UNIVERSITÀ
DEGLI STUDI
DI PADOVA

SEDE AMMINISTRATIVA

UNIVERSITÀ DEGLI STUDI DI PADOVA

DIPARTIMENTO DI SCIENZE CHIMICHE

CORSO DI DOTTORATO DI RICERCA IN: SCIENZE MOLECOLARI
CURRICOLO: SCIENZE CHIMICHE
CICLO XXXV

EXPLOITING CHIRALITY IN SELF-ASSEMBLED MOLECULAR CAGES

Coordinatore: Ch.mo Prof. Leonard Prins
Supervisore: Ch.mo Prof. Cristiano Zonta

Dottorando : Federico Begato

Summary

In the recent years, the research group in which this thesis has been carried out, has reported the synthesis of novel molecular cages based on tris(2-pyridylmethyl)amine (**TPMA**) complexes. These architectures have shown peculiar recognition properties for several molecules containing carboxylate anions.

This Ph.D. project has the aim to extend the applications of these supramolecular architectures in the field of chiral sensing taking advantage from molecular confinement, and to synthetize novel chiral structures for future applications in asymmetric catalysis. The introduction has the purpose to cover how chirality has been exploited in confined systems. While the first part regards the methodologies which have been used to prepare chiral architectures, in the second part of this chapter, the applications of chiral confined systems in asymmetric catalysis, guests recognition and sensing, and chiral amplification or induction have been explored. In the final part of the introduction, an overall overview of recent works regarding the synthesis and applications of supramolecular cages based on **TPMA** complexes ,developed in the research group in which this thesis has been carried out, have been presented.

In Chapter 1 the self assembly capability of the supramolecular cage in the presence of complex matrixes has been investigated. In this study, complex mixtures like wines and fruit juices have been employed in order to test if the cage could be able to selectively encapsulate and discriminate the dicarboxylic acids (tartaric, malic, and succinic acids) present in these matrixes. Moreover, the synthesis of a novel chiral zinc-**TPMA** complex has been reported, and the capability of the resulting chiral cage to act as Chiral Solvating Agent (CSA) for chiral dicarboxylic acids has been evaluated. This feature has been further exploited for the discrimination of the enantiomers of malic and tartaric acids present in wines and fruit juices using NMR.

In Chapter 2 the capability of the supramolecular architecture to act as stereodynamic probe for the recognition of chiral dicarboxylate anions has been explored employing circular dichroism. In particular, the cage showed a chiroptical enhancement of the dichroic signal in the presence of the tartrate anion as guest (*viz*. one order of magnitude higher than the other dicarboxylic acids). To investigate this phenomenon, a meticulous computational study was carried out. Moreover, stereodynamic properties of the cage combined with the capability to self-assemble in presence of complex mixtures has allowed the quantification of tartaric acid content in wines using circular dichroism.

In Chapter 3 the possibility to tune guests uptake or release from the cage has been explored. A novel approach based on the capability of 9,10-phenanthrenequinone to react with diamines subcomponents, thus allowing their selective removal or replacement has been developed. Using this procedure, reversible assembly and disassembly of the supramolecular architecture has been performed. Moreover, cage to cage conversions changing the size or the chirality of the diamine linkers were achieved, leading the selective uptake and release of (a)chiral guests.

In Chapter 4 a novel methodology based on [3,3]-sigmatropic Diaza-Cope rearrangement has been developed to obtain novel hydrolytically-stable chiral **TPMA**-based architectures. A detailed mechanistic study has been carried out in order to explain the effect of the guest length in the final thermodynamic distribution of the species involved during the reaction.

In the Appendices are contained the experimental details related to each chapter.

Riassunto

Negli ultimi anni, il gruppo di ricerca presso il quale è stata svolta questa tesi ha sviluppato nuove gabbie supramolecolari basate su complessi di tris(2-piridilmetil)ammina (**TPMA**). Queste strutture hanno dimostrato interessanti proprietà di riconoscimento verso diverse molecole contenenti anioni carbossilato.

Questo progetto di dottorato ha lo scopo di estendere le applicazioni di queste architetture supramolecolari nel campo del riconoscimento chirale traendo vantaggio dal confinamento molecolare, e di sintetizzare nuove strutture chirali per future applicazioni in catalisi asimmetrica.

L'introduzione ha la scopo di esporre come la chiralità sia stata impiegata in sistemi confinati. Mentre la prima parte riguarda le metodologie utilizzate per preparare strutture chirali, nella seconda parte di questo capitolo sono state esplorate le applicazioni di sistemi chirali confinati in catalisi asimmetrica, riconoscimento e sensing di molecole, e amplificazione o induzione di chiralità. Nella parte finale dell'introduzione è stata presentata una panoramica generale dei recenti lavori, riportati dal gruppo di ricerca presso il quale è stata svolta la tesi, sulla sintesi e applicazioni di gabbie supramolecolari basate su complessi di **TPMA**.

Nel Capitolo 1 è stata investigata la capacità di auto-assemblaggio della gabbia in presenza di matrici complesse. In questo studio, miscele complesse come vini e succhi di frutta sono state impiegate allo scopo di testare se la gabbia fosse in grado di incapsulare selettivamente e discriminare gli acidi dicarbossilici (tartarico, malico e succinico) presenti in queste matrici. È stata inoltre riportata la sintesi di un nuovo complesso di zinco-**TPMA** chirale, ed è stata valutata la capacità della gabbia chirale risultante di agire come Agente Chirale Solvatante (CSA) nei confronti di acidi dicarbossilici chirali. Questa caratteristica è stata poi sfruttata per la discriminazione degli enantiomeri dell'acido malico e tartarico presenti nei vini e nei succhi di frutta attraverso l'uso dell'NMR.

Nel Capitolo 2 è stata esplorata la capacità dell'architettura supramolecolare di agire come sensore stereodinamico per il riconoscimento di anioni dicarbossilato chirali utilizzando il dicroismo circolare. In particolare, la gabbia ha mostrato un'amplificazione del segnale chirottico in presenza dell'anione tartrato (un ordine di grandezza maggiore rispetto a quello degli altri acidi dicarbossilici). Per investigare questo fenomeno è stato effettuato uno studio computazionale approfondito. Combinando le proprietà stereodinamiche della gabbia con le capacità di auto-assemblarsi in presenza di matrici complesse è stato possibile quantificare il contenuto di acido tartarico nei vini utilizzando il dicroismo circolare.

Nel Capitolo 3 è stata esplorata la possibilità di modulare l'incapsulamento e il rilascio di molecole dalla gabbia. È stato quindi sviluppato un nuovo approccio basato sulla capacità del 9,10-fenantrenchinone di reagire con i componenti diamminici, permettendo così la loro rimozione o sostituzione selettiva. Utilizzando questa procedura è stato possibile ottenere il disassemblaggio/assemblaggio reversibile dell'architettura supramolecolare. Sono state inoltre effettuate trasformazioni gabbia-gabbia cambiando la grandezza o la chiralità della diammina, che hanno portato al rilascio o all'incapsulamento selettivo di specifiche molecole (a)chirali.

Nel Capitolo 4 è stata sviluppata una nuova metodologia basata sul riarrangiamento [3,3]-sigmatropico di Diaza-Cope allo scopo di ottenere nuove strutture basate su leganti **TPMA** idroliticamente stabili. Uno studio meccanicistico dettagliato è stato effettuato per spiegare l'effetto della lunghezza dell'ospite all'interno della gabbia sulla distribuzione termodinamica finale delle specie coinvolte durante la reazione.

Nelle appendici sono contenuti i dettagli sperimentali relativi ad ogni capitolo.

Declaration

Chapter 1 has been adapted from F. Begato, R. Penasa, G. Licini, C. Zonta, *Chem. Commun.* **2021**, *57*, 10019–10022. with permission from the Royal Society of Chemistry.

Chapter 2 has been adapted with permission from F. Begato, R. Penasa, G. Licini, C. Zonta, *ACS Sensors* **2022**, *7*, 1390–1394. with permission from the America Chemical Society.

Chapter 3 is submitted at Journal of the American Chemical Society.

Chapter 4 is submitted at Journal of the American Chemical Society.
The work was carried out in collaboration with Prof. Klaus Wurst at Department of General, Inorganic and Theoretical Chemistry University of Innsbruck A-6020 Innsbruck, Austria that refined the crystal structure.

Federico Begato, Padova 27/02/2023

Contents

Introduction

Exploiting Chirality in Confined Systems

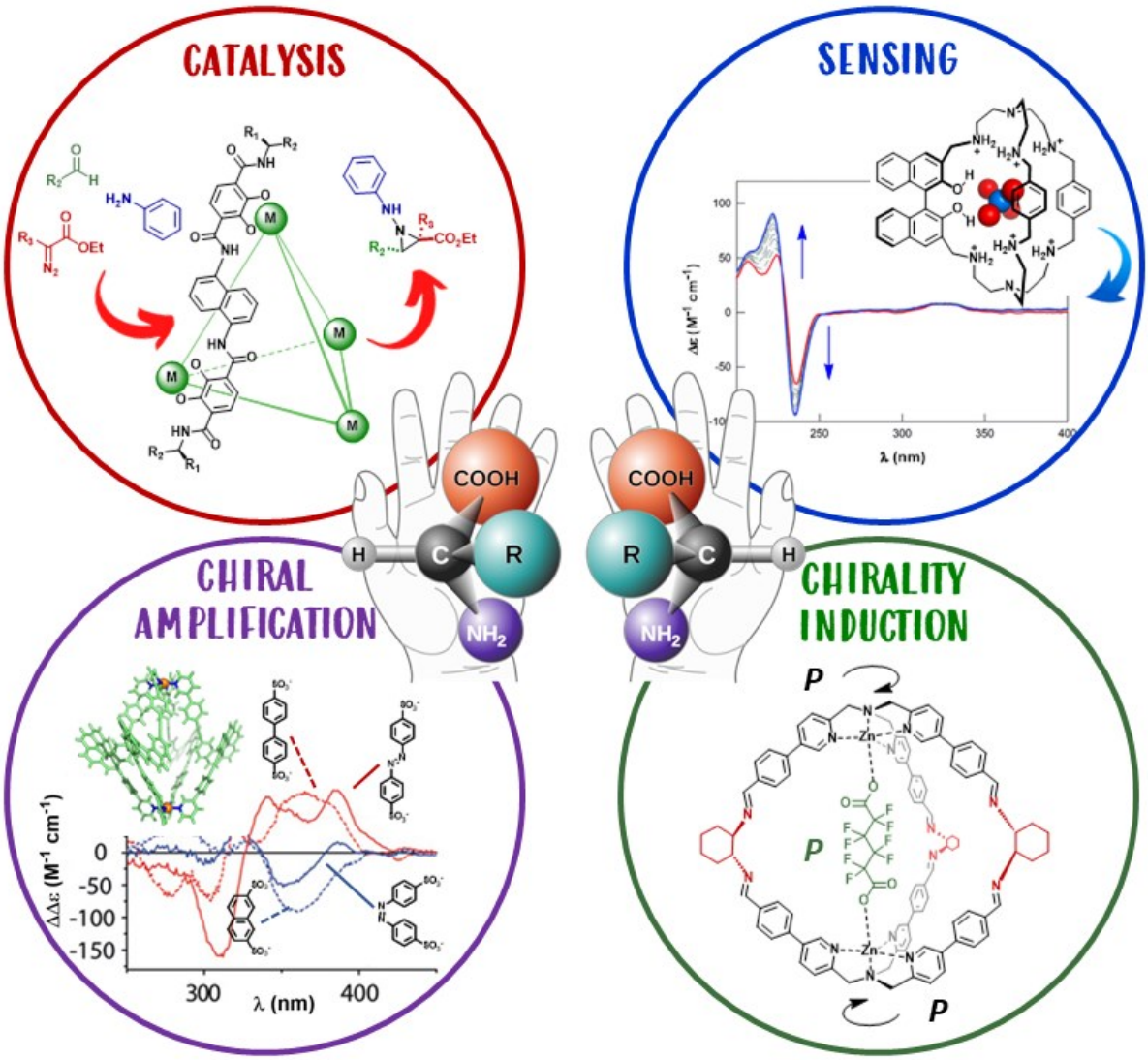

ABSTRACT Inspired by Nature, over the last decades, chemists have dedicated many efforts in order to develop artificial chiral supramolecules able to mimic biological systems. To obtain this capability there is the need to create a confined chiral environment in which one component of a racemic mixture could be preferentially bound through steric and electronic interaction. This introduction has the aim to show how chirality can be exploited in confined systems. After an overview of different methodologies that have been developed to obtain chiral molecular cages in Section I2, various applications of chiral confined architectures are presented. In section I3, the use of chiral nanocapsules in catalysis *(viz.* preorganization of the reactants inside the cavity, incorporation of the catalytic site in the structure of the architecture, and encapsulation of the catalyst within the cage) is described. In Section I4, the applications of enantiopure supramolecular cages in sensing and molecular recognition of specific analytes using different techniques (Circular Dichroism, NMR, Gas Chromatography) are reported. Afterwards, in Sections I.5 and I.6, the chiral amplification or induction upon encapsulation of chiral or achiral guests is described. In the last Section I7, an overall overview of recent works regarding the synthesis and applications of supramolecular cages based on tris(2-pyridylmethyl)amines (**TPMA**) scaffolds, developed in the research group in which this thesis has been carried out, are showed.

I1. Introduction

Confined structures have been one of the pillars in the journey of supramolecular chemistry. Since initial reports of Cram[1] and Lehn[2] on confined structures, the possibility to exploit shape-persistent organic molecules with permanent and accessible cavities has contributing to our actual knowledge of molecular recognition and how to take advantage of these recognition events in applications such as catalysis, sensing or separation.[3] Since the early reports, novel synthetic methodologies, mainly based on the use of metal-ligand or imine chemistry, have allowed a continuous development of the field. Giant structures, novel topologies, practical applications, and unexpected properties at the molecular levels are continuously emerging and rising the bar of innovation in supramolecular chemistry.[4] Chirality has been largely exploited in confined systems. This is either due to the implicit property of chiral subcomponents to direct stereochemically the development of the architectures, but also to the functions that only chiral systems can have. On the latter properties, while the initial purposes of chiral confined architectures were only directed to guest recognition and asymmetric transformations, chiroptical properties are emerging more intensively in the recent years.[5,6]

This introduction has as purpose to cover how chirality has been exploited in confined systems. While the first part regards the methodologies which have been used to prepare chiral architectures, in the second part of this chapter, the applications of chiral confined systems in asymmetric catalysis, guest recognition and sensing, and chiral amplification or induction have been explored. Finally, in the third part of the introduction, an overall overview of recent works regarding the synthesis and applications of tris(2-pyridylmethyl)amine **TPMA** architectures developed in the research group in which this thesis has been carried out, has been presented.

I2. Synthesis of Chiral cages

Three different methodologies can be employed for the preparation of chiral supramolecular cages. The first approach consists in the use of building blocks which already contain a fixed stereogenic element such as a classical carbon with four different substituents. This approach allows to obtain cages with a defined chirality which is defined by the initial units. In the second case, one or more of the constituents contain a labile stereogenic element. In these stereodynamic systems the final cage in usually present at room temperature in equilibria among the two enantiomeric forms. Shift of the equilibrium toward a preferential

enantiomeric form is usually obtained by the formation of a diasteroisomer using a chiral guest. The third methodology instead starts from employing achiral components, which due to elements of symmetry of the final structure, lead to a chiral architecture. In this latter case, a pair of enantiomeric cages with opposite chirality is usually obtained, which are not able to interconvert in solution at room temperature. Also in this case, an external enantiopure molecule can be used to separate the stereoisomers.

I2.1. Synthesis from Enantiopure building blocks

The use of enantiopure components to build chiral cages is the most frequently used methodology. While the first examples were related exclusively to purely organic systems, in recent years coordination-driven self assembly has emerged as a straightforward strategy to obtain complex metal-organic structures in high yields.[7]

I2.1.1. Organic cages

One of the early examples of purely organic chiral cage was firstly reported by Collet in 1981 (Figure 1). The formation for the first time of a D_3 symmetric chiral cryptophane **1** was obtained after six synthetic steps with an overall yield of 3%.[8] Later, Diederich *et al.* reported in 1997 a C_3 cage-like symmetric receptors **2a** and **2b**, containg two 1,3,5-triarylbenzene moieties held toghether by three amino acids spacers through peptide bonds.[9] The chirality of the cages was imparted by the stereocenters of the aminoacids, that allowed the formation of intramolecular H-bonds and thus an helical twist of the overall structrure. Nevertheless, due to the irreversible nature of reactions involved during the synthesis, the chiral receptors were obtained in low yield (<10%).

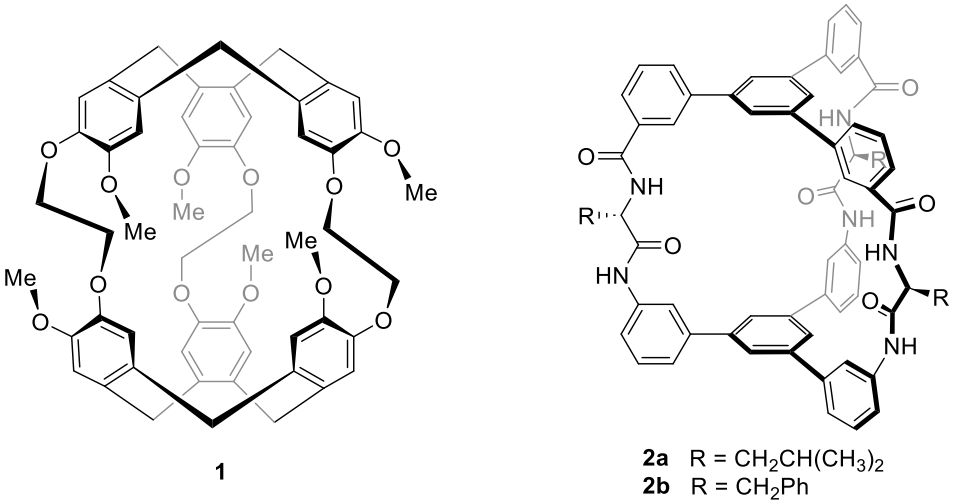

Figure 1. Chiral capsules reported by Collett (**1**) and Diederich (**2a**, **2b**). Adapted from ref. 8 and 9.

Since then, many efforts have been devoted to obtain chiral hosts in few synthetic steps and higher yields. One of the strategies that allowed to achieve this goal is the construction of self-assembled organic cages using dynamic covalent chemistry (DCC) instead of irreversible stepwise synthesis. DCC, which takes advantage of the reversible covalent bonds formation that works under thermodynamic control, has been widely used for the formation of more complex supramolecular architectures from relatively simple building blocks.[10,11] Under these conditions the system is free to explore all the accessible configurations and the final distribution of the species depends only on the relative stabilities of the products. Among the possible reversible bonds, imine condensation has been extensively used for the synthesis of large organic cages of defined shapes and sizes in excellent yields.[12,13]

One of the first example of dynamic covalent cage synthesis using imine bonds formation was reported by Warmuth in 2008.[14] In this work, a racemic mixture of C_3-trialkoxy-triformylcyclobenzylene **3** was heated at 80 °C with (*R*,*R*)-diaminocyclohexane *RR*-**CHDA** in the presence of catalytic amount of TFA furnishing the imine-based homochiral capsule (*PPRRR*)-**4** (Figure 2). Beside allowing the formation of the closed structure, heating the solution also led to the dynamic thermodynamic resolution of cyclotriveratrylene unit, obtaining the exclusive formation of the *P* enantiomer.[15] Precipitation and hydrolysis of the cage allowed the recovery of the enantiopure cryptoptophane that was further employed in combination of *p*-phenylendiamine **5** to obtain an enantiopure nano-cube **6** in 90% yield.

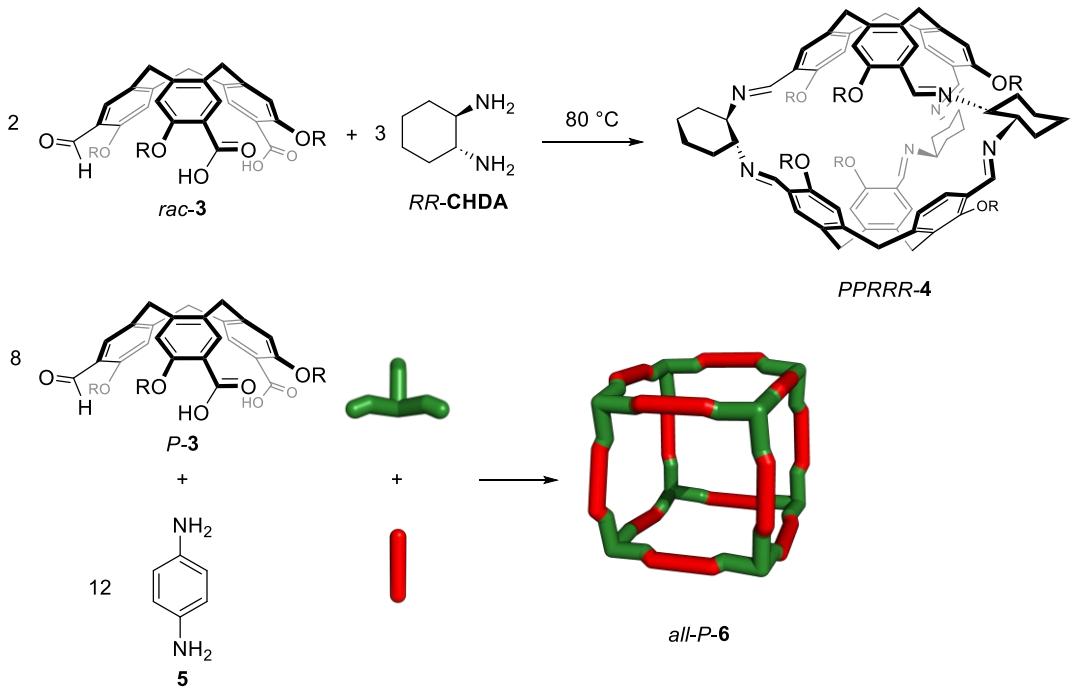

Figure 2. Synthesis of the enantiopure capsule (**4**) and nano-cube (**6**) reported by Warmuth. Adapted from 14.

Using a subcomponent self-assembly from *RR*-**CHDA** and triformyl benzene, Cooper *et al*. prepared a tetrahedral chiral cage **7** that can be isolated directly as crystalline solid (Figure 3).[16] These architectures presented permanent pore channels in the crystal structure that could be exploited for gas absorption. The same group took advantage of [8+12] imine condensation between tris(4-formyphenyl)amine and chiral diamines *RR*-**CHDA** and (*R*,*R*)-1,2-cyclohex-4-enediamine to generate large and shape persistent A_8B_{12} cages **8** and **9** through the formation of 24 new imine bonds.[17]

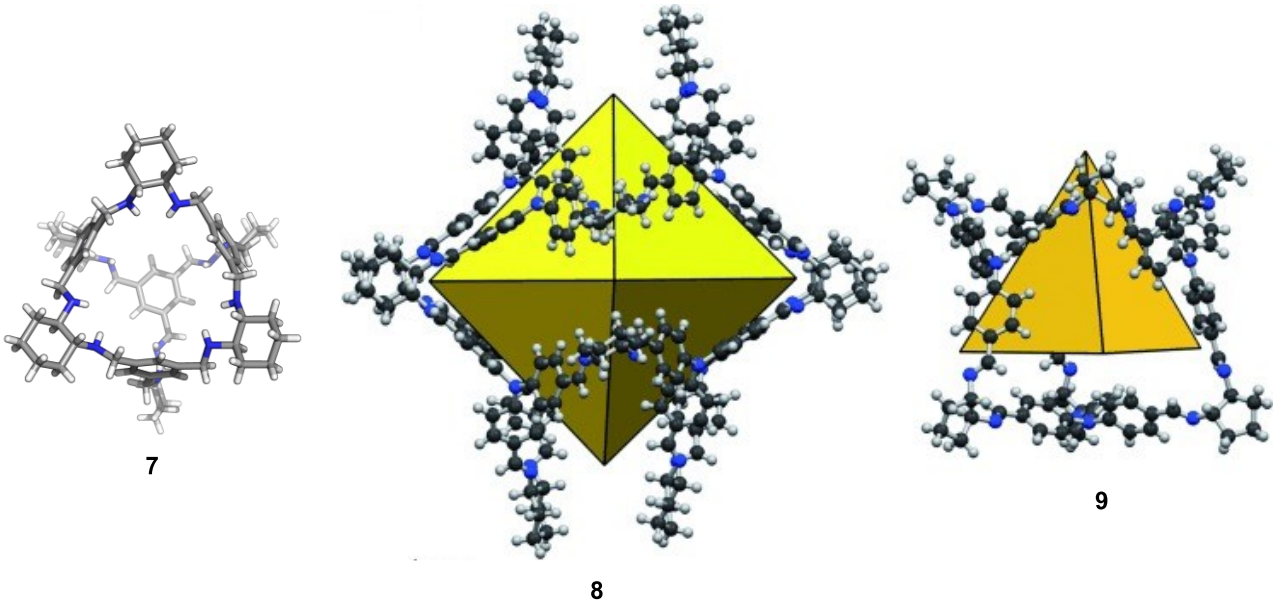

Figure 3. Imine-based molecular cages developed by Cooper. Adapted from ref. 16 and 17.

Scarso and coworkers synthetized in 2009 imine-linked (+)-syn-benzotricamphor derivative **11** that was able to selective encapsulate gaseous guest like ethane (Figure 4).[18] The chiral host was obtained through imine condensation between the syn benzotricamphor precursor **10** and ethylenediamine as linker. While in the previous cases the chiral element was in the diamine, in this case the chirality arised from the camphor building block.

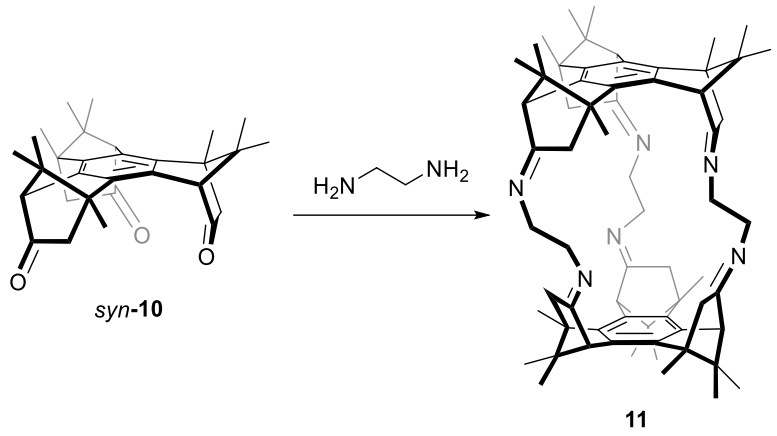

Figure 4. Synthesis of the (+)-syn-benzotricamphor derivative **11**. Adapted from ref. 18.

Taking advantage of the helical chirality of helicenes, Qiu *et al.* reported the synthesis of a [3+2]-type architecture **12** containing a triple stranded helical structure with three helicene units arranged in a propeller-like shape (Figure 5).[19] The formation of the cage was achieved starting from enantiopure helicene moieties, opportunely functionalized with aldehyde groups, through imine condensation with tris(2-aminoethyl)amine **TREN**. Crystal structure revealed that in the skeleton of **9** the three lateral arms were twisted into a triple helix fashion with a defined sense.

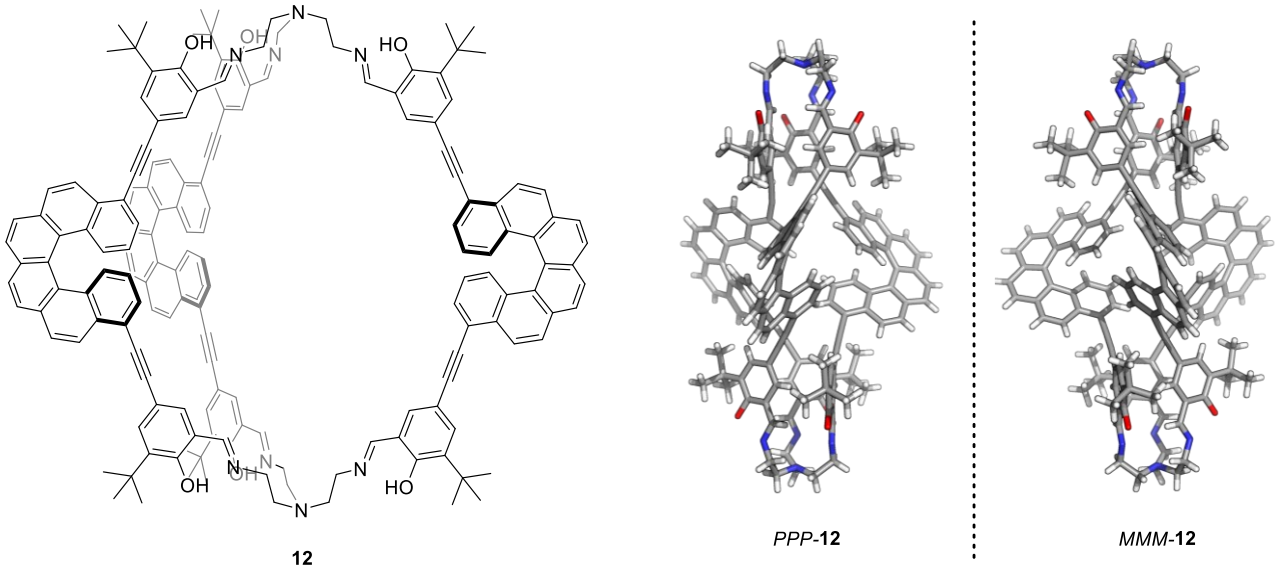

Figure 5. Triple stranded helical structure **12** reported by Qiu. Adapted from ref. 19.

Li *et al.* reported the use of chiral binaphthol derivatives to fabricate a chiral [2+3] **BINOL** based cage **14** through imine condensation (Figure 6).[20] More in detail, the supramolecular architecture was built up through the reaction between enantiopure **BINOL** building blocks **13** functionalized with aldehydic groups and **TREN**, leading the formation of the cage in almost quantitative yield.

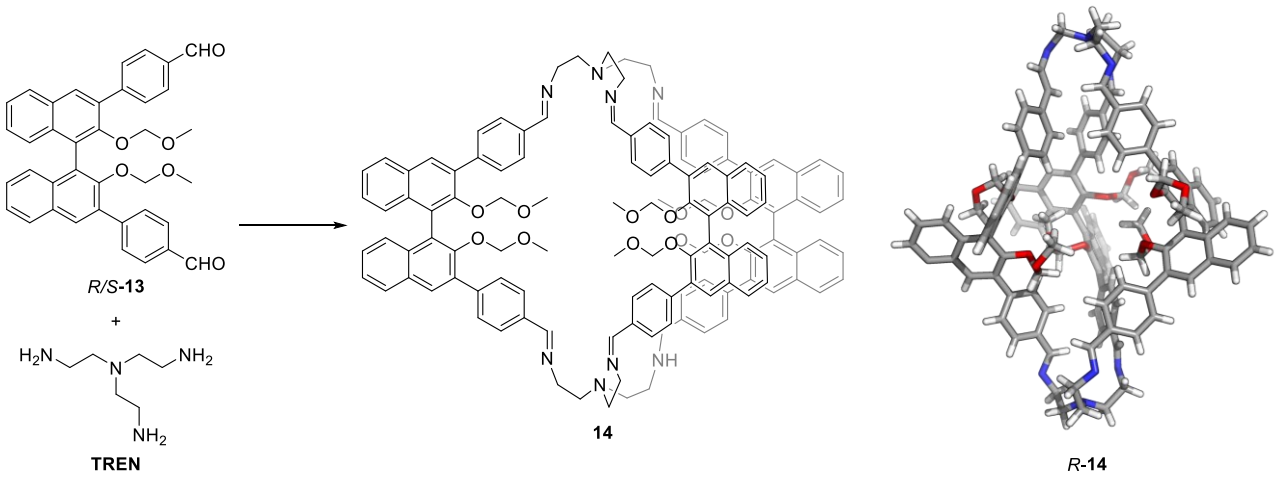

Figure 6. Synthesis of the **BINOL**-based architecture **14**. Adapted from ref. 20.

I2.1.2. Metal Organic cages

The field of self-assembled cages has been growing rapidly in the last decades. In particular, the use of metal-ligand coordination has been extensively exploited for the construction of supramolecular coordination complexes. Metal directed self-assembly, which takes advantage from directional, rather strong, and dynamic interactions, is a powerful tool to obtain architectures with well-defined shapes and sizes. Efficiency of this self-assembly method made it a powerful tool for the construction of chiral supramolecular architectures.[21–24] This methodology allowed the fabrication of discrete chiral metallo-cages due to the predictable outcome both in terms of composition and chirality.[25] The enantiopurity of the resulting system could be achieved by the use vertice-, edge-, and face-directed assembling strategies.[26] In the vertice-directed synthesis, the metal ions that are positioned at the vertex of the polyhedron, are surrounded by chiral auxiliaries, while in the other two approaches the chirality derives from linear (edge-directed) or planar (face-directed) ligands.[7]

In an early case, Stang *et al.* presented the first example of vertice-directed assembly, preparing chiral M_6L_4-type cages **17** from the self-assembly of tridentate ligand 1,3,5-tris[(4-pyridyl)ethynyl]benzene **15** and [(*R*)-(+)-BINAP]Pd^{II} and -Pt^{II} bis(triflates) **16** (Figure 7).[27] In this case, the six Pd(II) or Pt(II), that are positioned at the corners of the octahedron, were functionalized with the enantiopure **BINAP** as auxiliary and this dictated the formation of a *T*-symmetrical structure.

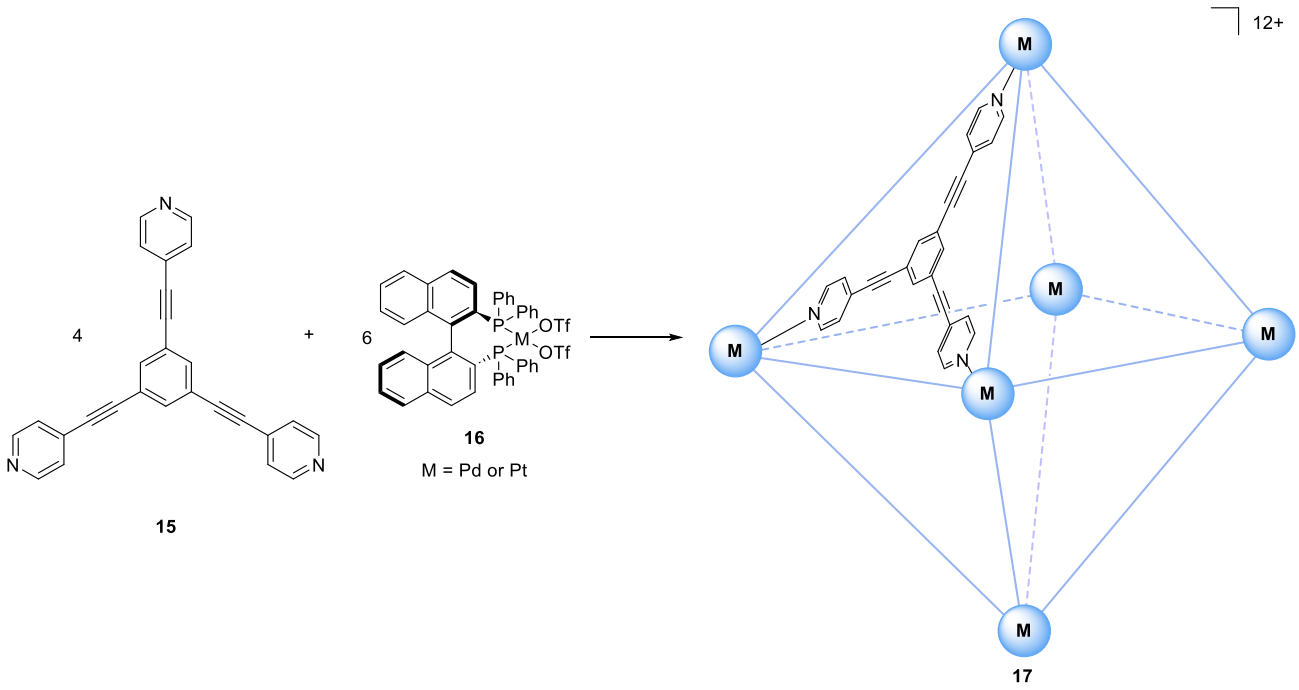

Figure 7. Synthesis of the enantiopure metal-organic octahedral cage **17**. Adapted from ref. 27.

With a similar strategy, Lusby and coworkers reported the first example of chiral Iridium-based nanocapsule **20**.[28] Starting from the resolved Δ- or Λ-[(Ir(ppy)$_2$Cl)$_2$] **18** and the subsequent self assembly with 1,3,5-tricyanobenzene ligands **19**, the authors were able to obtain the enantiopure Ir_6L_4 octahedral cage (Figure 8). Interestingly, the molecular architecture displayed emissive properties in tetrachloroethane, that were not observed in the simple mononuclear iridium complex. A possible explanation could be attributed to an inhibition of the nonradiative ligand dissociation pathways due to the rigidity of the octahedral capsule, that could allow the rise of the novel luminescence properties.

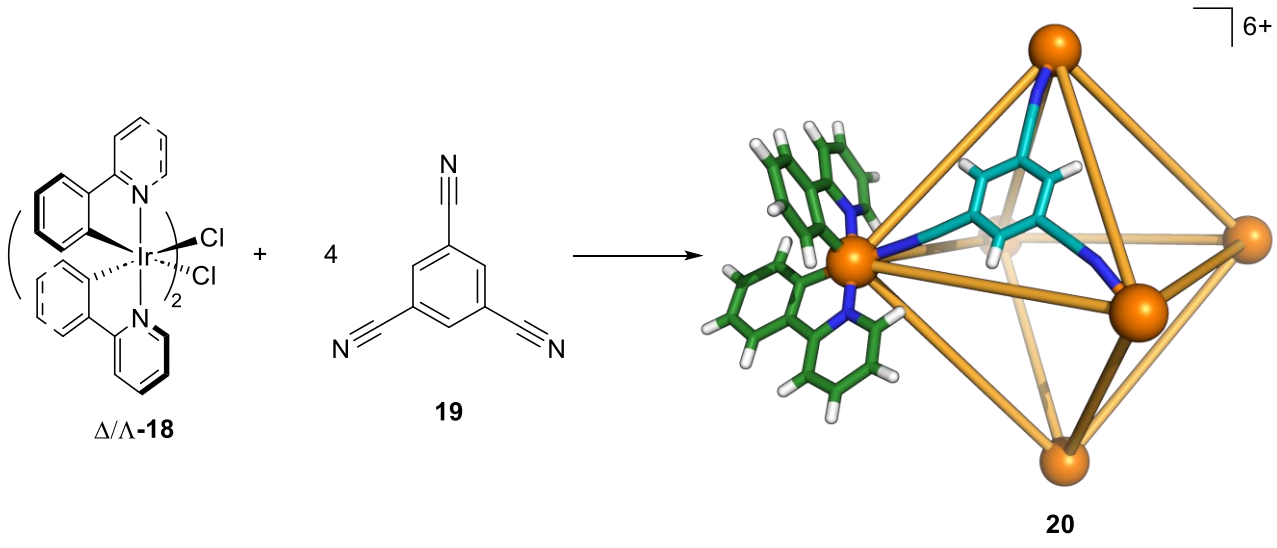

Figure 8. Synthesis of the enantiopure metal-organic octahedral cage **20**. Adapted from ref. 28.

Edge directed synthesis was used by the Nitschke group for the synthesis of chiral tetrahedral water soluble cage **23** by self-assembly of enantiopure diaminoterphenylene ligands **21**, formylpyridine **22** and Fe(II) metal ions (Figure 9).[29] It has to be noted that the stereochemistry of the glyceryl groups on the ligand dictated the handeness of the ligands around the iron (II) centers.

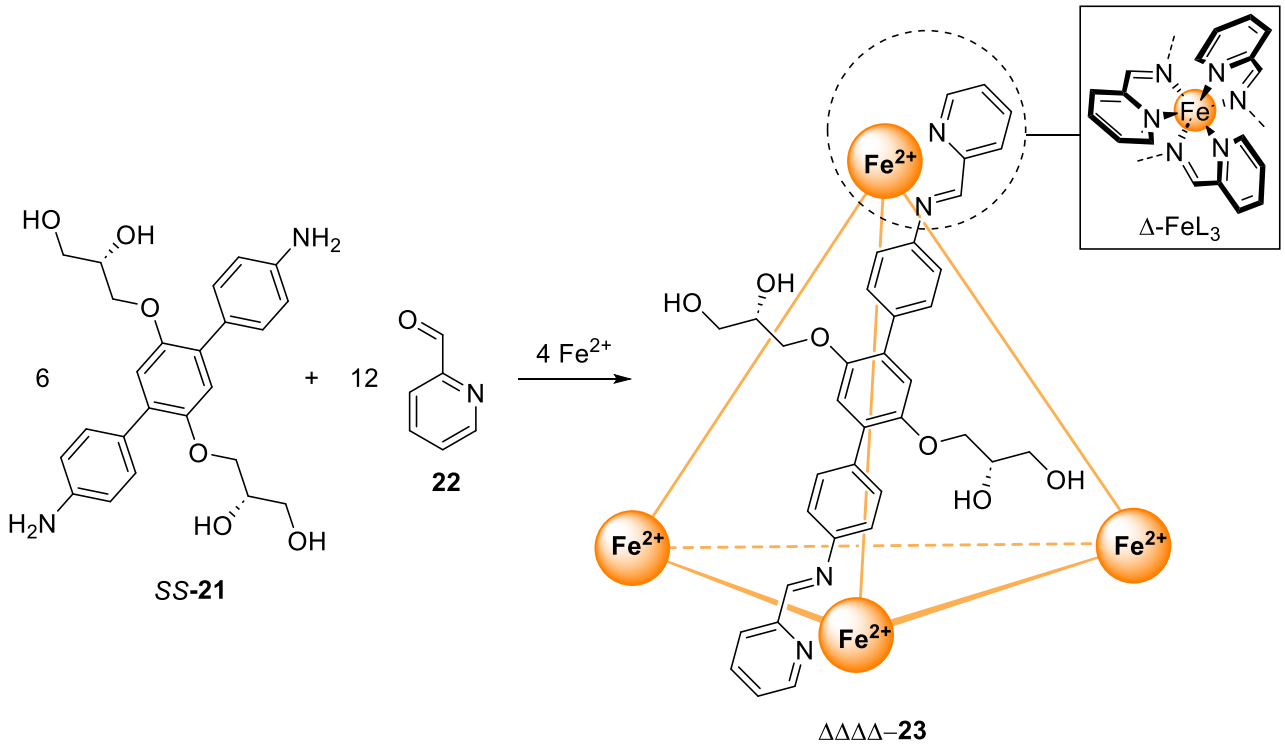

Figure 9. Enantioselective formation of capsule **23** by subcomponent self-assembly. Adapted from ref. 29.

A similar approach was reported by Raymond and coworkers that designed the synthesis of an enantiopure Ga_4L_6-type cage **25**.[30] The strategy was based on the self-assembly of a chiral terephthalamide-based ligand **24** opportunely modified at the vertexes with chiral-directing amide groups that allowed the isolation of a single diasteroisomer (Figure 10).

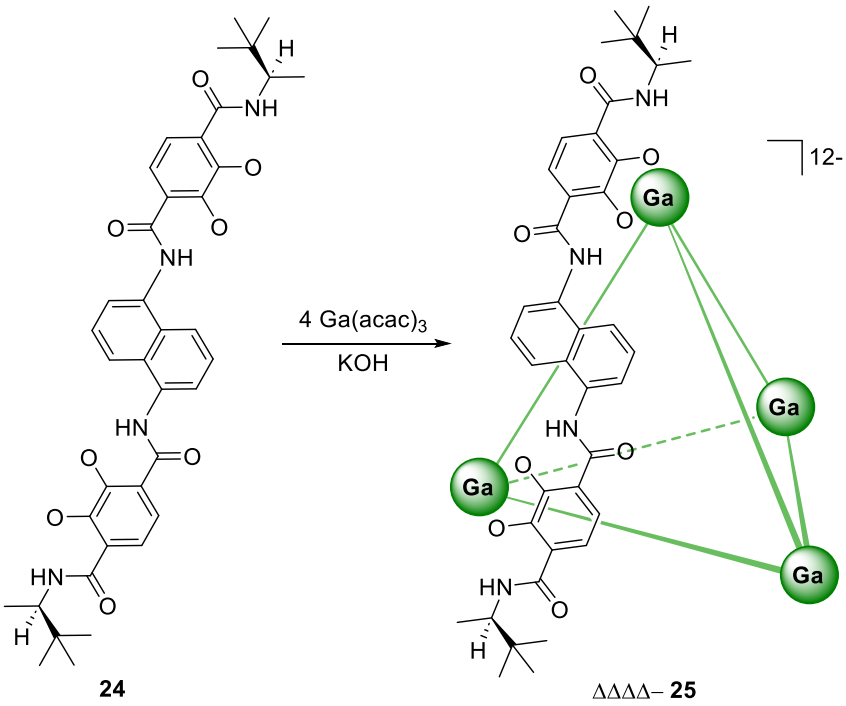

Figure 10. Synthesis of the molecular assembly **25**. Adapted from ref. 30.

Using planar ligand, Sun *et al*. reported face-directed self-assembly of chiral luminescent tetrahedral cages in combination with Europium ions.[31] More in detail, the group synthetized both enantiomers of 1,3,5- tris(4-aminophenyl)-benzene based ligands **26**, modified with a chiral unit, to obtain tris(tridentate) coordination scaffolds (Figure 11). These platforms were further employed to obtain chiral $Eu_4(L)_4$ **27** tetrahedral cages through a face-directed strategy. Interestingly, a narcissistic self-sorting process was observed when both enantiomers of the same ligand were mixed, leading to homochiral structures.

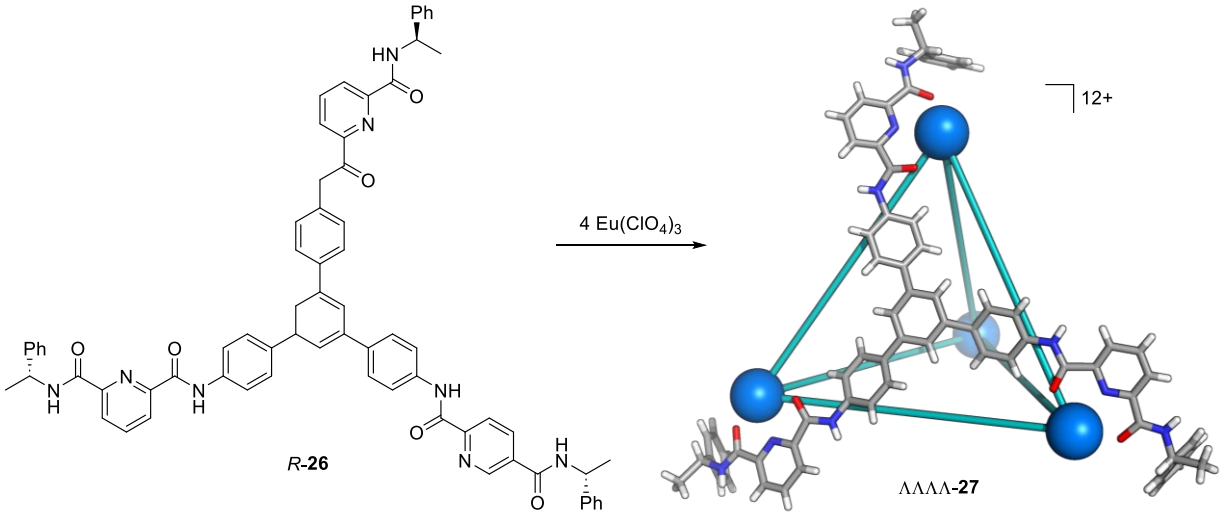

Figure 11. Synthesis of the enantiopure cage ΛΛΛΛ-**27** starting from the *R* enantiomer of ligand **26**. Adapted from ref. 31.

I2.2. Stereodynamic cages

Another method to realize chiral cages is the use of stereodynamic units as building blocks for the construction of the supramolecular architectures. Stereodynamic molecules are characterized by the presence of one interconverting stereogenic element in the molecular scaffold. Since the inversion barrier for the racemization is low, the two enantiomeric forms are in rapid equilibrium at room temperature. Due to this dynamic behavior, the addition of a chiral analyte able to bind the stereodynamic unit can move the system toward the diastereomeric regime thus leading to the formation of a preferential diastereoisomer.[32] Axially chiral aromatic frameworks, metal complexes capable of fast ligand sphere modifications, and propeller-like reporter units have been extensively exploited in the field of sensing using chiroptical techniques. [33] In this scenario, self-assembled hosts made up using stereodynamic units as building block, and capable to encapsulate chiral guests inside the void cavity, have been extensively explored for chiral sensing employing chiroptical analyses. Among metallo-supramolecular systems, the combination of achiral ligands and metal ions can originate discrete capsules with propeller (Λ/Δ) or helical (*M*/*P*) structures. Helicates are architectures in which the organic ligand fold around two or more metal ions with a helical twist. Without any stereogenic element, self-assembly of the achiral component leads to the formation of two helical interconvertible domains with opposite helicity. The inclusion of a chiral guest in the cavity leads to the formation of two diastereoisomers. The equilibrium is thus shifted toward the most stable species, generating an induced chiroptical signal that can be used for chiral analysis.[34,35]

Rancan and coworkers reported the formation of a quadruple stranded helicate **30** using bis-β-diketone-based ligands **28** and **29** and lanthanide or europium ions (Figure 12).[36] The equilibrium of the resulting racemic mixture was controlled by addition α-methylcholine **G**. The chiral induction was followed using either circular dichroism and circularly polarized luminescence and the chiroptical readout could be correlated with the enantiomeric excess of the asymmetric guest.

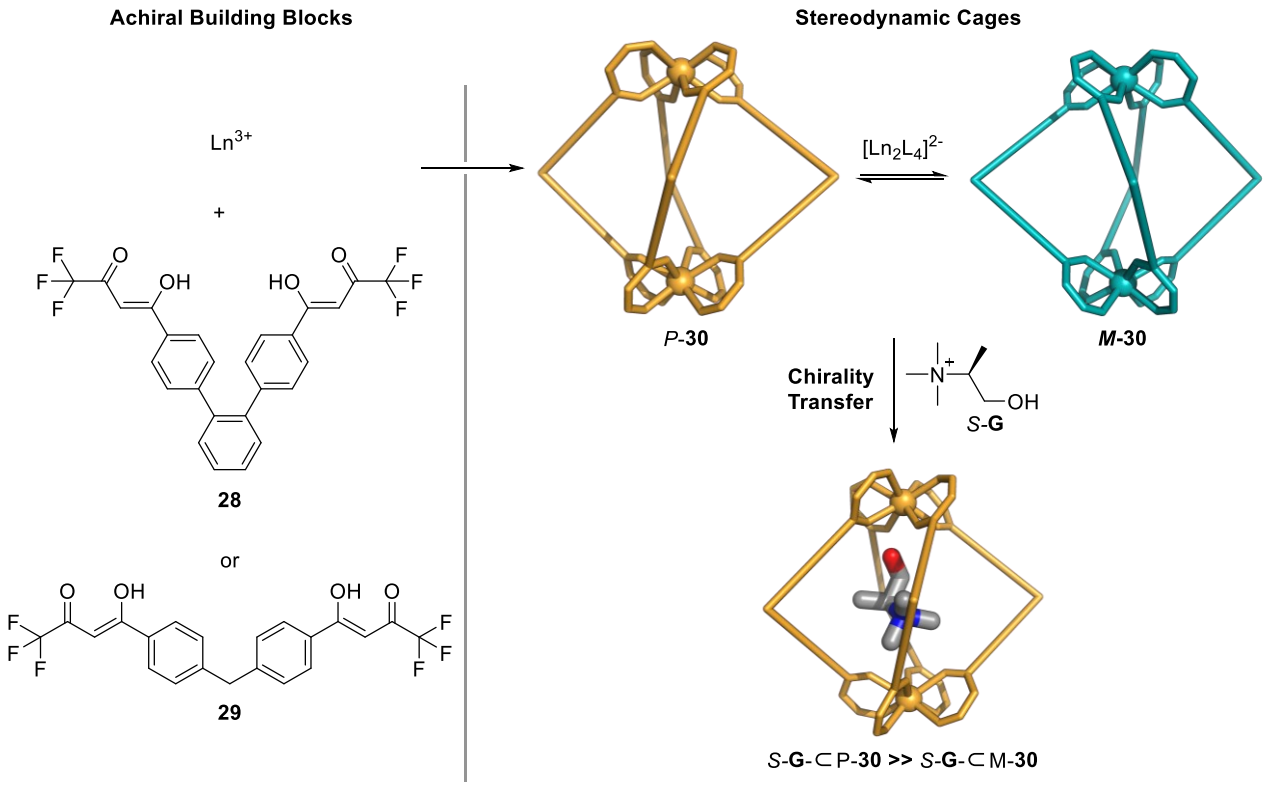

Figure 12. Self-assembly of a racemic mixture of quadruple-stranded helicate-cages **30** and hierarchical chirality transfer from the chiral guest to the host. Adapted from ref. 36.

Mukherjee *et a*l. reported a metal-coordinated cage in which trispyridyl donor ligand **31**, with a propeller shape, could self-assemble with *cis*-protected Pd(II) complexe **32** allowing the formation of an octahedral nanocapsule **33** (Figure 13).[37] The process led to the formation of a complex mixture of interconverting stereoisomers of the chiral cage. Due to the guanidium core, addition of *R*- or *S*-**BINOL** resulted in the encapsulation of the chiral guest through H-bond. The efficient diastereoselective interaction drove the equilibrium selectively toward a single enantiomeric species, allowing the formation of a strong CD signal that could be employed for the chiral sensing of **BINOL**.

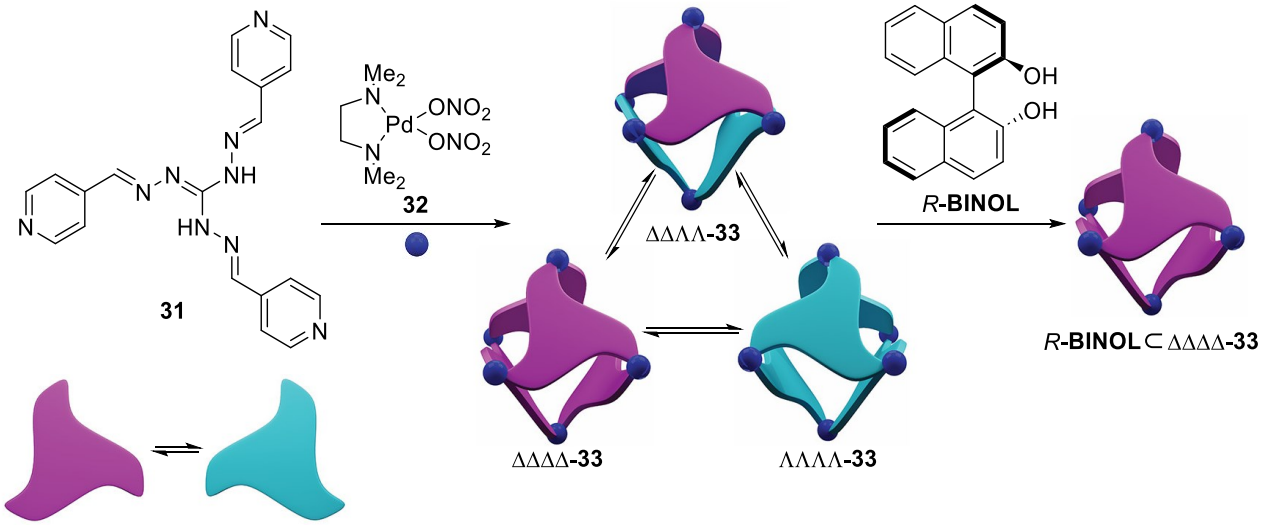

Figure 13. Schematic representation of the formation of enantiopure host−guest assembly *R*-**BINOL**⊂ΔΔΔΔ-**33**. Adapted from ref. 37.

Tetradentate complexes in which the ligand can assume a propeller like arrangement around the metal ion are an emerging class of scaffold in supramolecular chemistry. As example, complexes of tris-2-pyridilmethylamine (**TPMA**), triphenolamine (**TPA**), and triethanolamine (**TEA**) ligands usually display a bipyramidal trigonal geometry in which the ligand is twisted around the metal center in a helical C_3-symmetrical fashion. As a consequence, two enantiomeric forms of the complex that differ for the handedness of the arm twist, namely Λ (*M*) and Δ (*P*), are present (Figure 14).[38,39]

However, few example of purely steoreodynamic supramolecular cages built up using these type of complexes have been reported so far, and the field of chiral sensing still remains unexplored.

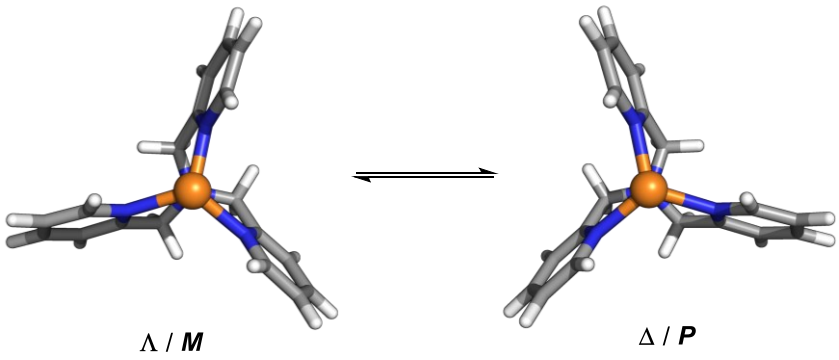

Figure 14. Λ (counterclockwise) and Δ (clockwise) conformation of **TPMA** ligands wrapped around a metal center.

Zonta *et al*. reported the synthesis of a chiral cage **35** using a modified **TPMA**-Zn complex **34**, chiral diamine *RR*-**CHDA** and aliphatic dicarboxylic acids $\mathbf{C_n}$ as guests (Figure 15).[40] The formation of the cage was achieved exploiting dynamic covalent chemistry, in particular the imine condensation between the **TPMA** complex bearing three aldehyde groups and the chiral diamine. The self-assembly of the chiral cage could in principle lead to the formation of two diastereoisomers in which the chirality of the diamine linker is fixed while both helicities of the **TPMA** scaffold could be present. However, thanks to the dynamic nature of the stereodynamic unit, the formation of the *RR*-Λ-**35** diastereoisomer with a preferential helicity was induced, depending on the configuration of the enantiopure diamine building blocks.

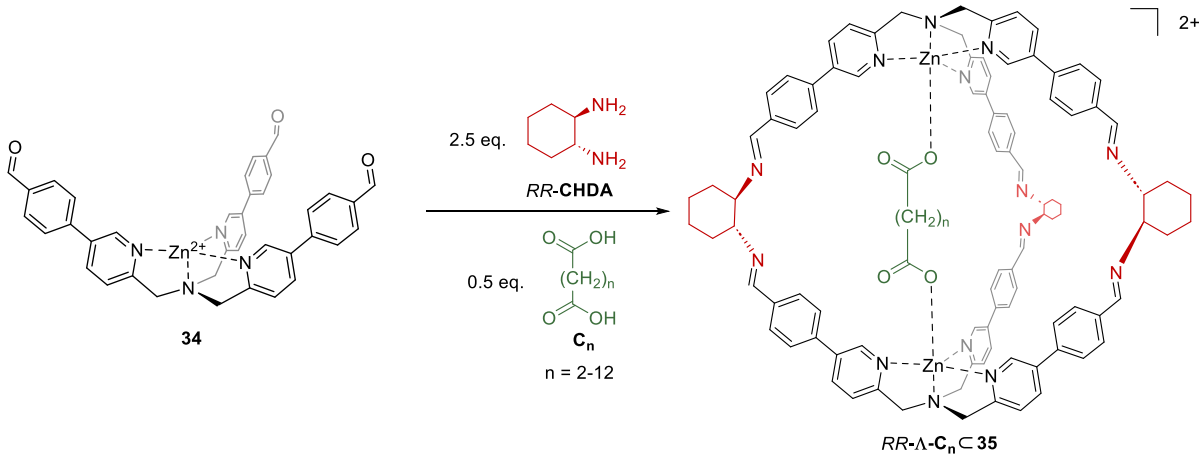

Figure 15. Self-assembly of the enantiopure host–guest assembly ***RR*-Λ-$\mathbf{C_n}$⊂35** starting from the stereodynamic **TPMA**-based zinc complex **34**. Adapted from ref. 40.

I2.3. Resolution of Chiral cage starting from Achiral Building blocks

As mentioned before, chiral cages can be also obtained starting from achiral building blocks. In this case, the final arrangement of the subcomponents determines the chirality of the structure and this is most of the time due to the twisted configuration that one of the achiral components assume upon coordination to the metal center. Without any chiral input the resulting structures can exists only in a racemic mixture of enantiomers and, usually, the interconversion barrier between the two species is higher enough to avoid the racemization. The most common methodology for the resolution of these systems is crystallization, in which the interaction with an asymmetric auxiliary is used to obtain diastereomeric species with different solubilities. [41]

One of the characteristic example of resolution was reported by Raymond and coworkers in which the interaction of enantiopure *S*-(+)-*N*-methylnicotinium cation *S*-**NIC** was used to

resolve the anionic gallium-based cage **36** (Figure 16).[42] More in detail, the enantiomeric tetrahedral assemblies were prepared from the self-assembly of bis-hydroxamate ligands and Ga(III) metal ions. The synthesis led to the formation of a racemic mixture of homoconfiguration clusters (ΛΛΛΛ or ΔΔΔΔ), in which the racemization is prevented due to the interconnection of the four metal centers in a rigid three-dimensional tetrahedral arrangement. Encapsulation and interaction with the catecholate groups of enantiopure cations *S*-**NIC** led the quantitative crystallization of the less soluble diastereoisomer ΔΔΔΔ species as confirmed by X-Ray, CD, and NMR techniques. While the other diastereomeric species could be recovered from mother liquors. Guest removal was finally performed using ion-exchange chromatography. This strategy was employed few years later by the same group for the resolution of the parent Aluminum and Iron structures.[43]

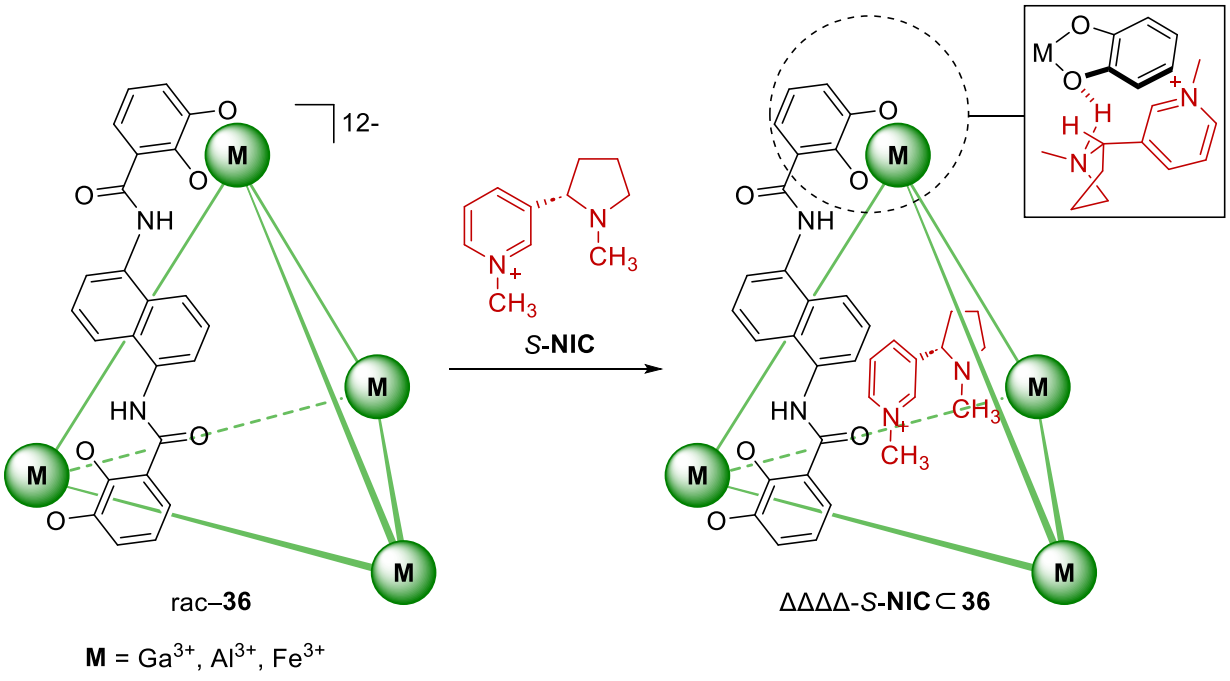

Figure 16. Schematic representation of the resolution of cage **36** upon interaction with chiral S-**NIC** that allowed the precipitation of the ΔΔΔΔ-*S*-**NIC⊂36** diastereoisomer. Adapted from ref. 42.

Zhang *et al.* reported the selective resolution of a water soluble tetrahedral cage **37** using (*R*)- or (*S*)-**BINOL**.[44] The $[Fe_4L_6]^{4-}$ type cage was obtained by mixing 4,4' -diaminobiphenyl-2,2' -disulfonic acid and 2-formylpyridine subcomponents with iron(II) and a base (Figure 17). Among all the possible stereoisomers, the self-assembly led to the formation of a racemic mixture of the homochiral configuration ΛΛΛΛ or ΔΔΔΔ. Interestingly, while chiral cationic resolving agents like L-1-hydroxymethyl-3-methylbutyl (trimethyl)- ammonium iodide and N-benzylcinchoninium chloride were not suitable for the resolution of the cage, *S*-***BINOL*** allowed the isolation of the enantiopure compounds.

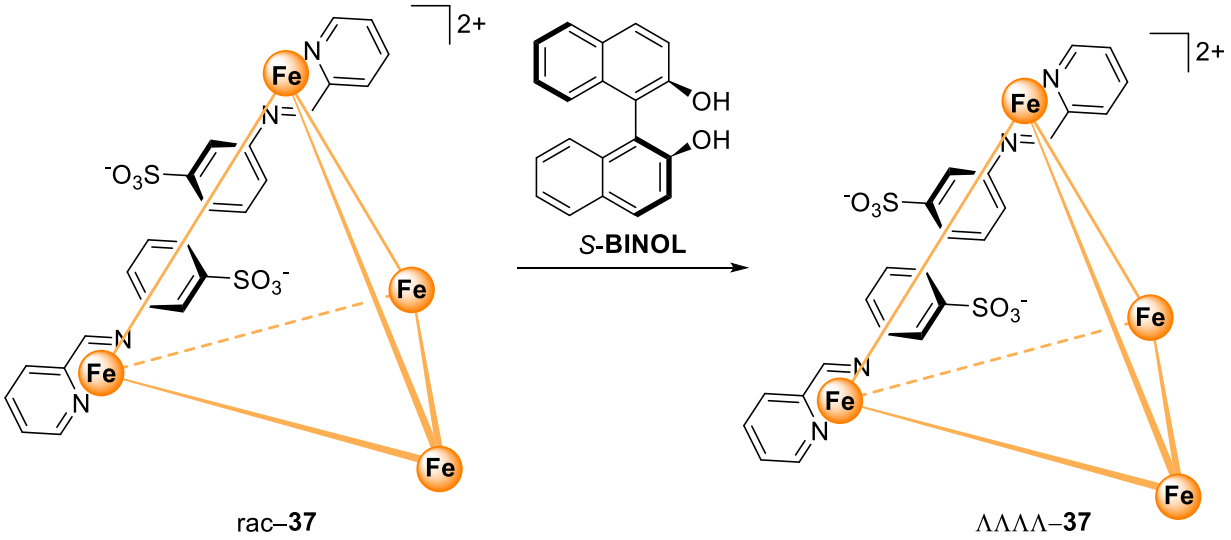

Figure 17. Schematic representation of the resolution of cage **37** using enantiopure *S*-**BINOL**. Removal of the **BINOL** was achieved after slow vapor diffusion of acetone in water/methanol solution of the cage. Adapted from ref. 44.

Beside chiral purely organic molecules, also chiral metal complexes has been employed for the optical resolution of chiral cages **38** by Zhang *et al.*[45] In this case, the two enantiomers ΛΛΛΛ-[Ti_4L_6] and ΔΔΔΔ-[Ti_4L_6] were completely resolved by addition of Δ-[Mn(*RR*-CHDA)$_3$] and Λ-[Mn(*SS*-CHDA)$_3$] **39** respectively (Figure 18).

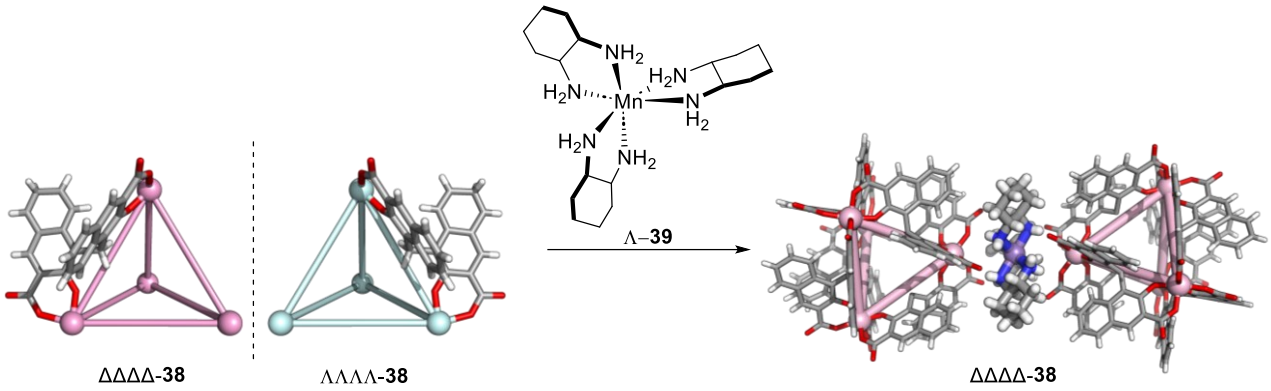

Figure 18. Optical resolution of ΔΔΔΔ-cage **38** by a Λ-[Mn(*RR*-DCH)$_3$] metal complex. Adapted from ref. 45.

I3. Catalysis

The high efficiency and specificity of enzymes has inspired chemists to pursue the discovery of novel artificial catalysts able to perform selective transformations.

In this scenario, molecular cages with defined void cavities able to mimic the unique features of the active sites of biological molecules have been extensively studied.[46] Thanks to the hydrophobic pockets and specific noncovalent interactions, nanocapsules can bind the substrates, stabilize transition states or reactive intermediates and allow selective catalysis. Moreover, enzymes are closely related to chirality since they are complex proteins built up by folding of chiral peptides. Consequently, the engineering of chiral supramolecular architectures able to establish specific interaction with chiral substates could open the possibility to unravel the complexity of natural biomolecules.[47]

Catalysis in confined spaces can occur in three different ways: *i)* by preorganization of the reactants inside the cavity, *ii)* incorporating catalytic sites, and *iii)* by encapsulation of the catalyst within the cage.

A pioneering work in stereoselective catalysis in confined spaces was reported Fujita *et al.* that performed enantioselective cross [2+2] photoaddition of fluoranthene **39** with a maleimide derivative **40** (Figure 19).[48] In this work, the well-defined void cavity allowed the preorganization of the substrates in a specific diastereomeric fashion, allowing the asymmetric induction during the process. The reaction occurred in an enantiopure octahedral cage **41** made through the self-assembly of 1,3,5-tricyanobenzene ligands Pd(II) metal centers coordinated with chiral diamine auxiliaries. By the simple chiral modification of the external vertices, the authors were able to perform the photoaddition in an asymmetric fashion inside the hydrophobic cavity of the capsule with enantiomeric excess of the products **42** up to 50%. It should be pointed out that the photochemical pericyclic reaction of fluoroanthrene derivatives does not occur, thus, in this case, confinement allowed a reaction that would otherwise be impossible to perform.

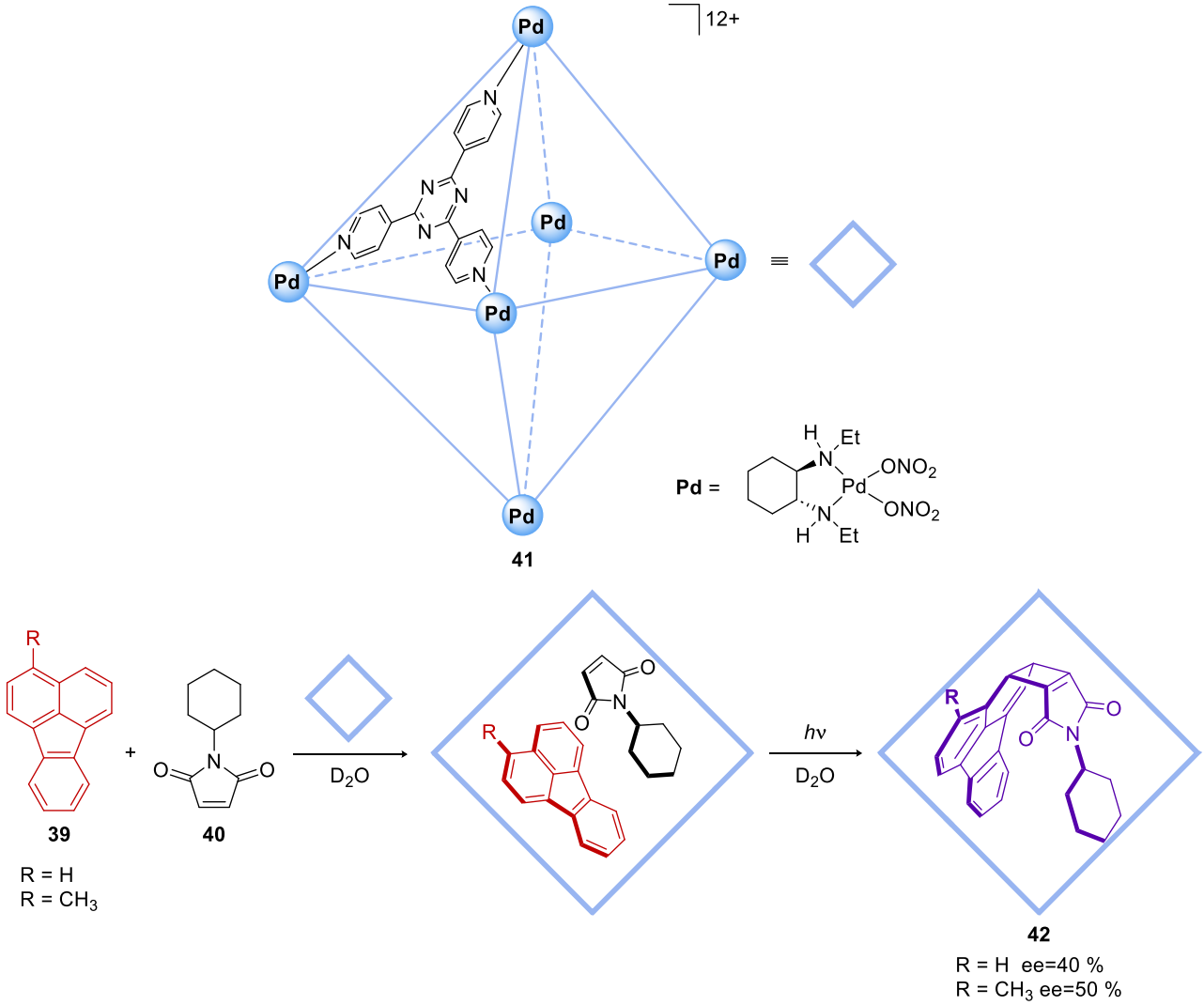

Figure 19. [2+2] Photoaddition reaction of **39** with **40** in cage **41**. Adapted from ref. 48.

In a similar way, Toste, Raymond and Bergman reported the enantioselective aza-Darzens reaction catalyzed by an enantiopure Ga(III), Al(III), and In(III)-based tetrahedral cages **43** (Figure 20).[49] The authors synthetized a library of chiral assemblies in order to demonstrate how the flexibility of the chiral host could influence the enantioselectivies during the reaction. By modification of the chiral amide-based ligand, a wide range of enantiopure molecular architectures were prepared. Moreover, it was seen that the variation of the external scaffold led to a substantial effect on the cage flexibility and host opening. Aza-Darzens condensation for the formation of trans-aziridine was then tested in the presence of catalytic amount of the chiral cages. Interestingly, the best performances in terms of enantioselectivities (99% e.e.) were observed with the most flexible hosts. This work highlighted that supramolecular nanocapsules cannot be seen as simple rigid containers in which the reaction occurred. It has instead emphasized how the dynamicity of the host, like in the enzymatic systems, could play a crucial role in reaction outcome.

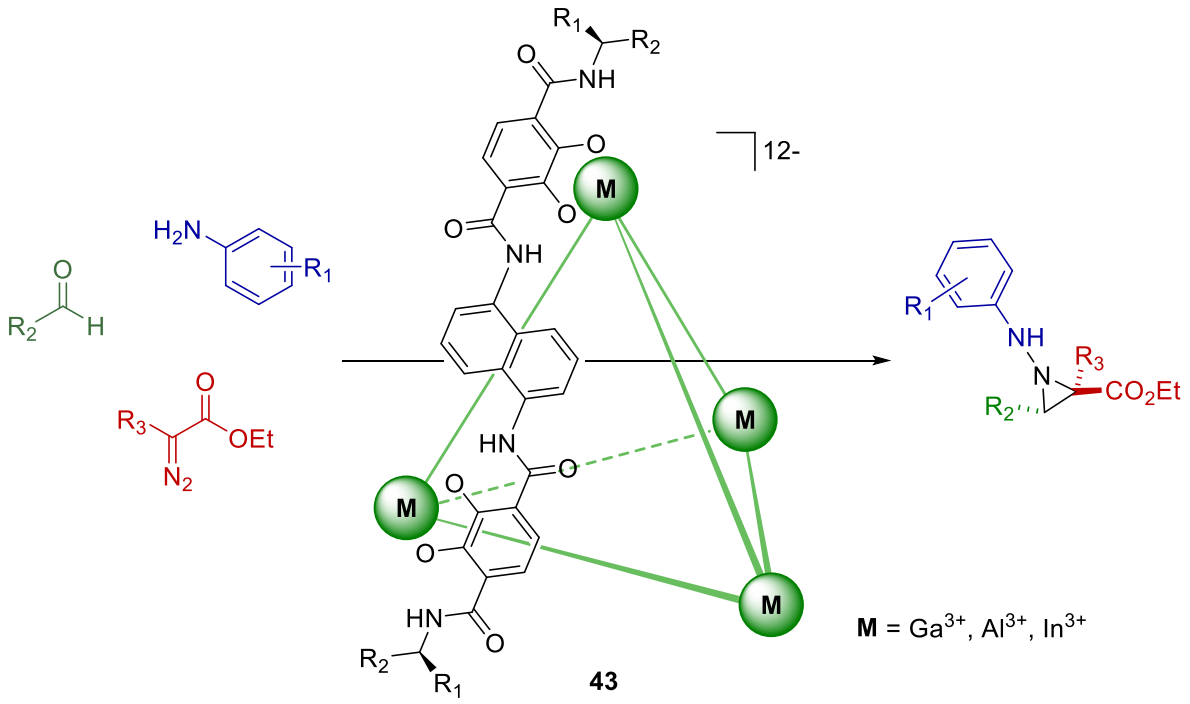

Figure 20. [2+2] Photoaddition reaction of **39** with **40** in cage **41**. Adapted from ref. 49.

Incorporation of a chiral catalyst inside the cavity of a supramolecular cage, either by covalent bonding or non-covalent interactions, is another efficient way to build chiral host-guest complexes able to promote asymmetric transformations. With this approach the supramolecular architecture acts as a molecular flask, resulting in greater control over guests selectivity and products regio- and stereo-selectivity in comparison to the free catalyst. Moreover, using this strategy, self-quenching and deactivation of the catalyst are prevented and the effective molarity could be dramatically increased.

Reek, Ribas and Costas groups reported the enantioselective hydroformylation performed in a tetragonal cage able to incorporate the monophosphoramidite-Rh(I) catalyst.[50] The construction of the nanocapsule **44** was based on Pd-carboxylate coordination bonds between two opposite Zn porphyrins bridged together by four macrocyclic assemblies (Figure 21). After the synthesis of the cage, encapsulation of the enantiopure Rh-catalyst was achieved through the coordination of the pyridine groups of the phosphoramidite-based complex to the Zn metal of the porphyrin scaffold, as confirmed by UV and NMR titrations. The host-guest adduct was further employed in the catalytic hydroformylation of styrene derivatives. The obtained results highlighted that the confinement of the catalyst improved both the efficiency and the stereoselectivity of the process in comparison to the free Rh-complex.

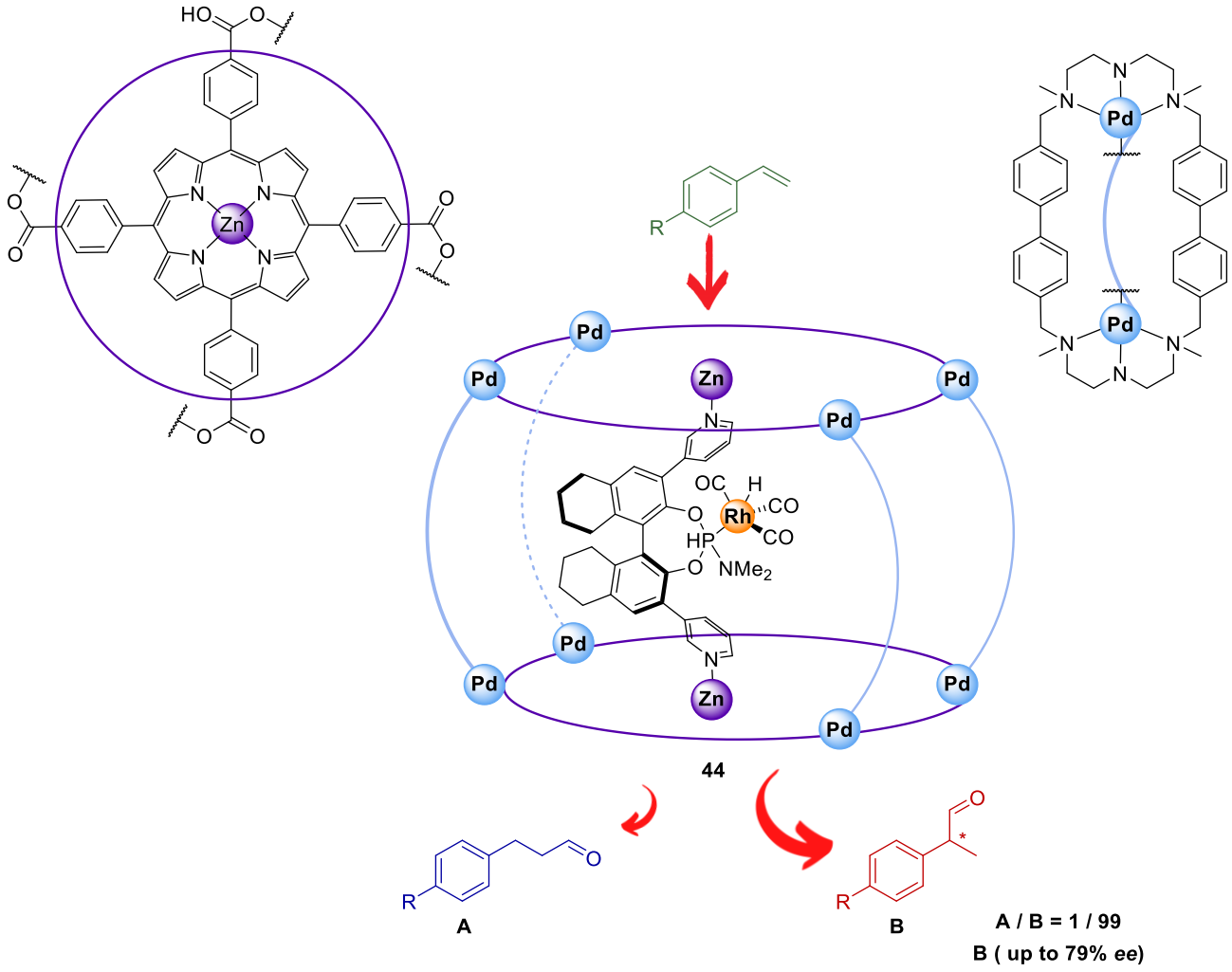

Figure 21. Schematic representation of the enantioselective hydroformylation performed in the tetragonal cage **44** that incorporates the monophosphoramidite-Rh(I) catalyst. Adapted from ref. 50.

Another efficient way to obtain stereoselective reaction using confined systems is to integrate the active site, usually a metal ion, in the structure of the cage. In this case the cavity of the structure still plays an important role since it can pre-organize and activate the substrate, preventing the aggregation of the catalysts and increasing the local concentration of the active center. Using this strategy, Su and coworkers developed a homochiral octahedral cage **45** and explored the photoinduced regio- and stereoselective oxidative biaryl coupling reaction (Figure 22).[51] The molecular container was synthetized through the coordination-driven assembly of palladium metal ions, that formed the vertices of the octahedron, and enantiopure phenanthroline-based ruthenium complexes, placed at the faces. The active species in this case was the embedded chiral ruthenium complex, that is a typical photo-driven hydrogen evolving catalyst. Due to the capability of cage **45** to encapsulate naphthol guests, by irradiation at 453 nm the system was able to perform an uncommon regiospecific 1,4-coupling to obtain the only formation of 4-(2-hydroxy-1-

naphthyl)-1,2-naphthoquinones in both high yield (up to 96%) and good enantiomeric excesses (up to 58%). The presence of the cage was found to be essential for the success of the photoinduced regio-and steoreoselective process, that otherwise usually produces the 1,1'-bi-2-naphtol coupled products. Moreover, a control experiment using the free Ruthenium complex showed that the coupling was inefficient under the same reaction conditions. These results proved that the encapsulation of the substrates inside the chiral confined space was the key factor in the stabilization of the reactive radical species.

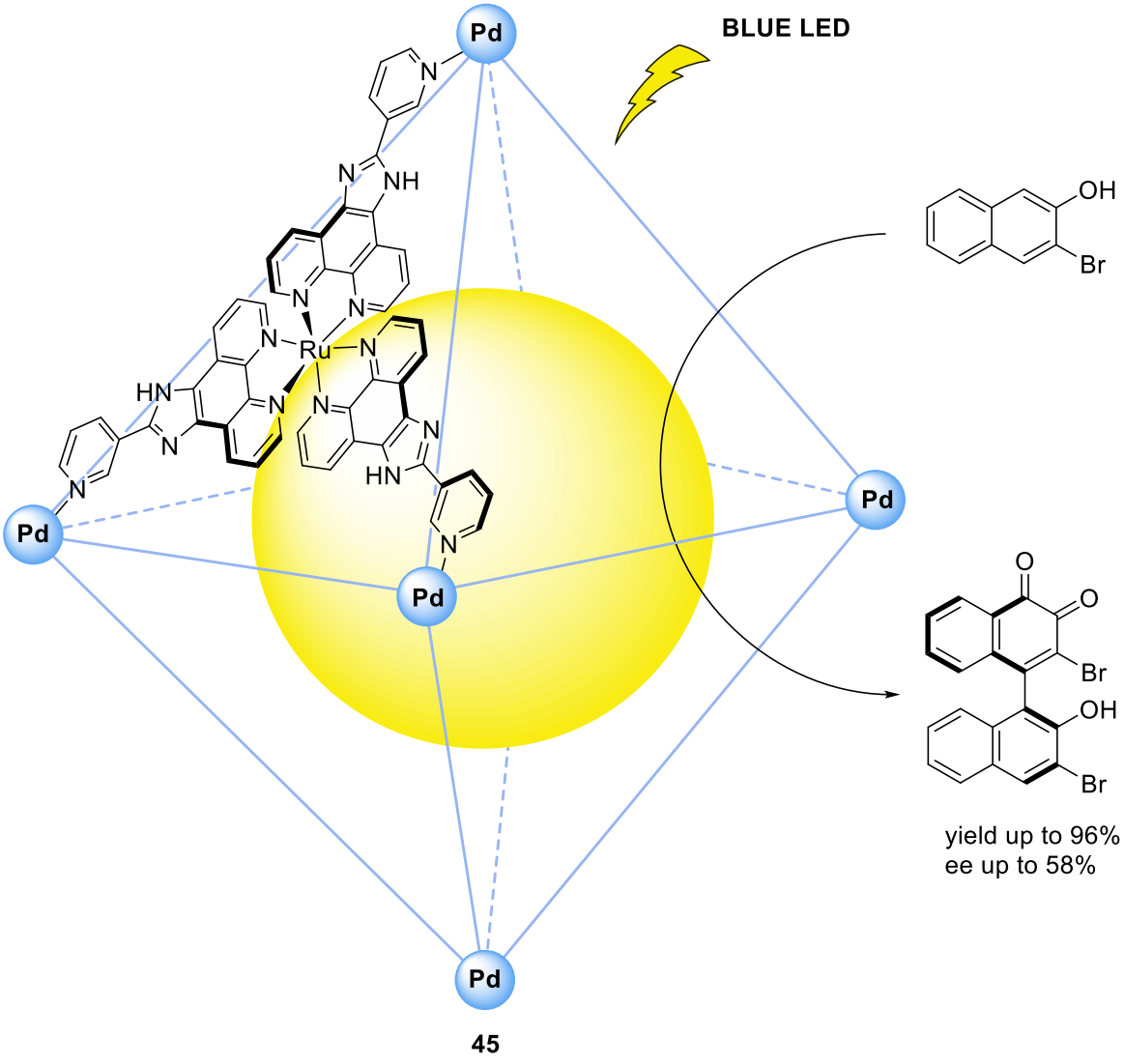

Figure 22. Schematic representation of the photoinduced biaryl coupling performed in the octahedral cage **45** that incorporates the monophosphoramidite-Rh(I) catalyst. Adapted from ref. 51.

I4. Sensing and recognition

Inspired by Nature, in which molecular recognition is the crucial process that allows all the biological functions, over the last decades, chemists have dedicated many efforts in order to develop artificial chiral supramolecules able to mimic natural systems.[52] In particular, the attention has been driven to the preparation of confined chiral environments in which one component of a racemic mixture could be preferentially bound through steric and electronic interactions. Among chemosensors, supramolecular cages have become an important class of molecules for the selective detection of wide variety of chemical and biological analytes.[53] Complexation of chiral or achiral guests within a chiral cage through noncovalent interaction led to the formation of a chiral host-guest complex that could be discriminated using chiroptical techniques (Circular Dichroism, Vibrational Circular Dichroism, Circular Polarized Luminescence), NMR, and Gas Chromatography. In this part of the introduction, an overview of supramolecular architectures employed in combination with analytical techniques for the molecular recognition and sensing of analytes will be presented.

I4.1. Circular Dichroism

Chiroptical supramolecular sensors are an emerging class of molecules for the selective detection of chemical and biologically analytes. In this context, circular dichroism is one of the most employed methods because it allows fast, reliable, and cheap analyses. The main disadvantage of this technique is the limited application to those molecules that does not possess any chromophore unit. To overcome this issue, the interaction of the analyte with a supramolecular sensor can be translated to a chiroptical output. [54]

Zonta *et al.* reported a chiral supramolecular cage that displayed an inversion of the CD signal upon the addition of different achiral dicarboxylic guests.[55] The supramolecular architecture **46** was built up exploiting imine condensation between two **TPMA**-based zinc complexes held together by (*R*,*R*)-1,2-diphenylethylenediamine linkers. An interestingly capability of the chiral host was found when dicarboxylate anions from succinic (**C_4**) to suberic acid (**C_8**) were encapsulated inside the structure (Figure 23). Using circular dichroism, it was possible to understand that the guest length acted as allosteric effector for the cage conformation. This effect was ascribed to the dia-stereodynamic nature of the cage which was determined by the two **TPMA** stereodynamic units and the six stereogenic carbon atoms of the three diamine linkers. Theoretical studies demonstrated that the guest length was able to induce the system to move toward opposite configurations, changing the

handedness of the helix of the two **TPMA** units together with a variation of the relative orientation of the diamine phenyl rings.

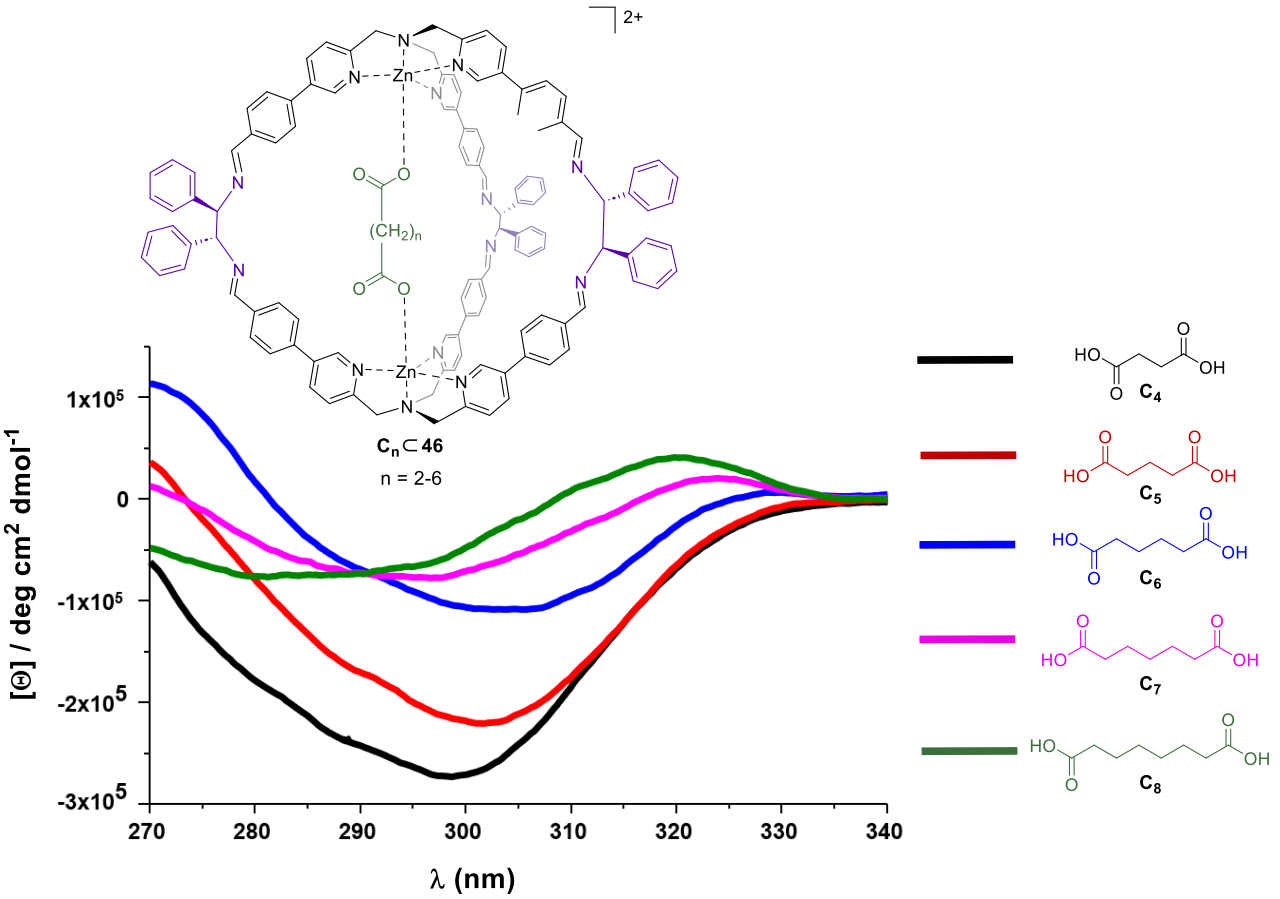

Figure 23. CD signal response of the chiral supramolecular cage **C_n⊂46**upon encapsulation of dicarboxylic acids with different chain lengths. Adapted from ref. 55.

Another example in which a chiral cage acted as chiroptical sensor for an achiral guest was reported by Amendola and coworkers that developed an asymmetric architecture **47** able to recognize and detect perrhenate (ReO_4^-) using circular dichroism in aqueous media (Figure 24).[56] Due to the similar features, ReO_4^- is usually used as surrogate of the hazardous pollutant TcO_4^- for binding studies, thus the development of sensors for this species have received considerable attention. The covalent chiral cage was synthetized in high yield usings reductive amination after the self-assembly of **TREN** precursors and enantiopure **BINOL**-based ligands. Upon addition, the binding of ReO_4^- was translated in a significant variation in the chiroptical output of the host. More in detail a blue shift accompanied by an increase of the signal intensity at both 222 and 235 nm was observed. This remarkable alteration was ascribed to the variation of the dihedral angle between the naphtyl planes of the binaphthyl chromophore units when the anionic guest is encapsulated inside the cavity

of the capsule. Interestingly, the chiroptical probe was effective also in the presence of complex matrixes like fruit juices.

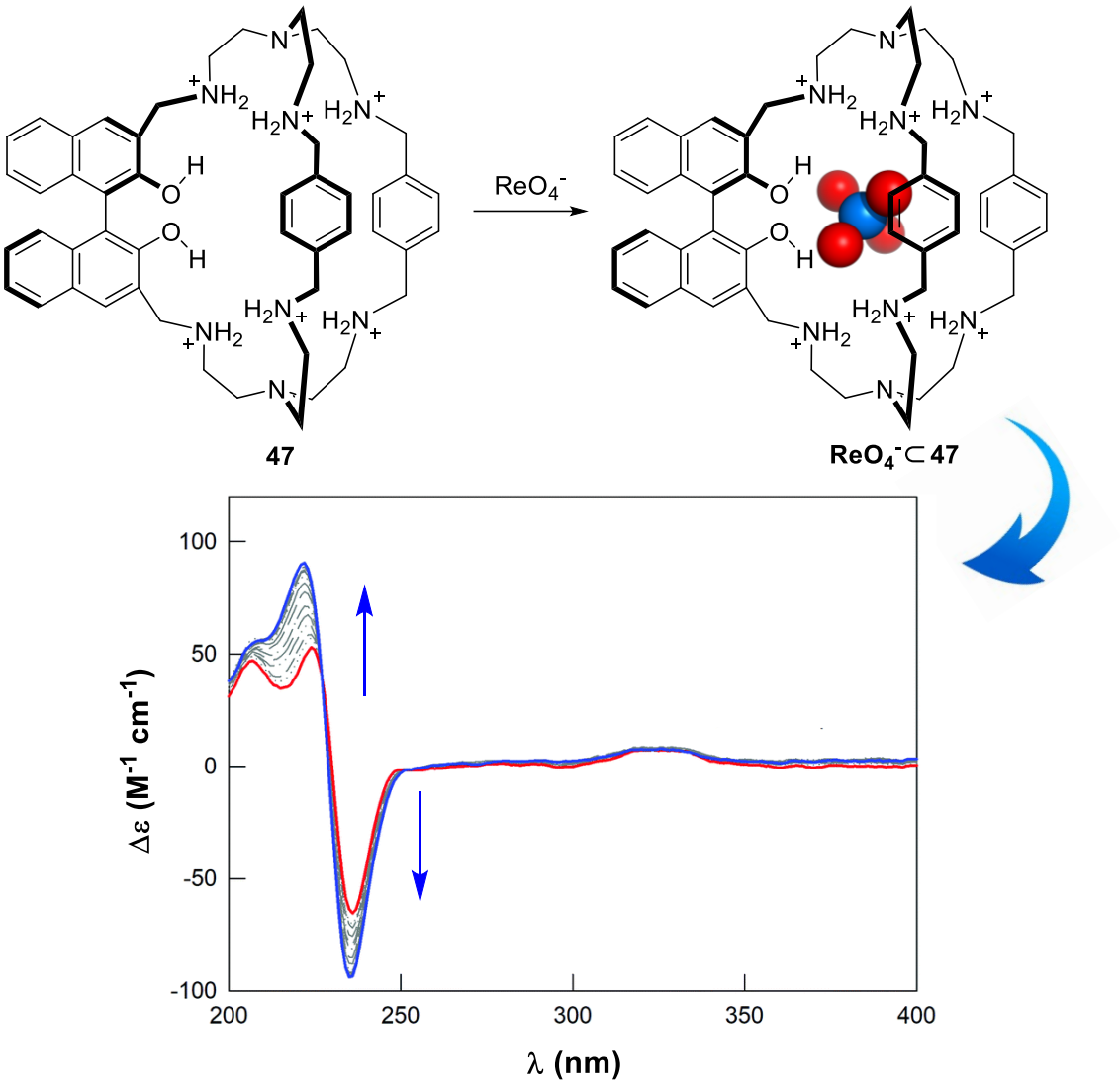

Figure 24. CD titration of cage **47** (0.1 mM in 0.05 M CF_3SO_3Na, pH 2) with $NaReO_4$ (red and blue lines: initial and final spectra, respectively). Adapted from ref. 56.

The Li group reported an homochiral octahedral cage able to recognize and detect enantiomeric guest in water using circular dichroism.[57] The anionic capsule was obtained by self-assembly of Ga^{3+} ions and hydrazone-based ligands, leading to the formation of an enantiomeric pair of homochiral octahedral cages **48** (Figure 25). Taking advantage of the hydrophobic cavity and the anionic nature of the capsule, recognition of a wide variety of chiral/achiral neutral and cationic guests was carried out in aqueous media. Due to the presence of both enantiomers of the cage, addition of the chiral analyte led to the formation of two diastereoisomers. The thermodynamic difference between these two species induced a shift in the equilibrium toward the most stable one as confirmed by both NMR and CD

spectra recorded during time. Moreover, due to the linear response of the induced CD signal, cage **48** was employed for the quantitative determination of the enantiomeric excess of different non racemic guests.

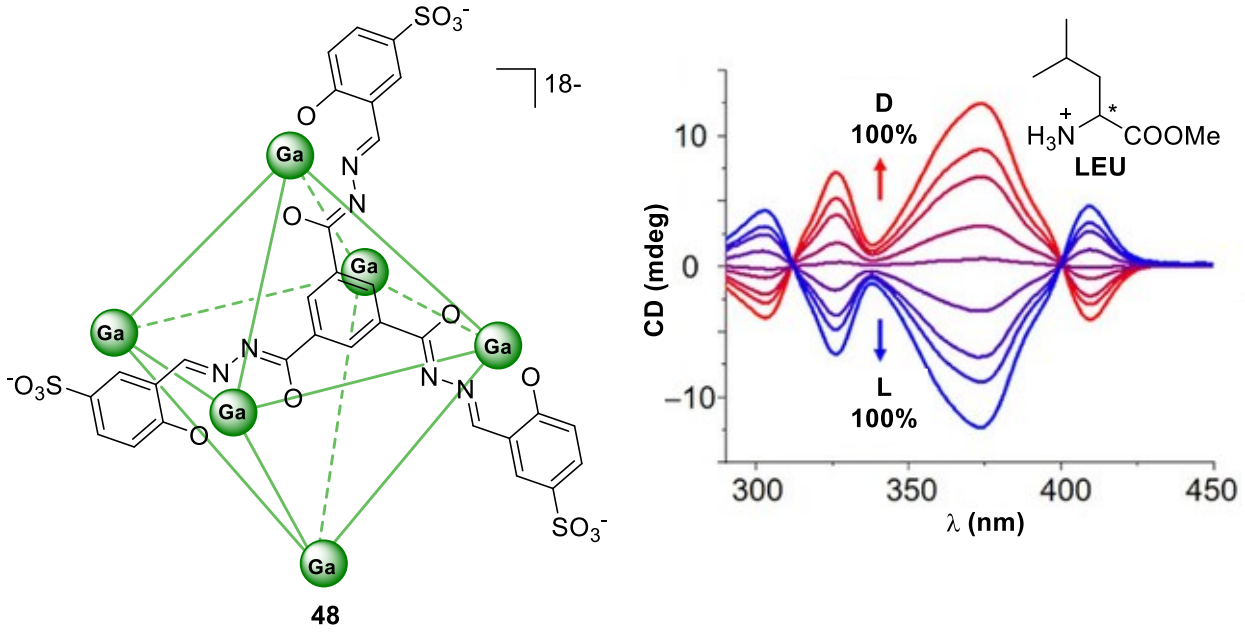

Figure 25. CD spectra of cage **48** (0.06 mM,H_2O, pH 7) in the presence of the ammonium salt of leucine methyl ester (**LEU**) (6 mM) with various *e.e.* values. Adapted from ref. 57.

Wu *et al.* reported a stereodyanamic helicate cage **50** that could act as chiroptical sensor for choline derivative sensing.[58] Choline and its derivatives, like acetylcholine, carnitine, and acetylcholine are extensively involved in human life since they are synthetic precursors of cell component, signaling molecules or have important pharmacological and nutritional functions. Since these analytes are CD silent, a supramolecular approach was developed to obtain a chiroptical induction through host-guest complexation. The helicate-based cage was built up using achiral amide-based ligand **49** through coordination of two PO_4^{3-} anions. The self-assembly led to a racemic mixture of stereodynamic triple stranded helicates **50**, in which both *M* and *P* conformers were in rapid equilibrium (Figure 26). The binding properties and the subsequent CD inductions were tested using seven chiral choline derivatives. Upon encapsulation of the chiral guest **51**, the equilibrium between the helicate conformers was shifted toward the preferential diastereoisomer, leading to the formation of an induced dichroic signal. This chiroptical signal could be correlated with the enantiomeric excess of the asymmetric guest, since a linear response was obtained varying the enantiopurity of the analyte.

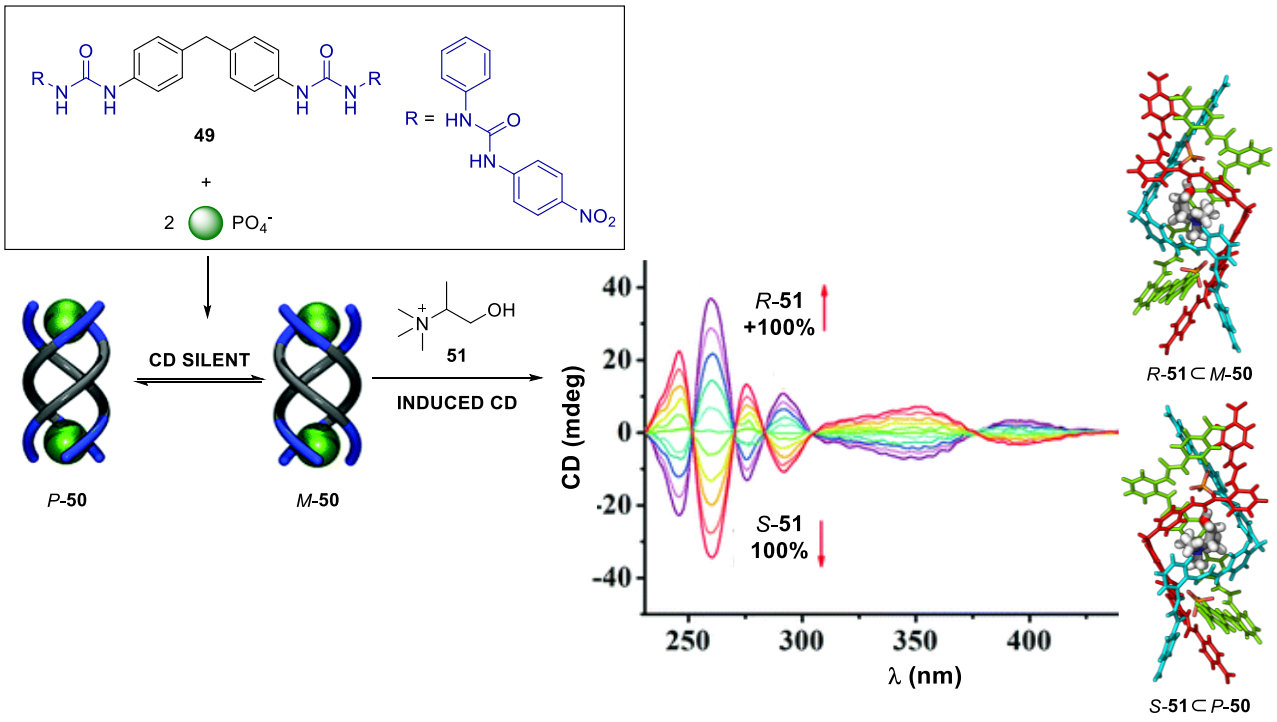

Figure 26. Synthesis of the stereodynamic helicate **50** and induced CD upon addition of guest **51** with various *e.e.* values. Adapted from ref. 58.

In this scenario, the biological importance of saccharides, in particular glucose, has resulted in an increasing interest in the development of molecular receptors able to recognize these analytes. Nevertheless, binding of carbohydrates in water is challenging due to the hydrophilic nature of these compounds. Davis and coworkers developed an achiral cage-like receptor **52** with outstanding selectivity for glucose, able to translate the binding event in a chiroptical signal.[59] Cage **52** was composed by two triethylmesitylene units held together by bis-ureidobenzenecarboxamido scaffolds functionalized with nonacarboxylate moieties in order to maintain the water solubility (Figure 27). Circular dichroism was found to be an efficient technique in order to study glucose sensing in biological matrices, due to the absence of chromophores in the scaffold of the chiral analyte, thus the influence on the receptor could be easily monitored. More in detail, addition of D-glucose **D-Glu** to a solution of receptor **52** produced a strong CD signal to the twist of the chromophore units of the cage. The high selectivity for glucose, that was achieved exploiting the specific interactions that this molecule was able to establish inside the void cavity of the host, implied that the presence of other interferent (for example L-glucose) could be negligible. This chiroptical probe was thus applied for the determination of the D-glucose content in human serum, that closely match standard biochemical procedures.

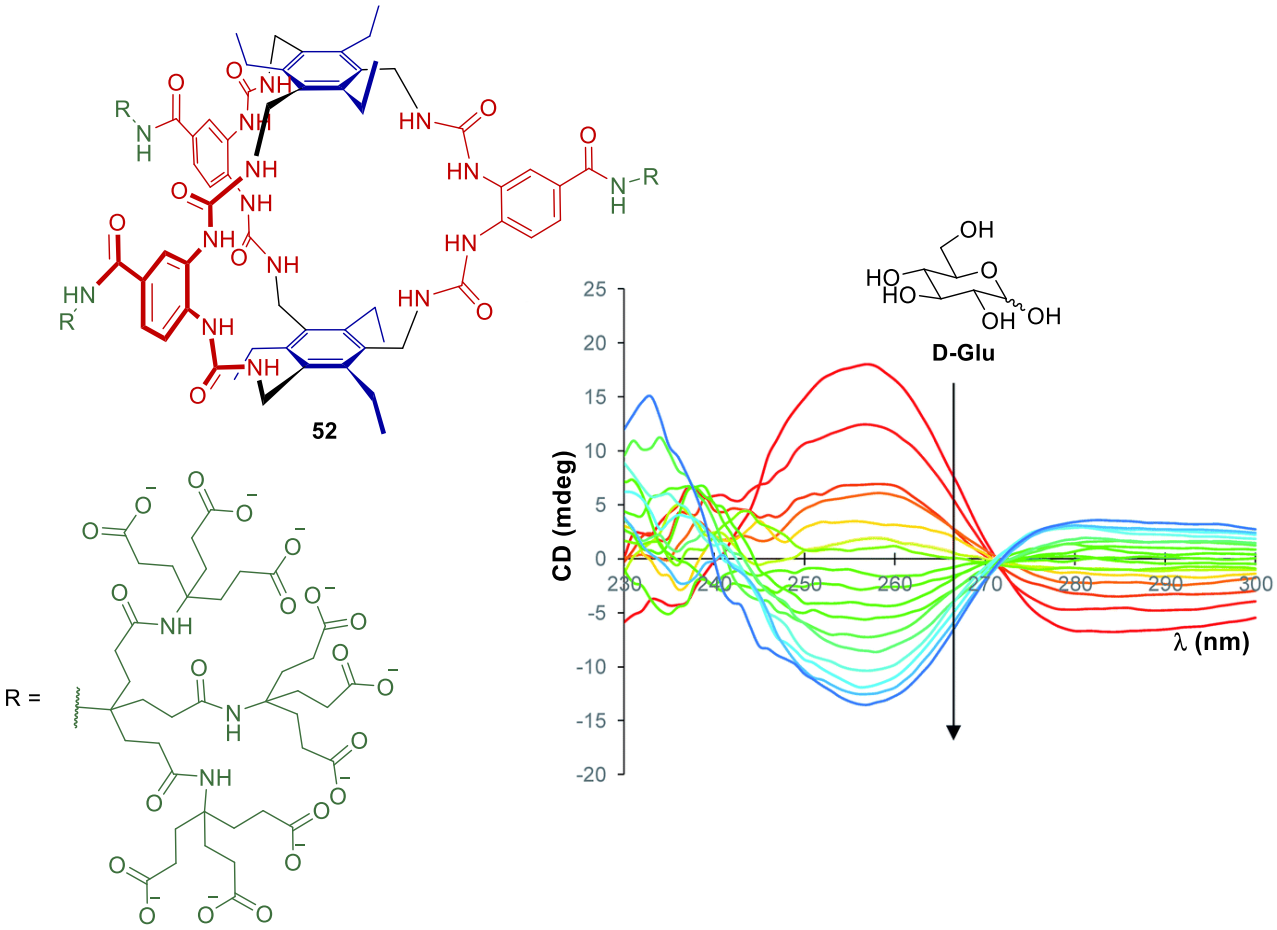

Figure 27. CD spectra from the titration of D-glucose into filtered, diluted, glucose-free human serum, in the presence of L-glucose (2 mM) and cage **52** (0.25 mM). Adapted from ref. 59.

I4.2. NMR

NMR spectroscopy is another useful technique for chiral discrimination that allow the unambiguous identification of the species in solution. However, to distinguish enantiomer through NMR, the interaction with a chiral molecule is necessary in order to obtain diastereomeric species that present distinct chemical shift.[60] In this field, the application of chiral supramolecular cages has allowed to obtain novel chiral solvating agents (CSA) able to discriminate enantiomers upon encapsulation through non covalent interactions, thus avoiding derivatization processes. Moreover, the protected environment created by the void cavity could allow the binding of apolar guests also in water media.

Enantiopure cryptophanes have been extensively employed in combination with NMR for chiral recognition of enantiomeric species. These supramolecular capsules have received increasing attention due to their capability to encapsulate atoms (xenon, alkali cations, anions) or small molecules (methane, halogenomethanes). Starting from the pioneering work of Collet and coworkers on chiral cryptophanes able to bind enantioriched CHFClBr,[61]

different works have reported on the capability of the structure to distinguish enantiomers by ^{1}H-NMR spectroscopy.

Buffeteau *et al*. reported the synthesis and the resolution of an enantiopure water-soluble cryptophane **53** composed off two hydroxy functionalized cyclotriveratrylene bowls connected by three ethoxy linkers.[62] Both enantiomers of propylene oxide **54** were then chosen as guests in order to test the capability of **54** to act as chiral solvating agent in aqueous solution (Figure 28). Interestingly, the formation of the two diastereomeric species after encapsulation of *R*-**54** and *S*-**54** inside the enantiopure host allowed the clear enantio-discrimination of the two species due to the strong shielding effect induced by the benzene walls of the capsule.

In a subsequent work the same authors employed the same capsule for the recognition of other oxirane derivatives in water obtaining efficient separation of the diastereotopic protons.[63]

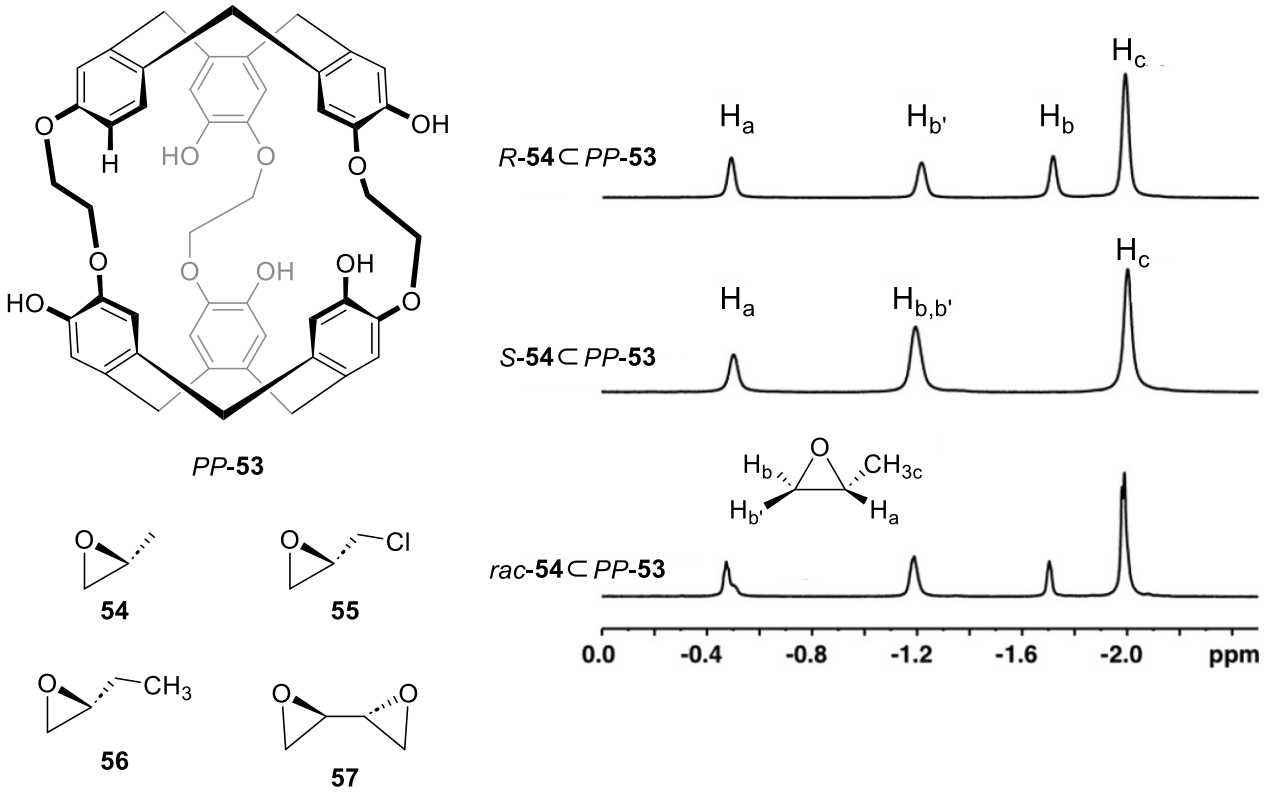

Figure 28. Structures of cryptophane *PP*-**53** and the chiral oxiranes used in the study (only a single stereoisomer is shown for each compound) and, partial ^{1}H-NMR spectra of *PP*-**53** in the presence of *R*-**54**, *S*-**54**, and *rac*-**54** in NaOD/D_2O solution. Adapted from ref. 62.

Hemi-cryptophane are another class of cage-like structures that have been largely exploited in sensing. In particular, these architectures have recently demonstrated the capability to encapsulate carbohydrates. One of the major problems in sugar recognition is that carbohydrate stereoisomers often differ from each other by the configuration of a single stereocenter, thus making their discrimination very difficult.[64] In this scenario, capsules played a crucial role since they can maximize the interactions of the analyte inside the void cavity, thus allowing a better selectivity. Martinez *et al*. reported a chiral hemi-cryptophane **58** that presented both polar and apolar domains and displayed notable enantioselectivities toward a wide range of sugar molecules that were studied using NMR.[65] Interestingly, switching the chirality of the host allowed a changing in the substrate selectivity. In particular, the *M*-**58** enantiomer was **Oct-*β*-glucose** selective while the *P*-**58** enantiomer displayed a **Oct-*β*-mannose** discrimination (Figure 29). This changing in the substrate discrimination could be attributed to different interaction of the substrates with inner asymmetric cavity of the host.

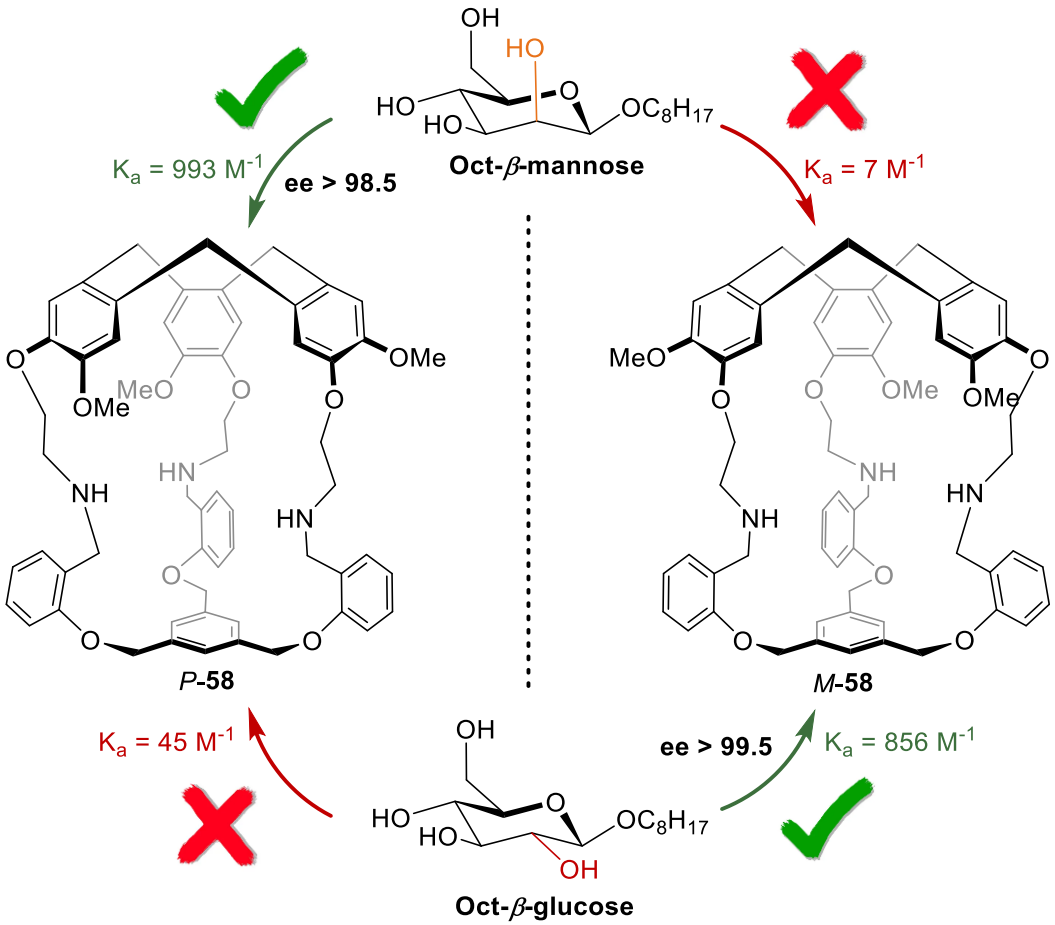

Figure 29. Schematic representation of the selectivity of both enantiomers of receptors **58** toward the sugar guests **Oct-*β*-glucose** and **Oct-*β*-mannose**. Adapted from ref. 65.

Raymond *et al*. developed a chiral self-assembled host able to recognize chiral natural products in a diastereoselctive fashion.[66] More in detail, the homochiral M_4L_6 cage **36** was synthetized as a racemic mixture from the coordination driven assembly of 1,5-biscatecholamide naphthalene and Gallium (III) ions (Figure 30). Even though cage **36** was mainly soluble in polar solvents like water, the inner cavity allowed to create a protected hydrophobic confined space. This property was exploited in a first instance for the encapsulation of aromatic guests in water media. The racemic cage was thus tested for chiral recognition of natural products. In the case of limonene, camphor, and fenchone a modest diastereoselectivity, up to 54% de, was observed. However, it was possible to highlight how small changes in the structure (size and shape) of the analytes had a huge impact on the diastereoselectivity.

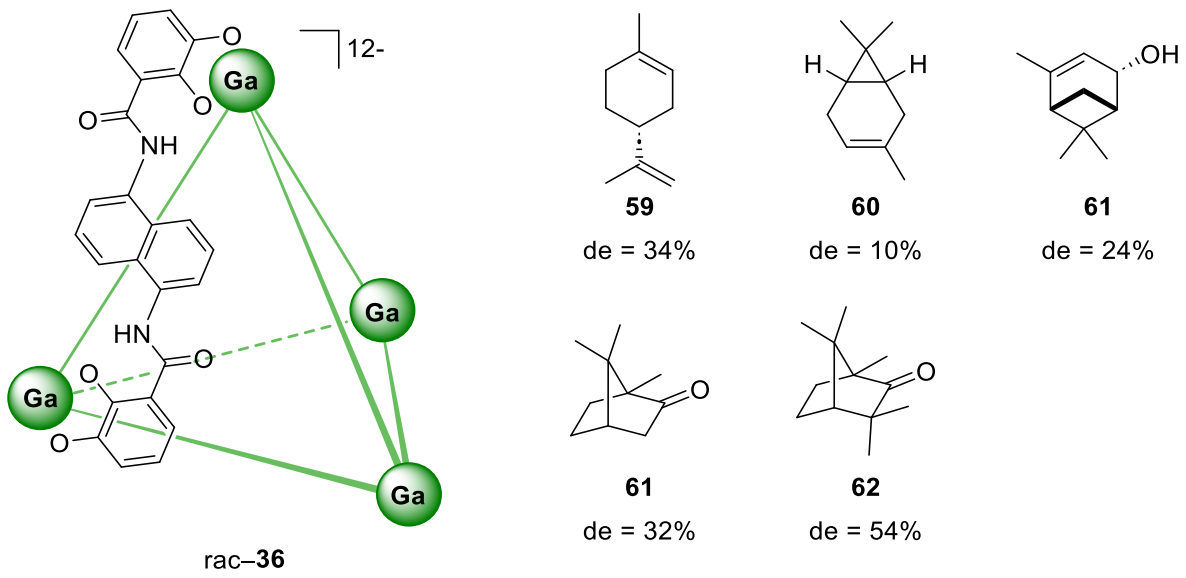

Figure 30. Scope of chiral guests recognition encapsulated in cage *rac*-**36**. Adapted from ref. 66.

I4.3. Gas Chromatography

Porous Organic Cages (POCs) have attracted the attention also for their applicability in material science. Unlike extend networks, porous organic materials, that are formed by discrete molecules held together through non-covalent interactions, have been extensively employed due to their high solubility in organic solvents.[67] This property could allow post-functionalization processes in order to adjust and modulate the final material.[68]

Due to the pore size, chiral POCs have become suitable alternative to the more common cyclodextrins, showing promising commercial applicability, as stationary phases for chiral separation in gas chromatography.[69,70]

Cooper *et al*. reported the use of imine-based cage **7** that could be coated inside a standard capillary column for chiral GC separation.[71] The homochiral tetrahedral cage was synthetized through imine-condensation between 1,3,5-triformylbenzene and *RR*-**CHDA** and showed an high level of permanent microporosity. Cage **7** was then coated to a capillary column and employed for the separation of racemic mixtures, demonstrating high selectivity for linear 2-hydroxy alkanes.

The same structure was also employed by the group of Yuang in a wider analyte scope.[72] More in detail, enantiopure cage **7** was diluted with a polysiloxane (OV-170) to obtain a chiral stationary phase for high-resolution GC. Excellent enantioselectivities were obtained for chiral alcohols, amines, diols, esters, ketones, ethers, alcohol amines and sulfoxides. In this work the authors showed that the cage-coated column displayed better recognition performances compared to other commercially available columns (Figure 31).

The work was subsequently extended by the same group that reported a column coated with a novel chiral cage built up exploiting imine condensation between 1,3,5-triformylbenzene and (*R*,*R*)-1,2-diphenylethylendiamine.[73] The novel stationary phase showed complementary recognition properties to the previously reported one, allowing the separation of alcohols, esters, ethers and epoxides.

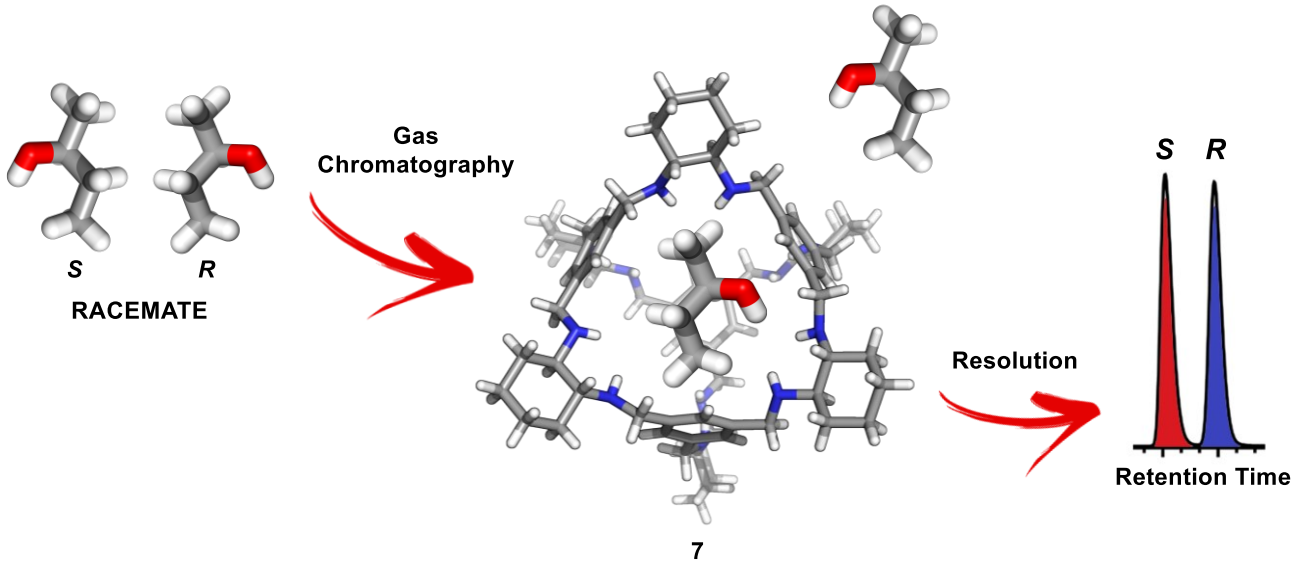

Figure 31. Schematic representation of the chromatoghraphic separation of chiral 2-butanol employing cage **7** as GC stationary phase. Adapted from ref. 72.

I5. Chiral amplification

Introduction of chirality in supramolecular cages can allow the preparation of responsive materials that could be employed in advanced applications like chiral optical devices, chiral functional materials, sensing and catalysis.[74]

Also in this case, the key feature to obtain these novel properties is the interaction, between the host and the guest. Upon binding, a reorganization of the chromophore units of the supramolecular architecture or the guest could occurred, and this is translated in a measurable chiroptical output. In this case, confinement of the molecule is not focused on sensing applications, but it is mainly directed toward obtaining novel optical properties that rise upon the formation of the host-guest complex. In this sense, Circular Dichroism and Circularly Polarized Luminesce have played a crucial role, since they enable to gain information about the stereochemistry or the change in conformation in both ground or exited state.[75]

In this scenario, Clever group reported a Pd_2L_4 coordination cage **64**, based on chiral helicene ligand, able to translate the changing in length of the guest in a chiroptical output.[76] The homochiral structure was obtained through the self assembly of an enantiopure helicene-based unit functionalized with pyridine groups that could coordinate to the Pd (II) ions, leading to the formation of the closed structure (Figure 32). Combining the flexibility of the cage upon encapsulation of anionic molecules with the strong CD signal displayed by the structure in solution, the authors investigated the potential use of the supramolecule as indicator for the guest size discrimination using circular dichroism. More in detail, encapsulation of shorter guests (**67** and **68**) resulted in an inversion of the CD band at 360 nm, compared to the one of the free host. On the contrary, the employment of longer molecules (**65** and **66**) led to an increase in intensity of the same band. This behavior was attributed to a tightness or expansion of the cage upon complexation, that was accompanied by a different helical pitch of the helicene units and thus to a different chiroptical output. This assumption was also confirmed by ion mobility mass spectrometry that revealed different gas-phase collisional cross-section for the systems.

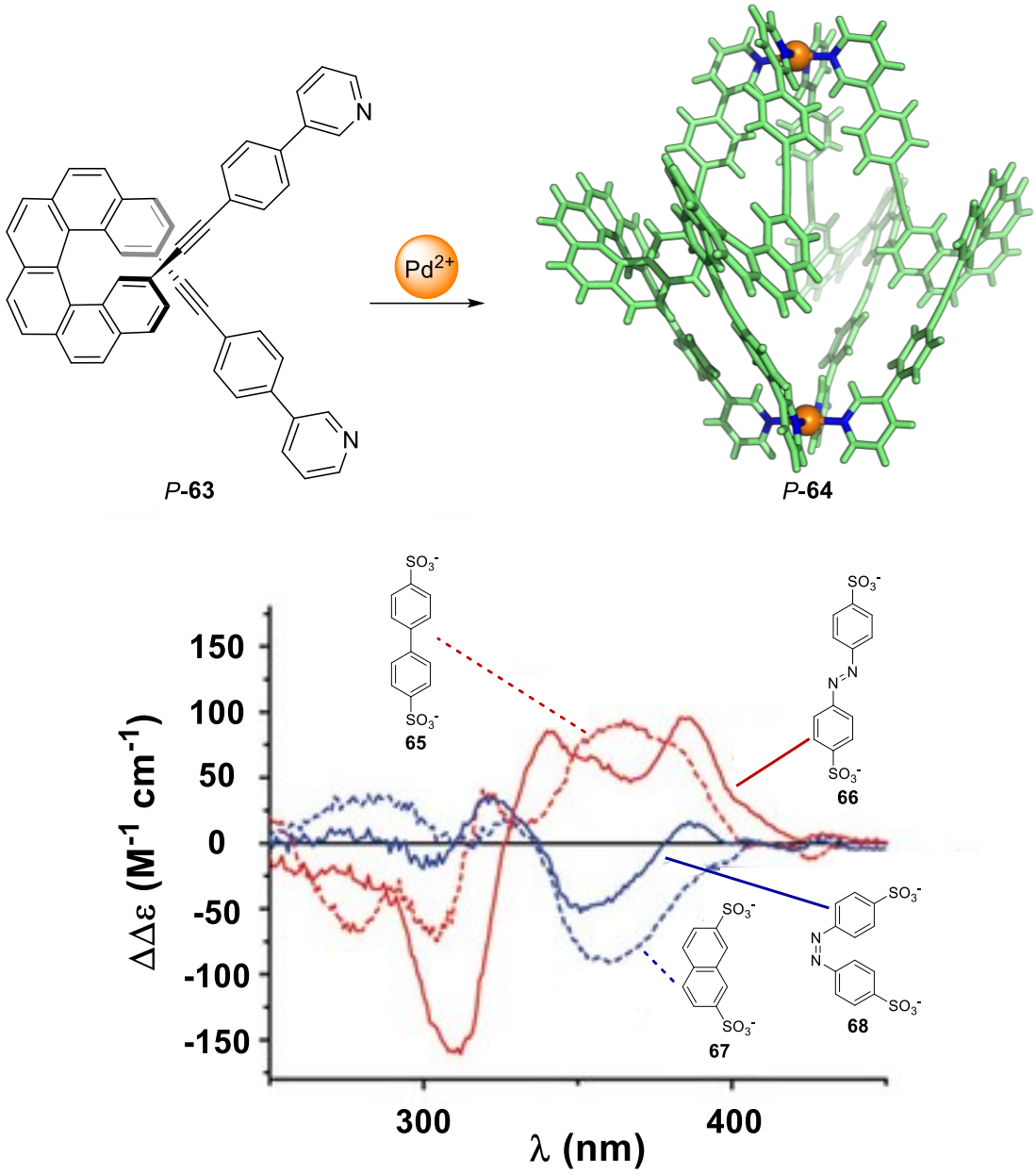

Figure 32. Synthesis of the enantiopure helicene-based cage **64** and difference CD spectra (free host CD spectra subtracted from the host–guest CD spectra) of the capsule upon encapsulation of different guests. Adapted from ref. 76.

Combining luminophore and chiral ligands, the same group developed an efficient way to obtain the exclusive formation of heteroleptic cages **71** with peculiar chiroptical properties derived from the cooperative effects between all the subcomponents.[77] In detail, the group synthetized Pd (II) cages combining enantiopure helicene-based ligands **69** and achiral banana-shaped bis-pyridyl ligand **70** having a fluorenone scaffold with emissive properties (Figure 33). The resulting cages, obtained through a shape-complementarity assembly (SCA) that allowed the non-statistical and precise arrangement of the ligands, had an inner void cavity able to encapsulate aliphatic bis-sulfonate guests. Interestingly, it was also

observed that even though the emissive properties of ligand *M/P* were completely quenched upon coordination to the palladium cation, the emission of the fluorenone-based skeleton was retained. Furthermore, as shown by CD spectra, the chiral information contained in the ligand *M/P*-**69** was transferred to the whole supramolecular architecture, resulting in a twist of the ligands around the metal ions. More interestingly, the synergistic effect between the imparted chirality, combined with the emissive properties of the non-chiral fluorenone ligand, allowed the rise of a CPL signal. Moreover, addition and encapsulation of an achiral bis-sulfonate guest **72** provided a changing in CPL output, leading to a bathochromic shifting and an amplification of the signal (4 fold increase of $|g_{lum}|$). This effect, as proved by both ion mobility mass spectrometry and DFT, was due to a contraction of the cage that resulted in a lower Pd-Pd distance. This example thus showed that only the combination of three elements, imparted chirality from ligand **69**, emissive properties from ligand **70**, and Pd cations to create the void cavity, could contribute to achieve novel properties that could not otherwise be obtained with the single components.

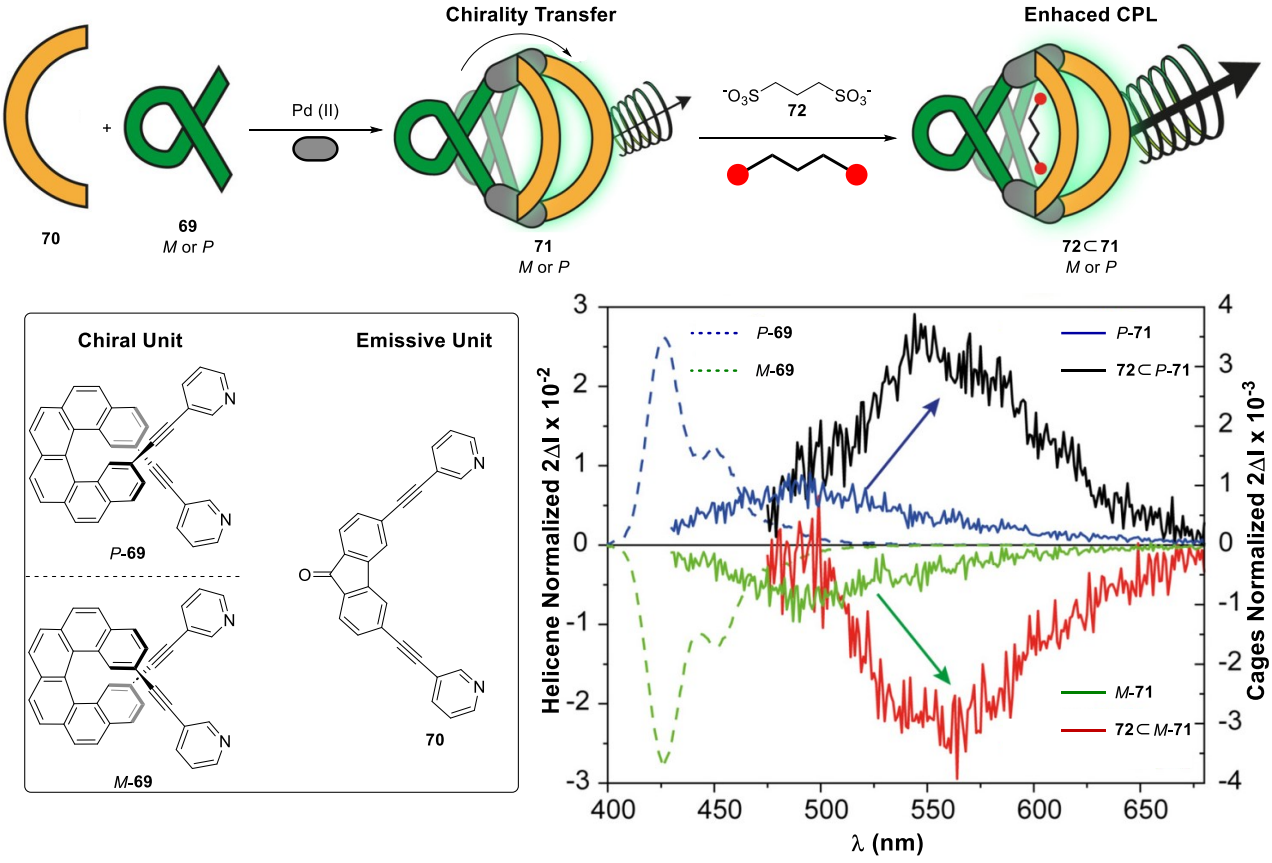

Figure 33. Schematic representation for the synthesis of the heteroleptic cage **71** and encapsulation of guest **72**. CPL spectra of ligands *M*/*P* **69**, heteroleptic cages *M*/*P*-**71**, and host–guest complexes **72**⊂*M*/*P*-**71**. Adapted from ref. 77.

Liu *et al*. reported the development of a chiral hexahedral cage **74** able to encapsulate achiral Dyes obtaining novel chiroptical properties resulting from confinement.[78] More in detail, the chiral architecture was prepared from the self-assembly of enantiopure pyridine-biphenyl- based ligands decorated with 18-crown-6 groups *R*/*S*-**73** and Pd (II) cations leading to the formation of a Pd_6L_{12} structure (Figure 34). Addition of potassium sulfonate boron-dipyrromethene (BODIPY) dyes (**75** or **76**) resulted in the complete encapsulation of the guest inside the cavity of the host. In particular, 1:2 stoichiometry was obtained with guest **75**, while 1:1 was achieved with the bigger guest **76**, as shown by both UV and NMR titration experiments. Interestingly, a novel band around 507 nm appeared in CD spectrum upon encapsulation of the guests inside the cage host, thus indicating that chirality of the cage was transferred to the achiral dyes. Moreover, the formation of the host-guest complex was accompanied to the rise of a broad CPL band around 550 nm, that was not observed with both the free cage and guests (due to the aggregation-caused quenching of the dyes), with $|g_{lum}|$ values around 10^{-3} -10^{-4}, that were increased by one order of magnitude in crystalline state. The obtained results highlighted that only encapsulation of the BODIPY into the hollow host, allowed to avoid the aggregation of the dye and induce a chirality in both ground and excited state.

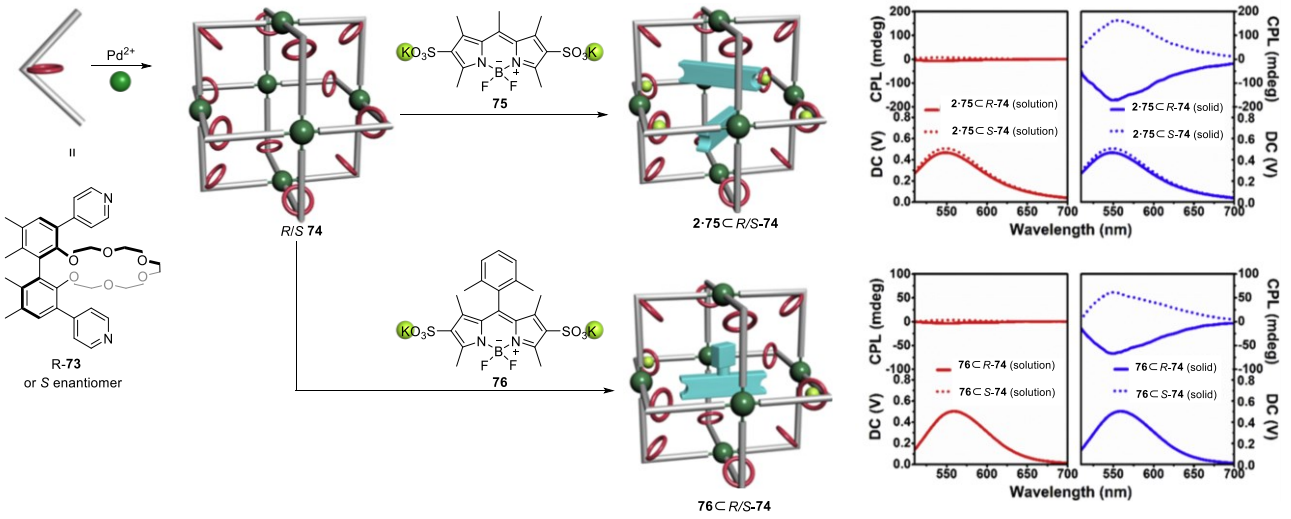

Figure 34. Schematic representation for the synthesis of cage **74** and encapsulation of guests **75** and **76**. CPL spectra of ligands *M*/*P* **69**, heteroleptic cages *M*/*P*-**74**, and host–guest complexes **75**⊂*M*/*P*-**74** and **76**⊂*M*/*P*-**74**. Adapted from ref. 78.

I6. Chirality Induction

The communication of the chiral information can be efficiently transmitted in both the host or the guest. In contrast to the previous paragraph in which the chirality induction was the means to obtain an enhancement or a tuning of the chiroptical output, here the transfer of chirality is a key feature in order to form chiral structures or to control the chirality of the guests.

As example, Yan *et al.* reported chiral lanthanide-based tetrahedral cages **79** that displayed chiral memory and CPL properties after the removal of the chiral auxiliary.[79] More in detail, the authors developed a strategy to obtain enantiopure Europium tetrahedral cages from the self-assembly of achiral components and the use of *S*-**BINAPO** as ancillary ligand (Figure 35). The employment of the steric hindered auxiliary allowed the successfully transfer of chirality to the overall structure **78** that presented only one helical configuration around the metal ion, as confirmed by both CD and X-Ray structures. Moreover, due to the emission properties of the Europium ions, a strong CPL signal was observed, accompanied with an outstanding luminescence quantum yield ($\Phi_{overall}$ = 81 %), which was un unprecedent value obtained for a lanthanide-based complex. More remarkably, the complete substitution of the chiral ancillary ligand with the achiral analogue bis[2-(diphenylphosphino)phenyl] ether oxide (**DPEPO**) resulted in the preservation of the chirality of the original cage after the exchange process, as confirmed by the excitation coupling signs in the CD spectrum that were retained. In addition, CPL signals were observed, and a final luminescence quantum yield equal to 68% was measured.

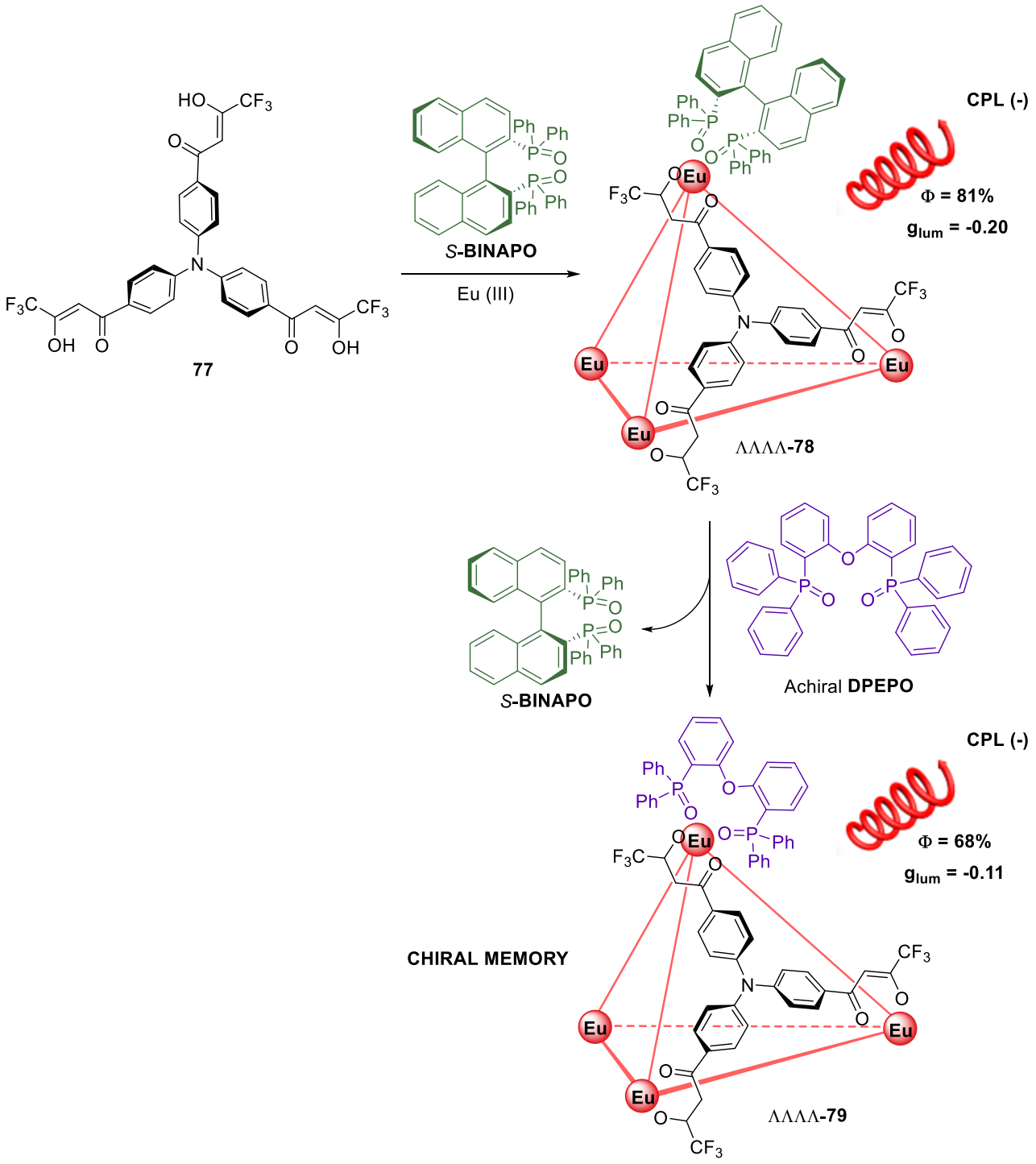

Figure 35. Schematic representation of the synthesis of cage **78** and subsequent substitution of *S*-**BINAPO** with **DPEPO** as ancillary ligand, leading to the formation of cage **79** with retention of the initial chirality. Adapted from ref. 79.

An example of chirality induction triggered by encapsulation of a chiral guest and irradiation with light was reported by Clever and coworkers that synthetized a Pd-based cage **81** that presented dithienylethene (DTE) units **80** in the ligand scaffold (Figure 36).[80] These photochromic components present the advantage to be intrinsic chiral since they display an helical arrangement of the chromophores and, upon irradiation, they can be reversibly

interconvert between the open and the close isomeric form. In absence of a chiral element, the DTE unit is present in a racemic mixture of *M* and *P* helix, and thus, after photoisomerization, both enantiomers of the close isomer are produced. However, it has been observed that if the closure of the DTE moiety is performed in a chiral environment, a chirality induction can be achieved. For this reason, the authors envisaged to perform the stereoselective closure of the DTE units of the cage in the presence of a chiral guest encapsulated in the inner cavity of the structure. Addition of enantiopure camphor sulfonate **82** to a solution of the cage in which the DTE moieties were in the open form, revealed a chirality transfer from the guest to the host, inducing a preferential helix conformation in the chromophore units. After irradiation with a 313 nm light, close-form of the cage **83** was obtained. The resulting structure presented a Cotton effect in the CD spectrum, thus indicating that an enantioenriched architecture (up to 25% of enantiomeric excess) was obtained due to the chiral induction of the guest. Interestingly, the closure of the structure was also accompanied with the ejection of the guest from the cage cavity.

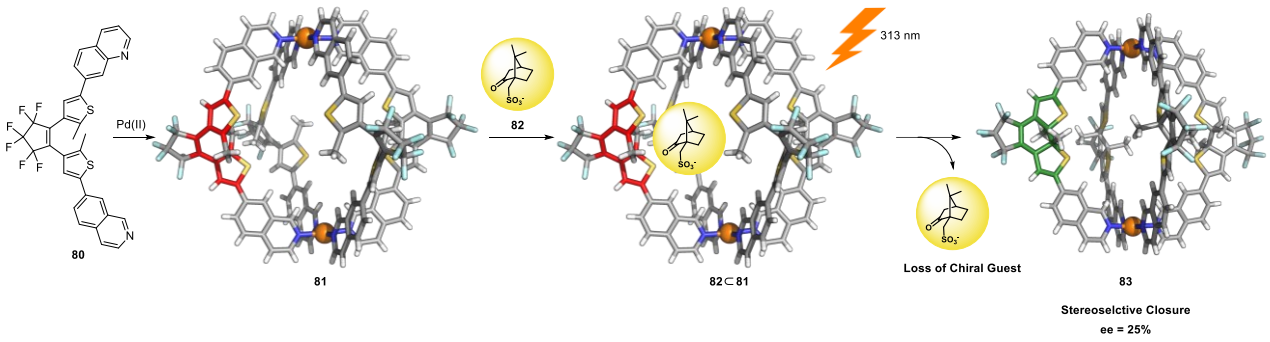

Figure 36. Schematic representation of the synthesis of cage **81** and subsequent encapsulation of guest **82**. Upon irradiation the stereoselective closure of the architecture is obtained (ee = 25%) with release of the guest. Adapted from ref. 80.

In the previous examples the chiral information was transferred from the chiral guest to the host. Nevertheless, the chirality transfer could also occur in the opposite sense, as shown by Zonta *et al.*[81] The group demonstrated that encapsulation of a perfluorinated dicarboxylic acid inside chiral cage **35** induced a preferential helical twist of the alkyl chain of the guest. The helical nature of perfluorinated alkanes is due to specific hyperconjugative interactions between the σ_{CC} and σ^*_{CF} orbitals and this results in the formation of two enantiomers with opposite helicity. More in detail, the host-guest complex was built up through a templated synthesis by mixing a modified **TPMA**-based zinc complex, *RR*-**CHDA**, and octafluoro adipic acid.**C$_6$F** (Figure 37). After the formation of system **C$_6$F⊂35**, VCD spectroscopy combined with DFT calculation were employed to investigate the chirality induction. From theoretical

studies, it was found that the *PP-P* isomer was the most stable conformation. The good agreement between the experimental and calculated VCD spectra highlighted that the most stable conformation found computationally was actually the preferential one present in solution, confirming that the chiral cage was able to impart a defined helicity sense to the achiral guest.

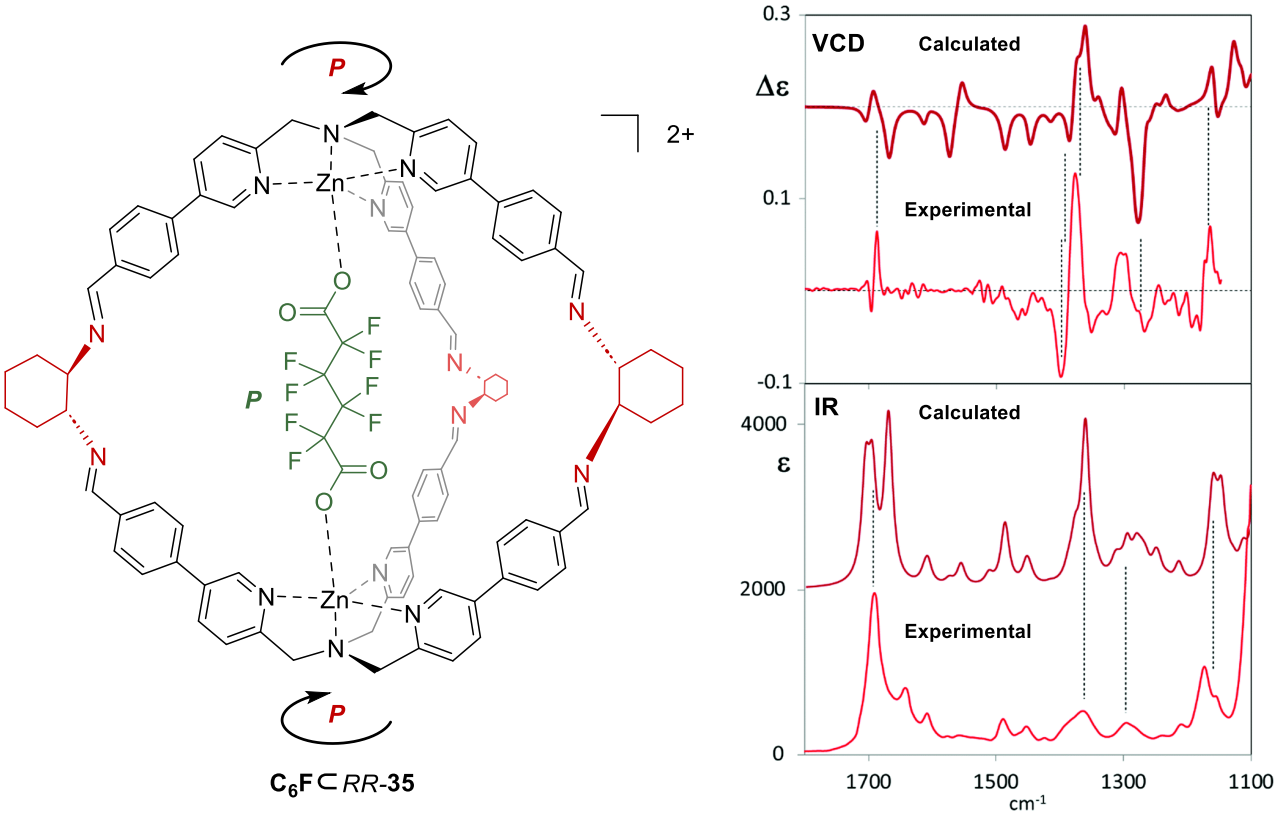

Figure 37. Most stable isomer *PP-P* of cage **C_6F⊂*RR*-35.** Comparison of experimental VCD spectra and IR absorption spectra of with calculated (upper traces) VCD and IR spectra of **C_6F⊂*RR*-35** with the two head groups in *P*,*P* configuration and with the *P* configuration of the fluorinated chain. Adapted from ref. 81.

I7. TPMA based molecular cages

Within the field of supramolecular cages, the research group in which this thesis has been carried out has reported the use of tris(2-pyridyl)methylamine **TPMA** as building block to obtain a metal-organic architectures with an internal cavity able to accommodate guests. While in the previous sections only chiral systems have been reported, in this paragraph an overall overview of recent works regarding the synthesis and applications of these architectures will be presented.

Due to the stability given by the polydentate nature of the ligand and the capability to coordinate a wide variety of metal ions, **TPMA** complexes have been extensively employed as catalysts for different reactions. Important application in catalysis with **TPMA** metal complexes have been achieved with cobalt, nickel and ruthenium for hydrogen production or carbon dioxide reduction, atom transfer radical addition and polymerization with copper, and olefine oxidation with iron and manganese.[82–84]

The novel self-assembled structure was built up through imine condensation between a modified **TPMA** zinc complex **34** bearing three aldehyde groups and diamine molecules Taking advantage from dynamic covalent chemistry (DCC), in particular imine bond formation, the system is able to equilibrate through an error-checking and self-correct toward the thermodynamic product. In this case, addition of ethylenediamine into a solution containing **TPMA** zinc complex **34** led to the formation of the supramolecular cage **84** in solution with a D_3 symmetry (Figure 38).[85]

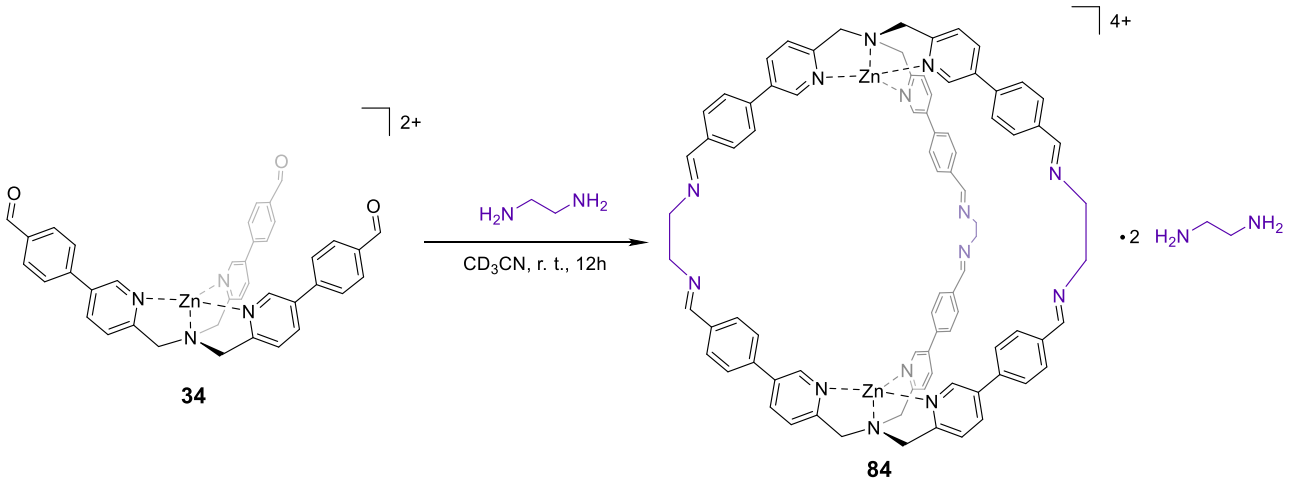

Figure 38. Synthesis of the **TPMA**-based molecular cage **84**. Adapted from ref. 85.

I7.1. Binding and Recognition properties

Inspired by the work of Anslyn and Canary on the sensing of carboxylic acid by **TPMA**-based complexes and the ability of Zinc to bind oxygen-donor ligands,[86] the molecular recognition properties of the cage toward dicarboxylate anions were initially investigated by the group. The addition of a stoichiometric amount of suberic acid **C_8** to a solution containing the empty cage resulted in a new set of ^{1}H-NMR signals, indicating the formation of the 1:1 host-guest complex. After this preliminary result, the binding capabilities of the cage toward diacids ranging from succinic acid (**C_4**) to tetradecandioic acid (**C_{14}**) were evaluated in order to understand how the slight structural variation in the guest length could affect the free energy of the encapsulation process. Interestingly, the binding constants determined via ^{1}H-NMR displayed a pseudo-Gaussian profile, centered on suberic acid (**C_8**) highlighting that encapsulation of shorter and longer diacids resulted in a higher thermodynamic cost for the conformational rearrangement for both the host and the guest (Figure 39).

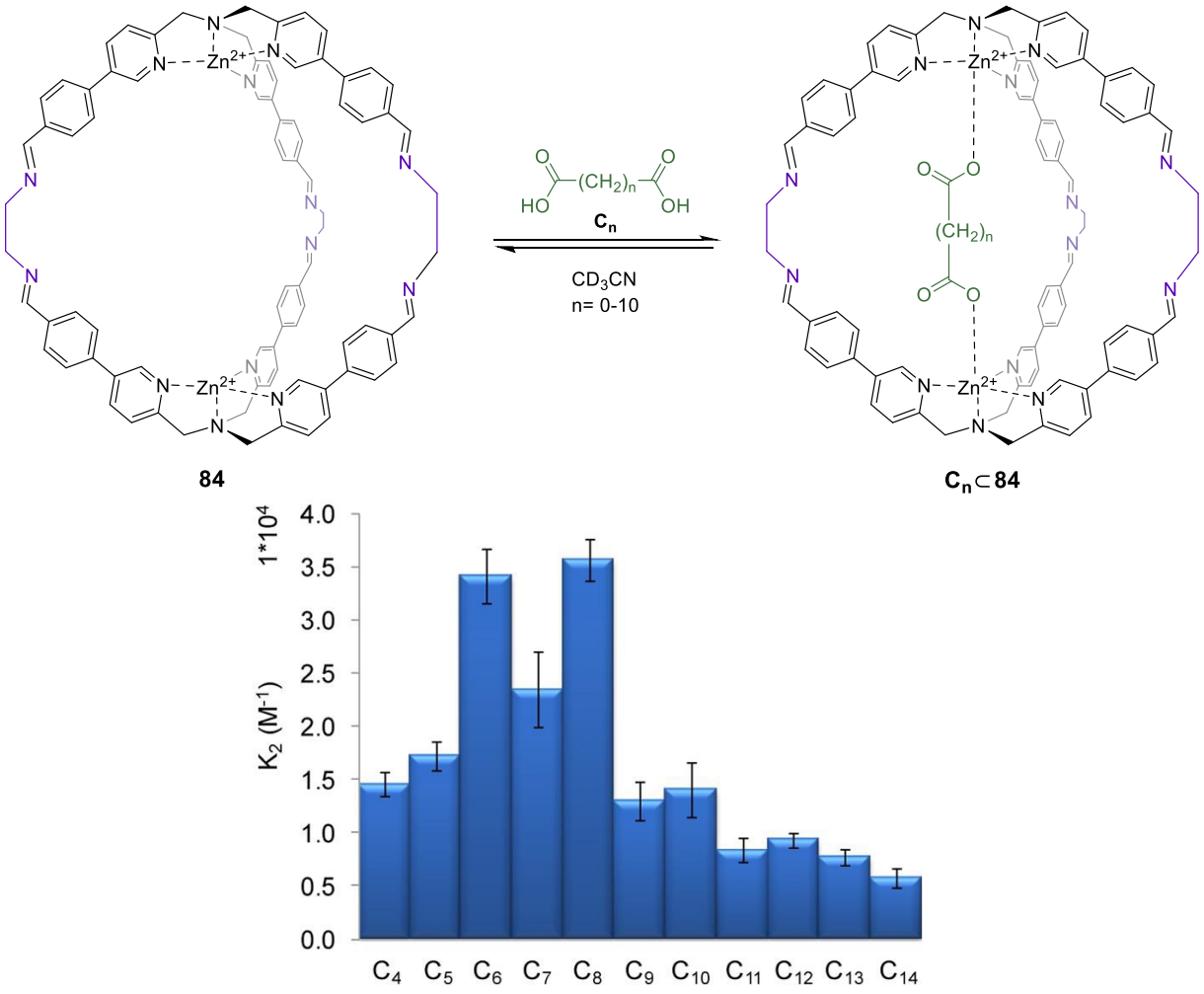

Figure 39. ^{1}H NMR binding constants (K_2) for the inclusion of diacids **C_4-C_{14}** within cage **84**. Perchlorate counteranions are removed for clarity. Adapted from ref. 85.

I7.2. Effect of the guest on the assembly and disassembly of the cage

Guest length could also affect the assembly or disassembly rate of the architecture. In particular, the presence of the diacid played a crucial role in the cage rate compared to the non-templated synthesis. More in detail, the templated synthesis showed a trend in the rate enhancement which resemble the binding constant profile (viz. a good binder is also a good templating agent). Also the disassembly rate of the imine-based structure upon addition of water strongly depends on the chain length of the diacid. Compared to the hydrolysis rate of the empty cage, shorter diacids allowed to slow down the disassembly process, while an higher rate was observed for longer guests. This behavior could be explained by the fact that guests with short chain length kept the two **TPMA** complexes together and the opening of the structure was associated with a strain gain to maintain the interaction of the carboxylates with both zinc metal centers. On the other hand, longer diacids tended to push toward both **TPMA** Zn units and this was due to the coiled conformation that these guests adopted within the cage, thus leading to a speed up of the hydrolysis reaction (Figure 40).

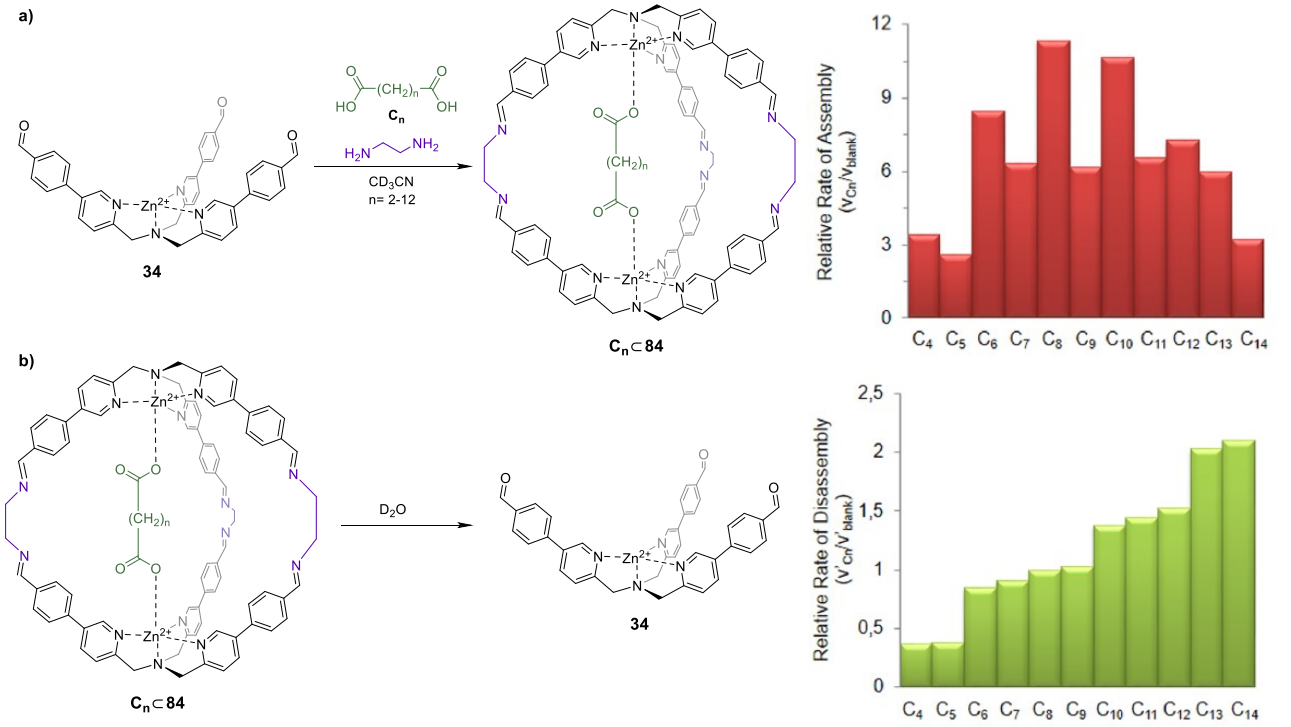

Figure 40. Initial rates of a) assembly and b) disassembly of cage **84** in the presence of dicarboxylic acids **C_4-C_{14}**. The graphs report the rate of assembly/disassembly relative to the black rate. Perchlorate counteranions are removed for clarity. Adapted from ref. 85.

I7.3. ESI-MS competition experiments

The initial results on the recognition properties of the cage with ethylenediamine as linker encouraged the research group to investigate the influence of the diamine linker on the binding capability of the system toward different dicarboxylic acids. For this purpose, the group developed a new, fast, and reliable method based on electron spray ionization (ESI-MS) in order to avoid the time-consuming binding experiments for each single cage by ^{1}H NMR.[87] More in detail, structures with different cavity size were obtained changing the diamine chain length and rigidity, and the recognition properties were studied using competition experiments (Figure 41).

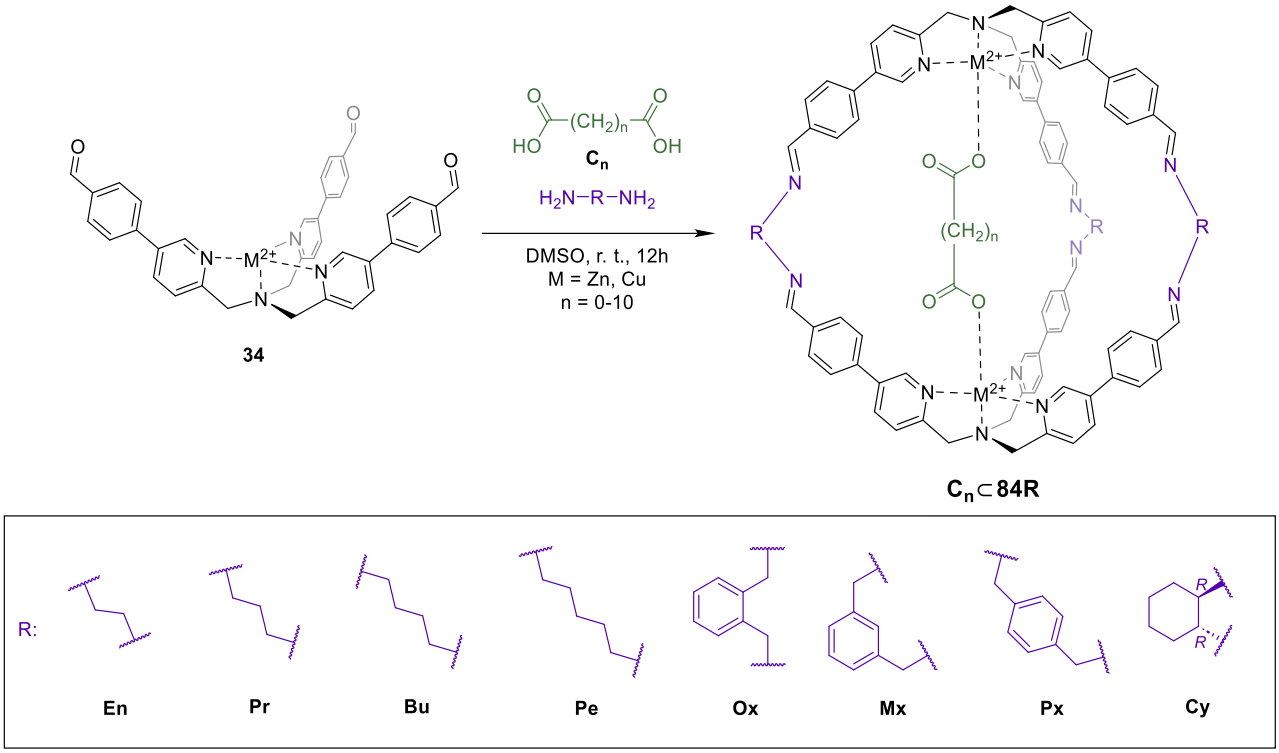

Figure 41. Synthesis of cages **C_{4+n}⊂84R**. Perchlorate counteranions are removed for clarity. (**En**: ethylenediamine, **Pr**: 1,3-diaminopropane, **Bu**: 1,4-diaminobutane, **Pe**: 1,5-diaminopentane, **Ox**: *o*-xylylenediamine, **Mx**: *m*-xylylenediamine, **Px**: *p*-xylylenediamine, **Cy**: 1,2-(*R*,*R*)-cyclohexyldiamine.

In order to validate the method, equimolar amount of diacids ranging from succinic **C_4** to tetradecandioic **C_{14}** were simultaneously added to a solution containing complex **34** and the ethylenenediamine, allowing the system to evolve toward the thermodynamic distribution. After 24 hours, the reaction mixture was analyzed, and as shown in Figure 42, the obtained relative ratio between the eleven inclusion species resembled the pseudo-Gaussian profile of the binding constants obtained via ^{1}H-NMR.

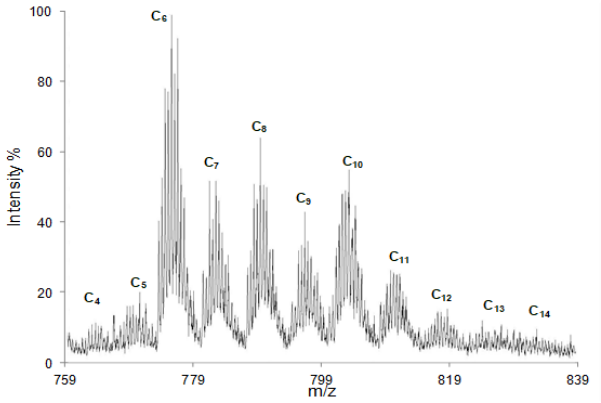

Figure 42. ESI-MS profile for the competition experiment of guests **C_4-C_{14}** in the presence of cage **84**. The information obtained are similar to those obtained from ^{1}H NMR (Figure 39). Adapted from ref. 87.

The same experiment was repeated for all the series of diamines and also employing copper TPMA complexes. From the obtained results, it was observed that the elongation of the diamine linker corresponded to a binding preference for longer dicarboxylic acids. For example, the cage with *p*-xylilenediamine as linker had the highest affinity for **C_{10}** and almost no affinity for shorter acids. In the same fashion, increased flexibility of the linker led to a wider distribution of the preferential guests (Figure 43).

It should be pointed out that this methodology allowed to study also Copper (II) **TPMA**-based supramolecular cages, whose analysis through ^{1}H-NMR spectroscopy would otherwise result highly complicate due to the paramagnetic nature of the metal.

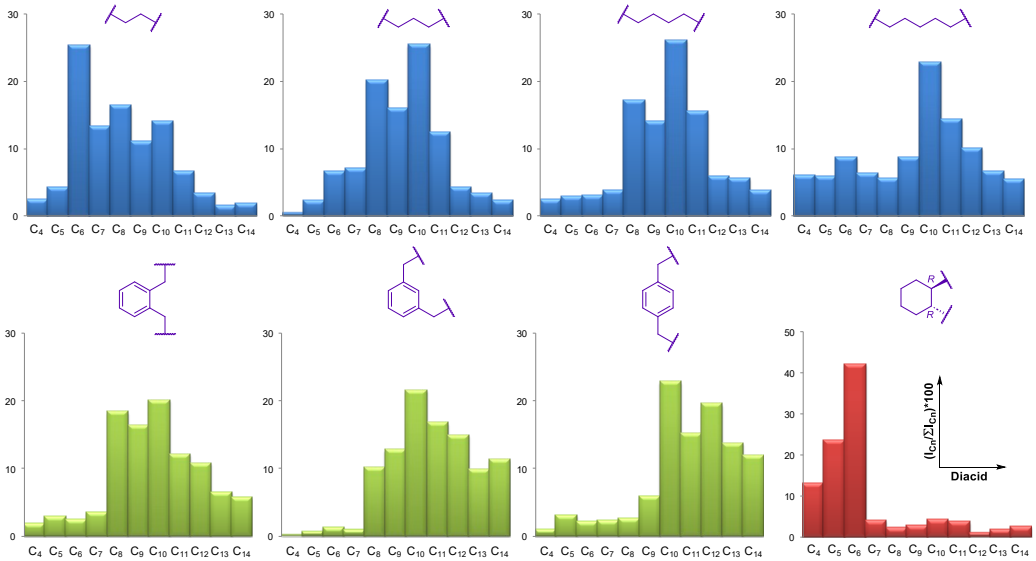

Figure 43. Synthesis of the supramolecular cage **84R** with different dicarboxylic acids ranging from succinic acid **C_4** to tetradecandioic acid **C_{14}** as guests and using different diamine (a-h) as linkers. b) ESI-MS selectivity profiles for cage **84R** in the competition experiments using different diacids guests and different diamine linkers. Adapted from ref. 87.

From the **C_{10}⊂84Pr·Cu** inclusion complex it was then possible to get a good quality crystal suitable for the X-ray diffraction (Figure 44). From the obtained crystal structure, it was observed that the distance between the two metal centers was equal to 15.4 Å, as a result of sebacic acid accommodation.

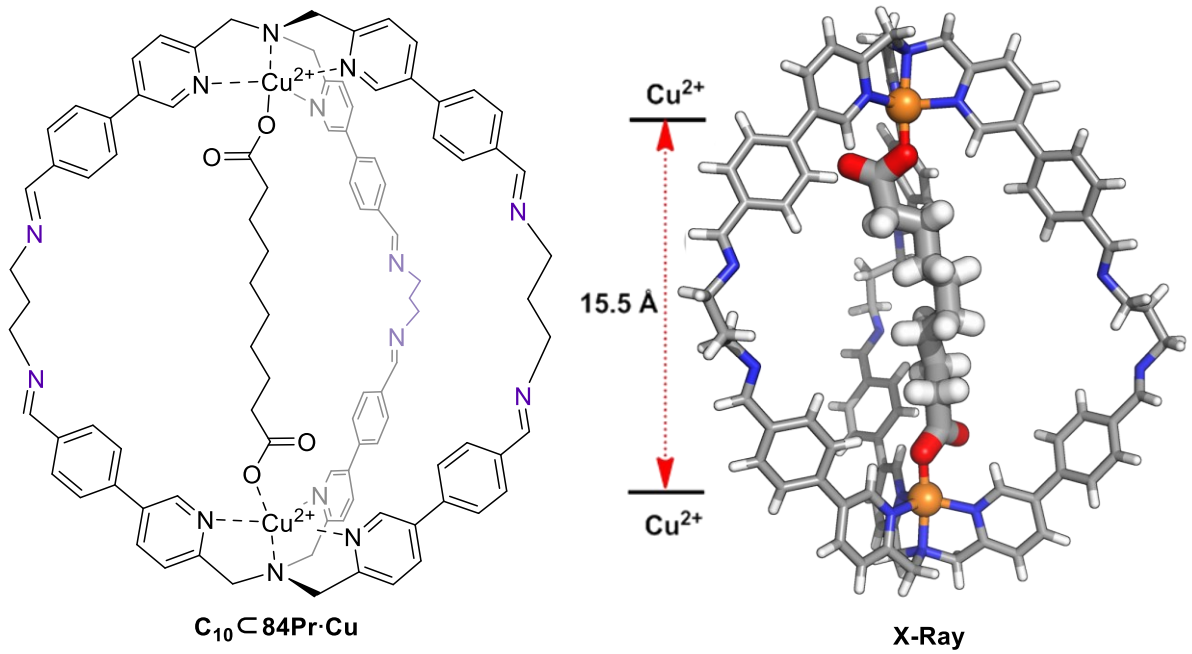

Figure 44. X-ray crystal structure of **C_{10}⊂84Pr·Cu**. Adapted from ref. 87.

I7.4. Encapsulation of aromatic carboxylic acids to quantify aromatic stacking interactions

Recently, the research group has reported the capability of the supramolecular cage **84** to interact with mono-carboxylic aromatic acids allowing the determination of the substituent effect on stacking interaction between the guests.[88] To investigate the encapsulation of the mono-carboxylic acid, a titration experiment with 4-nitrobenzoate was carried out, and from the subsequent additions of the benzoate it was possible to observe the formation of new set of peaks in the ^{1}H-NMR spectrum that could be attributed to the filled cage. Interestingly, only 1:2 cage-guest stoichiometry was observed, while no 1:1 host-guest complex was detected even at substoichiometric amount of the acid. Addition of two equivalents of the guest allowed the formation completely inclusion species.

As a result of the face-to-face geometry adopted by the two guests inside the cavity of the cage, the system was found to be an ideal candidate for the determination of the thermodynamic properties of aromatic stacking interactions between the two benzoates. Due to the simultaneously presence of many interactions between the acids and the cage,

a straightforward way could not be employed to determine directly the stacking interaction between the guests encapsulated. Nonetheless, it was possible to dissect all the aromatic stacking interactions from all the other contributions using the Double Mutant Cycle (DMC) approach, which has been used in different systems to quantify non-covalent interactions. For this purpose, the aliphatic n-hexanoate that cannot make aromatic interactions was taken as reference guest. Using DMC, it was possible to directly determine the aromatic stacking interaction between guests bearing different substituents. (Figure 45). The obtained results indicated that aromatic stacking interactions were dominated by short range local electrostatic interactions between the π-faces rather than by substituent dipole interactions

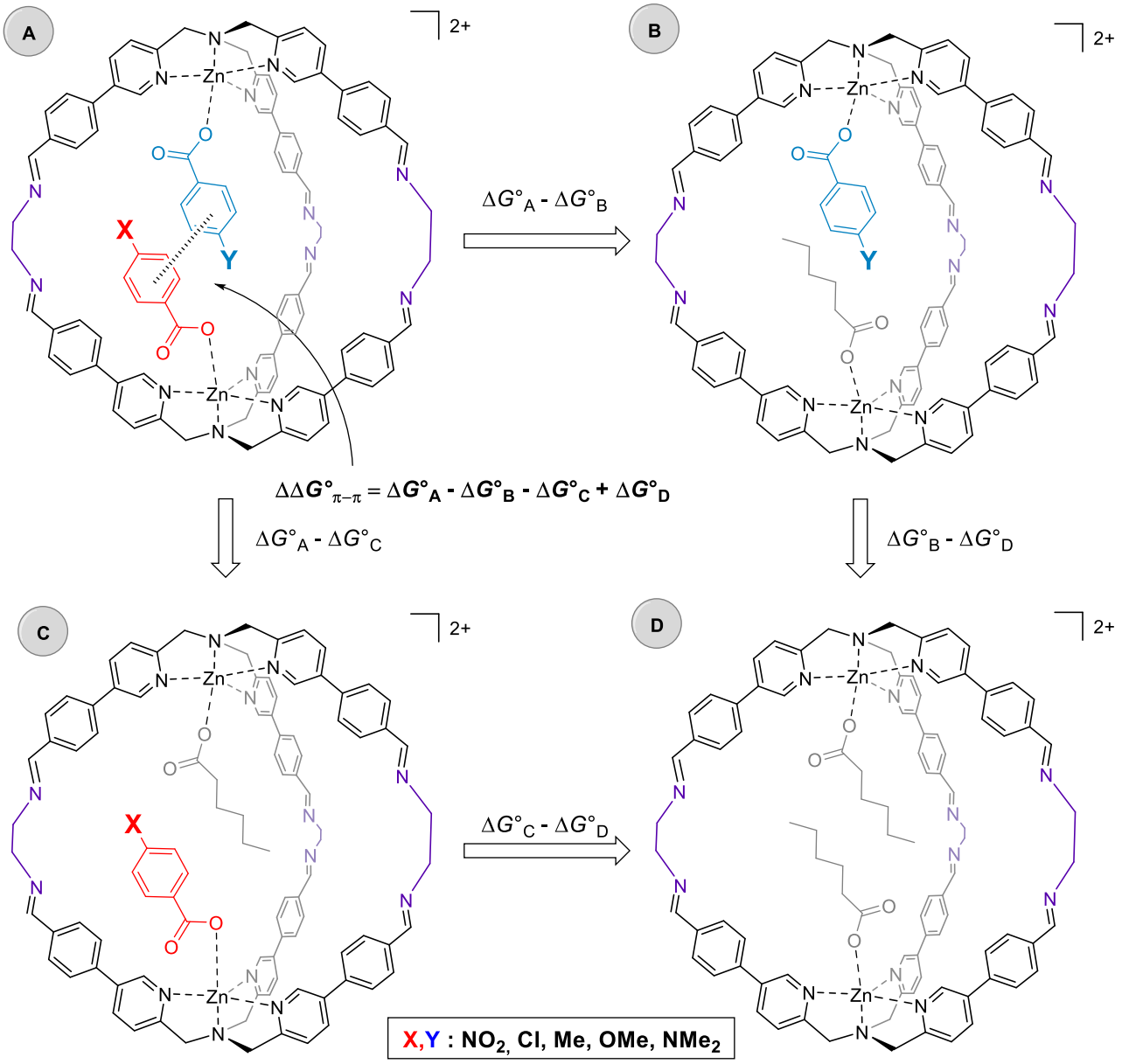

Figure 45. Chemical DMC for measuring the aromatic stacking interaction between two guests (perchlorate counteranions are removed for clarity). Adapted from ref. 88.

I8. Aim of the Thesis

In the recent years, the supramolecular cages developed in the research group where this thesis has been carried out have shown peculiar recognition properties for several carboxylate anions. In addition, as mentioned in the previous paragraphs, chiral supramolecular cages have shown promising functions in all the areas related to chirality. The overall Ph.D. project has the aim to extend the applications of the **TPMA**-based molecular cages in the field of chiral sensing taking advantage from confinement and to synthetize novel chiral structures for future applications in asymmetric catalysis.
In Chapter 1 the self assembly capability of the **TPMA**-based supramolecular cage in the presence of complex matrixes has been investigated. In this study, complex mixtures like wines and fruit juices have been employed in order to test if the cage could be able to selectively encapsulate and discriminate the dicarboxylic acids (tartaric, malic, and succinic acids) present in these matrixes. Moreover, the synthesis of a novel chiral Zinc-**TPMA** complex has been reported, and the capability of the resulting chiral cage to act as Chiral Solvating Agent (CSA) for chiral dicarboxylic acids has been evaluated. This feature has been further exploited for the discrimination of the enantiomers of malic and tartaric acids present in wines and fruit juices.
In Chapter 2 the capability of the supramolecular architecture to act as stereodynamic probe for the recognition of chiral dicarboxylate anions has been explored. The recognition capabilities of the cage in the presence of five different dicarboxylic acids have been tested using circular dichroism. The supramolecular structure in the presence of the tartrate anion as guest showed a chiroptical enhancement of the dichroic signal (*viz*. one order of magnitude higher than the other dicarboxylic acids). To investigate this phenomenon, a meticulous computational study was carried out on two supramolecular cages having the tartaric and malic acid (the closest related system) respectively encapsulated. Moreover, stereodynamic properties of the cage combined with the capability to self-assemble in presence of complex mixtures has allowed the quantification of tartaric acid content in wines using circular dichroism.
In Chapter 3 the possibility to tune guests uptake or release from the cage has been explored. A novel approach based on the capability of 9,10-phenanthrenequinone to react with diamines subcomponents, thus allowing their selective removal or replacement, has been developed. Using this procedure, the reversible assembly and disassembly of the cage with release and uptake of the guest was achieved. Moreover, the selective uptake and release of (a)chiral guests have been attempted through cage to cage conversions changing

the size or the chirality of the diamine linkers.

In Chapter 4 a novel methodology based on Diaza-Cope [3,3]-sigmatropic rearrangement has been developed to obtain a novel hydrolytically-stable chiral **TPMA**-based architectures. A detailed mechanistic study has been carried out in order to explain the effect of the guest length in the final thermodynamic distribution of the species involved during the reaction. This strategy has been further employed for the synthesis of novel tweezer-like structures. Finally, complexation of the novel water soluble cage has been performed.

I9. References

[1] J. C. Sherman, D. J. Cram, J. A. Bryant, . T Blanda, M. Vincenti, C. B. Knobler, *J. Chem. Soc.* **1991**, *113*, 7717–7727.
[2] B. Dietrich, J. M. Lehn, J. P. Sauvage, *J. Chem. Soc. Chem. Commun.* **1973**, 15–16.
[3] S. Zarra, D. M. Wood, D. A. Roberts, J. R. Nitschke, *Chem. Soc. Rev.* **2015**, *44*, 419–432.
[4] M. Mastalerz, *Angew. Chem. Int. Ed.* **2010**, *49*, 5042–5053.
[5] M. Pan, K. Wu, J.-H. Zhang, C.-Y. Su, *Coord. Chem. Rev.* **2019**, *378*, 333–349.
[6] L. Zhang, H. Liu, G. Yuan, Y.-F. Han, *Chinese J. Chem.* **2021**, *39*, 2273–2286.
[7] R. Chakrabarty, P. S. Mukherjee, P. J. Stang, *Chem. Rev.* **2011**, *111*, 6810–6918.
[8] J. Gabard, A. Collet, *J. Chem. Soc. Chem. Commun.* **1981**, 1137–1139.
[9] R. J. Pieters, J. Cuntze, M. Bonnet, F. Diederich, *J. Chem. Soc., Perkin Trans* **1997**, *2*.
[10] J. F. S. S. J. Rowan, S. J. Cantrill, G. R. L. Cousins, *Angew. Chem. Int. Ed.* **2002**, *41*, 898–952.
[11] P. T. Corbett, J. Leclaire, L. Vial, K. R. West, J. L. Wietor, J. K. M. Sanders, S. Otto, *Chem. Rev.* **2006**, *106*, 3652–3711.
[12] A. J. McConnell, C. S. Wood, P. P. Neelakandan, J. R. Nitschke, *Chem. Rev.* **2015**, *115*, 7729–7793.
[13] G. Zhang, M. Mastalerz, *Chem. Soc. Rev.* **2014**, *43*, 1934–1947.
[14] D. Xu, R. Warmuth, *J. Am. Chem. Soc.* **2008**, *130*, 7520–7521.
[15] A. Collet, *Tetrahedron* **1987**, *43*, 5725–5759.
[16] T. Tozawa, J. T. A. Jones, S. I. Swamy, S. Jiang, D. J. Adams, S. Shakespeare, R. Clowes, D. Bradshaw, T. Hasell, S. Y. Chong, C. Tang, S. Thompson, J. Parker, A. Trewin, J. Bacsa, A. M. Z. Slawin, A. Steiner, A. I. Cooper, *Nat. Mater.* **2009**, *8*, 973–978.
[17] K. E. Jelfs, X. Wu, M. Schmidtmann, J. T. A. Jones, J. E. Warren, D. J. Adams, A. I. Cooper, *Angew. Chemie* **2011**, *123*, 10841–10844.
[18] S. Tartaggia, A. Scarso, P. Padovan, O. De Lucchi, F. Fabris, *Org. Lett.* **2009**, *11*, 3926–3929.
[19] A. U. Malik, F. Gan, C. Shen, N. Yu, R. Wang, J. Crassous, M. Shu, H. Qiu, *J. Am. Chem. Soc.* **2018**, *140*, 2769–2772.
[20] E. Ramakrishna, J. D. Tang, J. J. Tao, Q. Fang, Z. Zhang, J. Huang, S. Li, *Chem. Commun.* **2021**, *57*, 9088–9091.
[21] M. Yoshizawa, J. K. Klosterman, M. Fujita, *Angew. Chem. Int. Ed.* **2009**, *48*, 3418–3438.
[22] S. J. Dalgarno, N. P. Power, J. L. Atwood, *Coord. Chem. Rev.* **2008**, *252*, 825–841.
[23] M. Fujita, M. Tominaga, A. Hori, B. Therrien, *Acc. Chem. Res.* **2005**, *38*, 369–378.
[24] M. M. J. Smulders, I. A. Riddell, C. Browne, J. R. Nitschke, *Chem. Soc. Rev.* **2013**, *42*, 1728–1754.
[25] A. M. Castilla, W. J. Ramsay, J. R. Nitschke, *Acc. Chem. Res.* **2014**, *47*, 2063–2073.
[26] L.-J. Chen, H.-B. Yang, M. Shionoya, *Chem. Soc. Rev.* **2017**, *46*, 2555–2576.
[27] P. J. Stang, B. Olenyuk, D. C. Muddiman, R. D. Smith, *Organometallics* **1997**, *16*, 3094–3096.
[28] O. Chepelin, J. Ujma, X. Wu, A. M. Z. Slawin, M. B. Pitak, S. J. Coles, J. Michel, A. C. Jones, P. E. Barran, P. J. Lusby, *J. Am. Chem. Soc.* **2012**, *134*, 19334–19337.
[29] J. L. Bolliger, A. M. Belenguer, J. R. Nitschke, *Angew. Chem. Int. Ed.* **2013**, *52*, 7958–7962.
[30] C. Zhao, Q.-F. Sun, W. M. Hart-Cooper, A. G. DiPasquale, F. D. Toste, R. G. Bergman, K. N. Raymond, *J. Am. Chem. Soc.* **2013**, *135*, 18802–18805.
[31] L.-L. Yan, C.-H. Tan, G.-L. Zhang, L.-P. Zhou, J.-C. Bünzli, Q.-F. Sun, *J. Am. Chem. Soc.* **2015**, *137*, 8550–8555.
[32] C. Wolf, K. W. Bentley, *Chem. Soc. Rev.* **2013**, *42*, 5408–5424.
[33] C. Bravin, E. Badetti, G. Licini, C. Zonta, *Coord. Chem. Rev.* **2021**, *427*, DOI 10.1016/j.ccr.2020.213558.
[34] M. Albrecht, in (Eds.: C.A. Schalley, F. Vögtle, K.H. Dötz), Springer Berlin Heidelberg, Berlin, Heidelberg, **2004**, pp. 105–139.
[35] M. Albrecht, *Chem. Rev.* **2001**, *101*, 3457–3497.
[36] M. Rancan, J. Tessarolo, A. Carlotto, S. Carlotto, M. Rando, L. Barchi, E. Bolognesi, R. Seraglia, G. Bottaro, M. Casarin, G. H. Clever, L. Armelao, *Cell Reports Phys. Sci.* **2022**, *3*, 100692.
[37] P. Howlader, S. Mondal, S. Ahmed, P. S. Mukherjee, *J. Am. Chem. Soc.* **2020**, *142*, 20968–20972.
[38] L. A. Joyce, M. S. Maynor, J. M. Dragna, G. M. da Cruz, V. M. Lynch, J. W. Canary, E. V. Anslyn, *J. Am. Chem. Soc.* **2011**, *133*, 13746–13752.
[39] P. Zardi, K. Wurst, G. Licini, C. Zonta, *J. Am. Chem. Soc.* **2017**, *139*, 15616–15619.
[40] C. Bravin, E. Badetti, R. Puttreddy, F. Pan, K. Rissanen, G. Licini, C. Zonta, *Chem. Eur. J.* **2018**, *24*, 2936–2943.
[41] Y.-J. Hou, K. Wu, Z.-W. Wei, K. Li, Y.-L. Lu, C.-Y. Zhu, J.-S. Wang, M. Pan, J.-J. Jiang, G.-Q. Li, C.-Y. Su, *J. Am. Chem. Soc.* **2018**, *140*, 18183–18191.
[42] A. J. Terpin, M. Ziegler, D. W. Johnson, K. N. Raymond, *Angew. Chem. Int. Ed.* **2001**, *40*, 157–160.
[43] A. V Davis, D. Fiedler, M. Ziegler, A. Terpin, K. N. Raymond, *J. Am. Chem. Soc.* **2007**, *129*, 15354–

15363.
[44] S. Wan, L.-R. Lin, L. Zeng, Y. Lin, H. Zhang, *Chem. Commun.* **2014**, *50*, 15301–15304.
[45] Y.-P. He, L.-B. Yuan, J.-S. Song, G.-H. Chen, Q. Lin, C. Li, L. Zhang, J. Zhang, *Chem. Mater.* **2018**, *30*, 7769–7775.
[46] B. Mitschke, M. Turberg, B. List, *Chem* **2020**, *6*, 2515–2532.
[47] C. Tan, D. Chu, X. Tang, Y. Liu, W. Xuan, Y. Cui, *Chem. Eur. J.* **2019**, *25*, 662–672.
[48] Y. Nishioka, T. Yamaguchi, M. Kawano, M. Fujita, *J. Am. Chem. Soc.* **2008**, *130*, 8160–8161.
[49] S. M. Bierschenk, J. Y. Pan, N. S. Settineri, U. Warzok, R. G. Bergman, K. N. Raymond, F. D. Toste, *J. Am. Chem. Soc.* **2022**, *144*, 11425–11433.
[50] C. García-Simón, R. Gramage-Doria, S. Raoufmoghaddam, T. Parella, M. Costas, X. Ribas, J. N. H. Reek, *J. Am. Chem. Soc.* **2015**, *137*, 2680–2687.
[51] J. Guo, Y.-W. Xu, K. Li, L.-M. Xiao, S. Chen, K. Wu, X.-D. Chen, Y.-Z. Fan, J.-M. Liu, C.-Y. Su, *Angew. Chem. Int. Ed.* **2017**, *56*, 3852–3856.
[52] M. Liu, L. Zhang, T. Wang, *Chem. Rev.* **2015**, *115*, 7304–7397.
[53] L. Tapia, I. Alfonso, J. Sola, *Org. Biomol. Chem.* **2021**, *19*, 9527–9540.
[54] G. Pescitelli, L. Di Bari, N. Berova, *Chem. Soc. Rev.* **2014**, *43*, 5211–5233.
[55] C. Bravin, G. Mason, G. Licini, C. Zonta, *J. Am. Chem. Soc.* **2019**, *141*, 11963–11969.
[56] R. Mobili, G. Preda, S. La Cognata, L. Toma, D. Pasini, V. Amendola, *Chem. Commun.* **2022**, *58*, 3897–3900.
[57] G. Wu, Y. Chen, S. Fang, L. Tong, L. Shen, C. Ge, Y. Pan, X. Shi, H. Li, *Angew. Chem. Int. Ed.* **2021**, *60*, 16594–16599.
[58] W. Zuo, Z. Huang, Y. Zhao, W. Xu, Z. Liu, X.-J. Yang, C. Jia, B. Wu, *Chem. Commun.* **2018**, *54*, 7378–7381.
[59] R. A. Tromans, S. K. Samanta, A. M. Chapman, A. P. Davis, *Chem. Sci.* **2020**, *11*, 3223–3227.
[60] T. J. Wenzel, C. D. Chisholm, *Chirality* **2011**, *23*, 190–214.
[61] J. Canceill, L. Lacombe, A. Collet, *J. Am. Chem. Soc.* **1985**, *107*, 6993–6996.
[62] A. Bouchet, T. Brotin, M. Linares, H. Ågren, D. Cavagnat, T. Buffeteau, *J. Org. Chem.* **2011**, *76*, 4178–4181.
[63] N. De Rycke, M. Jean, N. Vanthuyne, T. Buffeteau, T. Brotin, *European J. Org. Chem.* **2018**, *2018*, 1601–1607.
[64] A. Schmitt, B. Chatelet, D. Padula, L. Di Bari, J.-P. Dutasta, A. Martinez, *New J. Chem.* **2015**, *39*, 1749–1753.
[65] A. Long, O. Perraud, M. Albalat, V. Robert, J.-P. Dutasta, A. Martinez, *J. Org. Chem.* **2018**, *83*, 6301–6306.
[66] C. J. Hastings, M. D. Pluth, S. M. Biros, R. G. Bergman, K. N. Raymond, *Tetrahedron* **2008**, *64*, 8362–8367.
[67] J. R. Holst, A. Trewin, A. I. Cooper, *Nat. Chem.* **2010**, *2*, 915–920.
[68] T. Hasell, S. Y. Chong, K. E. Jelfs, D. J. Adams, A. I. Cooper, *J. Am. Chem. Soc.* **2012**, *134*, 588–598.
[69] D. W. Armstrong, W. Li, C. D. Chang, J. Pitha, *Anal. Chem.* **1990**, *62*, 914–923.
[70] V. Schurig, H.-P. Nowotny, *Angew. Chemie Int. Ed. English* **1990**, *29*, 939–957.
[71] A. Kewley, A. Stephenson, L. Chen, M. E. Briggs, T. Hasell, A. I. Cooper, *Chem. Mater.* **2015**, *27*, 3207–3210.
[72] J.-H. Zhang, S.-M. Xie, L. Chen, B.-J. Wang, P.-G. He, L.-M. Yuan, *Anal. Chem.* **2015**, *87*, 7817–7824.
[73] S.-M. Xie, J.-H. Zhang, N. Fu, B.-J. Wang, L. Chen, L.-M. Yuan, *Anal. Chim. Acta* **2016**, *903*, 156–163.
[74] H.-Y. Wong, W.-S. Lo, K.-H. Yim, G.-L. Law, *Chem* **2019**, *5*, 3058–3095.
[75] M. Quan, X.-Y. Pang, W. Jiang, *Angew. Chem. Int. Ed.* **2022**, *61*, e202201258.
[76] T. R. Schulte, J. J. Holstein, G. H. Clever, T. R. Schulte, J. J. Holstein, G. H. Clever, *Angew. Chem. Int. Ed.* **2019**, *58*, 5562–5566.
[77] K. Wu, J. Tessarolo, A. Baksi, G. H. Clever, *Angew. Chem. Int. Ed.* **2022**, *61*, DOI 10.1002/ANIE.202205725.
[78] X. Tang, H. Jiang, Y. Si, N. Rampal, W. Gong, C. Cheng, X. Kang, D. Fairen-Jimenez, Y. Cui, Y. Liu, *Chem* **2021**, *7*, 2771–2786.
[79] Y. Zhou, H. Li, T. Zhu, T. Gao, P. Yan, *J. Am. Chem. Soc.* **2019**, *141*, 19634–19643.
[80] R. J. Li, J. J. Holstein, W. G. Hiller, J. Andréasson, G. H. Clever, *J. Am. Chem. Soc.* **2019**, *141*, 2097–2103.
[81] C. Bravin, G. Mazzeo, S. Abbate, G. Licini, G. Longhi, C. Zonta, *Chem. Commun.* **2022**, *58*, 2152–2155.
[82] E. Benazzi, F. Begato, A. Niorettini, L. Destro, K. Wurst, G. Licini, S. Agnoli, C. Zonta, M. Natali, *J. Mater. Chem. A* **2021**, *9*, 20032–20039.
[83] T. G. Ribelli, M. Fantin, J.-C. Daran, K. F. Augustine, R. Poli, K. Matyjaszewski, *J. Am. Chem. Soc.* **2018**, *140*, 1525–1534.
[84] M. Borrell, M. Costas, *J. Am. Chem. Soc.* **2017**, *139*, 12821–12829.

[85] C. Bravin, E. Badetti, F. A. Scaramuzzo, G. Licini, C. Zonta, *J. Am. Chem. Soc.* **2017**, *139*, 6456–6460.
[86] L. A. Joyce, M. S. Maynor, J. M. Dragna, G. M. Da Cruz, V. M. Lynch, J. W. Canary, E. V. Anslyn, *J. Am. Chem. Soc.* **2011**, *133*, 13746–13752.
[87] C. Bravin, E. Badetti, R. Puttreddy, F. Pan, K. Rissanen, G. Licini, C. Zonta, *Chem. Eur. J.* **2018**, *24*, 2936–2943.
[88] C. Bravin, G. Licini, C. A. Hunter, C. Zonta, *Chem. Sci.* **2019**, *10*, 1466–1471.

Chapter 1

Straight from the Bottle! Wine and Juice Dicarboxylic Acids as Templates for Supramolecular Cage Self-Assembly

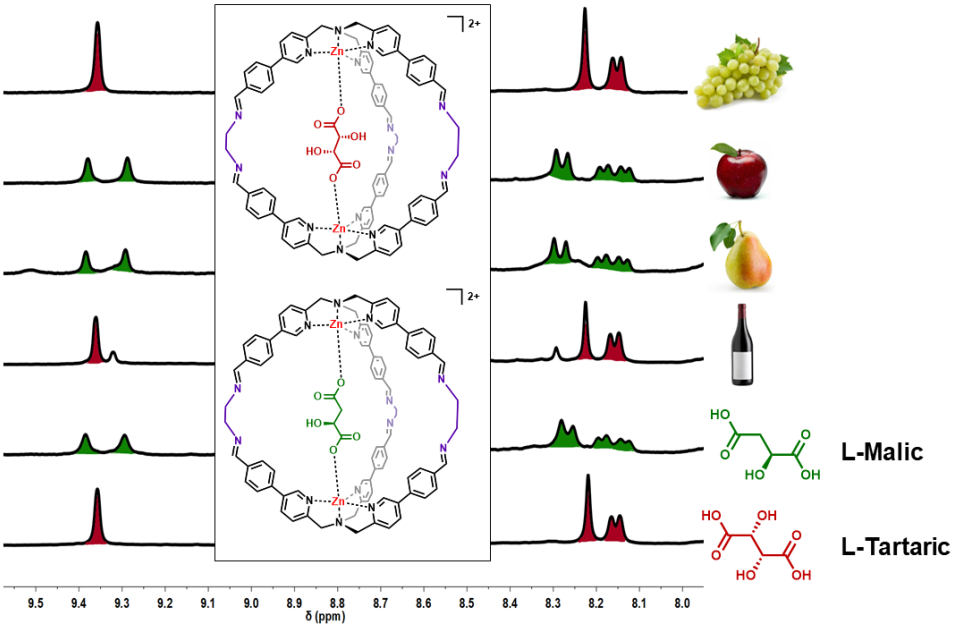

ABSTRACT Self-assembly processes have been the leading synthetic strategy for the preparation of elaborate molecular architectures. However, stringent chemical conditions are usually applied in order to favour the desired synthetic pathway. In this chapter, two imine based supramolecular cages able to self-assemble in the presence of a complex mixture like wine or fruit juices are presented. Taking advantage of diacids templating agents present in these matrixes the systems are able to form and to selectively encapsulate dicarboxylic systems present in the mixtures. This capability has been exploited to develop molecular systems able to report enantiomeric excess and composition of (a)chiral dicarboxylic acids in fruit juices and wines using ^{1}H-NMR.

1.1. Introduction

Thermodynamic driven assembly of small molecules in complex supramolecular architectures has offered the possibility to achieve molecular systems of increasing complexity in their size, topology and function.[1–6] Within the different methodologies, the use of coordination chemistry, also in combination with dynamic covalent imine condensation,[7–11] has been successfully applied for the synthesis of many different systems with noteworthy results especially in the field of supramolecular cages (Figure 1).[12–16]

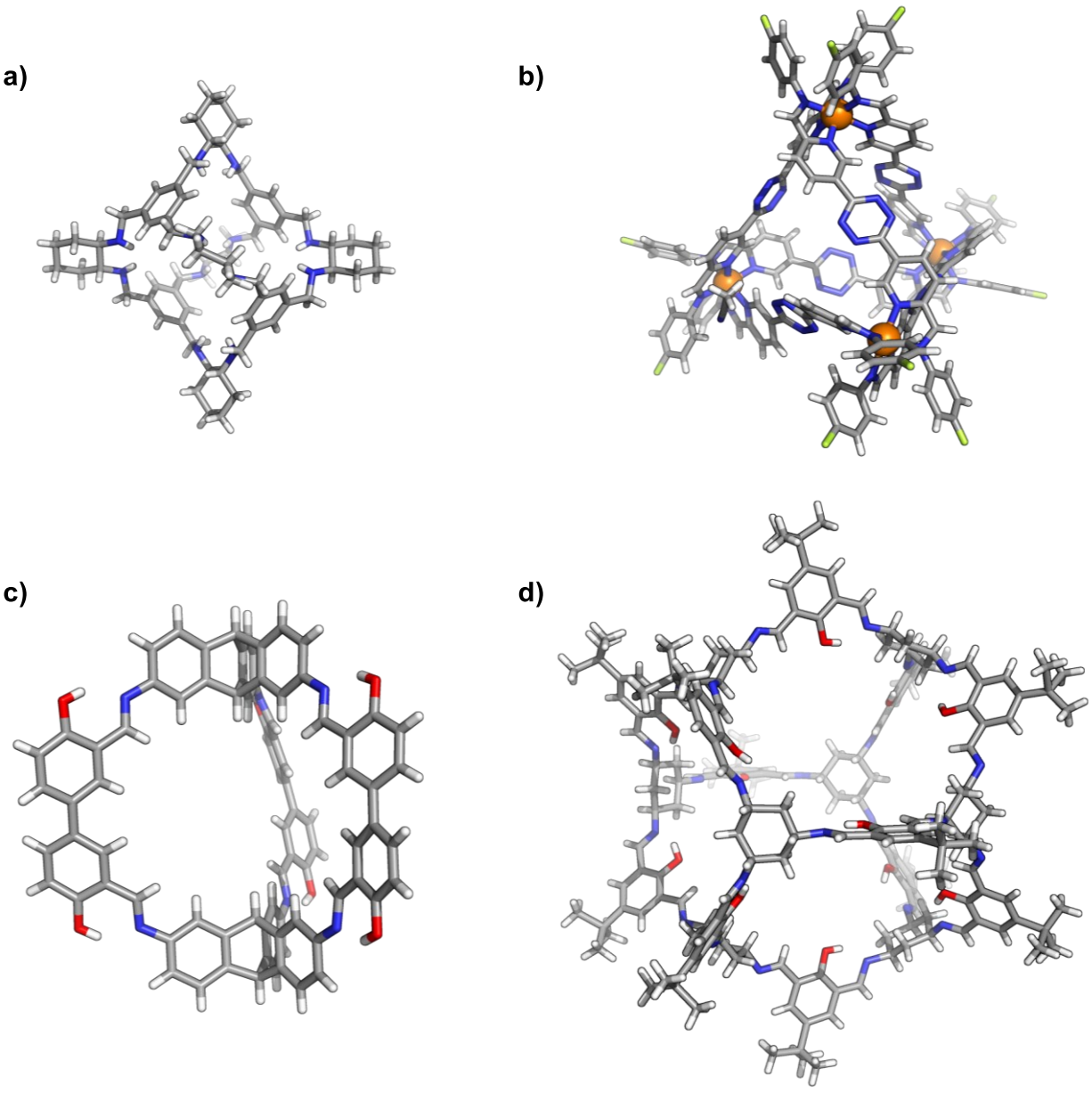

Figure 1. Molecular cages synthetized by a) Cooper,[8] b) Nitschke,[9] c) Mastalerz,[10] and d) Gawroński,[11] through imine condensation.

Even though novel strategies for in water synthesis of these complicate structures are emerging,[17–21] prerequisite for their formation is to perform the assembly in “ideal solutions” where the presence of correct stoichiometry, the absence of competing species, and “clean” solvents are often required. The realization of this chemistry in the presence of complex matrixes, where the variability of the molecular structures introduced in the mixture can compete with the self-assembly process, is a challenge that can results in novel practical applications for recognition chemistry.[22–27]

In this chapter, two imine based supramolecular cages able to assemble in the presence of complex matrixes have been reported. In particular, the natural occurrence of noticeable quantities of (a)chiral dicarboxylic acids in fruits,[28,29] and the corresponding juices was exploited to form self-assembled structures directly in these complex mixtures with the aim to gather quantitative information on dicarboxylic acids content and stereochemistry.

1.2. Results and Discussion

1.2.1. Self-Assembly of the cage in the presence of wine

As mentioned in the introduction, in recent years, the research group in which this thesis has been carried out, developed a series of novel **TPMA**-based supramolecular cages using dicarboxylic acids as templating agents.[30,31]

The high stability shown by the cage, also in the presence of high amounts of water, inspired the evaluation of the possibility to perform the cage self-assembly in the presence of wine, which contains enantiopure tartaric **L-Tar** (1-4 g/l) and malic **L-Mal** (0-4 g/l) diacids.[32,33] However, even if this complex mixture contains high amount of these two templating agents, the use of wine straight from the bottle is challenging for the self-assembly process due to the presence of many different organic compounds, water, and ethanol which can compete with the formation of the self-assembled system.

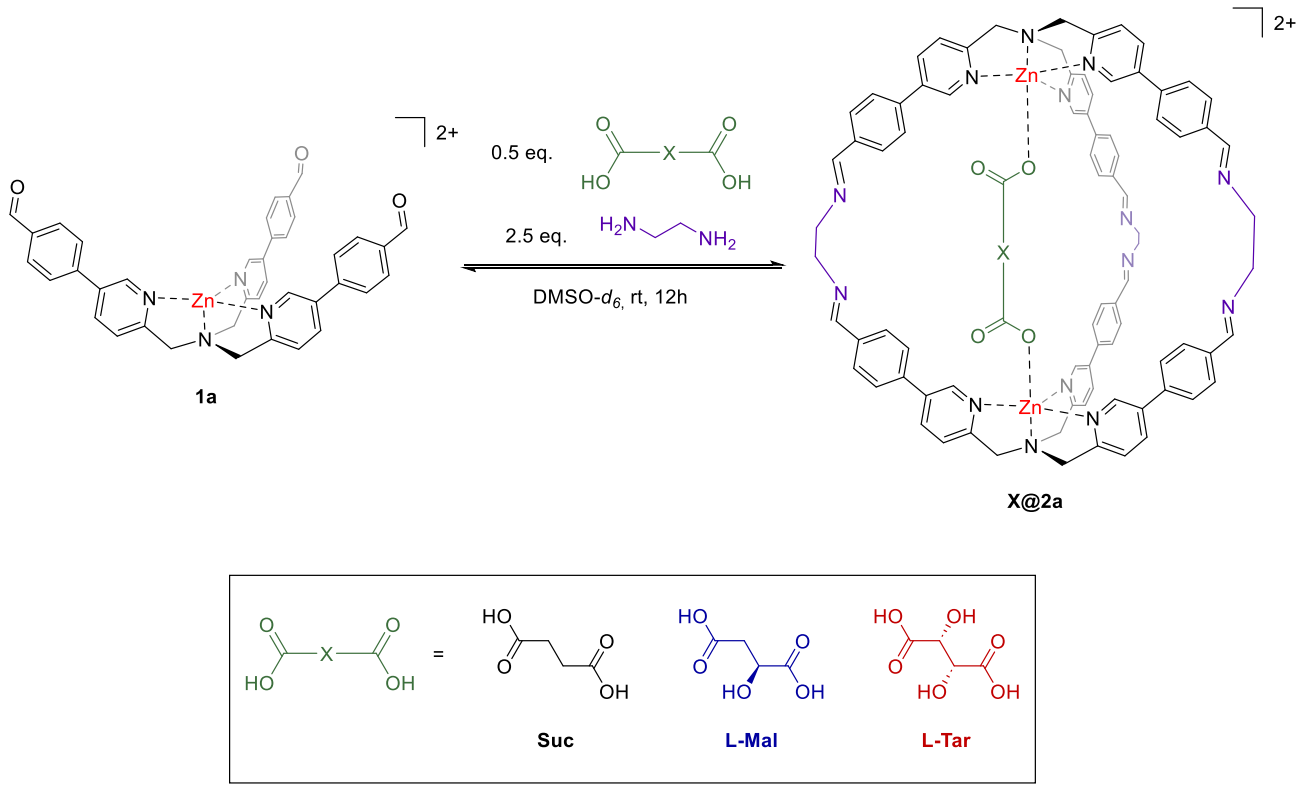

Scheme 1. Synthesis of **TPMA**-based cages **2a**. After the synthesis with commercially available pure diacids, synthesis have been performed using dicarboxylic acids present in complex mixtures. Perchlorates are removed for clarity.

Starting from these considerations, **L-Tar@2a** formation was attempted adding 15 µL of Valpolicella wine without any pretreatment (expected **L-Tar** content range 0.1 – 0.2 µmol) to a 0.5 mL solution of DMSO-d_6 (500 µL) containing 2.5 µmol of ethylenediamine and 1 µmol of the aldehyde-**TPMA**-based complex **1a** (Scheme 1).

The solution was left at room temperature overnight and subsequently analyzed by ^{1}H-NMR. As shown in Figure 2, the use of wine as source of **L-Tar** furnished a spectrum comparable with the cage synthetized using commercially available pure **L-Tar**.

In other words, **L-Tar@2a** self-assembled structure formed smoothly using a quantity close to the stoichiometric amount of templating agent coming from a water mixture containing several different molecules.

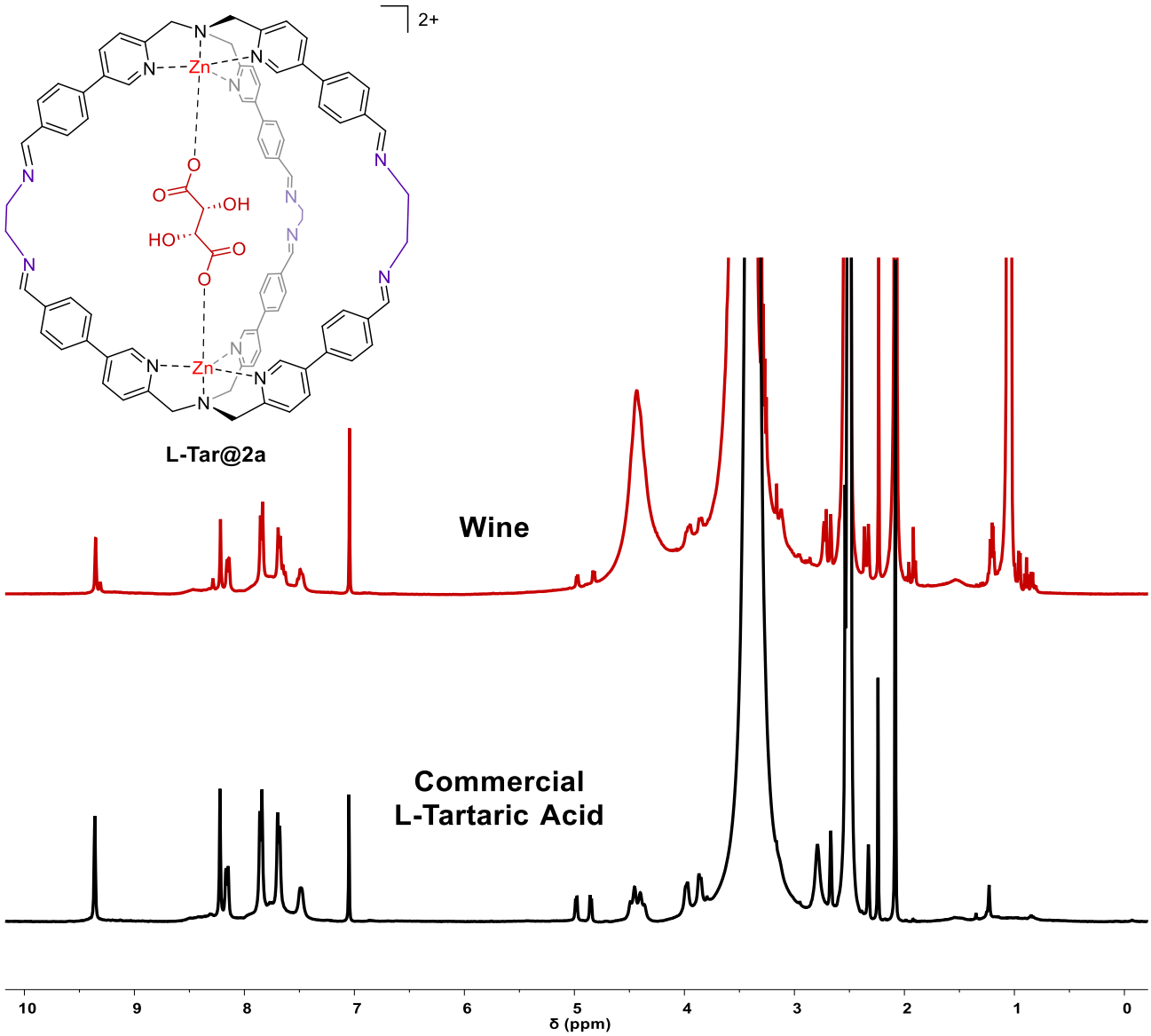

Figure 2. ^{1}H-NMR spectra (400 MHz, 301 K, DMSO-d_6) of the supramolecular cage **2a** formed adding commercially available **L-Tar** acid (black), and 15 µL of Valpolicella wine without pre-treatment (red) to 500 µL DMSO-d_6 solution containing 1 µmol of complex **1a** and 2.5 µmol ethylenediamine. Internal standard at 7.05 ppm is *p*-xylene. Perchlorates are removed for clarity.

This preliminary result encouraged the examination of the upper limit for wine content. For this reason, keeping constant the quantity of ethylenediamine and aldehyde complex **1a** in 0.5 mL solution of DMSO-d_6, solution containing increasing aliquots of wine have been prepared. After 12 hours, ^{1}H-NMR displayed clean cage formation for all samples up to 125 µL of wine (Figure 3). Even if at first instance the poor formation at high wine quantities seems related to the presence of water, high amount of wine induces a precipitation of the solution suggesting a low solubility of the system at high water contents.

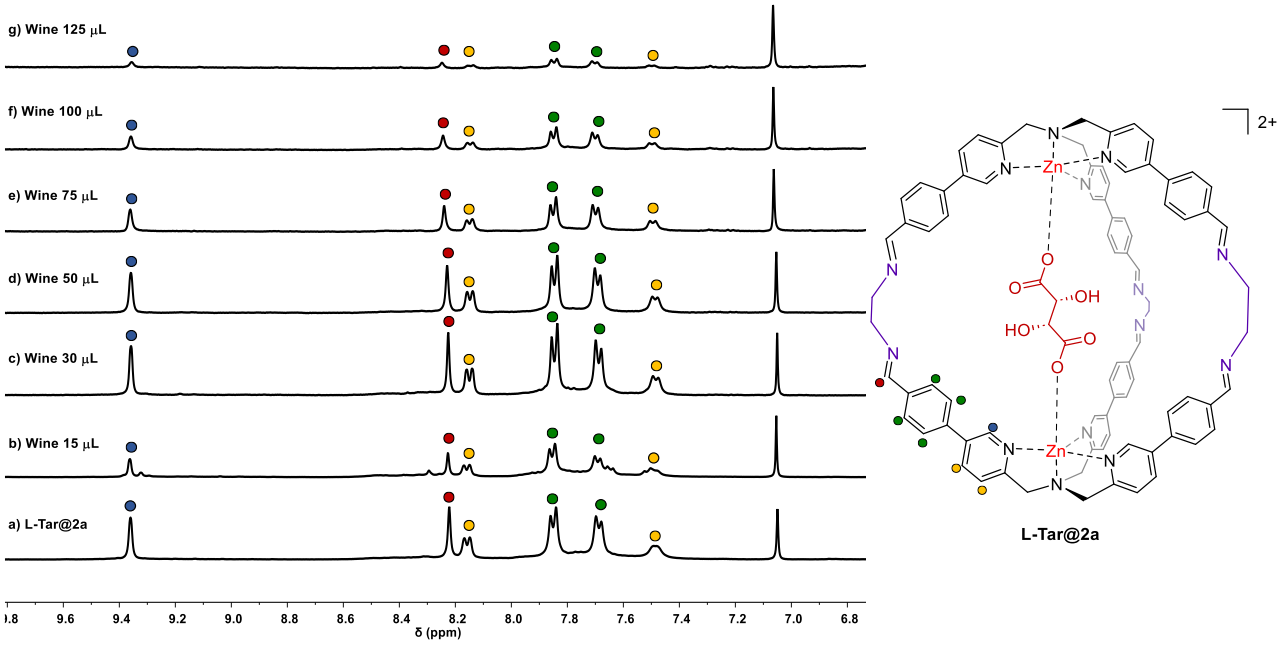

Figure 3. Partial ^{1}H-NMR spectra (400 MHz, 301 K, DMSO-d_6) of the supramolecular cage **2a** formed adding a) commercially available **L-Tar** acid (yield 96%), b) 15 µL (yield 43%), c) 30 µL (yield 94%), d) 50 µL (yield 72%), e) 75 µL (yield 33%), f) 100 µL (yield 22%), and g) 125 µL (yield 8%) of Valpolicella wine without pre-treatment to 500 µL DMSO-d_6 solution containing 1 µmol of complex **1a** and 2.5 µmol ethylenediamine. Internal standard at 7.05 ppm is p-xylene. Perchlorates are removed for clarity.

1.2.2. Discrimination of dicarboxylic acids in complex mixtures

The reliability of the self-assembly process in the presence of wine encouraged the examination of the capability of the structure to assemble in the presence of other fruit juices and wines. For this reason, the “scope” of the reaction has been tested across different matrixes containing dicarboxylic acids. In particular, 3 red wines (Valpolicella, Chianti, and Barbera), 3 white wines (Prosecco, Müller-Thurgau, and Chardonnay), 6 commercially available fruit juices (two blueberry, apple, pear , blueberry-grape, peach), and 3 freshly screwed juices (grape, blueberry, apple) have been used as templating source for the formation of cage **2a**.

In all the matrix sources the cage formed smoothly and, as shown by the ^{1}H-NMR (Figure 4, and Appendix 1, Figures A46-A60) tartaric, malic and succinic diacids can be discriminated and, using an internal standard, quantified (a comparison with HPLC analysis has been reported in Appendix 1, Section A1.18).

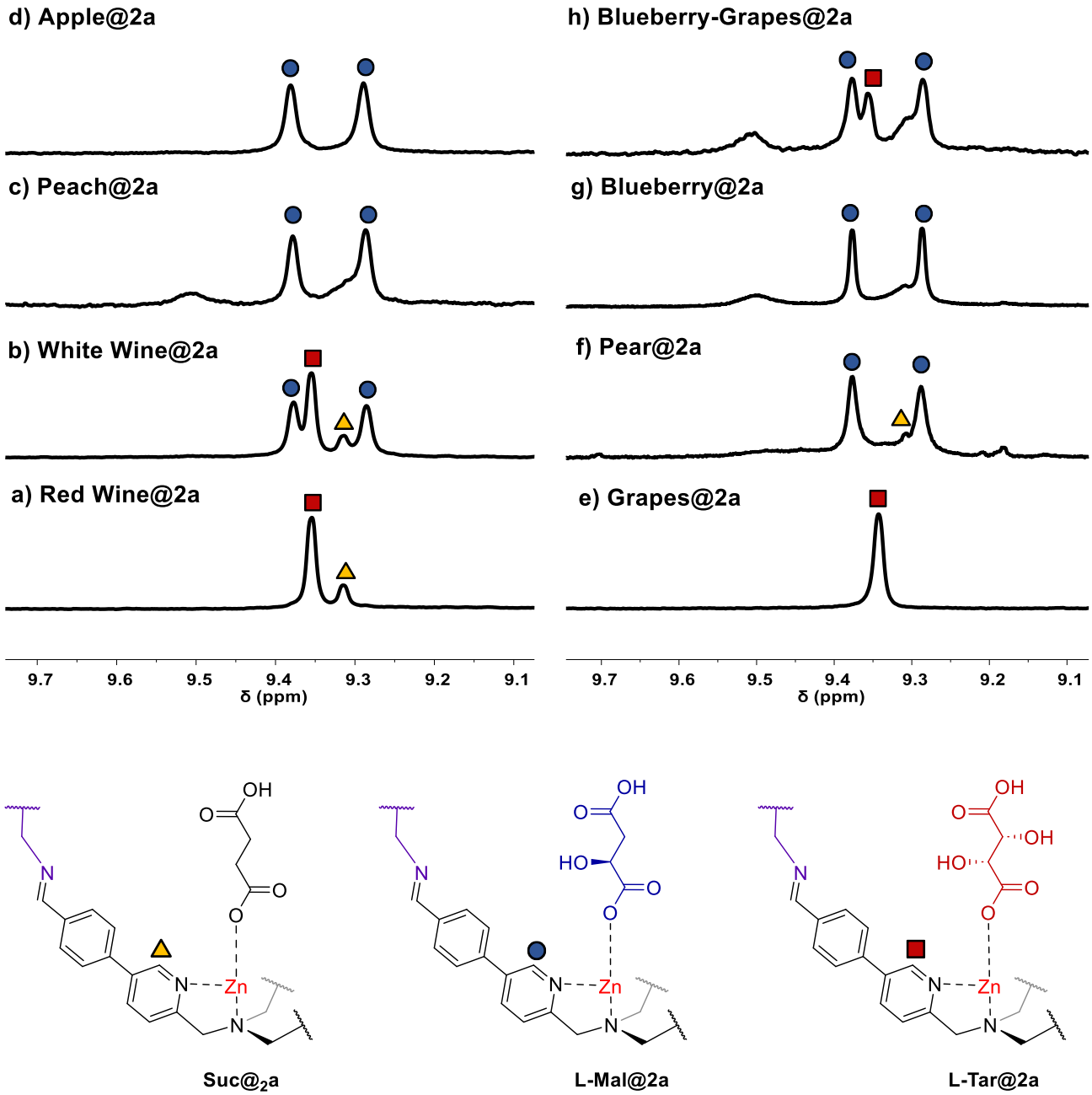

Figure 4. Partial ^{1}H-NMR spectra (400 MHz, 301 K, DMSO-d_6) of the supramolecular cage **2a** formed adding a) Chianti wine, b) Müller-Thurgau wine c) Peach juice, d) Apple juice, e) freshly squeezed Grapes juice, f) Pear juice, g) Blueberry juice, e) Blueberry-Grapes juice without pre-treatment to 500 µL DMSO-d_6 solution containing complex **1a** and ethylenediamine. Signals at 9.5 ppm and 9.33 ppm in c, g and h are ascribed to citric acid encapsulated inside the cage (Fig. S37).

1.2.3. Synthesis of a novel chiral cage

Due to the versatility of the self-assembly process, the possibility to prepare a chiral cage to be exploited as chiral solvating agents (CSA) for complex matrixes has been investigated.[34,35]

It should be highlighted that even if only **L-Mal** and **L-Tar** acids are present in natural fruits, racemic malic acid is sometime added to correct wine acidity.[36] On the other hand, only the **L-Tar** enantiomer can be added and the presence in solution of **D-Tar** is an index of infection by bacteria or adulteration.[37] The stereochemistry of these two diacids is usually monitored using HPLC or capillary electrophoresis,[38] nonetheless, the requirement of specific instrumentation and columns can made the use of ^{1}H-NMR a valuable alternative. Initial attempts for the synthesis of a chiral cage have been focused on the use of aldehyde **TPMA** complex **1a** in presence of a chiral diamine (1*R*,2*R*-(+)-diphenylethylenediamine).[39] However, even if this cage was formed using commercially available chiral diacids **L-Tar** and **L-Mal**, using wine as source of templating agent did not result in the cage assembly. For this reason, a second cage, incorporating a stereogenic element in one of the benzylic functions of the **TPMA** system, was specifically designed.

More in detail, **TPMA** metal complexes display a propeller-like arrangement of the ligand around the metal ion, and such disposition leads to the formation of two enantiomeric complexes that are characterized by a clockwise (P) or counter-clockwise (M) helicity .The inversion barrier for the racemization is low and the two enantiomeric forms are in rapid equilibrium in solution at room temperature (Figure 5).

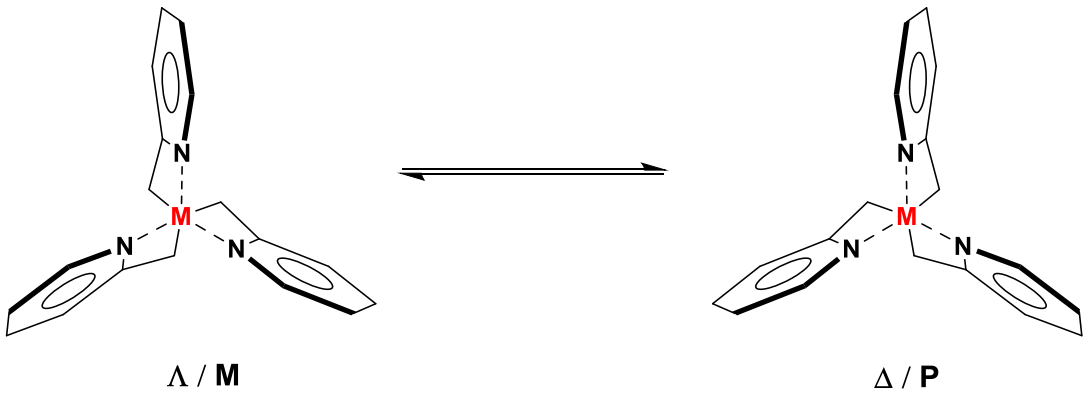

Figure 5. Λ (counterclockwise) and Δ (clockwise) conformation of **TPMA** ligands wrapped around a metal center.

Nevertheless, the group of Canary reported that the addition of a chiral methyl group in the benzylic position of one arm of the ligand leads the formation of two diastereoreomeric species upon complexation of the metal ion. The formation of two diastereoisomers could

induce a predominant propeller orientation, whose handedness is dictated by the absolute configuration of the stereocenter. Thus a *S* stereocenter induce a P (right-handed) propeller-like twist, whereas a *R* stereocenter would induce the opposite one (Figure 6). [40–42]

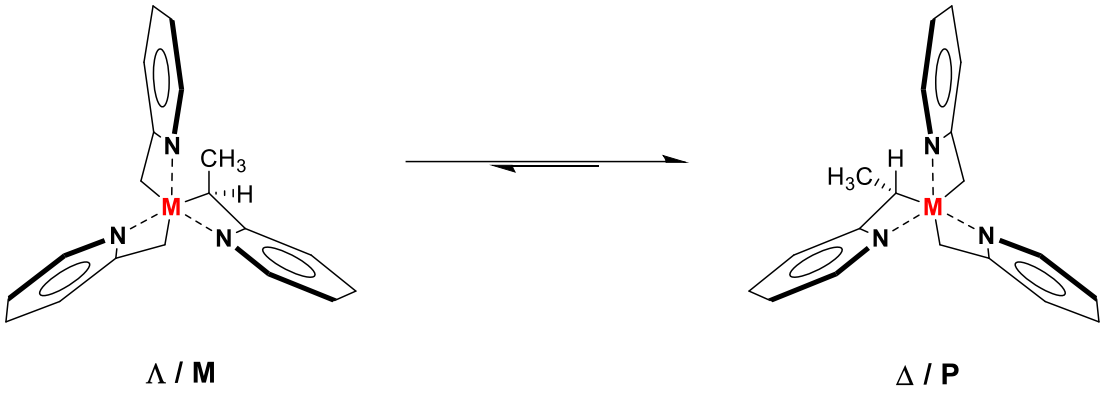

Figure 6. Chiral modified **TPMA** ligand with its relative conformational diasteromers coordinated to a generic metal ion (M). *S* stereocenter induces the preferential formation of P (right-handed) diastereoisomer.

Using a similar synthetic strategy, complex **(*R*)-1b** in which one arm of the tripodal ligand contained a defined stereogenic unit was prepared following the synthesis reported in Scheme 2 (enantiopurity assessments of **(*R*)-7** and complex **1b** are reported in Appendix 1, Section A1.10-13).

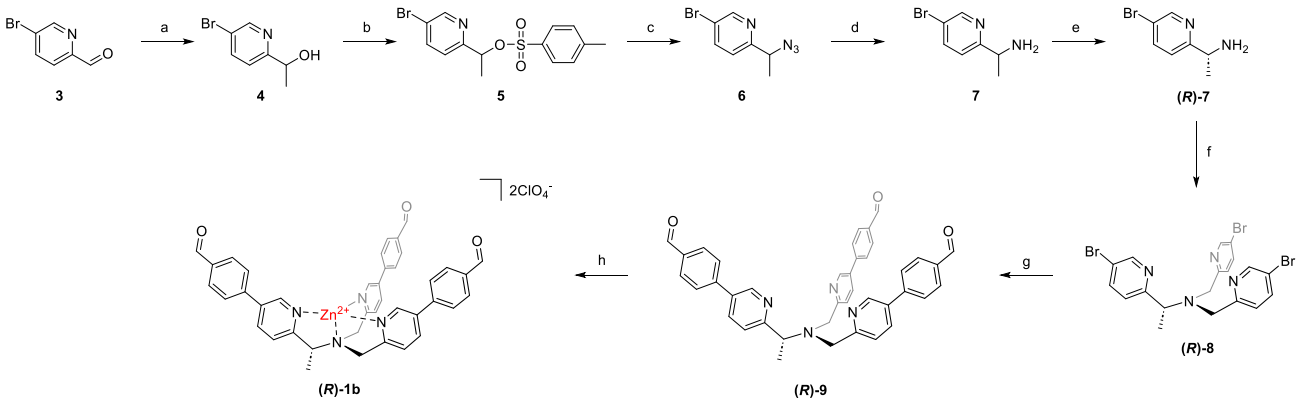

Scheme 2. Synthesis of complex **(*R*)-1b**: a) CH_3MgBr, THF dry, 0 °C, 2h, (95%), b) *p*-Toluenesulfonyl chloride, DMAP, CH_2Cl_2, 0 °C 10 min, rt 30 min (50%), c) NaN_3, DMSO, rt, 12h, (97%), d) PPh_3, H_2O, THF, r.t., 3d, (95%), e) 1. D-(-)-Tartaric acid, EtOH, 2. NaOH 2M, (41%, ee>99%), f) **3**, $NaBH(OAc)_3$, CH_2Cl_2 dry, N2, rt, 12h, (87%) g) 4-formylphenylboronic acid, $Pd(PPh_3)_4$, CsF, Toluene/H_2O/CH_3OH (1:1:0.5), N_2 , 90°C, 24 h (90%), h) 1. $Zn(ClO_4)_2$*$6H_2O$, CH_3CN, 2. Et_2O (95%, ee>90%).

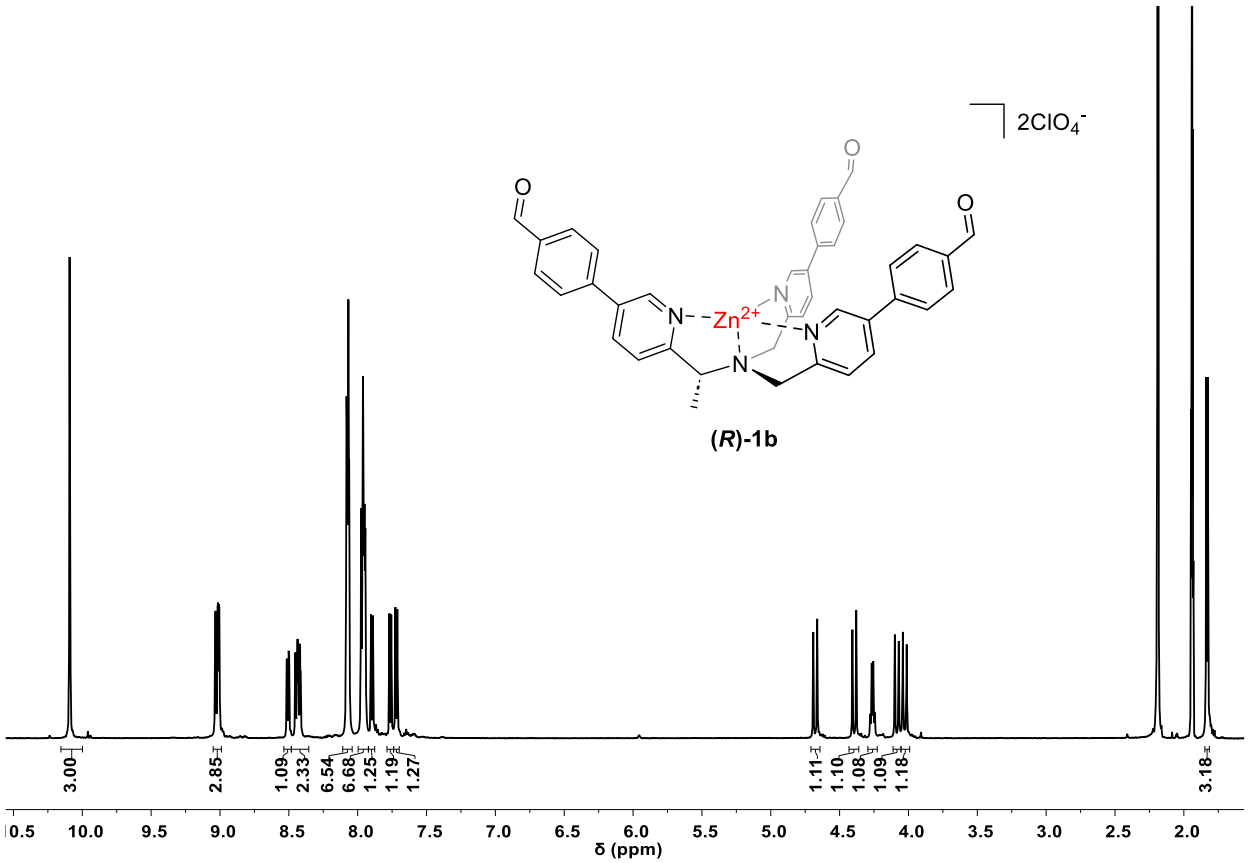

Figure 7. ^{1}H-NMR spectrum (600 MHz, 301 K, CD_3CN) of complex **(*R*)-1b**.

1.2.4. Chiral cage as Chiral Solvating Agent (CSA) in complex mixtures

With the enantiopure complex **(*R*)-1b** in hand, the chiral cage was initially assembled in DMSO-d_6 in the presence of succinic acid **Suc** as templating agent (Scheme 3) and, as confirmed by ^{1}H-NMR and ESI-HRMS characterizations, a complete conversion to the cage was observed (Figure 7).

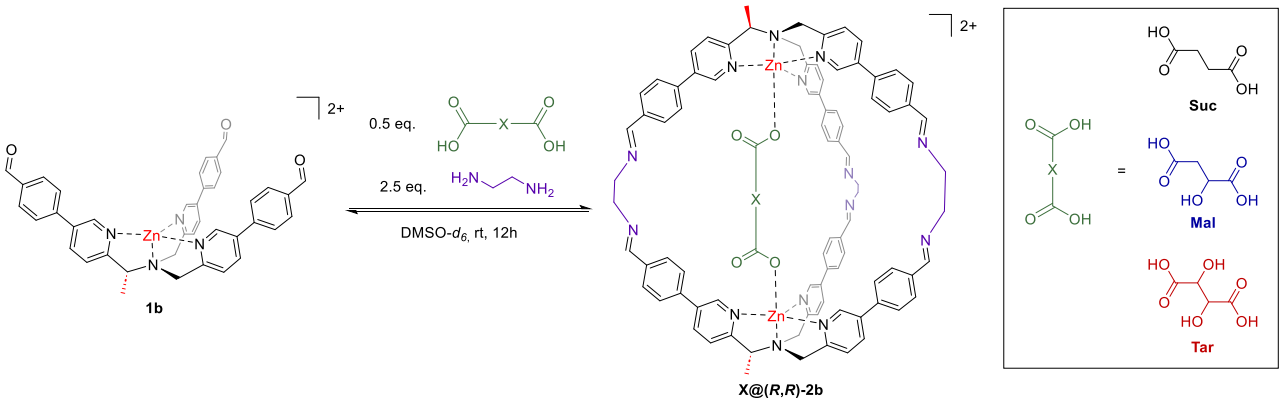

Scheme 3. Synthesis of **TPMA**-based cages **2a**. After the synthesis with commercially available pure diacids, synthesis have been performed using dicarboxylic acids present in complex mixtures. Perchlorates are removed for clarity.

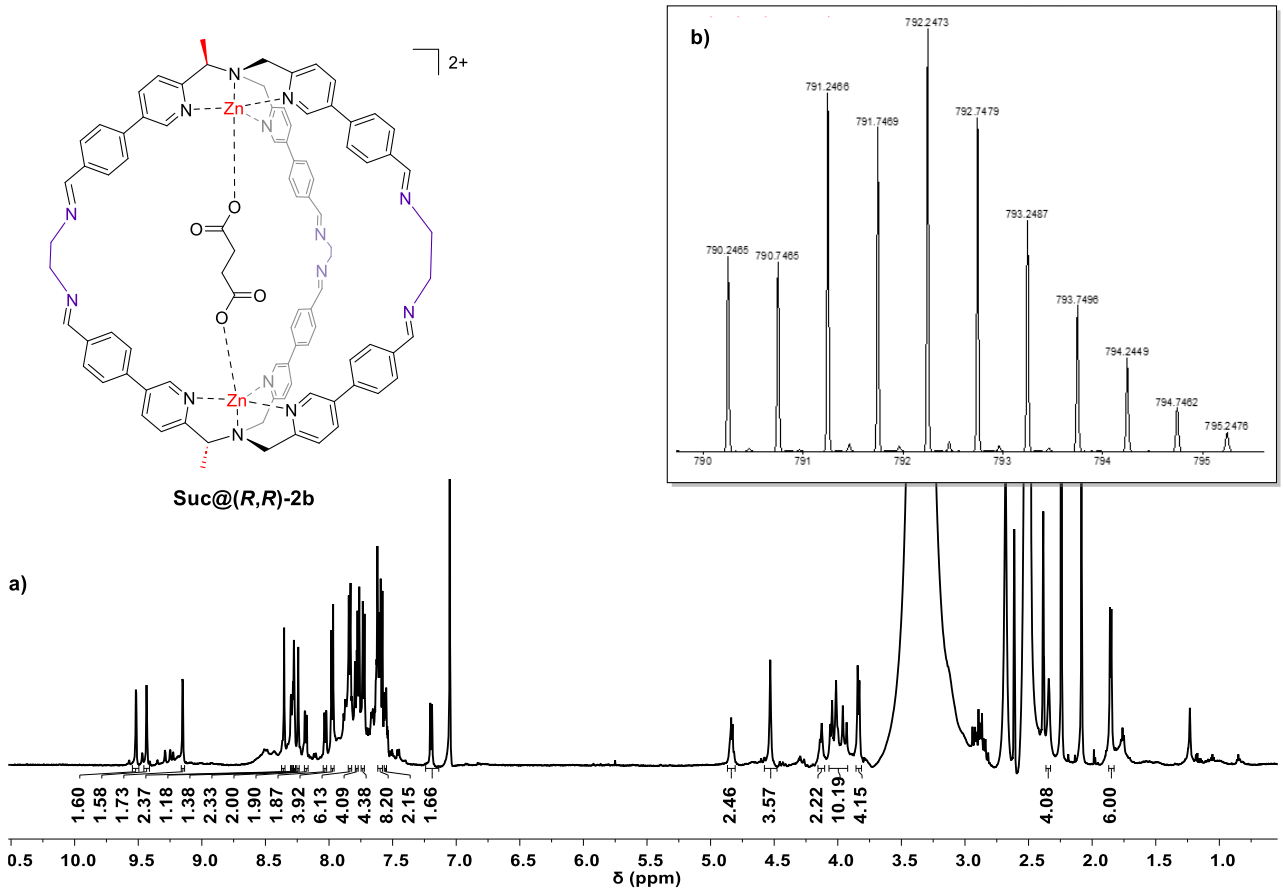

Figure 7. a) ^{1}H-NMR spectra (600 MHz, 301 K, DMSO-d_6) of the supramolecular cage **Suc@(*R*,*R*)-2b**. b) HRMS (ESI-TOF) of the cage. Perchlorates are removed for clarity.

It should be noted that, as a consequence of the presence of the methyl group only in one arm of the starting complex **(*R*)-1b**, three C_2 symmetric isomeric cages could be obtained depending on the relative orientation of the benzylic stereocenters (Appendix 1, Figure A12). Interestingly, ^{1}H-NMR reveals the preferential formation of one isomer among the three as witnessed by the number of α pyridine proton signals (Figure 8a).

The system was subsequently assembled in DMSO-d_6 using enantiopure samples of each pair of chiral **Tar** and **Mal** acids. In this case, α pyridine proton signals are sensible to the nature of the acid and to their configurations. While **Mal** acids, due to the its asymmetry, shows six different peaks for the predominant isomeric cage, in the case of C_2 symmetric **Tar** acids only three peaks are observed. More importantly, all the peaks do not overlap and it is possible to distinguish clearly among **Suc**, **L-Tar**, **L-Mal**, **D-Tar,** and **D-Mal** acids (Figure 8 and Appendix 1, Figures A38-A45).

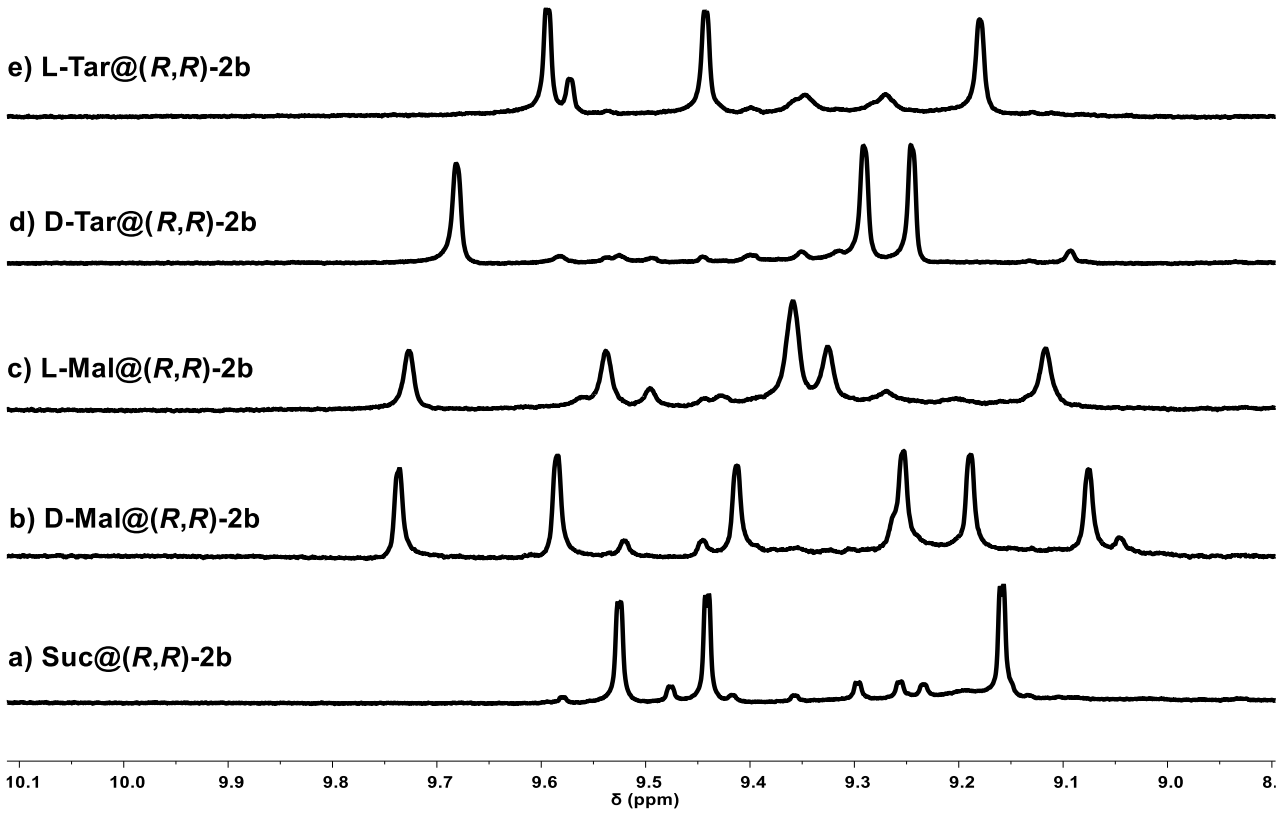

Figure. 8. Partial ^{1}H-NMR spectra (600 MHz, 301 K, DMSO-d_6) of the supramolecular cage **(*R,R*)-2b** formed adding a) **Suc** acid, b) **D-Mal** acid, c) **L-Mal** acid, d) **D-Tar** acid, e) **L-Tar** acid to the DMSO-d_6 solution containing complex **(*R*)-1b** and ethylenediamine.

Chiral cage **(*R,R*)-2b** self-assembly was subsequently attempted adding as templating agents diacids contained in wine and juices. Chiral cage **(*R,R*)-2b** assembles in all the tested complex matrixes displaying the typical pattern of the natural enantiomers **L-Tar** and **L-Mal** (Appendix 1, Figures A61-A72).

To test cage capability to sense unnatural enantiomers in the complex matrix, increasing amounts of unnatural **D-Tar** have been added to wine and used as templating agents for cage formation. As shown in Figure 9, as little as 2% e.e. of **D-Tar** was revealed at ^{1}H-NMR (Appendix 1, Section 1.15).

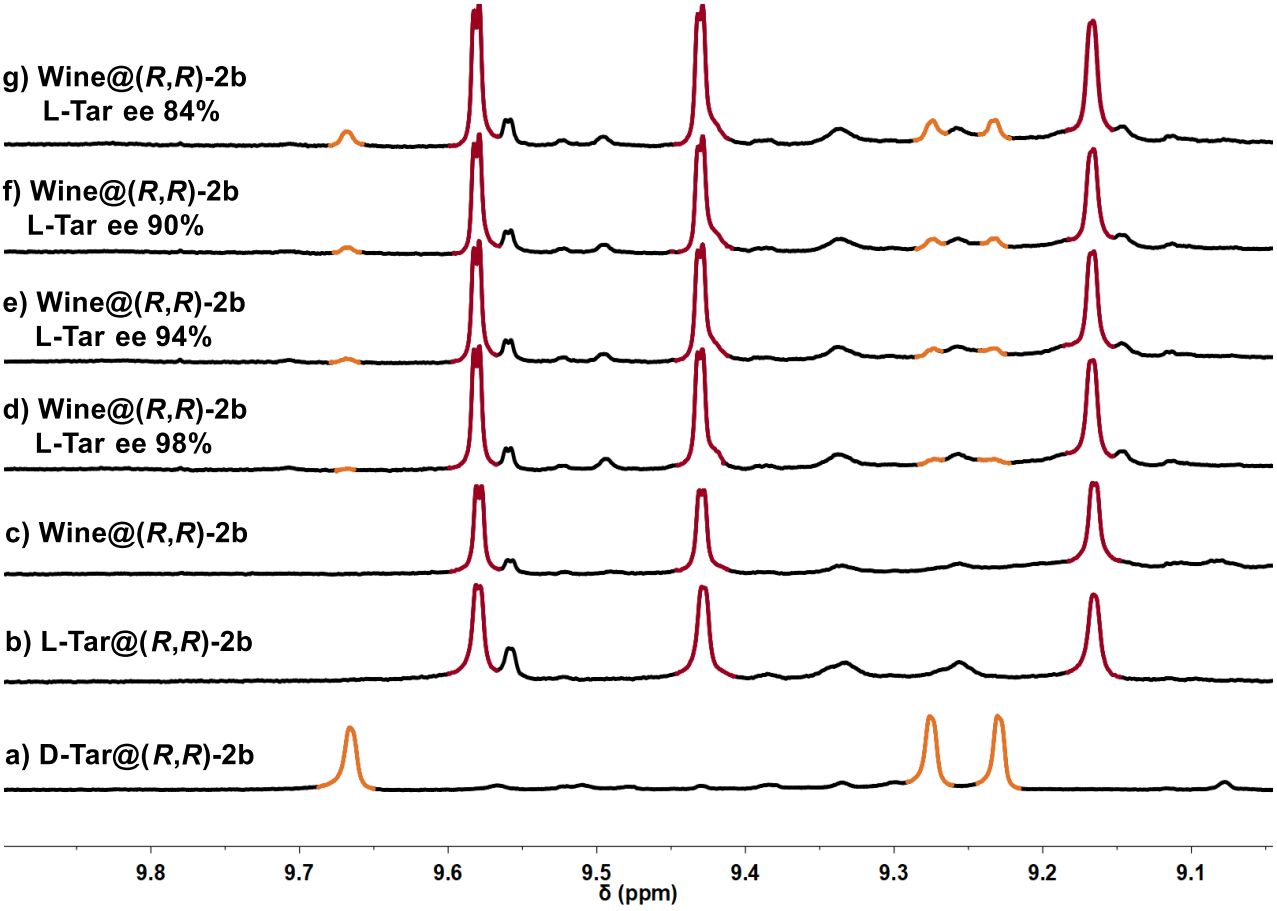

Figure 9. Partial ^{1}H-NMR spectra (600 MHz, 301 K, DMSO-d_6) of the supramolecular cage **(*R,R*)-2b** formed adding a) **D-Tar** acid, b) **L-Tar** acid, and Valpolicella wine with **L-Tar** c) pure, d) e.e. 98%, e) e.e. 94%, f) e.e. 90%, g) e.e. 84%, to the DMSO-d_6 solution containing complex **(*R*)-1b** and ethylenediamine.

1.3. Conclusions

In conclusion, two supramolecular cages able to self-assemble in presence of complex mixtures such as wine and fruit juices have been prepared. In particular, chiral cage **(*R,R*)-2b** acted as CSA for chiral dicarboxylates present in the complex mixtures differentiating enantiomers. It should be noted that even if several carboxylic acids CSAs supramolecular receptors have been developed, to the best of our knowledge systems able to differentiate among enantiomers of malic **Mal** and tartaric **Tar** acids in complex mixtures, where multiple potential analytes can bind to the recognition site, have not been reported. In particular, our system is able to exploit the selectivity typical of confined chemistry which, combined with the stability of a templated self-assembled structure, allows to overcome difficulties due to the presence of competing molecules. In addition, eventhough NMR methods, in general, are less sensitive compared with chromatographic methods, the reported results can open the possibility to have a novel dimension in the patterning typical of food chemistry.

1.4. Experimental Section

1.4.1. Synthesis of 1-(5-bromopyridin-2-yl)ethan-1-ol (4)

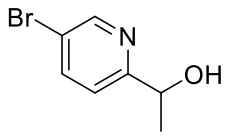

4

In a 250 mL double necked flask, 5-bromo-2-pyridinecarboxaldehyde **3** (10.00 g, 53.7 mmol) was dissolved in dry THF (180 mL) under N_2 and cooled to 0 °C. Methylmagnesium bromide (1.4 M in toluene/THF (3:1), 45.9 mL, 64.2 mmol) was added dropwise under stirring. After 2 h, the reaction mixture was diluted with EtOAc, washed with potassium phosphate buffer (1 M, pH 7), dried over $MgSO_4$ and the solvent was removed under reduced pressure. The crude product **4** was obtained as a brownish oil and used in the next step without further purifications (10.26 g, 50.8 mmol, 95%).

^{1}H NMR (300 MHz, $CDCl_3$) δ (ppm): 8.59 (d, *J* = 2.0 Hz, 1H), 7.80 (dd, *J* = 8.4, 2.3 Hz, 1H), 7.24 (d, *J* = 8.4 Hz, 1H), 4.86 (q, *J* = 6.4 Hz, 1H), 3.73 (s, 1H), 1.48 (d, *J* = 6.5 Hz, 2H).

ESI-MS (m/z): $[M+H]^+$ calcd. for $[C_7H_8BrNO+H]^+$, 202.00, found 201.93

1.4.2. Synthesis of 1-(5-bromopyridin-2-yl)ethyl 4-methylbenzenesulfonate (5)

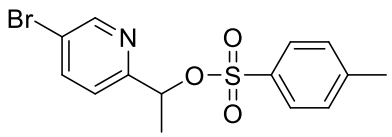

5

In a 250 mL flask, to a stirred solution of alcohol **4** (9.17 g, 45.4 mmol) and DMAP (11.09 g, 90.8 mmol) in CH_2Cl_2 (180 mL) p-toluenesulfonyl chloride (10.33 g, 54.2 mmol) was added at 0 °C. The mixture was stirred for 10 min at the same temperature and then overnight at room temperature. After 12 h, ice water was added to the reaction mixture and the mixture was extracted with CH_2Cl_2. The organic layer was washed with water and brine, dried over $MgSO_4$ and the solvent was removed under reduced pressure. The brownish oil was dissolved in CH_2Cl_2, and few milliliters of EtOH were added. The mixture was put in the fridge and after 24 h the pure product **5** was obtained as a pale brown crystalline solid that was washed with few milliliter of ice-cooled EtOH (8.10 g, 50 %).

^{1}H NMR (300 MHz, $CDCl_3$) δ (ppm): 8.50 (d, *J* = 2.4 Hz, 1H), 7.72 (dd, *J* = 8.3, 6.4 Hz, 4H), 7.29 – 7.20 (m, 4H), 5.55 (q, *J* = 6.6 Hz, 1H), 2.41 (s, 4H), 1.56 (d, *J* = 6.6, 3H).

^{13}C NMR (75 MHz, $CDCl_3$) δ (ppm): 157.35, 150.21, 144.94, 139.53, 133.95, 129.87, 127.99, 122.12, 120.21, 80.13, 21.76.

FT-IR (KBr) v (cm^{-1}): 2980, 2925, 1601, 1470, 1373, 1180, 1013.

ESI-MS (m/z): $[M+H]^+$ calcd. for $[C_{14}H_{14}BrNO_3S+H]^+$, 356.00 ; found 356.01.

1.4.3. Synthesis of 2-(1-azidoethyl)-5-bromopyridine (6)

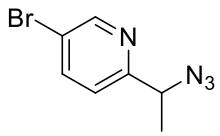

6

In a 250 mL flask, a mixture of tosylate **5** (6.95 g, 19.5 mmol) and sodium azide (5.07 g, 78.0 mmol) was stirred in DMSO (100 mL) at room temperature overnight. After the reaction was complete the mixture was diluted with 150 mL of 30% EtOAc in hexane and washed with water and brine. The organic layer was dried over $MgSO_4$ and the solvent was removed under reduced pressure. The pure product **6** was obtained as a yellow oil (4.28 g, 97%).

^{1}H NMR (300 MHz, $CDCl_3$) δ (ppm): 8.62 (d, *J* = 2.4 Hz, 1H), 7.82 (dd, *J* = 8.3, 2.4 Hz, 1H), 7.32 – 7.14 (m, 1H), 4.62 (q, *J* = 6.9 Hz, 1H), 1.57 (d, *J* = 6.9 Hz, 3H).

^{13}C NMR (75 MHz, $CDCl_3$) δ (ppm): 158.81, 150.62, 139.77, 122.06, 119.95, 61.10, 20.15.

FT-IR (CH_2Cl_2) v (cm^{-1}): 2985, 2923, 2094, 1578, 1463.

ESI-MS (m/z): $[M+H]^+$ calcd. for $[C_7H_7BrN_4+H]^+$, 227.00, found 226.94.

1.4.4. Synthesis of 1-(5-bromopyridin-2-yl)ethan-1-amine (7)

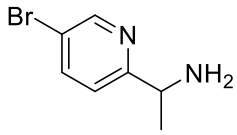

7

In a 500 mL flask, a mixture of azide **6** (4.28g, 18.8 mmol), triphenylphosphine (9.89 g, 37.7 mmol), and water (0.68 mL, 37.7 mmol), was stirred in THF at room temperature for 48 h. After that, water (0.68 mL, 37.7 mmol) was added and the reaction mixture was stirred for 24 h. The mixture was condensed under reduced pressure and the residual brown oil was distilled using a Kügelrohr apparatus, yielding the pure product **7** as a pale yellow oil (3.6 g, 95%) (bp 130 °C/0.1 mm Hg).

^{1}H NMR (300 MHz, $CDCl_3$) δ (ppm): 8.59 (d, *J* = 2.4 Hz, 1H), 7.76 (dd, *J* = 8.2, 2.3 Hz, 1H), 7.23 (d, *J* = 8.4 Hz, 1H), 4.13 (q, *J* = 6.7 Hz, 1H), 1.88 (s, 3H), 1.40 (d, *J* = 6.6 Hz, 3H).

^{13}C NMR (75 MHz, $CDCl_3$) δ (ppm): 164.41, 150.31, 139.28, 121.65, 118.70, 52.18, 24.53.

FT-IR (CH_2Cl_2) v (cm^{-1}): 3350, 3591, 2976, 2931, 1587, 1463, 1365.

ESI-MS (m/z): $[M+H]^+$ calcd. for $[C_7H_9BrN_2+H]^+$, 201.00, found 200.95

1.4.5. Synthesis of *R*-(+)-1-(5-bromopyridin-2-yl)ethan-1-amine ((*R*)-7)

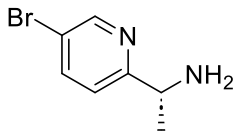

(*R*)-7

In a Schlenk apparatus, racemic 1-(5-bromopyridin-2-yl)ethan-1-amine **7** (4.10 g, 12.6 mmol) and D-(−)-tartaric acid (3.50 g, 23.3 mmol) were dissolved in 2 mL of boiling water. Then 10 mL of boiling EtOH were added to the mixture. The solution was cooled to room temperature. After 24 h, a white crystalline precipitate was observed. The supernatant was removed and the crystals washed with few milliliters of EtOH and Et_2O. Four recrystallizations of this precipitate from 8 mL of 95% EtOH gave the (−)-acid tartrate salt of *R*-(+)-amine (>99% e.e.). The salt was dissolved in 50 mL of 2 M NaOH and the solution was extracted with Et_2O. The organic layer was dried with $MgSO_4$ and concentrated under reduced pressure. The pure product (***R*)-7** was obtained as a pale yellow oil (0.85 g, 41%). The enantiomeric excess of (***R*)-7** has been reported via NMR using a reported procedure.[43]

$[\alpha]_D^{25}$ = +13.7° (c 0.02 g/mL, CH_2Cl_2)

1.4.6. Synthesis of *R*-(+)1-(5-bromopyridin-2-yl)-*N*,*N*-bis((5-bromopyridin-2-yl)methyl)ethan-1-amine ((*R*)-8)

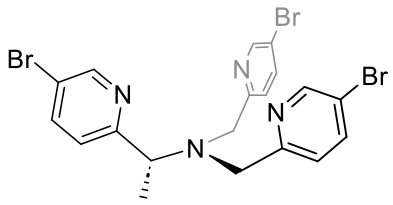

(*R*)-8

In a Schlenk apparatus, **(*R*)-7** (0.40 g, 2.2 mmol) and 5-bromo-2-pyridinecarboxaldehyde **3** (0.41 g, 2.2 mol) were dissolved in 15 mL of dry CH_2Cl_2 under N_2, and left under stirring for 1 h. Three aliquots of $NaBH(OAc)_3$ (0.15 g, 0.73 mmol) were added waiting 20 minutes between each addition. After that, 5-bromo-2-pyridinecarboxaldehyde **3** (0.41 g, 2.2 mol) was added and the mixture was left under stirring for 1 h. Three aliquots of $NaBH(OAc)_3$ (0.15 g, 0.73 mmol) were added waiting 20 minutes between each addition. After the reaction mixture was stirred for 12 h at room temperature. The solvent was removed under reduced pressure. The resulting brown oil was dissolved in EtOAc and the solution extracted with 0.1 M solution of KOH (3x25 mL). The organic phases were dried with $MgSO_4$ and the solvent was removed under reduced pressure. The crude product was chromatographed on neutral alumina (CH_2Cl_2/EtOAc = 9.5 : 0.5). The pure product (***R*)-8** was collected as a yellow oil (0.94 g, 87%).

$[\alpha]_D^{25}$ = +121.1° (c 0.02 g/mL, CH_2Cl_2)

^{1}H NMR (600 MHz, $CDCl_3$) δ (ppm): δ 8.65 (d, *J* = 2.4 Hz, 1H), 8.59 (d, *J* = 2.3 Hz, 2H), 7.80 (dd, *J* = 8.3, 2.4 Hz, 1H), 7.77 (dd, *J* = 8.3, 2.4 Hz, 2H), 4.02 (q, *J* = 6.8 Hz, 1H), 3.93 (d, *J* = 15.0 Hz, 2H), 3.72 (d, *J* = 15.0 Hz, 2H), 1.53 (d, *J* = 6.8 Hz, 3H).

^{13}C NMR (75 MHz, $CDCl_3$) δ (ppm): 160.45, 158.93, 150.24, 139.20, 138.96, 124.36, 119,36, 119.11, 59.96, 56.23, 14.91.

FT-IR (KBr) v (cm^{-1}): 2980, 2931, 2837 1573, 1468, 1362, 1084, 1007.

ESI-MS (m/z): $[M+H]^+$ calcd. for $[C_{19}H_{17}Br_3N_4+H]^+$, 538.90; found 538.93.

1.4.7. Synthesis of (*R*)-4,4'-((((1-(5-(4-formylphenyl)pyridin-2-yl)ethyl)azanediyl) bis(methylene))bis(pyridine-6,3-diyl))dibenzaldehyde ((*R*)-9)

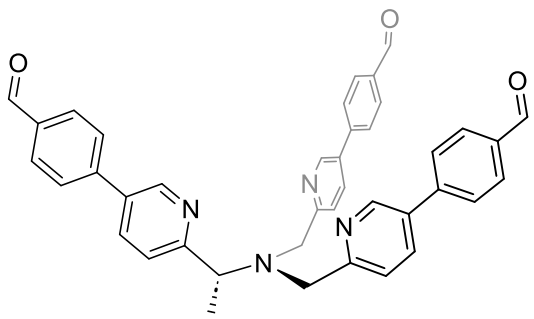

(*R*)-9

In a Schlenk apparatus, a mixture of (***R***)-**8** (0.465 g, 0.9 mmol), 4-formyphenylboronic acid (1.030 g, 6.9 mmol), $Pd(PPh_3)_4$ (0.100 g, 0.086 mmol) and CsF (1.88 g, 12.3 mmol) was dissolved in 10 mL of H_2O/toluene/CH_3OH (1:1:0.5). The mixture was stirred under N_2 for 24 h at 90 °C. The solvent was removed under reduced pressure. The resulting brown oil was dissolved in $CHCl_3$ and the solution washed with H_2O. the organic phases were dried over $MgSO_4$, filtered on Celite and the solvent was removed under reduced pressure. The resulting brown oil was precipitated by crystallization from THF/hexane to yield the product (***R***)-**9** as pale yellow solid.

$[\alpha]_D^{25}$ = +95.2° (c 0.01 g/mL, CH_2Cl_2)

^{1}H NMR (600 MHz, $CDCl_3$) δ (ppm): 10.12-10.10 (m, 3H), 8.92 (d, *J* = 2.4 Hz, 1H), 8.83 (d, *J* = 2.3 Hz, 2H), 8.03-7.99 (m, 6H), 7.96 (dd, *J* = 8.1, 2.4 Hz, 1H), 7.93 (dd, *J* = 8.1, 2.4 Hz, 2H), 7.81 – 7.72 (m, 8H), 7.70 (d, *J* = 8.1 Hz, 1H), 4.26 (q, *J* = 6.8 Hz, 1H), 4.16 (d, *J* = 15.1 Hz, 2H), 3.96 (d, *J* = 15.1 Hz, 2H), 1.70 (d, *J* = 6.8 Hz, 3H).

^{13}C NMR (75 MHz, $CDCl_3$) δ (ppm): 191.71, 161.97, 160.53, 147.60, 143.75, 135.81, 135.16, 134.92, 133.68, 130.54, 127.65, 123.08, 60.48, 56.71, 15.17.

FT-IR (KBr) v (cm^{-1}): 2977, 2934, 2827, 1701, 1600, 1211, 1172, 821.

ESI-MS (m/z): $[M+H]^+$ calcd. for $[C_{40}H_{32}N_4O_3 +H]^+$, 617.30; found 617.28.

1.4.8. Synthesis of complex (*R*)-1b

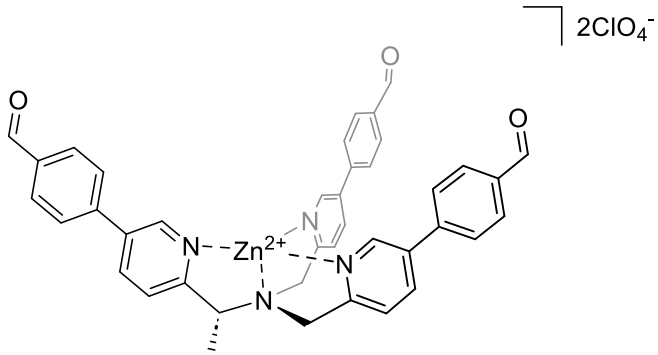

(***R***)-**1b**

To a suspension of ligand (***R***)-**9** (100 mg, 0.18 mmol) in CH_3CN (25 mL) zinc(II) perchlorate hexahydrate was added (67 mg, 0.18 mmol). The solution was stirred at room temperature for 1 h and the reaction was followed by ^{1}H-NMR and ESI-MS. At the end of the reaction Et_2O (25mL) was added, obtaining quantitatively a crystalline solid then centrifugated and dried. Complex (***R***)-**1b** resulted as pale yellow solid (154 mg, 95%).

$[\alpha]_D^{25}$ = +181.9° (c 0.01 g/mL, CH_3CN)

^{1}H NMR (600 MHz, CD_3CN) δ (ppm): δ 10.13 (m, 3H, CHO), 9.05 (d, *J* = 2.2 Hz, 1H, PyrH), 9.03 (d, *J* = 2.1 Hz, 1H, PyrH), 9.02 (d, *J* = 2.1 Hz, 1H, PyrH), 8.55 (dd, *J* = 8.4, 2.2 Hz, 1H, PyrH), 8.48 (dd, *J* = 8.3, 2.2 Hz, 1H, PyrH), 8.46 (dd, *J* = 8.2, 2.2 Hz, 1H, PyrH), 8.12-8.11 (m, 6H, ArH), 8.02 – 7.95 (m, 6H, ArH), 7.93 (d, *J* = 8.4 Hz, 1H, PyrH), 7.80 (d, *J* = 8.3 Hz, 1H, PyrH), 7.75 (d, *J* = 8.3 Hz, 1H, PyrH), 4.71 (d, *J* = 17.1 Hz, 1H, CH), 4.42 (d, *J* = 16.8 Hz, 1H, CH), 4.29 (q, *J* = 6.7 Hz, 1H, CH), 4.11 (d, *J* = 17.1 Hz, 1H, CH), 4.05 (d, *J* = 16.8 Hz, 1H, CH), 1.86 (d, *J* = 6.8 Hz, 3H, CH_3).

^{13}C NMR (151 MHz, CD_3CN) δ (ppm) 193.21, 159.00, 156.02, 155.84, 147.92, 147.81, 141.85, 141.71, 141.49, 138.05, 138.01, 137.85, 137.80, 137.77, 131.35, 129.24, 129.19, 126.41, 126.25, 125.41, 60.16, 55.41, 53.00, 12.47.

ESI-MS (m/z): $[M+Cl]^+$ calcd. for $[C_{40}H_{32}N_4O_3Zn+Cl]^+$, 715.15; found 715.25.

1.4.9. Synthesis of tris((5-bromopyridin-2-yl)methyl)amine 10

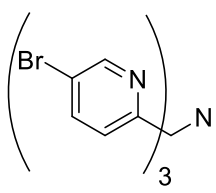

10

Compound **10** has been synthesized according to literature.[30].In a 250 ml double neck flask, anhydrous NH_4OAc (1.38 g, 17.9 mmol) and 5-bromo-2-pyridinecarboxaldehyde **3** (10.00 g, 53.7 mmol) were dissolved in dry CH_2Cl_2 (170 ml) under N_2 atmosphere and left under stirring for 1 h. Three aliquots of $NaBH(OAc)_3$ (3.80 g, 17.9 mmol) were added waiting one hour

each addition. After that the reaction was stirred for 12 h at room temperature. The solvent was removed under reduced pressure. The resulting white solid was dissolved in ethyl acetate and the solution extracted with 0.1 M solution of KOH (3x100 ml). the organic phases were dried on anhydrous $MgSO_4$ and the solvent was removed under reduced pressure. The resulting solid was precipitated by crystallization from THF/hexane to yield product **10** as a white solid (7.43 g, 79%).

^{1}H NMR (200 MHz, CDCl3) δ (ppm): 8.60 (d, 3H, *J* = 2.0 Hz, ArH), 7.78 (dd, 3H, *J* = 2.0 Hz, *J* = 8.0 Hz, ArH), 7.41 (d, 3H, *J* = 8.0 Hz, ArH), 3.81 (s, 6H, CH_2).

1.4.10. Synthesis of 4,4',4''-((nitrilotris(methylene))tris(pyridine-6,3-diyl))tribenzaldehyde 11

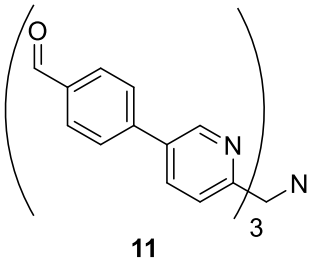

11

Compound **11** has been synthesized according to literature.[30] A mixture of **10** (3.00 g, 5.69 mmol), 4-formylphenylboronic acid (3.84 g, 25.6 mmol), $Pd(PPh_3)_4$ (65 mg, 0,0057 mmol, 1 mol%) and K_2CO_3 (5.51 g, 39.8 mmol) was dissolved in 60 ml of H_2O/toluene/CH_3OH (1:1:0.5). The mixture was stirred under N_2 for 48 h at 100°C. The solvent was removed under reduced pressure. The resulting yellow oil was dissolved in $CHCl_3$ and the solution extracted with H_2O (3x50 mL). The organic phases were dried on anhydrous $MgSO_4$, filtered on celite and then the solvent was removed under reduced pressure. The resulting solid was precipitated by crystallization from THF/hexane to yield product **1** as a pale-yellow solid (2.89 g, 82%).

^{1}H NMR (200 MHz, $CDCl_3$) δ (ppm): 10.11 (s, 3H, CHO), 8.89 (d, 3H, *J* = 2.0 Hz, PyrH), 8.02 (dd, 3H, *J* = 8.0 Hz, *J*= 2.0 Hz, PyrH), 7.97 (d, 6H, *J* = 8.25 Hz, ArH), 7.83 (d, 6H, *J* = 8.25 Hz, ArH), 7.72 (d, 3H, *J* = 8.0 Hz, PyrH), 4.09 (s, 6H, CH_2).

1.4.11. Synthesis of complex 1a

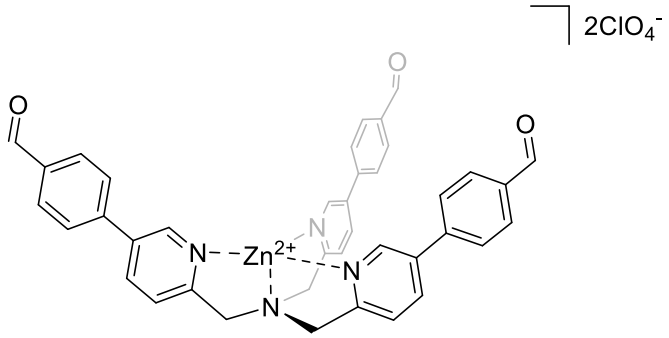

1a

Compound **1a** has been synthesized according to literature.[30] To a suspension of ligand **11** (100 mg, 0.017 mmol) in acetonitrile (15 ml) zinc (II) perchlorate hexahydrate was added (62 mg, 0.17 mmol) . The solution was stirred at room temperature for 1 h and the reaction was followed by ^{1}H NMR and ESI-MS. At the end of the reaction diethyl ether (25 ml) was added obtaining quantitatively a crystalline solid then centrifuged and dried. Complex **1a** results as a pale-yellow solid (128 mg, 90%).

^{1}H NMR (300 MHz, CD_3CN) δ (ppm): 10.09 (s, 3H, CHO), 8.82 (d, 3H, *J*= 2.0 Hz, PyrH), 8.44 (dd, 3H, *J*=8.0 Hz, *J*=2.0 Hz PyrH), 8.07 (d, 6H, *J*=8.0 Hz, ArH), 7.94 (d, 6H, *J*=8.0 Hz, ArH), 7.75 (d, 3H, *J*=8.0 Hz, PyrH), 4.40 (s, 6H,CH_2)

1.4.12. Synthesis of Cages X@2a and X@(*R*,*R*)-2b.

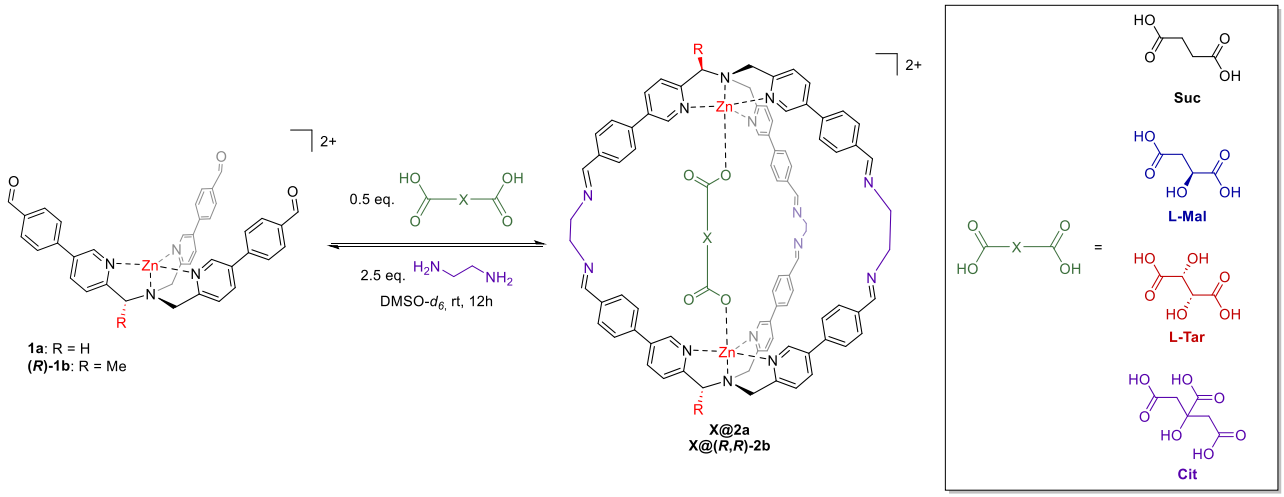

General procedure for the synthesis of molecular cages **X@2a** and **X@(*R*,*R*)-2b**. Perchlorate counterions are removed for clarity. Citric acid **Cit** has been employed as guest only in the presence of complex **1a**.

To 500 µL (1.0 µmol) of a solution 0.002 M of complex **1a** or **(*R*)-1b** in DMSO-d_6, 50 µL (0.5 µmol, with 2 eq. of triethylamine) of a solution 0.01 M in DMSO-d_6 of a dicarboxylic acid **X** and 125 µL (2.5 µmol) of a solution 0.02 M in DMSO-d_6 of ethylenediamine were added in a NMR tube. The mixture was left for 12 h at room temperature and checked *via* ^{1}H-NMR and ESI-MS. The yield for all the cages is >95% (Determined *via* ^{1}H-NMR based on internal standard *p*-xylene).

1.4.12.1. L-Tar@2a

^{1}H-NMR (600 MHz, DMSO-d_6) δ (ppm): 9.37 (s, 6H, PyrH), 8.23 (s, 6H, NH_{imm}), 8.16 (d, J = 7.5 Hz, 6H, PyrH), 7.85 (d, J = 7.8 Hz, 12H, ArH), 7.70 (d, J = 7.4 Hz, 12H, ArH), 7.50 – 7.48 (m, 6H, PyrH), 4.98 (d, J = 4.8 Hz, 2H, OH_{TAR}), 4.83 (d, J = 4.8 Hz, 2H, CH_{TAR}), 4.48 – 4.38 (m, 12H, CH_2-TPMA), 3.98 – 3.85 (m, 12H, CH_2-EDA).
HRMS (ESI-TOF) (*m/z*): [M^{2+}] calcd. for $[C_{88}H_{76}N_{14}O_6Zn_2]^{2+}$,776.2322 ; found 776.2319.

1.4.12.2. L-Mal@2a

^{1}H-NMR (600 MHz, DMSO-d_6) δ (ppm): 9.39 – 9.30 (m, 6H, PyrH), 8.28 – 8.26 (m, 6H, NH_{imm}), 8.18 – 8.13 (m, 6H, PyrH), 7.85 (d, J = 7.8 Hz, 12H, ArH), 7.66 – 7.63 (m, 12H, ArH), 7.53 – 7.49 (m, 6H, PyrH), 4.92 – 4.90 (m, 2H, OH_{MAL} – CH_{MAL}), 4.46 – 4.43 (m, 12H, CH_2-TPMA), 3.95 – 3.91 (m, 12H, CH_2-EDA), 2.84 – 2.79 (m, 2H, CH_2-MAL).

HRMS (ESI-TOF) (*m/z*): [M^{2+}] calcd. for [$C_{88}H_{76}N_{14}O_5Zn_2]^{2+}$, 768.2347; found 768.2348.

1.4.12.3. Suc@2a

^{1}H-NMR (600 MHz, DMSO-d_6) δ (ppm): 9.34 (s, 6H, PyrH), 8.29 (s, 6H, NH_{imm}), 8.16 (d, J = 8.1 Hz, 6H, PyrH), 7.85 (d, J = 8.4 Hz, 12H, ArH), 7.64 (d, 12H, J = 8.3 Hz, ArH), 7.51 (d, 6H, J = 8.2 Hz, PyrH), 4.45 (s, 12H, $CH_{2\text{-}TPMA}$), 3.96 (s, 12H, $CH_{2\text{-}EDA}$), 2.87 (s, 4H, $CH_{2\text{-}SUC}$).
HRMS (ESI-TOF) (*m/z*): [M^{2+}] calcd. for [$C_{88}H_{76}N_{14}O_4Zn_2]^{2+}$, 760.2373; found 760.2349.

1.4.12.4. Cit@2a

^{1}H-NMR (600 MHz, DMSO-d_6) δ (ppm): 9.50 – 9.34 (m, 6H, PyrH), 8.31 – 8.23 (m, 12H, NH_{imm}+ PyrH), 7.82 – 7.71 (m, 26H, ArH+PyrH), 7.51 (s, 4H, PyrH), 4.46 (s, 12H, $CH_{2\text{-}TPMA}$), 4.01 – 3.82 (m, 12H, $CH_{2\text{-}EDA}$), ($CH_{2\text{-}CIT}$, 4H, hidden by solvent).
HRMS (ESI-TOF) (*m/z*): [M^{2+}] calcd. for [$C_{90}H_{78}N_{14}O_7Zn_2]^{2+}$, 797.2374; found 797.2391.

1.4.12.5. L-Tar@(*R*,*R*)-2b

^{1}H NMR (600 MHz, DMSO-d_6) δ 9.59 – 9.17 (m, 6H, PyrH), 8.35 (d, *J* = 8.3 Hz, 2H, PyrH), 8.31 – 8.16 (m, 8H, NH_{imm}+PyrH), 8.01 – 7.99 (m, 4H, ArH+PyrH), 7.88 – 7.53 (m, 26H, ArH+PyrH), 7.09 (d, *J* = 8.2 Hz, 2H, PyrH), 5.03 (d, *J* = 4.6 Hz, 2H, OH_{TAR}), 4.99 – 4.92 (m, 2H, CH_{TPMA}), 4.90 (d, *J* = 4.6 Hz, 2H, CH_{TAR}), 4.62 – 4.58 (m, 2H, $CH_{2\text{-}TPMA}$), 4.52 – 4.47 (m, 2H, $CH_{2\text{-}TPMA}$), 4.24 – 4.13 (m, 4H, $CH_{2\text{-}TPMA}$), 3.96 – 3.87 (m, 4H, $CH_{2\text{-}EDA}$), 3.68 – 3.64 (m, 8H, $CH_{2\text{-}EDA}$), 1.84 (d, *J* = 6.6 Hz, 6H, $CH_{3\text{-}TPMA}$).
HRMS (ESI-TOF) (*m/z*): [M^{2+}] calcd. for [$C_{90}H_{80}N_{14}O_6Zn_2]^{2+}$, 790.2479; found 790.2465.

1.4.12.6. D-Tar@(*R*,*R*)-2b

^{1}H NMR (600 MHz, DMSO-d_6) δ 9.67 – 9.24 (m, 6H, PyrH), 8.29 – 8.19 (m, 12H, NH_{imm}+PyrH), 8.03 – 8.00 (m, 6H, NH_{imm}+PyrH), 7.85 – 7.80 (m, 8H, ArH+PyrH), 7.77 – 7.73 (m, 4H, ArH+PyrH), 7.64 – 7.54 (m, 10H, ArH+PyrH), 7.15 (d, *J* = 8.3 Hz, 2H), 4.94 – 4.92 (m, 4H, CH_{TPMA}+OH_{TAR}), 4.69 (d, *J* = 6.0 Hz, 2H, CH_{TAR}), 4.94 – 4.92 (m, 4H, $CH_{2\text{-}TPMA}$), 4.13 – 3.82 (m, 16H, $CH_{2\text{-}TPMA}$+$CH_{2\text{-}EDA}$), 1.85 (d, *J* = 6.8 Hz, 6H, $CH_{3\text{-}TPMA}$).
HRMS (ESI-TOF) (*m/z*): [M^{2+}] calcd. for [$C_{90}H_{80}N_{14}O_5Zn_2]^{2+}$, 790.2479; found 790.2465.

1.4.12.7. L-Mal@(*R*,*R*)-2b

^{1}H NMR (600 MHz, DMSO-d_6) δ 9.72 – 9.11 (m, 6H, PyrH), 8.39 – 8.12 (m, 9H, NH_{imm}+PyrH), 8.07 – 7.96 (m, 5H, PyrH), 7.89 – 7.56 (m, 26H, ArH+PyrH), 7.20 – 7.12 (m, 2H, PyrH), 4.97 – 4.86 (m, 6H, CH_{MAL}+OH_{MAL}+ CH-$_{TPMA}$), 4.56 – 4.52 (m, 4H, CH_2-$_{TPMA}$), 4.16 – 4.14 (m, 2H, CH_2-$_{TPMA}$), 4.03 – 3.77 (m, 12H, CH_2-$_{EDA}$), , 1.87 – 1.84 (m, 6H, CH_3-$_{TPMA}$), (CH_2-$_{MAL}$, 2H, hidden by solvent).
HRMS (ESI-TOF) (*m/z*): [M^{2+}] calcd. for [$C_{90}H_{80}N_{14}O_5Zn_2$]$^{2+}$, 782.2504; found 782.2457.

1.4.12.8. D-Mal@(*R*,*R*)-2b

^{1}H NMR (600 MHz, DMSO-d_6) δ 9.73 – 9.07 (m, 6H, PyrH), 8.36 – 8.15 (m, 8H, NH_{imm}+PyrH), 8.06 – 7.54 (m, 32H, ArH+PyrH), 7.18 – 7.12 (m, 2H, PyrH), 4.96 – 4.84 (m, 5H, CH_{MAL}+OH_{MAL}+CH-$_{TPMA}$), 4.57 – 4.50 (m, 4H, CH_2-$_{TPMA}$), 4.18 – 4.16 (m, 2H, CH_2-$_{TPMA}$), 4.08 – 3.75 (m, 13H, CH_2-$_{TPMA}$+CH_2-$_{EDA}$), , 1.86 – 1.83 (m, 6H, CH_3-$_{TPMA}$), (CH_2-$_{MAL}$, 2H, hidden by solvent).
HRMS (ESI-TOF) (*m/z*): [M^{2+}] calcd. for [$C_{90}H_{80}N_{14}O_6Zn_2$]$^{2+}$, 782.2504; found 782.2457.

1.4.12.9. Suc@(*R*,*R*)-2b

^{1}H NMR (600 MHz, DMSO-d_6) δ 9.53 – 9.15 (m, 6H, PyrH), 8.35 (s, 2H, NH_{imm}), 8.30 – 8.28 (m, 4H, NH_{imm}+PyrH), 8.24 (s, 2H, NH_{imm}), 8.19 – 8.17 (m, 2H, PyrH), 8.04 – 8.02 (m, 2H, PyrH), 7.97 (d, *J* = 8.3 Hz, 4H, ArH), 7.84 – 7.71 (m, 14H, ArH+PyrH), 7.62 – 7.58 (m, 8H, ArH+PyrH), 7.57 – 7.54 (m, 2H, PyrH), 7.20 (d, *J* = 8.3 Hz, 2H, PyrHf), 4.85 – 4.82 (m, 2H, CH-$_{TPMA}$), 4.53 (s, 4H, CH_2-$_{TPMA}$), 4.15 – 4.13 (m, 2H, CH_2-$_{TPMA}$), 4.06 – 3.93 (m, 10H, CH_2-$_{TPMA}$+CH_2-$_{EDA}$), 3.84 – 3.83 (m, 4H, CH_2-$_{EDA}$), 2.34 (s, 4H, CH_2-$_{SUC}$), 1.85 (d, *J* = 6.7 Hz, 6H, CH_3-$_{TPMA}$).
HRMS (ESI-TOF) (*m/z*): [M^{2+}] calcd. for [$C_{90}H_{80}N_{14}O_4Zn_2$]$^{2+}$, 774.2529; found 774.2508.

1.4.13. Synthesis of Cages in the presence of complex mixtures

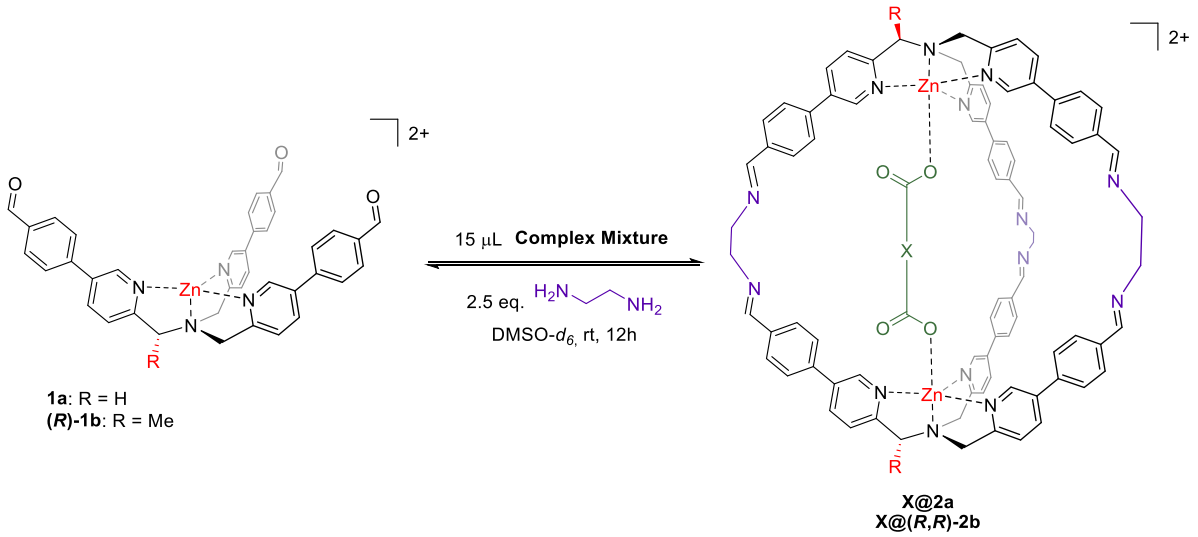

General procedure for the synthesis of molecular cages **X@2a** and **X@(*R*,*R*)-2b**. Perchlorate counterions are removed for clarity.

To 500 µL (1.0 µmol) of a solution 0.002 M of complex **1a** or **(*R*)-1b** in DMSO-d_6, 15 µL of Complex mixture without pre-treatment and 125 µL (2.5 µmol) of a solution 0.02 M in DMSO-d_6 of ethylenediamine were added in a NMR tube. The mixture was left for 12 h at room temperature and checked *via* ^{1}H-NMR and ESI-MS. The concentration of **L-Tar@2a**, **L-Mal@2a**, and **L-Suc@2a** was determined *via* ^{1}H-NMR based on internal standard *p*-xylene, Table A1).

1.5. References

[1] D. Fujita, Y. Ueda, S. Sato, H. Yokoyama, N. Mizuno, T. Kumasaka, M. Fujita, *Chem* **2016**, *1*, 91–101.
[2] R. S. Forgan, J. P. Sauvage, J. F. Stoddart, *Chem. Rev.* **2011**, *111*, 5434–5464.
[3] D. A. Leigh, J. J. Danon, S. D. P. Fielden, J. F. Lemonnier, G. F. S. Whitehead, S. L. Woltering, *Nat. Chem.* **2021**, *13*, 117–122.
[4] S. Pullen, J. Tessarolo, G. H. Clever, *Chem. Sci.* **2021**, *12*, 7269–7293.
[5] E. O. Bobylev, D. A. P. III, B. de Bruin, J. N. H. Reek, *Chem. Sci.* **2021**, *12*, 7696–7705.
[6] A. Brzechwa-Chodzyńska, W. Drożdż, J. Harrowfield, A. R. Stefankiewicz, *Coord. Chem. Rev.* **2021**, *434*, 213820.
[7] P. T. Corbett, J. Leclaire, L. Vial, K. R. West, J. L. Wietor, J. K. M. Sanders, S. Otto, *Chem. Rev.* **2006**, *106*, 3652–3711.
[8] M. Liu, M. A. Little, K. E. Jelfs, J. T. A. Jones, M. Schmidtmann, S. Y. Chong, T. Hasell, A. I. Cooper, *J. Am. Chem. Soc.* **2014**, *136*, 7583–7586.
[9] D. A. Roberts, B. S. Pilgrim, J. D. Cooper, T. K. Ronson, S. Zarra, J. R. Nitschke, *J. Am. Chem. Soc.* **2015**, *137*, 10068–10071.
[10] M. W. Schneider, I. M. Oppel, M. Mastalerz, *Chem. Eur. J.* **2012**, *18*, 4156–4160.
[11] P. Skowronek, B. Warżajtis, U. Rychlewska, J. Gawroński, *Chem. Commun.* **2013**, *49*, 2524–2526.
[12] S. Zarra, D. M. Wood, D. A. Roberts, J. R. Nitschke, *Chem. Soc. Rev.* **2015**, *44*, 419–432.
[13] A. J. McConnell, C. S. Wood, P. P. Neelakandan, J. R. Nitschke, *Chem. Rev.* **2015**, *115*, 7729–7793.
[14] P. Ballester, *Chem. Soc. Rev.* **2010**, *39*, 3810–3830.
[15] G. Zhang, M. Mastalerz, *Chem. Soc. Rev.* **2014**, *43*, 1934–1947.
[16] S. M. Jansze, G. Cecot, K. Severin, *Chem. Sci.* **2018**, *9*, 4253–4257.
[17] C. Givelet, J. Sun, D. Xu, T. J. Emge, A. Dhokte, R. Warmuth, *Chem. Commun.* **2011**, *47*, 4511–4513.
[18] Z. Lin, J. Sun, B. Efremovska, R. Warmuth, *Chem. - A Eur. J.* **2012**, *18*, 12864–12872.
[19] Y. Lei, Q. Chen, P. Liu, L. Wang, H. Wang, B. Li, X. Lu, Z. Chen, Y. Pan, F. Huang, H. Li, *Angew. Chem. Int. Ed.* **2021**, *60*, 4705–4711.
[20] S. Hong, M. R. Rohman, J. Jia, Y. Kim, D. Moon, Y. Kim, Y. H. Ko, E. Lee, K. Kim, *Angew. Chem. Int. Ed.* **2015**, *54*, 13241–13244.
[21] A. R. Stefankiewicz, M. R. Sambrook, J. K. M. Sanders, *Chem. Sci.* **2012**, *3*, 2326–2329.
[22] J. Sessler, *Supramol. Chem.* **2018**, *30*, 655–657.
[23] P. Rios, T. S. Carter, T. J. Mooibroek, M. P. Crump, M. Lisbjerg, M. Pittelkow, N. T. Supekar, G.-J. Boons, A. P. Davis, *Angew. Chem. Int. Ed.* **2016**, *55*, 3387–3392.
[24] M. Yamashina, M. Akita, T. Hasegawa, S. Hayashi, M. Yoshizawa, *Sci. Adv.* **2017**, *3*, e1701126.
[25] S. Kusaba, M. Yamashina, M. Akita, T. Kikuchi, M. Yoshizawa, *Angew. Chem. Int. Ed.* **2018**, *57*, 3706–3710.
[26] A. J. Plajer, E. G. Percástegui, M. Santella, F. J. Rizzuto, Q. Gan, B. W. Laursen, J. R. Nitschke, *Angew. Chem. Int. Ed.* **2019**, *58*, 4200–4204.
[27] M. Yamashina, T. Tsutsui, Y. Sei, M. Akita, M. Yoshizawa, *Sci. Adv.* **2019**, *5*, eaav3179.
[28] S. M. Butler, K. A. Jolliffe, *Org. Biomol. Chem.* **2020**, *18*, 8236–8254.
[29] S. N. Berry, L. Qin, W. Lewis, K. A. Jolliffe, *Chem. Sci.* **2020**, *11*, 7015–7022.
[30] C. Bravin, E. Badetti, F. A. Scaramuzzo, G. Licini, C. Zonta, *J. Am. Chem. Soc.* **2017**, *139*, 6456–6460.
[31] C. Bravin, E. Badetti, R. Puttreddy, F. Pan, K. Rissanen, G. Licini, C. Zonta, *Chem. Eur. J.* **2018**, *24*, 2936–2943.
[32] G. W. A. Fowles, *J. Wine Res.* **1992**, *3*, 25–41.
[33] J. Robinson, J. Harding, *The Oxford Companion to Wine, Third Edition*, Oxford University Press, **2014**.
[34] D. Parker, *Chem. Rev* **1991**, *91*, 1441–1457.
[35] T. J. Wenzel, J. D. Wilcox, *Chirality* **2003**, *15*, 256–270.
[36] S. Kodama, A. Yamamoto, A. Matsunaga, K. Mayakawa, *Electrophoresis* **2003**, *24*, 2711–2715.
[37] R. Knob, J. Petr, J. Ševčík, V. Maier, *J. Sep. Sci.* **2013**, *36*, 3426–3431.
[38] S. Kodama, A. Yamamoto, A. Matsunaga, Soga Tomoyoshi, Hayakawa Kazuichi, *Electrophoresis* **2001**, *22*, 3286–3290.
[39] C. Bravin, G. Mason, G. Licini, C. Zonta, *J. Am. Chem. Soc.* **2019**, *141*, 11963–11969.
[40] J. W. Canary, C. S. Allen, J. M. Castagnetto, Y. Wang, *J. Am. Chem. Soc.* **1995**, *117*, 8484–8485.
[41] J. W. Canary, S. Mortezaei, J. Liang, *Coord. Chem. Rev.* **2010**, *254*, 2249–2266.
[42] C. Bravin, E. Badetti, G. Licini, C. Zonta, *Coord. Chem. Rev.* **2021**, *427*, DOI 10.1016/j.ccr.2020.213558.
[43] Y. Pérez-Fuertes, A. M. Kelly, A. L. Johnson, S. Arimori, S. D. Bull, T. D. James, *Org. Lett.* **2006**, *8*, 609–612.

Chapter 2

Chiroptical Enhancement of Chiral Dicarboxylic Acids from Confinement in a Stereodynamic Supramolecular Cage

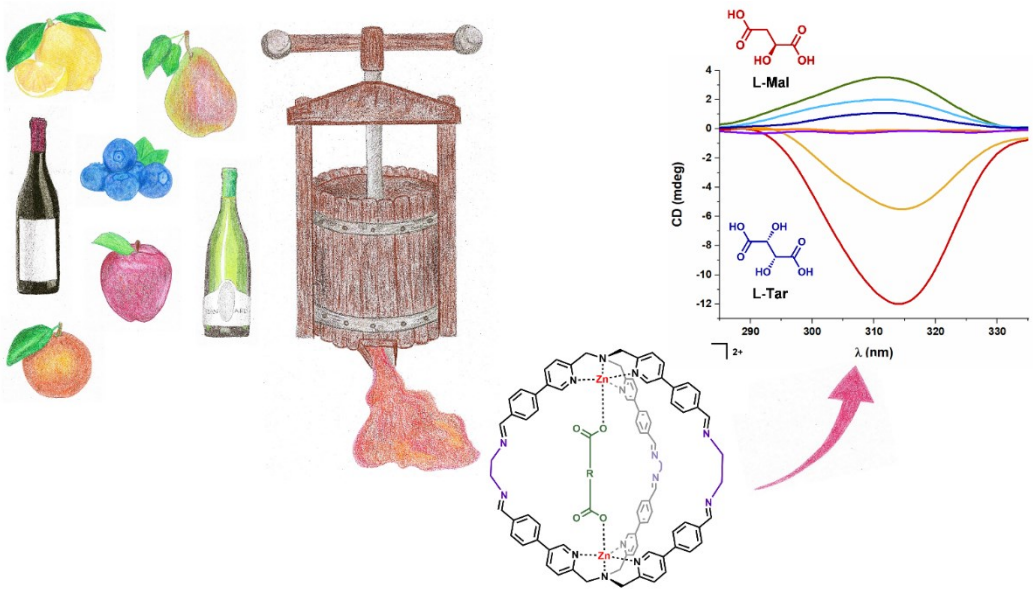

ABSTRACT The fundamental implications that chirality has in science and technology require continuous efforts for the development of fast, economic and reliable quantitative methods for enantiopurity assessment. Among the different analytical approaches, chiroptical techniques in combination with supramolecular methodologies have shown promising results in terms of both costs and time analysis. In this chapter, the capability of a tris(2-pyridylmethyl)amines (**TPMA**)-based supramolecular cage to amplify the Circular Dichroism (CD) signal of a series of chiral dicarboxylic acids also in the presence of a complex mixture has been presented. This feature has been used to quantify tartaric acid in wines and to discriminate different matrixes using Principal Component Analysis (PCA) of the raw CD data.

2.1. Introduction

Since Pasteur's tartrate experiment highlighting the significance of "dissymmetry", control of chirality at the molecular level has led to many technological and scientific advancements in physics, chemistry and life sciences.[1] Along with the progress of this area, the quantification of enantiomeric excess (e.e.) has urged the development of fast and effective methods. Within this context, promising results have been reported by the use of supramolecular approaches which have developed molecular sensors able to amplify chiroptical signal intensities.[2–11] The leading strategy in this field is represented by the use of chemosensors carrying a chromophore unit and a labile stereogenic element in fast racemization.[12–17] Interaction of these stereodynamic probes with a chiral analyte shifts the equilibrium among the two enantiomeric forms of the receptor toward a preferential diastereoisomer (Figure 1). The presence of chromophores allows to translate this bias in a signal which is detected using electronic circular dichroism (CD).

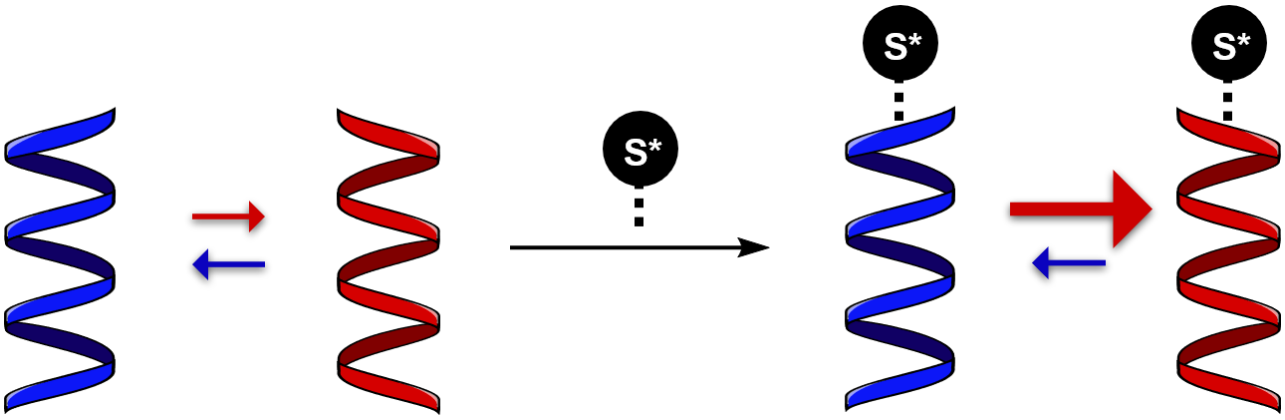

Figure 1. Schematic representation of a stereodynamic probe. Adapted from reference 25.

Among the different molecular architectures exploiting this feature, metal complexes of tris(2-pyridylmethyl)amine (**TPMA**)[18] ligands have gained considerable attention due to the seminal contributions of Canary[19,20], Anslyn[21,22] and, more recently, by the research group in which this thesis has been carried out.[23–25] These complexes exploit the propeller-like arrangement of the ligand around the metal centre, whose configuration is controlled by the interaction with the chiral analyte.

However, it should be noted that while these probes have shown a good capability to amplify CD signals of a wide variety of molecular systems, one unresolved issue remains their application in the presence of other possible interfering analytes. Indeed, while the versatility toward different functional groups can be considered an analytical strength, low specificity in the presence of complex mixtures or reaction crudes, just to cite some practical examples,

can represent a hampering weakness. In particular, the main drawback comes in those cases in which the presence of other chiral components within the analytical mixture can interfere with the chiroptical output.

As shown in chapter 1, the use of **TPMA** based supramolecular cages able to self-assemble in the presence of a complex mixture like wine or fruit juices has been reported.[26] In these mixtures cages were able to selectively encapsulate dicarboxylic acids present in the matrixes.

In this chapter, the chiroptical analytical employment of a **TPMA**-based cage has been studied. The obtained results highlighted that a confined stereodynamic structure can allow the e.e. determination of chiral dicarboxylic acids also in complex mixtures. The reported system displayed a preferential enhancement of the dichroic signal for tartaric acid which is more than one order of magnitude higher than the structural closest system malic acid.

2.2. Result and Discussion

2.2.1. Chiroptical properties of the supramolecular cage

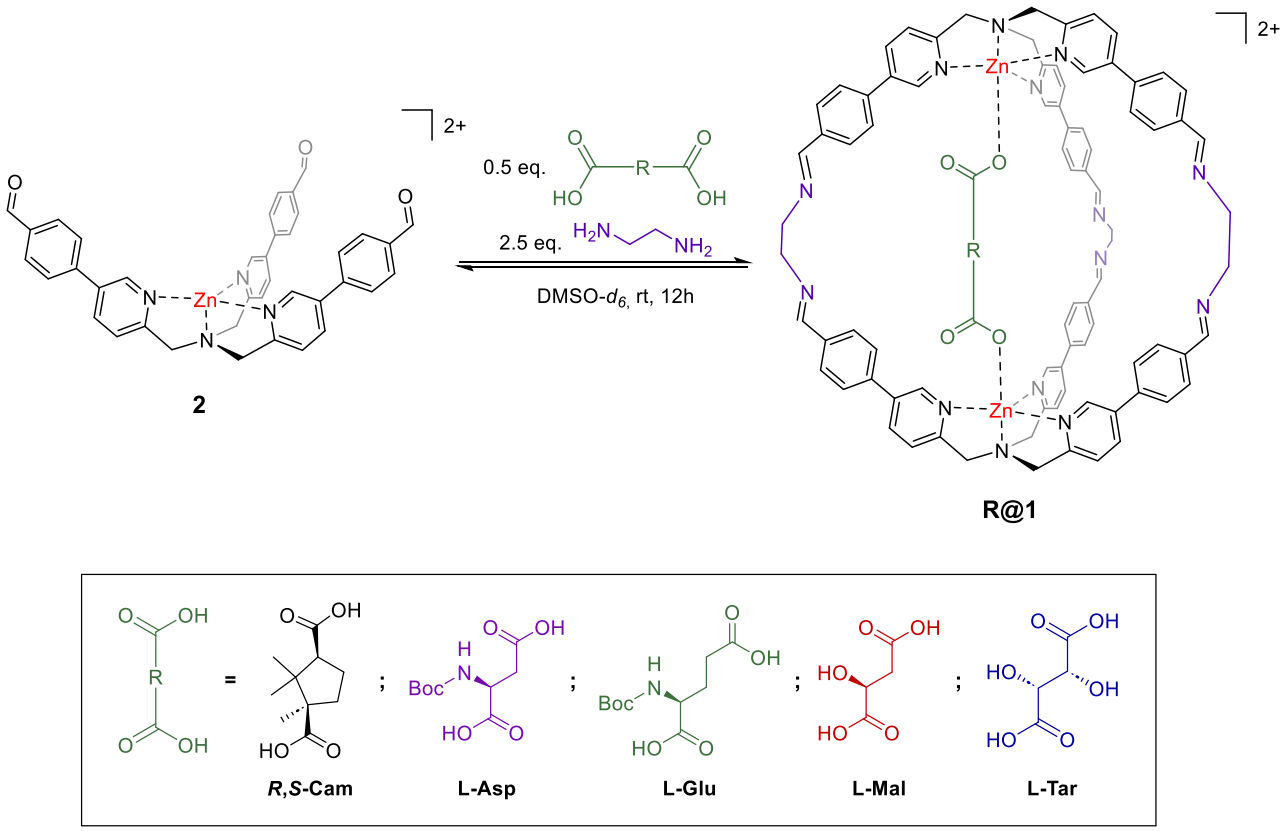

Scheme 1. Synthesis of cage **R@1** with different chiral dicarboxylic acids. Perchlorate counteranions have been removed for clarity.

In recent years, the research group has been interested in carboxylic acids sensing[27–30] using **TPMA**-based supramolecular cages.[31–33] The high affinity and selectivity of the system toward diacids, together with the capability to form in complex mixtures, prompted the investigation into the possibility to take advantage also of the stereodynamic features of the two **TPMA** units in chiral sensing.[34–36] For these reasons, in the first instance, the recognition capabilities and chiroptical properties of the molecular cage **1** have been studied toward: L-malic acid (**L-Mal**), L-tartaric acid (**L-Tar**), the amino acids *Boc*- L-glutamic acid (**L-Glu**), *Boc*-L-aspartic acid (**L-Asp**) and (1*R*,3*S*)-camphoric acid (***R,S*-Cam**). The enclosed cages were formed taking advantage of the imine based dynamic covalent chemistry process obtained by mixing the aldehyde precursor **2** with ethylenediamine in the presence of the chiral diacid in DMSO-d_6 (Scheme 1). After 12 hours, the formation of the cages was confirmed for all the systems by ^{1}H-NMR, 2D-NMR (COSY, DOSY) and ESI-MS analyses (Figure 2 and Appendix 2, Figures A18-A25).

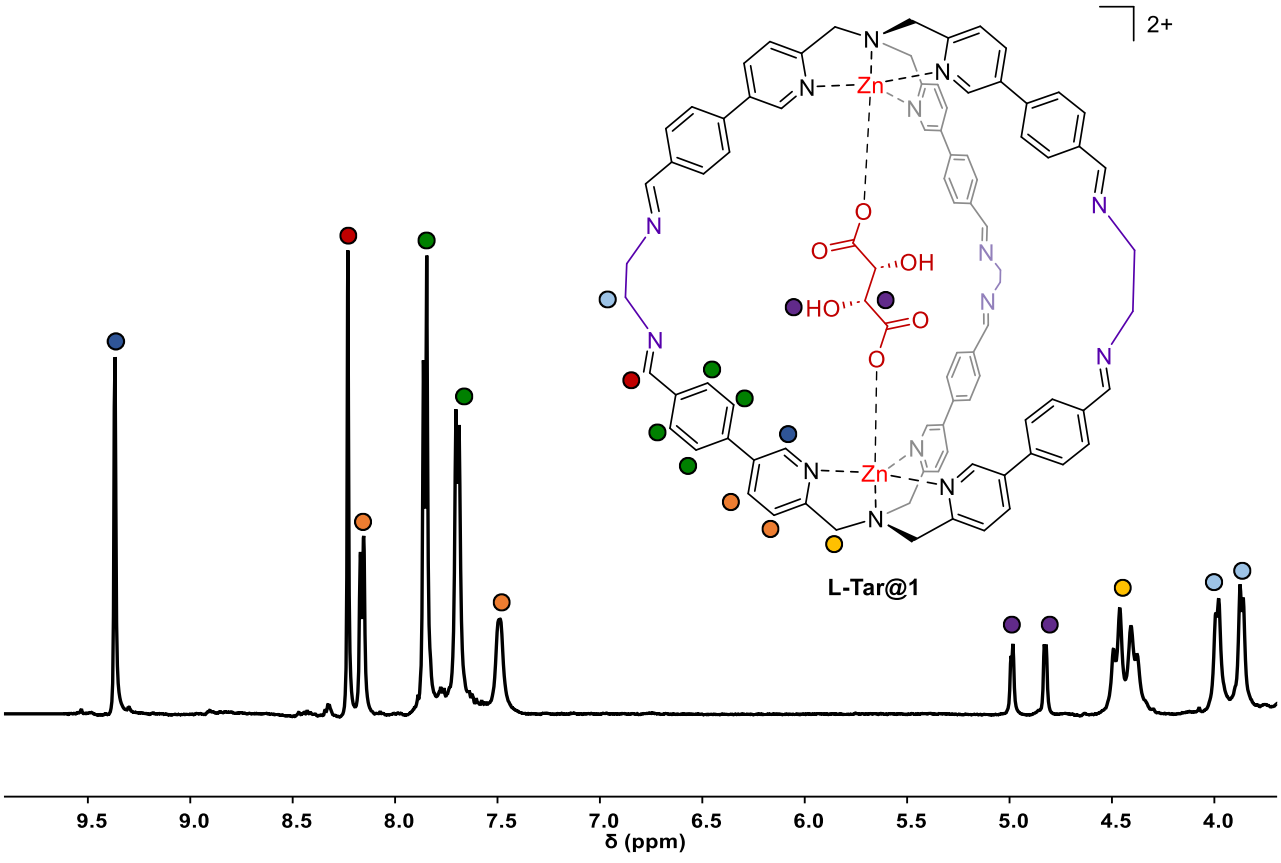

Figure 2. ^{1}H-NMR (DMSO-d_6, 400 MHz) spectrum of cage **L-Tar@2** (yield 92% based on internal standard p-xylene). Perchlorate counteranions have been removed for clarity.

Once cage systems were formed, dichroic signals were observed for all the five differently included cages in the spectral region between 260 nm and 350 nm, a region where the free diacids do not display any meaningful signal (Figure 3).

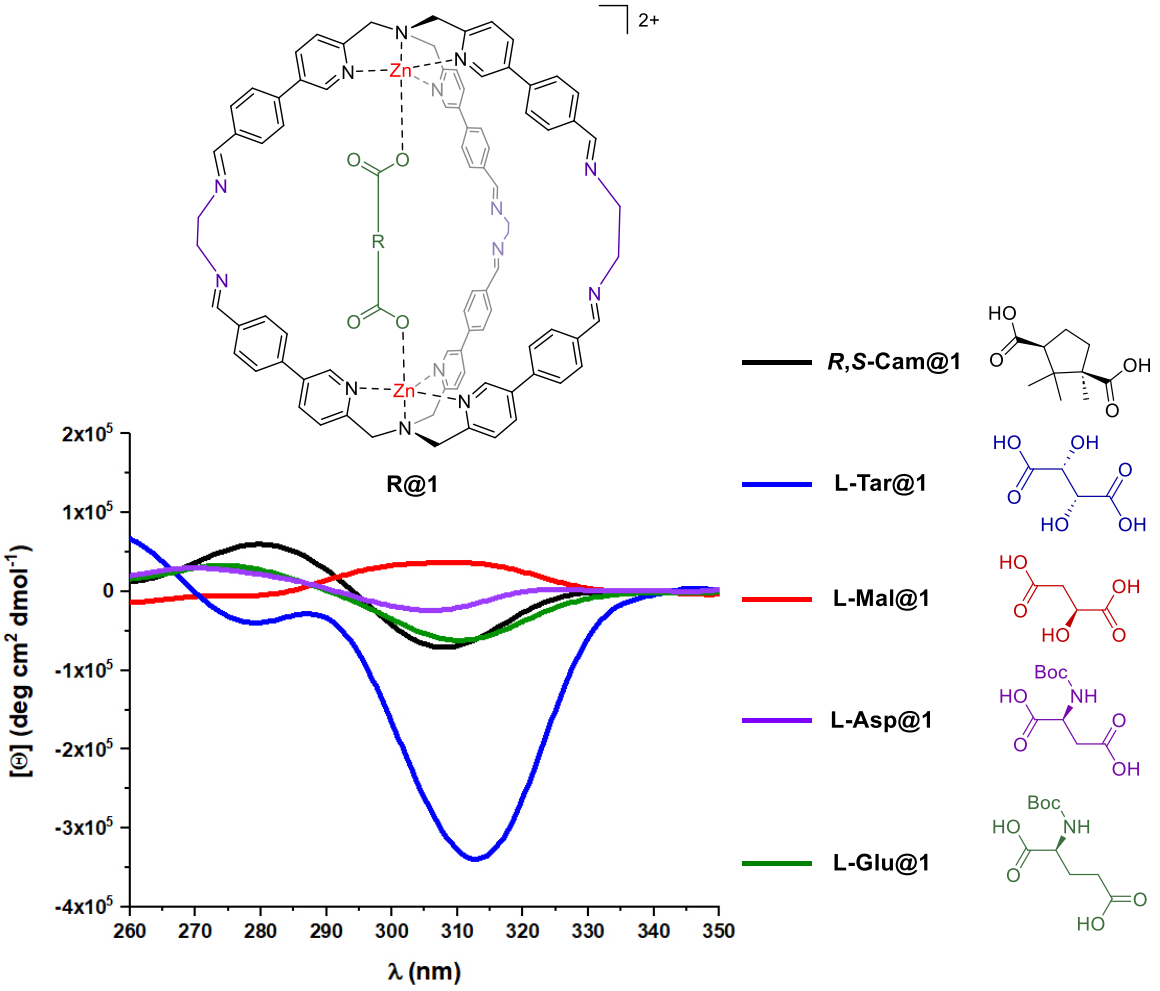

Figure 3. Circular dichroism spectra for the **R@1** series. Solution of molecular cages containing the different diacids have been analyzed using CD spectroscopy. Dichroic signals are observed for all diacid. Among them, **L-Tar** acid is furnishing the stronger signal. CD measurements were performed by diluting the synthesized cage with anhydrous DMSO to obtain a final concentration equal to $1.0 \cdot 10^{-5}$M (0.1 cm cuvette). The counterions are perchlorate for the cage.

Unexpectedly, while for four embedded diacids the intensities are in line with previously reported **TPMA** probes,[23] a higher signal enhancement was observed in the case of encapsulated tartaric acid **L-Tar@1** (Figure 3). This feature was also more remarkable considering that the closely related system incorporating malic acid **L-Mal@1**, which displayed a binding constant similar to **L-Tar@1** (Appendix 2, Section A2.7), had a signal intensity one order of magnitude lower (**L-Tar@1** [θ] = -3.5 and **L-Mal@1** [θ] = 0.36 deg cm^2 $dmol^{-1}$ 10^5 at 314 nm).

In order to test the capability of the system to act as probe for enantiomeric excess (e.e.) determination, the chiroptical response of the supramolecular system **1** in the presence of tartaric acid with different e.e. values has been studied. In particular, six different solution **Tar@1** with different e.e. values have been prepared and analyzed with the same procedure adopted for previous CD analysis. The investigations revealed a linearity in CD intensity response as a function of the e.e. of the guest suggesting a possible application of the system for e.e sensing (Figure 4).

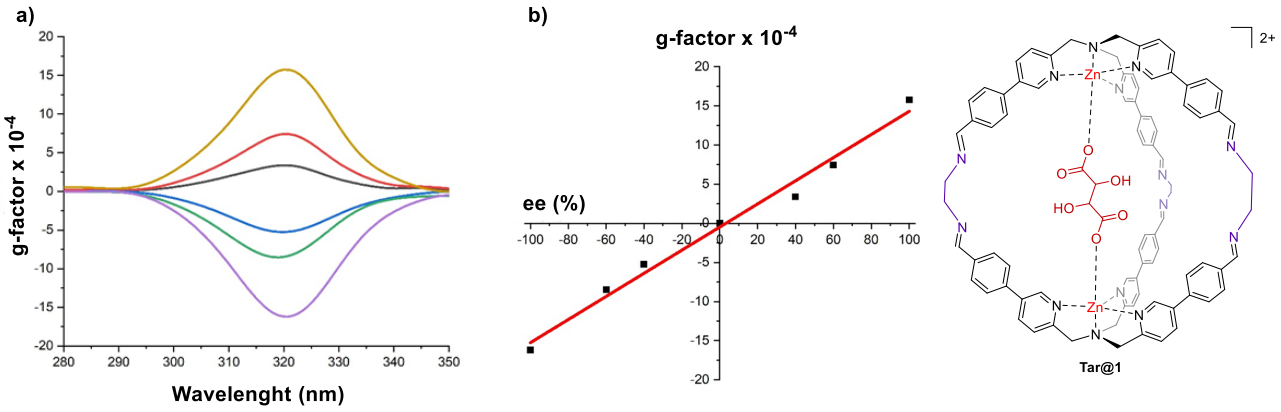

Figure 4. a) Anisotropy g-factor for the six samples of **Tar@1** analyzed, respectively with an ee (%) equal to +100, +60, +40, -40, -60 and -100; b) calibration curve obtained with the g-factor of the samples at 320 nm. The fitting equation curve is y=0.1478(±0.0083)x-0.48(±0.55), R^2=0.9814. The counterions are perchlorate for the cage.

2.2.2. Computational Studies

To clarify the origin of the signal enhancement in case of **L-Tar**, TD-DFT calculations on the **L-Mal@1** and **L-Tar@1** cages were carried out (Appendix 2, Section A2.4). More in detail, initially a conformational search was performed to identify the structures responsible of the observed signals. Possible conformations are ruled by the propeller-like arrangement of the ligand around the metal and the conformations of the enclosed diacids. The latter were essentially dictated by the intramolecular network of hydrogen bonds among hydroxyls and carboxylates (Figure 5). The lowest energy structures found for the two inclusion systems highlighted intramolecular hydrogen bonds within the diacids, two in the case of **L-Tar** versus one in the case of **L-Mal**. These hydrogen bonds were responsible for a shorter length of the guest in the case of **L-Tar@1** in comparison with **L-Mal@1.** This difference influenced the size of the cage and in its capability to adopt the two enantiomeric forms. The extra hydrogen bond in **L-Tar** induced a tightening in **L-Tar@1,** which corresponded to a higher

thermodynamic differentiation among the two diastereomeric forms of the cage in comparison to **L-Mal@1**. This difference in population was responsible of signal intensities as confirmed by the overlap between the calculated and the experimental CD spectra (Appendix 2, Figures A10-A11).

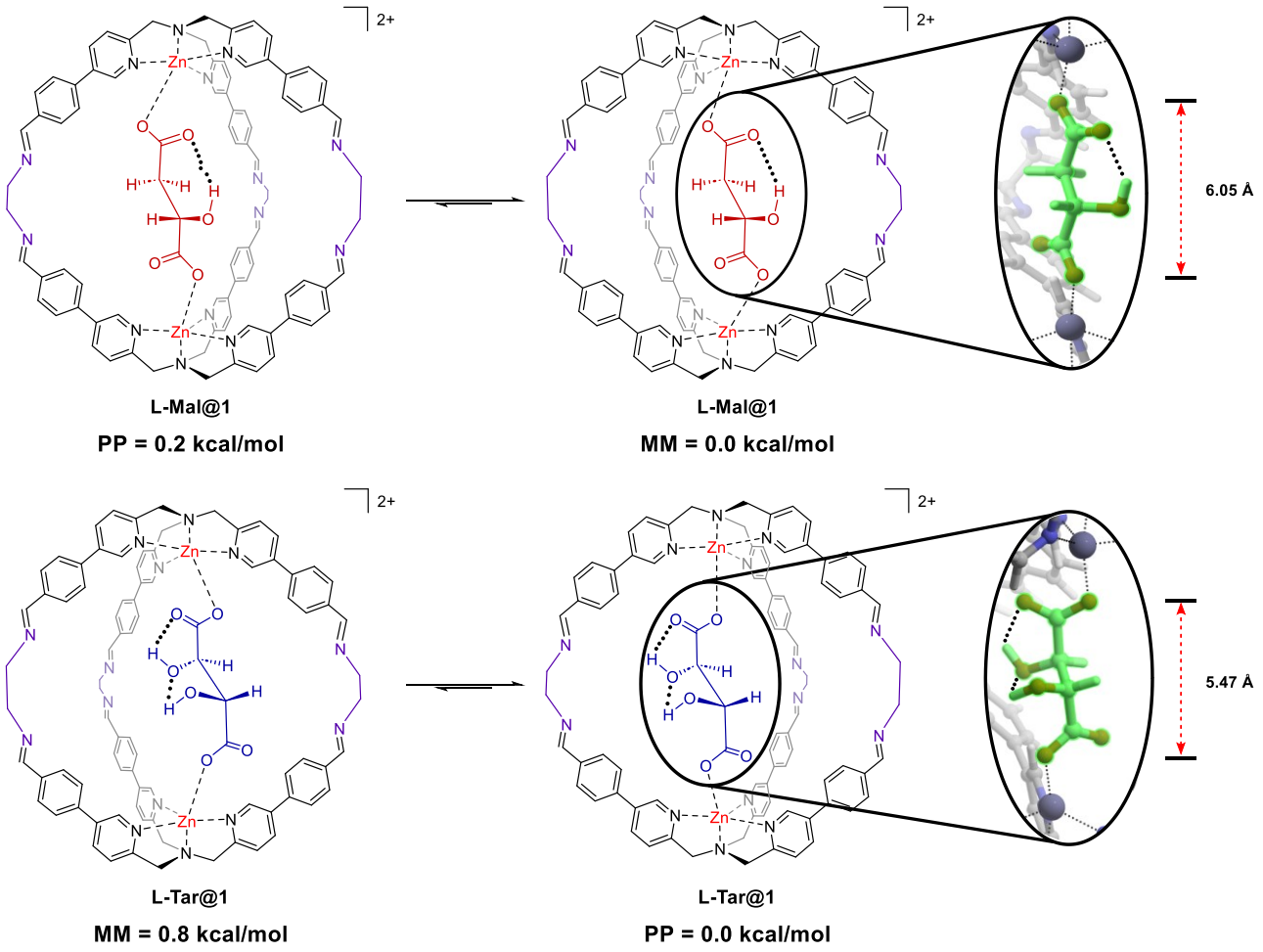

Figure 5. Diacids lead mainly to the formation of two diastereomeric conformations characterized by the opposite helicity of the **TPMA** unit (*MM* or *PP*) according to DFT calculations. Energy difference among the diastereomeric structures is 0.2 kcal/mol for the L Mal and 0.8 kcal/mol for the **L-Tar** acids. The higher energy difference calculated in the latter case is ascribable to the formation of two intramolecular hydrogen bonds, which results in a tightening of the cage (representative distances in **L-Mal@1** O-O 6.05 Å and Zn-Zn 9.67 Å, **L-Tar@1** O-O 5.47 Å and Zn-Zn 9.11 Å). Perchlorate counteranions have been removed for clarity.

2.2.3. Determination of L-Tartaric Acid content using CD

As showed in chapter 1, the capability of this system to form also in the presence of complex matrixes, such as fruit juices and wines, taking advantage of the templating capability of dicarboxylic acids present in these solutions has been reported.[26] Due to the "natural" chiral character of these templates, the chiroptical probe was tested using complex mixtures as source of the diacids. In the first experiment, the capability of the cage to preferentially enhance **L-Tar** signal was exploited to quantify wines tartaric acid content using Circular Dichroism. More in detail, the standard addition method was used to minimise the effect of the sample matrix.

In particular, cages synthesis has been optimized in the presence of wine, reducing the time of formation to 20 minutes (Figure 6).

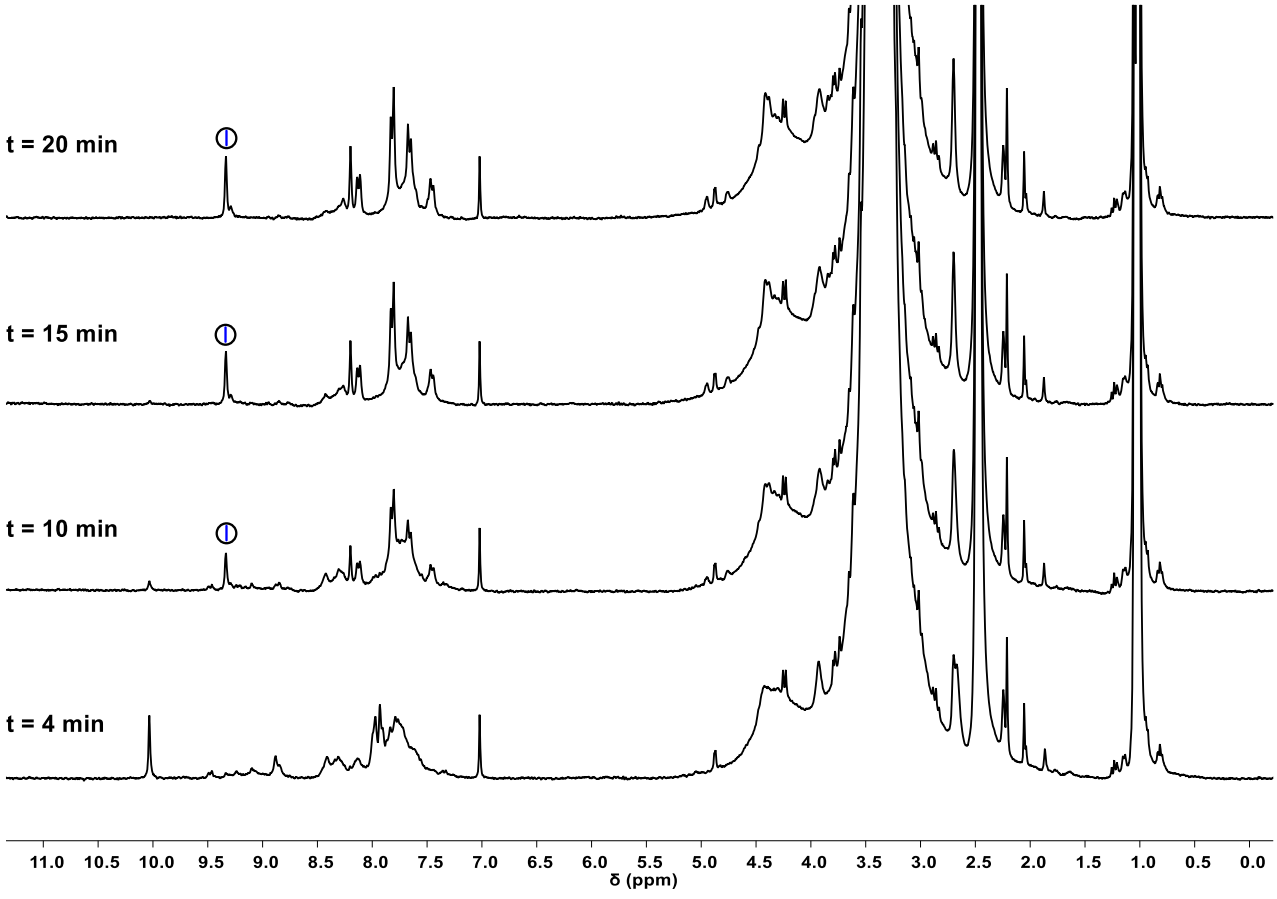

Figure 6. ^{1}H-NMR (300 MHz, 301 K, DMSO-d_6) of the cage formation at different times. The black circle indicates cage **1**, blue stick indicates the dicarboxylic acid **L-Tar**.

After these results, CD was subsequently used to quantify tartaric acid content in six wines using the standard addition method to minimise the effect of the sample matrix. In particular, cages have been assembled using the different wines and increasing aliquots of commercially available optically pure **L-Tar** (Figure 7 and Appendix 2, Figures A12-A17). The **L-Tar** content obtained by the CD investigation has been compared with **L-Tar** content measured using ^{1}H-NMR with an internal standard (Table 1 and Appendix 2, Table A7).[26]

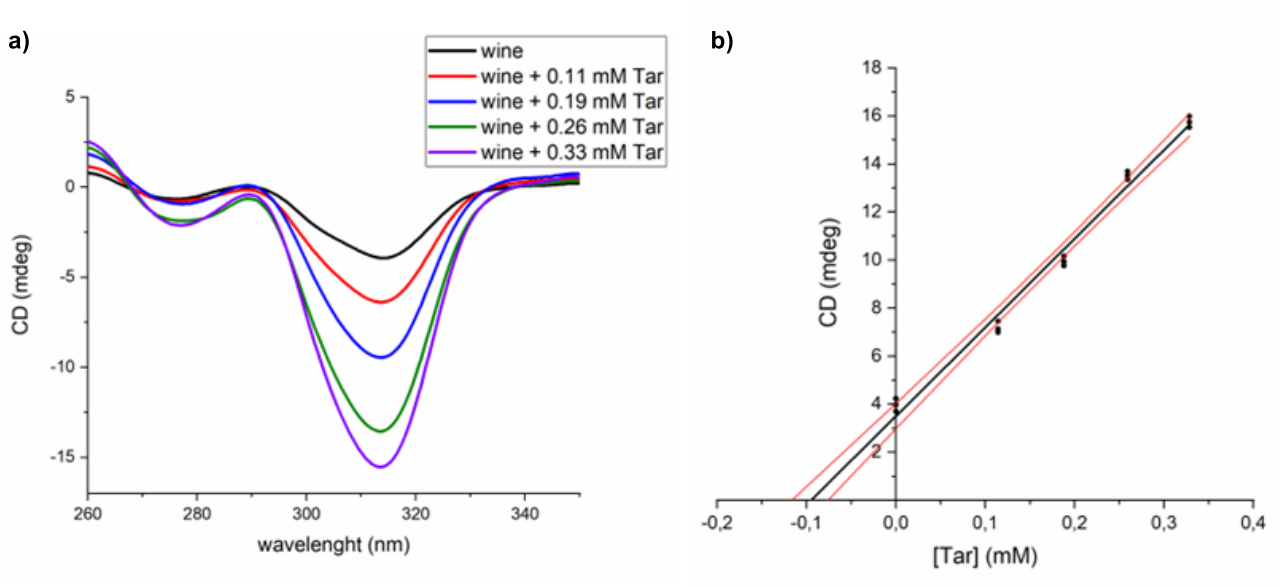

Figure 7. a) Circular Dichroism spectra in Ellipticity (mdeg) within the range 260-350 nm of the supramolecular system **1** with 5 µL of Chianti wine and different content in L-tartaric acid, respectively equal to 0.0×10^{-4} M (black line), 1.1×10^{-4} M (red line), 1.9×10^{-4} M (blue line), 2.6×10^{-4} M (green line), 3.3×10^{-4} M (violet line); b) the linear fit of the CD signal response of the supramolecular system **1** taking the point of the maximum CD signal at 314 nm. The fitting equation curve is y=36.91x+3.50, R^2=0.986. The abscissa intercept is equal to -0.095 ± 0.020 mM, corresponding to a Tartaric acid content equal to 2.28 ± 0.13 g/L.

Table 1. L-Tar acid content in different wines obtained with standard addition method and ^{1}H-NMR peaks integration in the presence of an internal standard.

WINE	TARTARIC ACID CONTENT	
	CD (g/L)	NMR (g/L)[a]
PROSECCO	1.1	1.3
CHIANTI	2.3	2.4
CHARDONNAY	1.7	1.5
BARBERA	2.5	2.5
MÜLLER-THURGHAU	1.2	1.5
VALPOLICELLA	2.2	2.0

[a] Values have been taken from ref. 26.

2.2.4. PCA Analysis

In a second experiment, cage synthesis was performed using 11 different juices and 6 wines as source of templating agent. CD of the resulting mixtures were registered and the collected data analysed using the Principal Component Analysis (PCA) method (Figure 8).[37,38] Even though the CD spectra seem mainly dictated by the **L-Tar** (*viz*. negative curves) and **L-Mal** (*viz*. positive curves) contents, PCA showed an effective degree of separation allowing a discrimination among the different "templating" matrixes. PC1 which accounted for more than 99% of the total variation, showed a direct correlation with **L-Tar** acid content. Wines with high **L-Tar** content were in the positive region of PC1, while two white wines were present in an intermediate region of PC1 axis. In this case, as shown by ^{1}H-NMR analysis, **L-Tar** content was low. All the other juices displayed a negative PC1 and discrimination was obtained along PC2. High **L-Mal** content systems (pears and apples) were in the positive PC2 region, while systems that did not present high contents of either **L-Mal** or **L-Tar** were in the negative PC2 region. It is also interesting to notice that PC1 and PC2 loadings strongly resembled CD spectra of **L-Tar** and **L-Mal** respectively (Appendix 2, Figures A31-A47). It should be highlighted that even if a naked eye impression over CD spectra in Figure 8 seemed uninformative, unexpectedly, the differences in CD spectra of the two natural diacids, (*e.g.* absolute value, intensity and maximum absorbance wavelength) were sufficient to furnish a distinct discrimination among the different natural matrixes.

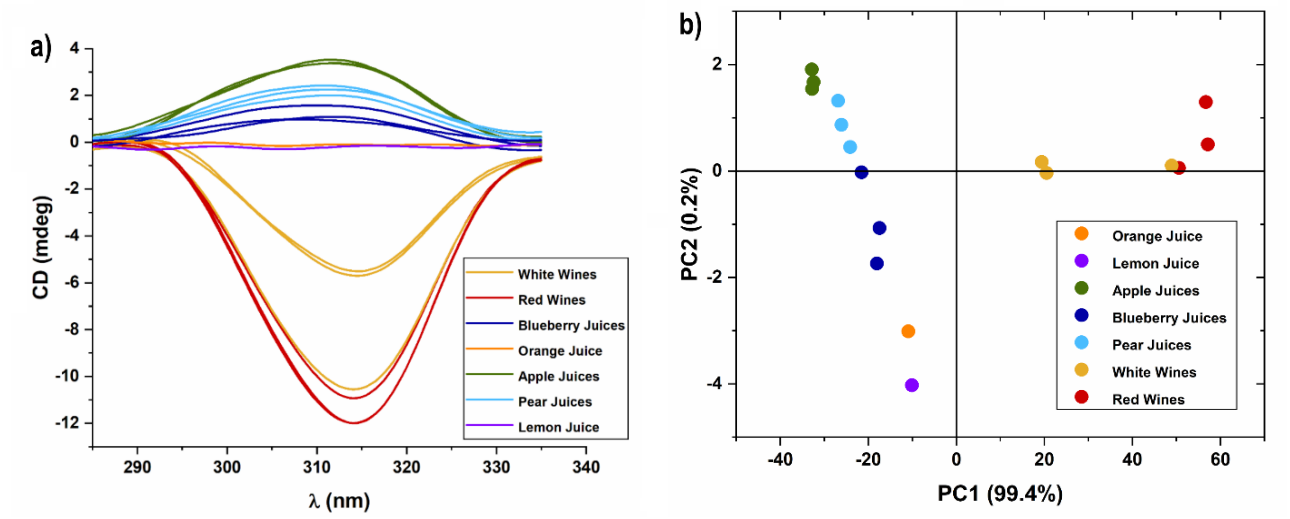

Figure 8. a) CD spectra of the supramolecular cage **1** formed upon addition of 15 µL of different fruit juices and wines without pre-treatment to a DMSO-d_6 solution containing 500 µL of the aldehyde zinc complex **2** and 125 µL of ethylenediamine, and b) PCA analysis. ^{1}H NMR of all the formed cages present in the PCA and relative **L-Tar** and **L-Mal** values are reported in Appendix 2, Section A2.11.

2.3. Conclusions

In conclusion, the capabilities of a supramolecular cage able: *i*) to act as sensor for chiral diacids, *ii*) to display a CD signal one order of magnitude higher for **L-Tar** in comparison with the structurally related **L-Mal**, *iii*) to report **L-Tar** content in wines and iv) to discriminate different juices using PCA have been reported. These results have been obtained combining the stereodynamic properties of the two **TPMA** units together with the properties arising from cage confinement. It should be stressed that dynamic covalent chemistry has already been successfully exploited in complex mixtures taking advantage of differential sensing in dynamic chemical networks.[39–41] However, the possibility to master the self-assembly of a defined molecular architecture in presence of a complex mixture and to report a signal urges to novel opportunities in the preparation of innovative functional supramolecular systems in more challenging matrices.

2.4. Experimental Section

2.4.1. Synthesis of Cages R@1

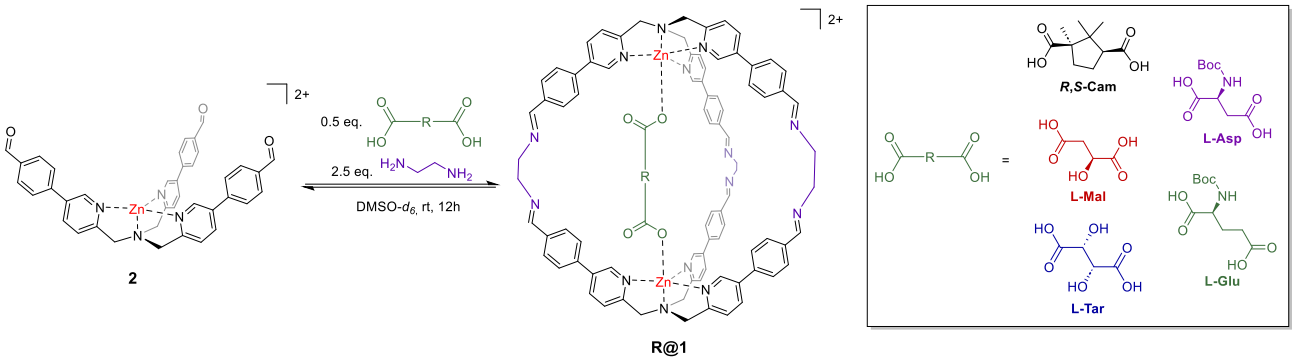

General procedure for the synthesis of molecular cages **R@1**. Perchlorate counterions are removed for clarity.

To 500 µL (1.0 µmol) of a solution 0.002 M of the aldehyde zinc complex **2** in DMSO-d_6, 50 µL (0.5 µmol) of a solution 0.01 M in DMSO-d_6 of a dicarboxylic acid **R** and 125 µL (2.5 µmol) of a solution 0.02 M in DMSO-d_6 of ethylenediamine were added in a NMR tube. The mixture was left overnight at room temperature and checked *via* ^{1}H-NMR and ESI-MS. The yield for all the cages is >90% (Determined *via* ^{1}H-NMR on internal standard *p*-xylene).

2.4.1.1. L-Tar@1

^{1}H-NMR (500 MHz, DMSO-d_6) δ (ppm): 9.37 (s, 6H, PyrH), 8.23 (s, 6H, NH_{imm}), 8.16 (d, J = 7.9 Hz, 6H, PyrH), 7.85 (d, J = 8.0 Hz, 12H, ArH), 7.70 (d, J = 7.4 Hz, 12H, ArH), 7.49 (s, 6H, PyrH), 4.98 (s, 2H, OH_{TAR}), 4.83 (d, J = 4.8 Hz, 2H, CH_{TAR}), 4.64 – 4.21 (m, 12H, CH_2-$_{TPMA}$), 3.98 (d, J = 7.5 Hz, 6H, CH_2-$_{EDA}$), 3.86 (d, J = 7.5 Hz, 6H, CH_2-$_{EDA}$).
MS (ESI-MS) (*m/z*): [M^{2+}] calcd. for $[C_{88}H_{76}N_{14}O_6Zn_2]^{2+}$, 776.2328; found 776.2319

2.4.1.2. L-Mal@1

^{1}H-NMR (500 MHz, DMSO-d_6) δ (ppm): 9.39 (s, 3H, PyrH), 9.30 (s, 3H, PyrH), 8.28 (s, 3H, NH_{imm}), 8.26 (s, 3H, NH_{imm}), 8.18 (d, 8.8 Hz, 3H, PyrH), 8.13 (d, 8.8 Hz, 3H, PyrH), 7.85 (d, J = 7.8 Hz, 12H, ArH), 7.66 – 7.63 (m, 12H, ArH), 7.52 (d, 8.2 Hz, 3H, PyrH), 7.48 (d, 8.2 Hz, 3H, PyrH), 4.92 – 4.90 (m, 2H, OH_{MAL} – CH_{MAL}), 4.45 – 4.42 (m, 12H, CH_2-$_{TPMA}$), 3.95 – 3.91 (m, 12H, CH_2-$_{EDA}$), 2.84 – 2.82 (m, 2H, $CH_{2\text{-}MAL}$).
MS (ESI-MS) (*m/z*): [M^{2+}] calcd. for $[C_{88}H_{76}N_{14}O_5Zn_2]^{2+}$, 768.2347; found 768.2348

2.4.1.3. *R,S*-Cam@1

^{1}H-NMR (500 MHz, DMSO-d_6) δ (ppm): 9.26 (s, 3H, PyrH), 9.23 (s, 3H, PyrH), 8.51 – 8.31 (m, 12H, NH_{imm} – PyrH), 7.90 – 7.84 (m, 12H, ArH), 7.80 – 7.69 (m, 12H, ArH), 7.65 – 7.62 (m, 6H, PyrH), 4.39 (b, m, 12H, CH_2 $_{TPMA}$), 3.91 (b, m, 12H, CH_2-$_{EDA}$), 2.85 (m, 2H, CH_{CAM}), 2.37 (m, 1H, CH_{CAM}), 1.99 (m, 1H, CH_{CAM}), 1.76 (m, 1H, CH_{CAM}), 1.60 – 1.53(m, 6H, CH_{CAM}), 1.23 – 1.13 (m, 3H, CH_{CAM}).
MS (ESI-MS) (*m/z*): [M^{2+}] calcd. for $[C_{94}H_{86}N_{14}O_4Zn_2]^{2+}$, 801.2764; found 801.2739

2.4.1.4. L-Glu@1

^{1}H-NMR (500 MHz, DMSO-d_6) δ (ppm): 9.31 (s, 3H, PyrH), 9.18 (s, 3H, PyrH), 8.23 – 8.21 (m, 12H, NH_{imm} – PyrH),), 7.80 – 7.75 (m, 12H, ArH), 7.72 – 7.60 (m, 12H, ArH), 7.57 – 7.54 (m, 6H, PyrH), 7.14 – 7.06 (b, m, 1H, NH_{GLU}), 4.32 – 4.24 (m, 3H, CH_2-$_{EDA}$ – CH_{GLU}), 3.83 (b, m, 12H, CH_2-$_{EDA}$), 1.27 (b, m, 2H, CH_{GLU}), 1.15 (b, m, 1H, CH_{GLU}), 1.08 (b, m, 1H, CH_{GLU}), 0.84 (b, m, 1H, CH_{GLU}), 0.75 (s, 9H, $CH_{3\text{-}GLU}$).
MS (ESI-MS) (*m/z*): [M^{2+}] calcd. for $[C_{94}H_{87}N_{15}O_6Zn_2]^{2+}$, 824.7768; found 824.7758

2.4.1.5. L-Asp@1

^{1}H-NMR (500 MHz, DMSO-d_6) δ (ppm): 9.34 – 9.31 (m, 6H, PyrH), 8.30 – 8.27 (m, 6H, NH_{imm}), 8.18 – 8.17 (m, 6H, PyrH), 7.84 – 7.82 (m,12H, ArH), 7.73 – 7.63 (m, 12H, ArH), 7.53 – 7.51 (m, 6H, PyrH), 7.30 – 7.28 (b, m, 1H, NH_{ASP}), 4.68 (b, m, 1H, CH_{ASP}), 4.44 (s, 12H, $CH_{2\text{-}TPMA}$), 3.94 (s, 12H, $CH_{2\text{-}EDA}$), 2.74 (s, 1H, CH_{ASP}), 1.24 (s, 1H, CH_{ASP}), 0.89 – 0.85 (b, m, CH_{ASP}), 0.62 (s, 9H, CH_{ASP}).
MS (ESI-MS) (*m/z*): [M^{2+}] calcd. for $[C_{93}H_{85}N_{15}O_6Zn_2]^{2+}$, 817.7690; found 817.7681

2.4.2. Synthesis of Cages in the presence of complex mixtures

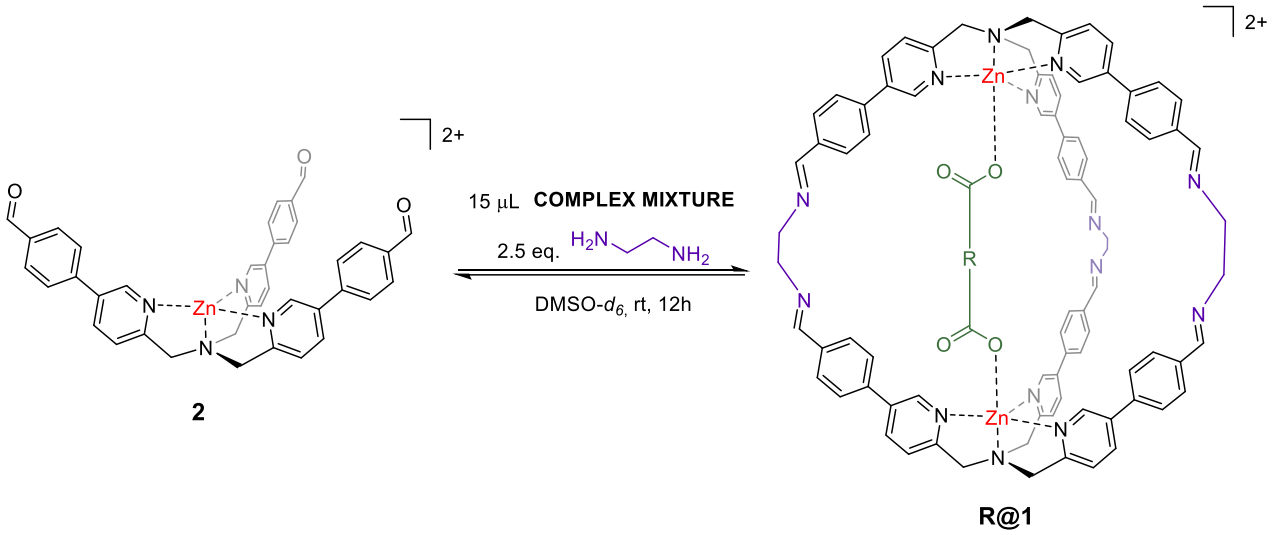

General procedure for the synthesis of molecular cages **R@1**. Perchlorate counterions are removed for clarity.

To 500 µL (1.0 µmol) of a solution 0.002 M the aldehyde zinc complex **2** in DMSO-d_6, 15 µL of complex mixture (wine or fruit juice) without pre-treatment and 125 µL (2.5 µmol) of a solution 0.02 M in DMSO-d_6 of ethylenediamine were added in a NMR tube. The mixture was left overnight compl at room temperature and checked *via* ^{1}H-NMR.

2.5. References

[1] J. R. Brandt, F. Salerno, M. J. Fuchter, *Nat. Rev. Chem.* **2017**, *1*, 45.
[2] G. Pescitelli, L. Di Bari, N. Berova, *Chem. Soc. Rev.* **2014**, *43*, 5211–5233.
[3] D. Leung, S. O. Kang, E. V. Anslyn, *Chem. Soc. Rev.* **2012**, *41*, 448–479.
[4] L. L. Wang, Z. Chen, W. E. Liu, H. Ke, S. H. Wang, W. Jiang, *J. Am. Chem. Soc.* **2017**, *139*, 8436–8439.
[5] Z. Chen, Q. Wang, X. Wu, Z. Li, Y. B. Jiang, *Chem. Soc. Rev.* **2015**, *44*, 4249–4263.
[6] L. A. Joyce, E. C. Sherer, C. J. Welch, *Chem. Sci.* **2014**, *5*, 2855–2861.
[7] D. L. Martínez-Zepeda, B. Meza-González, M. L. Álvarez-Hernández, I. J. Bazany-Rodríguez, A. R. Vilchis Néstor, F. Cortés-Guzmán, R. M. Gómez-Espinosa, J. Valdes-García, A. Dorazco-González, *Dye. Pigment.* **2021**, *188*, 109239.
[8] Y. Chen, L. Fu, B. Sun, C. Qian, S. Pangannaya, H. Zhu, J. Ma, J. Jiang, Z. Ni, R. Wang, X. Lu, L. Wang, *Chem. – A Eur. J.* **2021**, *27*, 5890–5896.
[9] F. Biedermann, W. M. Nau, *Angew. Chem. Int. Ed.* **2014**, *53*, 5694–5699.
[10] X. Huang, X. Wang, M. Quan, H. Yao, H. Ke, W. Jiang, *Angew. Chem. Int. Ed.* **2021**, *60*, 1929–1935.
[11] L.-L. Wang, M. Quan, T.-L. Yang, Z. Chen, W. Jiang, *Angew. Chemie* **2020**, *132*, 24025–24032.
[12] D. P. Iwaniuk, C. Wolf, *J. Am. Chem. Soc.* **2011**, *133*, 2414–2417.
[13] P. Zardi, K. Wurst, G. Licini, C. Zonta, *J. Am. Chem. Soc.* **2017**, *139*, 15616–15619.
[14] Z. A. De los Santos, C. Wolf, *J. Am. Chem. Soc.* **2016**, *138*, 13517–13520.
[15] H. G. Jeon, M. J. Kim, K. S. Jeong, *Org. Biomol. Chem.* **2014**, *12*, 5464–5468.
[16] K. W. Bentley, Y. G. Nam, J. M. Murphy, C. Wolf, *J. Am. Chem. Soc.* **2013**, *135*, 18052–18055.
[17] K. W. Bentley, D. Proano, C. Wolf, *Nat. Commun.* **2016**, *7*, 1–8.
[18] C. Bravin, E. Badetti, G. Licini, C. Zonta, *Coord. Chem. Rev.* **2021**, *427*, DOI 10.1016/j.ccr.2020.213558.
[19] S. Zahn, J. W. Canary, *Science* **2000**, *288*, 1404–1407.
[20] J. W. Canary, S. Mortezaei, J. Liang, *Coord. Chem. Rev.* **2010**, *254*, 2249–2266.
[21] L. A. Joyce, M. S. Maynor, J. M. Dragna, G. M. da Cruz, V. M. Lynch, J. W. Canary, E. V. Anslyn, *J. Am. Chem. Soc.* **2011**, *133*, 13746–13752.
[22] L. A. Joyce, J. W. Canary, E. V. Anslyn, *Chem. Eur. J.* **2012**, *18*, 8064–8069.
[23] F. A. Scaramuzzo, G. Licini, C. Zonta, *Chem. Eur. J.* **2013**, *19*, 16809–16813.
[24] R. Berardozzi, E. Badetti, N. A. Carmo dos Santos, K. Wurst, G. Licini, G. Pescitelli, C. Zonta, L. Di Bari, *Chem. Commun.* **2016**, *52*, 8428–8431.
[25] C. Bravin, G. Mason, G. Licini, C. Zonta, *J. Am. Chem. Soc.* **2019**, *141*, 11963–11969.
[26] F. Begato, R. Penasa, G. Licini, C. Zonta, *Chem. Commun.* **2021**, *57*, 10019–10022.
[27] S. M. Butler, K. A. Jolliffe, *Org. Biomol. Chem.* **2020**, *18*, 8236–8254.
[28] D. Curiel, M. Más-Montoya, G. Sánchez, *Coord. Chem. Rev.* **2015**, *284*, 19–66.
[29] P. A. Gale, E. N. W. Howe, X. Wu, M. J. Spooner, *Coord. Chem. Rev.* **2018**, *375*, 333–372.
[30] L. Chen, S. N. Berry, X. Wu, E. N. W. Howe, P. A. Gale, *Chem* **2020**, *6*, 61–141.
[31] C. Bravin, E. Badetti, F. A. Scaramuzzo, G. Licini, C. Zonta, *J. Am. Chem. Soc.* **2017**, *139*, 6456–6460.
[32] C. Bravin, E. Badetti, R. Puttreddy, F. Pan, K. Rissanen, G. Licini, C. Zonta, *Chem. Eur. J.* **2018**, *24*, 2936–2943.
[33] C. Bravin, A. Guidetti, G. Licini, C. Zonta, *Chem. Sci.* **2019**, *10*, 3523–3528.
[34] A. Akdeniz, L. Mosca, T. Minami, P. Anzenbacher, *Chem. Commun.* **2015**, *51*, 5770–5773.
[35] X. Mei, C. Wolf, *J. Am. Chem. Soc.* **2004**, *126*, 14736–14737.
[36] M. Tanasova, M. Anyika, B. Borhan, *Angew. Chem. Int. Ed.* **2015**, *54*, 4274–4278.
[37] R. Bro, A. K. Smilde, *Anal. Methods* **2014**, *6*, 2812–2831.
[38] J. T. Brindle, H. Antti, E. Holmes, G. Tranter, J. K. Nicholson, H. W. L. Bethell, S. Clarke, P. M. Schofield, E. McKilligin, D. E. Mosedale, D. J. Grainger, *Nat. Med.* **2002**, *8*, 1439–1445.
[39] M. Lafuente, J. Solà, I. Alfonso, *Angew. Chem. Int. Ed.* **2018**, *57*, 8421–8424.
[40] J. Solà, C. Jimeno, I. Alfonso, *Chem. Commun.* **2020**, *56*, 13273–13286.
[41] L. Tapia, I. Alfonso, J. Sola, *Org. Biomol. Chem.* **2021**, *19*, 9527–9540.

Chapter 3

Programmed Guest Confinement *via* Hierarchical Cage to Cage Transformations

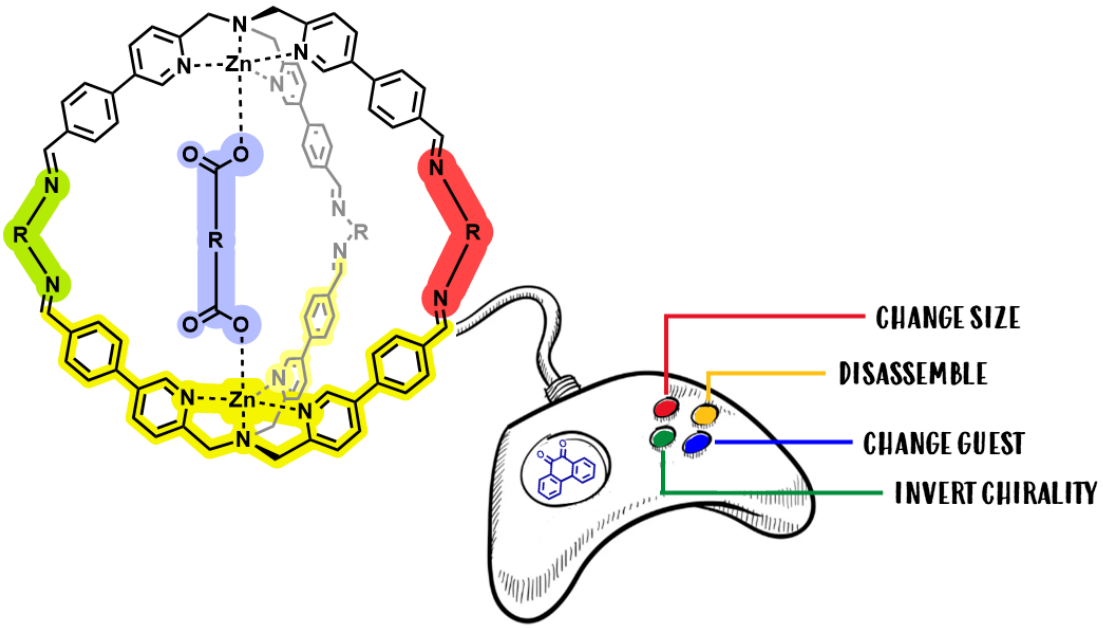

ABSTRACT Taking inspiration from Nature, where (bio)molecular geometry variations are exploited to tune a large variety of functions, supramolecular chemistry has continuously developed novel systems in which, as a consequence of a specific binding, structural changes occur. Among the different architectures, supramolecular cages have been continuously exploited for their capability to act as functional host where guests can be released in a controlled fashion. In this chapter, a novel methodology based on the use of phenanthrenequinone (**PHQ**) has been applied to selectively change the binding properties of a tris(2-pyridylmethyl)amine **TPMA** based cage. More in detail, changing the cage subcomponents has allowed to change the size of the system thus controlling inclusion ratio of two competing guests differing in size, and to switch the cage chirality thus controlling inclusion ratio of two enantiomeric competing guests.

3.1. Introduction

Uptake and release of guests using external stimuli is one of the emerging areas in the field of functional supramolecules.[1–3] Within this context, supramolecular cages have been continuously challenged for their intrinsic capability to act as functional host where guests can be released in a controllable fashion.[4–12]

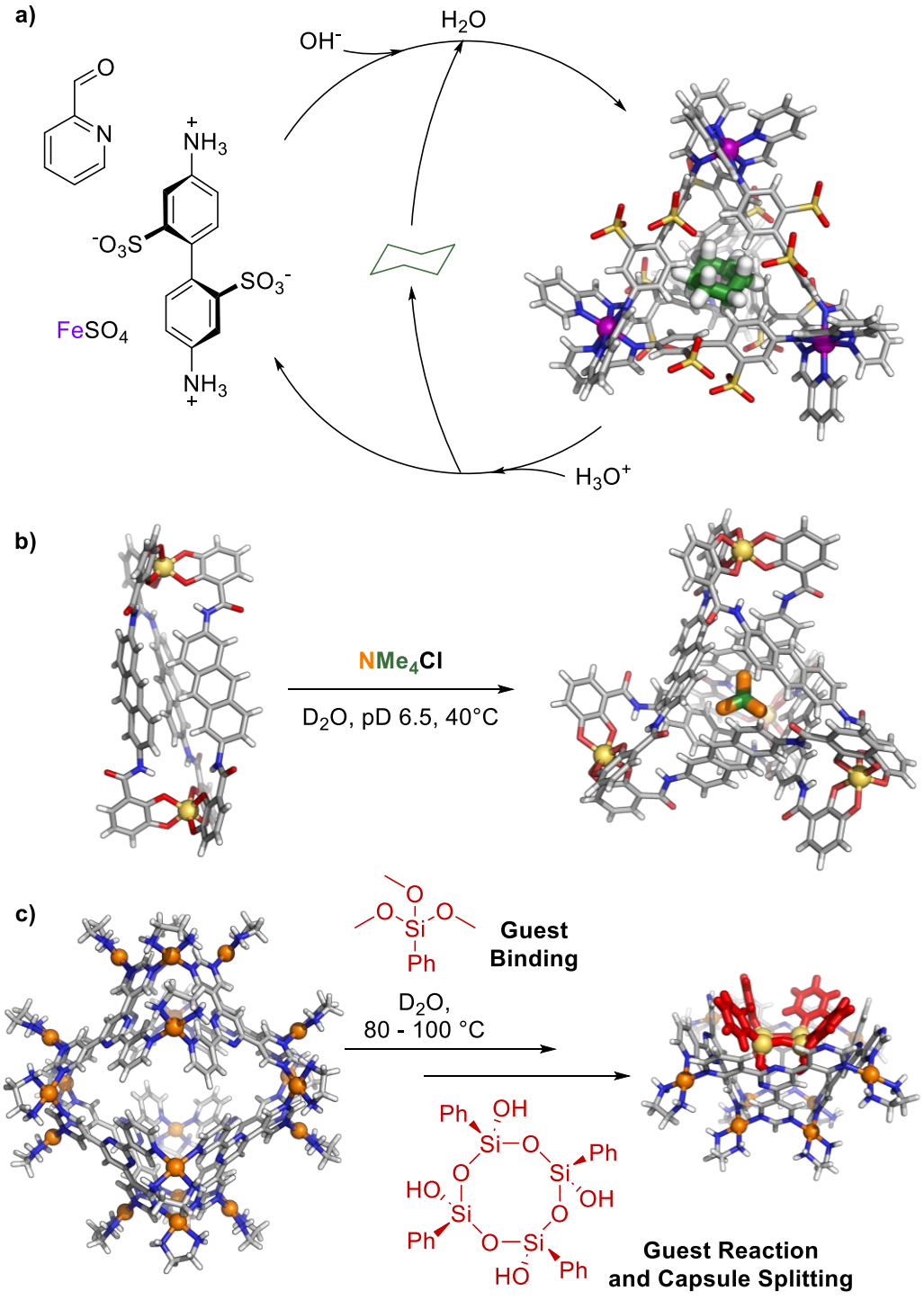

Figure 1. Examples of functional cages reported by a) Nitschke,[10] b) Raymond,[11] and c) Fujita.[12]

Due the dynamic nature of their bonds, assembled cages can transform between geometrically-distinct structures formed from the same set of components, giving opportunity to alter selectively their molecular structure as well as their functions.[13–16] The possibility to regulate guest uptake and release can open in principle to novel, and unexpected, properties in storage,[17,18] sensing,[19,20] and catalysis.[21] Common strategies for release of a guest from cages are based on: *i*) the presence of a stronger binder in solution which substitute the guest,[22,23], *ii*) disassembly of the host,[24,25] modification of the *iii*) guest (*viz*. protonation/deprotonation, oxidation/reduction, light)[26–30] or the *iv*) host by external factors (*viz*. ligand or subcomponent exchange).[31–33] The final goal is to mimic the biological complexity where chemical signals regulate activity via well-defined transformation of biomolecules.[34–36]

In the recent years the research group in which this thesis has been carried out has been interested in the phenomena related to confinement in supramolecular cages.[37] In particular, within the task of guest release, the group reported a delivery strategy that was taking advantage of the guest size to trigger its release by hydrolysis of a tris(2-pyridylmethyl)amine **TPMA** based supramolecular cage.[38] In this case, the architecture was built up using imine based Dynamic Covalent Chemistry (DCC) and hydrolyzed using water. However, water hydrolysis did not allow to: *i*) close the cycle and re-obtain the initial structure, *ii*) perform subsequent transformations or *iii*) to tune guest release. In other words, the addition of water within the DCC system coincides with end of the dynamic system. In the quest to gather additional control on guests release/uptake, the addition of a quinone was planned to offer the possibility to sequestrate diamines cage subcomponents allowing for their further transformation. In particular, in this chapter, a novel approach based on the capability of 9,10-phenanthrenequinone (**PHQ**) to react with diamines subcomponents is reported. This approach has allowed the selective removal or replacement of the diamines linkers leading cage disassembly or cage to cage transformations. This methodology enabled the selective switch of the cage binding properties towards competing guests present in solution. This strategy was successfully optimized to obtain: *i*) reversible assembly and disassembly of the cage with release and uptake of the guest, *ii*) hierarchical cage size transformation with differential release and uptake of competing guests in solution differing only in molecular size and *iii*) cage chirality inversion with allows to alternatively enclose in the cage two enantiomeric diacids competing in solution.

3.2. Results and Discussion

The molecular system under study is based on **TPMA** supramolecular cages that have been studied in the group in recent years.[38] These architectures assemble in solution taking advantage of the capability of aldehydic subcomponent **1** to bind carboxylates that pre-organize the system for the assembly.[39] The system is highly stable and, as reported in chapter 1 and 2, it can forms also in the presence of natural matrixes and high amount of water.[40,41] The system is built up using diamines and, as it has been shown, molecular size and characteristics of the diamines can be used to finely tailor recognition properties of the system.[39] As mentioned in the introduction, **PHQ** is known to form a stable adducts with either ethylendiamine (**EDA**)[42]or diaminocyclohexane (**CHDA**)[43] and its use in the presence of a formed cage was investigated.

3.2.1. Cage Assembly/Disassembly/Assembly (Case I)

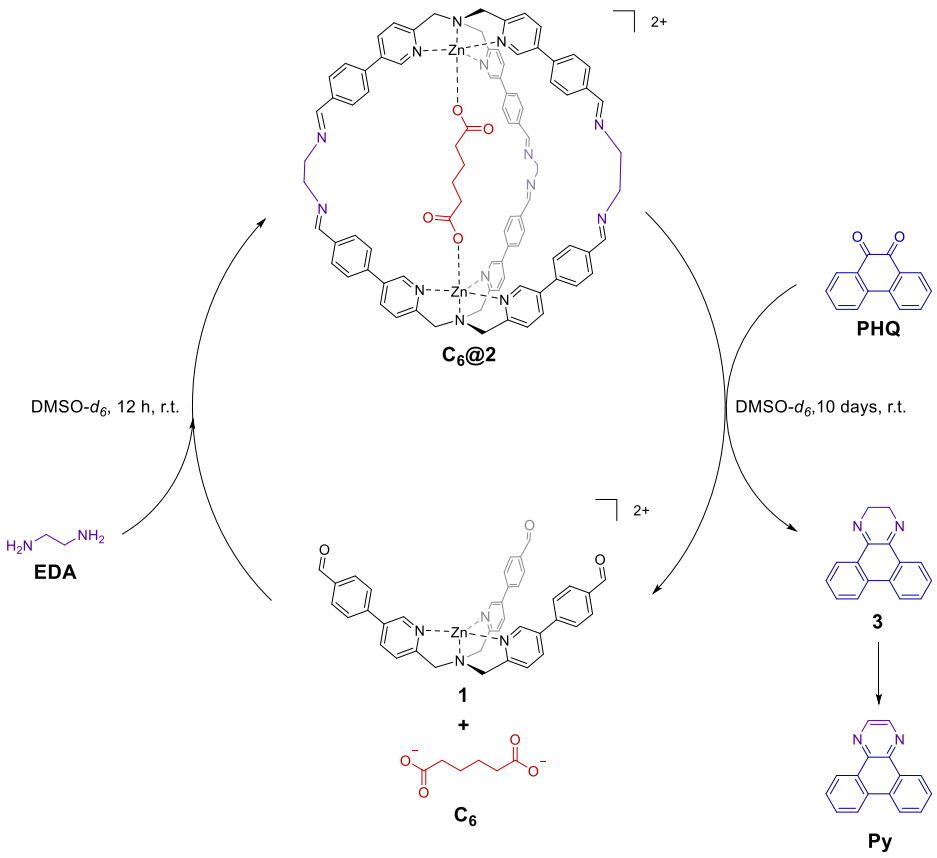

Scheme 1. Reaction scheme of the disassembly and assembly of the cage allowing guest release and uptake. Perchlorate counteranions have been removed for clarity.

The disassembly capability of **PHQ** was tested in the presence of a formed cage containing adipic acid **C$_6$** (Scheme 1). Cage **C$_6$@2**, which was formed in DMSO-*d$_6$* in the presence of complex **1** (1 eq.), ethylenediamine **EDA** (2.5 eq.) and **C$_6$** (0.5 eq.) as guest showing a 4:1 ratio among bound and unbound **C$_6$** and an overall yield of 95% in cage formation (Figure 2a). Subsequent addition of a stoichiometric amount of **PHQ** resulted in the complete cage disassembly after 10 days, as shown by the disappearance of the imine peak at 8.4 ppm, the ethylenediamine arm of the cage at 4 ppm, and the concomitant formation of the aldehyde peak of complex **1** at 10 ppm (Figure 2b). The disassembly was accompanied by the release of the guest in solution, obtaining 1:3 ratio among bound and unbound **C$_6$**. In this condition the acid was bound to the zinc aldehyde complex **1**. **EDA** was then added leading to the re-formation of cage **C$_6$@2**, generating a cycle in which the diacid guest was caught and released from solution. Re-formation of the cage was almost quantitative (85%). This was also reflected in the bound and unbound **C$_6$** ratio which was 2.5:1 (Figure 2c). The latter value is also influenced by the dilution of the system which occurs during the additions. It should also be noted that the initial dihydropyrazine system **3** slowly evolved to the pyrazine aromatic system **Py** due to the long times required for the disassembly**.**

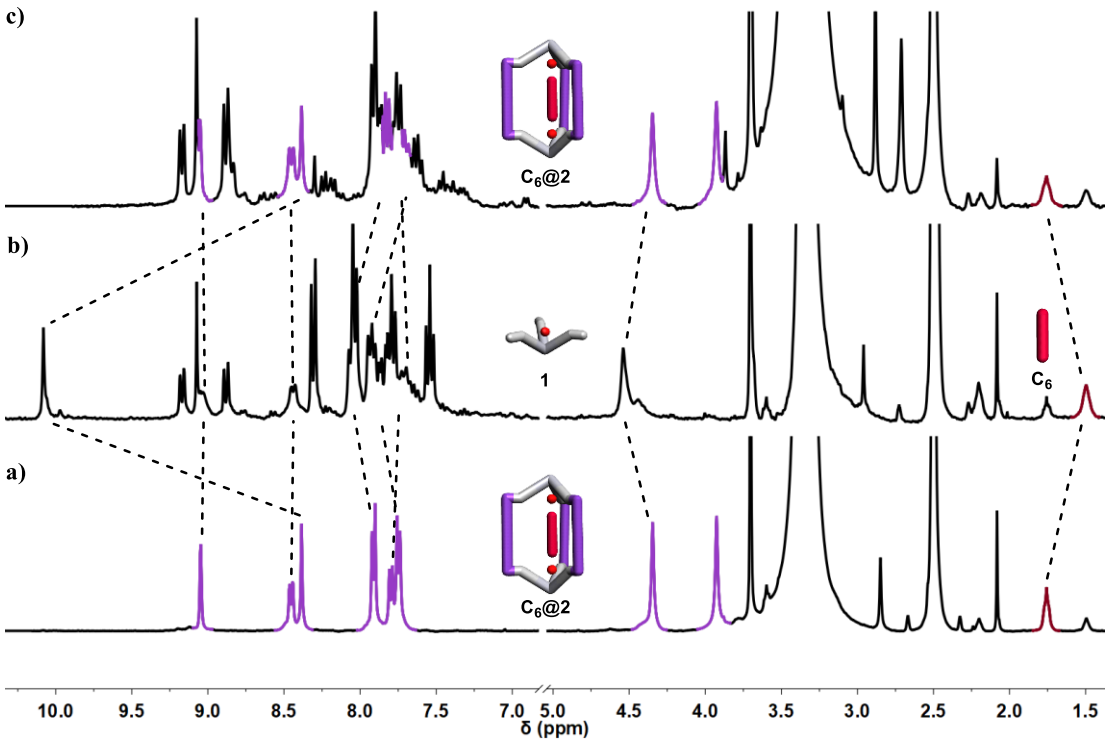

Figure 2. Partial ^{1}H-NMR (DMSO-*d$_6$*, 400 MHz) of a) cage **C$_6$@2**, b) complex **1** obtained from the disassembly of the cage using **PHQ**, and c) cage **C$_6$@2** re-formed after the addition of **EDA** to the mixture. Trimethoxy benzene was used as internal standard.

3.2.2. Cage-to-Cage One Guest (Case II)

The capability of **PHQ** to promote cage disassembly opened to the investigation of a second chemical cycle in which two diamines differing in length, **EDA** and *p*-xylylenediamine (***p*-XDA**), were introduced in the cycle with the purpose to switch cage geometry (Scheme 2). A chemically programmed change in cage size should lead to an increased metal-metal distance, thus in a different binding capability of the system toward the same guest. It should be also noted that **PHQ** offered the "perfect" geometry to form a 1:1 adduct with **EDA**, while with ***p*-XDA** could form only less favored 2:2 stoichiometric adducts or polymeric structures.

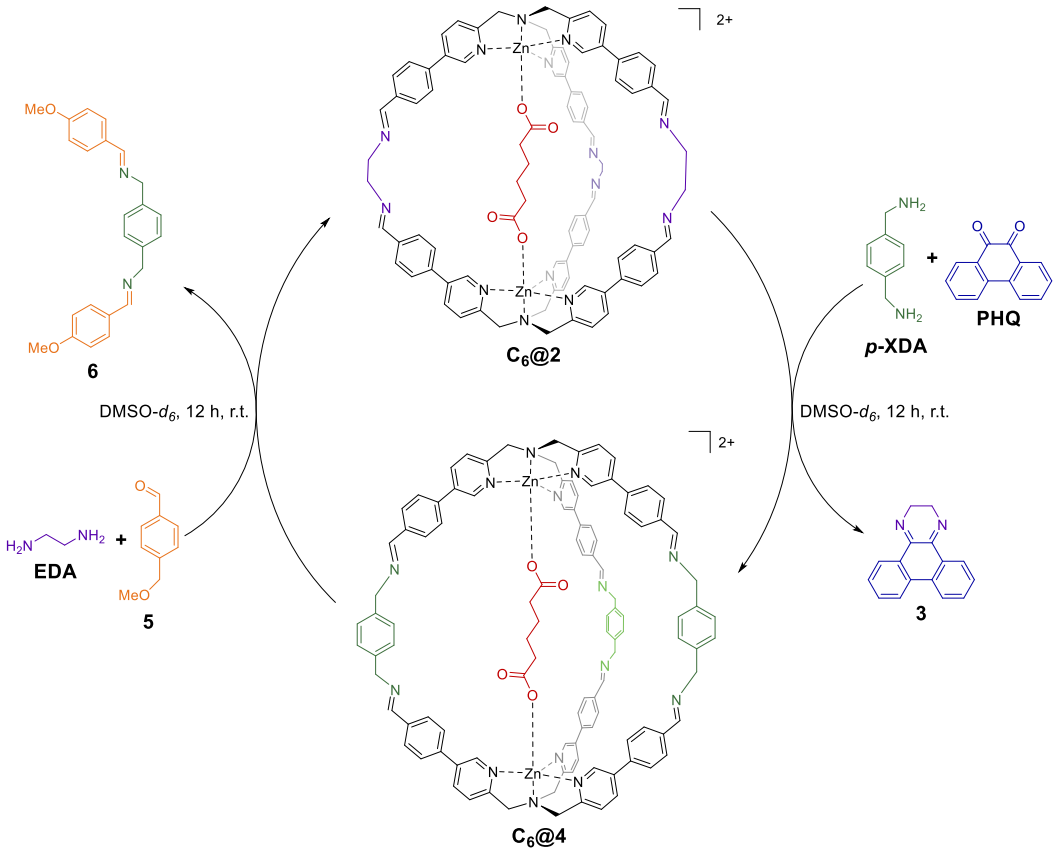

Scheme 2. Reaction scheme of the cage to cage conversion allowing the change in the size of the structure. Perchlorate counteranions have been removed for clarity.

In this second experiment, after the **C6@2** cage formation with **EDA** in which the ratio between the bound and unbound acid was 4:1 (Figure 3a), ***p*-XDA** (2.5 eq. in respect to the initial aldehyde **1**) was added simultaneously with **PHQ** (2.5 eq.). ^{1}H-NMR spectra was not changing after 12 h indicating a preferential conversion to **C6@4** (Figure 3b). However, ESI-MS showed still the presence of a minor species, which is a cage linked by two ***p*-XDA** and one **EDA** (Appendix 3, Figure A3). As a consequence of this exchange, encapsulated and free **C6** ratio changed to 1.2:1. Conversion to the initial cage was possible with addition of *p*-

anisaldehyde **5** (2.5 eq.) and **EDA** (2.5 eq.) with an overall yield of 72% obtaining 2:1 ratio among bound and unbound **C_6** (Figure 3c). The latter step was not driven to completeness by a specific sequestrator, as in the previous transformations, but by the thermodynamic stability of the cage **C_6@2**. This Case II represents an example in which cage to cage transformations allowed a change in geometry and, as a consequence, to different binding capabilities toward the only guest present in solution.

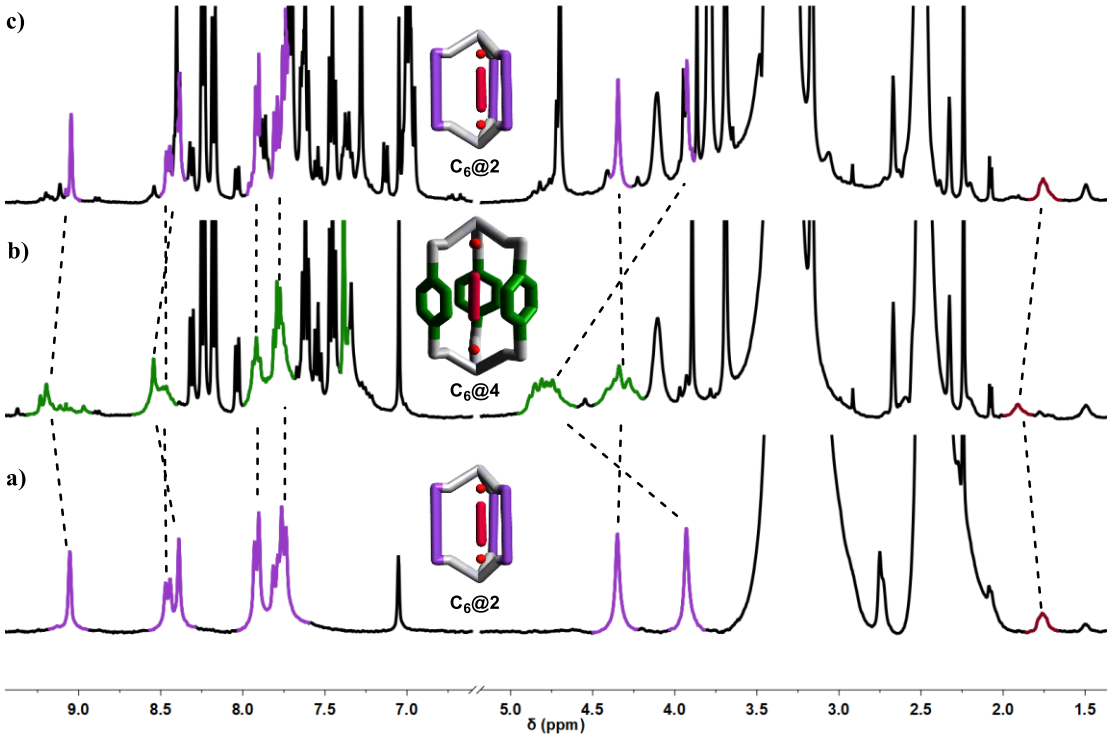

Figure 3. Partial ^{1}H-NMR (DMSO-d_6, 400 MHz) of a) cage **C_6@2**, b) cage **C_6@4** obtained after the addition of **PHQ** and ***p*-XDA** to cage **C_6@2**, and c) cage **C_6@2** obtained after the addition of **EDA** and *p*-anisaldehyde **5** to cage **C_6@4**. *P*-xylene was used as internal standard.

3.2.3. Cage-to-Cage Competing Guests (Case III)

Once the methodology for cage-to-cage was in hand, to obtain complete uptake and release of a guest a different experiment in which two diacids of different lengths were in competition in solution was conceived (Scheme 3).

In the first step, cage **C_{10}@2** was quantitively formed in DMSO-d_6 in the presence of complex **1** (1 eq.), **EDA** (2.5 eq.) and sebacic acid **C_{10}** (0.5 eq.) as guest (Figure 4a). The addition to this solution of adipic acid **C_6** (0.5 eq.) led to the complete encapsulation of the shorter diacid and the full release of **C_{10}** (Figure 4b). The selective displacement was a consequence of the higher binding constant of **C_6**, in comparison to the longer **C_{10}**, for the **EDA** linked cage.[38]

This phenomenon was also confirmed by a titration experiment followed by ^{1}H-NMR (Appendix 3, Figure A6). More in detail, guest switch was confirmed by new sets of signals in the ^{1}H-NMR spectrum in the region of the benzylic protons at 4.3 ppm of the **TPMA** arms and the α-protons of the pyridine ring at 9.0 ppm ring. In the third transformation step, the addition of ***p*-XDA** (2.5 equiv.) and **PHQ** (2.5 equiv.) led to subsequent the cage-to-cage transformation in quantitative yield (Figure 4c). More in detail, as a consequence of **EDA** trapping by the quinone, ***p*-XDA** linked caged was formed. The newly formed cage had a higher preference for the $\mathbf{C_{10}}$ in virtue of the longer metal-metal distance.[39] While in this case a complete guests switch was obtained as a consequence of cage "resizing", other experiments in which competing dicarboxylic acids lengths were varied, ranging from $\mathbf{C_4}$ to $\mathbf{C_{10}}$, led to different switch ratio in the first step (Appendix 3, Section 3.3.1).

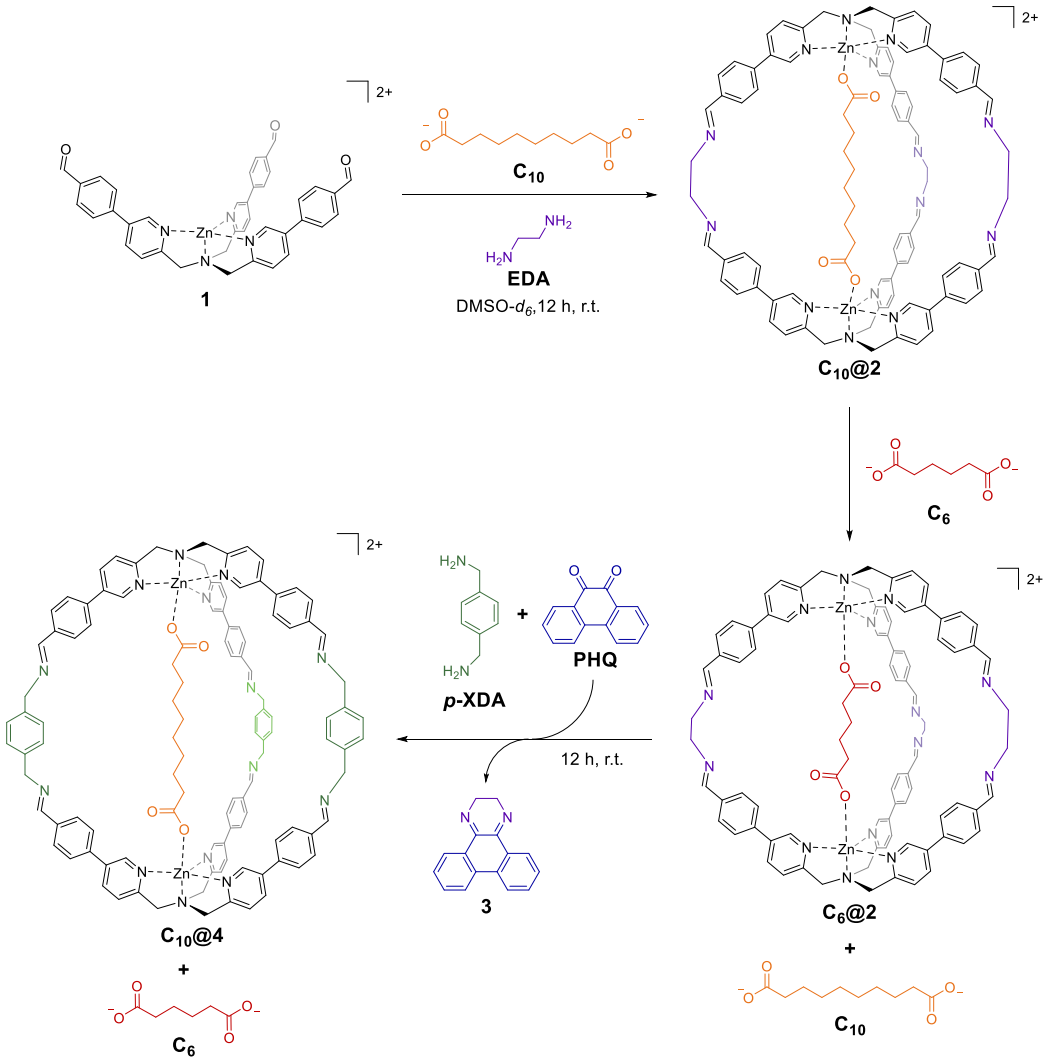

Scheme 3. Reaction scheme of the cage to cage transformation accompanied by the selective uptake and release of the guests in solution. Perchlorate counteranions have been removed for clarity.

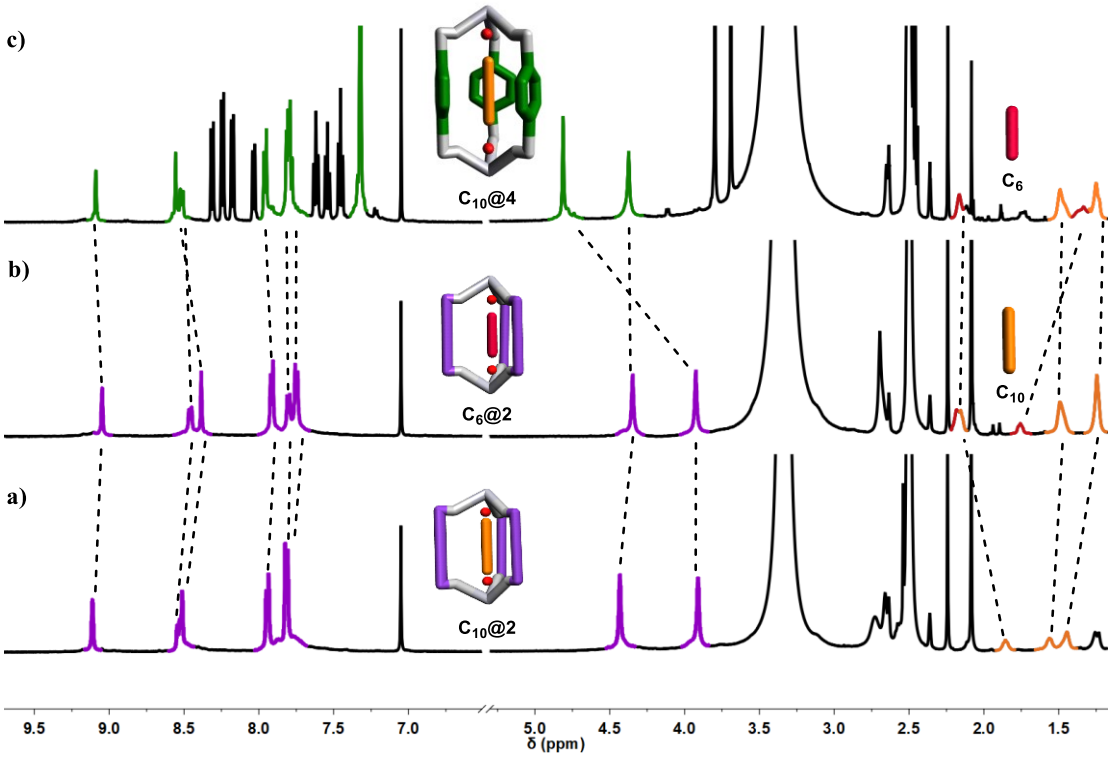

Figure 4. Partial ^{1}H-NMR (DMSO-d_6, 500 MHz) of a) cage **C_{10}@2**, b) cage **C_6@2** obtained after the addition of a stoichiometric amount of **C_6** to cage **C_{10}@2** with the complete exchange of the guest, and c) cage **C_{10}@4** obtained after the addition of **PHQ** and ***p*-XDA** to the mixture of cage **C_6@2** and **C_{10}**. *P*-xylene is used as internal standard.

3.2.4. Cage-to-Cage Enantiomeric Competing Guests (Case IV)

PHQ methodology was also challenged in the chiral realm. The latter experiment was planned with the idea to have enantiomeric guests competing with a cage which was alternatively switched in chirality by subcomponents exchange. As reported by others, **PHQ** is able to form stable adducts also with 1,2-diaminocyclohexane.[43] Taking advantage of this capability, an experiment in which two enantiomeric dicarboxylates could be selectively encapsulated upon chirality switching of the cage has been conceived. At the beginning of this fourth proof case, cage was synthesized in DMSO-d_6 using complex **1** (1 eq), *R*,*R*-diaminocyclohexane ***RR*-CHDA** (2.5 eq) in the presence of a racemic mixture of L and D dibenzoyl tartaric acid (0.5 eq each) (Scheme 4). These two guests competed for the inclusion in the chiral formed cage and, by integration of the NMR peaks of the two diastereoisomers, a remarkable preference toward D-enantiomer inclusion was observed (d.r. 17:1) (Figure 5a and Appendix 3, Figure A8). In other words, diastereoisomer ***RR*-D-Dibenz@7** was highly stable leaving L dibenzoyl tartaric acid free in solution.

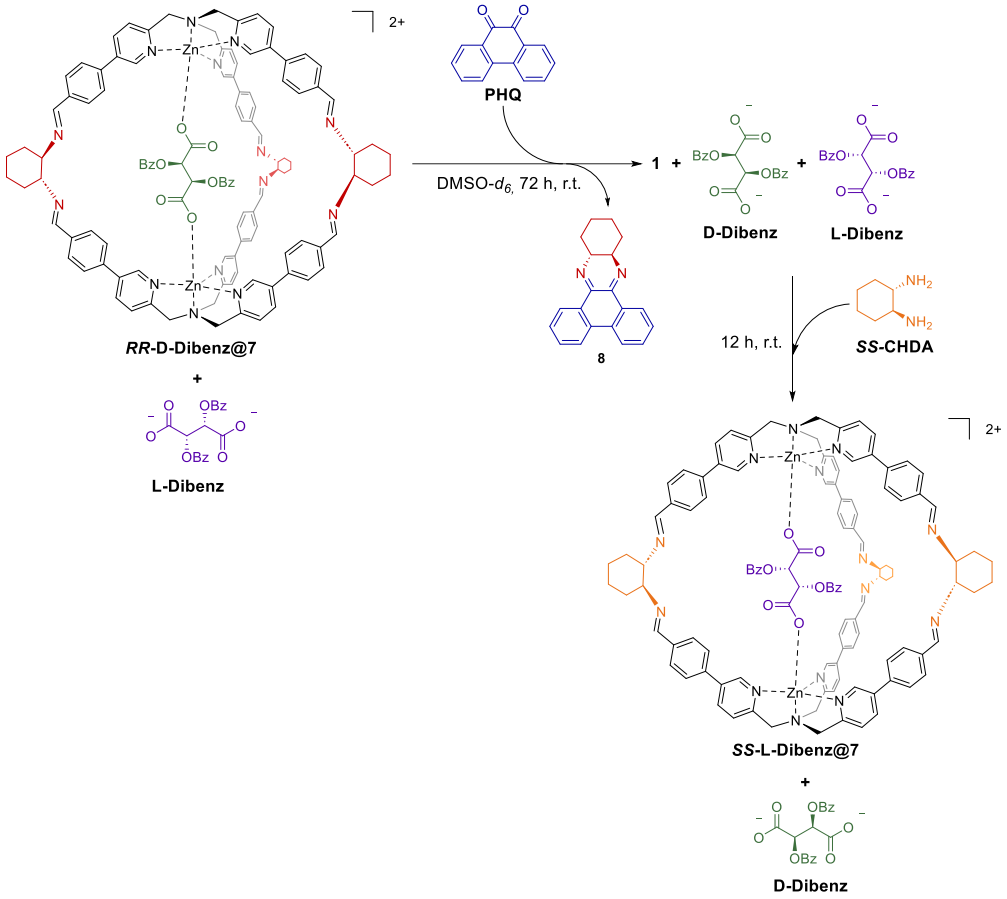

Scheme 4. Reaction scheme of the enantiomeric guest release and uptake modulated by the cage to cage conversion. Perchlorate counteranions have been removed for clarity.

Addition of **PHQ** (2.5 eq) led to the complete cage disassembly and sequestration of the chiral diamine after 72 h. This was confirmed by the disappearance of the imine peak at 8.5 ppm and the formation of the aldehyde peak at 10 ppm (Figure 5b).

Subsequent addition of *S*,*S*-diaminocyclohexane ***SS*-CHDA** (2.5 eq) drove the reaction mixture toward the formation of the enantiomeric cage ***SS*-L-Dibenz@7** and the exchange of the other enantiomeric form of the guest in 55% yield (Figure 5c and Appendix 3, Figure A10). The selective exchange of the two enantiomers was also confirmed using a pseudo-racemic mixture to have a better ^{1}H NMR resolution (Appendix 3, Section 3.5.3). To the best of our knowledge this is the first example in which uptake and release of two enantiomeric molecules can be selectively performed.

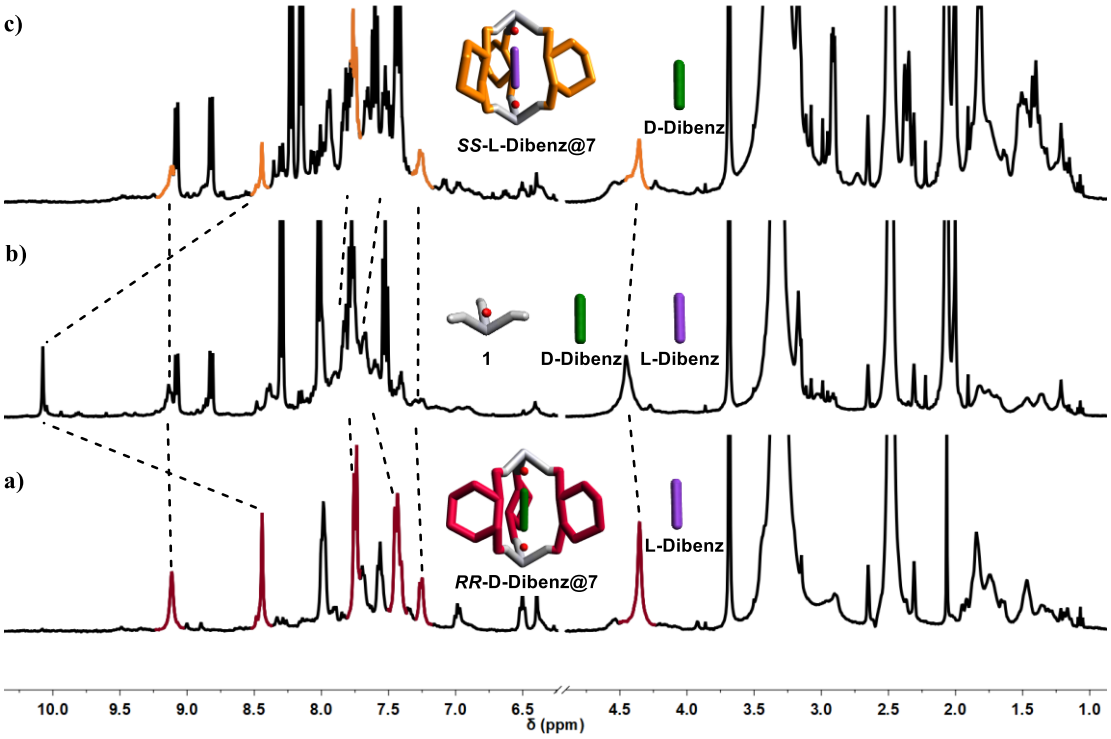

Figure 5. Partial ^{1}H-NMR (DMSO-d_6, 400 MHz) of a) cage ***RR*-D-Dibenz@7** (d.r. 17:1 between the two guests), b) complex **1** obtained from the disassembly of the cage using **PHQ** (dihydropyrazine system **8** slowly evolved to the pyrazine aromatic system), and c) 12 h after the addition of ***SS*-CHDA** that led to the formation of cage ***SS*-L-Dibenz@7** and the exchange in the selectivity for the two guests. Trimethoxy benzene is used as internal standard.

3.3. Conclusions

In conclusion, in this study, a novel quinone based strategy for selective guest release and uptake which was based either on cage disassembly/assembly or cage to cage conversions was conceived. Guests uptake and release has been successfully optimized allowing: *i*) reversible assembly and disassembly of the cage with release and uptake of the guest, *ii*) cage to cage conversions with switch in affinity toward guests of different sizes, and *iii*) inversion in cage chirality with the concomitant and selective uptake and release of two enantiomeric diacids. Due to the wide use of imine DCC methodology in the formation of supramolecular architectures, this methodology could pave the way to the selective release and uptake in other architectures that take advantage of diamine DCC chemistry.

3.4. Experimental Section

3.4.1. Synthesis of Cages R@2

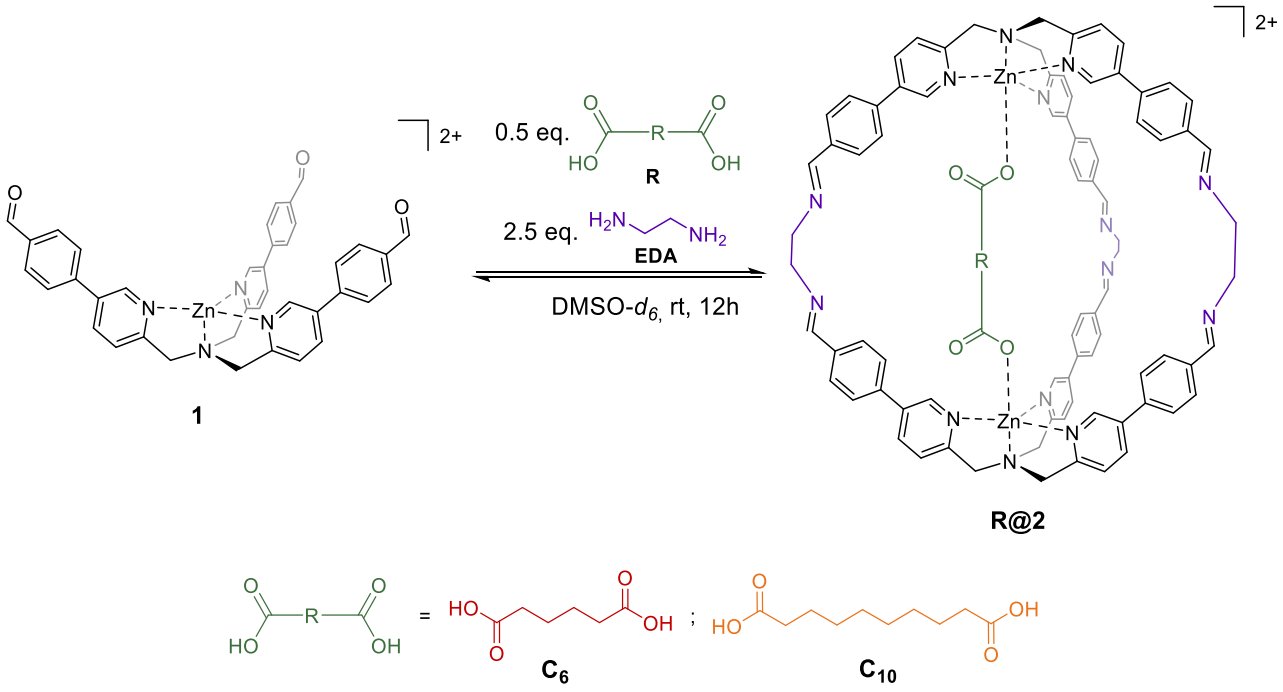

General procedure for the synthesis of molecular cages **R@2**.[39] Perchlorate counterions are removed for clarity.

To 500 µL (1.0 µmol) of a solution 0.002 M of the aldehyde zinc complex **1** in DMSO-d_6, 25 µL (0.5 µmol) of a solution 0.02 M in DMSO-d_6 of a dicarboxylic acid **R** and 125 µL (2.5 µmol) of a solution 0.02 M in DMSO-d_6 of ethylenediamine **EDA** were added in a NMR tube. The mixture was left overnight at room temperature and checked *via* ^{1}H-NMR. The yield for all the cages is >95% (Determined *via* ^{1}H-NMR on internal standard *p*-xylene).

3.4.1.1. C_6@2

^{1}H-NMR (400 MHz, DMSO-d_6) δ (ppm): 9.04 (s, 6H, PyrH), 8.46 (d, J = 8.2, 6H, PyrH), 8.38 (s, 6H, NH_{imm}), 7.91 (d, J = 8.0 Hz, 12H, ArH), 7.80 (d, J = 8.3 Hz, 6H, PyrH), 7.75 (d, J = 8.0 Hz, 12H, ArH), 4.35 (s, 12H, $CH_{2\text{-TPMA}}$), 3.93 (s, 12H, $CH_{2\text{-EDA}}$), 1.78 – 1.74 (m, 4H, $CH_{2\text{-acid}}$) (4H, $CH_{2\text{-acid}}$, hide by solvent).

MS (ESI-MS) (*m/z*): [M^{2+}] calcd. for $[C_{90}H_{80}N_{14}O_4Zn_2]^{2+}$, 774.25; found 774.23

3.4.1.2. C_{10}@2

^{1}H-NMR (500 MHz, DMSO-d_6) δ (ppm): 9.11 (s, 6H, PyrH), 8.54 (d, J = 8.3, 6H, PyrH), 8.51 (s, 6H, NH_{imm}), 7.94 (d, J = 8.0 Hz, 12H, ArH), 7.82 – 7.81 (m, 18H, PyrH + ArH), 4.43 (s, 12H, $CH_{2\text{-}TPMA}$), 3.91 (s, 12H , $CH_{2\text{-}EDA}$), 1.88 – 1.82 (m, 6H, $CH_{2\text{-}acid}$), 1.60 – 1.54 (m, 6H, $CH_{2\text{-}acid}$), 1.49 – 1.40 (m, 6H, $CH_{2\text{-}acid}$)
MS (ESI-MS) (m/z): [M^{2+}] calcd. for $[C_{94}H_{88}N_{14}O_4Zn_2]^{2+}$, 804.28; found 804.31

3.4.2. Synthesis of Cages R@4

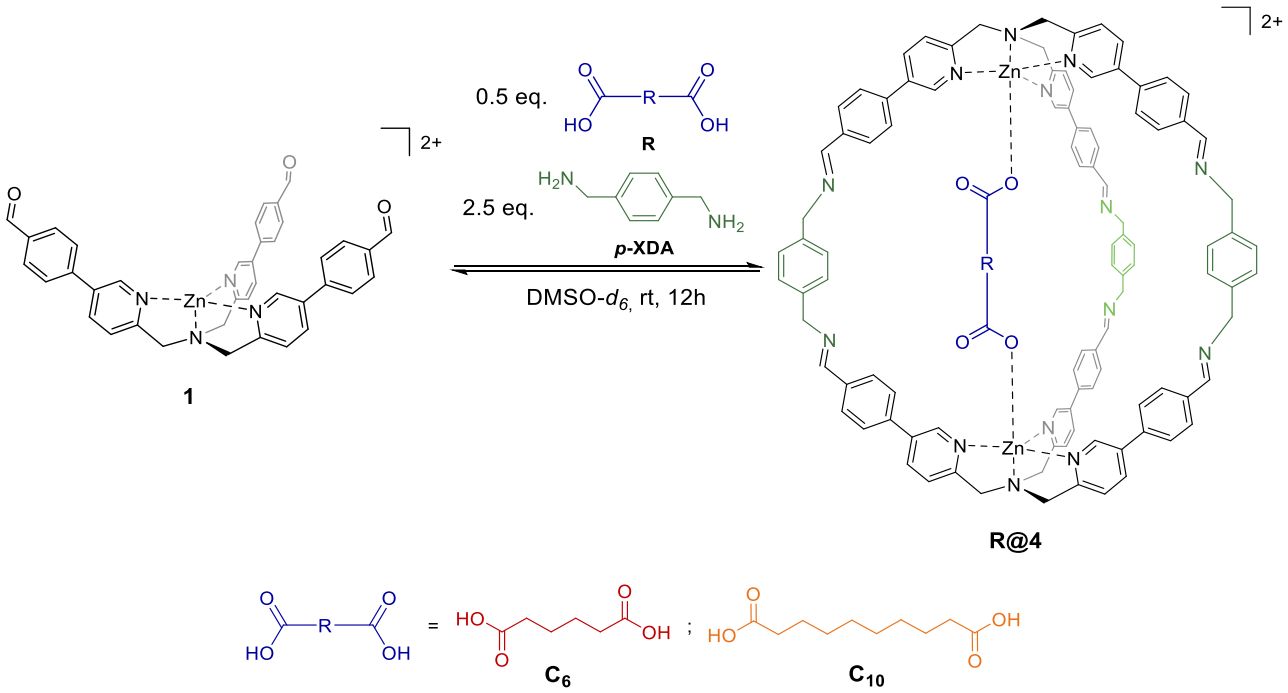

General procedure for the synthesis of molecular cages **R@5**.[39] Perchlorate counterions are removed for clarity.

To 500 µL (1.0 µmol) of a solution 0.002 M of the aldehyde zinc complex **1** in DMSO-d_6, 25 µL (0.5 µmol) of a solution 0.02 M in DMSO-d_6 of a dicarboxylic acid **R** and 125 µL (2.5 µmol) of a solution 0.02 M in DMSO-d_6 of *p*-xylylenediamine ***p*-XDA** were added in a NMR tube. The mixture was left overnight at room temperature and checked *via* ^{1}H-NMR. The yield for all the cages is >95% (Determined *via* ^{1}H-NMR on internal standard *p*-xylene).

3.4.2.1. C_6@4

^{1}H-NMR (400 MHz, DMSO-d_6) δ (ppm): 9.33 – 8.89 (m, 6H, PyrH), 8.63 – 8.35 (m, 12H, NH_{imm}+ PyrH), 8.09 – 7.84 (m, 12H, ArH), 7.77 (m, 18H, PyrH + ArH), 7.38 (s, 12H, $ArH_{p\text{-}xylDA}$), 4.79 (m, 12H, $CH_{2\text{-}TPMA}$), 4.49 – 4.06 (m, 12H, $CH_{2\text{-}pxylDA}$),1.98 – 1.84 (m, 6H, $CH_{2\text{-}acid}$), 1.25 – 1.18 (m, 2H, $CH_{2\text{-}acid}$).

MS (ESI-MS) (*m/z*): [(M^{2+}-C_6)+2Cl^-] calcd. for $[C_{102}H_{84}Cl_2N_{14}Zn_2]^{2+}$, 853.24; found 853.27

3.4.2.2. C_{10}@4

^{1}H-NMR (400 MHz, DMSO-d_6) δ (ppm): 9.09 (s, 6H, PyrH), 8.56 (s, 6H, NH_{imm}), 8.52 (d, *J* = 8.2, 6H, PyrH), 7.96 (d, *J* = 8.0 Hz, 12H, ArH), 7.88 – 7.62 (m, 18H, PyrH + ArH), 7.36 (s, 12H, $ArH_{p\text{-}xylDA}$), 4.81 (s, 12H, $CH_{2\text{-}TPMA}$), 4.38 (s, 12H, $CH_{2\text{-}pxylDA}$), 1.76 – 1.72 (m, 6H, $CH_{2\text{-}acid}$), 1.35 – 1.23 (m, 12H, $CH_{2\text{-}acid}$).

MS (ESI-MS) (*m/z*): [M^{2+}] calcd. for $[C_{112}H_{100}N_{14}O_4Zn_2]^{2+}$, 918.33; found 918.38

3.4.3. Synthesis of Cages *RR*-R@7

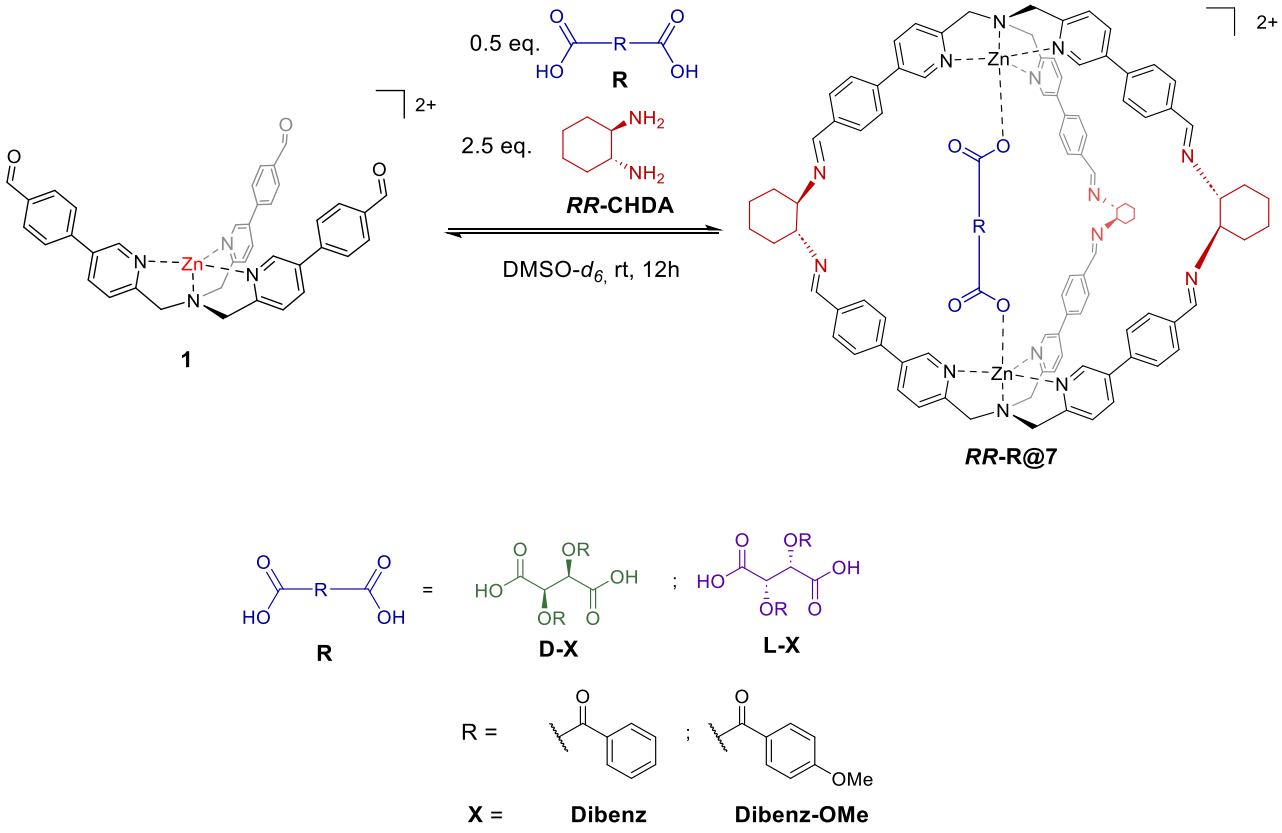

General procedure for the synthesis of molecular cages ***RR*-R@7**. Perchlorate counterions are removed for clarity.

To 500 µL (1.0 µmol) of a solution 0.002 M of the aldehyde zinc complex **2** in DMSO-d_6, 50 µL (0.5 µmol) of a solution 0.02 M in DMSO-d_6 of a dicarboxylic acid **R** and 125 µL (2.5 µmol) of a solution 0.02 M in DMSO-d_6 of *R*,*R*-cyclohexyldiamine ***RR*-CHDA** were added in a NMR tube. The mixture was left overnight at room temperature and checked *via* ^{1}H-NMR. The yield for all the cages is >95% (Determined *via* ^{1}H-NMR on internal standard 1,3,5-trimetoxybenzene).

3.4.3.1. *RR*-D-Dibenzoyl@7

^{1}H-NMR (400 MHz, DMSO-d_6) δ (ppm): 9.14 (s, 6H, PyrH), 8.46 (s, 6H, NH_{imm}), 8.01 (d, *J* = 8.0 Hz, 6H, PyrH), 7.77 (d, *J* = 7.9 Hz, 12H, ArH), 7.48z – 7.39 (m, 18H, ArH + PyrH), 7.28 (d, *J* = 7.3 Hz, 4H, $ArH_{benzoyl}$), 7.03 – 6.99 (m, 2H, $ArH_{benzoyl}$), 6.56 – 6.52 (m, 4H), 6.42 (s, 2H, $CH_{benzoyl}$), 4.38 (s, 12H, CH_2-$_{TPMA}$), 1.88 – 1.83 (m, 6H, CH_2-$_{cyclohexDA}$), 1.69 – 1.64 (m, 6H, CH_2-$_{cyclohexDA}$), 1.52 – 1.49 (m, 6H, CH_2-$_{cyclohexDA}$), 1.18 – 1.14 (m, 6H, CH_2-$_{cyclohexDA}$).
MS (ESI-MS) (*m/z*): $[M^{2+}]$ calcd. for $[C_{114}H_{102}N_{14}O_8Zn_2]^{2+}$, 963.33; found 963.36

3.4.3.2. *RR*-L-Dibenzoyl @7

^{1}H-NMR (400 MHz, DMSO-d_6) δ (ppm): 9.02 (s, 6H, PyrH), 8.31 (s, 6H, NH_{imm}), 8.08 (d, J = 8.1 Hz, 6H, PyrH), 7.71 – 7.65 (m, 16H, ArH + $ArH_{benzoyl}$), 7.52 (d, J = 8.2 Hz, 6H, PyrH), 7.38 – 7.36 (m, 14H, ArH + $ArH_{benzoyl}$), 7.01 – 6.97 (m, 4H, $ArH_{benzoyl}$), 6.29 (s, 2H, $CH_{benzoyl}$), 4.38 (m, 12H, CH_2-$_{TPMA}$), 1.88 – 1.84 (m, 6H, CH_2-$_{cyclohexDA}$), 1.68 – 1.63 (m, 6H, CH_2-$_{cyclohexDA}$), 1.52 – 1.49 (m, 6H, CH_2-$_{cyclohexDA}$), 1.19 – 1.14 (m, 6H, CH_2-$_{cyclohexDA}$).
MS (ESI-MS) (*m/z*): $[M^{2+}]$ calcd. for $[C_{114}H_{102}N_{14}O_8Zn_2]^{2+}$, 963.33; found 963.36

3.4.3.3. *RR*-D-Dibenzoyl-OMe@7

^{1}H-NMR (400 MHz, DMSO-d_6) δ (ppm): 9.50 – 8.75 (m, 6H, PyrH), 8.63 – 8.30 (m, 6H, NH_{imm}), 8.19 – 7.96 (m, 6H, PyrH), 7.88 – 7.31 (m, 33H, ArH + PyrH + $ArH_{benzoyl}$), 7.17 (d, *J* = 7.9 Hz, 1H, $ArH_{benzoyl}$), 7.01 – 6.97 (m, 2H, $ArH_{benzoyl}$), 6.49 (s, 1H, $CH_{benzoyl\ I}$), 6.23 (s, 1H, $CH_{benzoyl}$), 6.03 (d, *J* = 8.0 Hz, 2H, $ArH_{benzoyl}$), 5.91 (d, *J* = 7.9 Hz, 1H, $ArH_{benzoyl}$, 4.53 – 4.09 (m, 12H, CH_2-$_{TPMA}$), 3.86 – 3.79 (m, 6H, CH_3-$_{benzoy}$) 1.89 – 1.82 (m, 8H, CH_2-$_{cyclohexDA}$), 1.67 – 1.62 (m, 4H, CH_2-$_{cyclohexDA}$), 1.51 – 1.44 (m, 4H, CH_2-$_{cyclohexDA}$), 1.17 – 1.12 (m, 8H, CH_2-$_{cyclohexDA}$).
MS (ESI-MS) (*m/z*): $[M^{2+}]$ calcd. for $[C_{116}H_{106}N_{14}O_{10}Zn_2]^{2+}$, 993.34; found 993.40

3.4.3.4. *RR*-L-Dibenzoyl-Ome@7

^{1}H-NMR (400 MHz, DMSO-d_6) δ (ppm): 9.39 – 8.74 (m, 6H, PyrH), 8.50 – 8.30 (m, 6H, NH_{imm}), 8.20 – 8.01 (m, 6H, PyrH), 7.93 – 7.37 (m, 32H, ArH + PyrH + $ArH_{benzoyl}$), 7.30 (d, *J* = 7.9 Hz, 1H, $ArH_{benzoyl}$), 7.19 (d, *J* = 7.9 Hz, 2H, $ArH_{benzoyl}$), 7.04 (d, *J* = 8.7 Hz, 1H, $ArH_{benzoyl}$), 6.80 (d, *J* = 7.8 Hz, 1H, $ArH_{benzoyl}$), 6.49 (d, *J* = 8.0 Hz, 2H, $ArH_{benzoyl}$), 6.31 (d, *J* = 8.6 Hz, 1H, $ArH_{benzoyl}$). 6.08 (s, 2H, $CH_{benzoyl}$), 4.52 – 4.27 (m, 12H, CH_2-$_{TPMA}$), 3.71 (s, 6H, CH_3-$_{benzoy}$), 1.90 – 1.82 (m, 8H, CH_2-$_{cyclohexDA}$), 1.66 – 1.61 (m, 4H, CH_2-$_{cyclohexDA}$), 1.52 – 1.45 (m, 4H, CH_2-$_{cyclohexDA}$), 1.19 – 1.14 (m, 8H, CH_2-$_{cyclohexDA}$).

MS (ESI-MS) (*m/z*): [M^{2+}] calcd. for $[C_{116}H_{106}N_{14}O_{10}Zn_2]^{2+}$, 993.34; found 993.40

3.5. References

[1] W. C. Geng, J. L. Sessler, D. S. Guo, *Chem. Soc. Rev.* **2020**, *49*, 2303–2315.
[2] G. Szalóki, V. Croué, V. Carré, F. Aubriet, O. Alévêque, E. Levillain, M. Allain, J. Aragó, E. Ortí, S. Goeb, M. Sallé, *Angew. Chemie* **2017**, *129*, 16490–16494.
[3] I. A. Riddell, M. M. J. Smulders, J. K. Clegg, J. R. Nitschke, *Chem. Commun* **2011**, *47*, 459.
[4] N. Ahmad, H. A. Younus, A. H. Chughtai Abd, F. Verpoort, *Chem. Soc. Rev* **2015**, *44*, 6804-6849.
[5] T. R. Cook, P. J. Stang, *Chem. Rev.* **2015**, *115*, 7001–7045.
[6] S. Zarra, D. M. Wood, D. A. Roberts, J. R. Nitschke, *Chem. Soc. Rev.* **2015**, *44*, 419–432.
[7] M. Han, D. M. Engelhard, G. H. Clever, *Chem. Soc. Rev.* **2014**, *43*, 1848–1860.
[8] S. Mukherjee, P. S. Mukherjee, *Chem. Commun* **2014**, *50*, 2248.
[9] K. Harris, D. Fujita, M. Fujita, *Chem. Commun* **2013**, *49*, 6703–6712.
[10] P. Mal, D. Schultz, K. Beyeh, K. Rissanen, J. R. Nitschke, *Angew. Chem. Int. Ed.* **2008**, *47*, 8297–8301.
[11] M. Scherer, D. L. Caulder, D. W. Johnson, K. N. Raymond, *Angew. Chem. Int. Ed.* **1999**, *38*, 1587–1592.
[12] S. Wang, T. Sawada, M. Fujita, *Chem. Commun.* **2016**, *52*, 11653–11656.
[13] M. Scherer, D. L. Caulder, D. W. Johnson, K. N. Raymond, K. N. Raymond, M. Scherer, D. L. Caulder, D. W. Johnson, *Angew. Chem. Int. Ed* **1999**, *38*, 1588–1592.
[14] F. J. Rizzuto, J. R. Nitschke, *Nat. Chem.* **2017**, *9*, 903–908.
[15] P. Cheng, L. Cai, S. Li, S. Hu, D. Yan, L. Zhou, Q. Sun, *Angew. Chemie* **2020**, *132*, 23775–23779.
[16] R. Sekiya, M. Fukuda, R. Kuroda, *J. Am. Chem. Soc.* **2012**, *134*, 10987–10997.
[17] M. M. Deegan, M. R. Dworzak, A. J. Gosselin, K. J. Korman, E. D. Bloch, *Chem. - A Eur. J.* **2021**, *27*, 4531–4547.
[18] M. Mastalerz, M. W. Schneider, I. M. Oppel, O. Presly, *Angew. Chem. Int. Ed.* **2011**, *50*, 1046–1051.
[19] P. A. Gale, E. N. W. Howe, X. Wu, M. J. Spooner, *Coord. Chem. Rev.* **2018**, *375*, 333–372.
[20] L. Chen, S. N. Berry, X. Wu, E. N. W. Howe, P. A. Gale, *Chem* **2020**, *6*, 61–141.
[21] Y. Xue, X. Hang, J. Ding, B. Li, R. Zhu, H. Pang, Q. Xu, *Coord. Chem. Rev.* **2021**, *430*, 213656.
[22] N. Kishi, M. Akita, M. Yoshizawa, *Angew. Chemie* **2014**, *126*, 3678–3681.
[23] C. Colomban, G. Szalóki, M. Allain, L. Gómez, S. Goeb, M. Sallé, M. Costas, X. Ribas, *Chem. - A Eur. J.* **2017**, *23*, 3016–3022.
[24] P. Mal, D. Schultz, K. Beyeh, K. Rissanen, J. R. Nitschke, J. R. Nitschke, K. Beyeh, K. Rissanen, D. Schultz, *Angew. Chem. Int. Ed.* **2008**, *47*, 8297–8301.
[25] J. E. M. Lewis, E. L. Gavey, S. A. Cameron, J. D. Crowley, *Chem. Sci.* **2012**, *3*, 778–784.
[26] W. Cullen, S. Turega, C. A. Hunter, M. D. Ward, *Chem. Sci.* **2014**, *6*, 625–631.
[27] M. M. J. Smulders, S. Zarra, J. R. Nitschke, *J. Am. Chem. Soc.* **2013**, *135*, 7039–7046.
[28] W. Y. Sun, T. Kusukawa, M. Fujita, *J. Am. Chem. Soc.* **2002**, *124*, 11570–11571.
[29] C. Colomban, G. Szalóki, M. Allain, L. Gómez, S. Goeb, M. Sallé, M. Costas, X. Ribas, *Chem. – A Eur. J.* **2017**, *23*, 3016–3022.
[30] G. H. Clever, S. Tashiro, M. Shionoya, *J. Am. Chem. Soc.* **2010**, *132*, 9973–9975.
[31] A. J. McConnell, C. M. Aitchison, A. B. Grommet, J. R. Nitschke, *J. Am. Chem. Soc.* **2017**, *139*, 6294–6297.
[32] S. Akine, M. Miyashita, T. Nabeshima, *Chem. - A Eur. J.* **2019**, *25*, 1432–1435.
[33] E. Benchimol, B.-N. T. Nguyen, T. K. Ronson, J. R. Nitschke, *Chem. Soc. Rev* **2022**, *51*, 5101–5135.
[34] R. Nussinov, *Chem. Rev.* **2016**, *116*, 6263–6266.
[35] S. Raman, *Biochemistry* **2018**, *57*, 376–382.
[36] S. M. Butler, K. A. Jolliffe, *Org. Biomol. Chem.* **2020**, *18*, 8236–8254.
[37] C. Bravin, J. A. Piękoś, G. Licini, C. A. Hunter, C. Zonta, *Angew. Chem. Int. Ed.* **2021**, *60*, 23871–23877.
[38] C. Bravin, E. Badetti, F. A. Scaramuzzo, G. Licini, C. Zonta, *J. Am. Chem. Soc.* **2017**, *139*, 6456–6460.
[39] C. Bravin, E. Badetti, R. Puttreddy, F. Pan, K. Rissanen, G. Licini, C. Zonta, *Chem. Eur. J.* **2018**, *24*, 2936–2943.
[40] F. Begato, R. Penasa, G. Licini, C. Zonta, *Chem. Commun.* **2021**, *57*, 10019–10022.
[41] F. Begato, R. Penasa, G. Licini, C. Zonta, *ACS Sensors* **2022**, *7*, 1390–1394.
[42] R. Van Belzen, R. A. Klein, W. J. J. Smeets, A. L. Spek, R. Benedix, C. J. Elsevier, *Recl. des Trav. Chim. des Pays-Bas* **1996**, *115*, 275–285.
[43] M. L. Jimeno, J. L. G. de Paz, J. Rodriguez, M. Rodriguez, C. Ochoa, *An. Quim.* **1994**, *90*, 423–431.

Chapter 4

Freeze the Dynamic! Combining Imine Condensation Chemistry with [3,3] Diaza-Cope Rearrangement for the Formation of Chiral Supramolecular Architectures

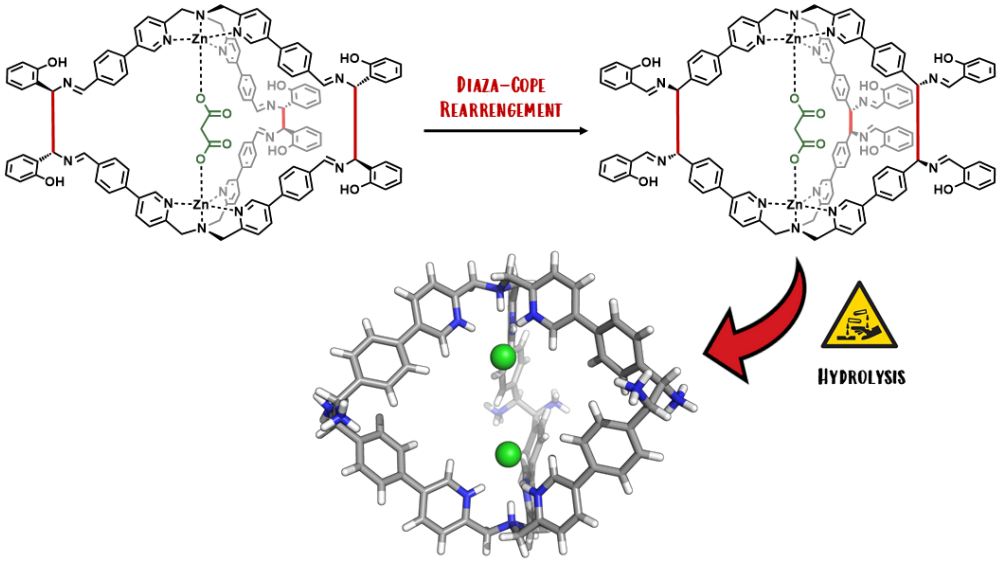

ABSTRACT Dynamic Covalent Chemistry has opened the supramolecular chemistry community toward molecular architectures of increasing complexity. In recent years, the research group took advantage of imine DCC chemistry to prepare novel **TPMA** based supramolecular cages for molecular recognition applications. However, the versatility of this approach had as major drawback the intrinsic hydrolytic lability of imines that hampered some of their applications. In this chapter, a novel synthetic strategy that combines the thermodynamic driven formation of a supramolecular structure using imine chemistry, together with a consecutive [3,3]-sigmatropic rearrangement which allows for the formation of chiral hydrolytically stable structures in a one-pot reaction is herein presented. A preliminary mechanistic analysis and the scope of the reaction has also been discussed.

4.1. Introduction

Dynamic covalent chemistry (DCC), has been widely used for the formation of supramolecular architectures from relatively simple building blocks.[1–4] Among the possible reversible bonds, imine condensation has been extensively used for the synthesis of large organic cages of defined shapes and sizes in excellent yields.[5–7] This powerful capability arises from the dynamic nature of imine bond that offers to the building subcomponents the possibility to experience an “error-checking” process which allows to obtain primarily the most stable thermodynamic assembly.[8–10] However, the chemical versatility can be a drawback since the presence of acids and nucleophiles could lead to the hydrolysis of the of the C=N bond, thus limiting the functional applicability of the resulting architectures.

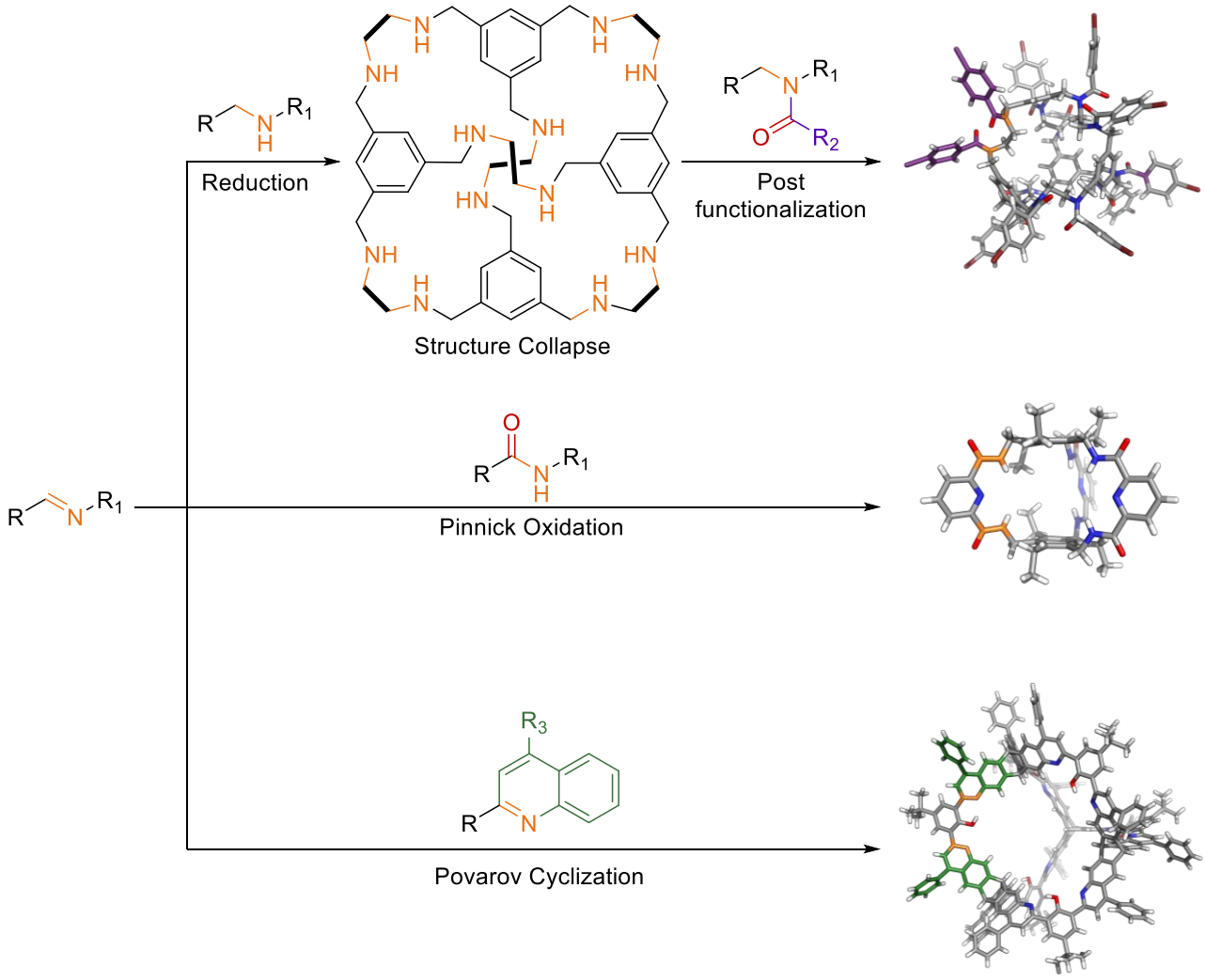

Figure 1. Strategies developed to make hydrolytically-stable cages starting from the imine architectures.[11–13]

A possibility to transform imines in more chemically stable bonds is offered by the reduction to the corresponding amines using hydrides.[14–16] However, it has been observed that the reduction to the corresponding amine leads to a greater degree of flexibility of the structure and this can be accompanied by a collapse of the shape-persistency and a loss of porosity in solid state.[17,18] Nevertheless, this property could be recovered by a post functionalization reaction of the resulting amine cage in order to change the functional properties (*e.g.* solubility, porosity, etc.).[11,19,20] Other possibilities to stabilize imine cages have been reported by Mastalerz which, using either a Pinnick oxidation[12,21] or a Povarov cyclization,[13] was able to prepare stable cage derivatives (Figure 1). However, these examples required the isolation of the precursors, and the overall yields of the final products were usually moderate. In addition, to the best of our knowledge, examples of chemical "stabilization" regarding chiral imine cages have not been reported.

The research group in which this thesis has been carried out has also largely exploit DCC imine chemistry in the recent years for the synthesis of tris(2-pyridylmethyl)amine **TPMA**-based supramolecular cages.[22] Beside high yields offered by this approach, the group further took advantage of the dynamic nature of imine chemistry to: *i*) trigger their assembly and disassembly in solution,[23] *ii*) use them as differential sensors for dicarboxylic acids,[24] and *iii*) synthesize these structures in complex matrixes.[25,26] However, while the reversibility of the imine bond is offering a versatility that can be successfully exploited in sensing, attempts to extend the application of our reported systems were hampered by imine lability. In addition, the use of reducing agents to form more stable systems (*e.g.,* $NaBH_4$ or $NaBHOAc_3$) resulted in very low conversions and, due the nature itself of the reduced compound (*viz*. a polypyridine amine system), it was possible to develop efficient reactions work-up.

In this chapter, a novel synthetic strategy which combines the advantages of imine chemistry (*viz*. formation of the thermodynamic product) with the formation of stable C-C bonds among the "dynamic" subcomponents offered by a [3,3]-sigmatropic rearrangement has been reported. Using this methodology, three novel hydrolytically stable chiral architectures have been prepared in high yields in a one-pot reaction. The molecular factors influencing the rearrangement reactivity, mechanistic insights of the novel formed cage and the crystal structure of the formed chiral cage have been also presented.

4.2. Results and Discussion

4.2.1. Synthesis of a novel Hydrolytically stable Chiral Cage

In recent years the group has extensively employed aldehydic system **1** in combination with different diamines for the preparation of different **TPMA**-based cages.[27] In the quest for the preparation of chiral diamines subcomponents,[28] the reaction developed by Chin which offers the possibility to prepare chiral diamines starting from (*R*,*R*)-1,2-Bis(2-Hydroxyphenyl)ethylenediamine **(*R*,*R*)-HPEDA** and any type of aldehyde (Scheme 1) has been encountered.[29] This procedure consists in a imine formation followed by a stereospecific [3,3]-sigmatropic Diaza-Cope rearrangement (DCR) (Scheme 1).[30] The shift of the rearrangement equilibrium is driven by the formation of strong resonance-assisted hydrogen bonds (RAHB) by the phenolic groups in the rearranged product which after hydrolysis results in the novel diamine in which a carbon-carbon bond between the initial aldehydes is formed.[31,32]

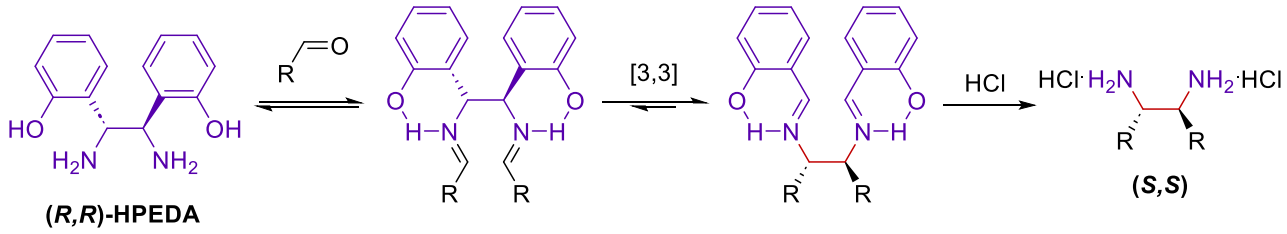

Scheme 1. [3,3]-sigmatropic Diaza-Cope rearrangement for the synthesis of chiral diamines.

Taking inspiration by this powerful reaction, the possibility to apply this strategy for the synthesis of novel chiral and hydrolytically stable **TPMA**-based architectures has been envisioned.

More in detail, aldehyde zinc(II) complex **1** (1 eq) was mixed with **(*R*,*R*)-HPEDA** (2.5 eq) in the presence of malonic acid **C_3** acid (0.5 eq) in a mixture of CD_3CN and 5% of DMSO-d_6 (Scheme 2).

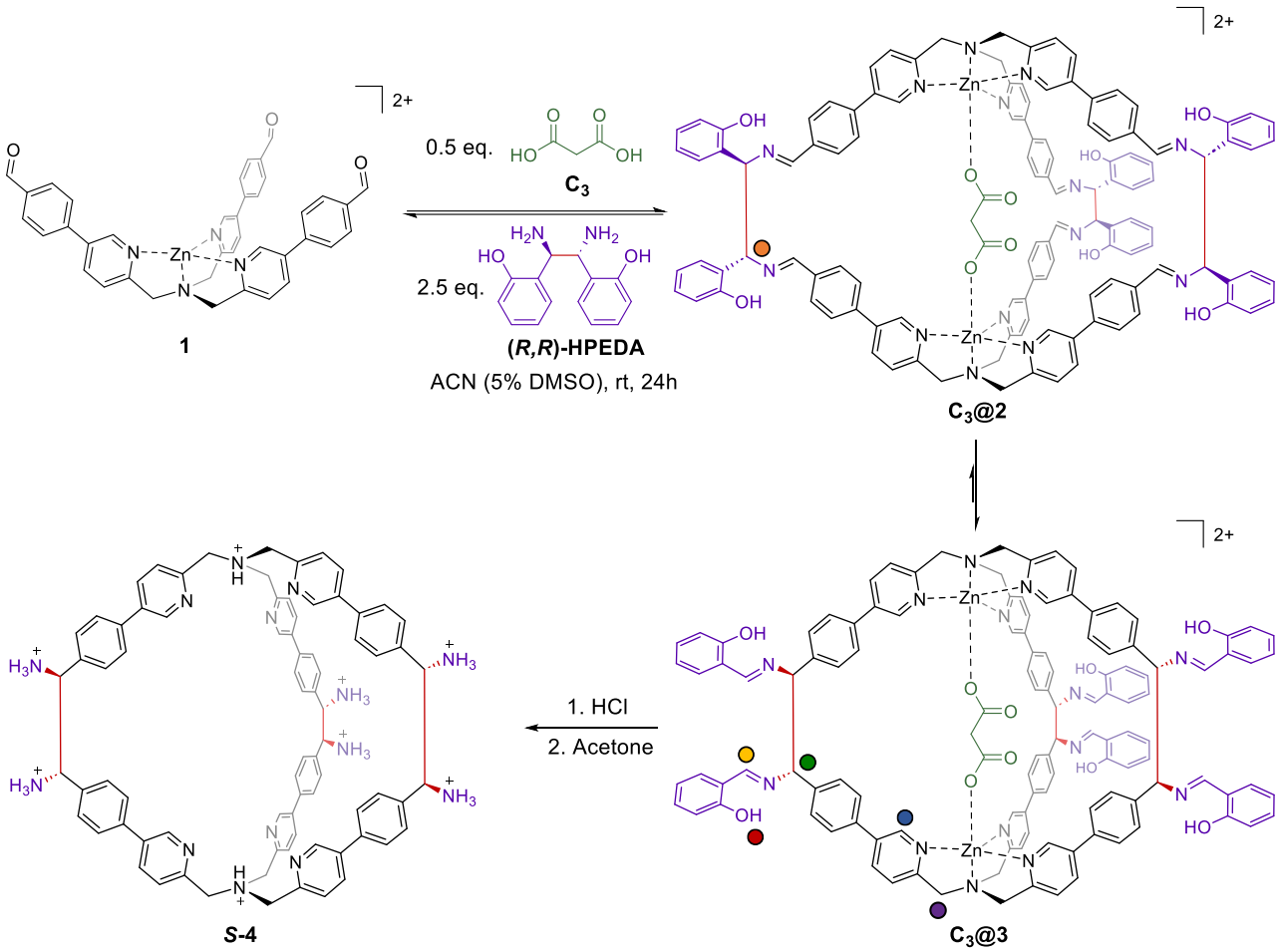

Scheme 2. Reaction scheme for the [3,3]-sigmatropic Diaza-Cope rearrangement for the synthesis of chiral **TPMA**-based cage. Perchlorate and chloride counteranions are removed for clarity.[33]

As shown in Figure 2, ^{1}H NMR kinetic profile of the mixture showed the complete disappearance of the aldehyde peak at 10.05 ppm and the appearance of the proton imine signal at 8.60 ppm (Figure 2 – yellow dots). In addition, a signal at 13.03 ppm (Figure 2 – red dots), which was indicative of the characteristic RAHB proton of the rearranged system, started to appear after 1 hour. At the beginning of the reaction, ^{1}H-NMR spectra also highlight the formation of cage **C$_3$@2**, confirmed by the singlet at 5.40 ppm corresponding to the CH protons of the unrearranged diamine (Figure 2 – orange dots). As the reaction proceed, this peak became broad, and barely visible after 24 hours when the reaction was subjected to hydrolysis using HCl to recover the poli-pyridine ammonium salt ***S*-4** in both high yield (87%) and purity.

The obtained compound, recrystallized from acetone, was completely water soluble and showed a high stability at low pH (*e.g.* addition of DCl to pH= 1 showed a ^{1}H-NMR stable for more than two weeks) (Appendix 4, Figure A63).

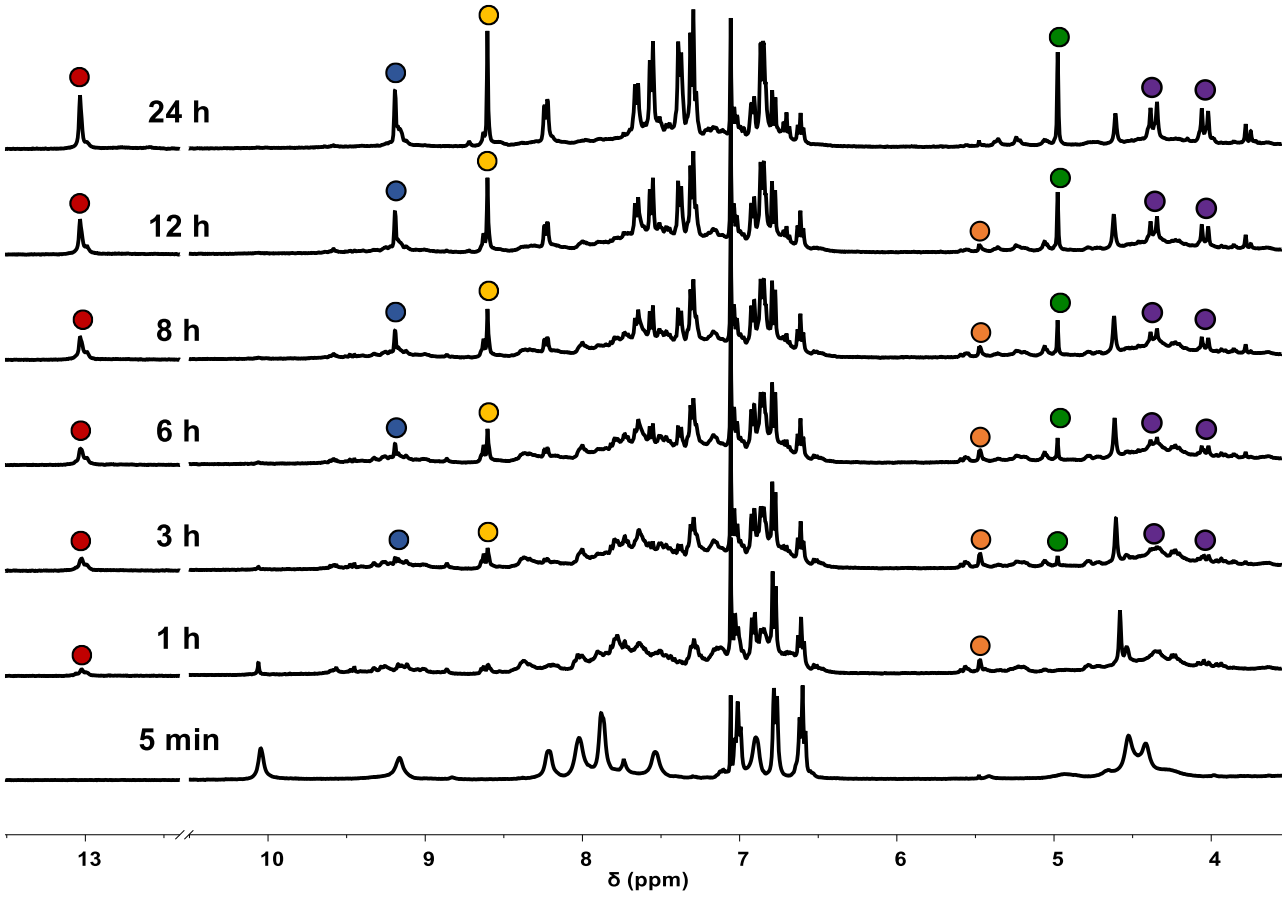

Figure 2. Partial ^{1}H-NMR (400 MHz, 301 K, CD_3CN with 5% DMSO-d_6) spectra in time progression of complex **1** after the addition of 2.5 equiv. of **(*R*,*R*)-HPEDA** and 0.5 equiv. of **C_3**. Times are related to the addition of **C_3** and **(*R*,*R*)-HPEDA** to the solution of complex **1**.

4.2.2. Crystal structure

X-ray diffraction of ***S*-4** single-crystals, obtained by slow evaporation of a water/DMSO solution, disclosed a C_3 symmetry for the architecture in the solid state in which the two **TPMA** units adopt an opposite propeller arrangement. As a consequence of the stereospecific character of the reaction, it was possible to assign the *S* configuration for the six newly formed stereocenters. Crystal packing revealed in addition an intrinsic porosity with a honeycomb arrangement of the cages, that is driven by salt bridges formed by the chloride anions and the cage ammonium groups (Figure 3 and Appendix 4, Figure A20).

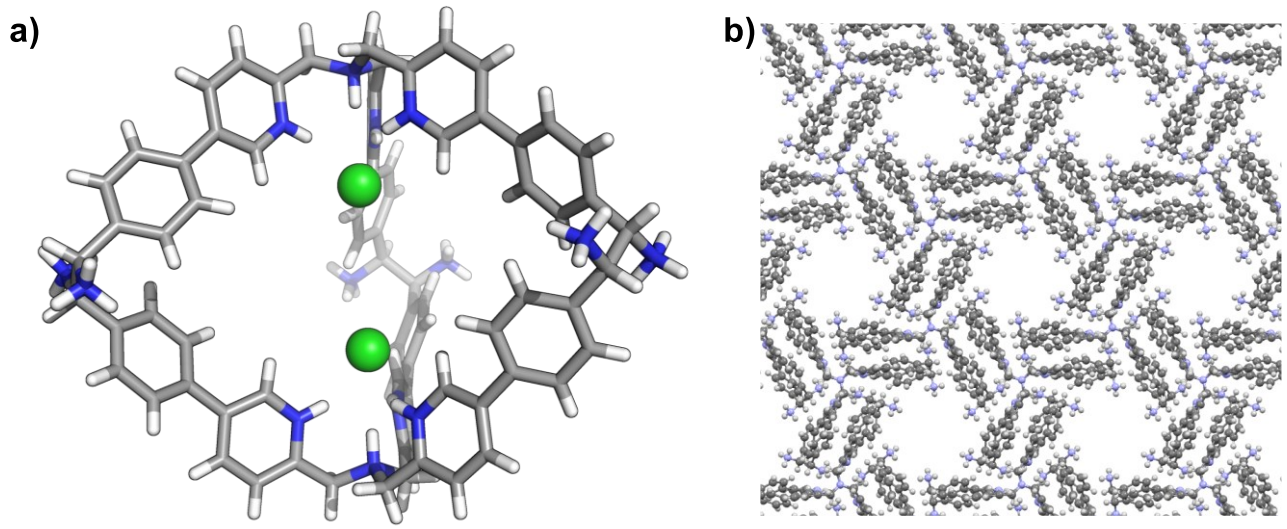

Figure 3. a) Single-crystal X-ray structure of cage ***S*-4**. b) pore system of cage ***S*-4** in the crystal structure. Chlorides and solvent molecules are removed for clarity.

4.2.3. Mechanistic Analysis

To gather more information on the different steps involved in the cage **3** formation, rearrangement kinetic for six different diacids of different lengths (**C_3-C_8**) was monitored via ^{1}H-NMR using an internal standard to have quantitative information of the species (Figure 4 and Appendix 4, Section 4.3).

For all the guests, aldehyde system **1** was completely converted after 24 hours (Figure 4 – black dots). As expected, the first products to rise were the imine cages **C_n@2** as witnessed by the characteristic benzylic peak around 5.4 ppm (Figure 4 – blue dots). Indeed, as it has been already reported, the templated formation of the imine cages is fast for all the guests.[23]

For all the systems, after this initial stage, it was also possible to monitor the formation of rearranged structures due to the formation of the characteristic RAHB peak which indicates the amount of **C_n@3** completely rearranged structure but also of partially rearranged intermediates (*viz.* intermediate structures where only one or two arms of the system have rearranged).

However, it was possible to directly quantify rearranged **C_n@3** using the benzylic protons signal around 5.0 ppm (Figure 3 – red dots) and thus partially rearranged structures (Figure 4 – green dots) by difference with initial aldehyde concentration. The overall analysis of product distribution along the kinetic experiment clearly highlighted a picture where the length of the diacid strongly ruled product distribution in solution. While **C_3** shifted the equilibrium toward the completely rearranged system **C_3@3**, longer diacids favored products where partially or non rearranged structures are present.

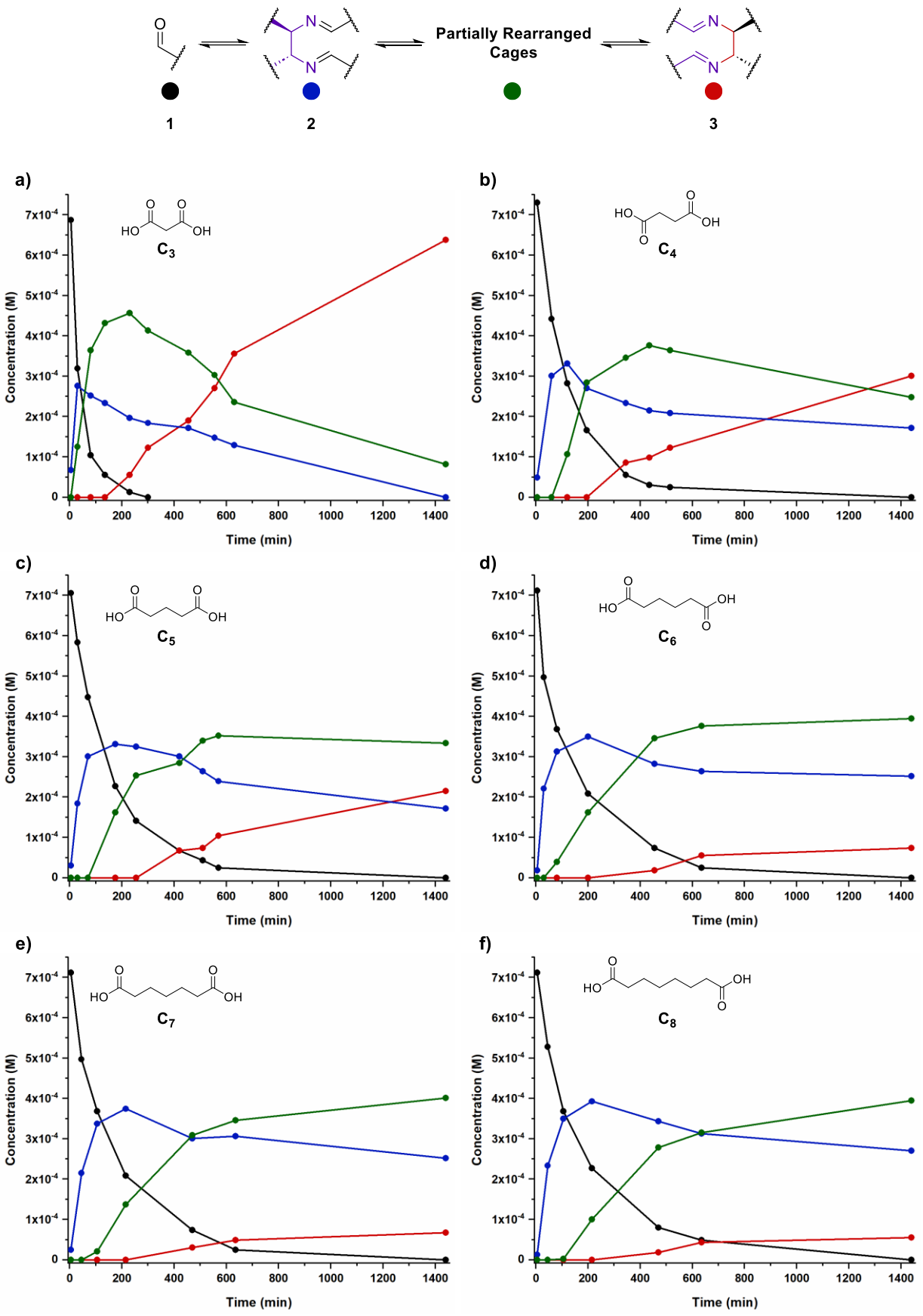

Figure 4. Kinetic profiles for the formation of rearranged cage in the presence of a) malonic acid (**C3**), b) succinic acid (**C4**), c) glutaric acid (**C5**), d) adipic acid (**C6**), e) pimelic acid (**C7**), and f) suberic acid (**C8**). Concentrations have been determined via ^{1}H-NMR using 1,3,5-Trimetoxybenzene as internal standard.

Taking into account that a chair like transition state in which the two carbon imine bonds are in close proximity have been postulated in previous works for the rearrangement,[30] the shorter diacid has the capability to pre-organize all the three arms of the system in a the correct conformation as confirmed by computational studies that have been carried out (Figure 5).

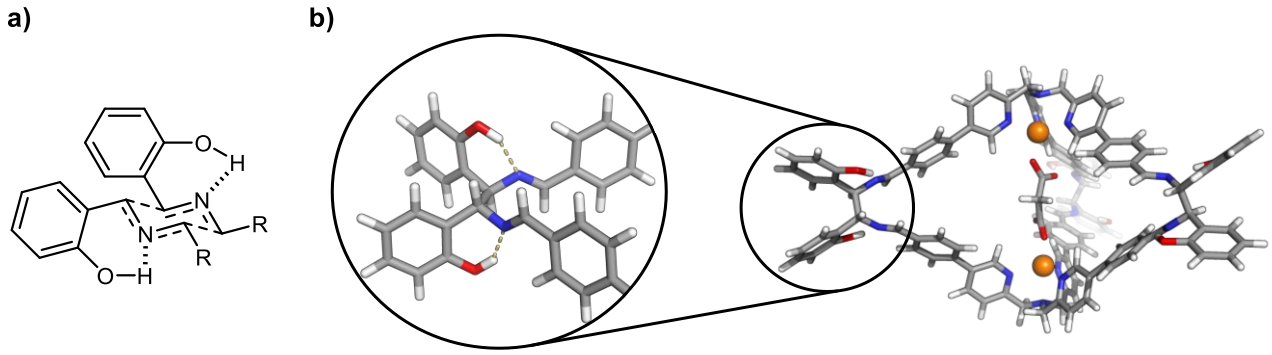

Figure 5. a) Diaza-Cope transition state[32] and, b) highlight of the imine conformation in cage **C_3@3** obtained by DFT calculations.

On the other hand, longer diacids favor a different thermodynamic distribution which tend to be similar for diacids longer than glutaric acid **C_5** (Figure 4d-f).

In order to have further confirmation of the dynamic nature of the system up to the end of the reaction, suberic acid **C_8** was used as templating agent and, after 24 hours, ^{1}H-NMR revealed the formation of only 8% of rearranged **C_8@3** (Figure 3d). Addition at this point of malonic acid **C_3** led to a re-equilibration of the system toward **C_3@3** (Figure 6).

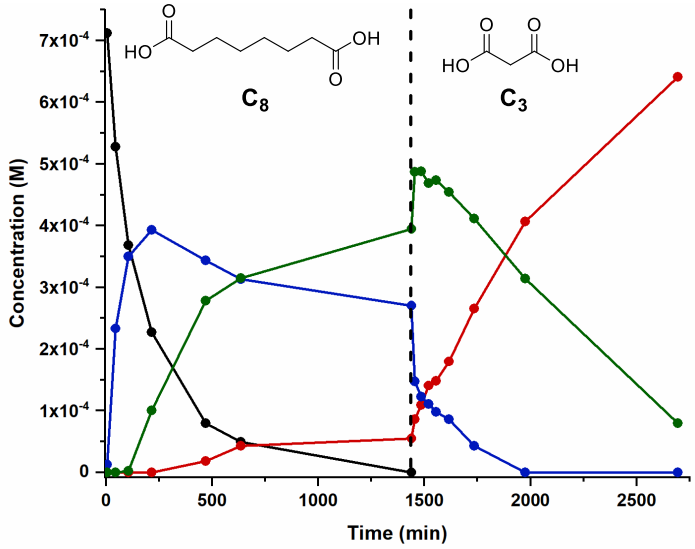

Figure 6. Kinetic profiles for the formation of rearranged cage in the presence of suberic acid (**C_8**) with the addition of malonic acid (**C_3**) after 24 hours. Concentrations have been determined via ^{1}H-NMR using 1,3,5-Trimetoxybenzene as internal standard.

4.2.4. Synthesis of novel "tweezer-like" structures and metal complexation

The scope of the novel reaction was tested with two others starting **TPMA** based structures with one, or two, aldehyde groups with the aim to verify the versatility of the reaction and to test if a different degree of closure was influencing the course of the reaction (Scheme 3 and Scheme 4)

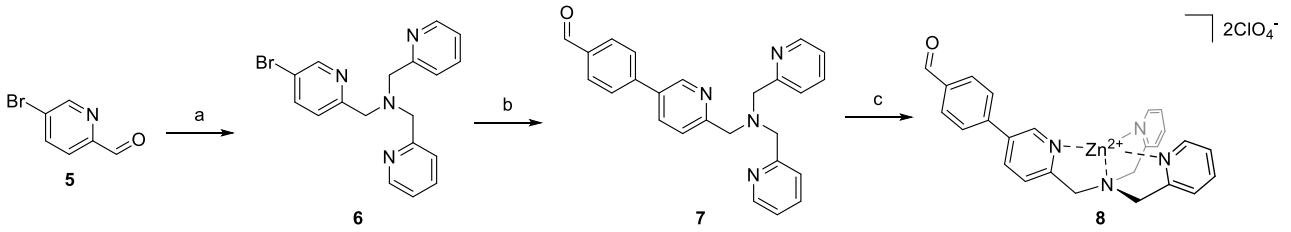

Scheme 3. Synthesis of complex **11**: a) Di-(2-picolyl)amine, $NaBH(OAc)_3$, CH_2Cl_2 dry, N2, rt, 12h, (64%) g) 4-formylphenylboronic acid, $Pd(PPh_3)_4$, K_2CO_3, Toluene/H_2O/CH_3OH (1:1:0.5), N_2 , 100 °C, 48 h (75%), h) 1. $Zn(ClO_4)_2$*$6H_2O$, CH_3CN, 2. Et_2O (96%).

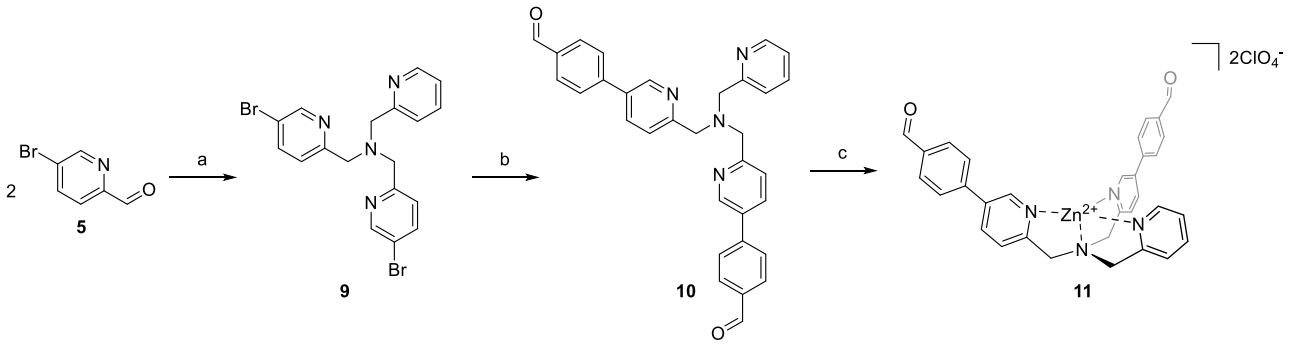

Scheme 4. Synthesis of complex **14**: a) 2-picolylamine, $NaBH(OAc)_3$, CH_2Cl_2 dry, N2, rt, 12h, (71%) b) 4-formylphenylboronic acid, $Pd(PPh_3)_4$, K_2CO_3, Toluene/H_2O/CH_3OH (1:1:0.5), N_2 , 100 °C, 48 h (67%), h) 1. $Zn(ClO_4)_2$*$6H_2O$, CH_3CN, 2. Et_2O (94%).

Interestingly the reactions, templated also in this case with malonic acid **C_3**, proceed through the formation of the rearranged products. Hydrolysis of the reaction mixture after 24 hours furnished both the chiral architectures ***S*-12** and ***S*-13** in high yields and purity (Figure 7).

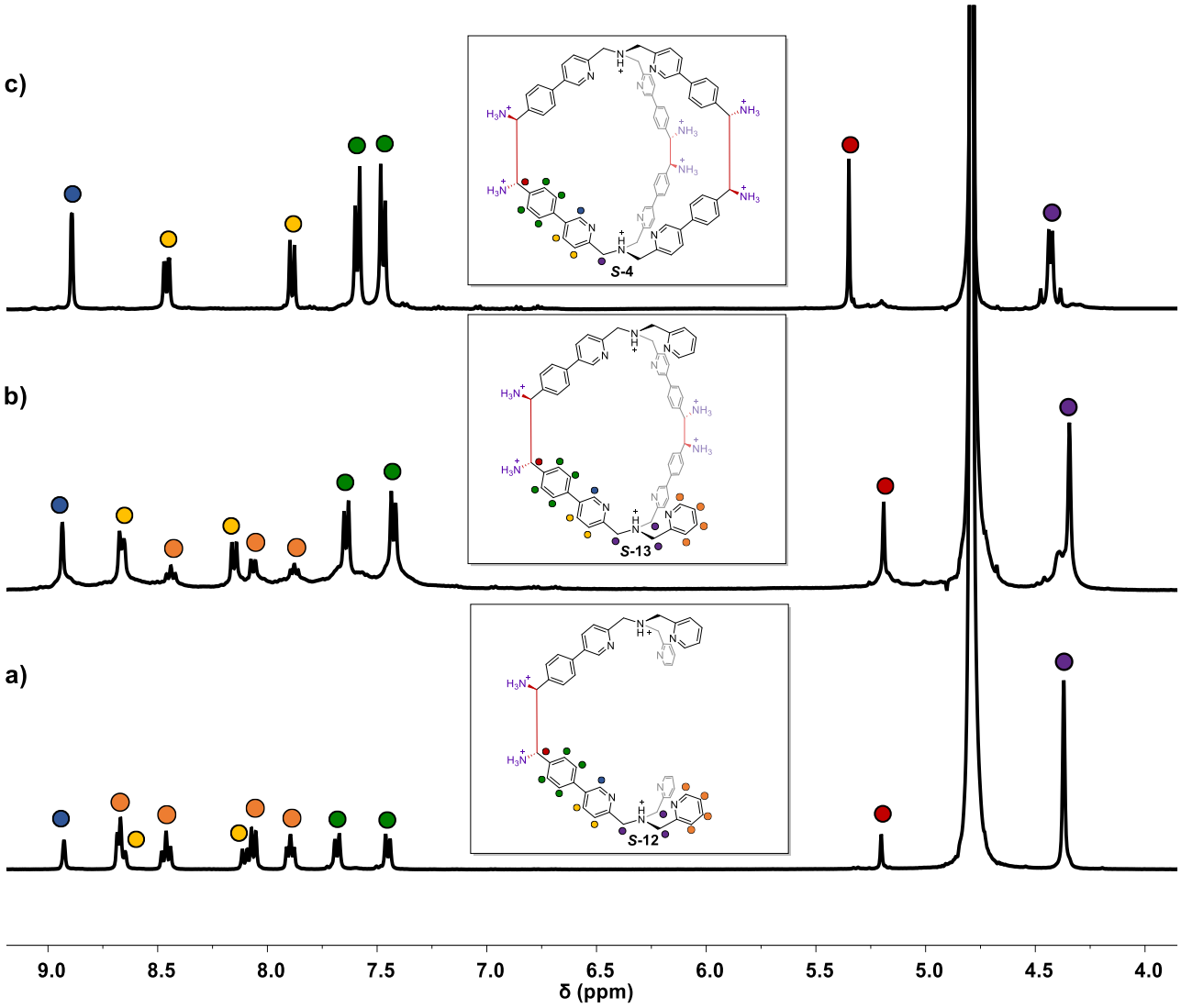

Figure 7. ^{1}H-NMR (400 MHz, 301 K, D_2O) spectra of **TPMA**-based architectures developed using Diaza-Cope rearrangement. Chlorides counteranions are removed for clarity.

Finally, to test the complexation capabilities of the novel cage, a stoichiometric amount of zinc(II) chloride was added to a solution of ***S*-4** in water.

As shown in Figure 8, the complexation occurred, as confirmed by the shift of the signals in the NMR spectrum and by the ESI-MS spectrum (Figure 8b and Appendix 4, Figure A47). Addition of acetone of the aqueous solution allowed the recovery of the zinc cage ***S*-Zn-4** in almost quantitative yield (93%).

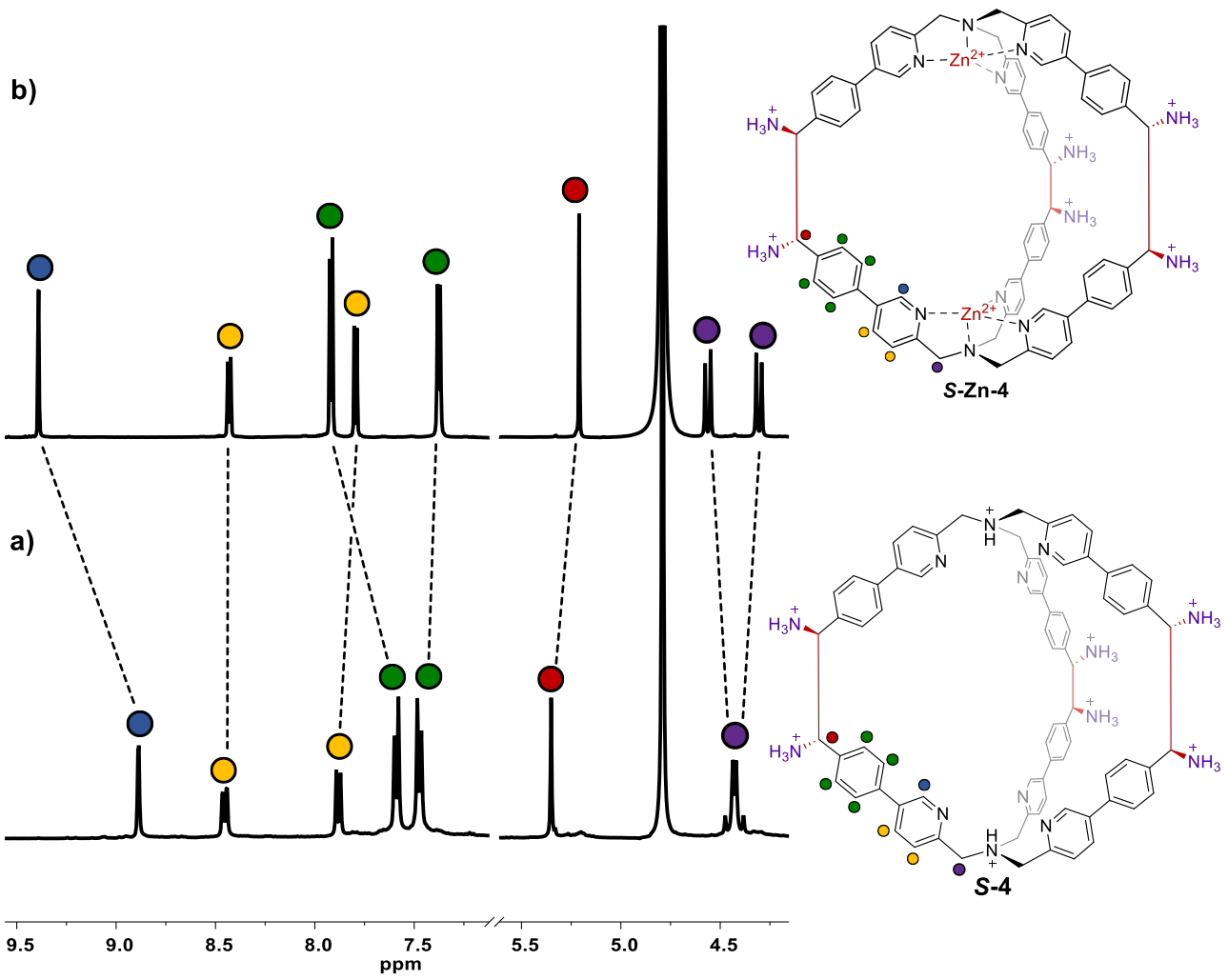

Figure 8. ^{1}H-NMR (400 MHz, 301 K, D_2O) spectra of a) cage ***S*-4**, and b) cage ***S*-Zn-4** after complexation with $ZnCl_2$. Chloride counteranions are removed for clarity.

4.3. Conclusions

In conclusion, the use of imine chemistry combined with [3,3]-sigmatropic rearrangement for the formation of supramolecular architectures has been reported for the first time. This novel strategy has opened to the preparation of novel chiral **TPMA**-based systems which are intrinsically hydrolytically stable due to the formation of C-C bonds. Among the structures, a novel C_3 symmetric cage has been prepared and it has shown to retain its structure also in the solid state. Preliminary studies of the reaction have shown the decisive role of the molecular length of the templating guest in the outcome of the reaction. Moreover, the re-complexation of the cage ligand has been performed opening for future studies where different metals could be exploited for their catalytic or recognition properties.

4.4. Experimental Section

4.4.1. Synthesis of 1-(5-bromopyridin-2-yl)-N,N-bis(pyridin-2-ylmethyl)methanamine (6)

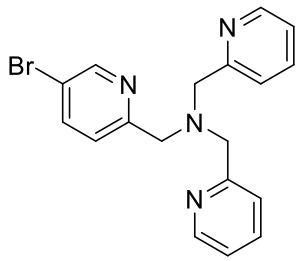

6

Compound **6** has been synthesized according to literature.[34] In a Schlenk apparatus, 5-bromopicolinaldehyde **8** (1.6 g, 8.33 mmol) and bis(pyridin-2-ylmethyl)amine (1.5 mL, 8.6 mmol) were dissolved in 15 mL of dry CH_2Cl_2 under N_2, and left under stirring for 1 h. Three aliquots of $NaBH(OAc)_3$ (0.59 g, 2.78 mmol, each addition) were added waiting 20 minutes between each addition. After the reaction mixture was stirred overnight at room temperature. The solvent was removed under reduced pressure. The resulting brown oil was dissolved in EtOAc and the solution washed with 0.1 M solution of KOH (3x100 mL). The organic phases were dried with $MgSO_4$ and the solvent was removed under reduced pressure. The resulting brown oil was precipitated by crystallization from THF/Hexane to yield the product **6** as a pale yellow solid. (1.97 g, 5.34 mmol, 64%).

^{1}H NMR (300 MHz, $CDCl_3$) δ 8.66 – 8.30 (m, 3H), 7.75 (dd, *J* = 8.3, 2.4 Hz, 1H), 7.67 – 7.62 (m, 2H), 7.56 – 7.44 (m, 3H), 7.20 – 7.06 (m, 2H), 3.87 (s, 4H), 3.84 (s, 2H).

4.4.2. Synthesis of 4-(6-((bis(pyridin-2-ylmethyl)amino)methyl)pyridin-3-yl)benzaldehyde (7)

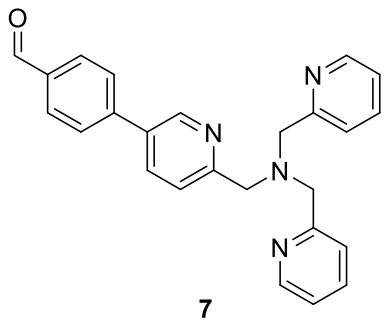

7

A mixture of **6** (2.84 g, 6.50 mmol), (4-formylphenyl)boronic acid (2.44 g, 16.2 mmol), 0.075 g (0.065 mmol, 1%) of $Pd(PPh_3)_4$, and K_2CO_3 (3.37 g, 24.9 mmol) was dissolved in 60 mL of H_2O/toluene/CH_3OH (1:1:0.5). The mixture was stirred under N_2 for 48 h at 100 °C. The solvent was removed under reduced pressure. The resulting brown oil was dissolved in $CHCl_3$ and the solution washed with H_2O. The organic phases were dried over $MgSO_4$, filtered on Celite and the solvent was removed under reduced pressure. The resulting brown oil was precipitated by crystallization from THF/hexane to yield the product **7** as pale yellow solid (1.92 g, 4.88 mmol, 75%)

^{1}H NMR (300 MHz, $CDCl_3$) δ 10.05 (s, 1H), 8.78 (d, *J* = 2.4, 1H), 8.54 – 8.52 (m, 2H), 7.98 – 7.95 (m, 2H), 7.88 (dd, *J* = 8.1, 2.4 Hz, 1H), 7.72 – 7.56 (m, 6H), 7.47 – 7.44 (m, 1H), 7.16 – 7.11 (m, 1H), 3.94 – 3.91 (m, 6H).

^{13}C NMR (50 MHz, $CDCl_3$) δ 191.91, 159.78, 159.40, 149.36, 147.79, 136.68, 135.27, 133.82, 132.20, 130.66, 128.84, 128.60, 127.80, 123.29, 122.29, 60.44, 60.05.

HRMS (m/z): $[M+H]^+$ calcd. for $[C_{25}H_{22}N_4O+H]^+$, 395.1866; found 395.2062.

4.4.3. Synthesis of complex 8

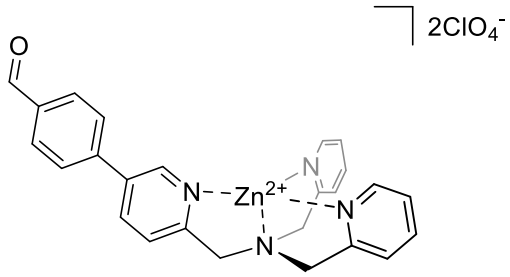

8

To a suspension of ligand **7** (100 mg, 0.25 mmol) in CH_3CN (15 mL) zinc(II) perchlorate hexahydrate was added (94 mg, 0.25 mmol). The solution was stirred at room temperature for 1 h and the reaction was followed by ^{1}H-NMR and ESI-MS. At the end of the reaction Et_2O (25 mL) was added, obtaining quantitatively a crystalline solid then centrifugated and dried. Complex **8** resulted as pale yellow solid (160 mg, 96%).

^{1}H NMR (300 MHz, CD_3CN) δ 10.08 (s, 1H), 8.96 (d, *J* = 1.7 Hz, 1H), 8.80 (d, *J* = 4.9 Hz, 2H), 8.41 (d, *J* = 8.2 Hz, 1H), 8.14 (t, *J* = 7.8 Hz, 3H), 8.08 – 8.05 (m, 2H), 7.96 – 7.93 (m, 2H), 7.73 – 7.68 (m, 3H), 7.63 – 7.61 (m, 2H), 4.34 – 4.31 (m, 6H).

^{13}C NMR (50 MHz, CD_3CN) δ 193.26, 156.19, 155.82, 149.45, 147.79, 143.10, 141.88, 141.39, 138.01, 137.70, 131.29, 129.22, 126.48, 126.21, 126.09, 57.98, 57.78.

HRMS (m/z): $[M+ CHOO]^+$ calcd. for $[C_{25}H_{22}N_4OZn+CHOO]^+$, 503.1056; found 503.1049.

4.4.4. Synthesis of 1-(5-bromopyridin-2-yl)-N-((5-bromopyridin-2-yl) methyl)-N-(pyridin-2-ylmethyl)methanamine (9)

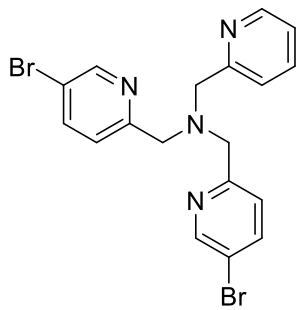

9

In a Schlenk apparatus, 5-bromopicolinaldehyde **5** (1.8 g, 9.7 mmol) and 2-picolylamine (1.0 mL, 9.7 mmol) were dissolved in 40 mL of dry CH_2Cl_2 under N_2, and left under stirring for 1 h. Three aliquots of $NaBH(OAc)_3$ (0.68 g, 3.24 mmol, each addition) were added waiting 20 minutes between each addition. Then, 5-bromopicolinaldehyde **5** (1.8 g, 9.7 mmol) was added and the solution was stirred for 1 h.

Three aliquots of $NaBH(OAc)_3$ (0.68 g, 3.24 mmol, each addition) were added waiting 20 minutes between each addition. After the reaction mixture was stirred overnight at room temperature. The solvent was removed under reduced pressure. The resulting brown oil was dissolved in EtOAc and the solution washed with 0.1 M solution of KOH (3x100 mL). The organic phases were dried with $MgSO_4$ and the solvent was removed under reduced pressure. The resulting brown oil was precipitated by crystallization from THF/Hexane to yield the product **9** as a pale yellow solid. (3.07 g, 5.89 mmol, 71%).

^{1}H NMR (300 MHz, $CDCl_3$) δ 8.54 – 8.48 (m, 3H), 7.74 – 7.69 (m, 2H), 7.65 – 7.57 (m, 1H), 7.46 – 7.39 (m, 3H), 7.14 – 7.08 (m, 1H), 3.82 – 3.79 (m, 6H).

^{13}C NMR (50 MHz, $CDCl_3$) δ 158.79, 157.78, 150.16, 149.25, 139.05, 136.49, 124.46, 123.13, 122.19, 119.10, 60.12, 59.41.

HRMS (m/z): $[M+H]^+$ calcd. for $[C_{18}H_{16}Br_2N_4+H]^+$, 446.9814; found 446.9850.

4.4.5. Synthesis of 4,4'-((((pyridin-2-ylmethyl)azanediyl)bis(methylene)) bis(pyridine-6,3-diyl))dibenzaldehyde (10)

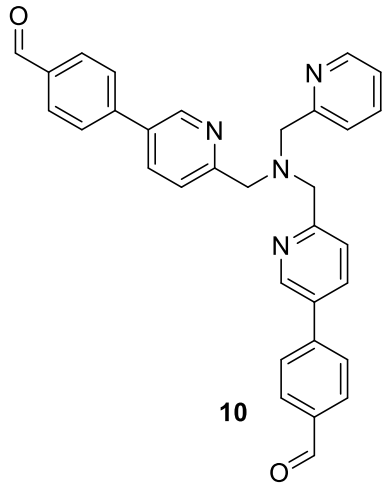

10

A mixture of **9** (2.50 g, 5.62 mmol), (4-formylphenyl)boronic acid (2.94 g, 19.7 mmol), 0.075 g (0.065 mmol, 1%) of $Pd(PPh_3)_4$, and K_2CO_3 (4.08 g, 29.5 mmol) was dissolved in 60 mL of H_2O/toluene/CH_3OH (1:1:0.5). The mixture was stirred under N_2 for 48 h at 100 °C. The solvent was removed under reduced pressure. The resulting brown oil was dissolved in $CHCl_3$ and the solution washed with H_2O. The organic phases were dried over $MgSO_4$, filtered on Celite and the solvent was removed under reduced pressure. The resulting brown oil was precipitated by crystallization from THF/hexane to yield the product **10** as pale yellow solid (1.87 g, 3.76 mmol, 67%)

^{1}H NMR (400 MHz, $CDCl_3$) δ 10.06 (s, 1H), 8.81 (d, *J* = 1.9 Hz, 2H), 8.56 (d, *J* = 4.4 Hz, 1H), 7.97 (d, *J* = 8.2 Hz, 4H), 7.90 (d, *J* = 8.1 Hz, 2H), 7.73 – 7.71 (m, 5H), 7.68 – 7.61 (m, 2H), 7.52 – 7.44 (m, 1H), 7.19 – 7.15 (m, 1H), 4.00 – 3.96 (m, 6H).

^{13}C NMR (101 MHz, $CDCl_3$) δ 191.80, 159.47, 159.11, 149.31, 147.74, 143.79, 136.68, 135.82, 135.23, 133.83, 132.16, 130.58, 127.71, 123.34, 122.30, 60.35, 59.98.

HRMS (m/z): $[M+H]^+$ calcd. for $[C_{32}H_{26}N_4O_2+H]^+$, 499.2129; found 499.2427.

4.4.6. Synthesis of complex 11

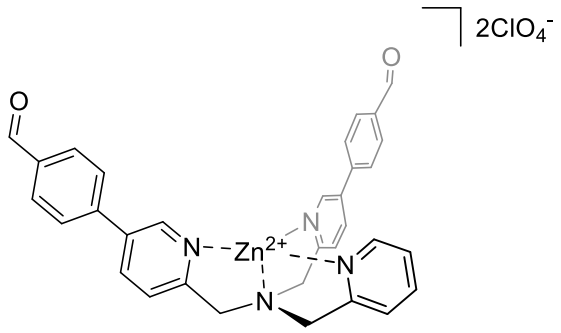

11

To a suspension of ligand **10** (100 mg, 0.20 mmol) in CH_3CN (15 mL) zinc(II) perchlorate hexahydrate was added (74 mg, 0.20 mmol). The solution was stirred at room temperature for 1 h and the reaction was followed by ^{1}H-NMR and ESI-MS. At the end of the reaction Et_2O (25mL) was added, obtaining quantitatively a crystalline solid then centrifugated and dried. Complex **11** resulted as pale yellow solid (143 mg, 94%).

^{1}H NMR (300 MHz, CD_3CN) δ 10.10 (s, 2H), 8.98 (d, *J* = 1.8 Hz, 2H), 8.82 (d, *J* = 4.9 Hz, 1H), 8.44 (dd, *J* = 8.2, 2.2 Hz, 2H), 8.17 (td, *J* = 7.8, 1.6 Hz, 1H), 8.09 – 8.06 (m, 4H), 7.94 – 7.92 (m, 4H), 7.77 – 7.65 (m, 3H), 7.58 – 7.52 (m, 1H), 4.39 – 4.37 (m, 6H).

^{13}C NMR (75 MHz, CD_3CN) δ 193.22, 156.15, 155.77, 149.40, 147.76, 143.12, 141.84, 141.37, 137.98, 137.68, 133.21, 131.30, 129.14, 126.49, 126.22, 58.02, 57.80.

HRMS (m/z): $[M+CHOO]^+$ calcd. for $[C_{32}H_{26}N_4O_2Zn+CHOO]^+$, 607.1318; found 607.1331.

4.4.7. Synthesis of compound *S*-4

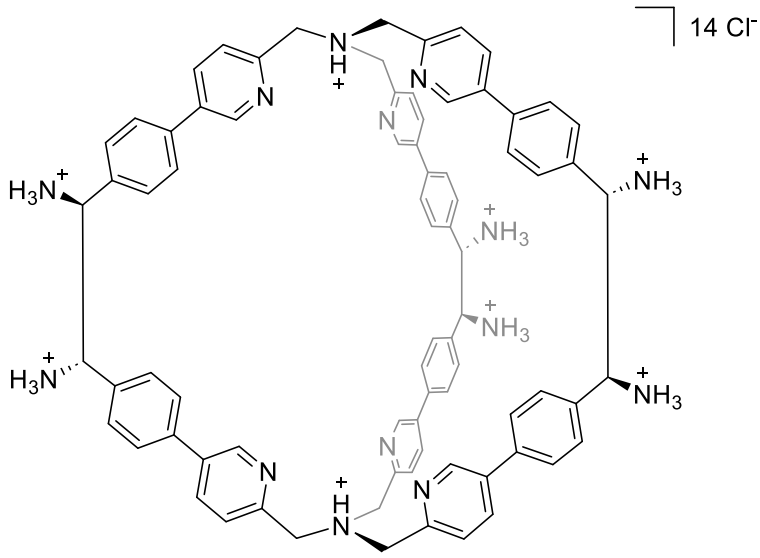

***S*-4**

In a 100 mL flask, 70 mg (80 μmol) of complex **1** were dissolved in 40 mL of dry. Then 2.02 mL (40 μmol) of a solution 0.02 M of malonic acid **C_3** in dry acetonitrile were added under stirring. Finally, 3.38 mL(202 μmol) of a solution 0.06 M of **(*R*,*R*)-HPEDA** in a mixture of dry acetonitrile/dry DMSO (1:1) were added with dropwise using a syringe pump (rate 0.8 mL/h). The solution was stirred for 24 h and the solvent was removed leading the residual DMSO. Then 2 mL of HCl 37% were added to the

residual DMSO and the solution stirred for 1 h. After 1 h, 1 mL of water was added and then 20 mL of acetone were added under vigorous stirring leading to the precipitation of a yellow powder. After centrifugation and removal of the solvent, the precipitate was dissolved in 1 mL of water and 1 mL of HCl 37% and stirred for an additional hour. Then 20 mL of acetone were added leading to bright yellow precipitate that was centrifugated and washed an additional time with acetone. (61 mg, 87%)

^{1}H NMR (400 MHz, D_2O) δ 8.71 (s, 6H), 8.26 (d, *J* = 8.7 Hz, 1H), 7.69 (d, *J* = 8.3 Hz, 6H), 7.47 (d, *J* = 8.0 Hz, 12H), 7.36 (d, *J* = 8.0 Hz, 12H), 5.23 (s, 6H), 4.33 – 4.24 (m, 12H).

^{13}C NMR (101 MHz, D_2O) δ 151.76, 142.93, 141.14, 137.35, 135.45, 133.16, 129.02, 128.18, 127.26, 58.64, 56.98.

HRMS (m/z): $[M+2H]^{2+}$ calcd. for $[C_{78}H_{72}N_{14}+2H]^{2+}$, 603.3105; found 603.3113.

Elemental analysis C. 54.72; H, 5.15; N, 11.58. Required: C. 54.60; H, 5.05; N, 11.43.

4.4.8. Synthesis of compound *S*-12

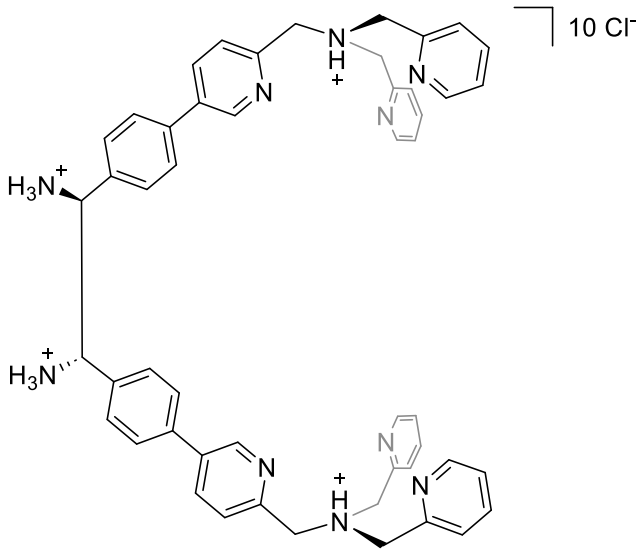

***S*-12**

In a 100 mL flask, 53 mg (80 µmol) of complex **8** were dissolved in 40 mL of dry. Then 2.0 mL (40 µmol) of a solution 0.02 M of malonic acid **C_3** in dry acetonitrile were added under stirring. Finally, 2.01 mL(121 µmol) of a solution 0.06 M of **(*R*,*R*)-HPEDA** in a mixture of dry acetonitrile/dry DMSO (1:1) were added with dropwise using a syringe pump (rate 0.8 mL/h). The solution was stirred for 24 h and the solvent was removed leading the residual DMSO. Then 2 mL of HCl 37% were added to the residual DMSO and the solution stirred for 1 h. After 1 h, 1 mL of water was added and then 5 mL of MeOH were added under vigorous stirring leading to the precipitation of a yellow powder. After centrifugation and removal of the solvent, the precipitate was dissolved in 1 mL of water and 1 mL of HCl 37% and stirred for an additional hour. Then 4 mL of MeOH were added leading to bright yellow precipitate that was centrifugated and washed an additional time with acetone and dried under vacuum.

After few hours the precipitate tends to be deliquescent leading to a slightly brown oil. (48 mg, 78%)

^{1}H NMR (400 MHz, D_2O) δ 8.94 (s, 2H), 8.70 – 8.66 (m, 6H), 8.48 (t, *J* = 7.7 Hz, 4H), 8.13 – 8.06 (m, 6H), 7.91 (t, *J* = 6.7 Hz, 4H), 7.70 (d, *J* = 8.2 Hz, 4H), 7.46 (d, *J* = 8.2 Hz, 4H), 5.22 (s, 2H), 4.38 (s, 12H).

^{13}C NMR (101 MHz, D_2O) δ 152.42, 151.18, 149.09, 146.61, 143,29, 141.45, 139.95, 136.27, 134.16, 130.89, 129.82, 129.26, 129.07, 128.23, 57.97, 57.56, 57.32.

HRMS (m/z): $[M+2H]^{2+}$ calcd. for $[C_{50}H_{48}N_{10}+2H]^{2+}$, 395.2104; found 395.2062.

4.4.9. Synthesis of compound *S*-13

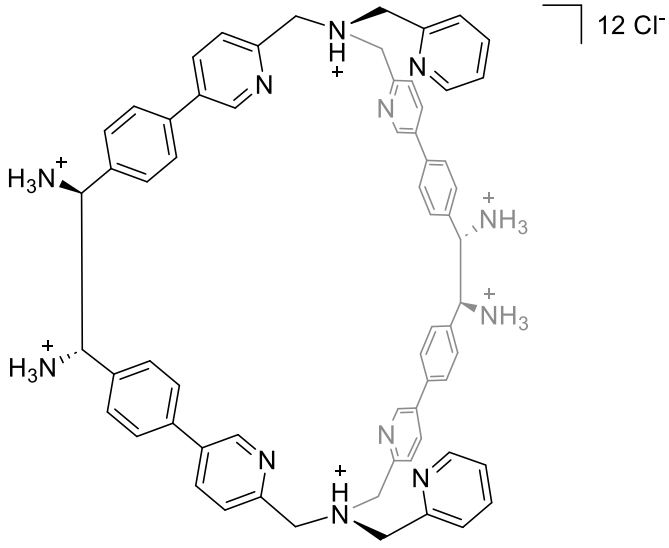

***S*-13**

In a 100 mL flask, 61 mg (80 µmol) of complex **11** were dissolved in 40 mL of dry. Then 2.00 mL (40 µmol) of a solution 0.02 M of malonic acid **C_3** in dry acetonitrile were added under stirring. Finally, 2.66 mL(160 µmol) of a solution 0.06 M of **(*R*,*R*)-HPEDA** in a mixture of dry acetonitrile/dry DMSO (1:1) were added with dropwise using a syringe pump (rate 0.4 mL/h). The solution was stirred for 24 h and the solvent was removed leading the residual DMSO. Then 2 mL of HCl 37% were added to the residual DMSO and the solution stirred for 1 h. After 1 h, 1 mL of water was added and then 20 mL of acetone were added under vigorous stirring leading to the precipitation of a yellow powder. After centrifugation and removal of the solvent, the precipitate was dissolved in 1 mL of water and 1 mL of HCl 37% and stirred for an additional hour. Then 20 mL of acetone were added leading to bright yellow precipitate that was centrifugated and washed an additional time with acetone and dried under vacuum. (53 mg, 81%)

^{1}H NMR (400 MHz, D_2O) δ 8.94 (s, 4H), 8.68 – 8.65 (m, 6H), 8.44 (t, *J* = 7.8 Hz, 2H), 8.15 (d, *J* = 8.4 Hz, 4H), 8.07 (d, *J* = 8.0 Hz, 2H), 7.90 – 7.86 (m, 2H), 7.64 (d, *J* = 8.1 Hz, 8H), 7.43 (d, *J* = 8.0 Hz, 8H), 5.19 (s, 4H), 4.39 – 4.35 (m, 12H).

^{13}C NMR (101 MHz, D_2O) δ 150.95, 149.72, 147.54, 145.19, 141.80, 139.96, 138.48, 134.71, 133.05, 129.27, 128.26, 127.71, 127.59, 126.61, 56.76, 56.10, 55.83.

HRMS (m/z): $[M+2H]^{2+}$ calcd. for $[C_{64}H_{60}N_{12}+2H]^{2+}$, 499.2605; found 499.2610.

4.4.10. Synthesis of compound Zn-*S*-4

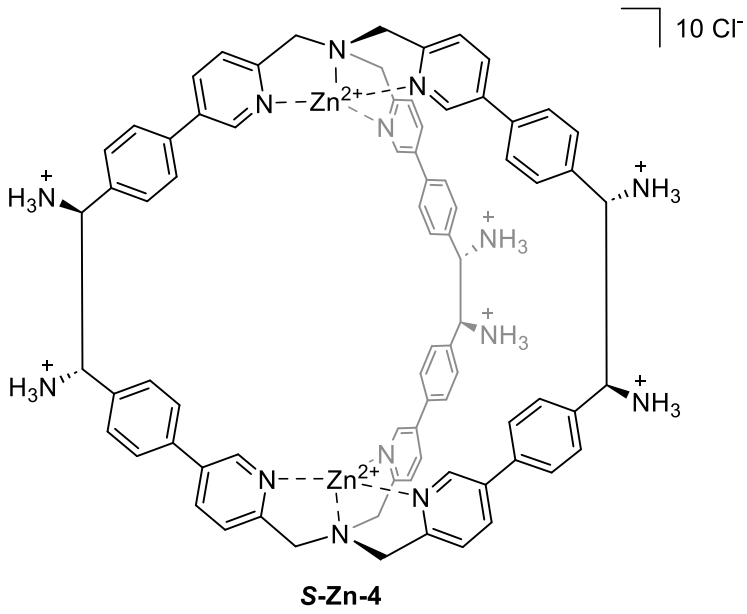

***S*-Zn-4**

To a solution of ligand ***S*-4** (100 mg, 0.06 mmol) in H_2O (2 mL), zinc(II) chloride was added (16 mg, 0.12 mmol). The solution was stirred at room temperature for 1 h and then acetone (15 mL) was added, obtaining a bright yellow solid that was centrifugated. After centrifugation and removal of the solvent, the precipitate was washed with 15 mL of acetone and dried under vacuum. Complex ***S*-Zn-4** resulted as bright yellow solid (93 mg, 93%).

^{1}H NMR (400 MHz, D_2O) δ 9.39 (s, 6H), 8.43 (d, *J* = 8.2, 6H), 7.92 (d, *J* = 8.0 Hz, 12H), 7.79 (d, *J* = 8.2 Hz, 6H), 7.38 (d, *J* = 8.0 Hz, 12H), 5.21 (s, 6H), 4.58 – 4.29 (m, 12H).

^{13}C NMR (50 MHz, D_2O) δ 154.57, 146.97, 140.45, 138.32, 137.20, 129.91, 129.39, 128.52, 125.23, 56.16, 55.78.

HRMS (m/z): $[M+2Cl]^{2+}$ calcd. for $[C_{78}H_{72}N_{14}Zn_2+2Cl]^{2+}$, 701.2001; found 701.1989.

4.5. References

[1] J. F. S. S. J. Rowan, S. J. Cantrill, G. R. L. Cousins, *Angew. Chem. Int. Ed.* **2002**, *41*, 898–952.
[2] P. T. Corbett, J. Leclaire, L. Vial, K. R. West, J. L. Wietor, J. K. M. Sanders, S. Otto, *Chem. Rev.* **2006**, *106*, 3652–3711.
[3] M. Mastalerz, *Angew. Chemie - Int. Ed.* **2010**, *49*, 5042–5053.
[4] T. Tozawa, J. T. A. Jones, S. I. Swamy, S. Jiang, D. J. Adams, S. Shakespeare, R. Clowes, D. Bradshaw, T. Hasell, S. Y. Chong, C. Tang, S. Thompson, J. Parker, A. Trewin, J. Bacsa, A. M. Z. Slawin, A. Steiner, A. I. Cooper, *Nat. Mater.* **2009**, *8*, 973–978.
[5] A. J. McConnell, C. S. Wood, P. P. Neelakandan, J. R. Nitschke, *Chem. Rev.* **2015**, *115*, 7729–7793.
[6] G. Zhang, M. Mastalerz, *Chem. Soc. Rev.* **2014**, *43*, 1934–1947.
[7] T. Mitra, K. E. Jelfs, M. Schmidtmann, A. Ahmed, S. Y. Chong, D. J. Adams, A. I. Cooper, *Nat. Chem.* **2013**, *5*, 276–281.
[8] K. Acharyya, P. S. Mukherjee, *Angew. Chem.* **2019**, *131*, 8732–8745.
[9] S. Zarra, D. M. Wood, D. A. Roberts, J. R. Nitschke, *Chem. Soc. Rev.* **2015**, *44*, 419–432.
[10] P. Ballester, *Chem. Soc. Rev.* **2010**, *39*, 3810–3830.
[11] J. L. Culshaw, G. Cheng, M. Schmidtmann, T. Hasell, M. Liu, D. J. Adams, A. I. Cooper, *J. Am. Chem. Soc.* **2013**, *135*, 10007–10010.
[12] J. C. Lauer, A. S. Bhat, C. Barwig, N. Fritz, T. Kirschbaum, F. Rominger, M. Mastalerz, *Chem. - A Eur. J.* **2022**, *28*, DOI 10.1002/CHEM.202201527.
[13] P. E. Alexandre, W. S. Zhang, F. Rominger, S. M. Elbert, R. R. Schröder, M. Mastalerz, *Angew. Chem. Int. Ed.* **2020**, *59*, 19675–19679.
[14] M. Mastalerz, M. W. Schneider, I. M. Oppel, O. Presly, *Angew. Chem. Int. Ed.* **2011**, *50*, 1046–1051.
[15] N. Planas, A. L. Dzubak, R. Poloni, L. C. Lin, A. McManus, T. M. McDonald, J. B. Neaton, J. R. Long, B. Smit, L. Gagliardi, *J. Am. Chem. Soc.* **2013**, *135*, 7402–7405.
[16] K. Acharyya, P. S. Mukherjee, *Chem. – A Eur. J.* **2015**, *21*, 6823–6831.
[17] Y. Jin, B. A. Voss, R. D. Noble, W. Zhang, *Angew. Chem.* **2010**, *122*, 6492–6495.
[18] Y. Jin, B. A. Voss, A. Jin, H. Long, R. D. Noble, W. Zhang, *J. Am. Chem. Soc* **2011**, *133*, 6650–6658.
[19] M. Liu, M. A. Little, K. E. Jelfs, J. T. A. Jones, M. Schmidtmann, S. Y. Chong, T. Hasell, A. I. Cooper, *J. Am. Chem. Soc.* **2014**, *136*, 7583–7586.
[20] Xin-Yue Hu, Wen-Shan Zhang, Frank Rominger, Irene Wacker, R. R. Schröder, Michael Mastalerz, *Chem. Commun.* **2017**, *53*, 8616–8619.
[21] A. S. Bhat, S. M. Elbert, W. S. Zhang, F. Rominger, M. Dieckmann, R. R. Schröder, M. Mastalerz, *Angew. Chem. Int. Ed.* **2019**, *58*, 8819–8823.
[22] C. Bravin, E. Badetti, G. Licini, C. Zonta, *Coord. Chem. Rev.* **2021**, *427*, DOI 10.1016/j.ccr.2020.213558.
[23] C. Bravin, E. Badetti, F. A. Scaramuzzo, G. Licini, C. Zonta, *J. Am. Chem. Soc.* **2017**, *139*, 6456–6460.
[24] C. Bravin, A. Guidetti, G. Licini, C. Zonta, *Chem. Sci.* **2019**, *10*, 3523–3528.
[25] F. Begato, R. Penasa, G. Licini, C. Zonta, *Chem. Commun.* **2021**, *57*, 10019–10022.
[26] F. Begato, R. Penasa, G. Licini, C. Zonta, *ACS Sensors* **2022**, *7*, 1390–1394.
[27] C. Bravin, E. Badetti, R. Puttreddy, F. Pan, K. Rissanen, G. Licini, C. Zonta, *Chem. Eur. J.* **2018**, *24*, 2936–2943.
[28] C. Bravin, G. Mason, G. Licini, C. Zonta, *J. Am. Chem. Soc.* **2019**, *141*, 11963–11969.
[29] H. Kim, M. Staikova, A. J. Lough, J. Chin, *Org. Lett.* **2009**, *11*, 157–160.
[30] H. Kim, Y. Nguyen, C. P. H. Yen, L. Chagal, A. J. Lough, B. M. Kim, J. Chin, *J. Am. Chem. Soc.* **2008**, *130*, 12184–12191.
[31] J. Chin, F. Mancin, N. Thavarajah, D. Lee, A. Lough, D. S. Chung, *J. Am. Chem. Soc.* **2003**, *125*, 15276–15277.
[32] H.-J. Kim, H. Kim, G. Alhakimi, E. J. Jeong, N. Thavarajah, L. Studnicki, A. Koprianiuk, A. J. Lough, J. Suh, J. Chin, *J. Am. Chem. Soc.* **2005**, *127*, 16370–16371.
[33] Elemental analysis of compound ***S-4*** highlight the presence of 14 choride anions. This is due to the protonation of the pyridine nitrogen atoms.
[34] E. Benazzi, F. Begato, A. Niorettini, L. Destro, K. Wurst, G. Licini, S. Agnoli, C. Zonta, M. Natali, *J. Mater. Chem. A* **2021**, *9*, 20032–20039.

Conclusions

In this Ph.D thesis, novel applications of the **TPMA**-based molecular cage have been reported. Moreover, the synthesis of a hydrolytically stable chiral architecture has been achieved.

In Chapter 1 the capability of the **TPMA**-based supramolecular cage to self-assemble in the presence of complex mixtures has been reported. The system was able to exploit the selectivity typical of confined chemistry which, combined with the stability of a templated self-assembled structure, allowed to overcome difficulties due to the presence of competing molecules. This study has allowed *(i)* to test the capability of the **TPMA**-based supramolecular cage to self-assembly in the presence of challenging complex mixtures like different wines and fruit juices and discriminate the dicarboxylic acids present in these matrixes, *ii)* to test the self-assembly capability of the cage in the presence of high amount of complex mixture, *iii)* to synthetize a chiral cage able to act Chiral Solvating Agent (CSA) for chiral dicarboxylic acids and exploit this capacity for the discrimination of the enantiomers of chiral malic and tartaric acids in complex mixtures.

In Chapter 2, the supramolecular cage has been employed as stereodynamic probe for the recognition of chiral dicarboxylate anions. In particular, sensing capabilities of the supramolecular architecture toward chiral dicarboxylic acids have been tested using circular dichroism. This work has demonstrated *(i)* the ability of the cage to act as stereodynamic probe using a wide range of dicarboxylic acids, *(ii)* to display a preferential enhancement of the dichroic signal of tartaric acid (*viz*. one order of magnitude higher than the structural closest system malic acid). The latter property has been clarified from computational studies, that highlighted that the formation of a hydrogen bonds network in the guest is responsible for the signal enhancement. Furthermore, the combination of the stereodynamic properties with the capability of the cage to self-assemble in a solution of complex media has allowed to build calibration curves for the assessment of the tartaric acid content in wines using circular dichroism.

In Chapter 3, a novel approach based on the capability of 9,10-phenanthrenequinone (**PHQ**) to react with diamines subcomponents, which allows their selective removal or replacement leading cage disassembly or cage to cage transformations has been developed. This methodology has been successfully optimized allowing to have: *i*) reversible assembly and disassembly of the cage with release and uptake of the guest, *ii*) hierarchical cage size transformation with differential release and uptake of guests in solution and *iii*) cage chirality

inversion which allows to alternatively enclose in the cage two enantiomeric diacids. In Chapter 4, the use of imine chemistry together with [3,3]-sigmatropic rearrangement to obtain novel hydrolytically stable chiral **TPMA**-based architectures in high yields and purity has been reported. A study of the rearrangement process has been carried out to understand the effect of the guest length in the rearrangement reaction. This strategy has led to the formation of a novel cage able to retain the structure also in solid state and the scope of the reaction has been extended to different **TPMA**-based structures. Moreover, the metalation of the novel cage has been performed. This could be exploit in future studies with different metals to obtain novel catalytic properties from confinement and the presence of two catalytic sites in the same structure.

APPENDIX

A1. Appendix to Chapter 1

A1.1. Self Assembly with different amount of Wine

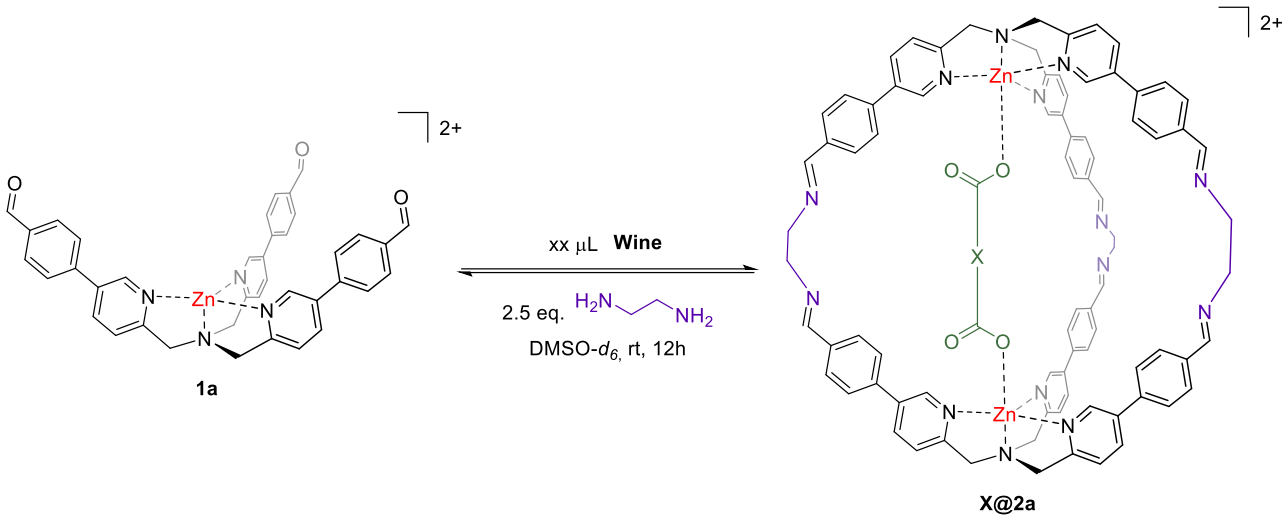

General procedure for the synthesis of molecular cage **X@2a** using different quantities of Valpolicella wine. Perchlorate counterions are removed for clarity.

To 500 µl (1.0 µmol) of a solution 0.002 M of complex **1** in DMSO-d_6 different amount of Valpolicella wine (15 µL, 30 µL, 50 µL, 75 µL, 100 µL, and 125 µL) without pre-treatment were added (triethylamine was added to correct the acidity of wine). In order to keep the concentration constant, DMSO-d_6 was added to reach the final volume of 625 µL. Then, 125 µL (2.5 µmol) of a solution 0.02 M in DMSO-d_6 of ethylenediamine were added slowly under stirring. The mixture was left for 12 h at room temperature and checked *via* ^{1}H-NMR using p-xylene as internal standard.

A1.1.1. Addition of 15 µL of wine

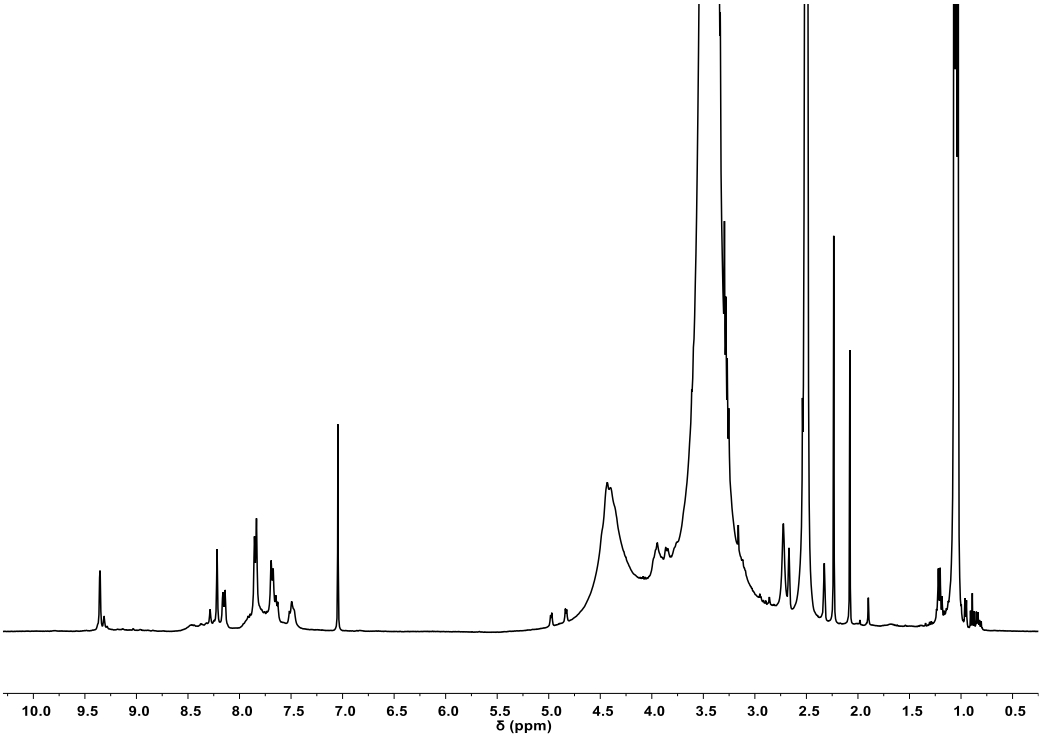

Figure A1. ^{1}H-NMR spectrum (400 MHz, 301 K, DMSO-d_6) of the mixture obtained using 15 µL of wine (yield 43% based on p-xylene).

A1.1.2. Addition of 30 µL of wine

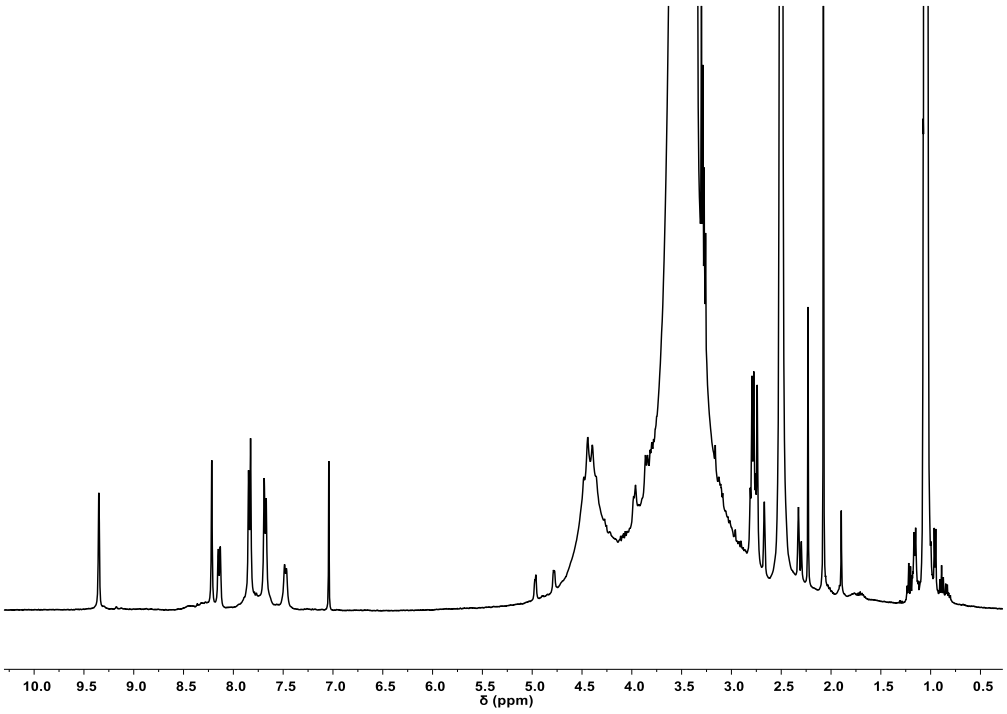

Figure A2. ^{1}H-NMR spectrum (400 MHz, 301 K, DMSO-d_6) of the mixture obtained using 30 µL of wine (yield 94% based on p-xylene).

A1.1.3. Addition of 50 µL of wine

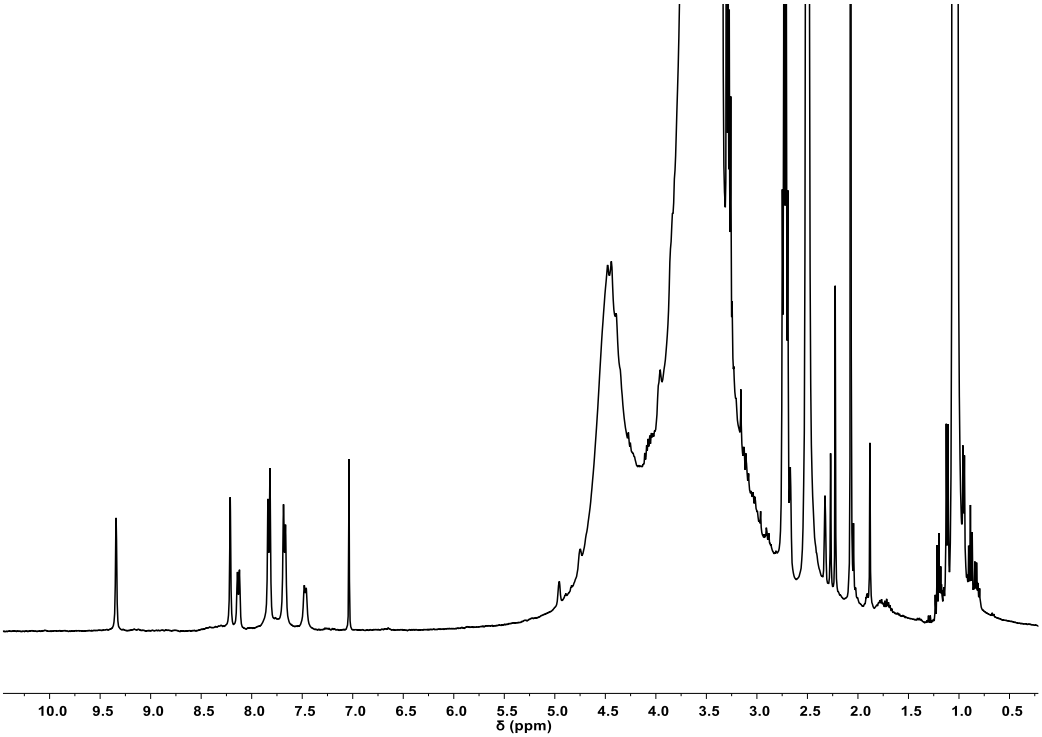

Figure A3. ^{1}H-NMR spectrum (400 MHz, 301 K, DMSO-d_6) of the mixture obtained using 50 µL of wine (yield 72% based on p-xylene).

A1.1.4. Addition of 75 µL of wine

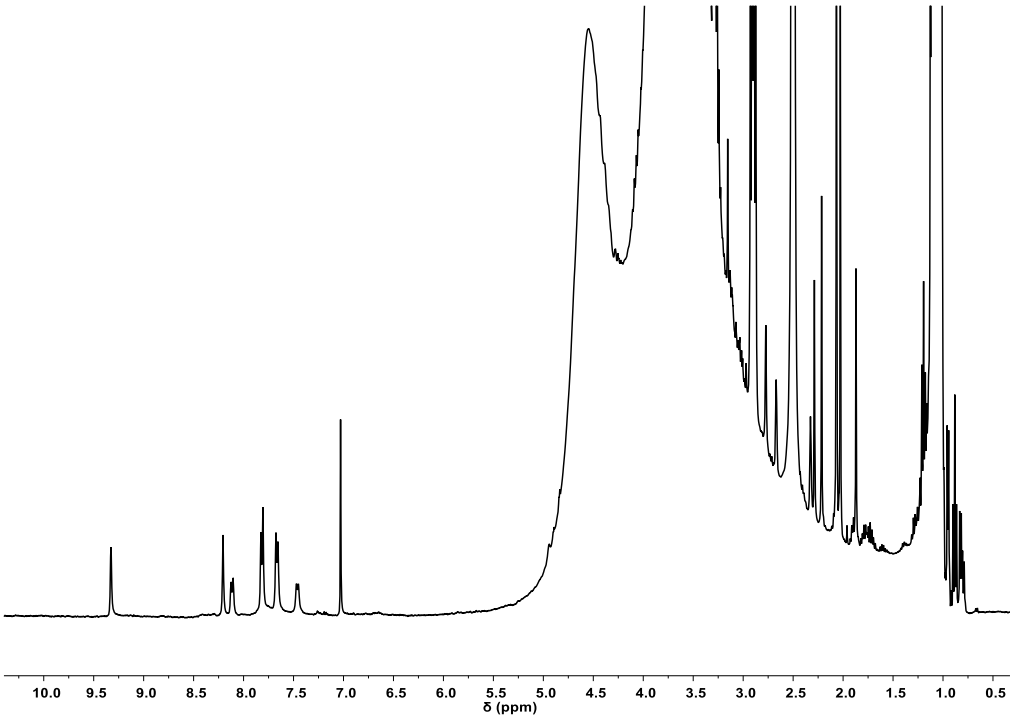

Figure A4. ^{1}H-NMR spectrum (400 MHz, 301 K, DMSO-d_6) of the mixture obtained using 75 µL of wine (yield 33% based on p-xylene).

A1.1.5. Addition of 100 µL of wine

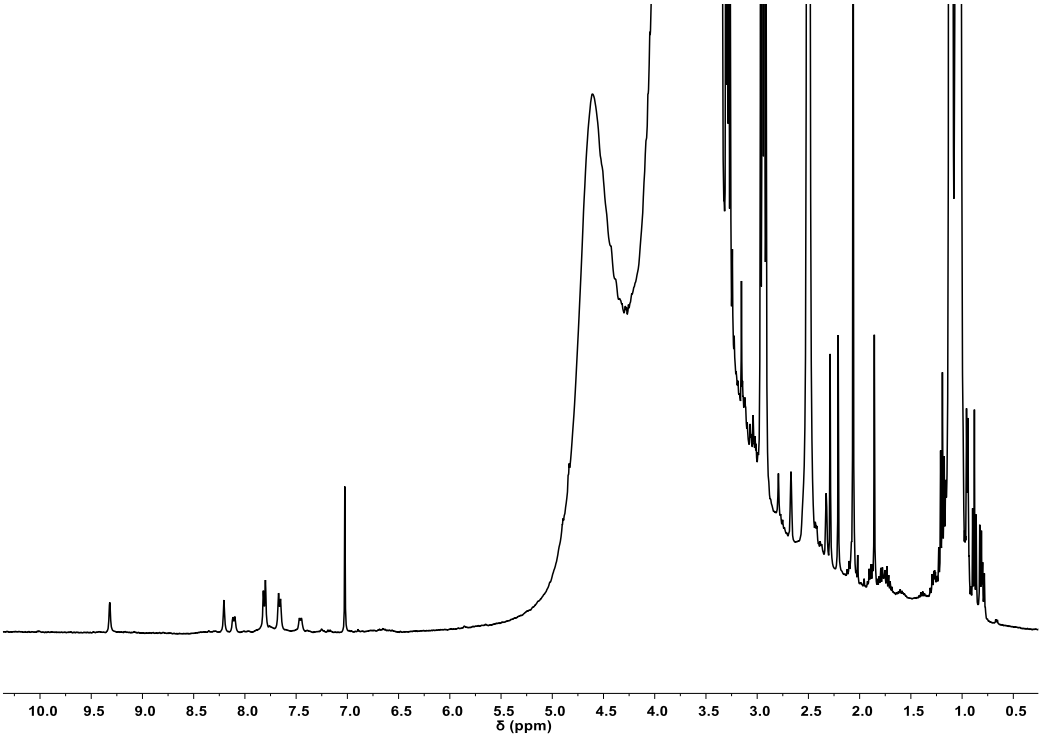

Figure A5. ^{1}H-NMR spectrum (400 MHz, 301 K, DMSO-d_6) of the mixture obtained using 100 µL of wine (yield 22% based on p-xylene)..

A1.1.6. Addition of 125 µL of wine

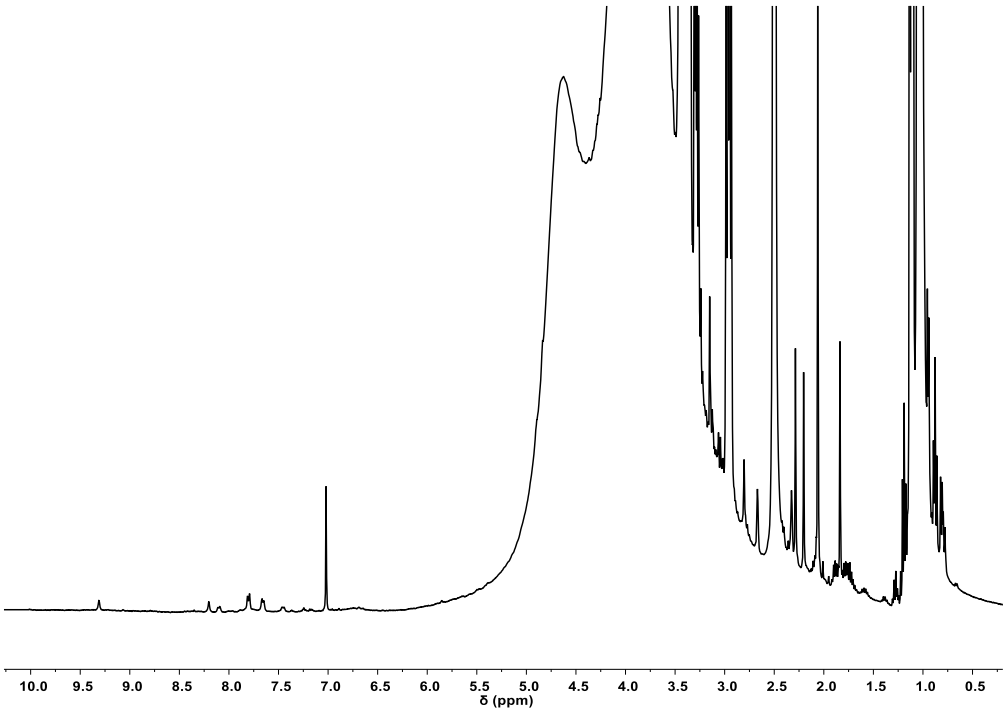

Figure S6. ^{1}H-NMR spectrum (400 MHz, 301 K, DMSO-d_6) of the mixture obtained using 125 µL of wine (yield 8% based on p-xylene).

A1.2. ECD measurement

ECD measurement was performed diluting complex **(*R*)-1b** with CH_3CN to obtain a final concentration equal to $1.0 \cdot 10^{-5}$M (0.1 cm cuvette). The CD spectrum was measured in millidegrees and reported in G value.

A1.3. CD spectrum of complex (*R*)-1b

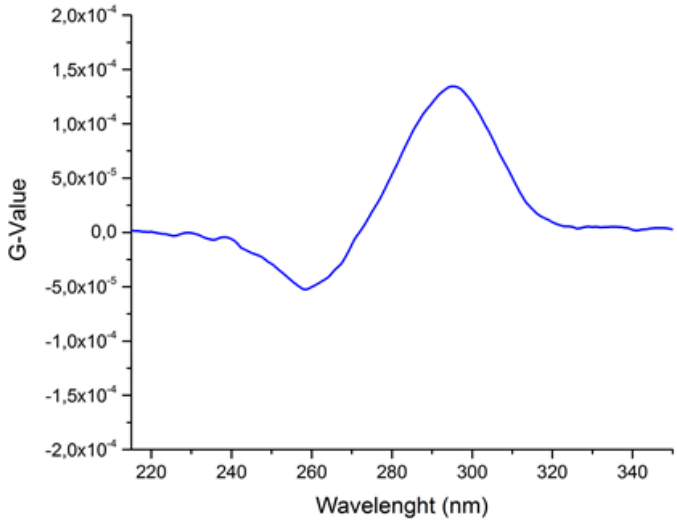

Figure A7. ECD spectrum of complex **(*R*)-1b**.

A1.4. Determination of the enantiomeric excess of (*R*)-7

The enantiomeric excess of the chiral amine ***R*-7** has been determined using a procedure reported by Bull *et al.*[1] To obtain the derivatization, 1.0 equiv. of boronic acid **11**, 1.1 equiv. of **(*S*)-BINOL** and 1.0 equiv. of the racemic amine **7** was dissolved in $CDCl_3$ in the presence of 4 Å molecular sieves and the ^{1}H-NMR was acquired after 5 minutes. The reaction led to the formation of rigid diastereoisomeric imino-boronate esters **(*S*-*R*)- 7** and **(*S*-*S*)-7**

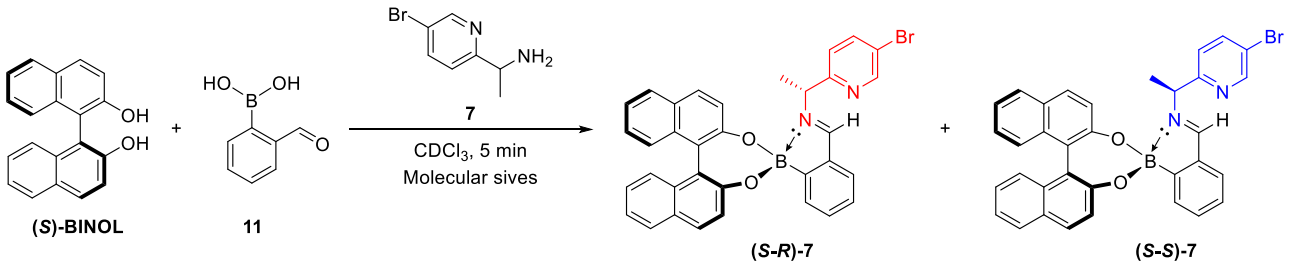

The ^{1}H-NMR spectrum of racemic **7** showed a good separation of the doublet of the methyl group, the quartet of the benzylic proton, and the imine proton due to the significantly different anisotropic effects experienced by the amine fragments in the presence of more than one aryl substituent. As expected, the racemic mixture presented the doubling of the signal in a 1:1 ratio, making this method suitable for the determination of the enantiomeric excess of the crystallized amines (Figure S8).

As shown in Figure A9, the ^{1}H-NMR of ***R*-27**, after four crystallizations, showed the presence of only one diastereomer in solution, with the disappearance of the signals of the second specie, indicating the complete resolution of the enantiomer. The absolute configuration of the enantiomer has been attributed from the work of Bull taking α-phenylethylamine as reference.

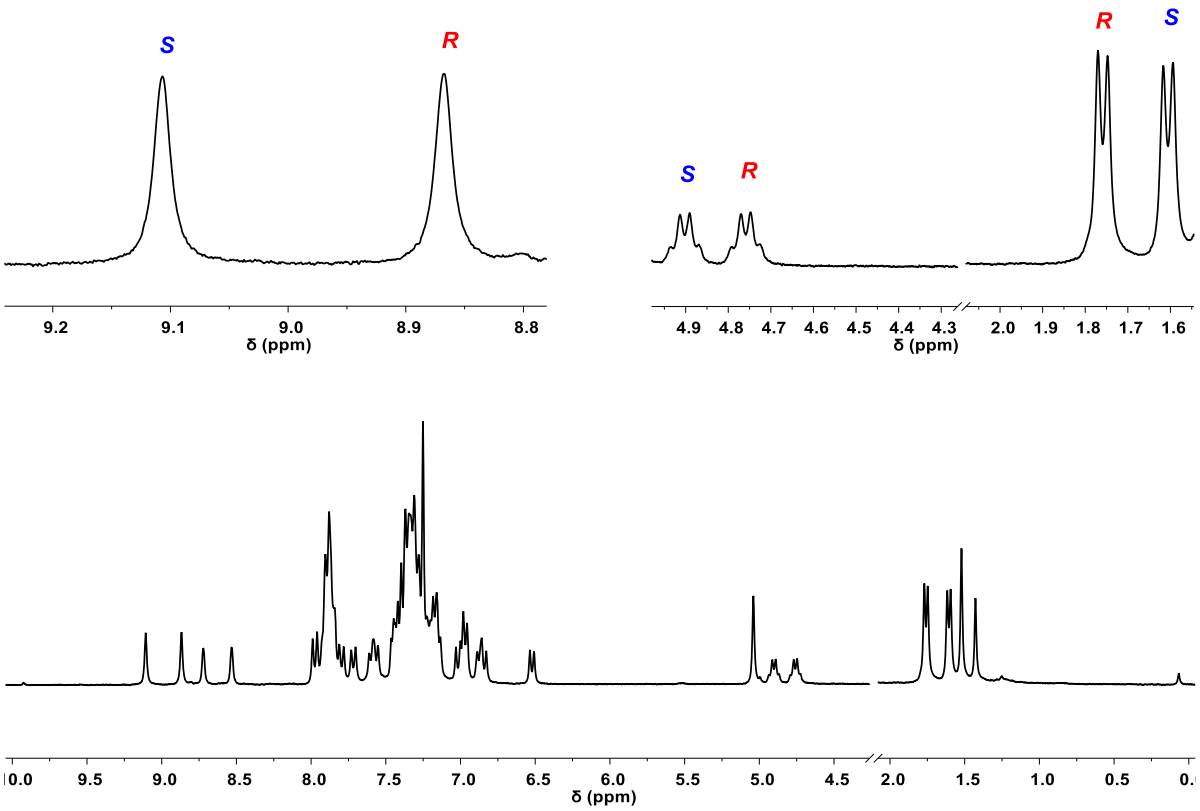

Figure A8. ^{1}H-NMR ($CDCl_3$, 300 MHz) spectrum of racemic mixture **(*S*-*R*)-7** and **(*S*-*S*)-7**.

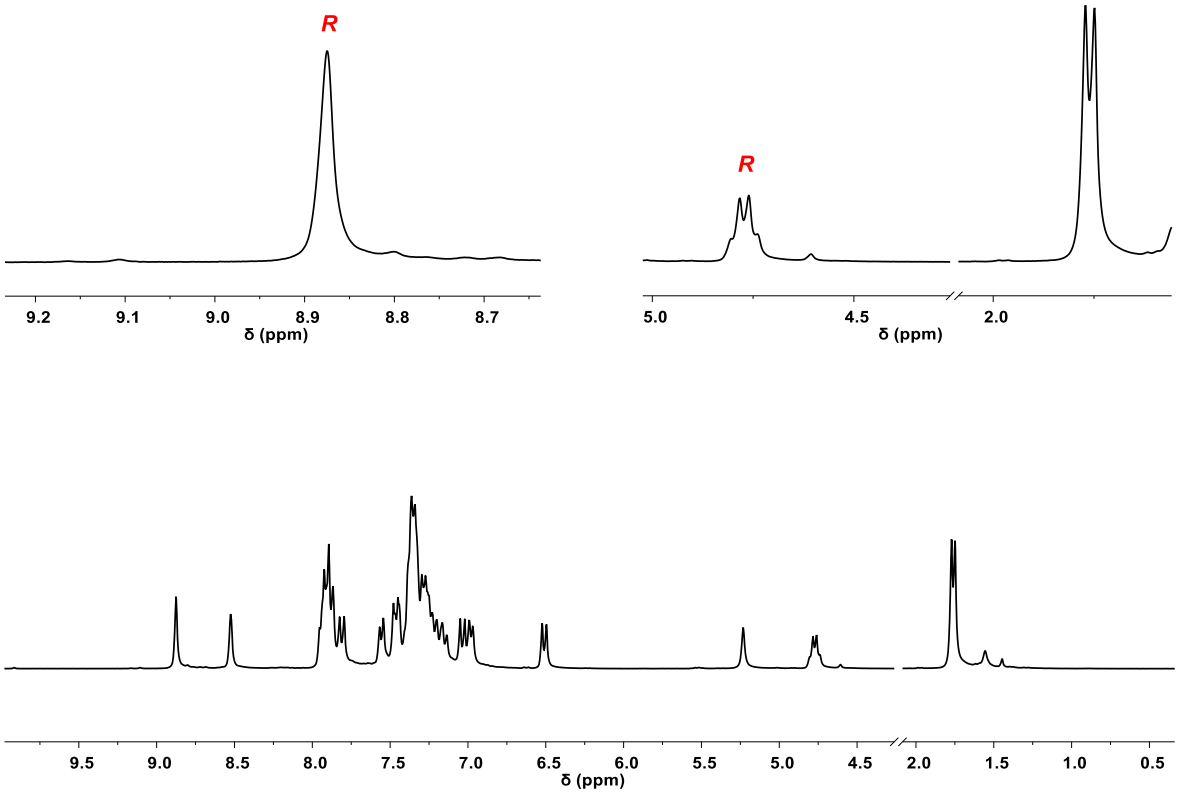

Figure A9 ^{1}H-NMR ($CDCl_3$, 300 MHz) spectrum of **(*S*-*R*)-7**.

A1.5. Procedure for the enantiomeric excess determination of 1-(5-bromopyridin-2-yl)ethan-1-amine (7)

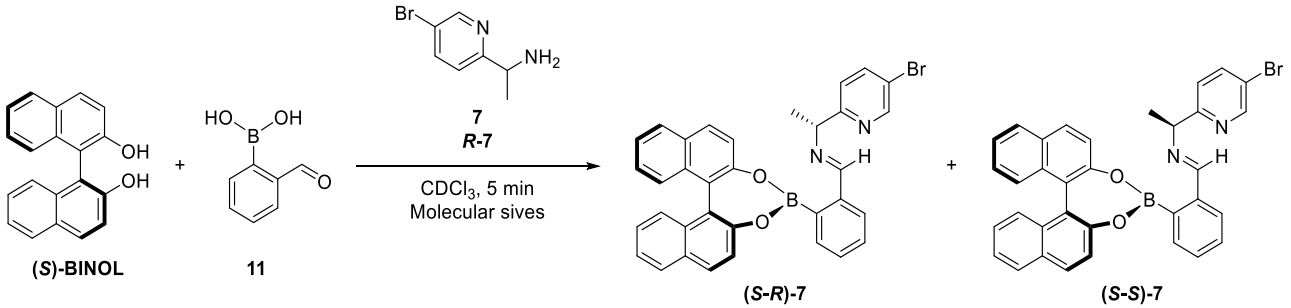

In a vial, 1.1 equiv. of (*S*)-(−)-1,1'-Bi(2-naphthol) **(*S*)-BINOL**, 1.0 equiv. of 2-formylphenylboronic acid **8** and 1.0 equiv. of 1-(5-bromopyridin-2-yl)ethan-1-amine **7** or (***R***)-**7** were dissolved in 2 mL of $CDCl_3$ in the presence of 4 Å molecular sieves. The ^{1}H-NMR spectrum of an aliquot was acquired after 5 minutes.

A1.6. Determination of the enantiomeric excess of zinc complex (*R*)-1b

Since it was not possible to find a method for the quantification of enantiomeric excess of the ligand (***R*)-9** using neither chiral chromatography nor chiral derivatization, the attention was focused on the zinc complex (***R*)-1b**.

The capability of the zinc complex to bind chiral carboxylic acid was exploited to determine its enantiomeric excess using NMR technique.

To analyze the optical purity of the both zinc complexes (***R*)-1b** using NMR analysis, (*S*)-(+)-2-methoxy-2-phenylacetic acid **12** was employed as CSR

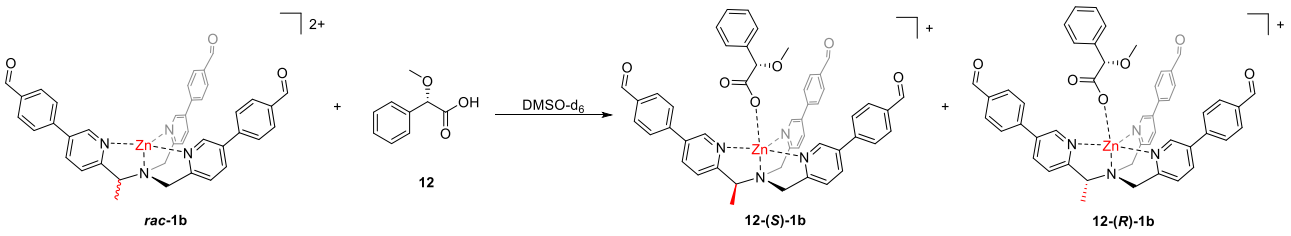

Adding chiral acid **12** to a solution of the racemic complex ***rac*-1b** in DMSO-d_6 allowed to observe a doubling of the signals in the region of the α pyridine protons between 8.90 ppm and 9.30. From the relative ratio of the areas of the signals it was possible to estimate directly the enantiomeric excess of the complex, considering the experimental error of the NMR technique. As shown in Figure S10, the racemic complex presented two doubling peaks with the same areas.

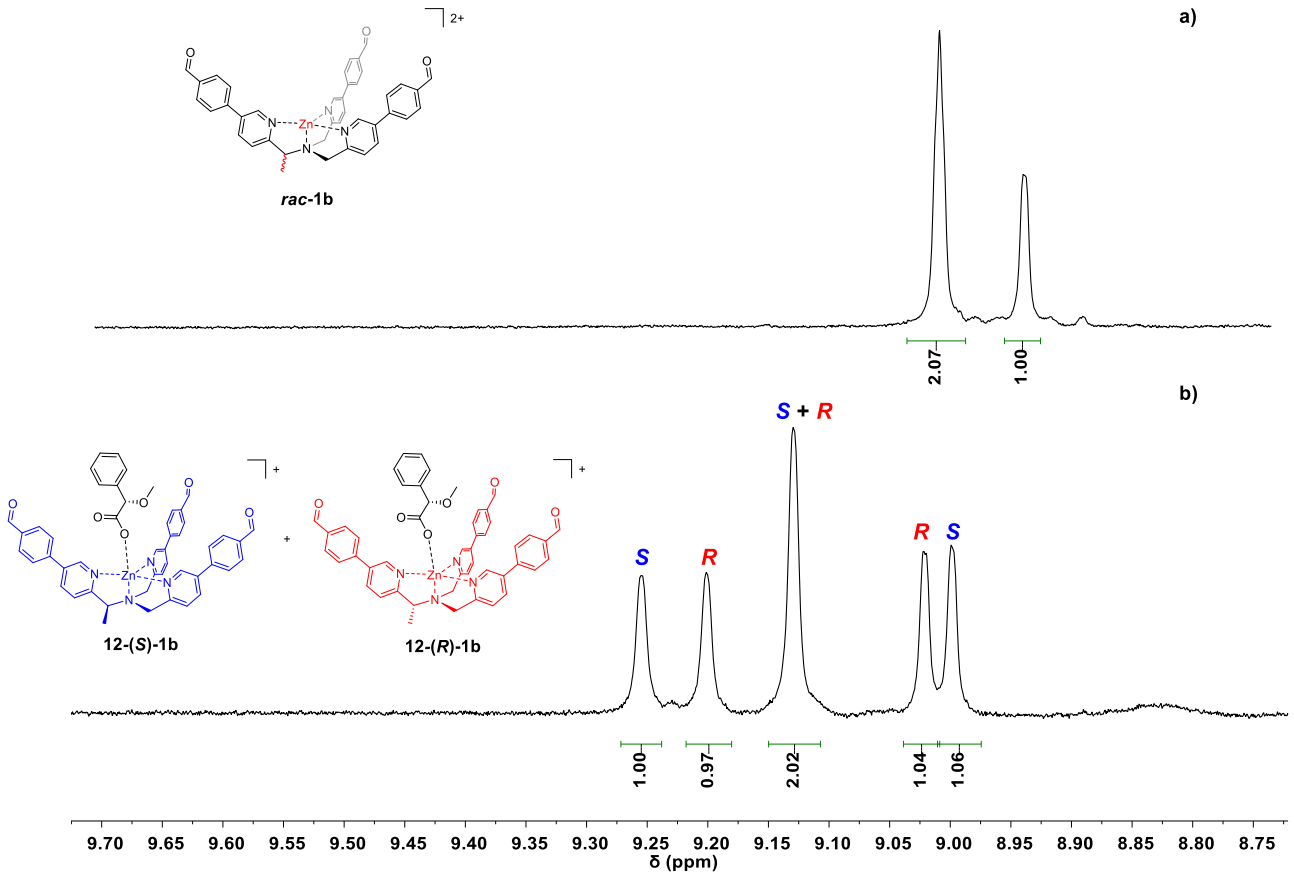

Figure A10. ^{1}H-NMR (DMSO-d_6, 600 MHz) spectrum of a) ***rac*-1b** complex, b) ***rac*-1b** complex after the addition of (*S*)-(+)-2-methoxy-2-phenylacetic acid **12**. From the relative ratio of the areas it was possible to estimate the enantiomeric excess.

The enantiomeric excess of zinc complex (***R*)-1b,** has been reported in Figure A11.

From the relative ratio of the areas of the obtained signals, more than 90% of enantiomeric excess was estimated.

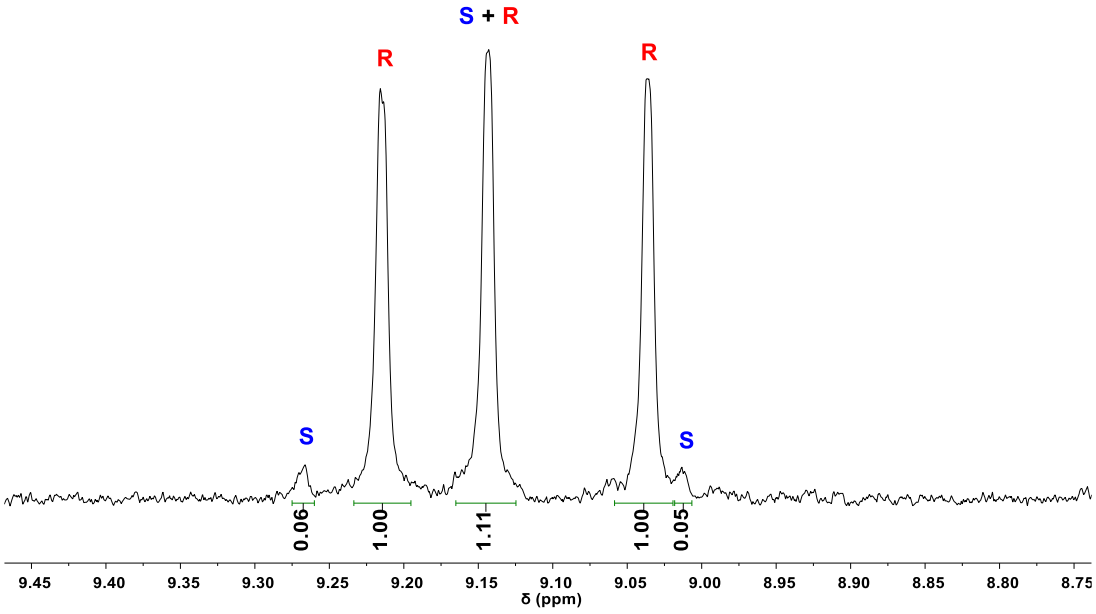

Figure A11. ^{1}H-NMR (DMSO-d_6, 600 MHz) spectrum (***R*)-1b** complex after the addition of (S)-(+)-2-methoxy-2-phenylacetic acid **12**. From the relative ratio of the areas it was possible to estimate an enantiomeric excess of more than 90%.

A1.7. General procedure for the enantiomeric excess determination of the complex.

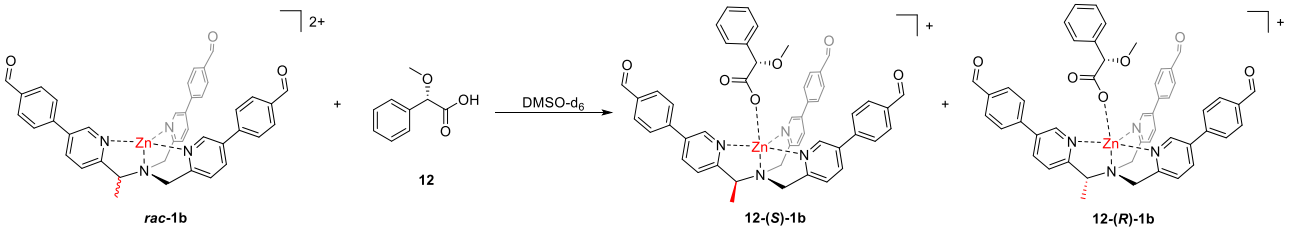

To 400 µL (1.0 µmol) of a 0.002 M solution of complex (***R*)-1b** in DMSO-d_6, 122 µL (1.0 µmol) of a 0.01 M solution of (*S*)-(+)-2-methoxy-2-phenylacetic acid **12** in DMSO-d_6 of were added in a NMR tube. The mixture was checked *via* ^{1}H-NMR.

A1.8. Stereochemical considerations on the possible cages present in solution

Due to presence of a stereocenter in one arm of the **TPMA** complexes, during the cage formation more than one assembly could be obtained. In particular, three different structures could be formed using (***R***)**-1b** complex. The resulting structures are all diastereoisomers since there is not any symmetry operation that could interconvert them to each other (Figure A12).

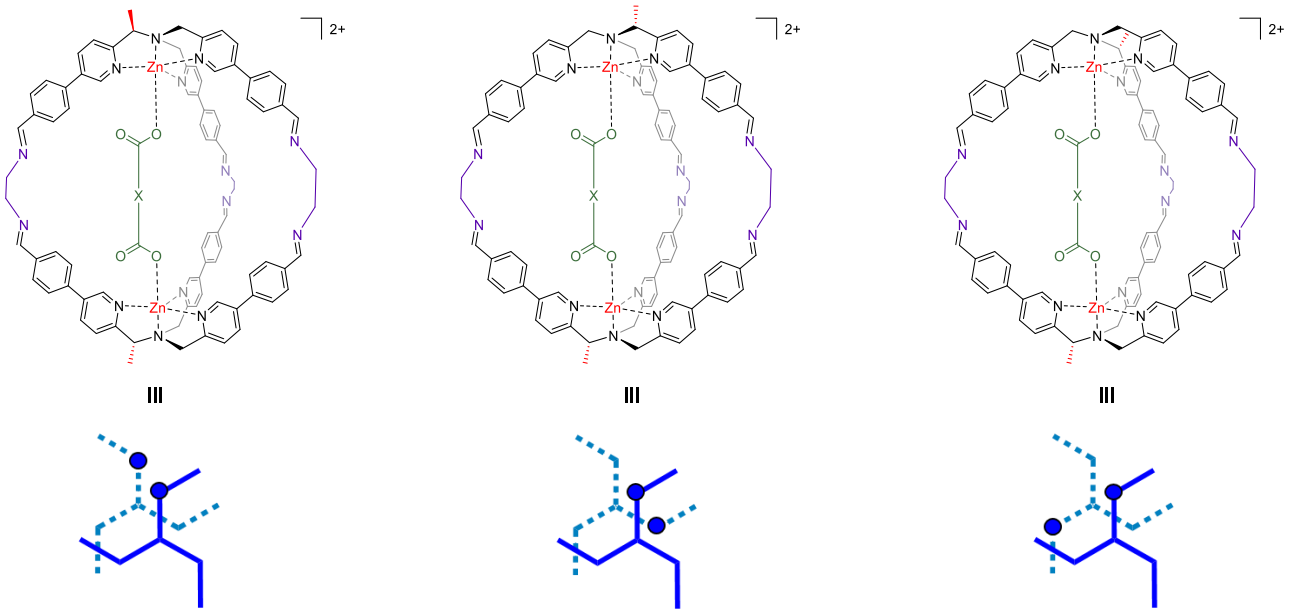

Figure A12. Different diastereoisomers of cages **X@**(***R,R***)**-2b** formed in solution using enantiopure complex (***R***)**-1b**.

A1.9. Addition of D-tar to Wine@(*R*,*R*)-2b

In order test cage capability to sense unnatural enantiomers in the complex matrix, increasing amounts of unnatural **D-Tar** have been added to Valpolicella wine and used as templating agents for cage formation. After determination of L-Tartaric acid content in Valpolicella wine using ^{1}H-NMR (2.3 g/L, Figure S49) different amount of **D-Tar** acid has been added to obtain different enantiomeric excesses. Since cage **X@(*R*,*R*)-2b** is chiral, **DL-Tar** (0.2 eq.) was added to a solution of complex **(*R*)-1b** and ethylenediamine in order to understand if there was no preference in binding for one of the two chiral dicarboxylic acids. As shown in Figure S13 no preference was observed.

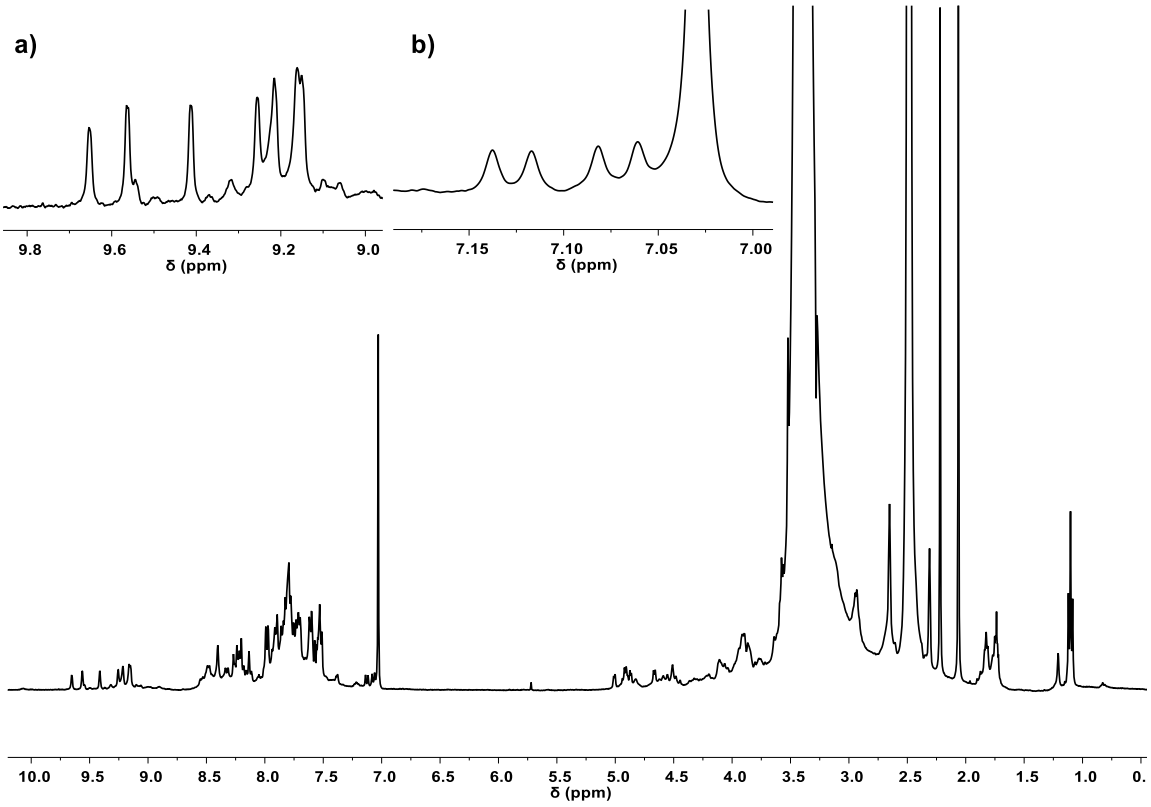

Figure A13. ^{1}H-NMR spectrum (600 MHz, 301 K, DMSO-d_6) of cage **DL-Tar@(*R*,*R*)-2b**, a) α-pyridine protons region, and b) pyridine proton region.

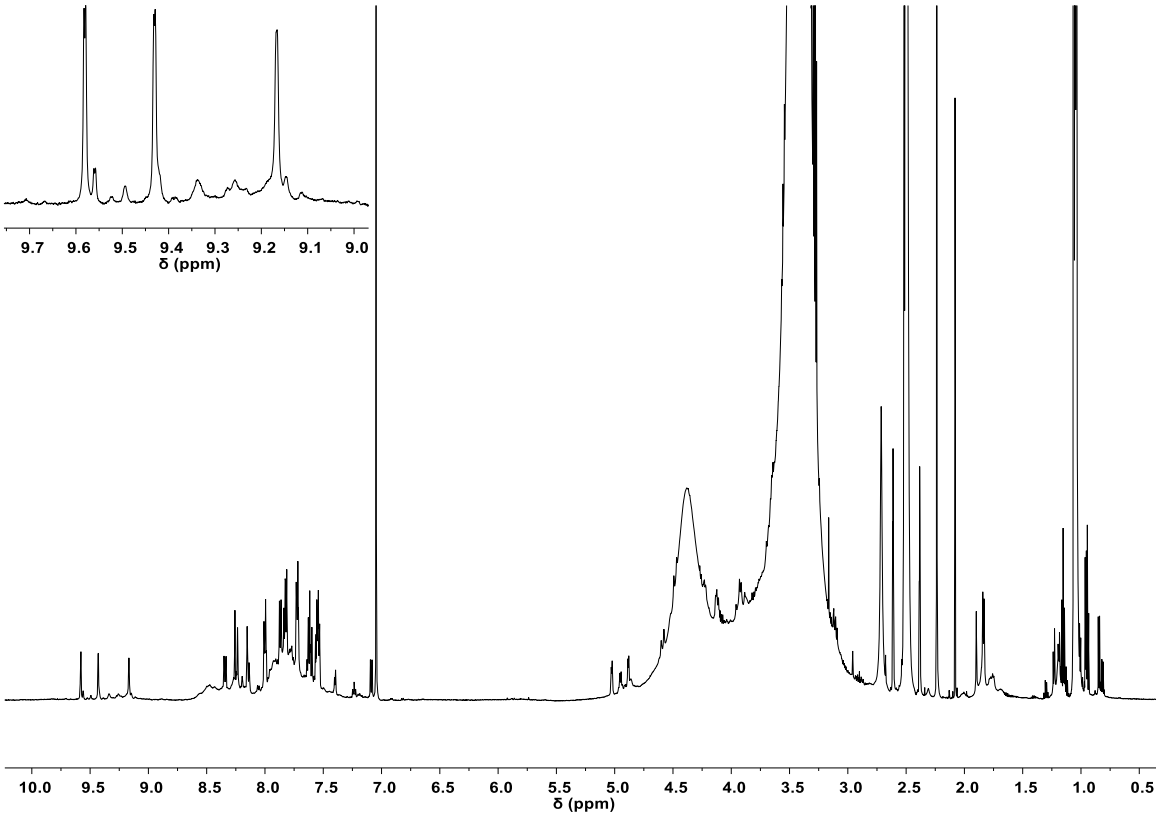

Figure A14. ^{1}H-NMR spectrum (600 MHz, 301 K, DMSO-d_6) of cage **Wine@(*R*,*R*)-2b** with **D-Tar** in order to obtain an enantiomeric excess equal to 98%.

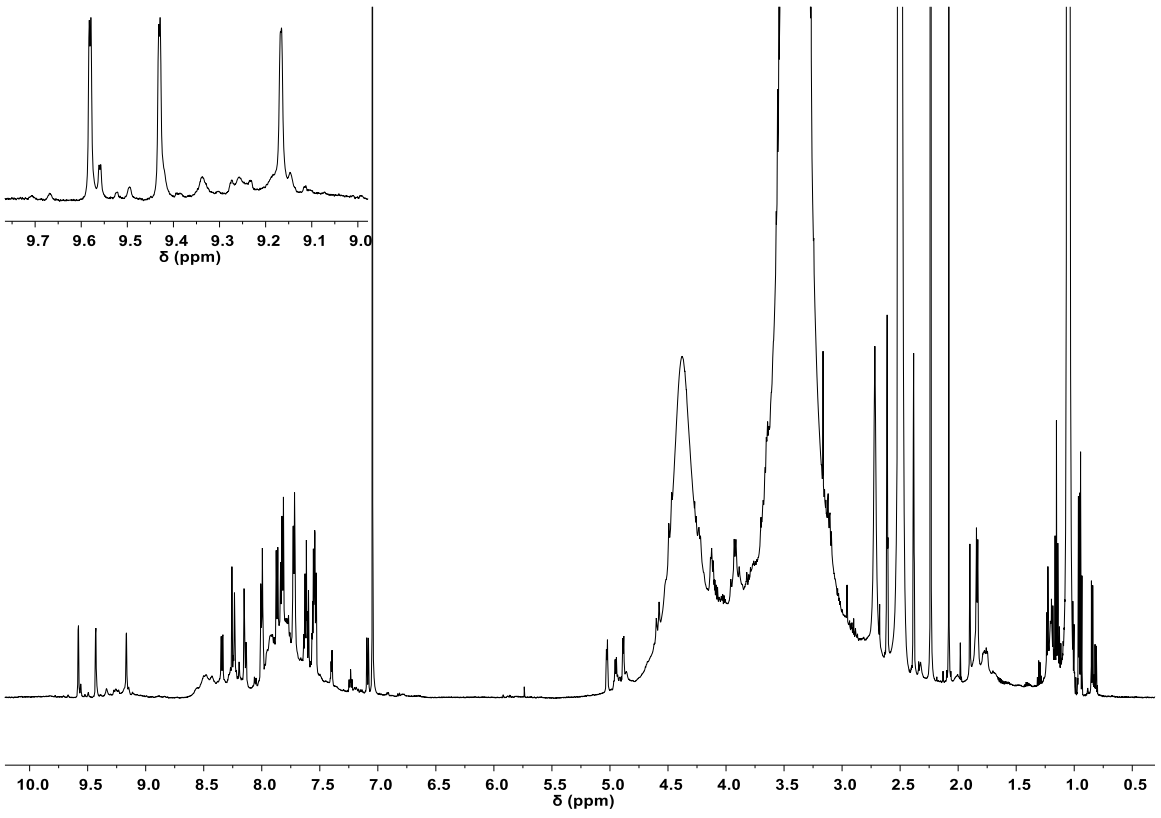

Figure A15. ^{1}H-NMR spectrum (600 MHz, 301 K, DMSO-d_6) of cage **Wine@(*R*,*R*)-2b** with **D-Tar** in order to obtain an enantiomeric excess equal to 94%.

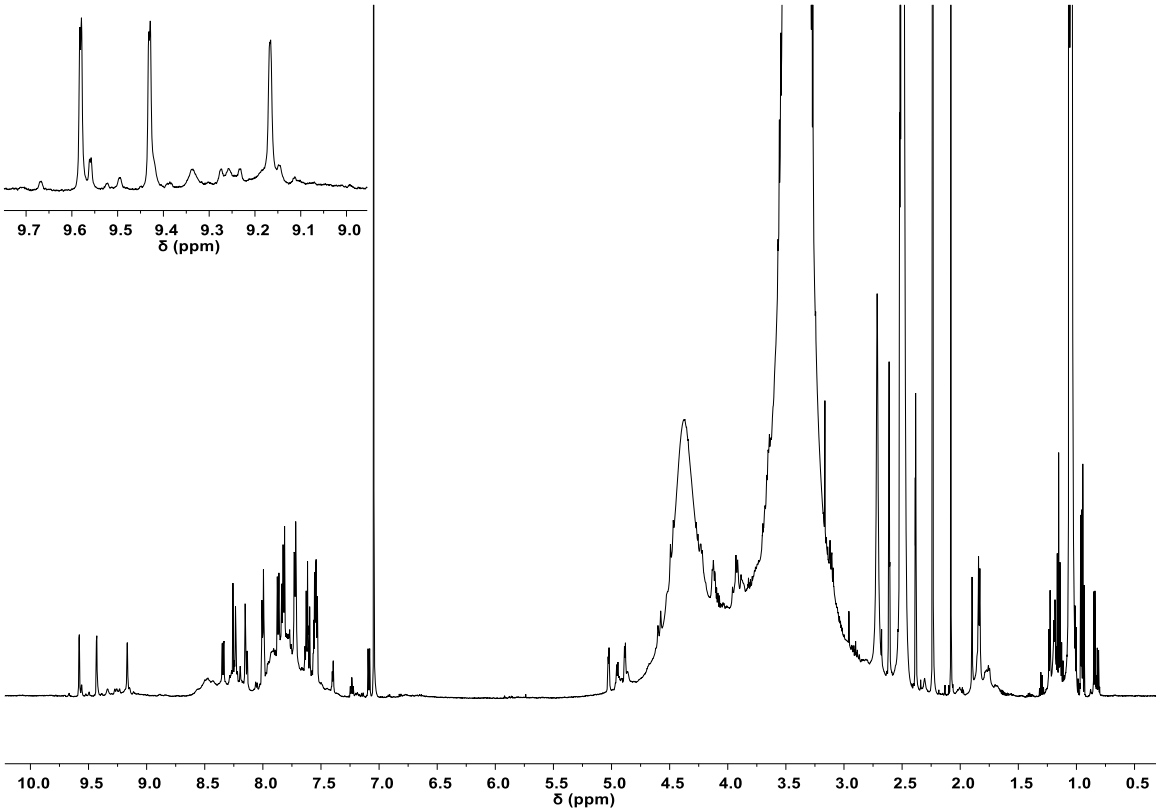

Figure A16. ^{1}H-NMR spectrum (600 MHz, 301 K, DMSO-d_6) of cage **Wine@(*R*,*R*)-2b** with **D-Tar** in order to obtain an enantiomeric excess equal to 90%.

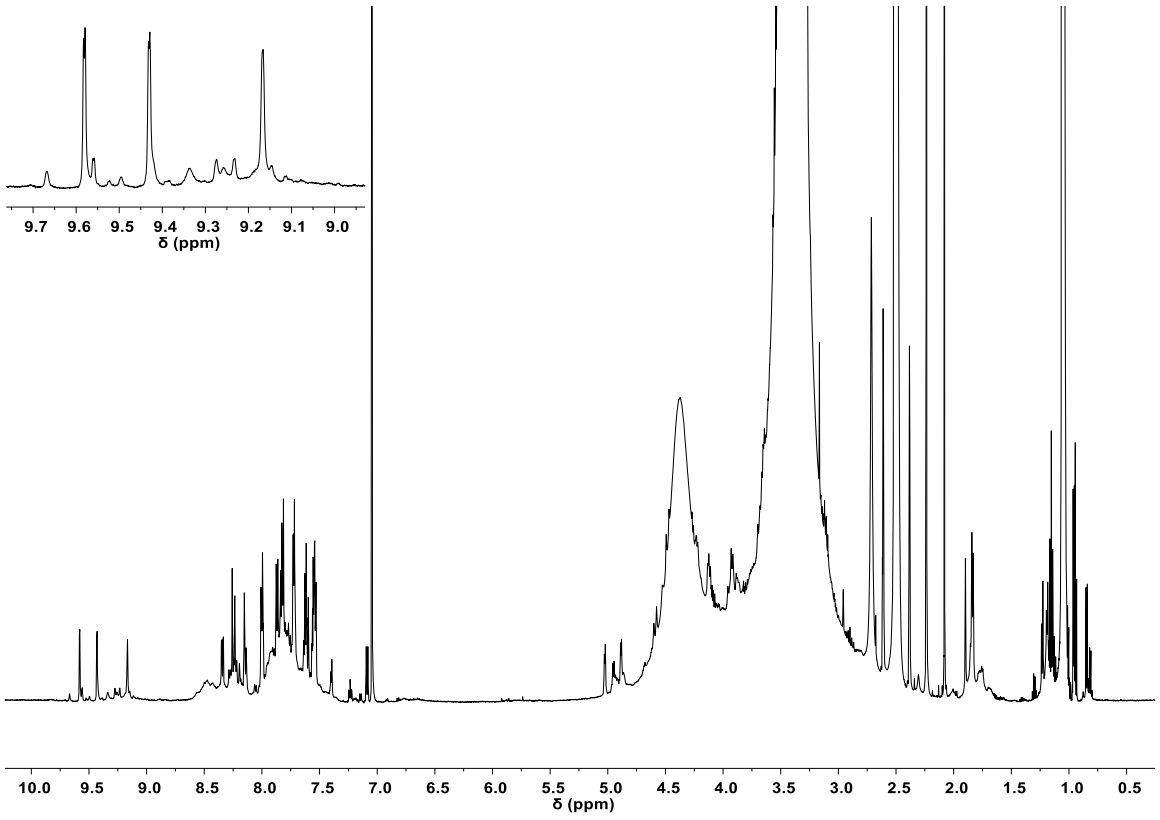

Figure A17.^{1}H-NMR spectrum (600 MHz, 301 K, DMSO-d_6) of cage **Wine@(*R*,*R*)-2b** with **D-Tar** in order to obtain an enantiomeric excess equal to 84%.

A1.10. NMR characterization

A1.10.1. 1-(5-bromopyridin-2-yl)ethan-1-ol (4)

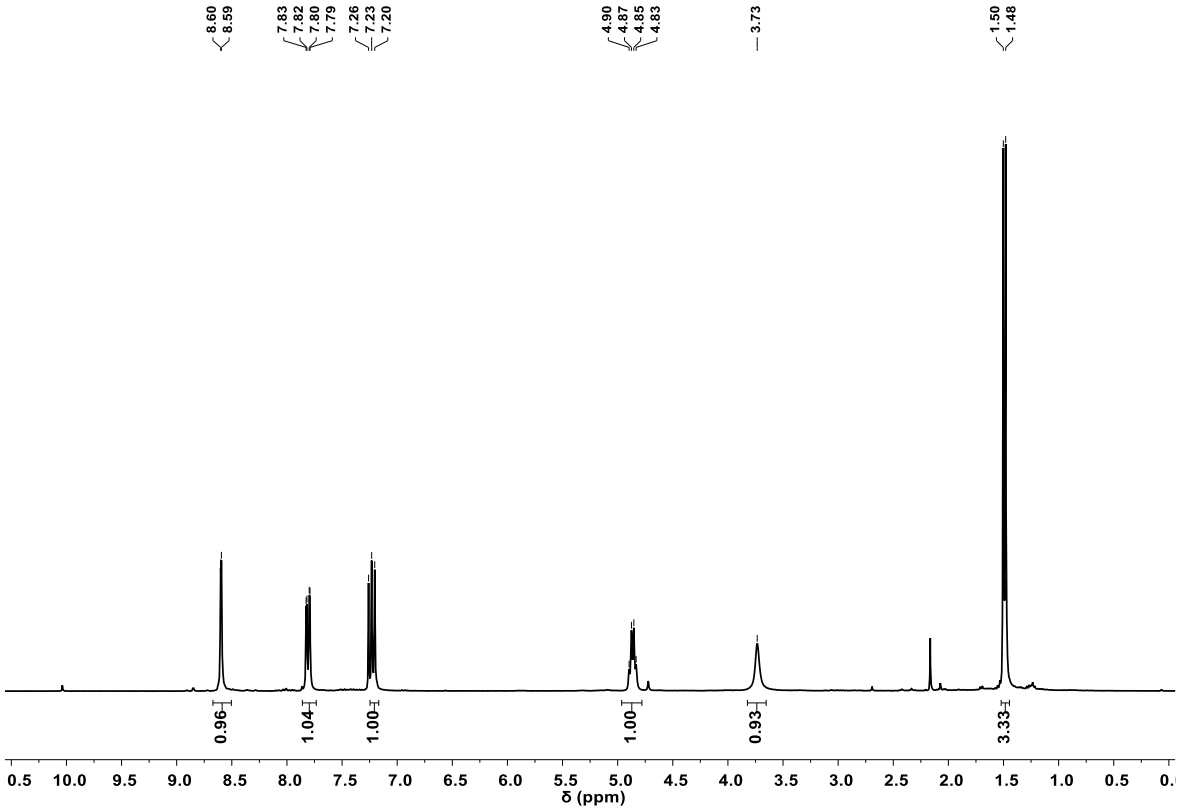

Figure A18. ^{1}H-NMR spectrum (300 MHz, 301 K, $CDCl_3$) of **4**.

A1.10.2. 1-(5-bromopyridin-2-yl)ethyl 4-methylbenzenesulfonate (5)

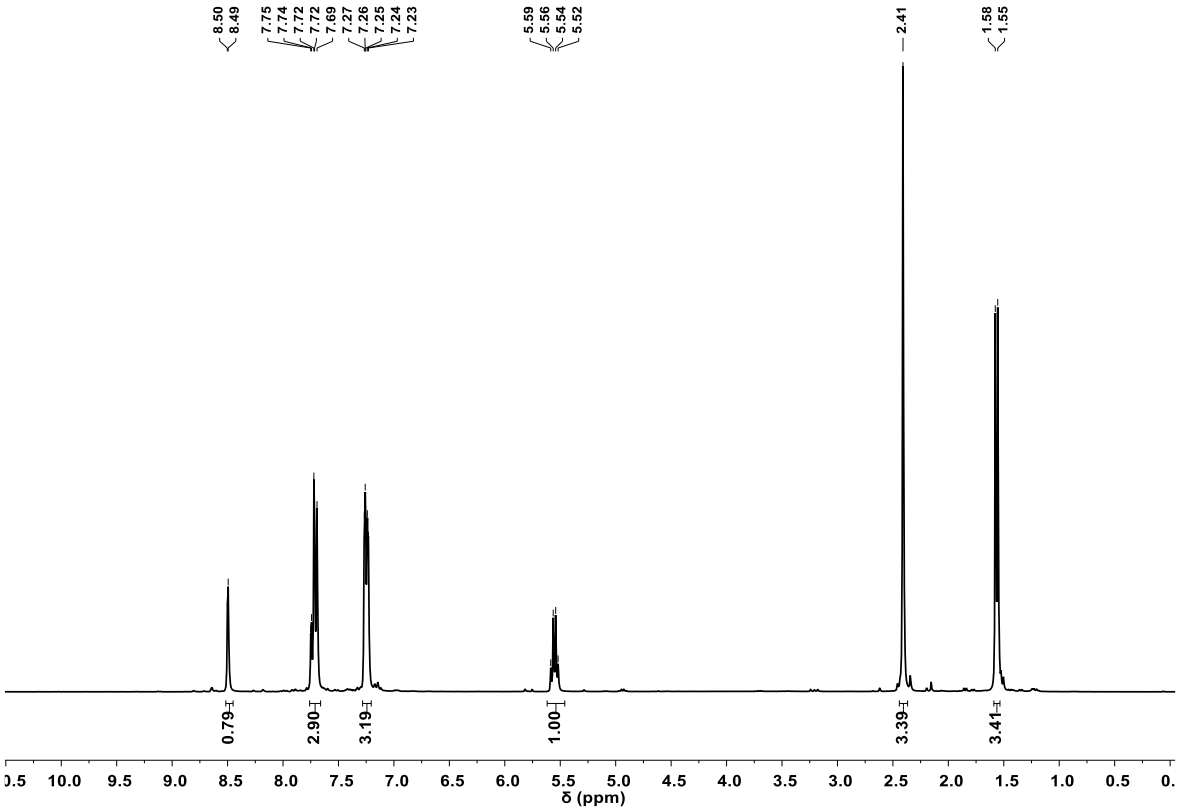

Figure A19. ^{1}H-NMR spectrum (300 MHz, 301 K, $CDCl_3$) of **5**.

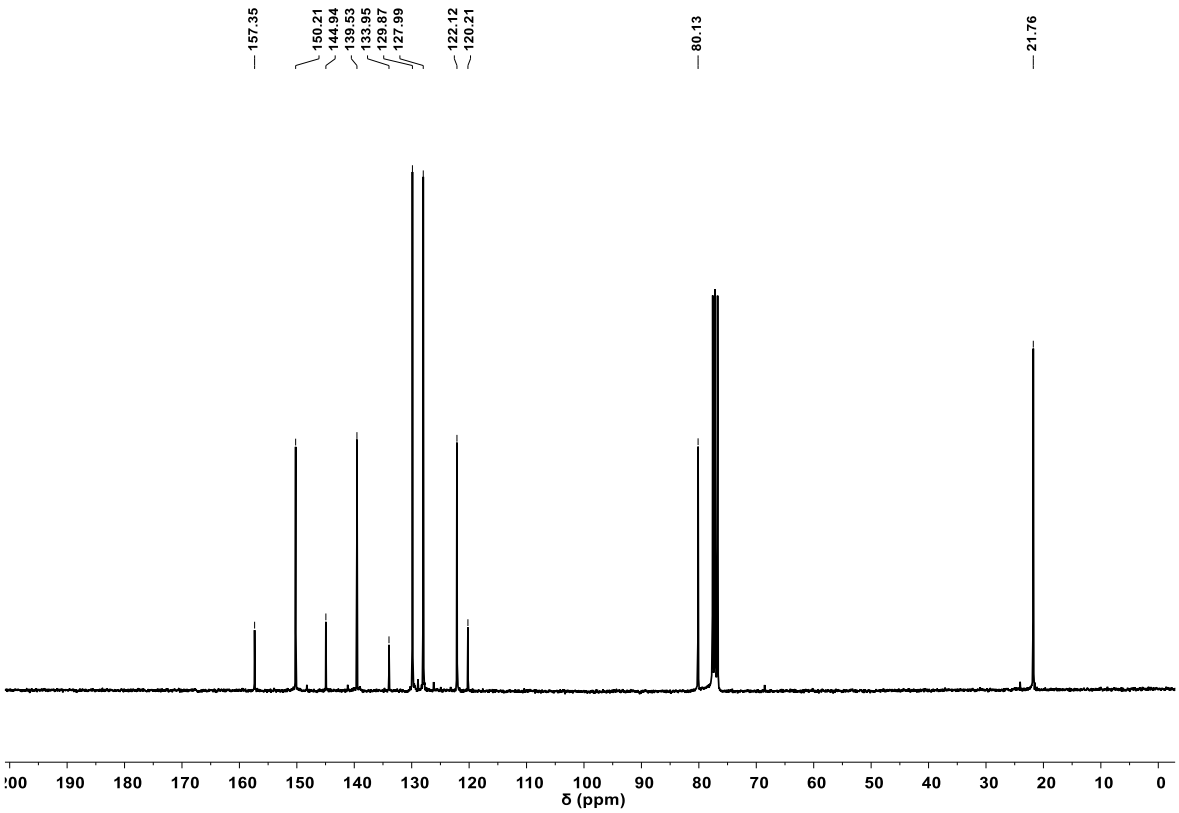

Figure A20. ^{13}C-NMR spectrum (75 MHz, 301 K, $CDCl_3$) of **5**.

A1.10.3. 2-(1-azidoethyl)-5-bromopyridine (6)

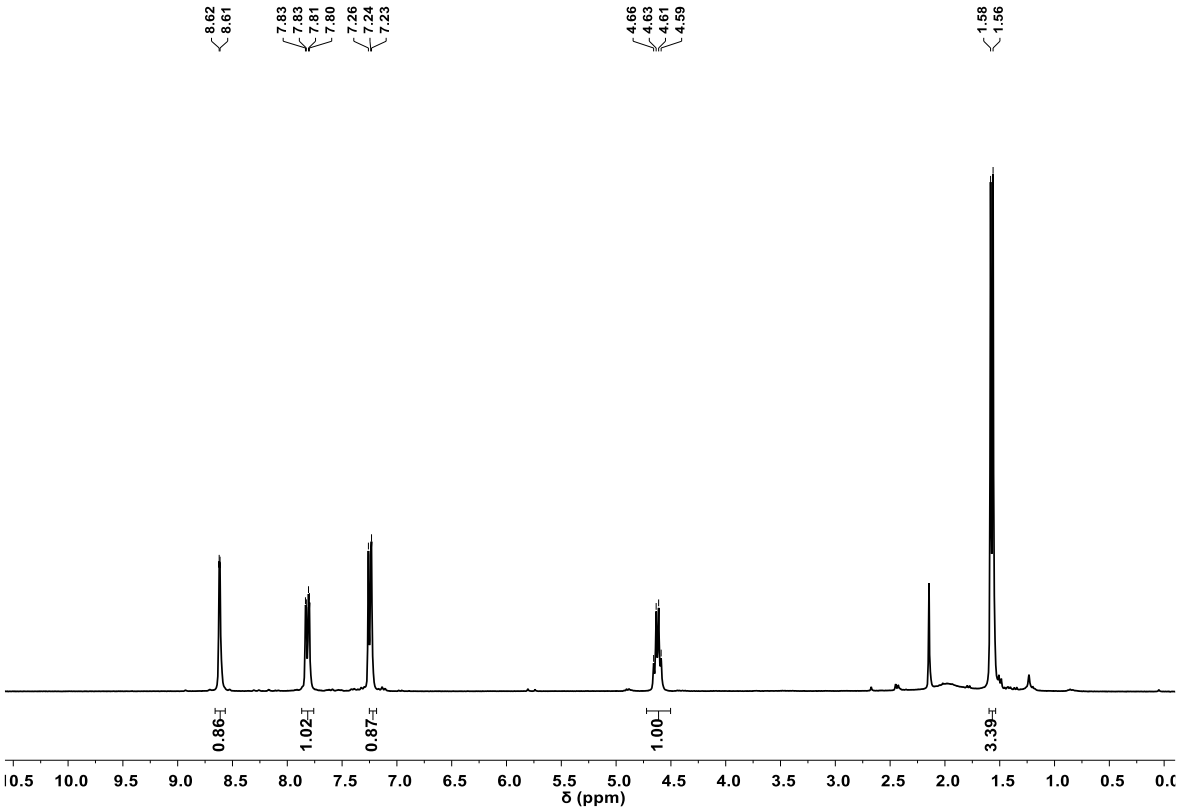

Figure A21. ^{1}H-NMR spectrum (300 MHz, 301 K, $CDCl_3$) of **6**.

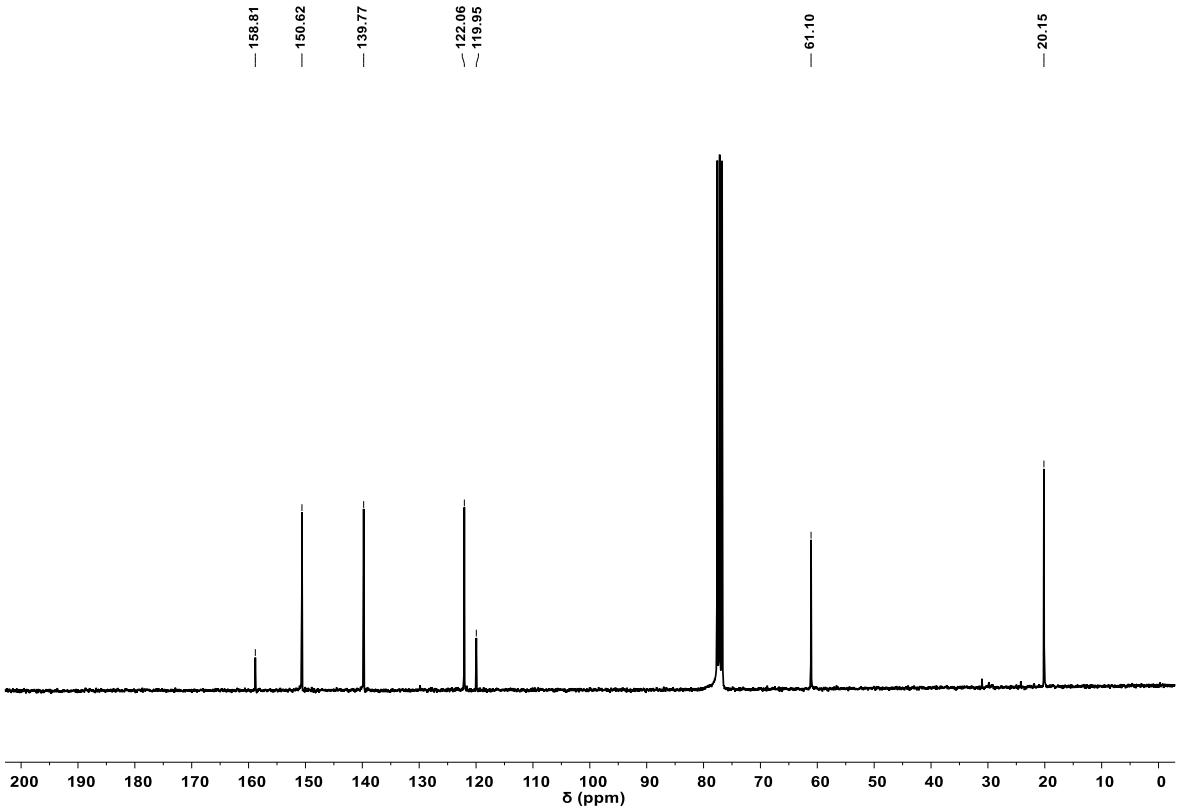

Figure A22. ^{13}C-NMR spectrum (75 MHz, 301 K, $CDCl_3$) of **6**.

A1.10.4. 1-(5-bromopyridin-2-yl)ethan-1-amine (7)

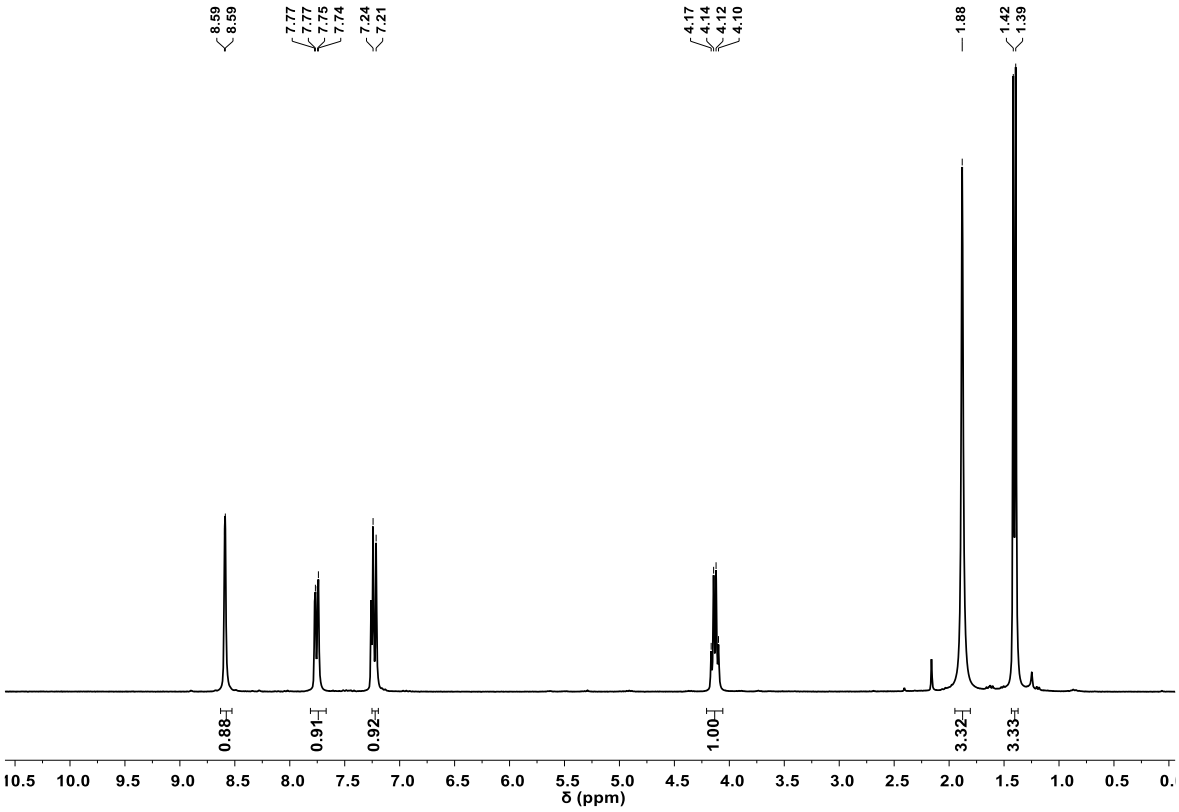

Figure A23. ^{1}H-NMR spectrum (300 MHz, 301 K, $CDCl_3$) of **7**.

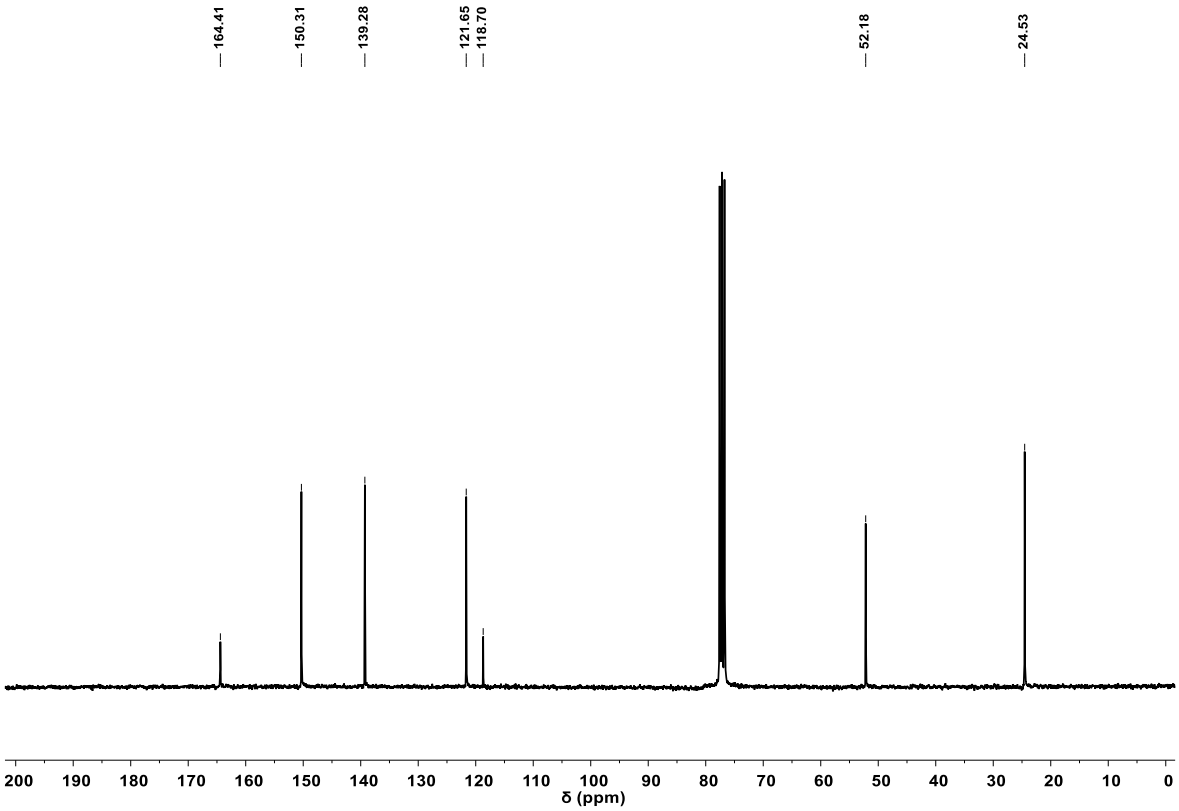

Figure A24. ^{13}C-NMR spectrum (75 MHz, 301 K, $CDCl_3$) of **7**.

A1.10.5. *R*-(+)1-(5-bromopyridin-2-yl)-*N*,*N*-bis((5-bromopyridin-2-yl)methyl)ethan-1-amine ((*R*)-8)

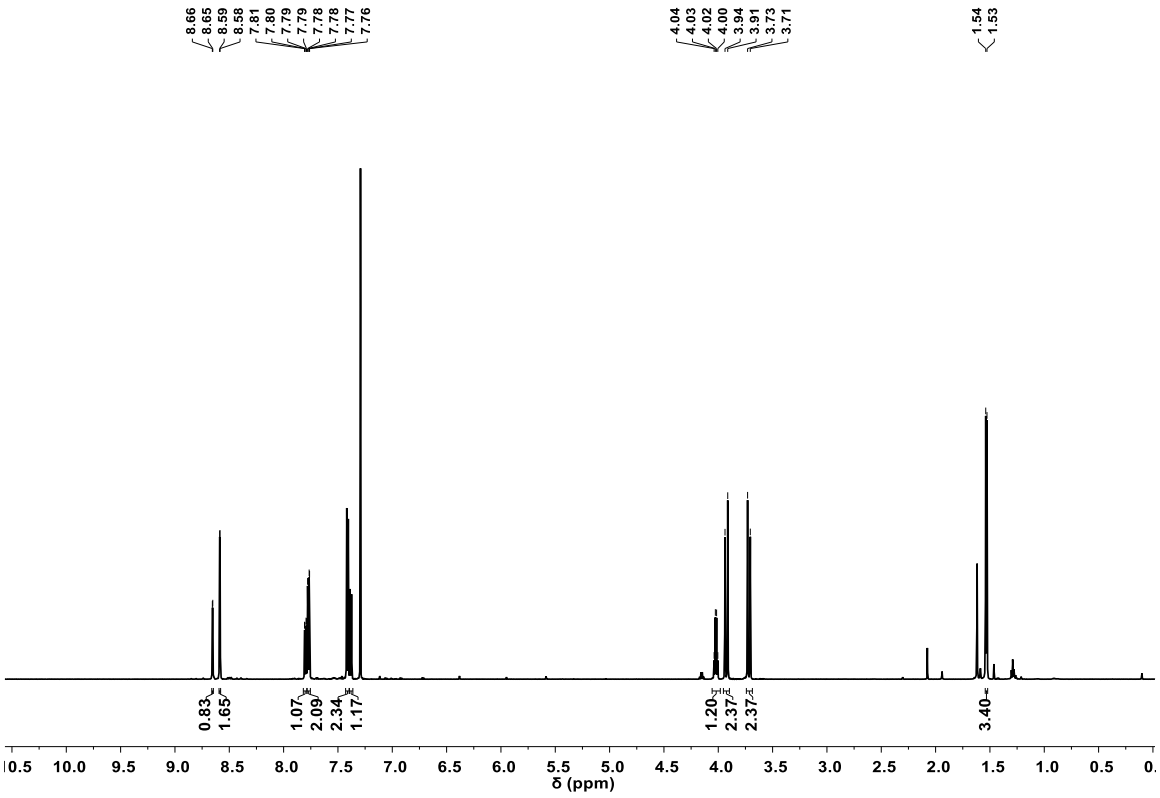

Figure A25. ^{1}H-NMR spectrum (600 MHz, 301 K, $CDCl_3$) of **(*R*)-8**.

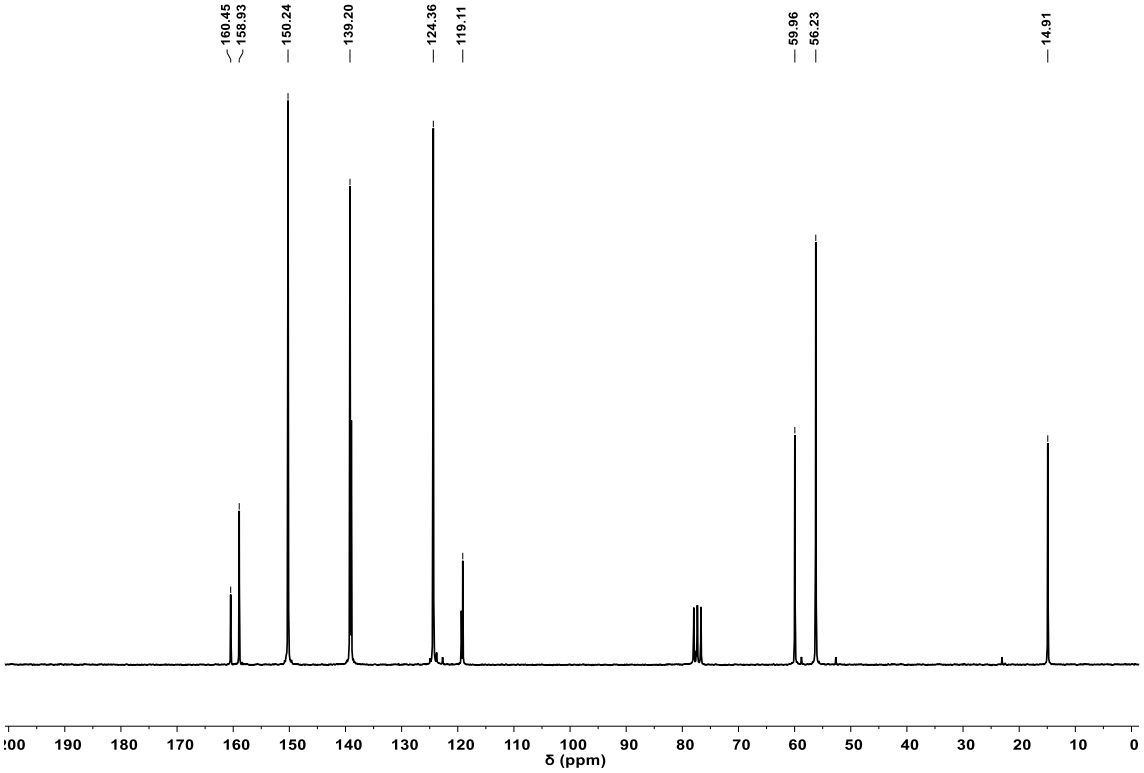

Figure A26. ^{13}C-NMR spectrum (75 MHz, 301 K, $CDCl_3$) of **(*R*)-8**.

A1.10.6. (*R*)-4,4'-((((1-(5-(4-formylphenyl)pyridin-2-yl)ethyl)azanediyl) bis(methylene)) bis(pyridine-6,3-diyl))dibenzaldehyde ((*R*)-9)

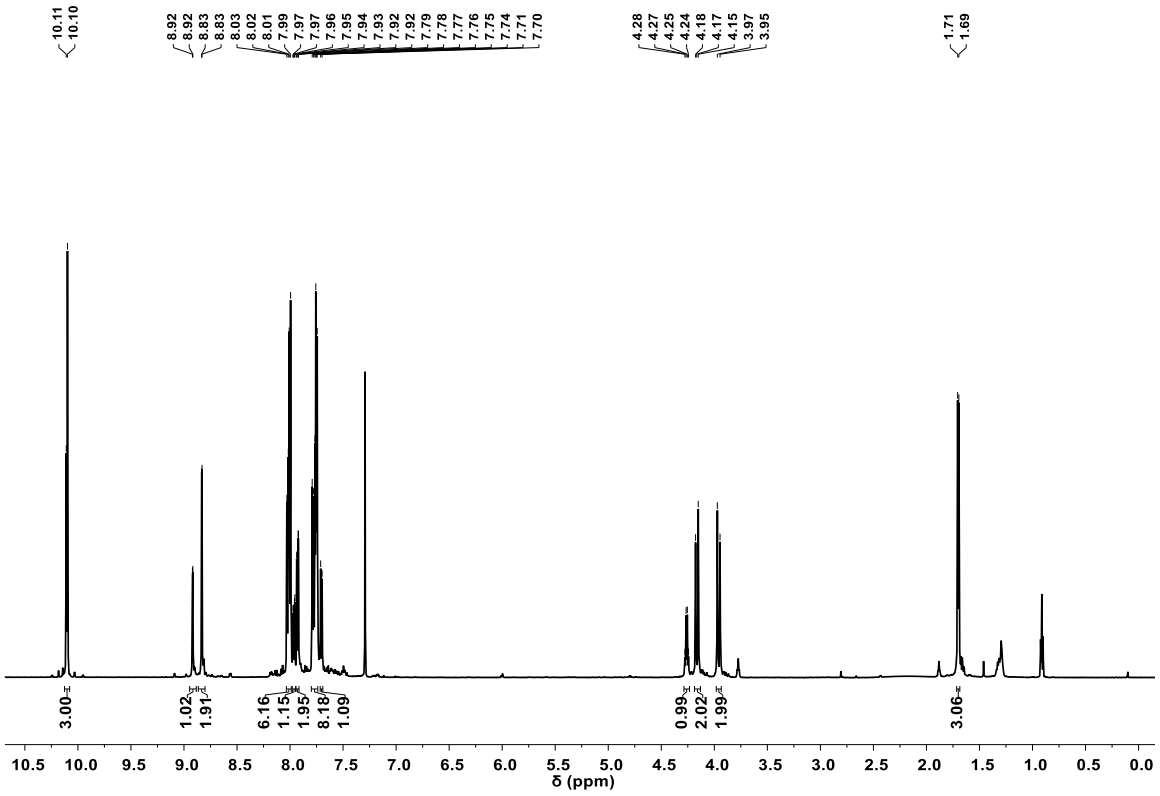

Figure A27. ^{1}H-NMR spectrum (600 MHz, 301 K, $CDCl_3$) of **(*R*)-9**.

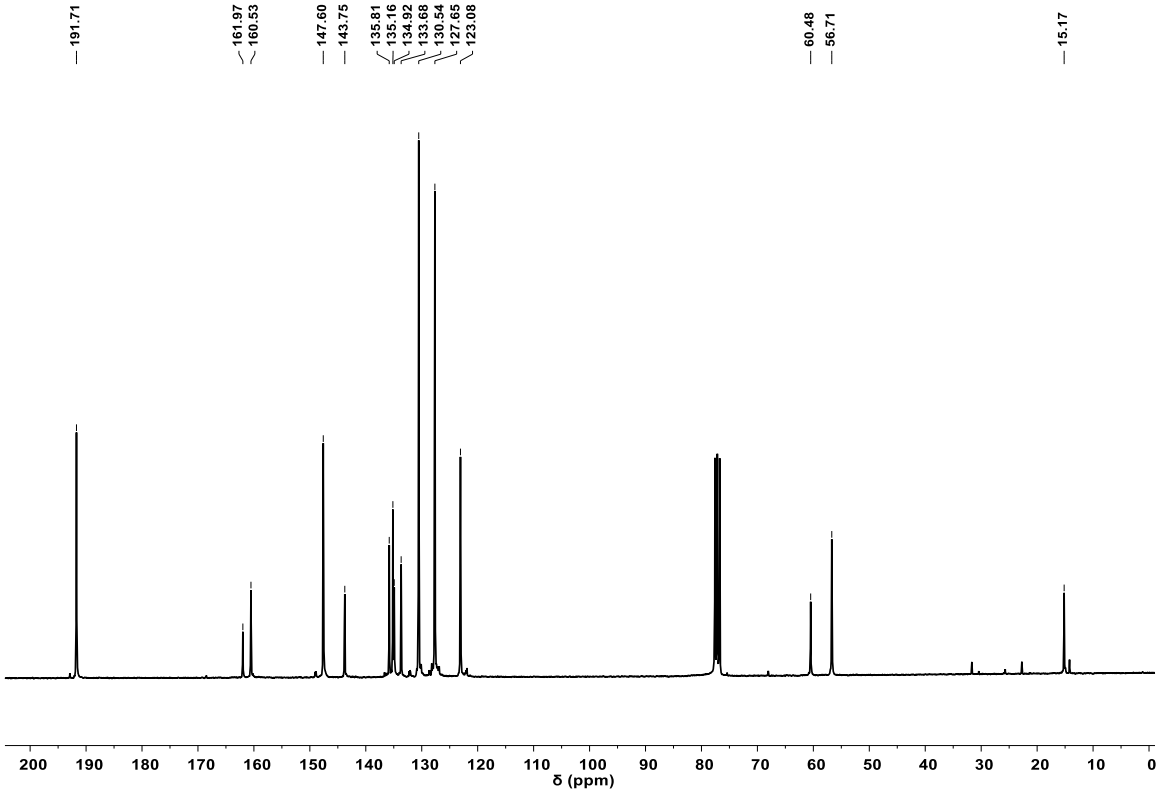

Figure A28. ^{13}C-NMR spectrum (75 MHz, 301 K, $CDCl_3$) of **(*R*)-9**.

A1.10.7. Complex (*R*)-1b

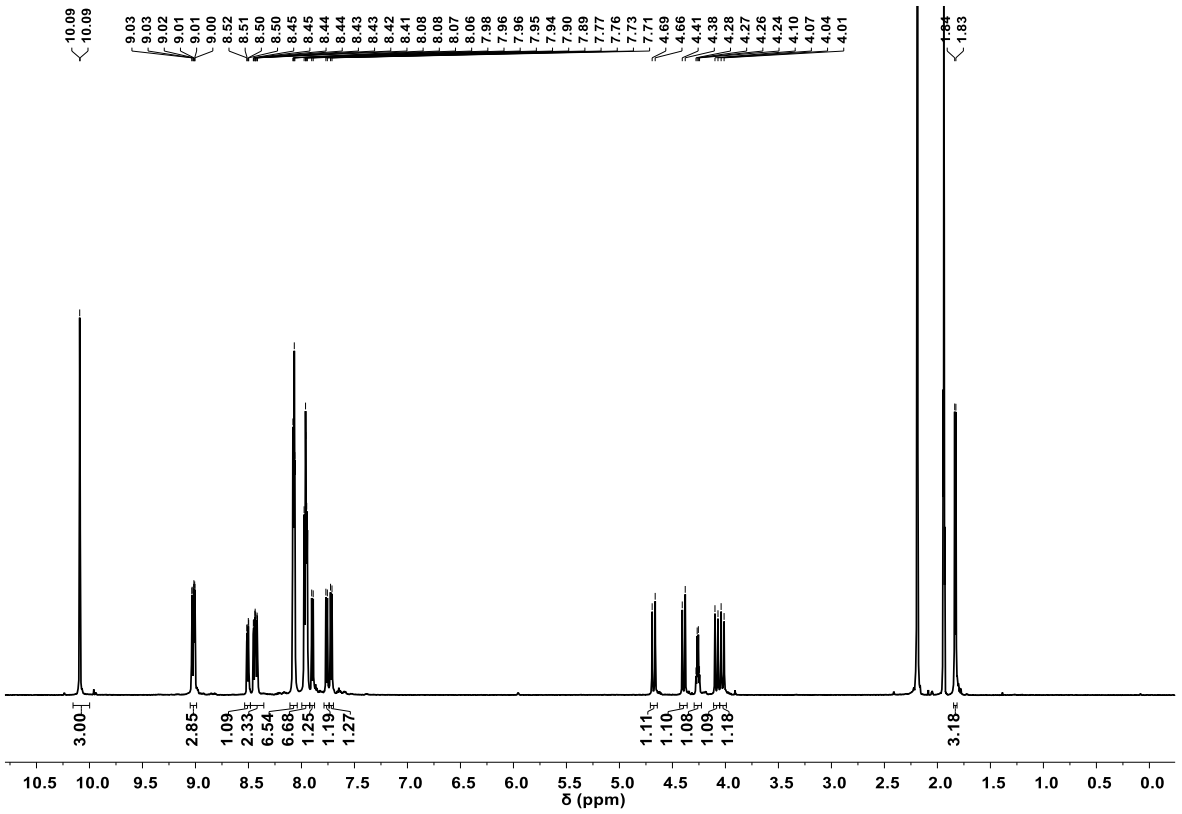

Figure A29. ^{1}H-NMR spectrum (600 MHz, 301 K, CD_3CN) of complex **(*R*)-1b**.

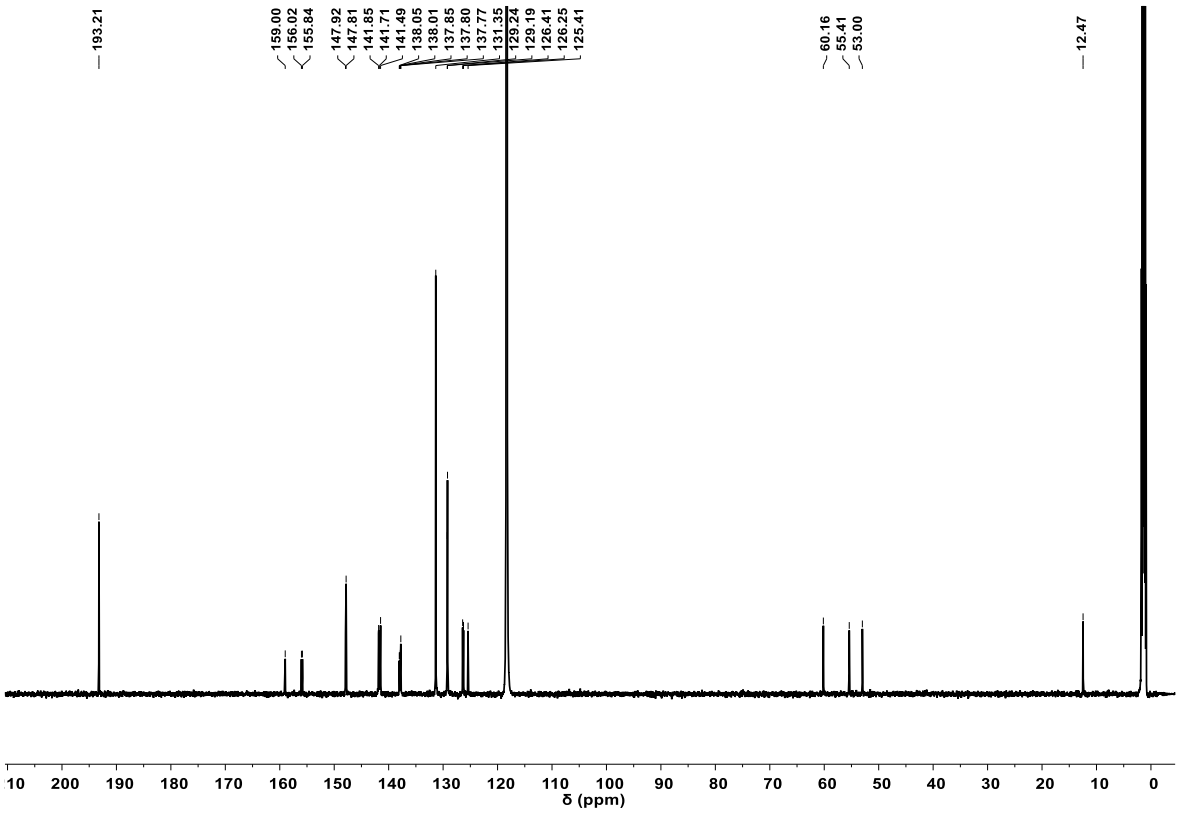

Figure A30. ^{13}C-NMR spectrum (151 MHz, 301 K, CD_3CN) of complex **(*R*)-1b**.

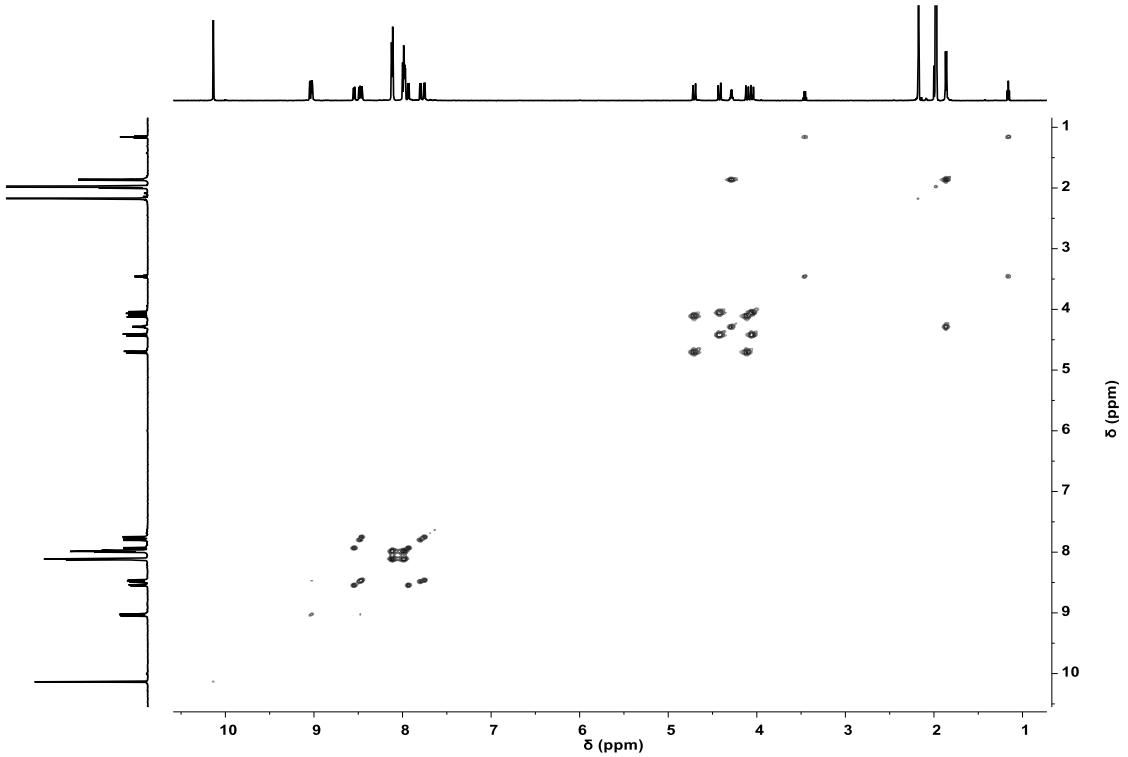

Figure A31. ^{1}H-^{1}H COSY spectrum (600 MHz, 301 K, CD_3CN)) of complex **(*R*)-1b**.

A1.10.8. L-Tar@2a

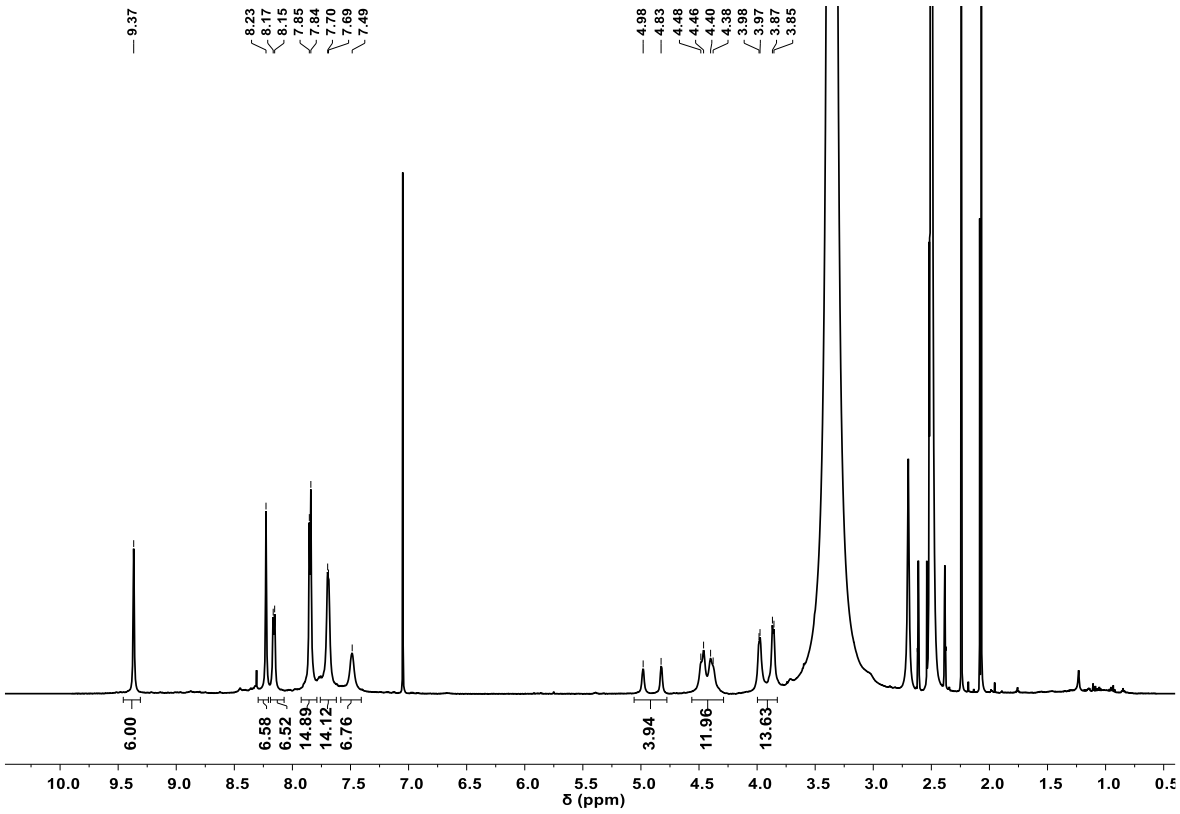

Figure A32. ^{1}H-NMR spectrum (600 MHz, 301 K, DMSO-d_6) of cage **L-Tar@2a**.

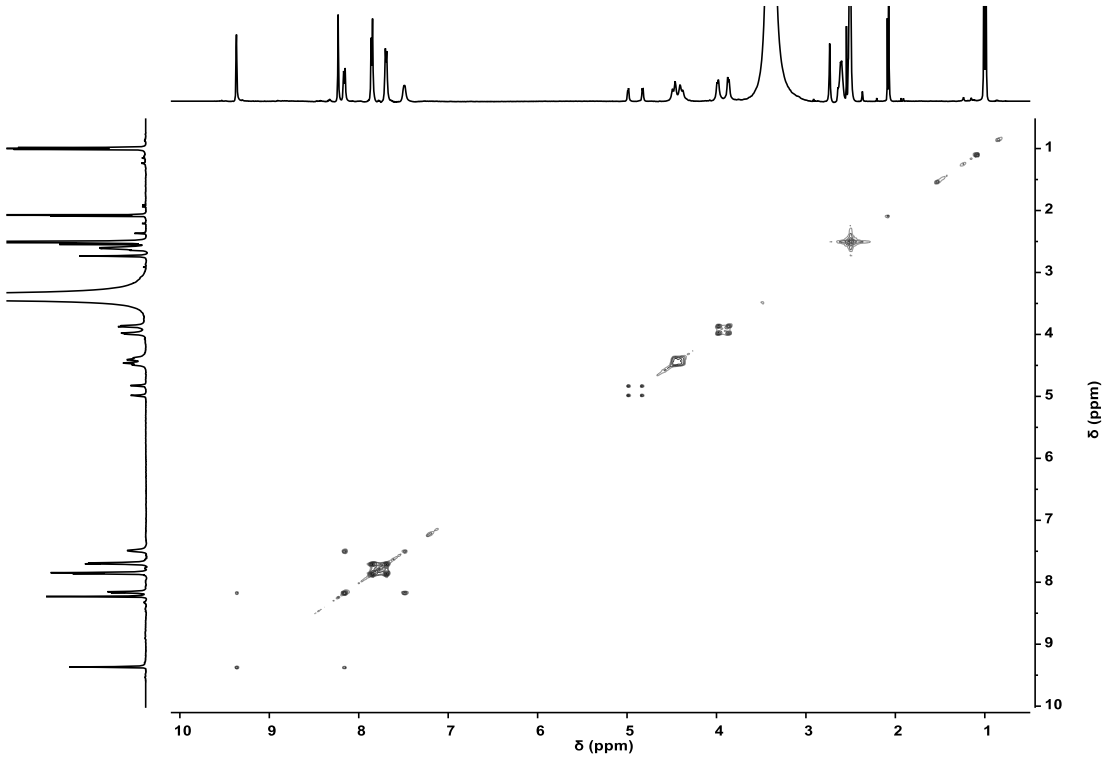

Figure A33. ^{1}H-^{1}H COSY spectrum (400 MHz, 301 K, DMSO-d_6) of cage **L-Tar@2a**.

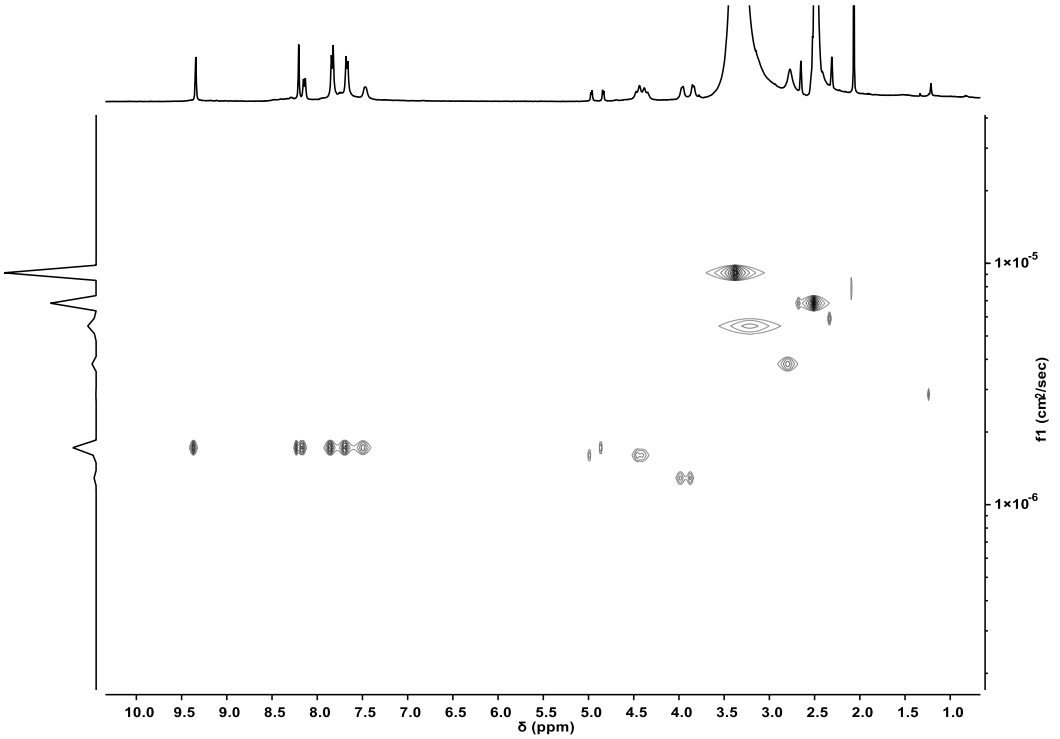

Figure A34. DOSY spectrum (400 MHz, 301 K, DMSO-d_6) of cage **L-Tar@2a**. The diffusion coefficient for the molecular cage **L-Tar@2a** was calculated to be 1.63 x 10^{-10} m^2 s^{-1}, corresponding to a hydrodynamic radius (r_H) of 6.8 Å. The hydrodynamic radius was calculated using Stokes-Einstein equation.[2,3]

A1.10.9. L-Mal@2a

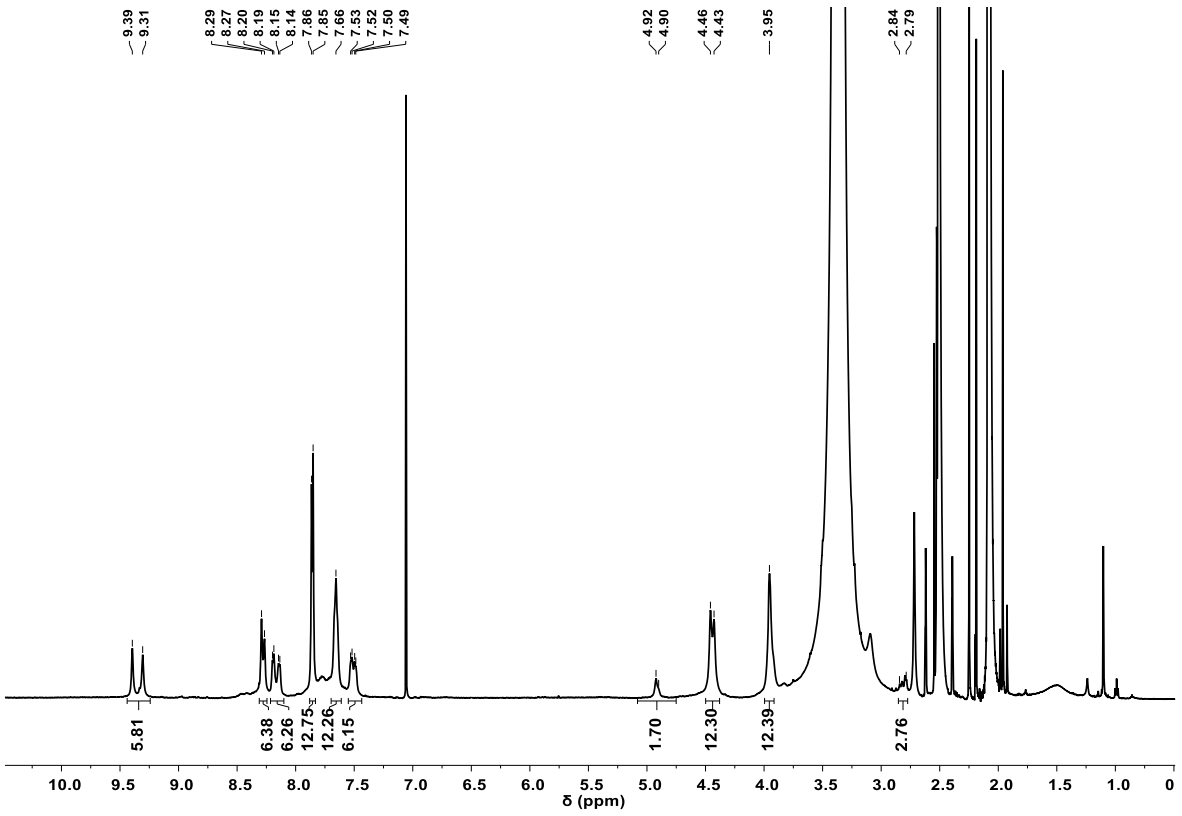

Figure A35. ^{1}H-NMR spectrum (600 MHz, 301 K, DMSO-d_6) of cage **L-Mal@2a**.

A1.10.10. Suc@2a

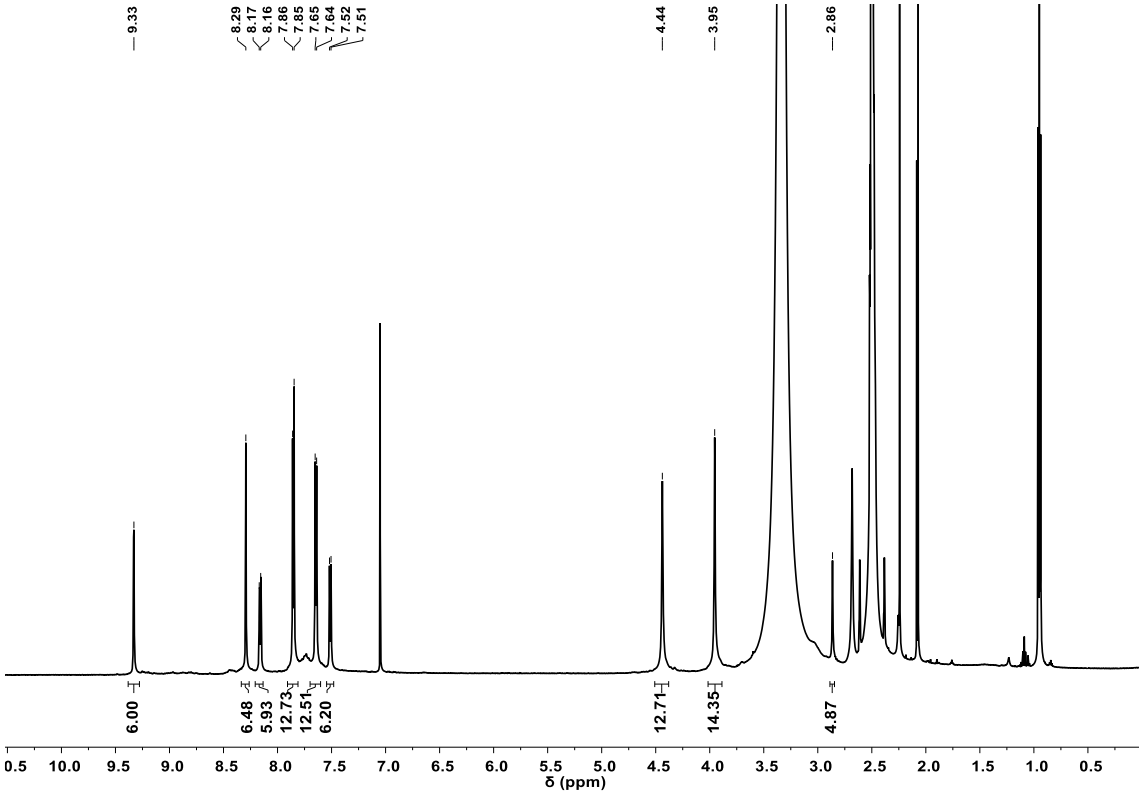

Figure A36. ^{1}H-NMR spectrum (600 MHz, 301 K, DMSO-d_6) of cage **Suc@2a**.

A1.10.11. Cit@2a

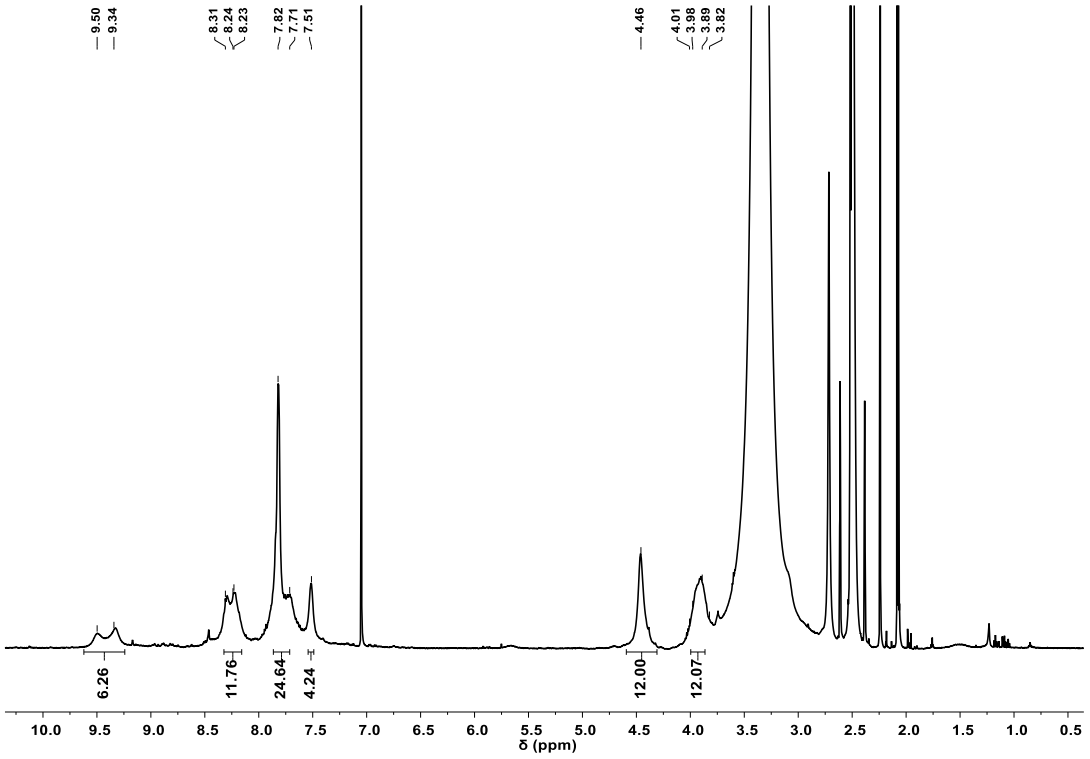

Figure A37. ^{1}H-NMR spectrum (600 MHz, 301 K, DMSO-d_6) of cage **Cit@2a**.

A1.10.12. L-Tar@(*R*,*R*)-2b

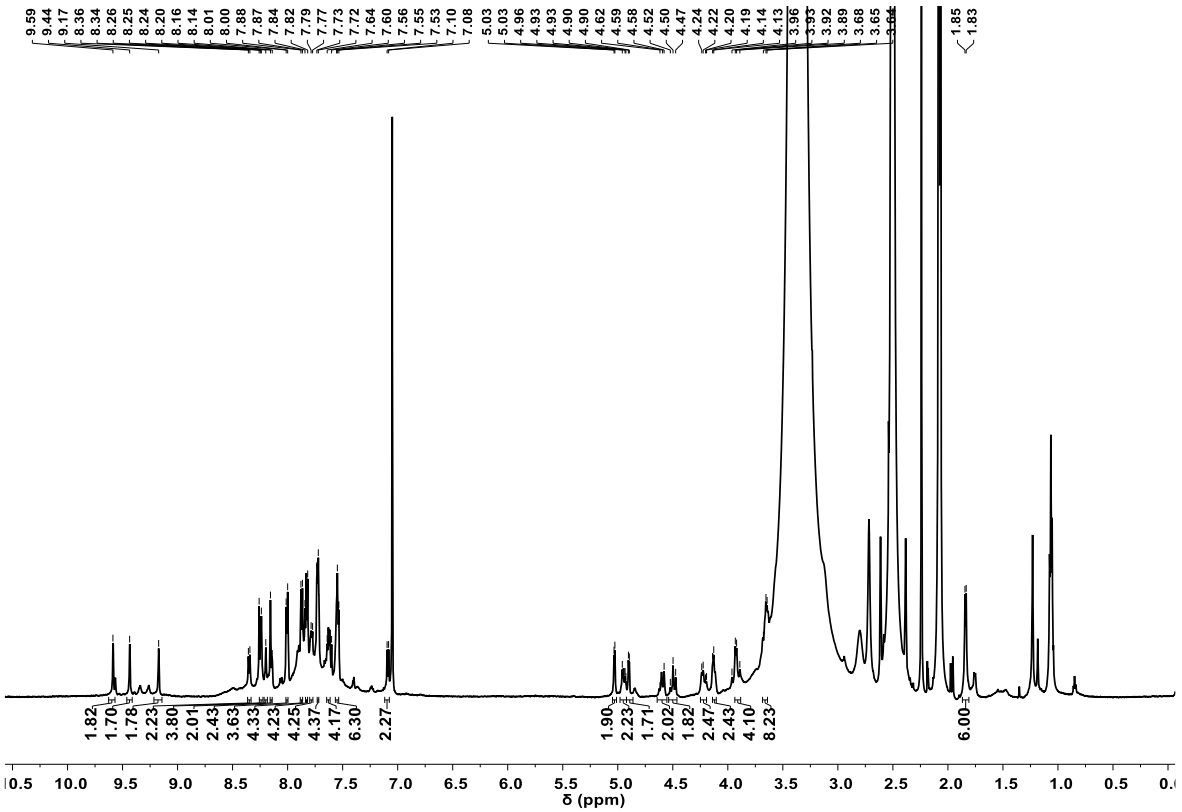

Figure A38. ^{1}H-NMR spectrum (600 MHz, 301 K, DMSO-d_6) of cage **L-Tar@(*R*,*R*)-2b**.

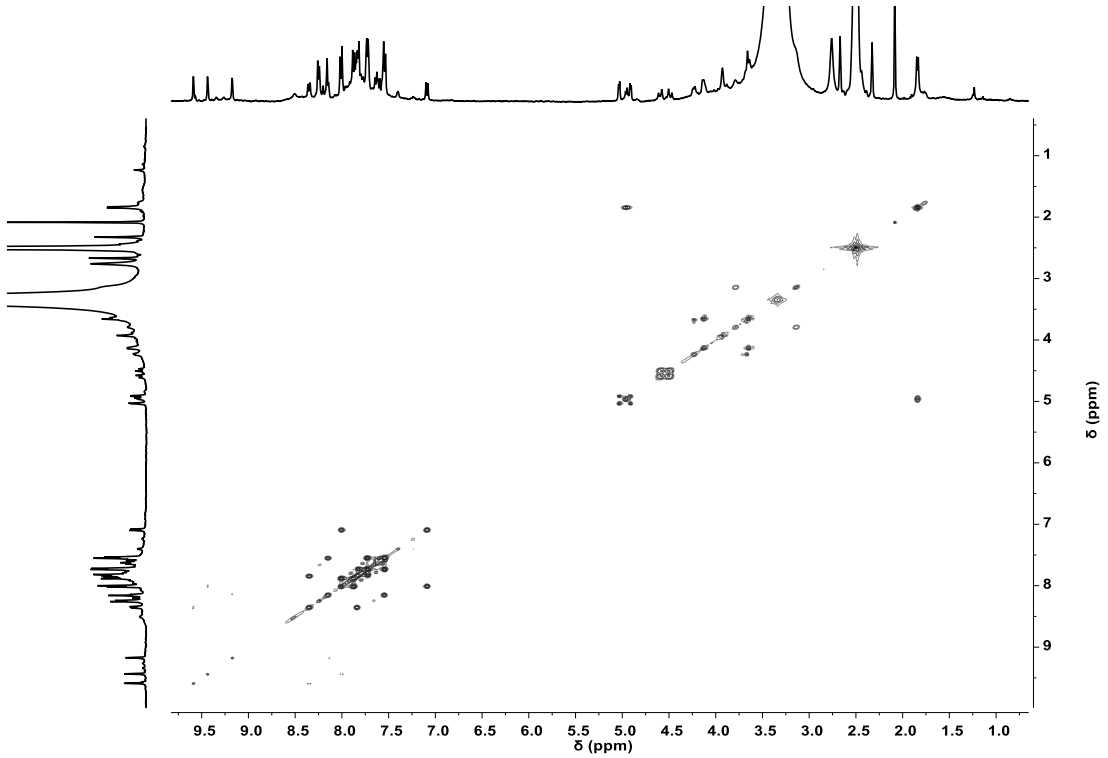

Figure A39. ^{1}H-^{1}H COSY spectrum (400 MHz, 301 K, DMSO-d_6) of cage **L-Tar@(*R*,*R*)-2b**.

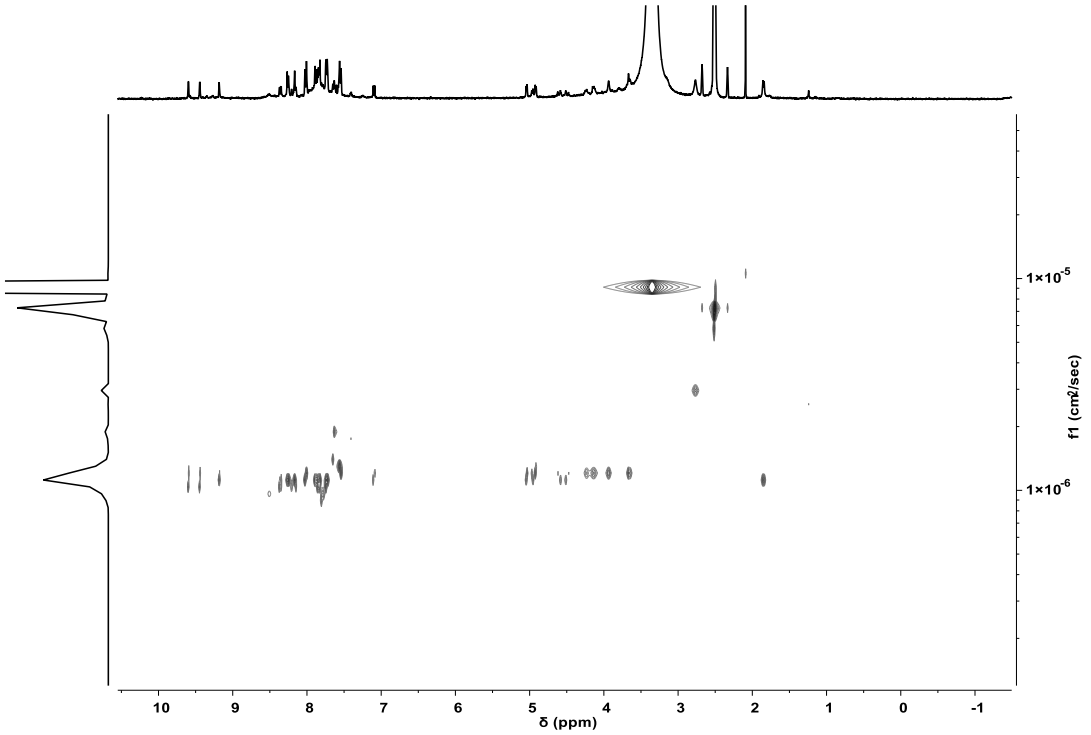

Figure A40. DOSY spectrum (400 MHz, 301 K, DMSO-d_6) of cage **L-Tar@(*R*,*R*)-2b**. The diffusion coefficient for the molecular cage **L-Tar@(*R*,*R*)-2b** was calculated to be 1.22 x 10^{-10} m^2 s^{-1}, corresponding to a hydrodynamic radius (r_H) of 9.08 Å. The hydrodynamic radius was calculated using Stokes-Einstein equation.[2,3]

A1.10.13. D-Tar@(*R*,*R*)-2b

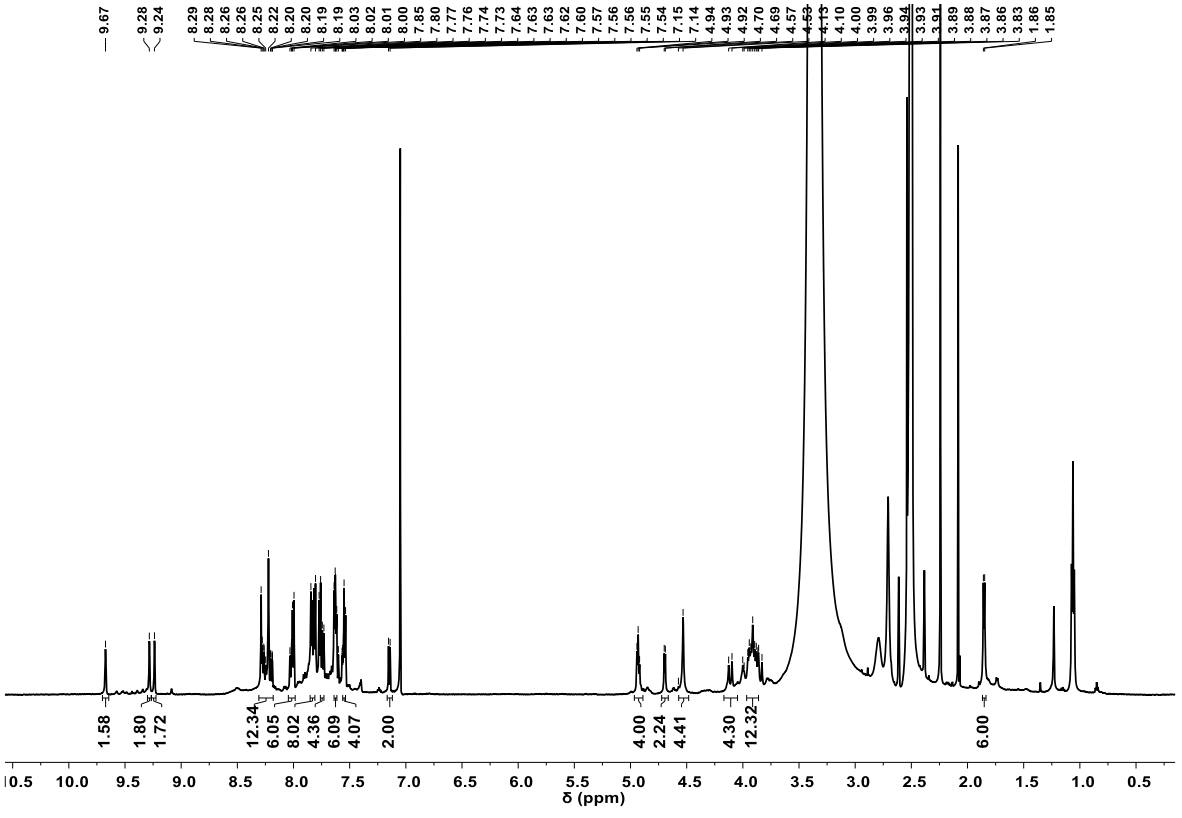

Figure A41. ^{1}H-NMR spectrum (600 MHz, 301 K, DMSO-d_6) of cage **D-Tar@(*R*,*R*)-2b**.

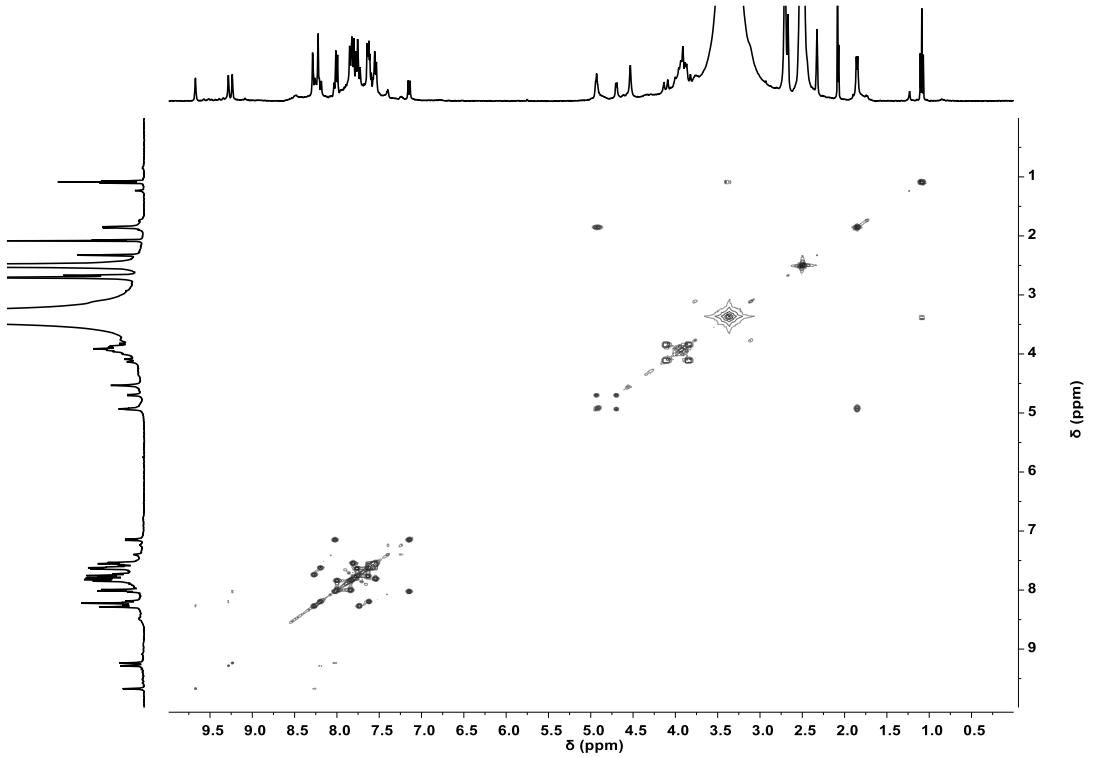

Figure A42. ^{1}H-^{1}H COSY spectrum (400 MHz, 301 K, DMSO-d_6) of cage **D-Tar@(*R*,*R*)-2b**.

A1.10.14. L-Mal@(*R*,*R*)-2b

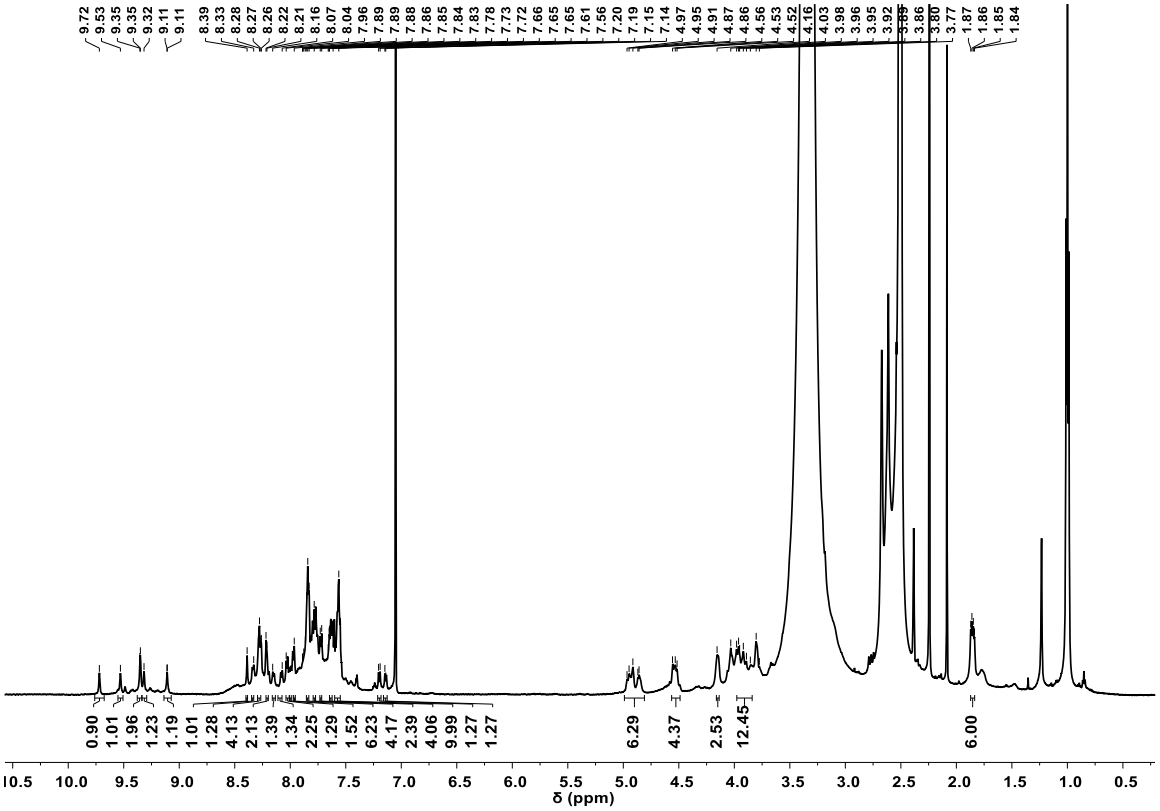

Figure A43. ^{1}H-NMR spectrum (600 MHz, 301 K, DMSO-d_6) of cage **L-Mal@(*R*,*R*)-2b**.

A1.10.15. D-Mal@(*R*,*R*)-2b

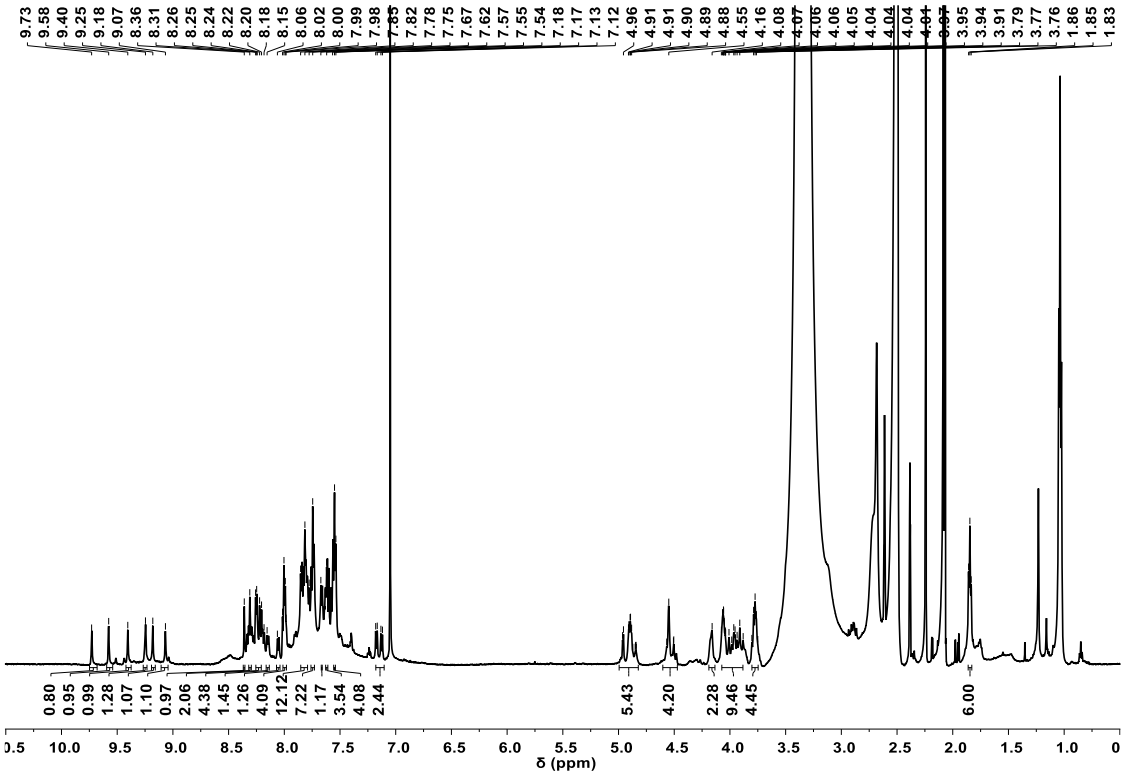

Figure A44. ^{1}H-NMR spectrum (600 MHz, 301 K, DMSO-d_6) of cage **D-Mal@(*R*,*R*)-2b**.

A1.10.16. Suc@(*R*,*R*)-2b

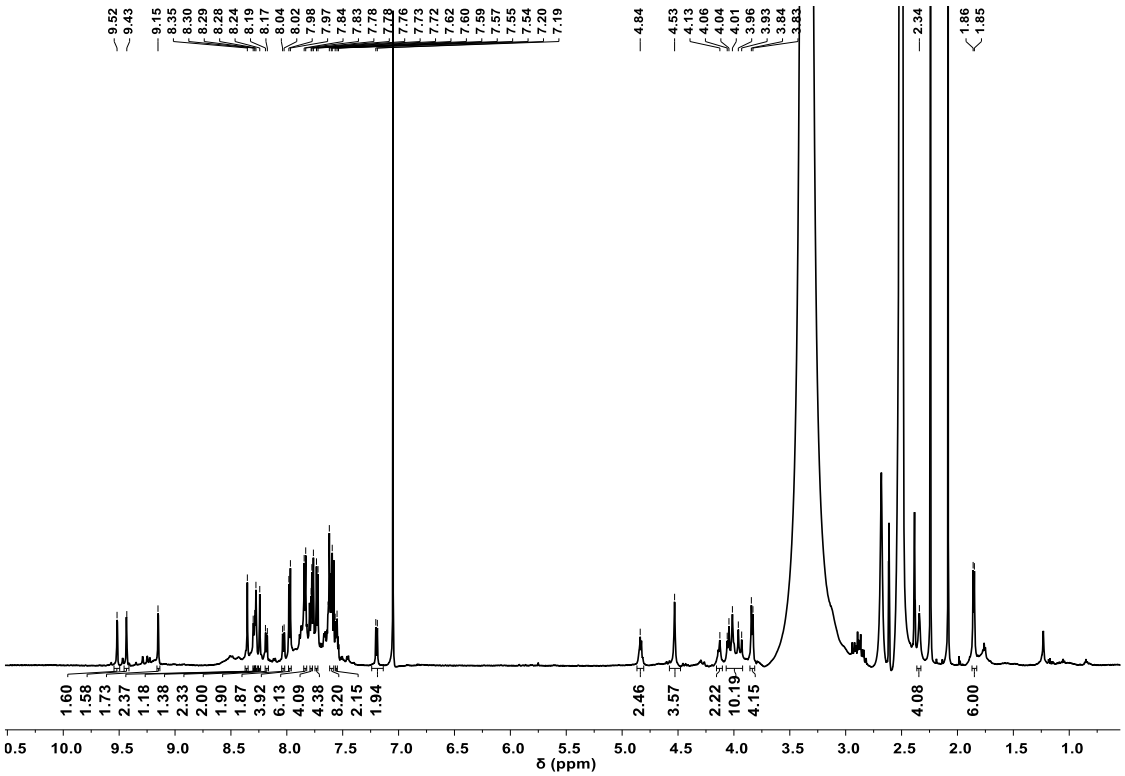

Figure A45. ^{1}H-NMR spectrum (600 MHz, 301 K, DMSO-d_6) of cage **Suc@(*R*,*R*)-2b**.

A1.10.17. Prosecco@2a

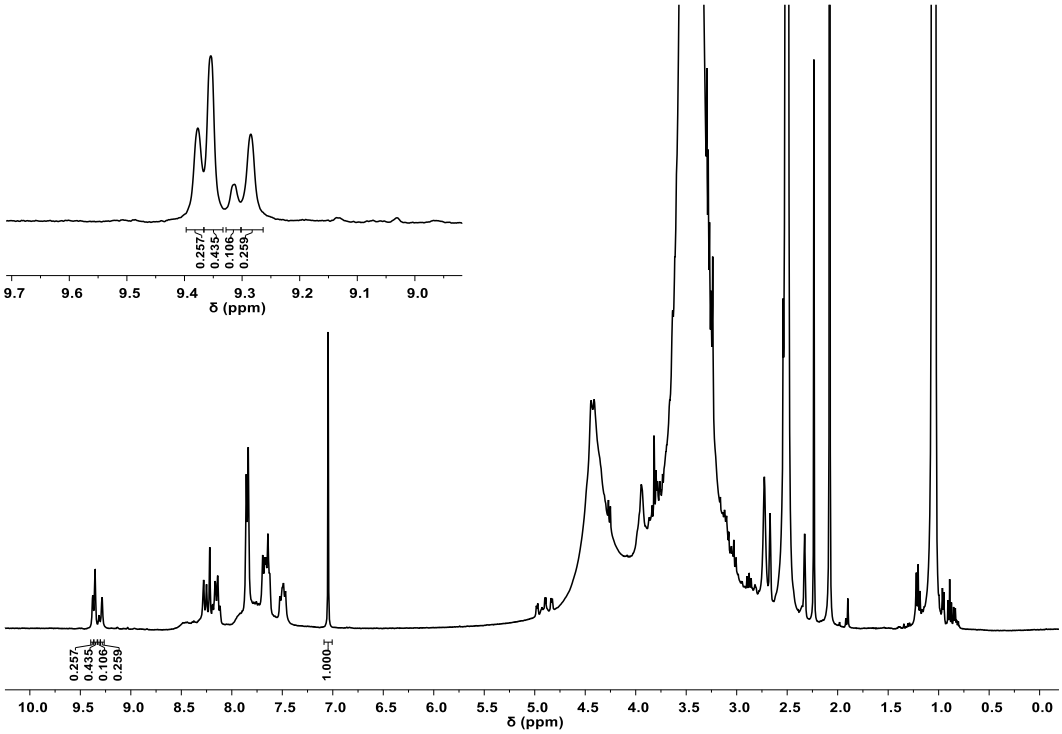

Figure A46. ^{1}H-NMR spectrum (400 MHz, 301 K, DMSO-d_6) of the system formed adding Prosecco wine without pre-treatment to the DMSO-d_6 solution containing complex **1a** and ethylenediamine.

A1.10.18. Chianti@2a

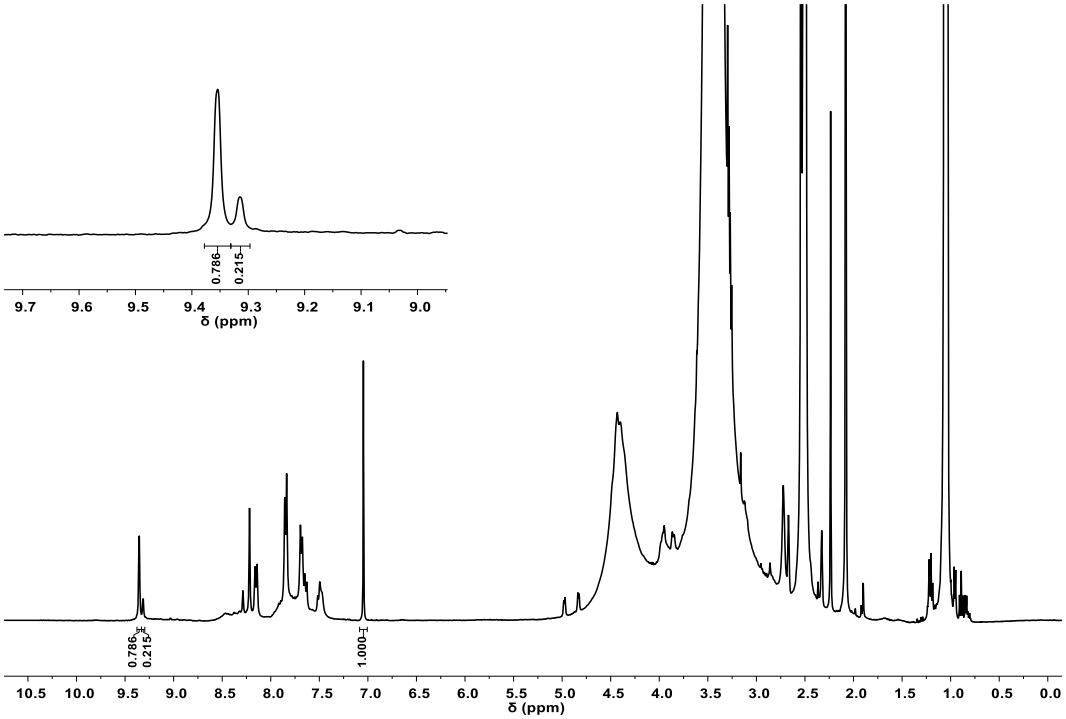

Figure A47. ^{1}H-NMR spectrum (400 MHz, 301 K, DMSO-d_6) of the system formed adding Chianti wine without pre-treatment to the DMSO-d_6 solution containing complex **1a** and ethylenediamine.

A1.10.19. Chardonnay@2a

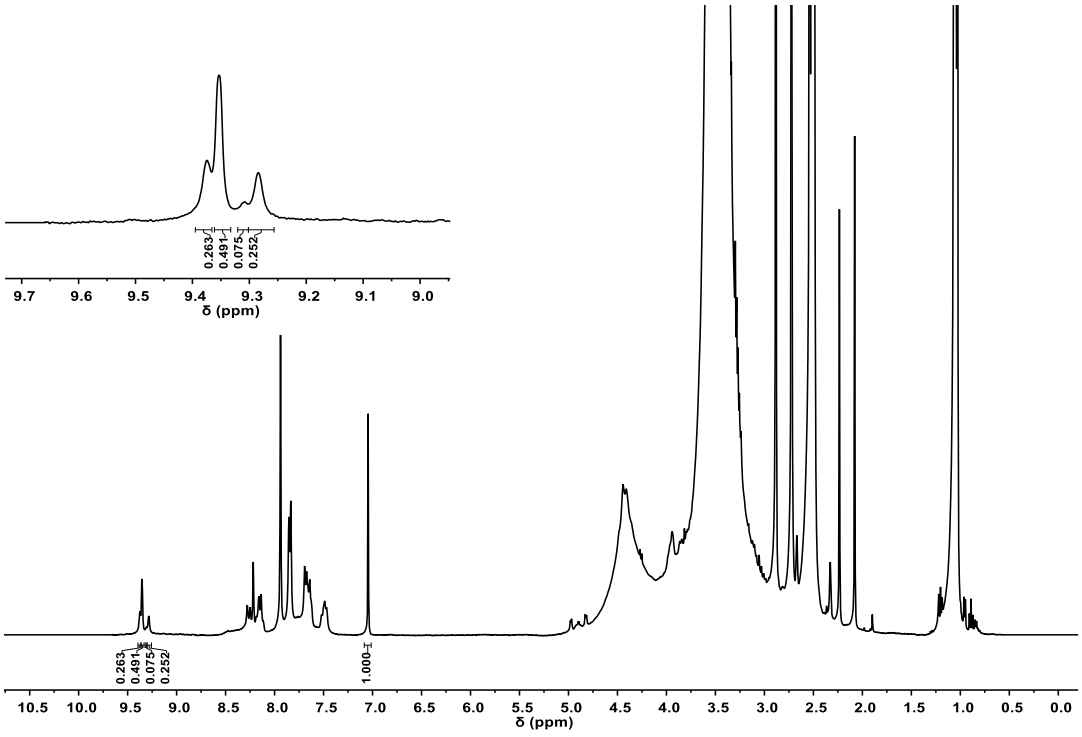

Figure A48. ^{1}H-NMR spectrum (400 MHz, 301 K, DMSO-d_6) of the system formed adding Chardonnay wine without pre-treatment to the DMSO-d_6 solution containing complex **1a** and ethylenediamine.

A1.10.20. Valpolicella@2a

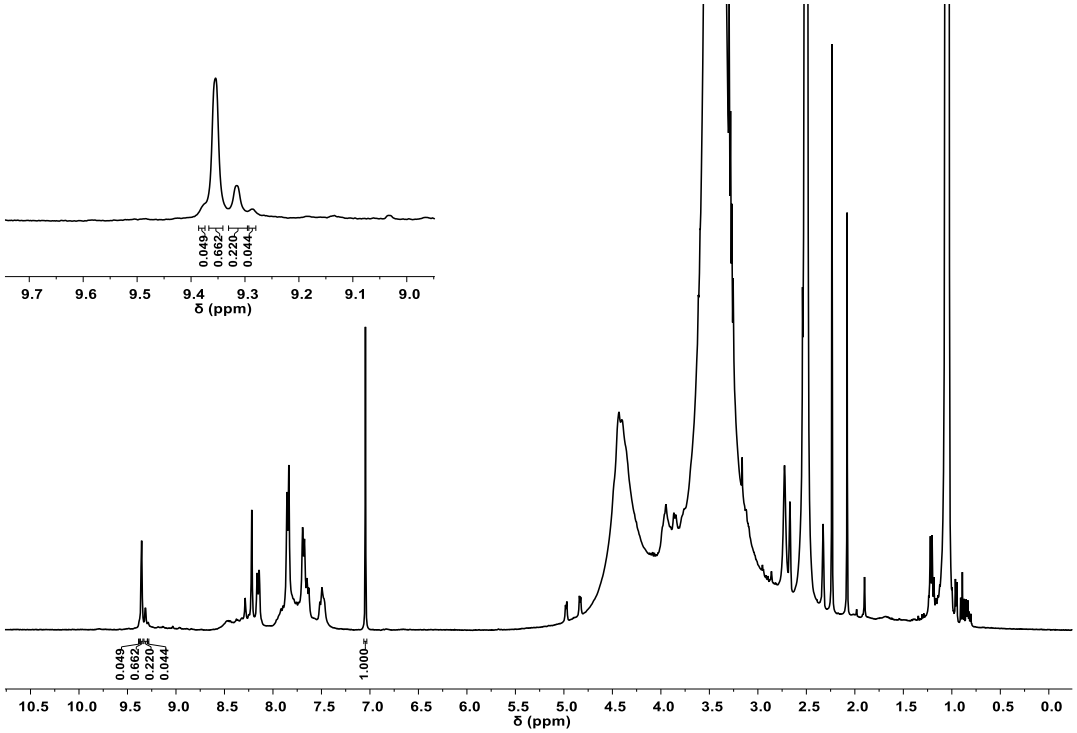

Figure A49. ^{1}H-NMR spectrum (400 MHz, 301 K, DMSO-d_6) of the system formed adding Valpolicella wine without pre-treatment to the DMSO-d_6 solution containing complex **1a** and ethylenediamine.

A1.10.21. Müller-Thurgau@2a

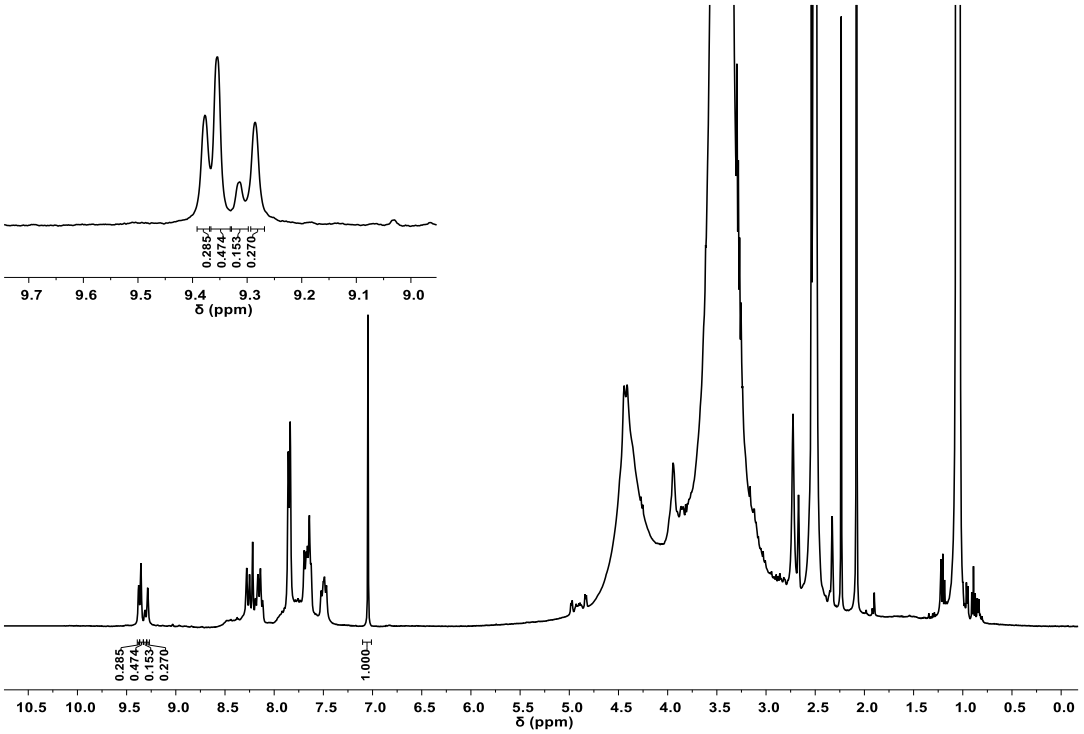

Figure A50. [1]H-NMR spectrum (400 MHz, 301 K, DMSO-d_6) of the system formed adding Müller-Thurgau wine without pre-treatment to the DMSO-d_6 solution containing complex **1a** and ethylenediamine.

A1.10.22. Barbera@2a

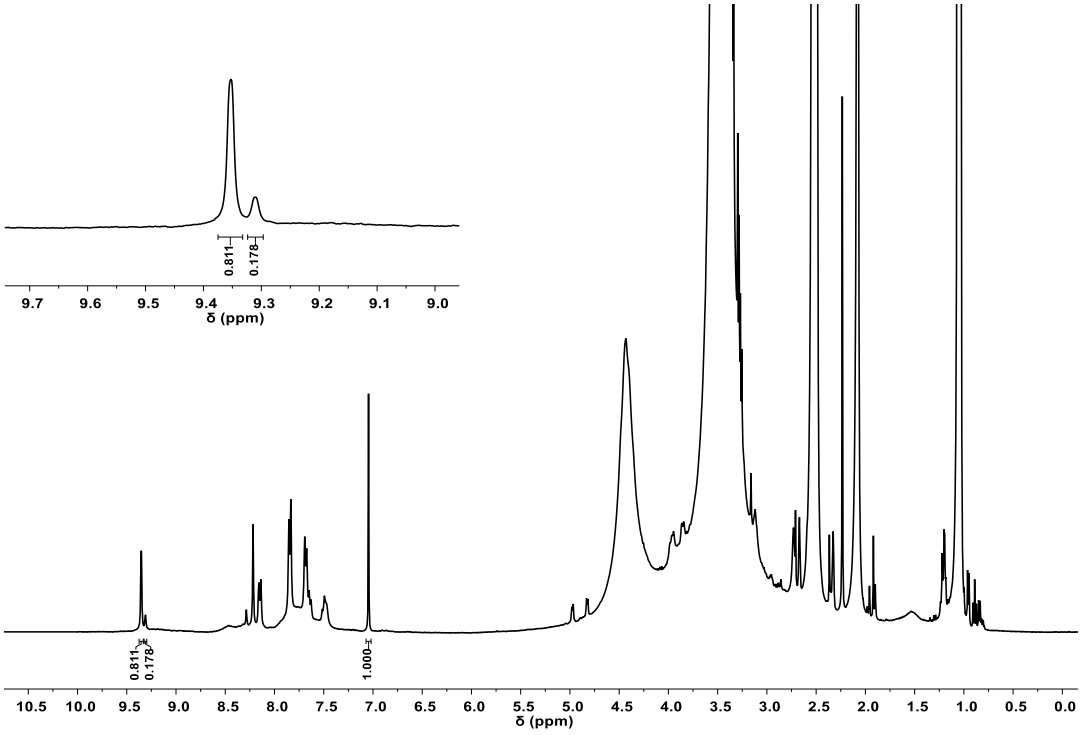

Figure A51. [1]H-NMR spectrum (400 MHz, 301 K, DMSO-d_6) of the system formed adding Barbera wine without pre-treatment to the DMSO-d_6 solution containing complex **1a** and ethylenediamine.

A1.10.23. Grapes Juice Squeezed@2a

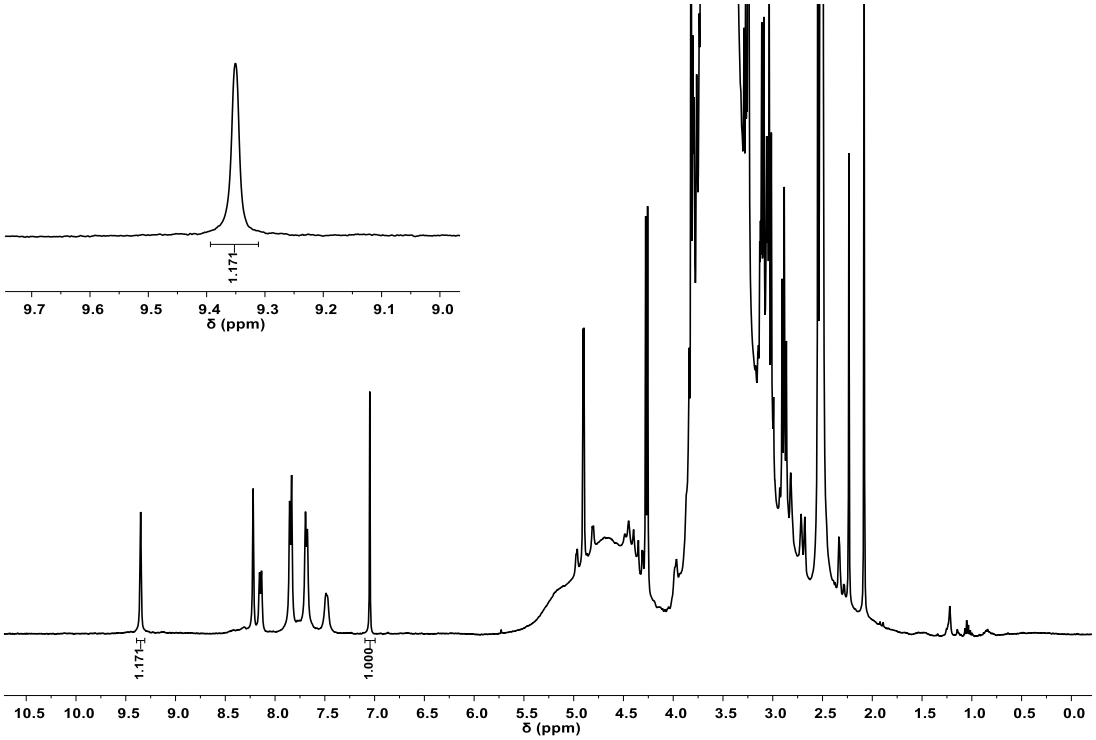

Figure A52. ^{1}H-NMR spectrum (400 MHz, 301 K, DMSO-d_6) of the system formed adding freshly squeezed grapes juice without pre-treatment to the DMSO-d_6 solution containing complex **1a** and ethylenediamine.

A1.10.24. Blueberry Alcenera@2a

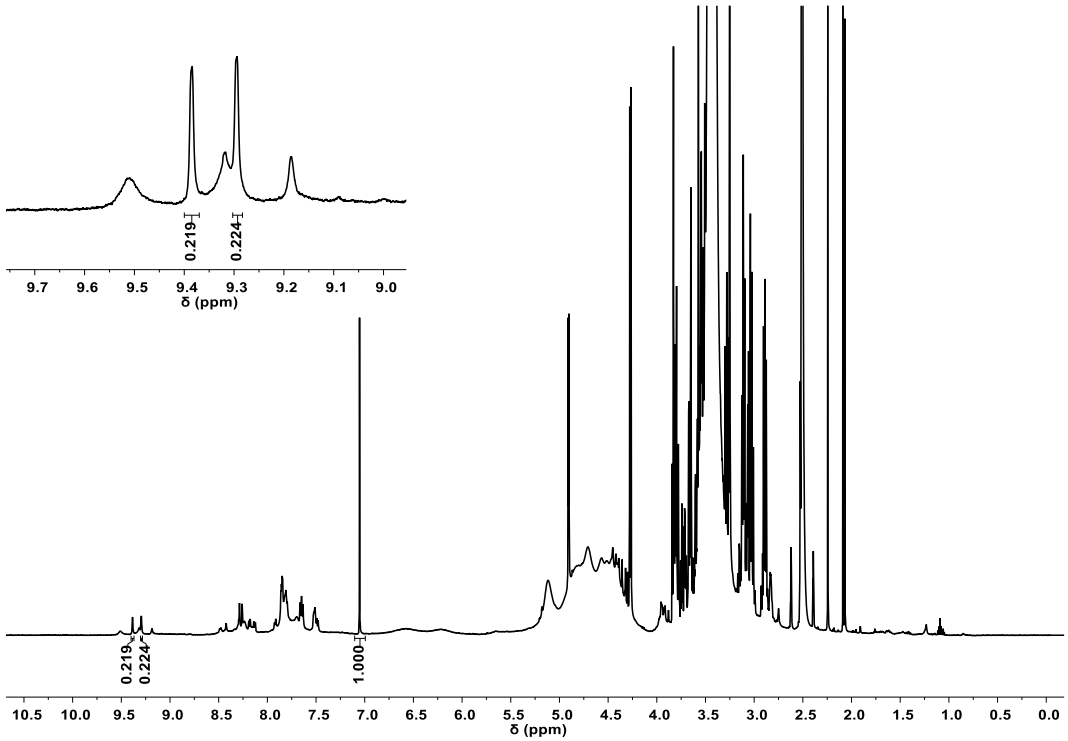

Figure A53. ^{1}H-NMR spectrum (600 MHz, 301 K, DMSO-d_6) of the system formed adding Blueberry juice without pre-treatment to the DMSO-d_6 solution containing complex **1a** and ethylenediamine.

A1.10.25. Blueberry Zuegg@2a

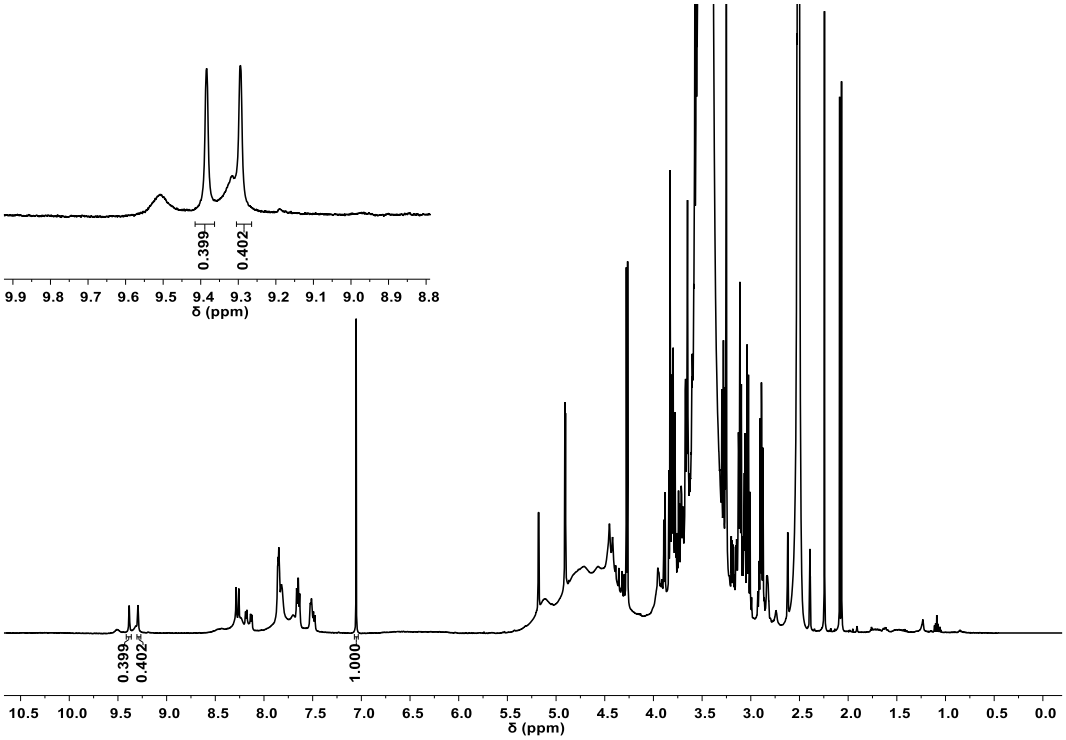

Figure A54. ^{1}H-NMR spectrum (400 MHz, 301 K, DMSO-d_6) of the system formed adding Blueberry juice without pre-treatment to the DMSO-d_6 solution containing complex **1a** and ethylenediamine.

A1.10.26. Blueberry Juice Squeezed@2a

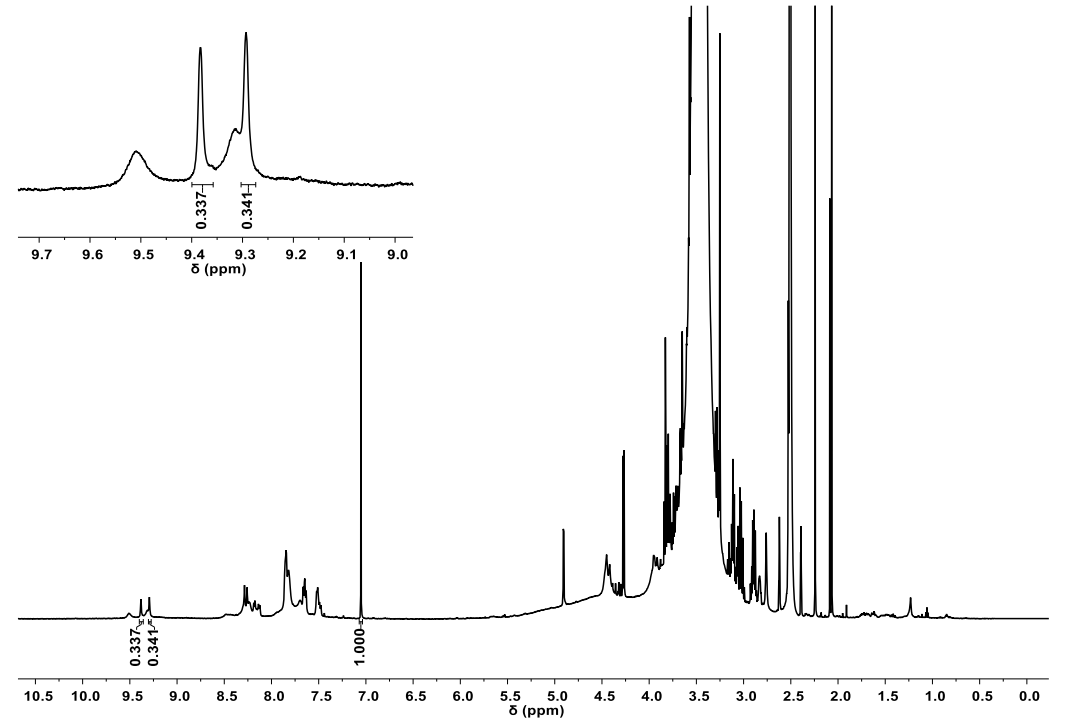

Figure A55. ^{1}H-NMR spectrum (600 MHz, 301 K, DMSO-d_6) of the system formed adding freshly squeezed Blueberry juice without pre-treatment to the DMSO-d_6 solution containing complex **1a** and ethylenediamine.

A1.10.27. Apple Juice@2a

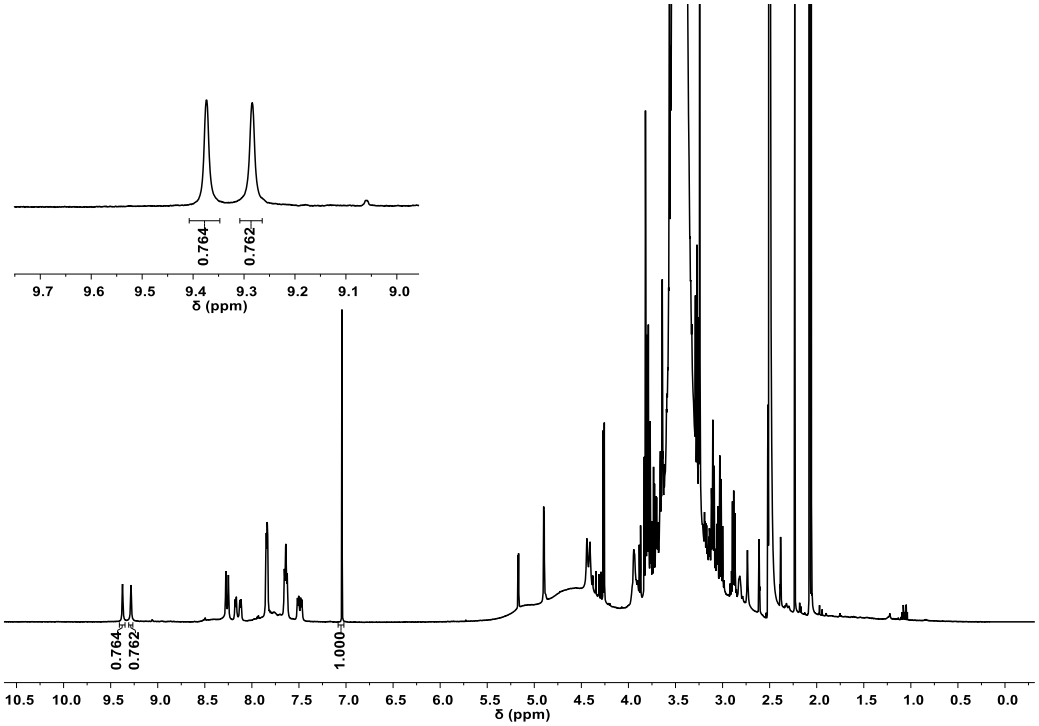

Figure A56. ^{1}H-NMR spectrum (400 MHz, 301 K, DMSO-d_6) of the system formed adding Apple juice without pre-treatment to the DMSO-d_6 solution containing complex **1a** and ethylenediamine.

A1.10.28. Apple Juice Squeezed@2a

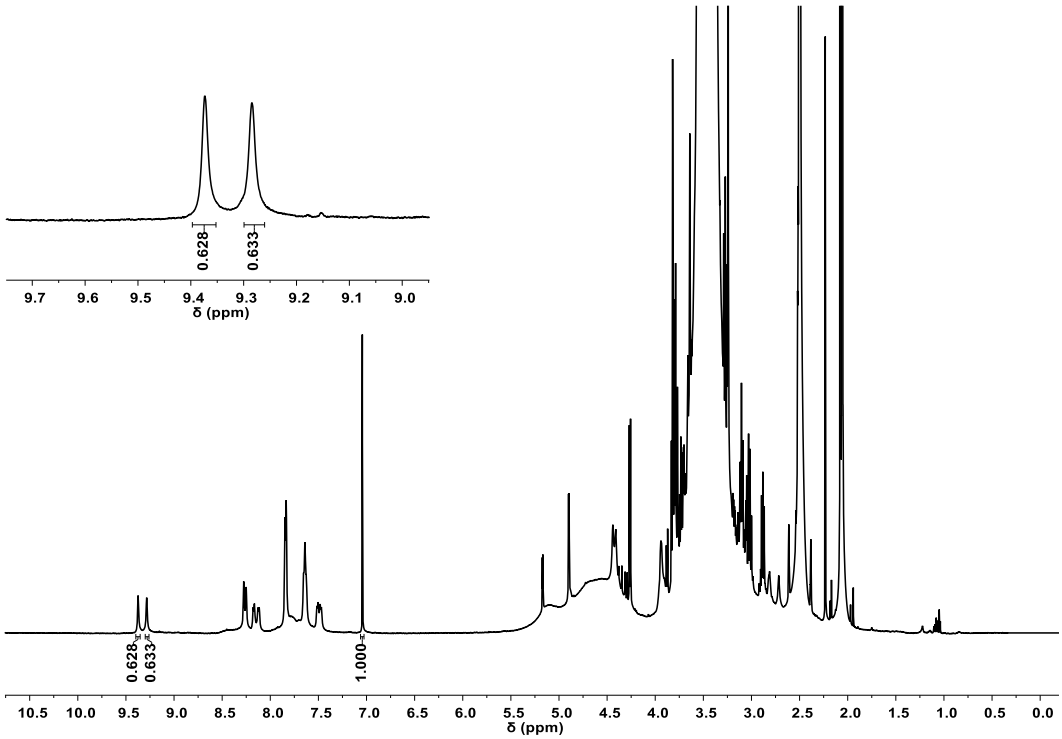

Figure A57. ^{1}H-NMR spectrum (600 MHz, 301 K, DMSO-d_6) of the system formed adding freshly squeezed Apple juice without pre-treatment to the DMSO-d_6 solution containing complex **1a** and ethylenediamine.

A1.10.29. Pear Juice@2a

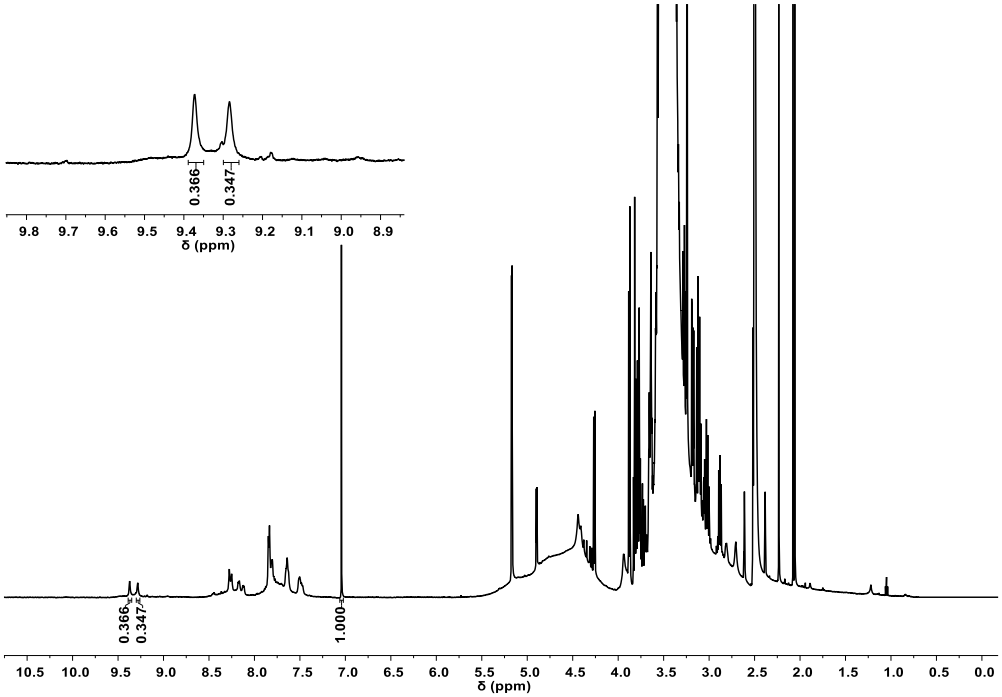

Figure A58. ^{1}H-NMR spectrum (400 MHz, 301 K, DMSO-d_6) of the system formed adding Pear juice without pre-treatment to the DMSO-d_6 solution containing complex **1a** and ethylenediamine.

A1.10.30. Blueberry-Grape Juice@2a

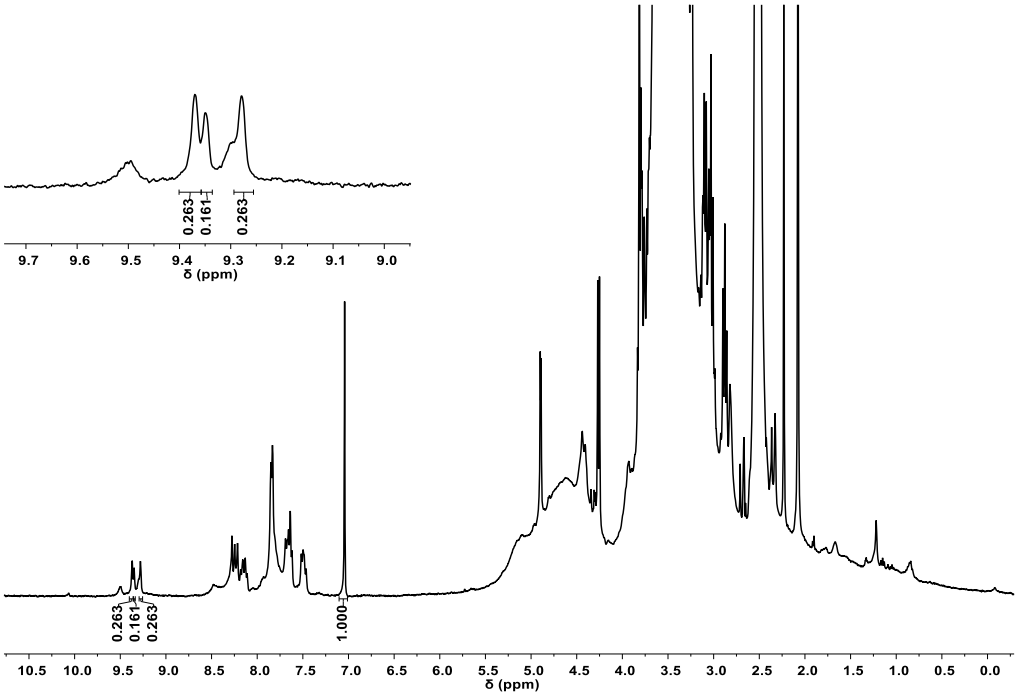

Figure A59. ^{1}H-NMR spectrum (400 MHz, 301 K, DMSO-d_6) of the system formed adding Blueberry-Grape juice without pre-treatment to the DMSO-d_6 solution containing complex **1a** and ethylenediamine.

A1.10.31. Peach Juice@2a

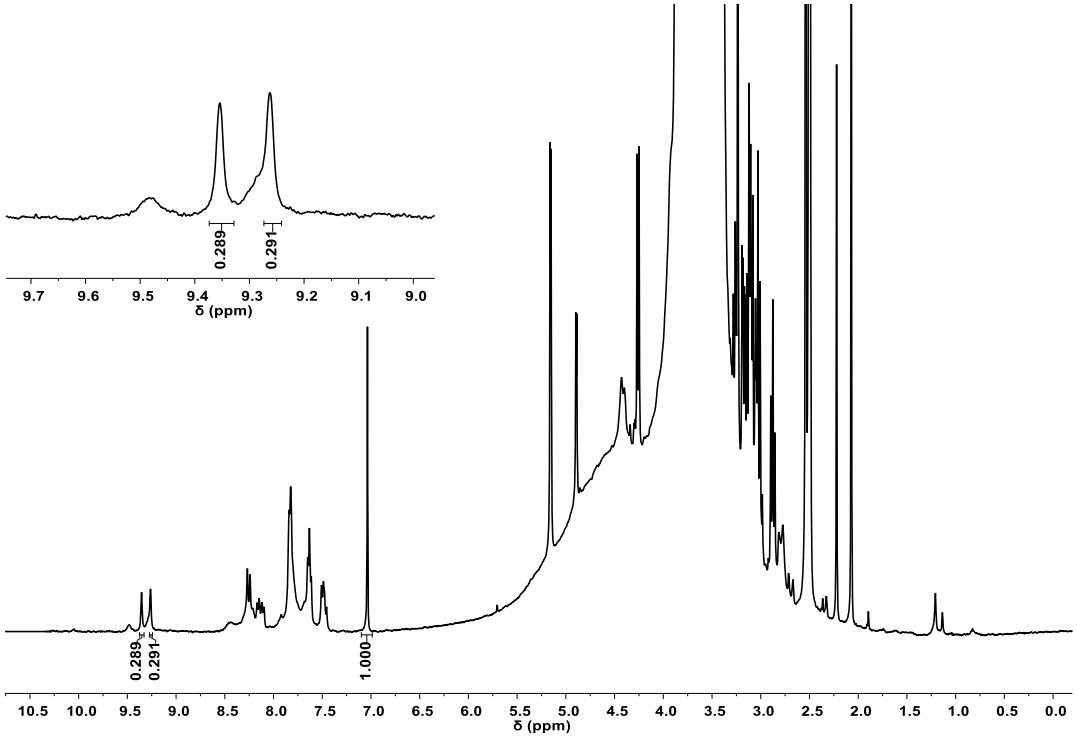

Figure A60. ^{1}H-NMR spectrum (400 MHz, 301 K, DMSO-d_6) of the system formed adding Peach juice without pre-treatment to the DMSO-d_6 solution containing complex **1a** and ethylenediamine.

A1.10.32. Prosecco@(*R*,*R*)-2b

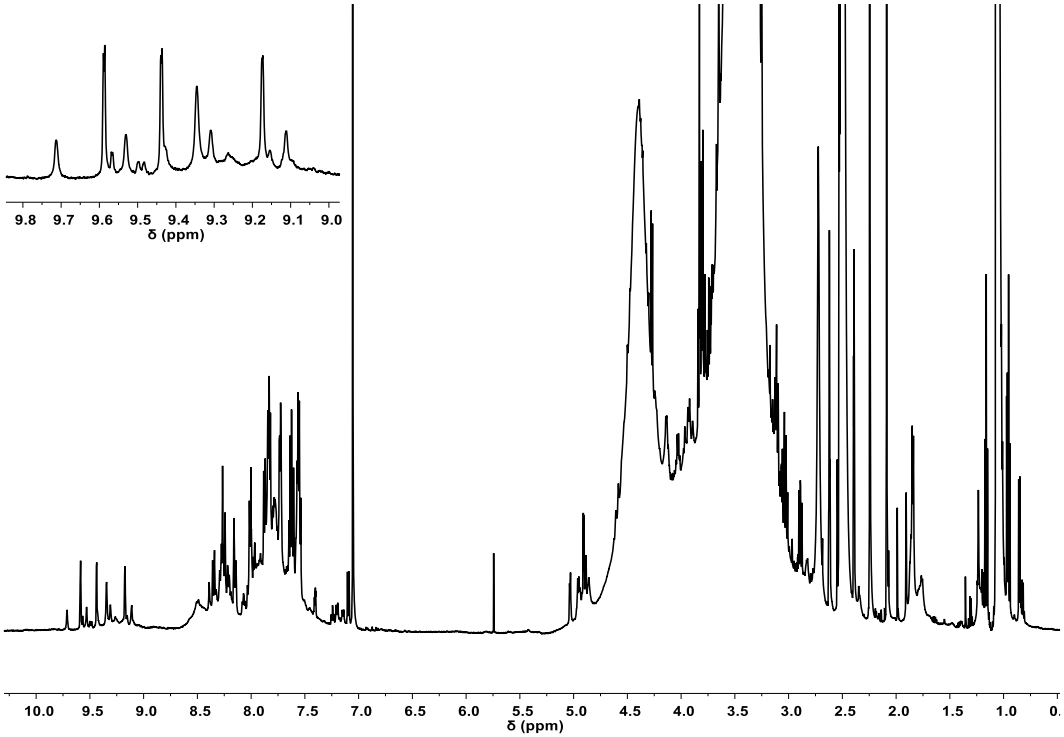

Figure A61. ^{1}H-NMR spectrum (600 MHz, 301 K, DMSO-d_6) of the system formed adding Prosecco Wine without pre-treatment to the DMSO-d_6 solution containing complex **(*R*)-1b** and ethylenediamine.

A1.10.33. Chianti@(*R*,*R*)-2b

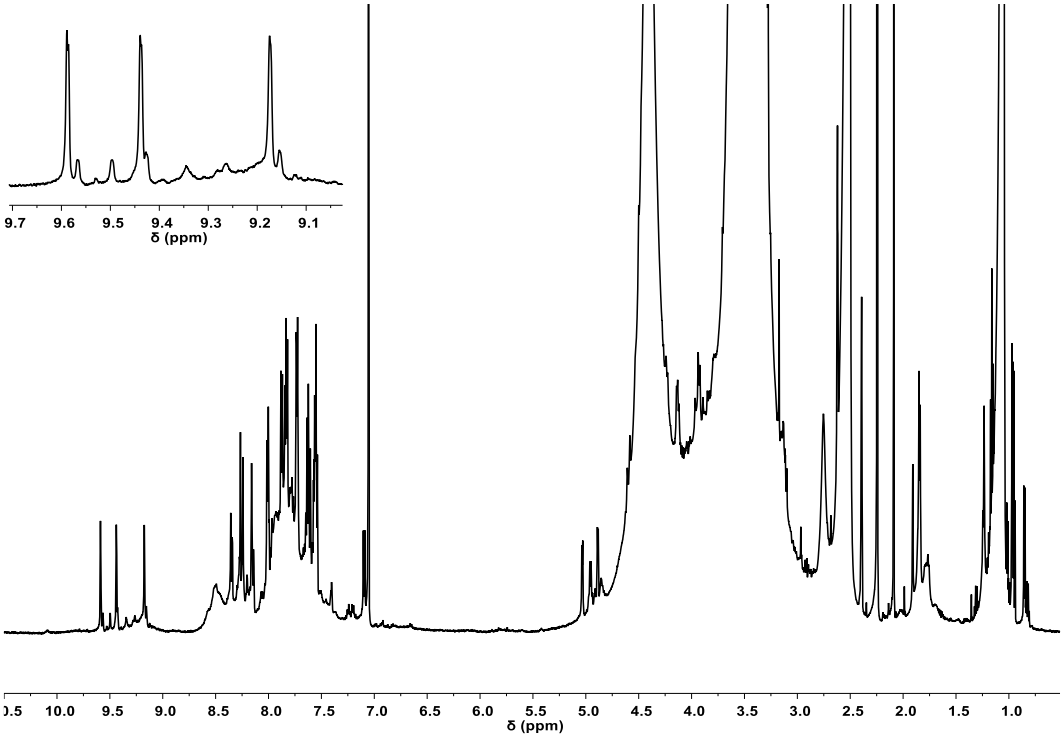

Figure A62. ^{1}H-NMR spectrum (600 MHz, 301 K, DMSO-d_6) of the system formed adding Chianti Wine without pre-treatment to the DMSO-d_6 solution containing complex **(*R*)-1b** and ethylenediamine.

A1.10.34. Chardonnay@(*R*,*R*)-2b

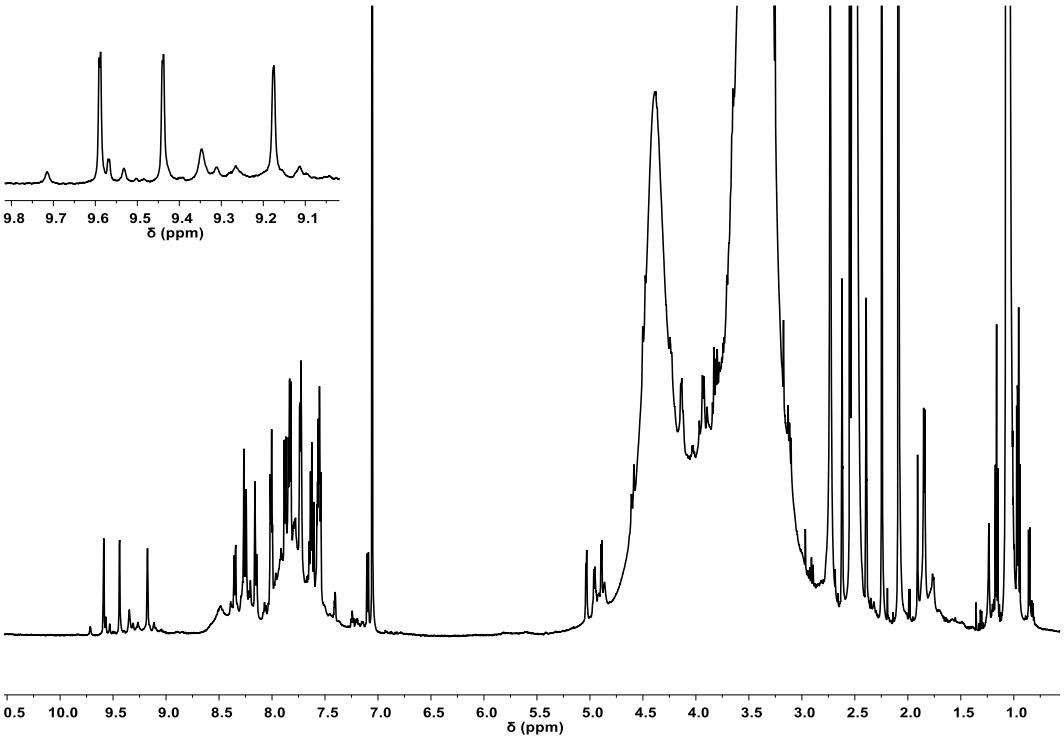

Figure A63. ^{1}H-NMR spectrum (600 MHz, 301 K, DMSO-d_6) of the system formed adding Chardonnay Wine without pre-treatment to the DMSO-d_6 solution containing complex **(*R*)-1b** and ethylenediamine.

A1.10.35. Valpolicella@(*R*,*R*)-2b

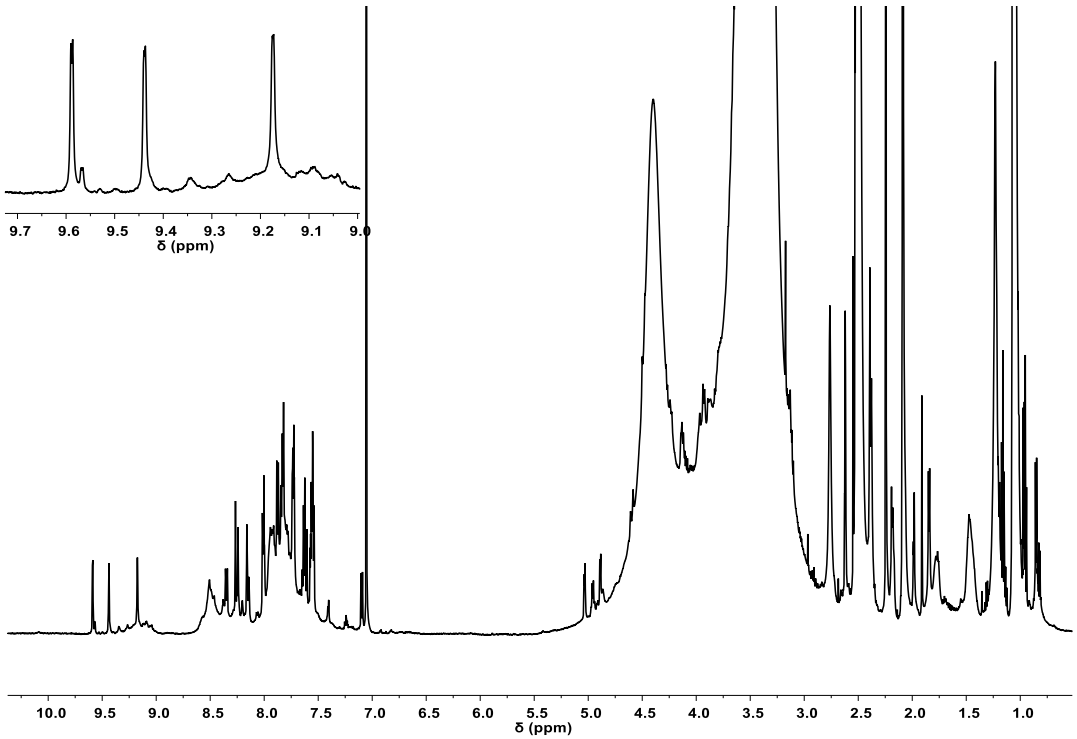

Figure A64. ^{1}H-NMR spectrum (600 MHz, 301 K, DMSO-d_6) of the system formed adding Valpolicella Wine without pre-treatment to the DMSO-d_6 solution containing complex **(*R*)-1b** and ethylenediamine.

A1.10.36. Müller-Thurgau@(*R*,*R*)-2b

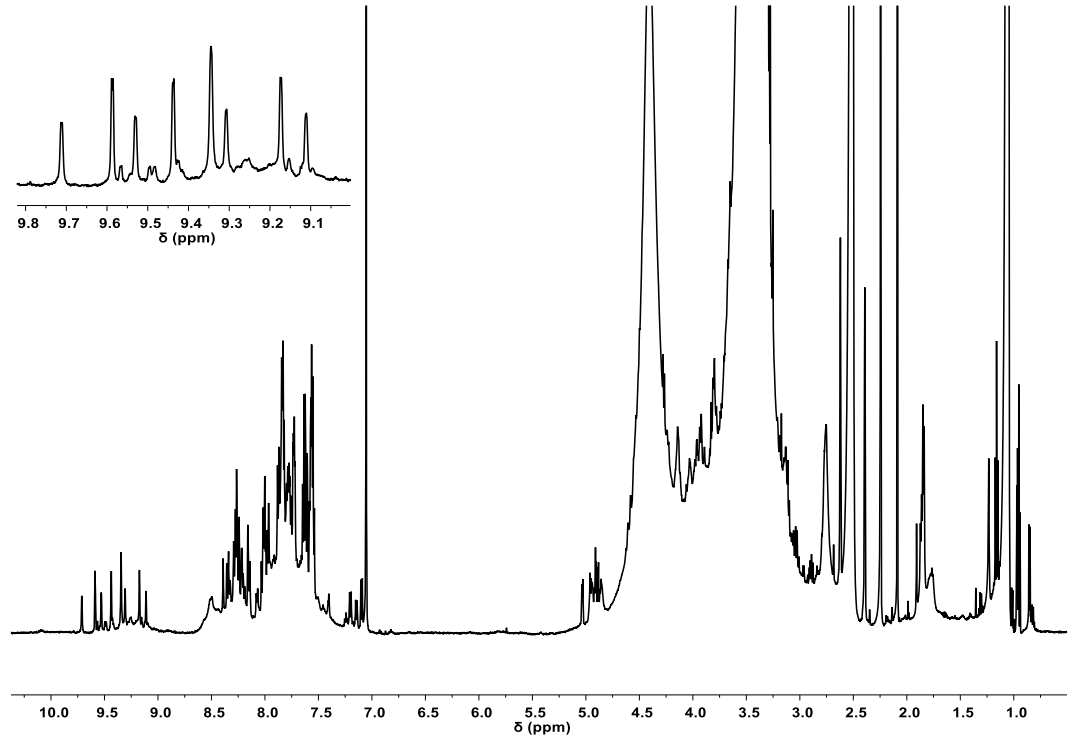

Figure A65. ^{1}H-NMR spectrum (600 MHz, 301 K, DMSO-d_6) of the system formed adding Müller-Thurgau Wine without pre-treatment to the DMSO-d_6 solution containing complex **(*R*)-1b** and ethylenediamine.

A1.10.37. Barbera@(*R*,*R*)-2b

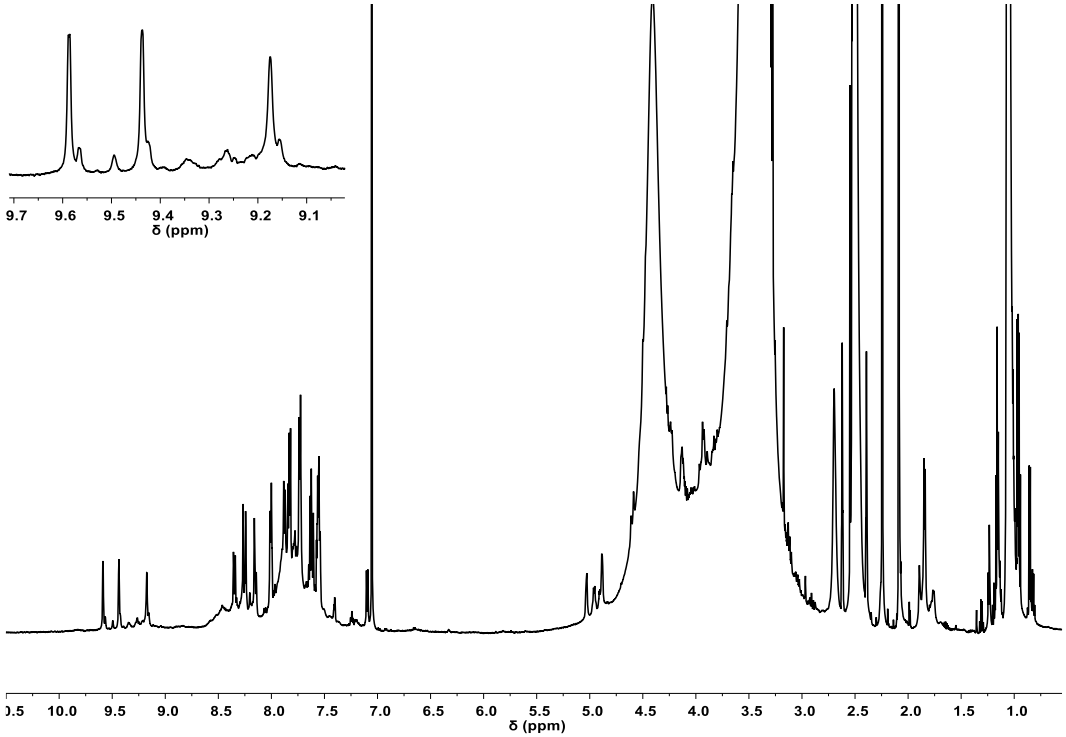

Figure A66. [1]H-NMR spectrum (600 MHz, 301 K, DMSO-d_6) of the system formed adding Barbera Wine without pre-treatment to the DMSO-d_6 solution containing complex **(*R*)-1b** and ethylenediamine.

A1.10.38. Blueberry Juice Alcenera@(*R*,*R*)-2b

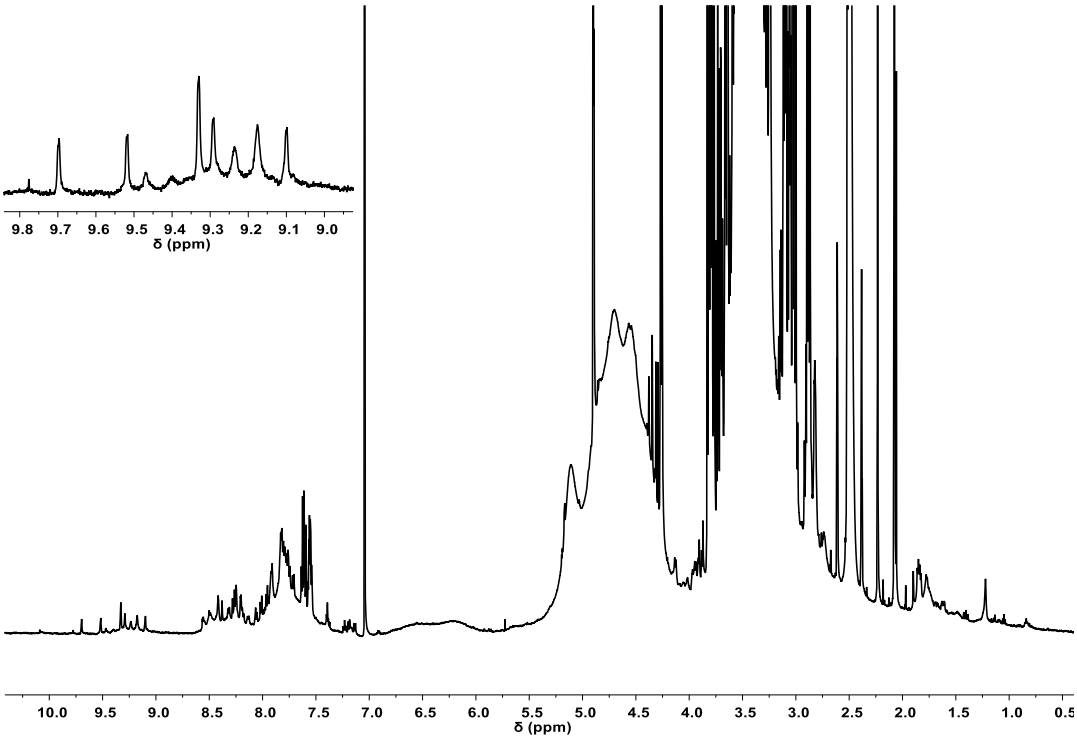

Figure A67. [1]H-NMR spectrum (600 MHz, 301 K, DMSO-d_6) of the system formed adding Blueberry Juice without pre-treatment to the DMSO-d_6 solution containing complex **(*R*)-1b** and ethylenediamine.

A1.10.39. Blueberry Juice Zuegg@(*R*,*R*)-2b

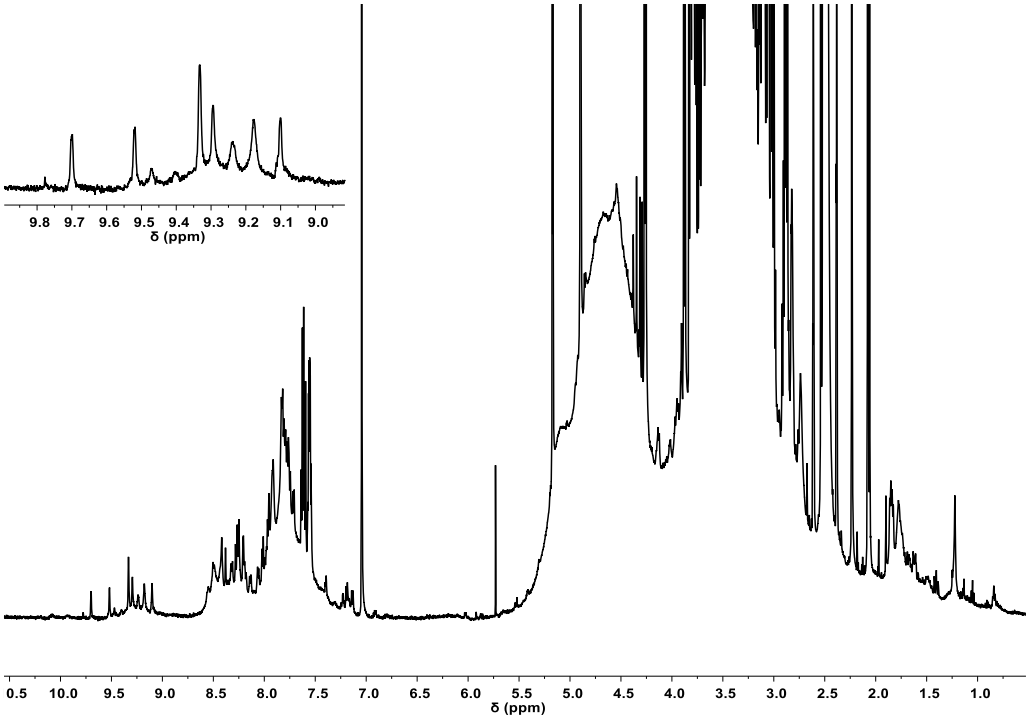

Figure A68. ^{1}H-NMR spectrum (600 MHz, 301 K, DMSO-d_6) of the system formed adding Blueberry Juice without pre-treatment to the DMSO-d_6 solution containing complex **(*R*)-1b** and ethylenediamine.

A1.10.40. Blueberry Juice Squeezed@(*R*,*R*)-2b

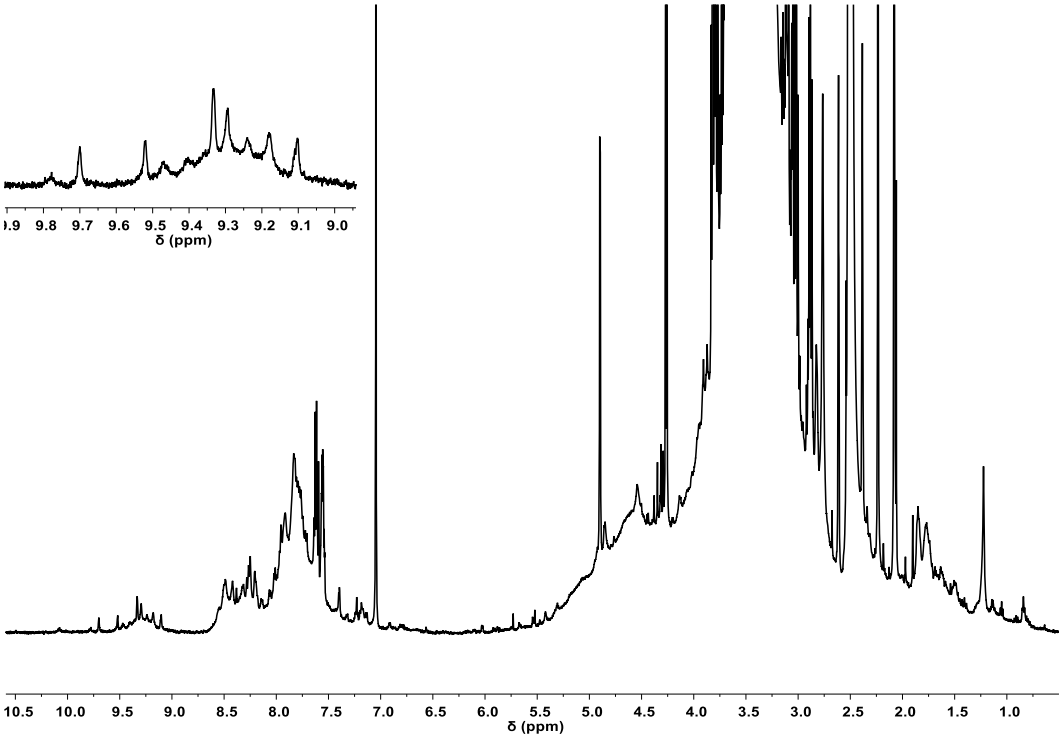

Figure A69. ^{1}H-NMR spectrum (600 MHz, 301 K, DMSO-d_6) of the system formed adding freshly squeezed Blueberry Juice without pre-treatment to the DMSO-d_6 solution containing complex **(*R*)-1b** and ethylenediamine.

A1.10.41. Apple Juice@(*R*,*R*)-2b

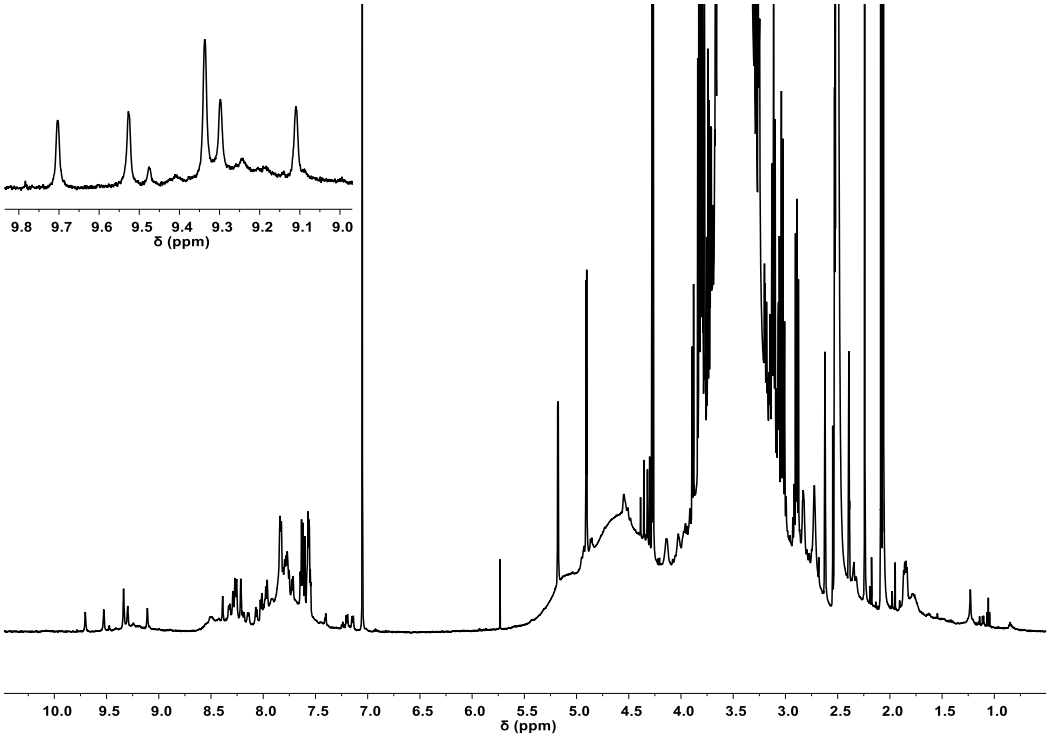

Figure A70. ^{1}H-NMR spectrum (600 MHz, 301 K, DMSO-d_6) of the system formed adding Apple Juice without pre-treatment to the DMSO-d_6 solution containing complex **(*R*)-1b** and ethylenediamine.

A1.10.42. Apple Squeezed@(*R*,*R*)-2b

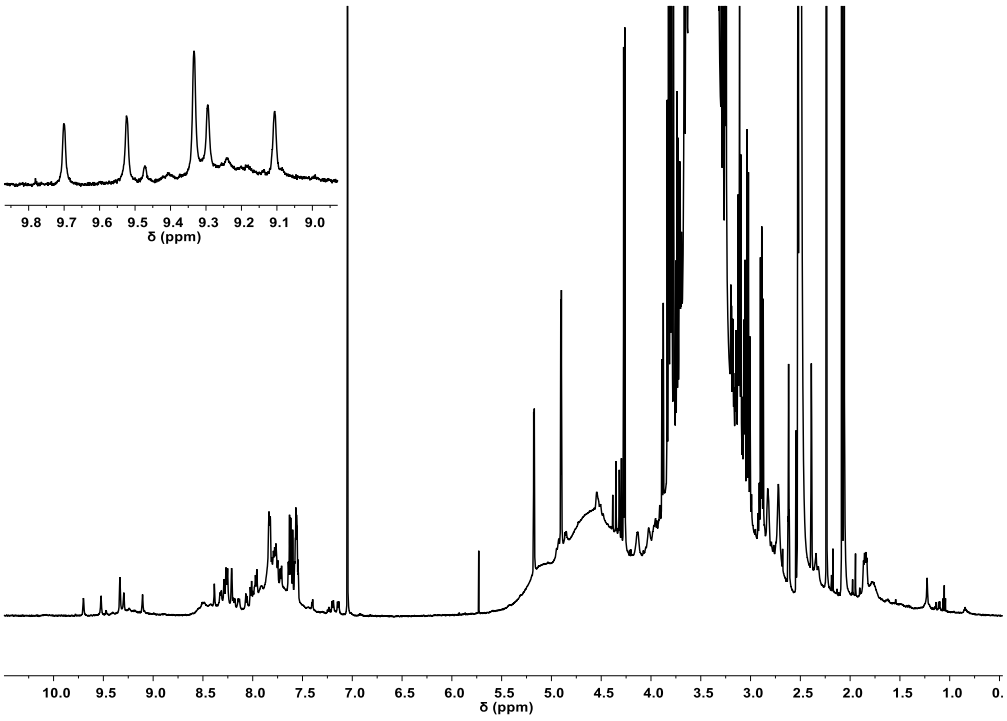

Figure A71. ^{1}H-NMR spectrum (600 MHz, 301 K, DMSO-d_6) of the system formed adding freshly squeezed Apple Juice without pre-treatment to the DMSO-d_6 solution containing complex **(*R*)-1b** and ethylenediamine.

A1.10.43. Pear Juice@(*R*,*R*)-2b

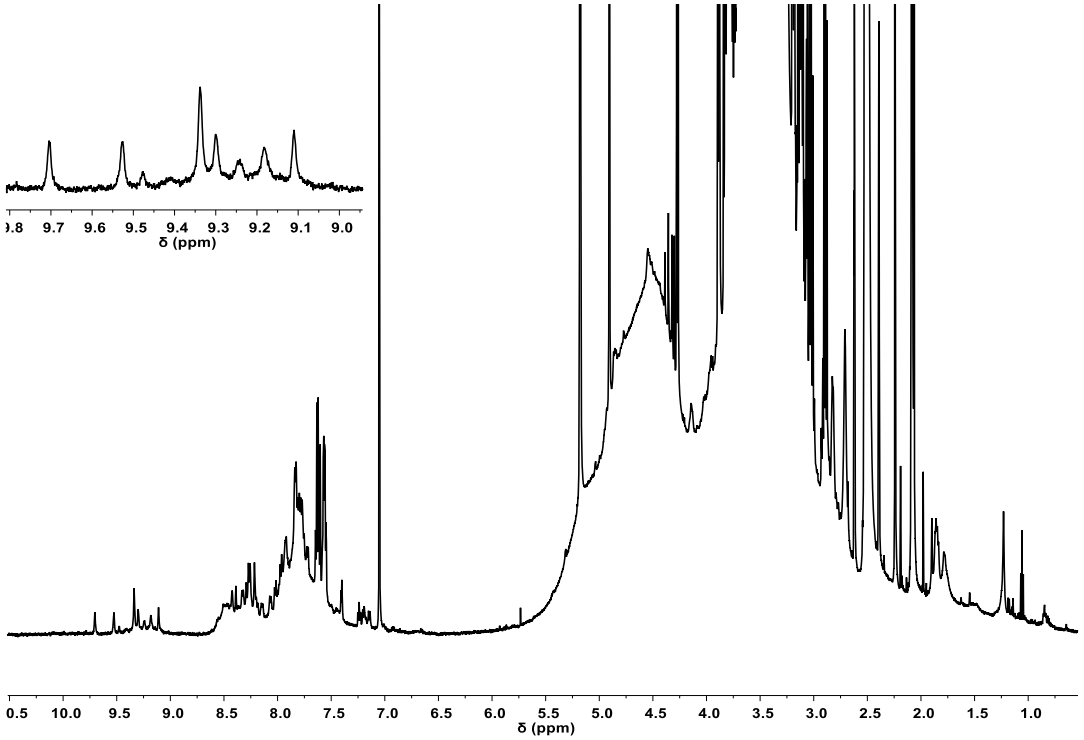

Figure A72. ^{1}H-NMR spectrum (600 MHz, 301 K, DMSO-d_6) of the system formed adding Pear Juice without pre-treatment to the DMSO-d_6 solution containing complex **1b** and ethylenediamine.

A1.11. Quantification of Dicarboxylic acids Content in Complex mixtures

In order to determine the concertation of Tartaric, Malic, and Succinic acids in the complex mixtures, the concentration of cages **L-Tar@2a, L-Mal@2a,** and **L-Suc@2a** has been determined using *p*-xylene as internal standard.

Table A1. Quantification of Tartaric, Malic, and Succinic acids content in the complex mixtures.

Complex Mixture	Tartaric Acid (g/L)	Malic Acid (g/L)	Succinic Acid (g/L)
Prosecco	1.3	1.6	0.3
Chianti	2.4	n.d	0.7
Chardonnay	1.5	1.6	0.2
Valpolicella	2.0	0.3	0.7
Müller-Thurgau	1.5	1.7	0.5
Barbera	2.5	n.d	0.5
Grapes Juice Squeezed	3.6	n.d	n.d
Blueberry Alcenera	n.d	1.4	n.d*
Blueberry Zuegg	n.d	2.5	n.d*
Blueberry Juice Squeezed	n.d	2.1	n.d*
Apple Juice	n.d	4.7	n.d
Apple Juice Squeezed	n.d	3.9	n.d
Pear Juice	n.d	2.1	n.d
Blueberry-Grape Juice	0.5	1.6	n.d*
Peach Juice	n.d	1.8	n.d*

*The peak of succinic acid could be overlapped to the citric acid peak at 9.33 ppm

A1.12. Chromatographic Analysis

In order to verify the reliability of the quantification of Tartaric, Malic, and Succinic acids *via* ^{1}H-NMR using the supramolecular cage **2a** as probe, a chromatographic analysis has been performed.

The HPLC method parameters have been reported in Table A2.

Table A2. HPLC Method Parameters.

HPLC Method Parameters	
Column	Eurospher II 100-5 C18, 5 µm, 4.6 x 250 mm
Mobile Phase	Isocratic, 25 mM K-phosphate buffer; pH 2.4
Flow Rate	1.5 mL/min. (~ 2600 psi)
Oven Temp.	30 °C
UV detection	Wavelength: 210 nm
Injection Volume	20 µL

The Chromatogram of the mixtures of the three dicarboxylic acids is reported in Fig. S73.

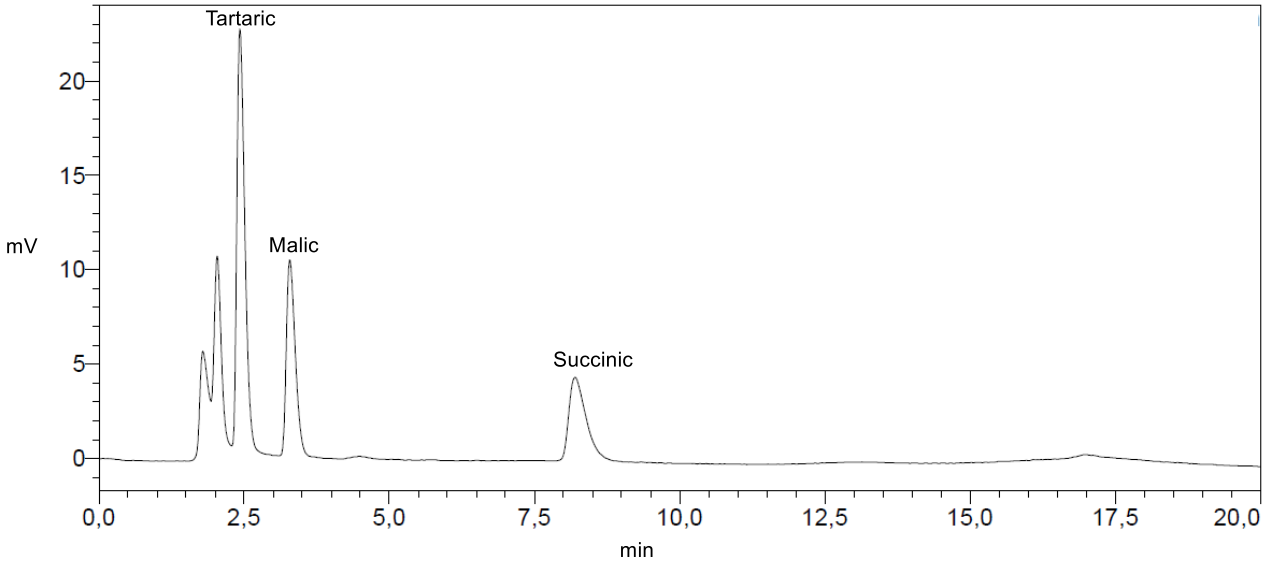

Figure A73. Chromatogram of the mixture of Tartaric (ret. time 2.43 min), Malic (ret. time 3.29 min), and Succinic (ret. time 8.20 min) acids.

For calibration purposes, five solutions with different concentrations (ranging from 20 to 1000 ppm) have been prepared for Tartaric, Malic, and Succinic acids (Fig. A74-A76).

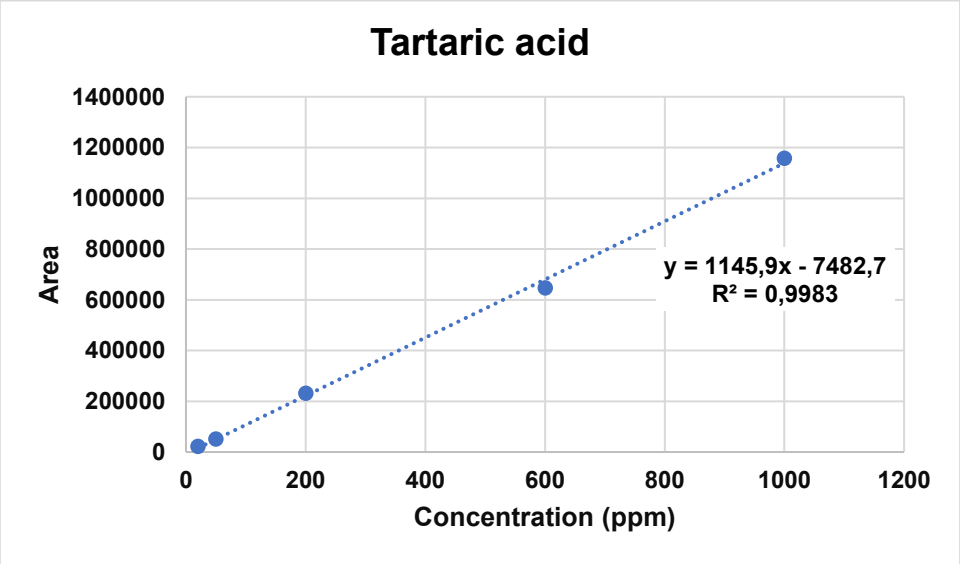

Fig A74. Calibration curve for Tartaric acid.

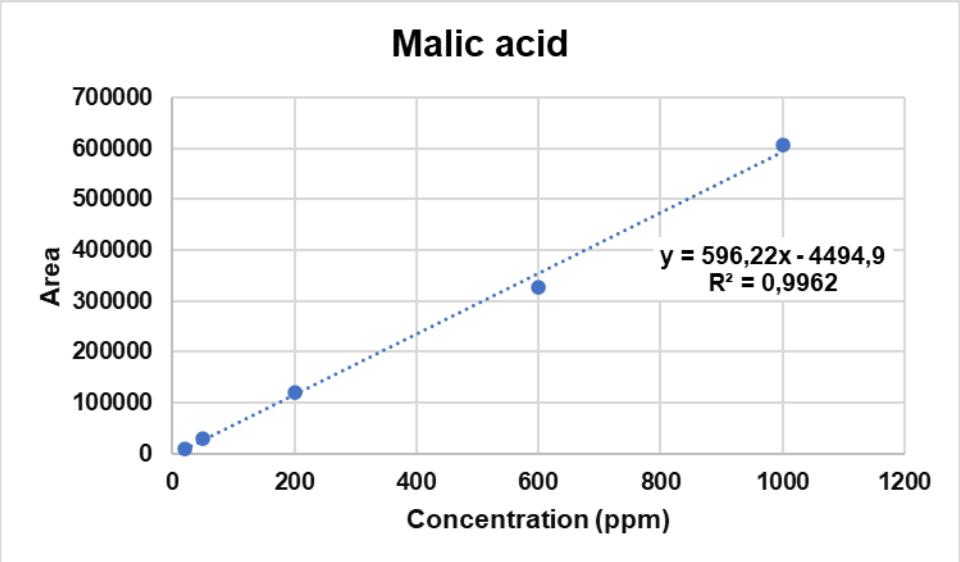

Fig A75 Calibration curve for Malic acid.

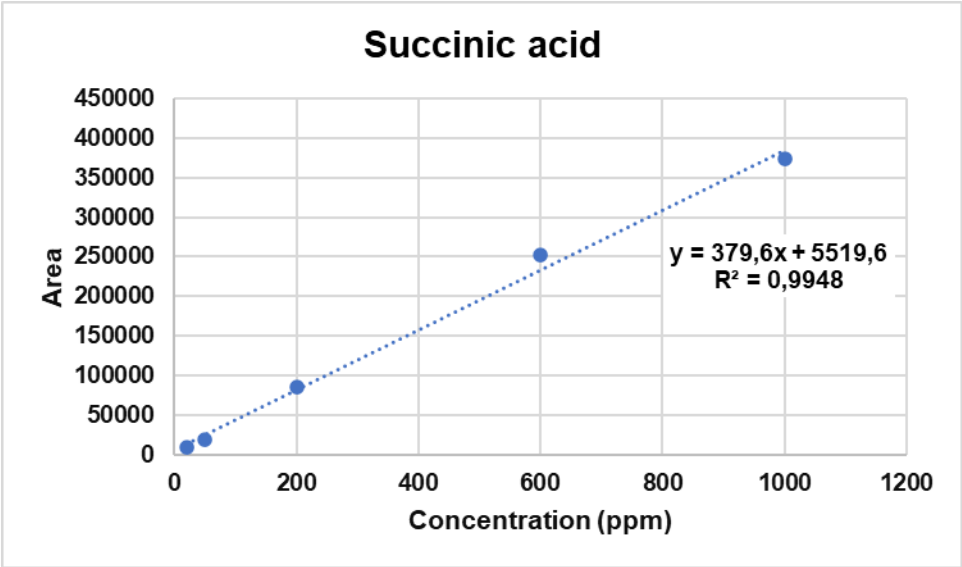

Fig A76. Calibration curve for Succinic acid.

Commercial red wine (Valpolicella), white wine (Müller-Thurgau), and apple juice have been diluted 5:1 with HPLC-grade water, filtered and then injected.

The three chromatograms are reported in Figure A77.

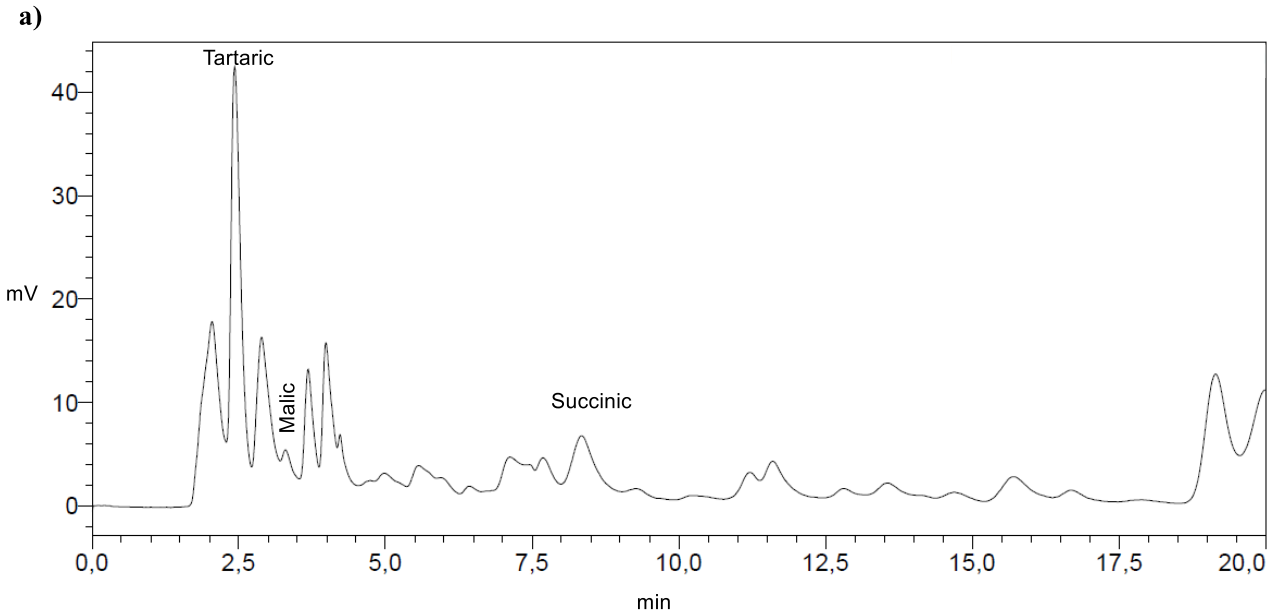

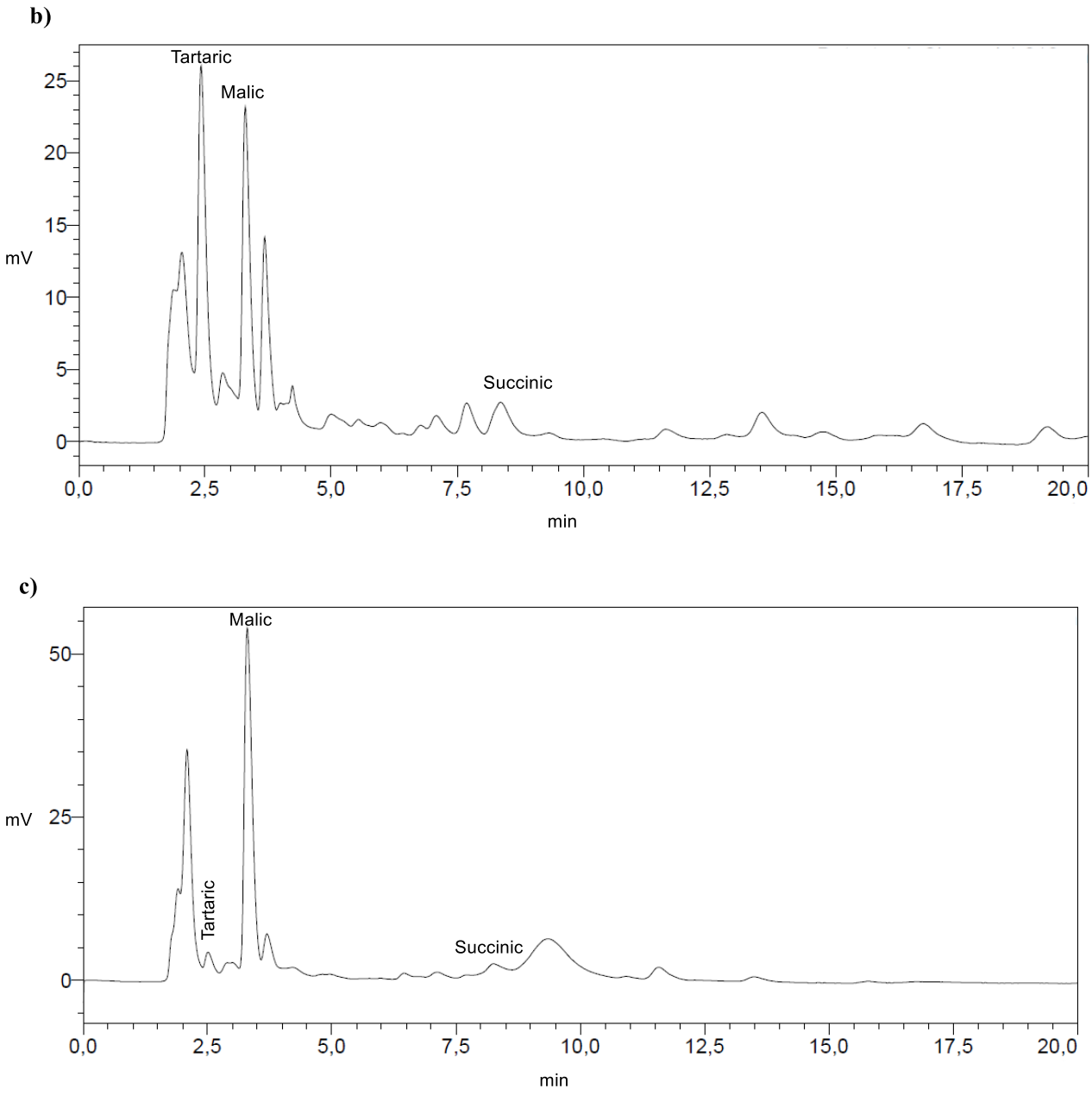

Figure A77. Chromatogram of a) Valpolicella wine, b) Müller-Thurgau wine, and c) apple juice.

As reported in Table A3 a good agreement between the two measurements has been found.

Table A3. Quantification of Tartaric, Malic, and Succinic acids content in the complex mixtures with HPLC and *via* ^{1}H-NMR using cage **2a** as probe.

Complex Mixtures		**HPLC (g/L)**	**^{1}H-NMR (g/L)**
Valpolicella Wine	Tartaric	1.8	2.0
	Malic	0.2	0.3
	Succinic	0.9	0.7
Müller-Thurgau Wine	Tartaric		1.5
	Malic	1.7	1.7
	Succinic	0.6	0.5
Apple Juice	Tartaric	0.1	n.d.*
	Malic	4.6	4.7
	Succinic	0.1	n.d.*

* In the case of apple juice tartaric and succinic acids were not observed in the ^{1}H-NMR spectrum (Fig A56). This could be probably due to the fact that the concentration of malic acid is such high that the cage is completely saturated by malic acid.

A1.13. ESI-MS Characterization

A1.13.1. ESI-MS spectrum of 4

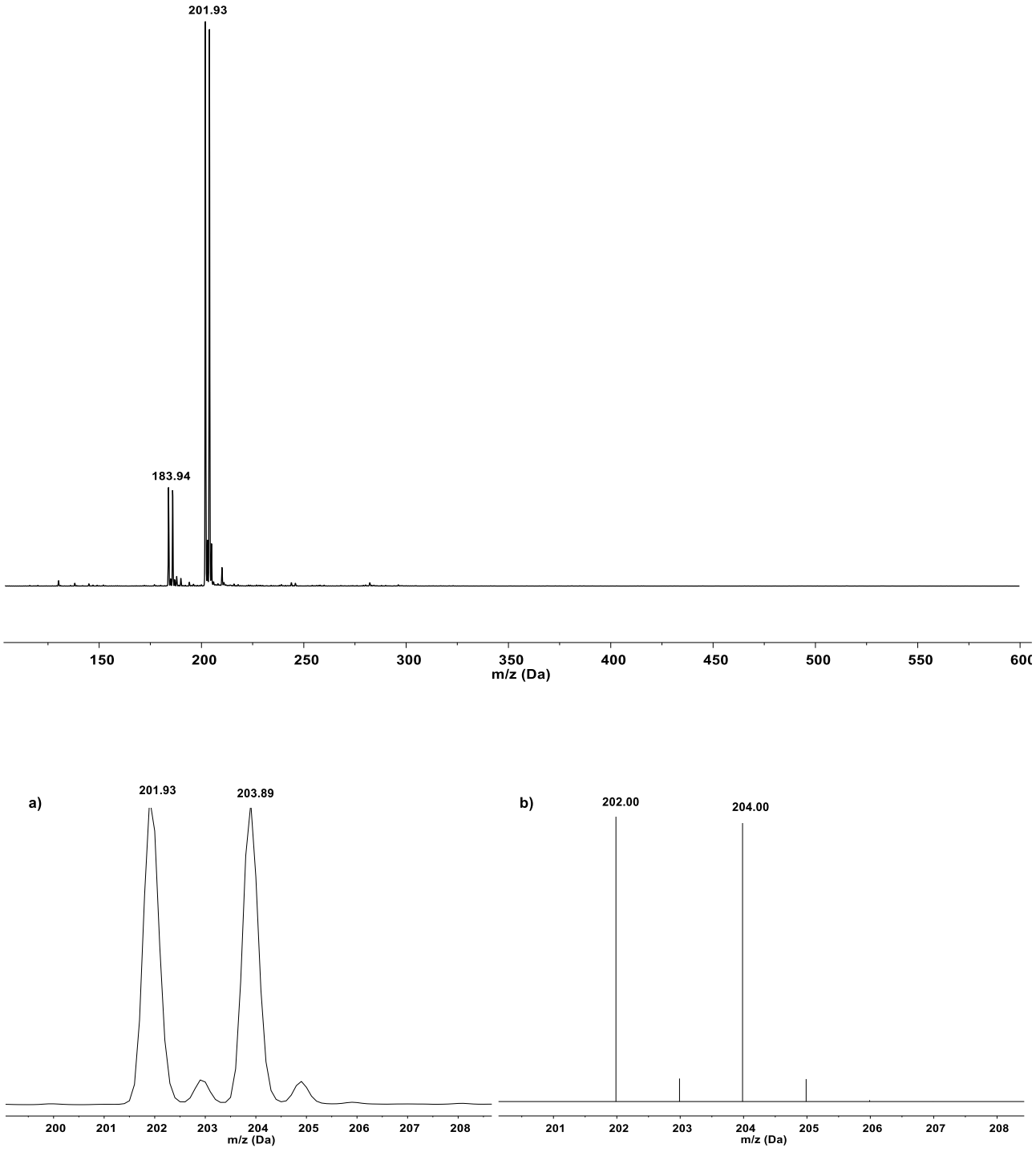

Figure A78. a) Experimental, and b) calculated ESI-MS pattern of **4** for $[M+H]^+$ adducts in CH_3CN/0.1% HCOOH.

A1.13.2. ESI-MS spectrum of 5

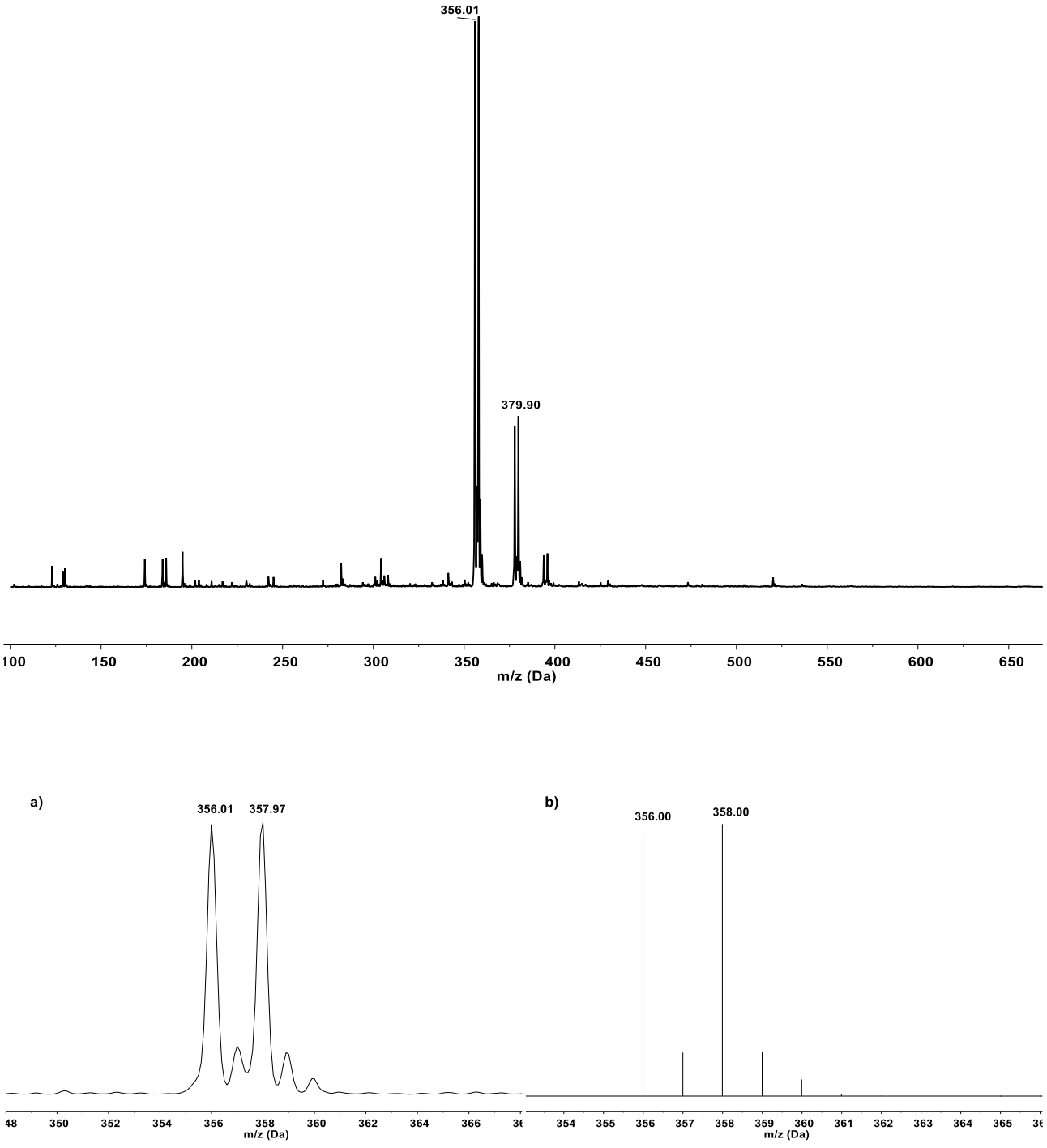

Figure A79. a) Experimental, and b) calculated ESI-MS pattern of **5** for $[M+H]^+$ adducts in CH_3CN/0.1% HCOOH.

A1.13.3. ESI-MS spectrum of 6

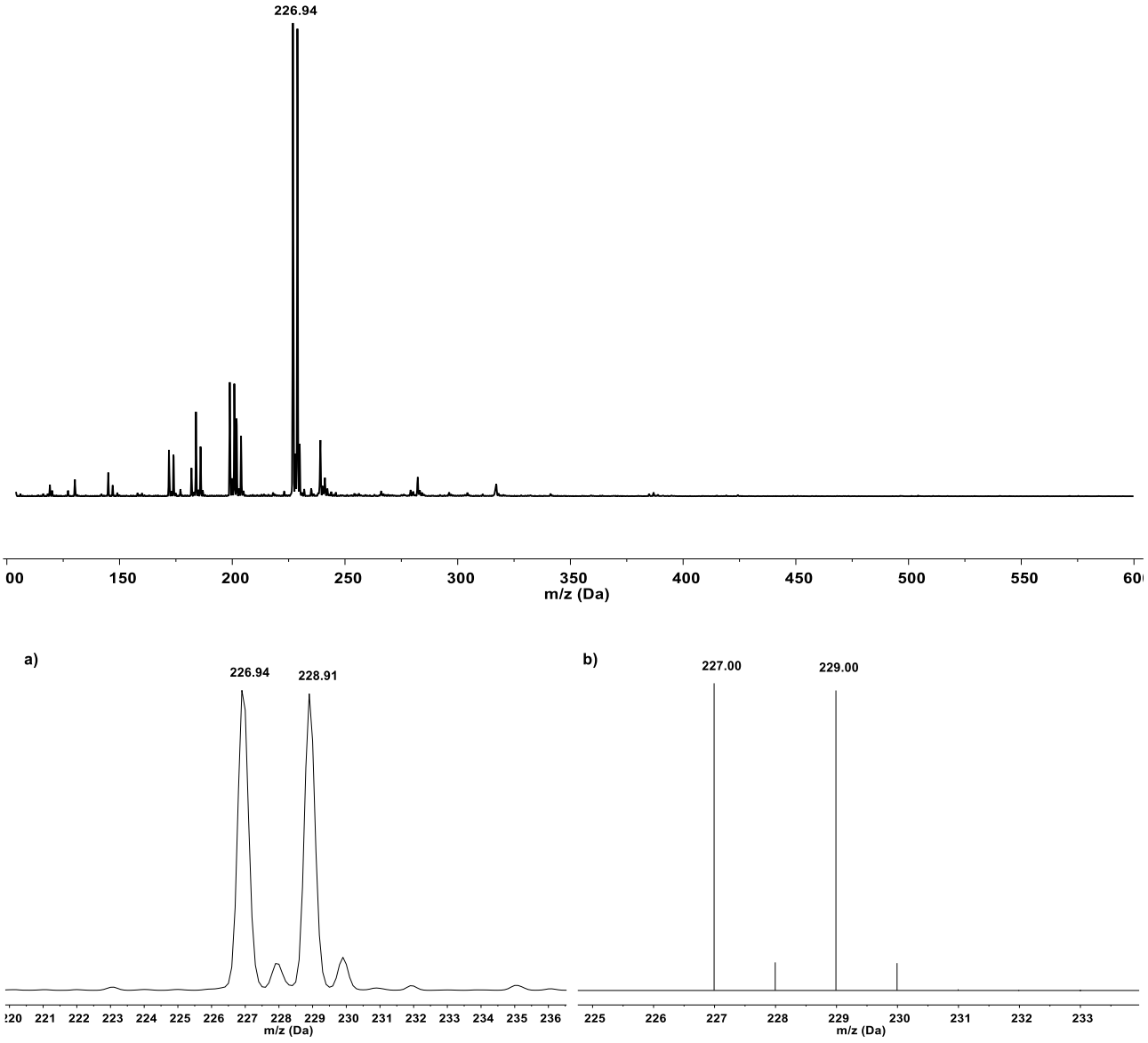

Figure A80. a) Experimental, and b) calculated ESI-MS pattern of **6** for $[M+H]^+$ adducts in CH_3CN/0.1% HCOOH.

A1.13.4. ESI-MS spectrum of 7

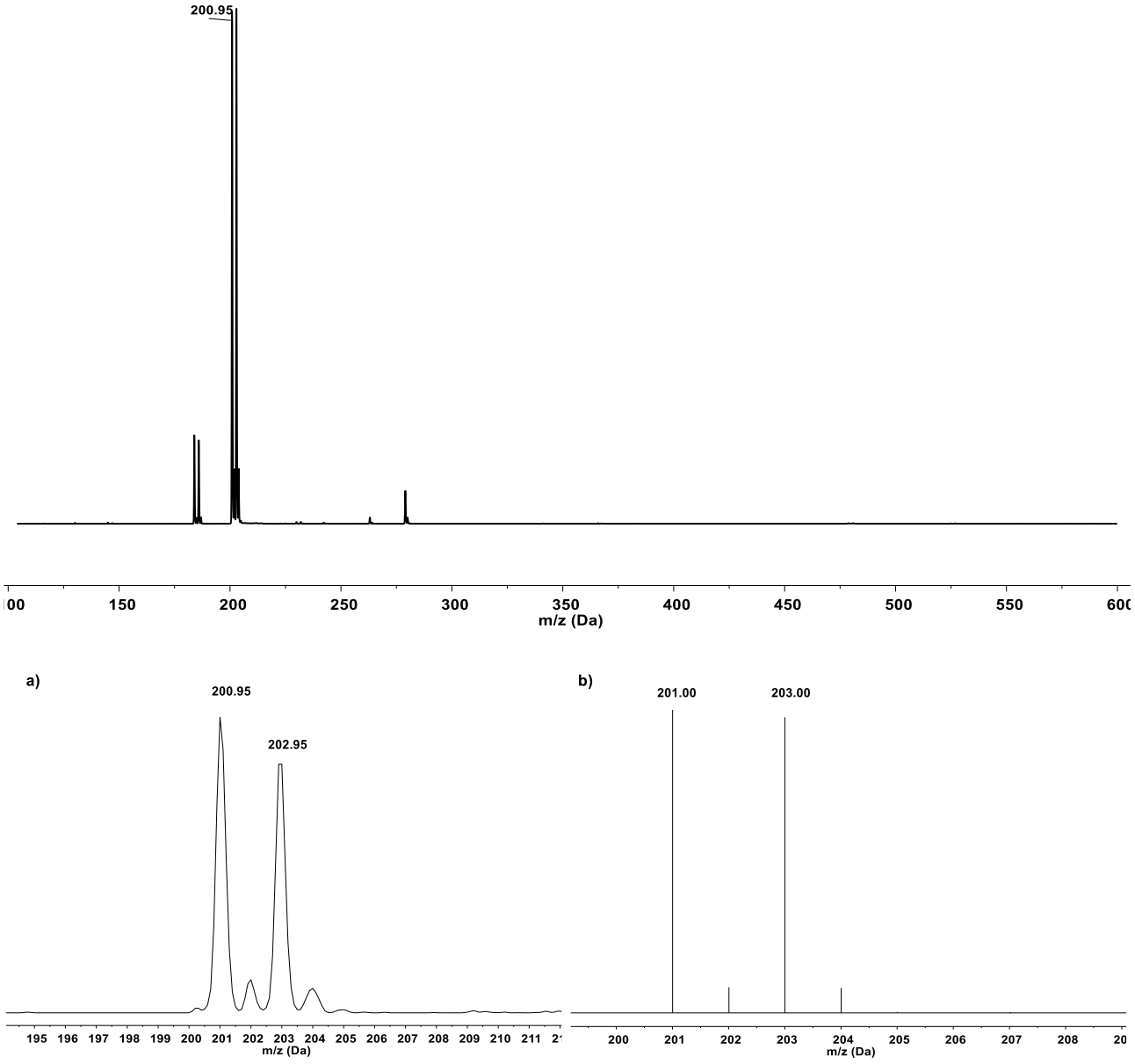

Figure A81. a) Experimental, and b) calculated ESI-MS pattern of **7** for $[M+H]^+$ adducts in CH_3CN/0.1% HCOOH.

A1.13.5. ESI-MS spectrum of (*R*)-8

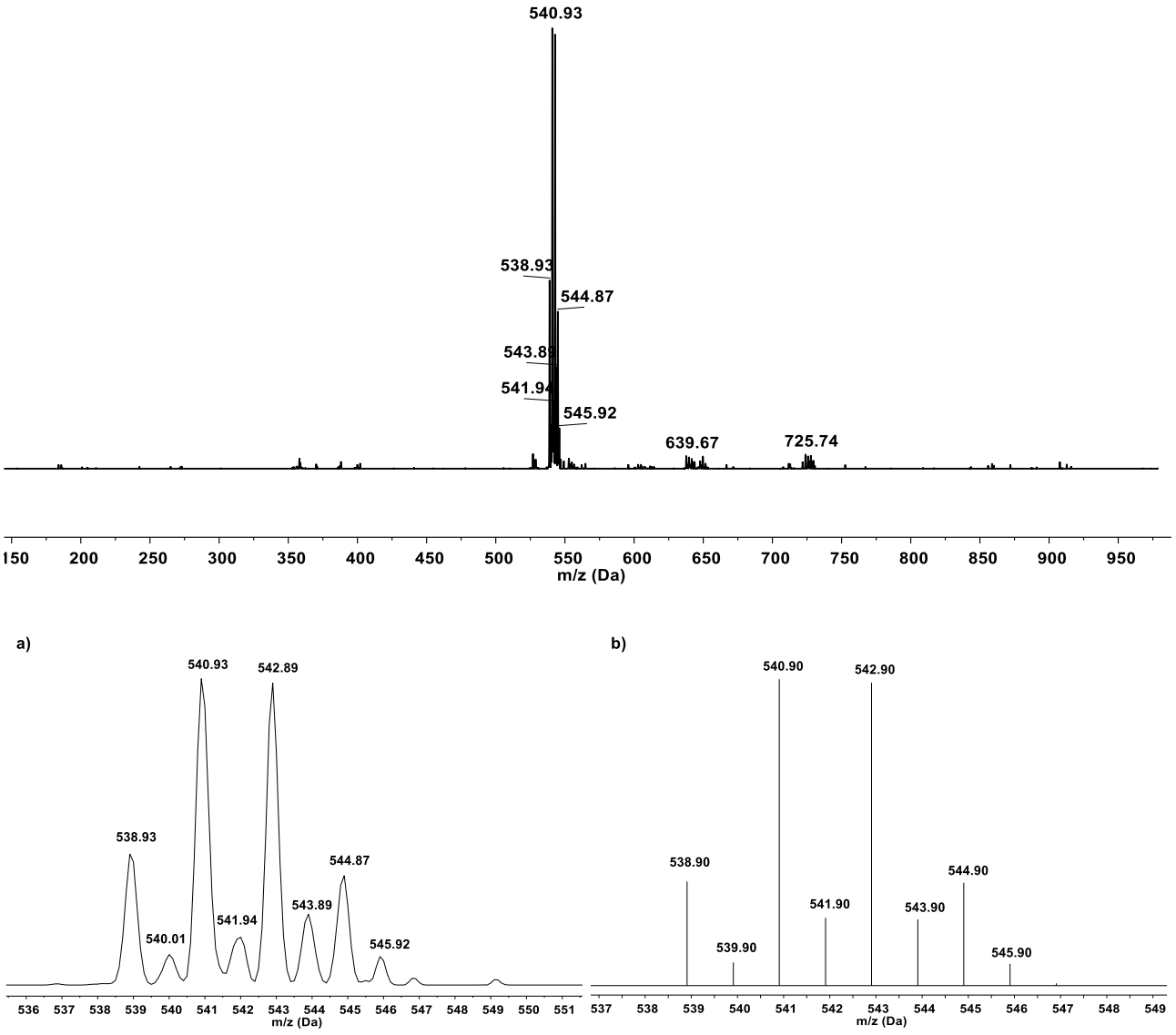

Figure A82. a) Experimental, and b) calculated ESI-MS pattern of **(*R*)-8** for $[M+H]^+$ adducts in CH_3CN/0.1% HCOOH.

A1.13.6. ESI-MS spectrum of (*R*)-9

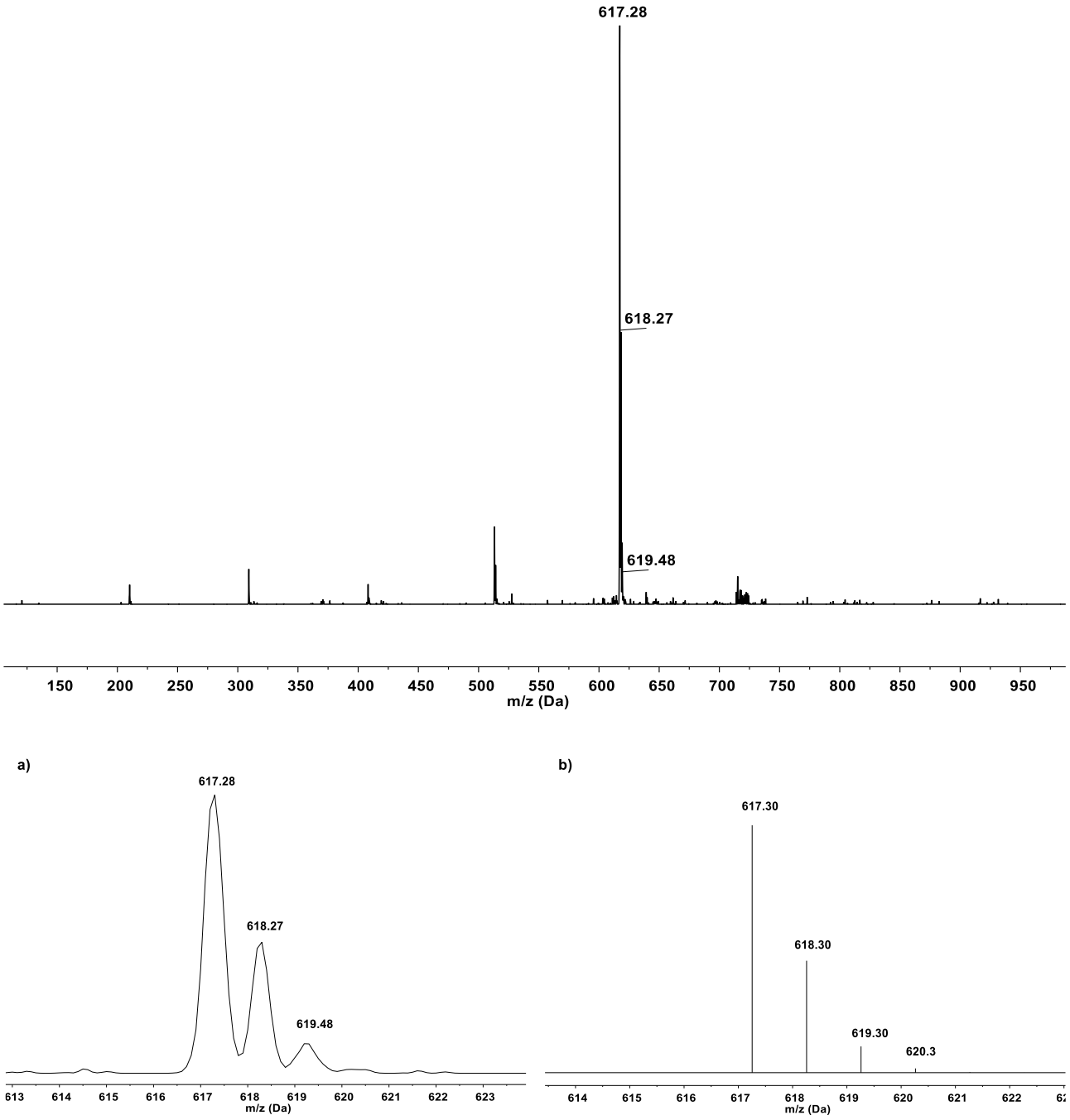

Figure A83. a) Experimental, and b) calculated ESI-MS pattern of **(*R*)-9** for $[M+H]^+$ adducts in CH_3CN/0.1% HCOOH.

A1.13.7. ESI-MS spectrum of (*R*)-1b

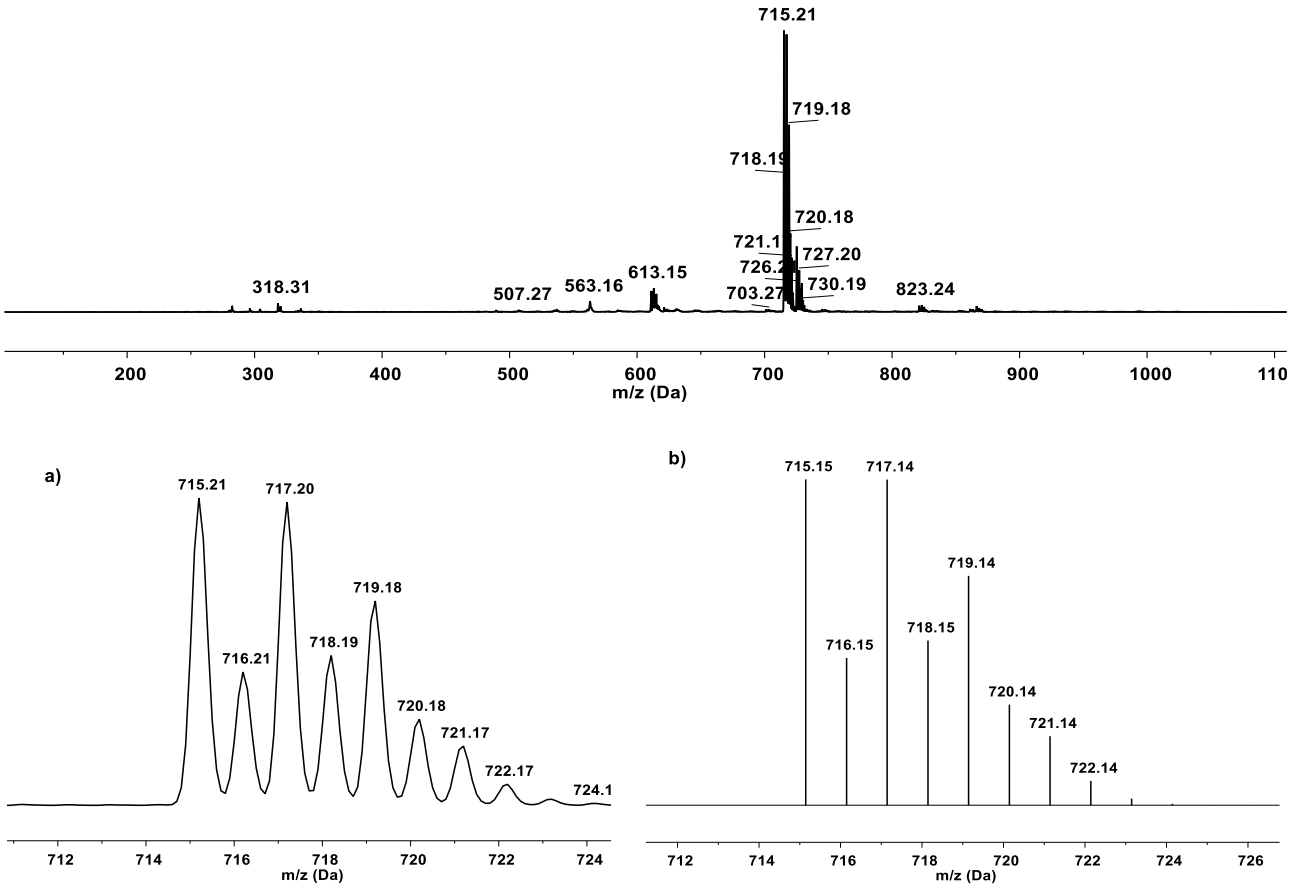

Figure A84. a) Experimental, and b) calculated ESI-MS pattern of **(*R*)-1b** corresponding to $[C_{40}H_{32}N_4O_3Zn + Cl]^+$ in CH_3CN/0.1% HCOOH.

A1.13.8. ESI-MS spectrum of L-Tar@(*R,R*)-2b

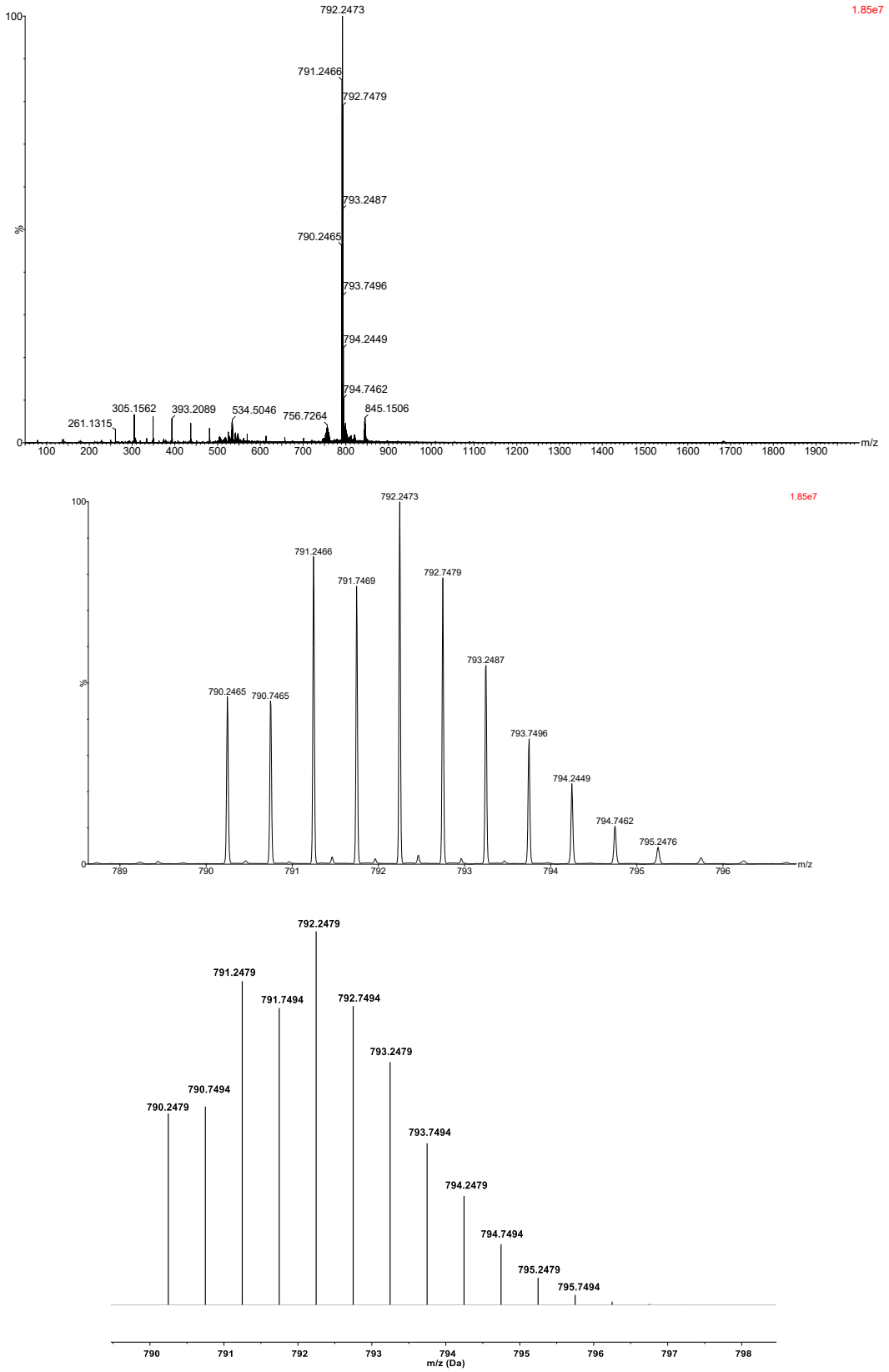

Figure A85. Experimental (top), and calculated (bottom) HRMS (ESI-TOF) pattern of **L-Tar@(*R,R*)-2b** corresponding to $[C_{90}H_{80}N_{14}O_6Zn_2]^{2+}$ in CH_3CN/0.1% HCOOH.

A1.14. References

[1] Y. Pérez-Fuertes, A. M. Kelly, A. L. Johnson, S. Arimori, S. D. Bull, T. D. James, *Org. Lett.* **2006**, 8, 609–612.

[2] R. Evans, Z. Deng, A. K. Rogerson, A. S. McLachlan, J. J. Richards, M. Nilsson, G. A. Morris, *Angew. Chem. Int. Ed.* **2013**, 52, 3199–3202.

[3] A. Macchioni, G. Ciancaleoni, C. Zuccaccia, D. Zuccaccia, *Chem. Soc. Rev.* **2008**, 37, 479–489.

A2. Appendix to Chapter 2

A2.1. CD measurements

CD measurements were performed diluting with anhydrous DMSO the synthesized cage to obtain a final concentration equal to $1.0 \cdot 10^{-5}$M (0.1 cm cuvette). The CD spectra were measured in millidegrees, normalized for the concentration of the cage and reported as [Θ], following the formula:

$$[\Theta] = \frac{\Theta}{C \cdot l}$$

Where [Θ] is the molar ellipticity, Θ is the CD value registered from the instrument (expressed in mdeg), *C* is the concentration of the sample, expressed in (mol/L) and *l* is the optical path (expressed in cm).

A2.2. CD spectra of Cages R@1

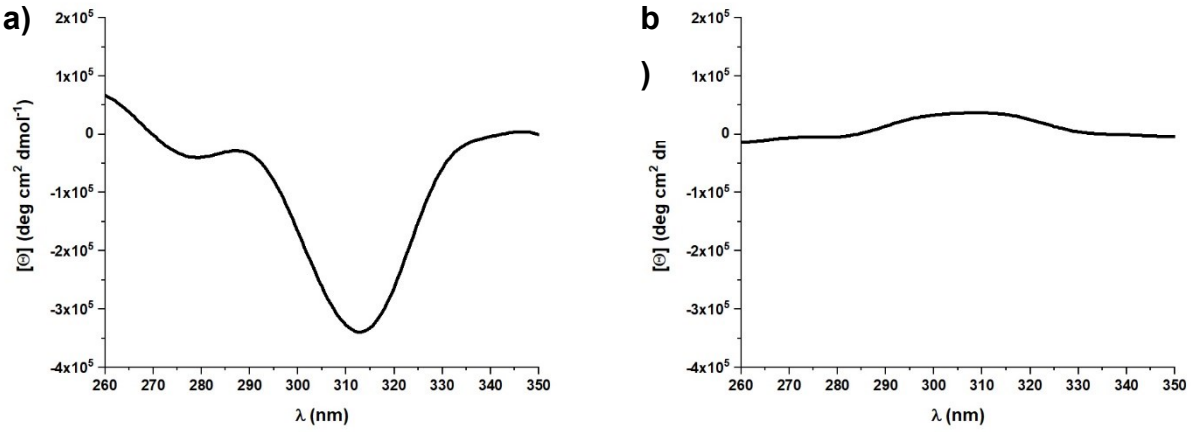

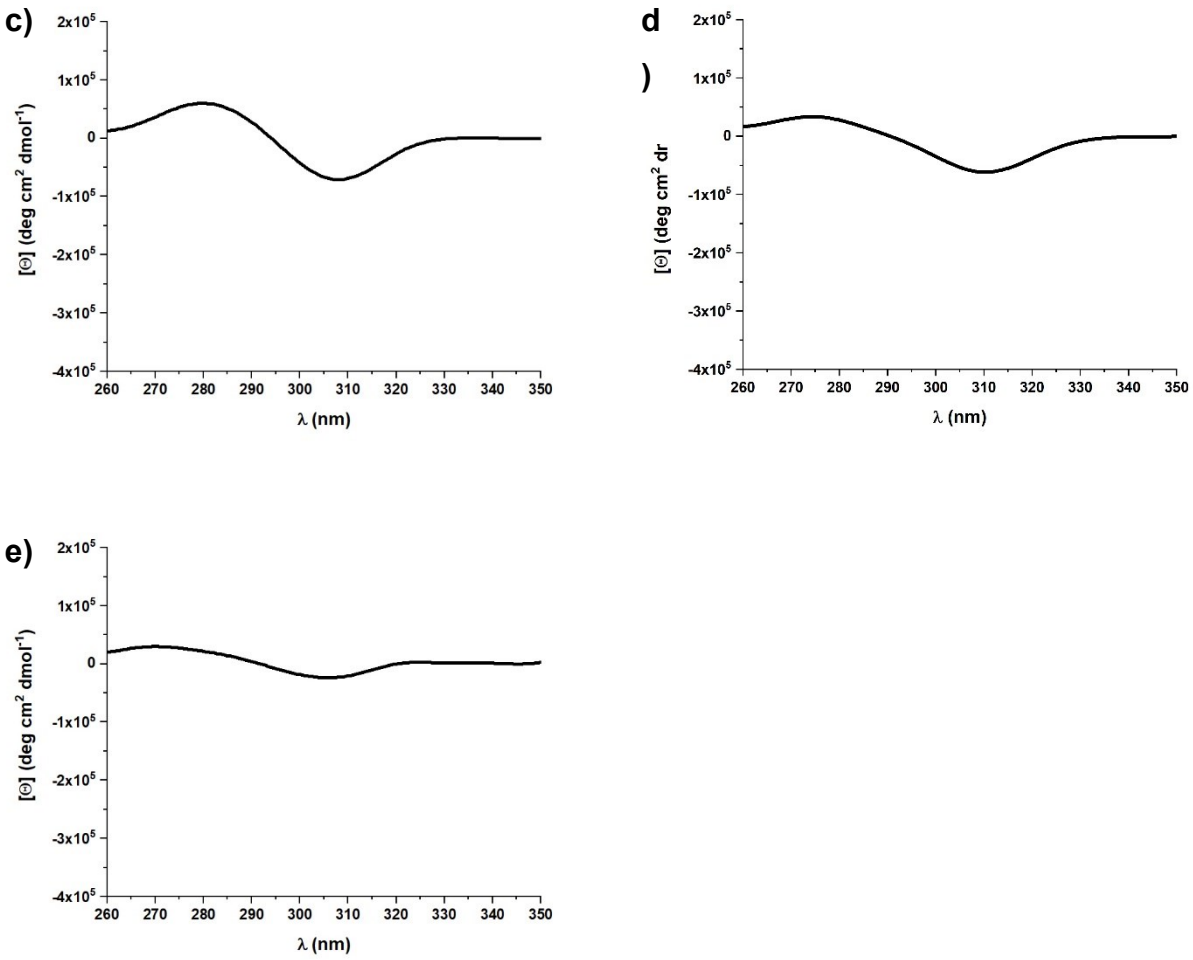

Figure A1. Molar ellipticity spectra of cage **R@1**, a) L-**Tar@1**, b) L-**Mal@1**, c) ***R,S*-Cam@1**, d) L-**Glu@1**, e) L-**Asp@1**. The CD spectra were recorded in anhydrous DMSO at 25°C ($1.0 \cdot 10^{-5}$ M, l=0.1 cm).

A2.3. Enantiomeric Excess curve for Tar@1

To 500 µL (1.0 µmol) of a solution 0.002 M of the aldehyde zinc complex **2** in DMSO-d_6, 50 µL (0.5 µmol) of a solution 0.01 M in DMSO-d_6 of tartaric acid with different enantiomeric excess (+100, +60, +40, -40, -60. -100) and 125 µL (2.5 µmol) of a solution 0.02 M in DMSO-d_6 of ethylenediamine were added in vial and then diluted with anhydrous DMSO the synthesized cage to obtain a final concentration equal to $1.0 \cdot 10^{-5}$M (0.1 cm cuvette).

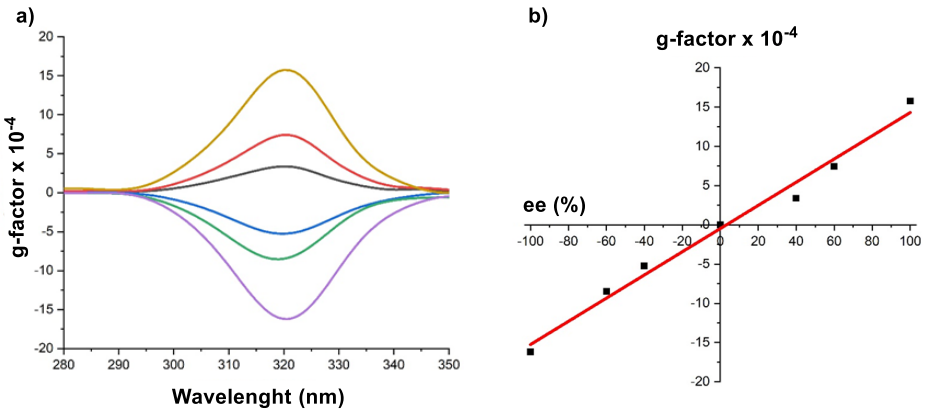

Figure A2. a) Anisotropy g-factor for the six samples of L-tartaric acid analyzed, respectively with an ee (%) equal to +100, +60, +40, -40, -60 and -100; b) calibration curve obtained with the g-factor of the samples at 320 nm. The fitting equation curve is y=0.1478(±0.0083)x-0.48(±0.55), R^2=0.9814.

A2.4. Computational section

A2.4.1. Conformational Analysis

Manual conformational search was run with Gaussian 16 package (DFT B3LYP/6-31G(d)), with default grids and loose convergence criteria.[1-4] The guests chosen for the computational investigation are the D-Tartaric acid and L-malic acid. Three stereogenic elements have been varied to generate eight different starting structures for the conformational search. In particular: *i*) the TPMA helix helicity sense (Figure A3), *ii*) the dihedral angle between the pyridine ring and the imine ring (Figure A4), *iii*) the dihedral angle of the imine bond relative to the aromatic ring (Figure A5).

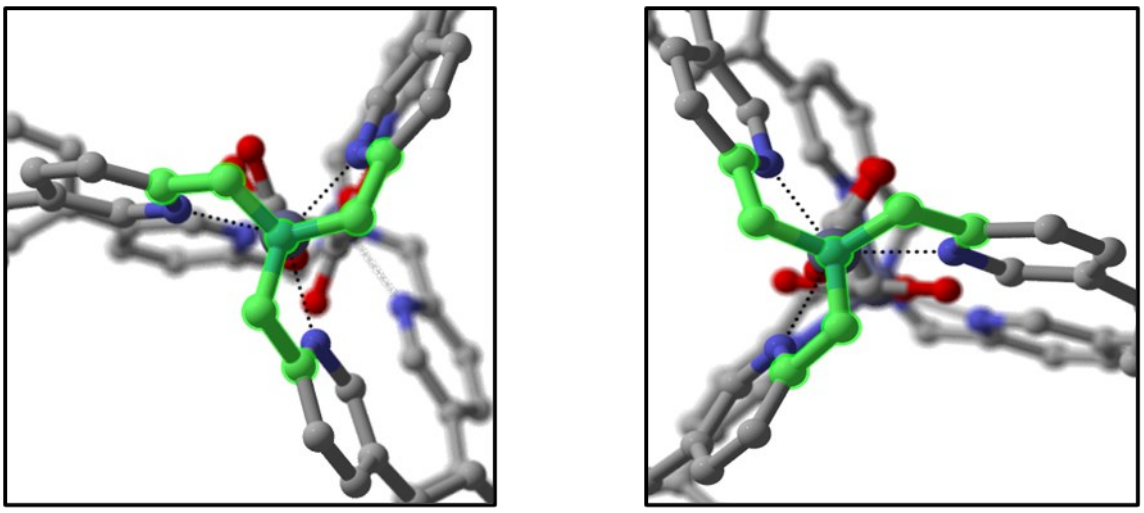

Figure A3. Helix conformation clockwise **Δ** (left) and counterclockwise **Λ** (right) of **TPMA**. Hydrogen atoms are removed for clarity.

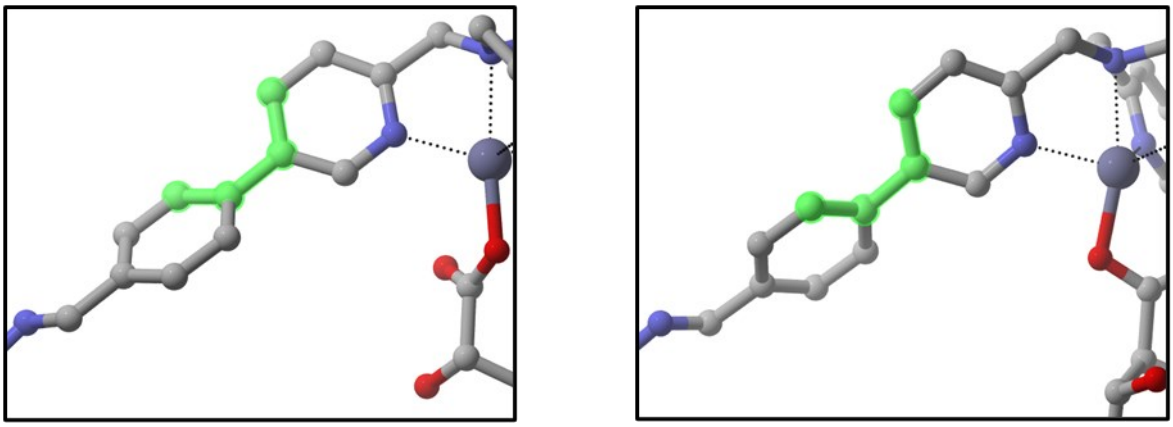

Figure A4. Dihedral angle formed between the pyridine-ring of **TPMA** and the phenyl-ring: example of positive angle on left (**+**) and negative angle on right (**-**). Hydrogen atoms are removed for clarity.

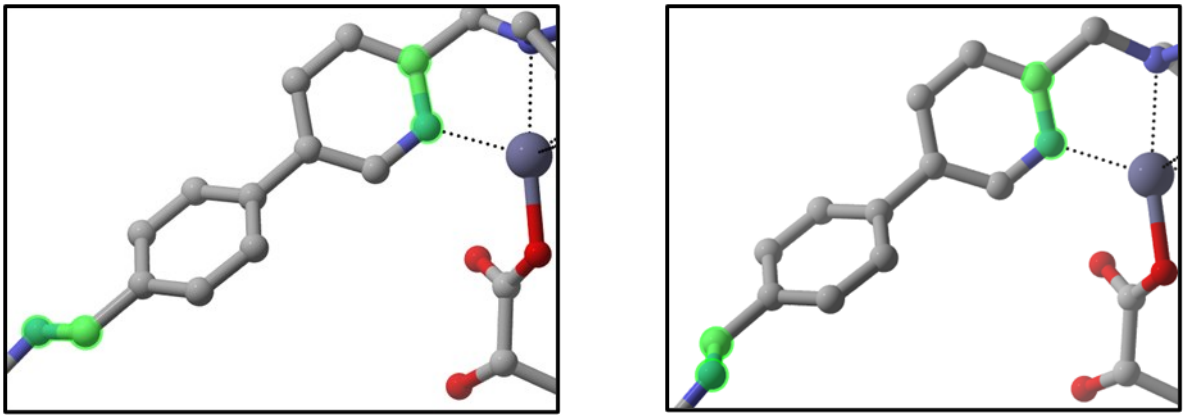

Figure A5. Orientation of the C=N bond of the imine group respect the C-N highlighted on the **TPMA** pyridine ring: C=N forms an angle **>|90°|** (left); C=N forms an angle **<|90°|** (right). Hydrogen atoms are removed for clarity.

Table A1. Classification of conformations assumed by cages stereoisomers: the propeller direction of **TPMA**, **Λ** (counterclockwise), **Δ** (clockwise); the sign of dihedral angle formed between the pyridine-ring of **TPMA** and the phenyl-ring **(+** for a positive angle, **-** for a negative angle); the orientation of the C=N bond of the imine group respect the C-N bond on the **TPMA** pyridine ring (angle **<|90°|** or **>|90°**|).

Conformers	**Helix**	**Dihedral Angle Pyr-Ar**	**Dihedral Angle Pry-Imine**
I	Λ	-	<|90°|
II	Δ	-	<|90°|
III	Λ	+	<|90°|
IV	Λ	+	>|90°|
V	Δ	+	<|90°|
VI	Δ	+	>|90°|
VII	Λ	-	>|90°|
VIII	Δ	-	>|90°|

A2.4.2. Dicarboxylic Acid Coordination

The search for the more stable cage conformation was then followed by a conformational analysis over the dicarboxylic acids, trying to expand the number minima explored on the potential energy surface. Due to the large energy difference of the two conformations **I** and **V** among the others, this search was done only with these two conformations of the cage. In Figure A6 and Figure A7 the four possible conformers for D-Tartaric acid and five for L-Malic acid are shown. The changes are mainly driven by the different network of hydrogen bonds formed within the molecule itself.

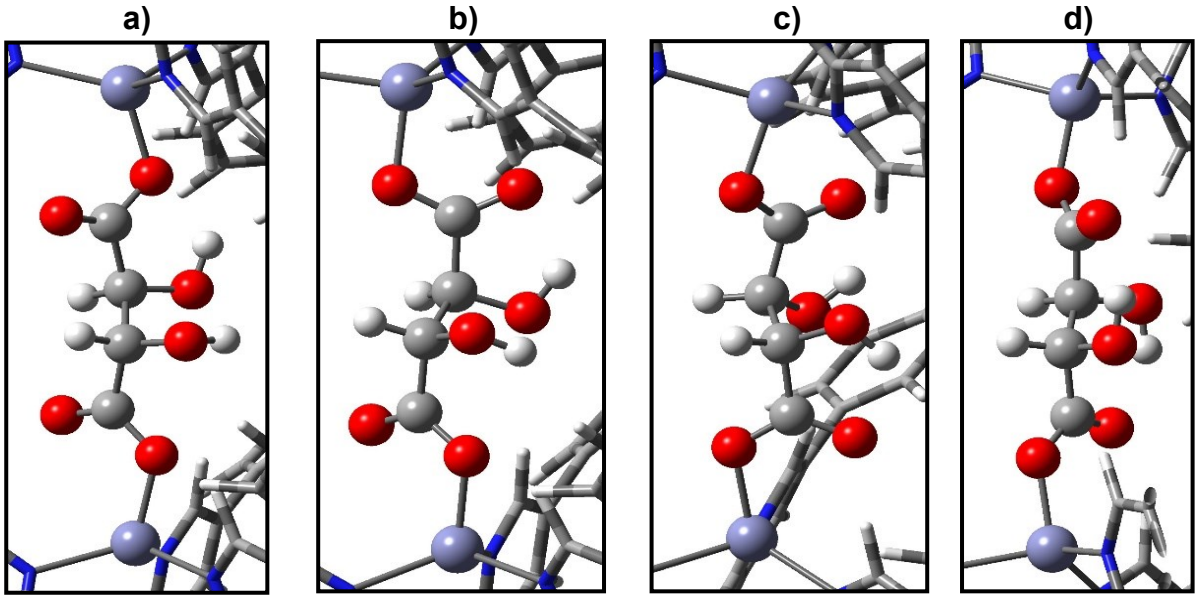

Figure A6. Most stable monodentate oxygen coordination of the D-Tartaric acid within the supramolecular cage **1** (a-d).

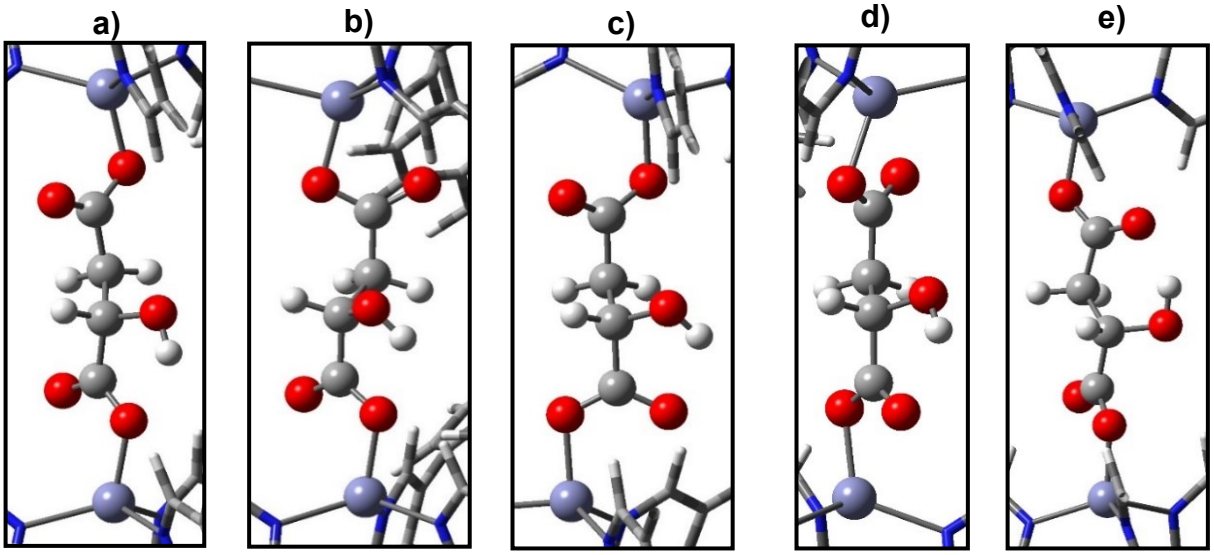

Figure A7. Most stable monodentate oxygen coordination of the L-Malic acid within the supramolecular cage **1** (a-e).

A2.4.3. Meso Structures

In the last part of the computational search structures with opposite helicity of the two **TPMA** zinc complexes have been considered (pseudo-meso). The dihedral angle between the pyridine ring and the phenyl ring (Figure A4) were also manually varied while the dihedral angle of the imine bond relative to the pyridine ring (Figure A5) was kept <|90°| since the most stable conformers calculated so far had this stereoconformation. The most stable dicarboxylic acid coordination was used for the calculation, i.e. **c)** for the D-Tartaric acid (Figure A6) and **e)** for the L-Malic acid (Figure A7). The classification of the different meso conformers is shown in Table A2.

Table A2. Classification of the four meso conformers computed: the propeller direction of **TPMA**, **Λ** (counterclockwise), **Δ** (clockwise) and the sign of dihedral angle formed between the pyridine-ring of **TPMA** and the phenyl-ring (**+** for a positive angle, **-** for a negative angle)**.** The dihedral angle of the imine bond relative to the pyridine ring was kept **<|90°|**.

Conformers	Helicity	Dihedral Angle Pyr-Ar
IX	Δ - Λ	+ / +
X	Δ - Λ	+ / -
XI	Λ - Δ	- / -
XII	Λ - Δ	+ / -

The conformational search over the four meso structures reveal the presence of other two good conformers, namely the IX and XI (Table A3). For both the diacid tested, they resulted close in energy to the best stable structures previously found.

A2.4.4. Energy calculation of the most stable conformers

Sixteen different conformations were obtained by changing the three stereogenic elements of the cage and the diacid coordination. Relative energies are calculated by the difference from the most stable conformation energy. **D-Tar@1** conformers summarized in Table A3 and **L-Mal@1** summarized in Table A4.

Table A3. Energy difference calculated from the minimum energy value for each conformation (kcal/mol).

Entry	D-Tar@1 Cage Conformers	Diacid Coordination	Energy	Relative Energy (kcal/mol)
1	I	a)	-8175.138165	1.4
2	II	a)	-8175.101767	24.3
3	III	a)	-8175.102165	24.0
4	IV	a)	-8175.094548	28.8
5	V	a)	-8175.138076	1.5
6	VI	a)	-8175.108308	20.2
7	VII	a)	-8175.107316	20.8
8	VIII	a)	-8175.105409	22.0
9	I	b)	-8175.139124	0.8
10	V	b)	-8175.140442	0.0
11	I	c)	-8175.137799	1.7
12	V	c)	-8175.136376	2.6
13	I	d)	-8175.138976	0.9
14	V	d)	-8175.137965	1.6
15	I	e)	-	-
16	V	e)	-	-
17	IX	b)	-8175.139461	0.6
18	X	b)	-8175.116636	14.9
19	XI	b)	-8175.138348	1.3
20	XII	b)	-8175.118944	13.5

Highlighted in green the lowest energetical conformation and in yellow the second and third best.

Table A4. Energy difference calculated from the minimum energy value for each conformation (kcal/mol). Highlighted in green the lowest energetical conformation and in yellow the second and third best.

Entry	L-Mal@1 Cage Conformers	Diacid Coordination	Energy	Relative Energy (kcal/mol)
1	I	a)	-8099.925810	1.9
2	II	a)	-8099.888734	25.2
3	III	a)	-8099.894008	21.9
4	IV	a)	-8099.893184	22.4
5	V	a)	-8099.925888	1.9
6	VI	a)	-8099.899173	18.7
7	VII	a)	-8099.897083	20.0
8	VIII	a)	-8099.895155	21.2
9	I	b)	-8099.921843	4.4
10	V	b)	-8099.923900	3.1
11	I	c)	-8099.927789	0.7
12	V	c)	-8099.926030	1.8
13	I	d)	-8099.921695	4.5
14	V	d)	-8099.920683	5.2
15	I	e)	-8099.928891	0.0
16	V	e)	-8099.928610	0.2
17	IX	e)	-8099.926993/ -8099.925047[a]	1.2 / 2.4[a]
18	X	e)	-8099.905595/ -8099.904361[a]	14.6 / 15.4[a]
19	XI	e)	-8099.926250/ -8099.926511[a]	1.7 / 1.5[a]
20	XII	e)	-8099.916133/ -8099.924247[a]	8.0 / 2.9[a]

[a)]: two coordination of the malic acid are possible, the left one with the hydroxyl group pointing the **Δ** conformation of the zinc complex, the right one pointing the **Λ**.

Table A3 and Table A4 summarize the conformational search conducted for the supramolecular cages **D-Tar@1** and **L-Mal@1**. As it is possible to see, there are some conformations relatively close in energy and others considerably far from the best one. To consider that the energy difference is expressed in kcal/mol, and therefore a small value difference determines a relatively large difference in the Boltzmann population. As example, considering two best structures with an energy difference equal to 0.5 kcal/mol, their corresponding population will be 70% for the best conformation and 30% for the second one.

In the case of **L-Mal@1**, two structures resulted significantly close in energy (Entry 15 and 16). Noteworthy, these two conformations are characterized by an opposite **TPMA** helicity and thus opposite CD spectra. As a result, the contemporary presence of both the conformations in solution, could be the explanation of the low intensity of the experimental CD signal measured for this system.

A2.4.5. B3LYP/6-31G(d) Best minimized structures

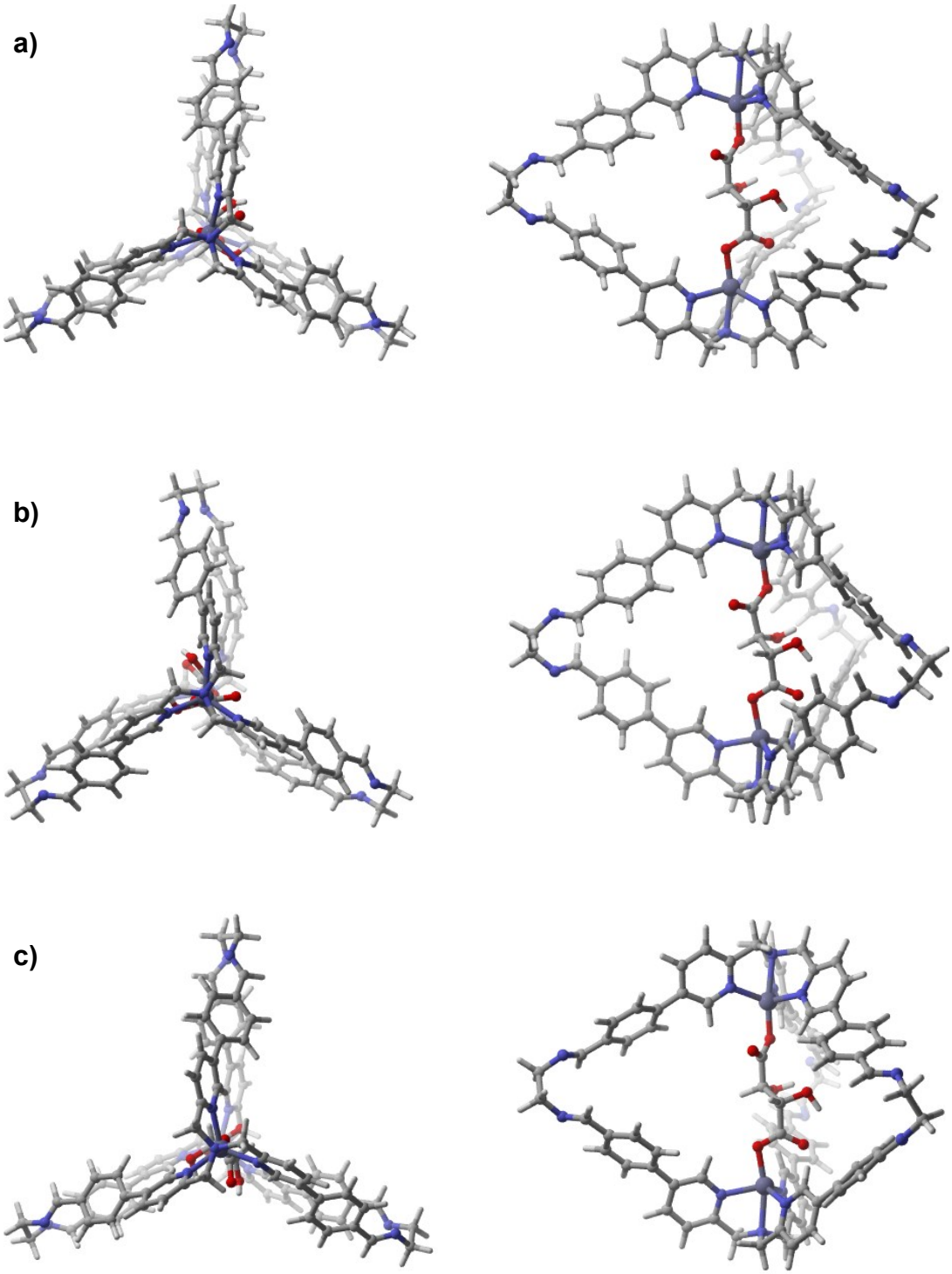

Figure A8. B3LYP/6-31G(d) minimized structures for the cage **D-Tar@1** a) entry 10, b) entry 17, c) entry 9.

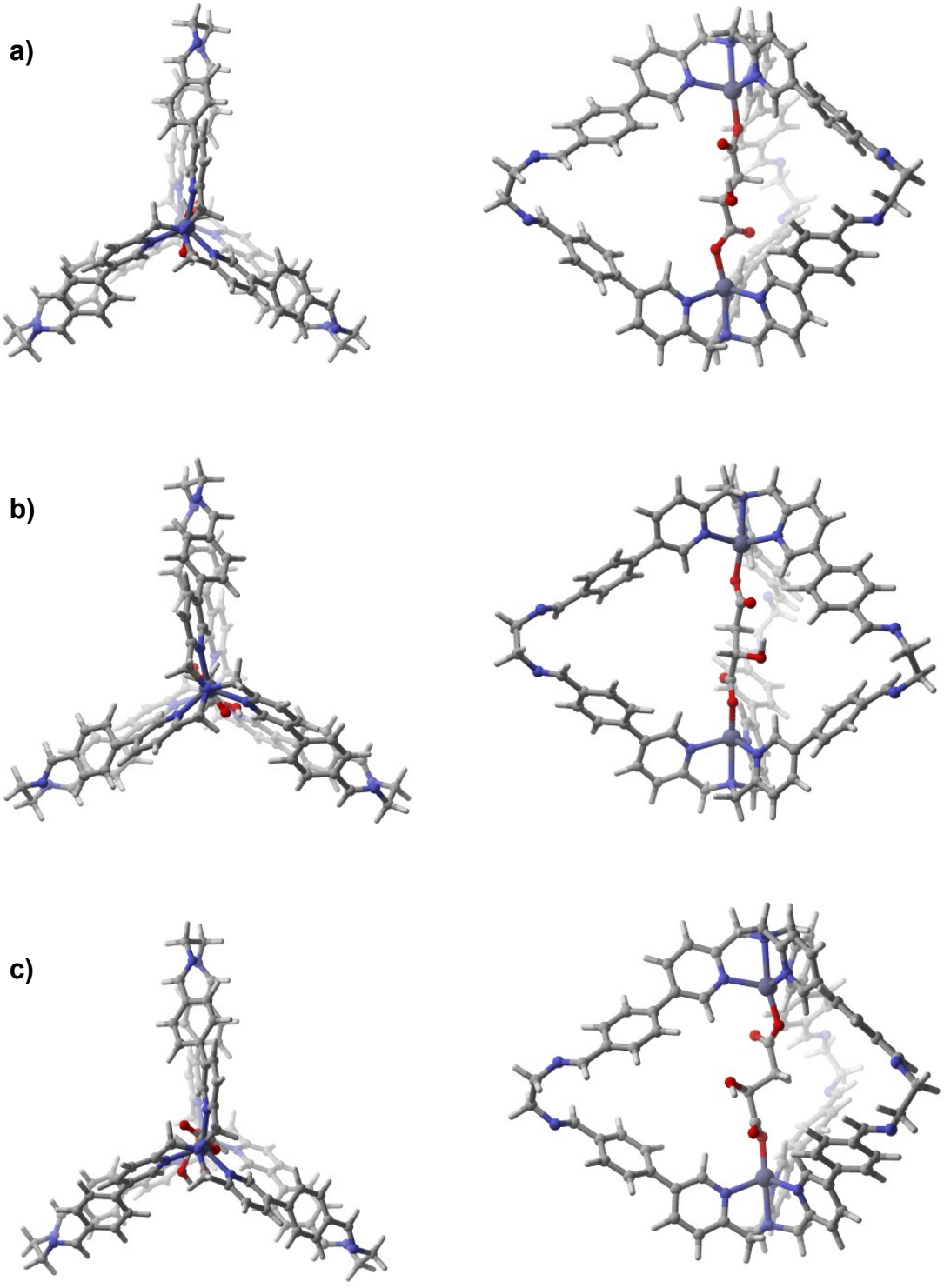

Figure A9. B3LYP/6-31G(d) minimized structures for the cage **L-Mal@1** a) entry 15, b) entry 16, c) entry 11.

A2.4.6. TD-DFT Calculations

Once obtained the energy distribution of the conformers, TD-DFT B3LYP/6-31G(d) calculations were performed to simulate the CD spectrum. The calculations were carried out over 50 excited states for the three best conformational structures found for the supramolecular systems **D-Tar@1** and **L-Mal@1** and Boltzmann-weighted ECD spectrum was then obtained with SpecDis software,[3] by using the population data shown in Table A5 and the bandwidth σ that gives the best superimposition of the spectra. To do this, the program maximize the *similarity factor S*, a parameter proposed by Bultinck[5] based on the cosine similarity equation.

Table A5. Energy difference in kcal/mol with their respective population (%) for the three best structures of the supramolecular systems **D-Tar@1** and **L-Mal@1**.

D-Tar@1		
Entry	**ΔG (kcal/mol)**	**Population (%)**
10	0.0	62
17	0.6	22
9	0.8	16

L-Mal@1		
Entry	**ΔG (kcal/mol)**	**Population (%)**
15	0.0	49
16	0.2	36
11	0.7	15

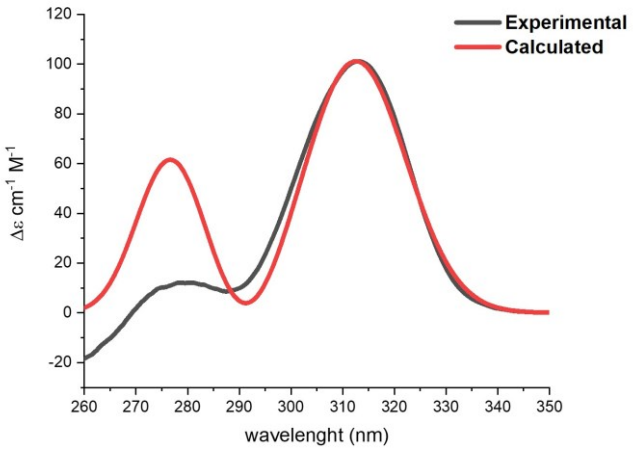

Figure A10. Experimental (black) molar ellipticity and calculated (red) CD spectra of **D-Tar@1** cage. The UV-shift and the best fitting bandwidth are equal to -29 nm and 0.15 eV respectively. The scale ratio experimental:calculated is 1:0.3521.

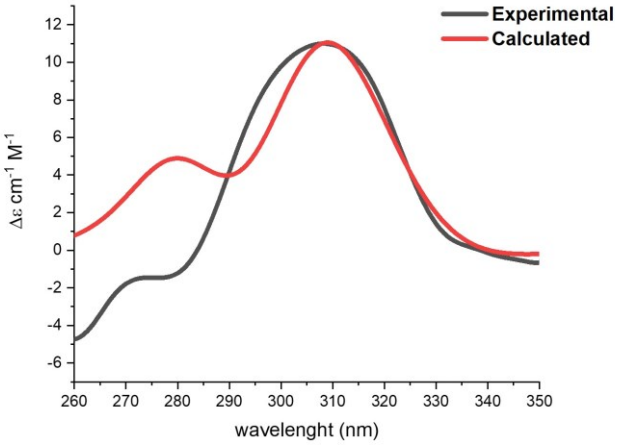

Figure A11. Overlay of experimental molar ellipticity and calculated CD spectra of **L-Mal@1** cage. The UV-shift and the best fitting bandwidth are equal to -29 nm and 0.20 eV respectively. The scale ratio experimental:calculated is 1:0.7724.

A2.5. Calibration Curves for the different wines

A2.5.1. General Procedure for the Standard addition Method

To 5 vials containing 500 µL (1.0 µmol) of a solution 0.002 M of the Zinc complex **2** in DMSO, 10 µL (Prosecco, Müller Thurgau) or 5 µL (Chardonnay, Chianti, Barbera, Valpolicella) of wine were added in each vial. Then, increasing amount of a solution 0.005 M of **L-Tar** in DMSO were added. Finally, 125 µL (2.5 µmol) of a solution 0.02 M in DMSO of ethylenediamine were added. For the CD analysis, 150 µL of the mixture were diluted to 1 mL with dry DMSO and analyzed. The measurements were repeated three times.
The standard deviation has been calculated using the equation:

$$s_x = \frac{t \cdot s_{y/x}}{m} \sqrt{\frac{1}{N} + \frac{(\bar{y})^2}{m^2 \sum (x_i - \bar{x})^2}}$$

A2.5.2. Prosecco

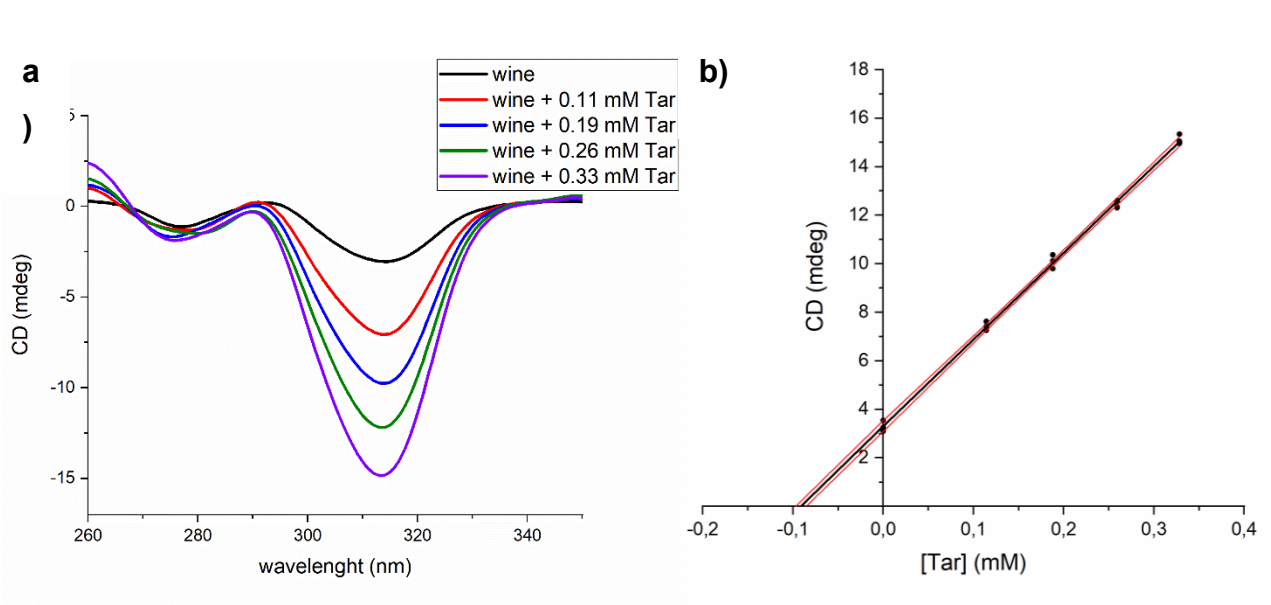

Figure A12. a) Circular Dichroism spectra in Ellipticity (mdeg) within the range 260-350 nm of the supramolecular system **1** with 10 µL of Prosecco wine and different content in L-tartaric acid, respectively equal to 0.0×10^{-4} M (black line), 1.1×10^{-4} M (red line), 1.9×10^{-4} M (blue line), 2.6×10^{-4} M (green line), 3.3×10^{-4} M (violet line); b) the linear fit of the CD signal response of the supramolecular system **1** taking the point of the maximum CD signal at 314 nm. The fitting equation curve is y=35.72x+3.31, R^2=0.997. The abscissa intercept is equal to -0.093 ± 0.008 mM, corresponding to a Tartaric acid content equal to 1.11 ± 0.05 g/L.

A2.5.3. Chianti

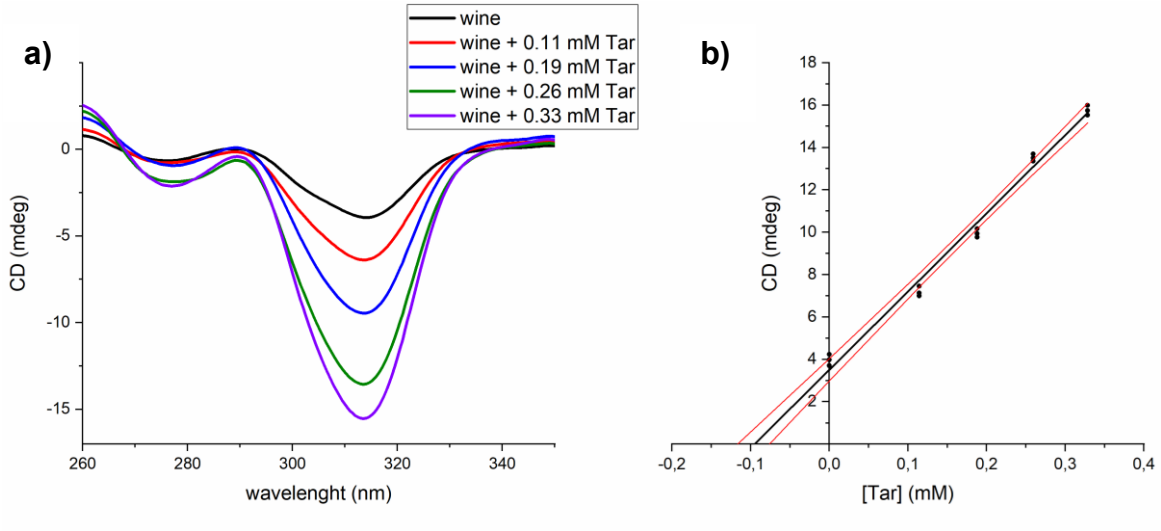

Figure A13. a) Circular Dichroism spectra in Ellipticity (mdeg) within the range 260-350 nm of the supramolecular system **1** with 5 µL of Chianti wine and different content in L-tartaric acid, respectively equal to 0.0×10^{-4} M (black line), 1.1×10^{-4} M (red line), 1.9×10^{-4} M (blue line), 2.6×10^{-4} M (green line), 3.3×10^{-4} M (violet line); b) the linear fit of the CD signal response of the supramolecular system **1** taking the point of the maximum CD signal at 314 nm. The fitting equation curve is y=36.91x+3.50, R^2=0.986. The abscissa intercept is equal to -0.095 ± 0.020 mM, corresponding to a Tartaric acid content equal to 2.28 ± 0.13 g/L.

A2.5.4. Chardonnay

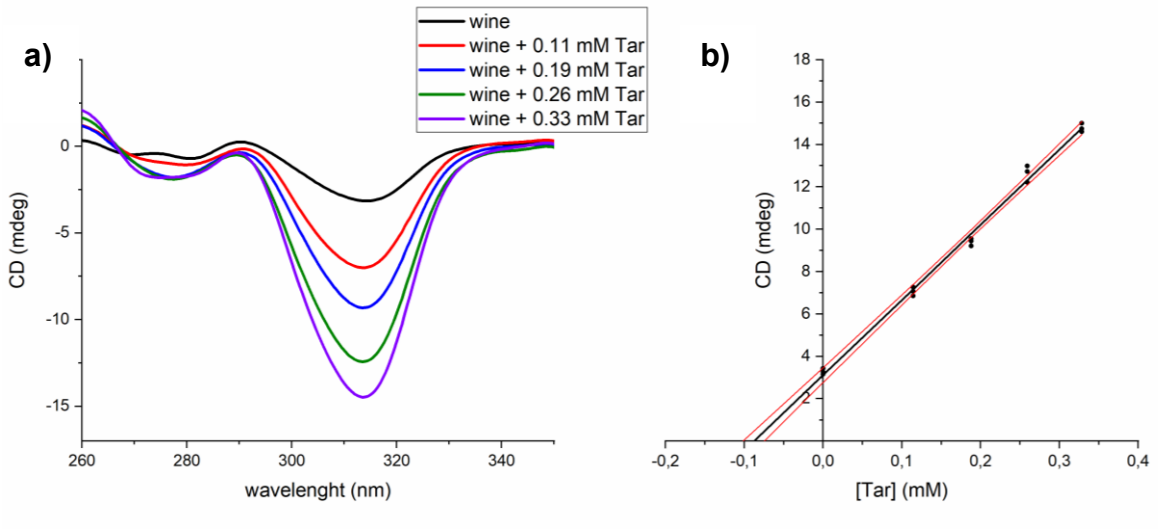

Figure A14. a) Circular Dichroism spectra in Ellipticity (mdeg) within the range 260-350 nm of the supramolecular system **1** with 5 µL of Chardonnay wine and different content in L-tartaric acid, respectively equal to 0.0×10^{-4} M (black line), 1.1×10^{-4} M (red line), 1.9×10^{-4} M (blue line), 2.6×10^{-4} M (green line), 3.3×10^{-4} M (violet line); b) the linear fit of the CD signal response of the supramolecular system **1** taking the point of the maximum CD signal at 314 nm. The fitting equation curve is y=35.51x+3.11, R^2=0.993. The abscissa intercept is equal to -0.087 ± 0.013 mM, corresponding to a Tartaric acid content equal to 1.68 ± 0.09 g/L.

A2.5.5. Valpolicella

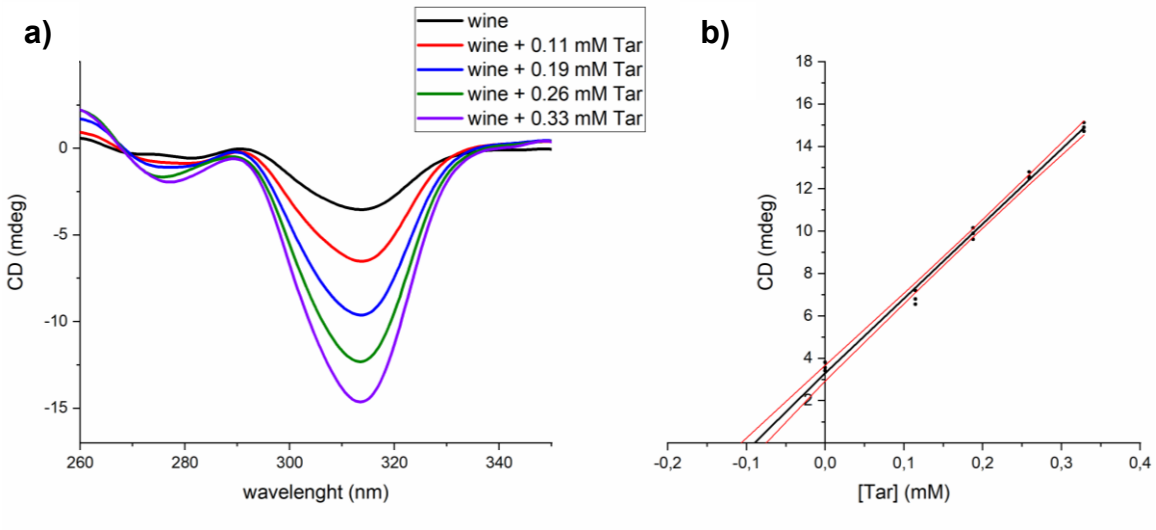

Figure A15. a) Circular Dichroism spectra in Ellipticity (mdeg) within the range 260-350 nm of the supramolecular system **1** with 5 µL of Valpolicella wine and different content in L-tartaric acid, respectively equal to $0.0x10^{-4}$ M (black line), $1.1x10^{-4}$ M (red line), $1.9x10^{-4}$ M (blue line), $2.6x10^{-4}$ M (green line), $3.3x10^{-4}$ M (violet line); b) the linear fit of the CD signal response of the supramolecular system **1** taking the point of the maximum CD signal at 314 nm. The fitting equation curve is y=35.24x+3.30, R^2=0.991. The abscissa intercept is equal to -0.094 ± 0.015 mM, corresponding to a Tartaric acid content equal to 2.24 ± 0.09 g/L.

A2.5.6. Müller-Thurgau

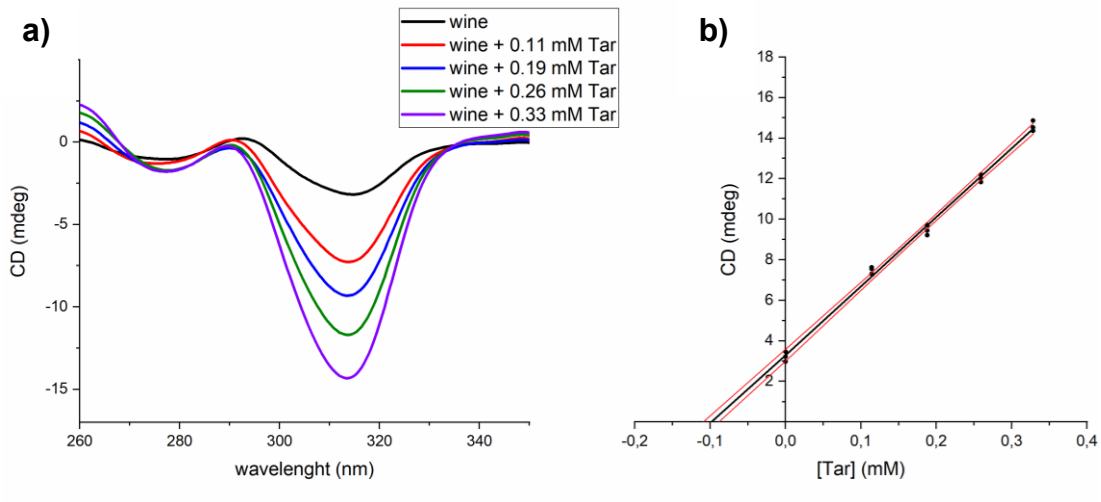

Figure A16. a) Circular Dichroism spectra in Ellipticity (mdeg) within the range 260-350 nm of the supramolecular system **1** with 10 µL of Müller-Thurgau wine and different content in L-tartaric acid, respectively equal to $0.0x10^{-4}$ M (black line), $1.1x10^{-4}$ M (red line), $1.9x10^{-4}$ M (blue line), $2.6x10^{-4}$ M (green line), $3.3x10^{-4}$ M (violet line); b) the linear fit of the CD signal response of the supramolecular system **1** taking the point of the maximum CD signal at 314 nm. The fitting equation curve is y=34.04x+3.29, R^2=0.995. The abscissa intercept is equal to -0.097± 0.012 mM, corresponding to a Tartaric acid content equal to 1.16 ± 0.08 g/L.

A2.5.7. Barbera

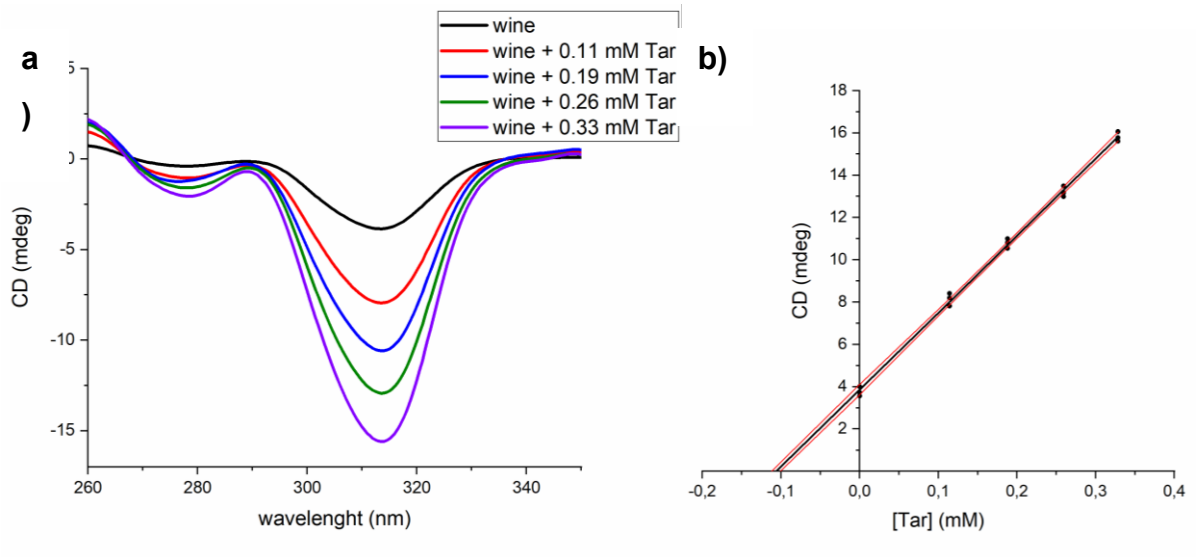

Figure A17. a) Circular Dichroism spectra in Ellipticity (mdeg) within the range 260-350 nm of the supramolecular system **1** with 5 µL of Barbera wine and different content in L-tartaric acid, respectively equal to $0.0x10^{-4}$ M (black line), $1.1x10^{-4}$ M (red line), $1.9x10^{-4}$ M (blue line), $2.6x10^{-4}$ M (green line), $3.3x10^{-4}$ M (violet line); b) the linear fit of the CD signal response of the supramolecular system **1** taking the point of the maximum CD signal at 314 nm. The fitting equation curve is y=36.44x+3.85, R^2=0.997. The abscissa intercept is equal to -0.106± 0.010 mM, corresponding to a Tartaric acid content equal to 2.54 ± 0.06 g/L.

A2.6. NMR and ESI-MS Characterization

A2.6.1. L-Tar@1

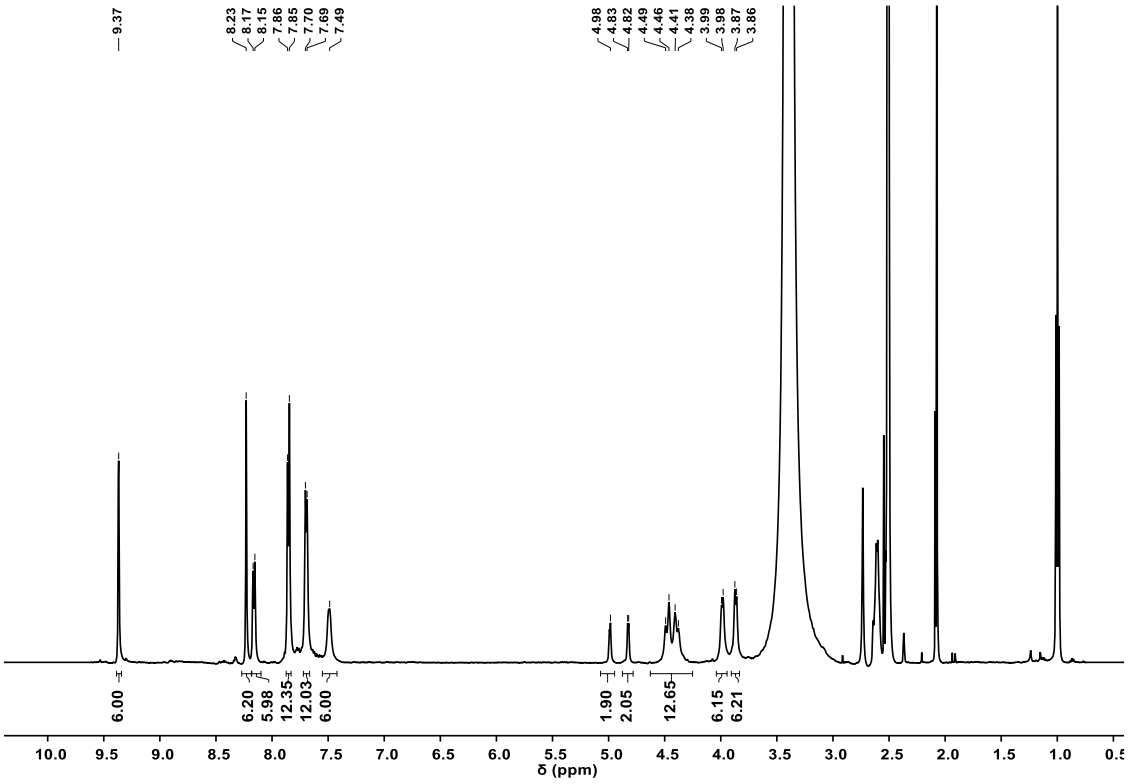

Figure A18. ^{1}H-NMR spectrum (500 MHz, 301 K, DMSO-d_6) of cage **L-Tar@1**.

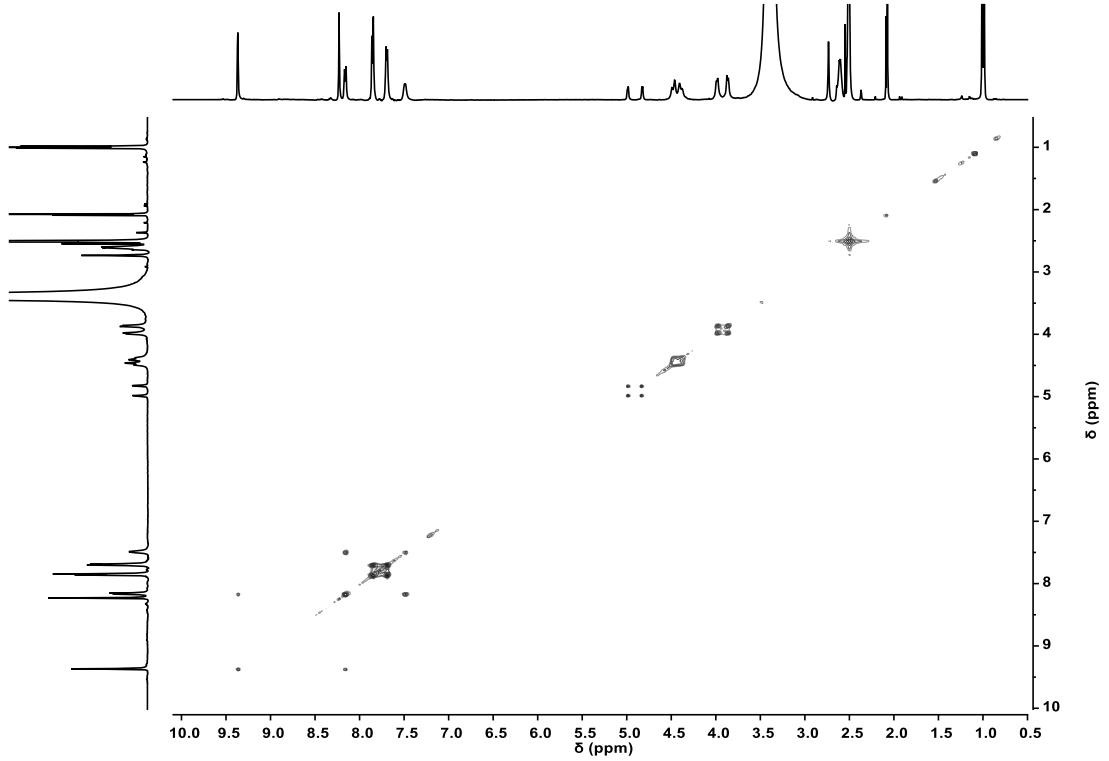

Figure A19. ^{1}H-^{1}H COSY spectrum (500 MHz, 301 K, DMSO-d_6) of cage **L-Tar@1**.

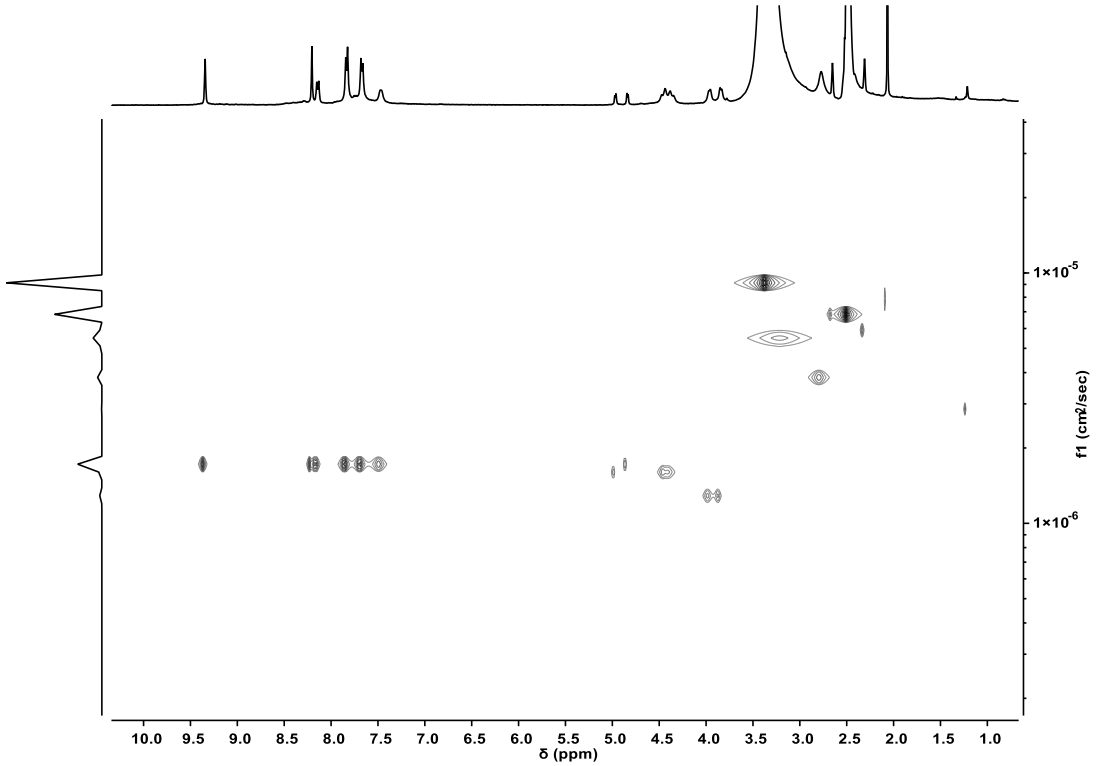

Figure A20. DOSY spectrum (400 MHz, 301 K, DMSO-d_6) of cage **L-Tar@1**. The diffusion coefficient for the molecular cage **Tar@1** was calculated to be 1.63 x 10^{-10} m^2 s^{-1}, corresponding to a hydrodynamic radius (r_H) of 9.8 Å. The hydrodynamic radius was calculated using Stokes-Einstein equation.[6-7]

A2.6.2. L-Mal@1

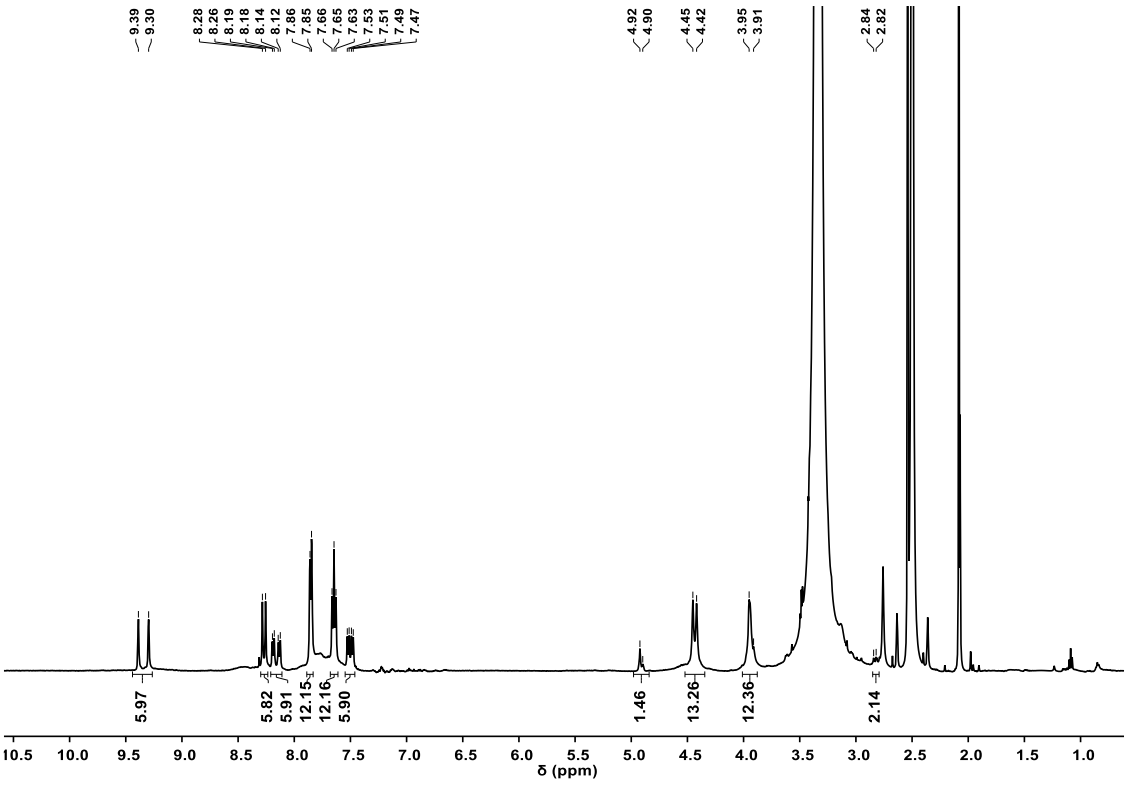

Figure A21. ^{1}H-NMR spectrum (500 MHz, 301 K, DMSO-d_6) of cage **L-Mal@1**.

A2.6.3. *R,S*-Cam@1

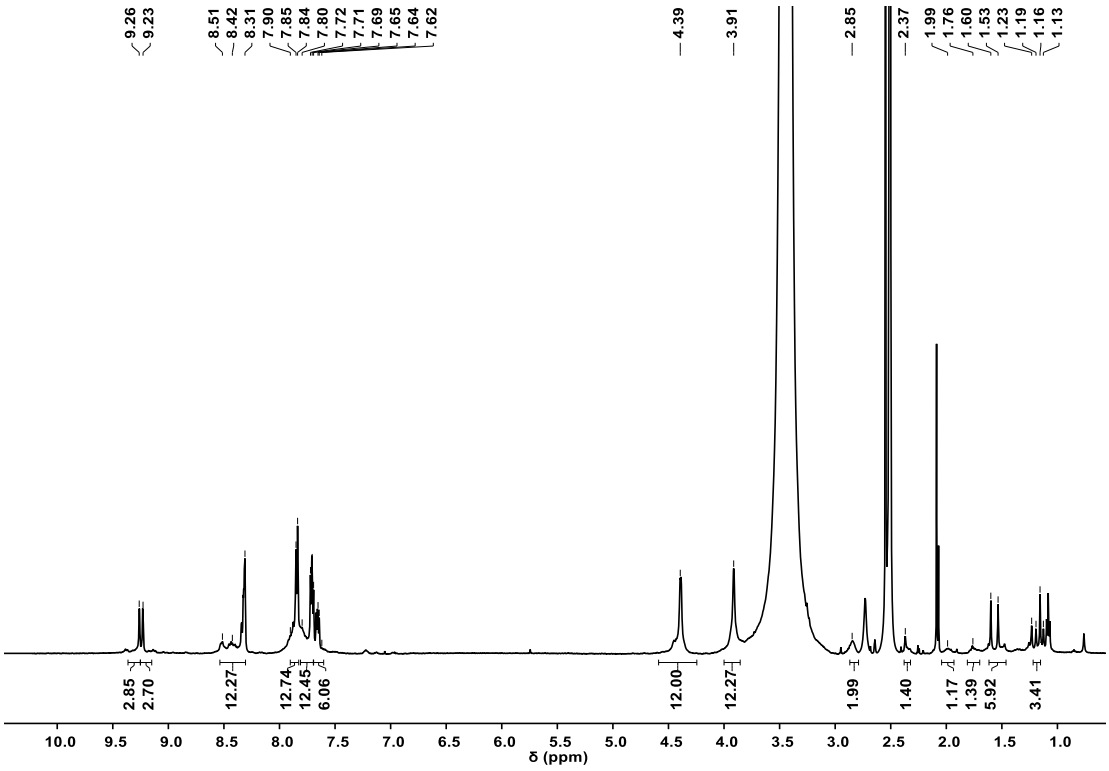

Figure A22. ^{1}H-NMR spectrum (500 MHz, 301 K, DMSO-d_6) of cage ***R,S*-Cam@1**.

A2.6.4. L-Glu@1

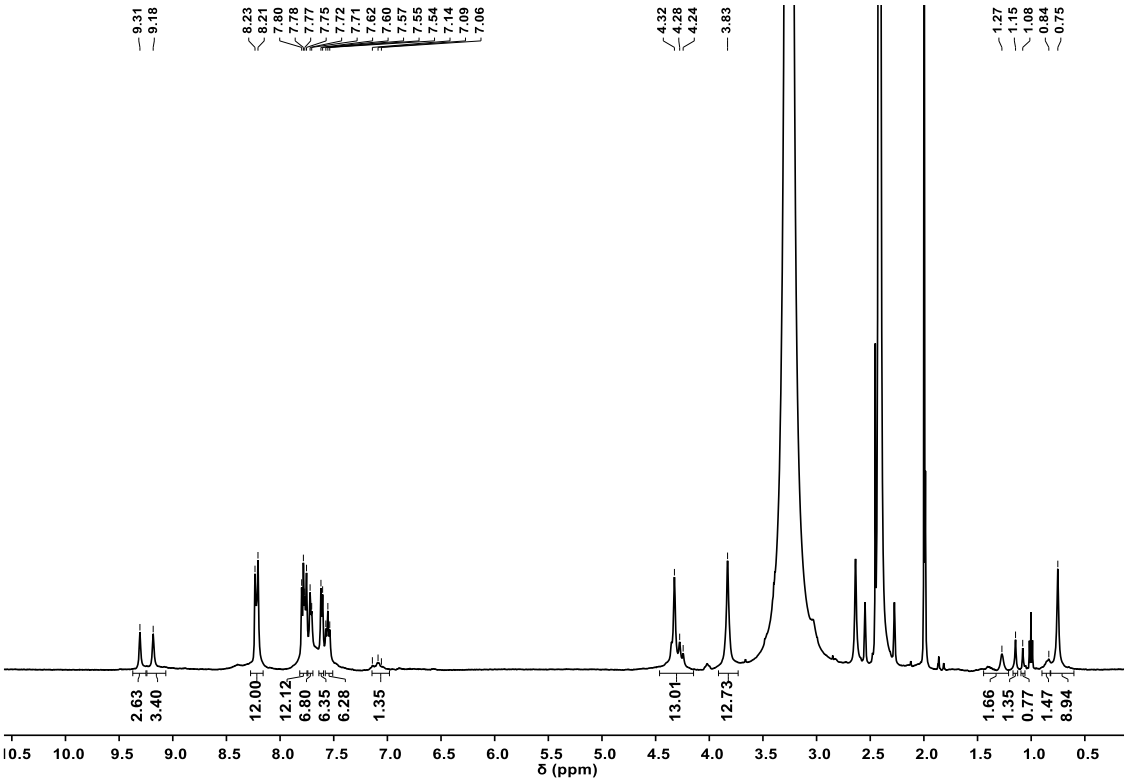

Figure A23. ^{1}H-NMR spectrum (500 MHz, 301 K, DMSO-d_6) of cage **L-Glu@1**.

A2.6.5. L-Asp@1

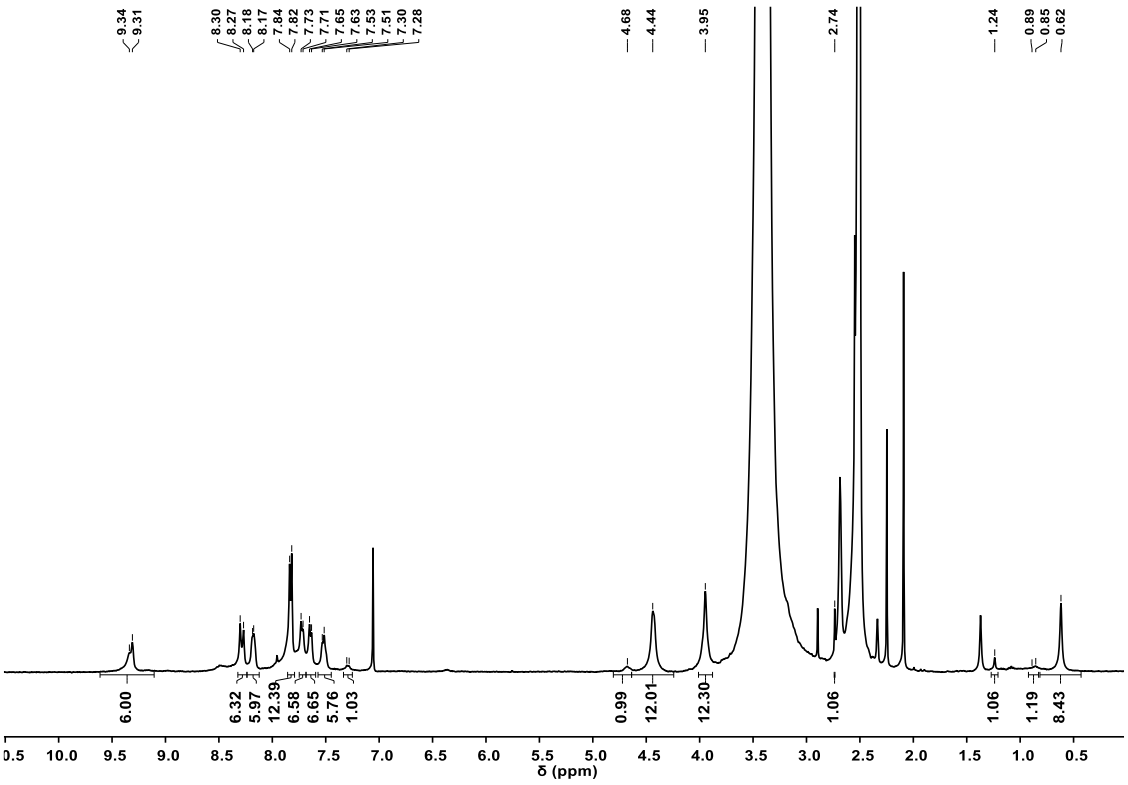

Figure A24. ^{1}H-NMR spectrum (500 MHz, 301 K, DMSO-d_6) of cage **L-Asp@1**.

A2.6.6. ESI-MS spectrum L-Tar@1

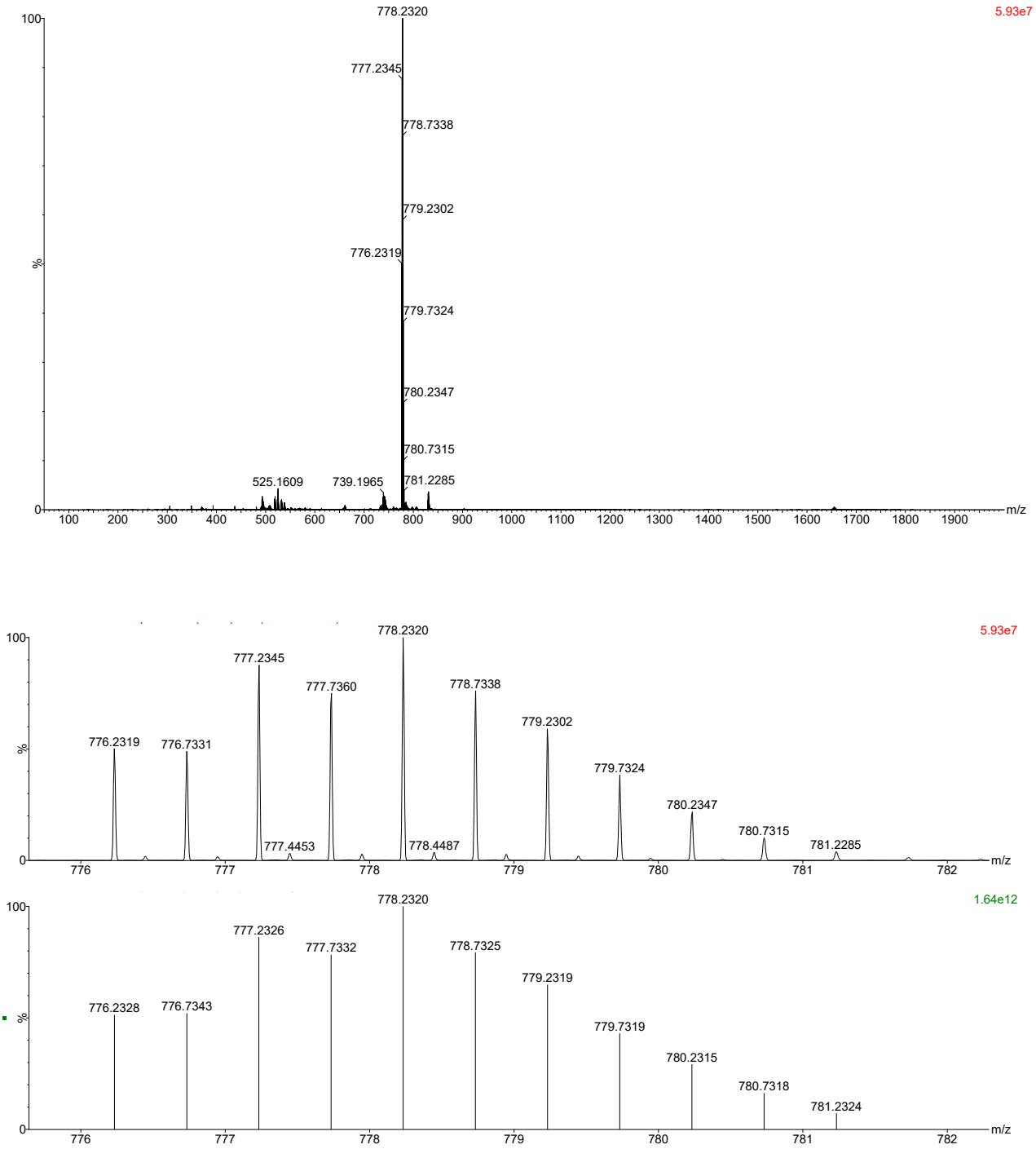

Figure A25. Experimental (top), and calculated (bottom) HRMS (ESI-TOF) pattern of **L-Tar@1** corresponding to $[C_{88}H_{76}N_{14}O_6Zn_2]^{2+}$ in CH_3CN/0.1% HCOOH.

A2.7. Binding constant determination

To 500 µL (0.5 µmol) of a solution 0.001 M of the cage **1** (based on *p*-xylene standard) in DMSO-d_6, 30 µL (0.36 µmol) of a solution 0.012 M in DMSO-d_6 of *p*-xylene were added. Small aliquots of the guest solution were titrated into this NMR tube. The solution was allowed to equilibrate at room temperature during 30 seconds before acquiring the ^{1}H NMR spectrum.

Due to the slow exchange regime, the determination of binding constant was possible thanks to the direct integration of the signals of the pyridine ring α proton of the filled cage and the empty cage in the region between 9.5 ppm and 8.5 ppm using equation:

$$K_b = \frac{[HG]}{[H][G]}$$

where the concentrations of [H] and [HG] have been determined by direct integration of the peaks, [G] has been determined by difference between added $[G]_0$ and measured [HG]. The NMR spectrum of the empty cage shows unsymmetric signals in DMSO. In particular, in the region of the pyridine ring α proton 9.3 ppm and 8.5 ppm. [H] has been determined by the sum of the integrals of this region. Reported binding constants are the average value of the four binding constants measure after addition of 0.2, 0.4, 0.6 and 0.8 equivalents.

The binding constant values for each dicarboxylic acid (**L-Tar** and **L-Mal**) are displayed in Table A6.

Table A6. Binding constant values for **L-Tar** and **L-Mal** acids.

Diacid	**K_b (M^{-1})**	**± σ (M^{-1})**
L-Tar	$1.1 \cdot 10^5$	$1.7 \cdot 10^4$
L-Mal	$1.3 \cdot 10^5$	$2.3 \cdot 10^4$

A2.7.1. Titration Experiment of L-Tartaric Acid with Molecular Cage 1

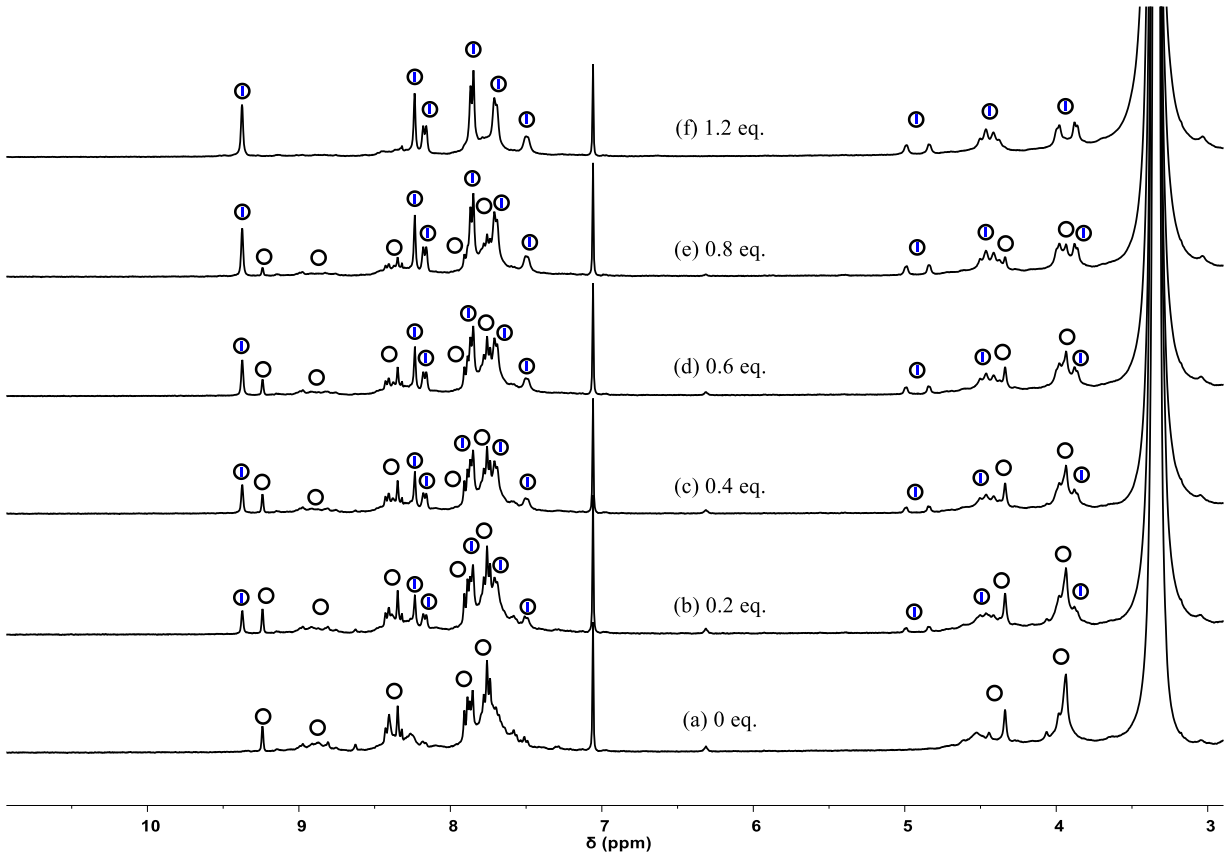

Figure A26. ^{1}H-NMR inclusion experiments (400 MHz, 301 K, DMSO-d_6). Addition of **L-Tar** in the preformed cage **1** in DMSO-d_6. The black circle indicates cage **1** blue stick indicates the dicarboxylic acid **L-Tar**. (a) Preformed cage **1** (0.001 M cage). (b)-(e) Addition of sub-stoichiometric amounts (0.2-0.8 equiv) of **L-Tar** results in the formation of a new species which could be attributed to 1:1 H:G complex. (f) Addition of 1.2 equiv of **L-Tar** totally shift the system to the new species **L-Tar@1**.

A2.7.2. Titration Experiment of L-Malic Acid with Molecular Cage 1

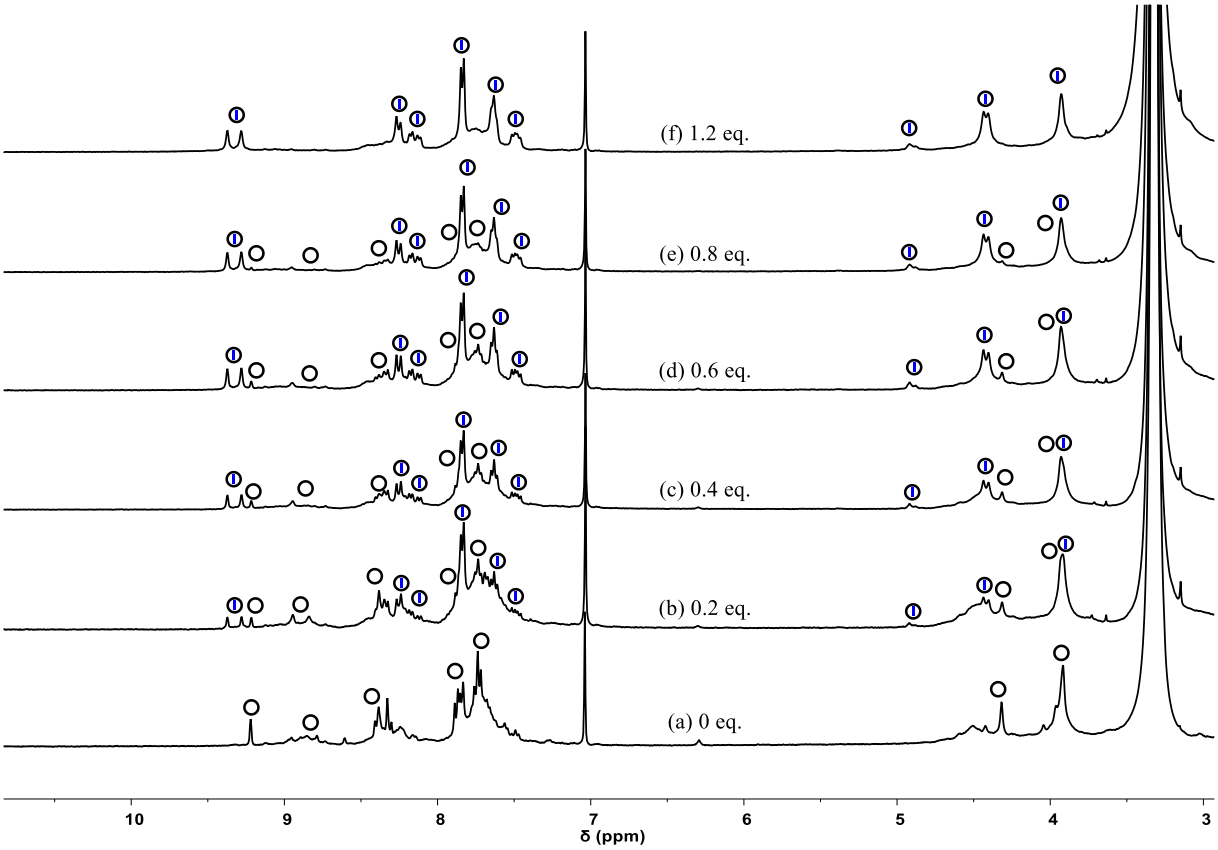

Figure A27. ^{1}H-NMR inclusion experiments (400 MHz, 301 K, DMSO-d_6). Addition of **L-Mal** in the preformed cage **1** in DMSO-d_6. The black circle indicates cage **1** blue stick indicates the dicarboxylic acid **L-Mal**. (a) Preformed cage **1** (0.001 M cage). (b)-(e) Addition of sub-stoichiometric amounts (0.2-0.8 equiv) of **L-Mal** results in the formation of a new species which could be attributed to 1:1 H:G complex. (f) Addition of 1.2 equiv of **L- Mal** totally shift the system to the new species **L-Mal@1**.

A2.8. Kinetic Experiment of Cage Formation Using Wine as Template

To 500 µL (1.0 µmol) of a solution 0.002 M of the zinc complex **2** in DMSO-d_6, 15 µL of red wine without pre-treatment and 125 µL (2.5 µmol) of a solution 0.02 M in DMSO-d_6 of ethylenediamine were added in a NMR tube. The cage formation was checked *via* ^{1}H-NMR and the complete assembly and encapsulation of L-**Tar** acid was observed after 20 minutes.

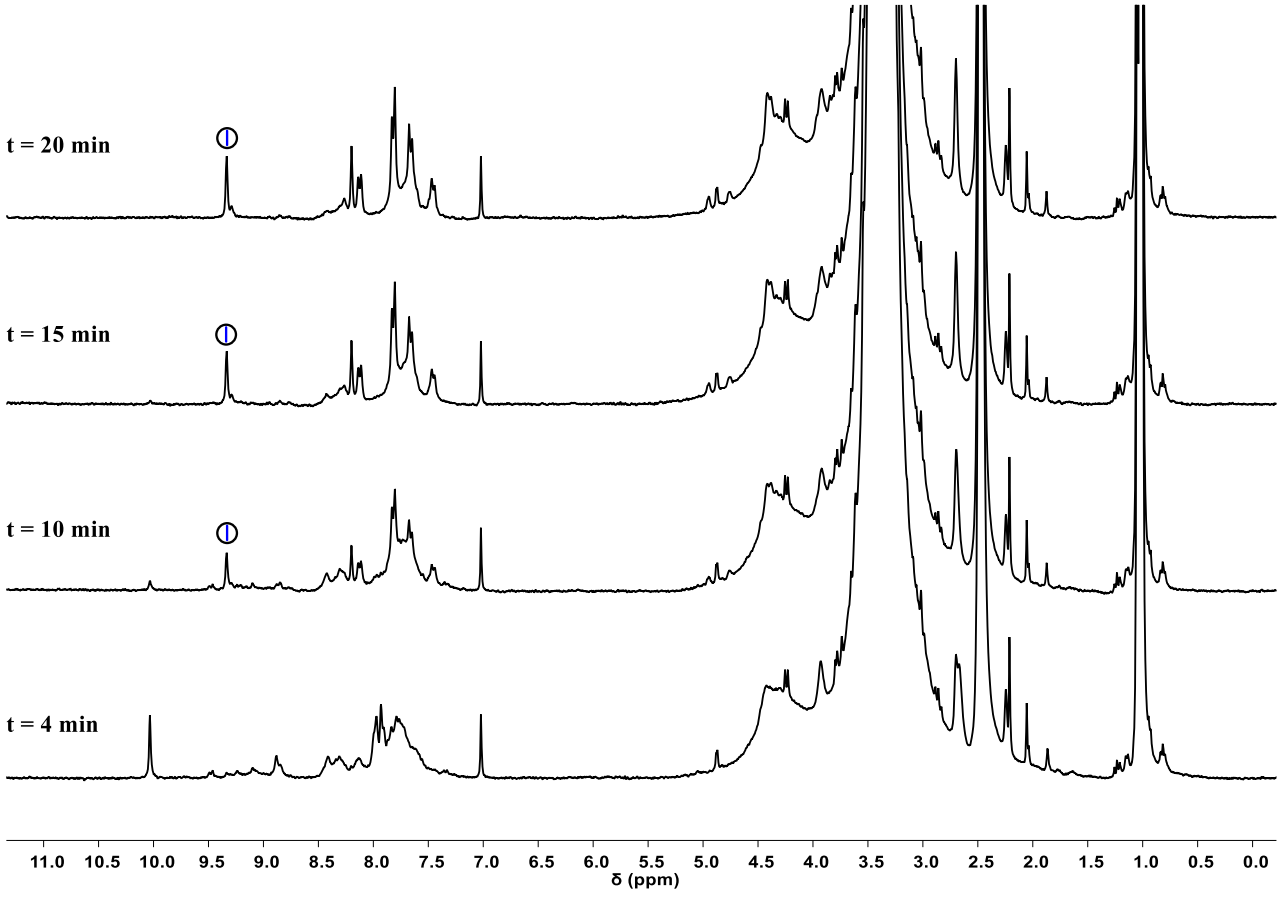

Figure A28. ^{1}H-NMR (300 MHz, 301 K, DMSO-d_6) of the cage formation at different times. The black circle indicates cage **1**, blue stick indicates the dicarboxylic acid L-**Tar**.

A2.9. Procedure for CD Data analysis with PCA

General Procedure

To 500 µL (1.0 µmol) of a solution 0.002 M of zinc complex **2** in DMSO-d_6, 15 µL (0.5 µmol) of complex mixture and 125 µL (2.5 µmol) of a solution 0.02 M in DMSO-d_6 of ethylenediamine were added. The mixture was left for 12 h at room temperature.
For the CD analysis, 200 µL of the mixture were diluted to 1 mL with dry DMSO and analyzed.
As complex mixtures, 3 red wines, 3 white wines, 3 Apple juices, 3 Pear juices, 3 Blueberry juices, 1 orange juice, and 1 lemon juice have been employed.
All the different mixtures were purchased at the local market in Padova.

The CD spectra were processed with Spectra Manager Version 2.15.3.1 and transformed into an xy coordinate sheet file. The non-vanishing portion of the spectra relative to the interval between 285 – 335 ppm were selected and analyzed with OriginPro 2018 (64-bit) SR1 b9.5.1.195. The data set was represented by a $n * m$ matrix X, where the n rows represent the number of points acquired during the measurement and the m columns represented the experiments characterized by a different complex mixture. In detail, the matrix was composed by a n=101 rows relative to the points of the spectra and m=13 columns relative to the number of complex mixtures utilized. Once the matrix was created, the Principal Component Analysis (PCA) was performed through the PCA for Spectroscopy script implemented into Origin which performs principal component analysis for spectra (IR, Fluorescence, UV-Vis, Raman, etc.). This tool allows to easily obtain a loading score as a plot in function of the PC1 (or PC2) and the wavelength of the spectra. In the case of PCA obtained from spectra data this kind of loading score result much clear and informative since the high number of the data points make the usual loading score (PC1 vs PC2) too crowded and complicated to understand.
The resulting PCA bidimensional plots were obtained from the score and coeff matrix from the pca function, considering the first and second principal components which account for the 99.6% of the total variance of the data set.

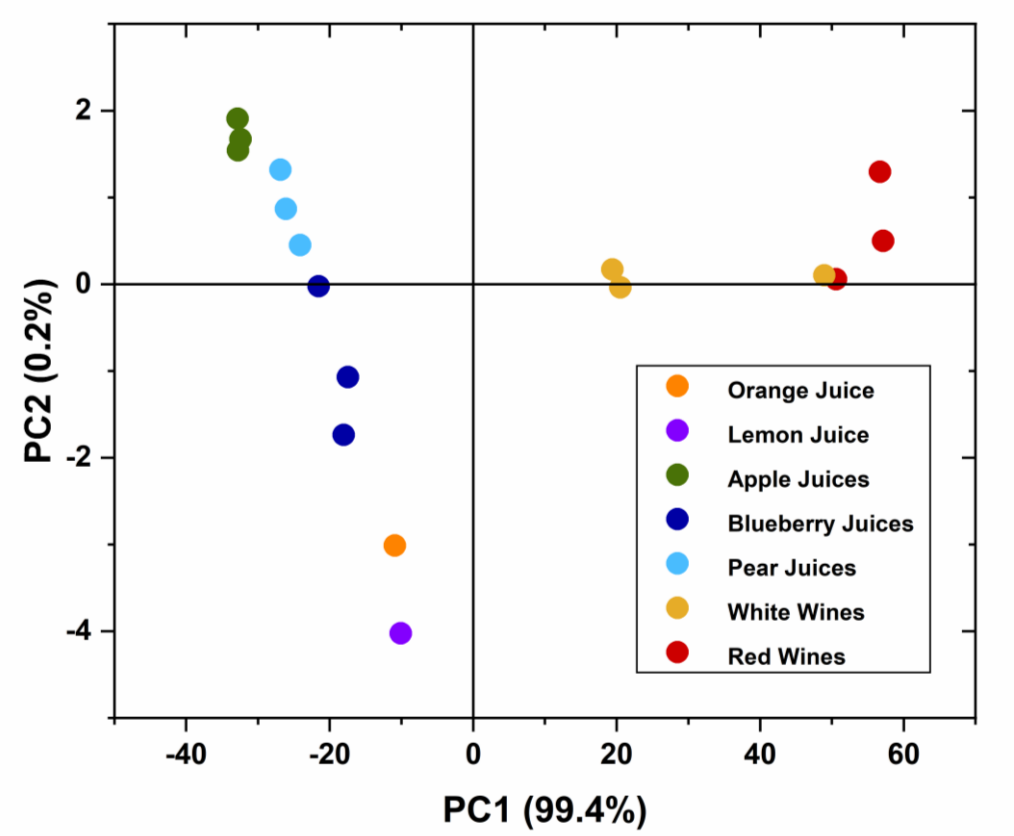

Figure A29. Scores plot of the first two principal components of the CD intensities matrix PCA.

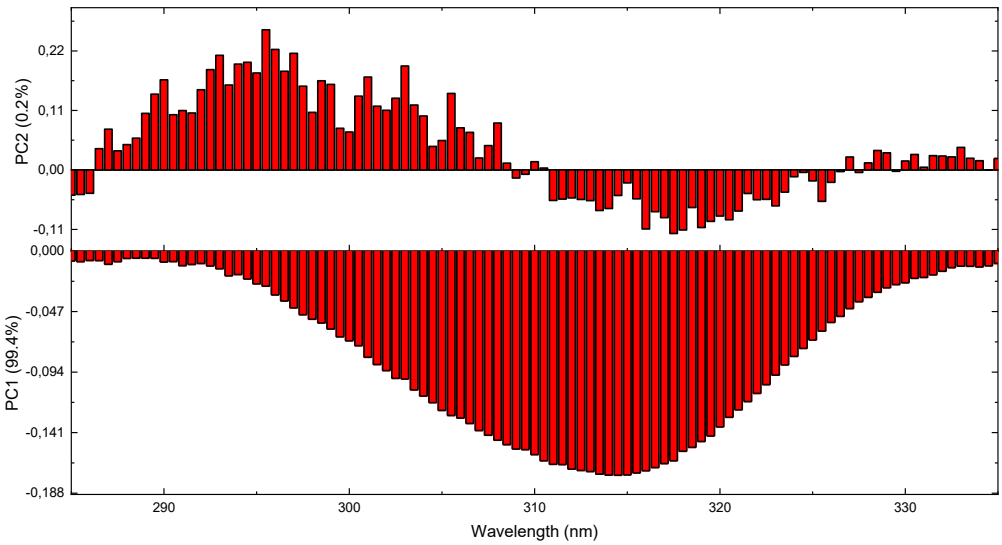

Figure A30. Loadings plot of the first two principal components along the wavelength interval 280-335 nm.

A2.10. Circular Dichroism Spectra

A2.10.1. Prosecco@1

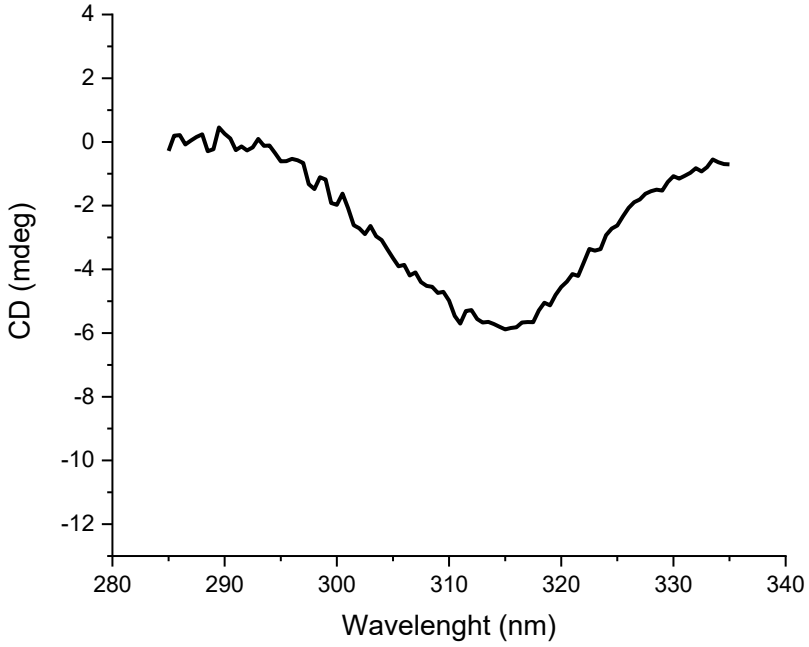

Figure A31. CD spectrum of cage **R@1** formed using Prosecco wine as complex mixture.

A2.10.2. Chardonnay@1

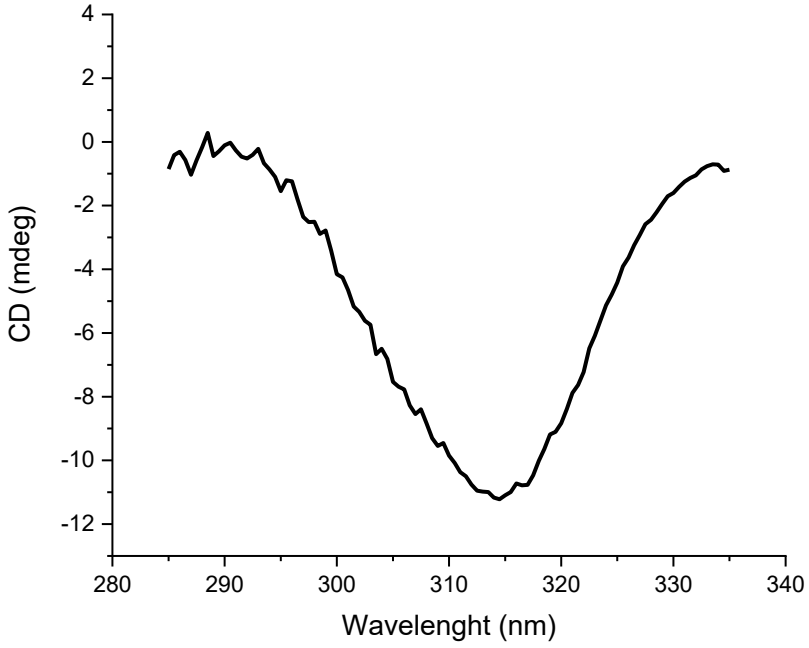

Figure A32. CD spectrum of cage **R@1** formed using Chardonnay wine as complex mixture.

A2.10.3. Chianti@1

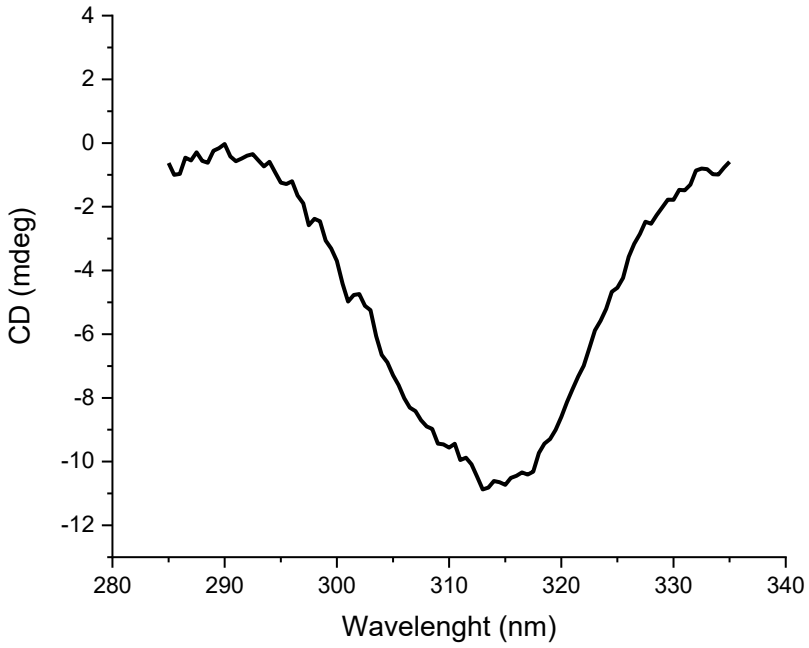

Figure A33. CD spectrum of cage **R@1** formed using Chianti wine as complex mixture.

A2.10.4. Valpolicella@1

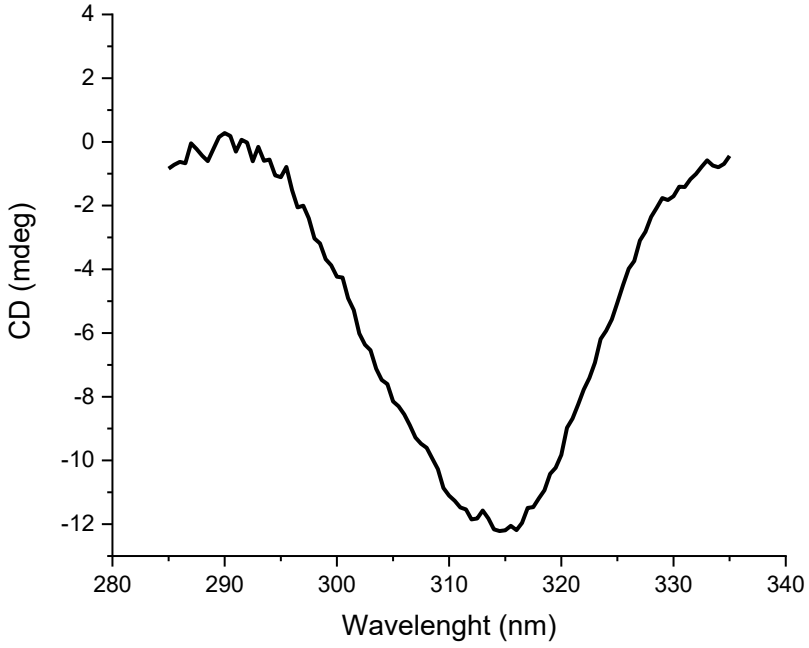

Figure A34. CD spectrum of cage **R@1** formed using Valpolicella wine as complex mixture.

A 1 Müller-Thurgau@1

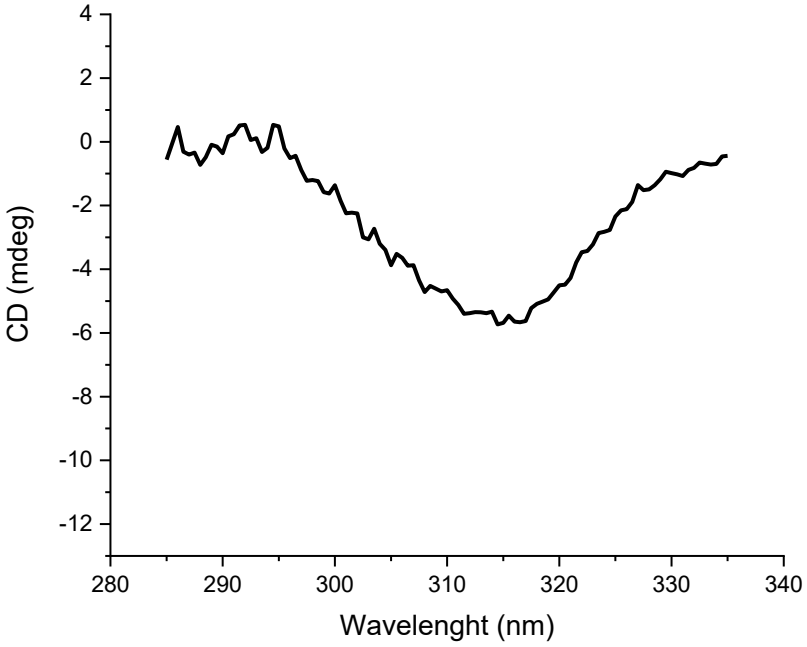

Figure A35. CD spectrum of cage **R@1** formed using Müller-Thurgau wine as complex mixture.

A 2 Barbera@1

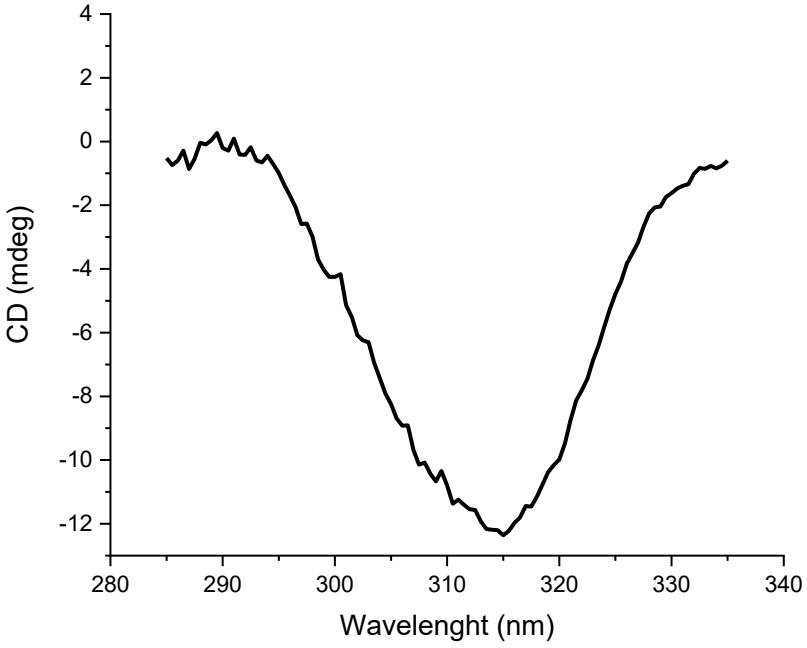

Figure A36. CD spectrum of cage **R@1** formed using Barbera wine as complex mixture.

A2.10.5. Blueberry juice-1@1

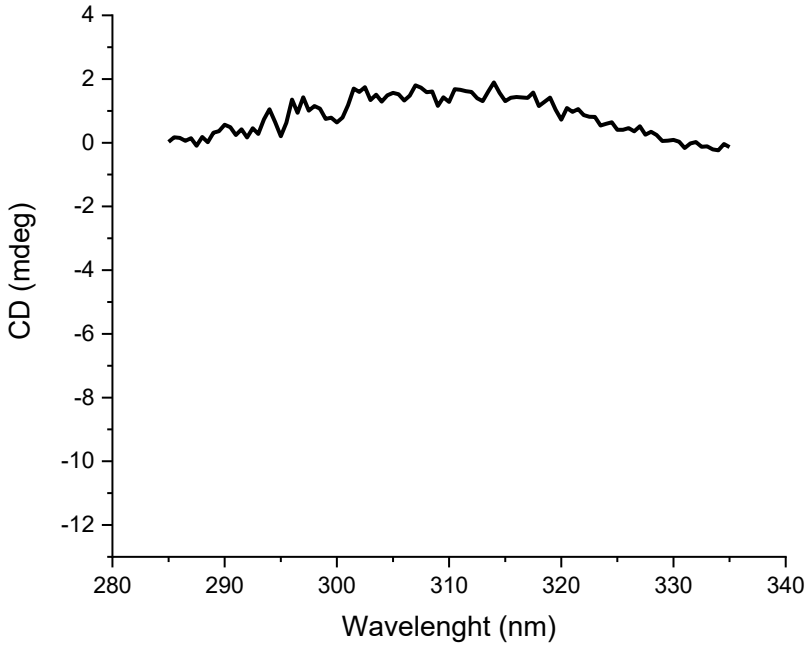

Figure A37. CD spectrum of cage **R@1** formed using Blueberry juice as complex mixture.

A2.10.6. Blueberry juice-2@1

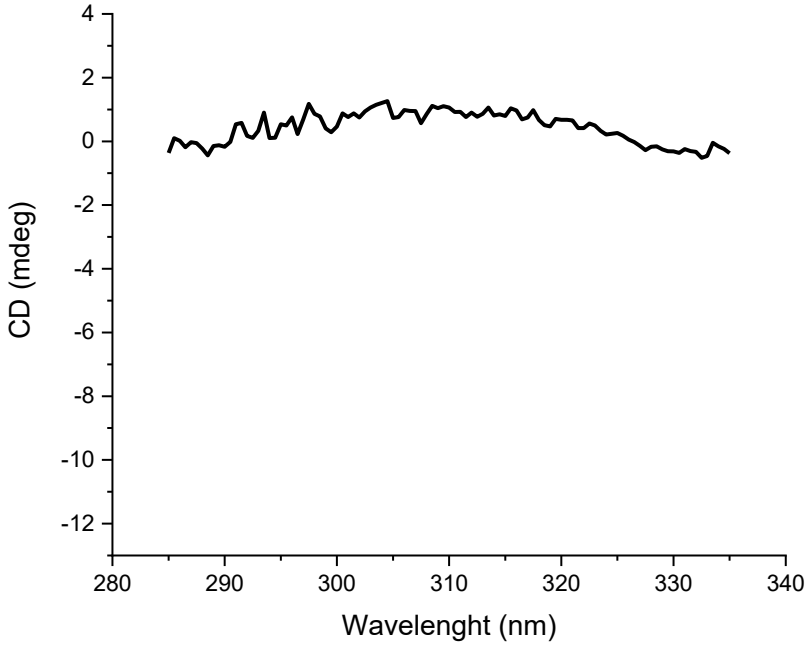

Figure A38. CD spectrum of cage **R@1** formed using Blueberry juice as complex mixture.

A2.10.7. Blueberry juice-3@1

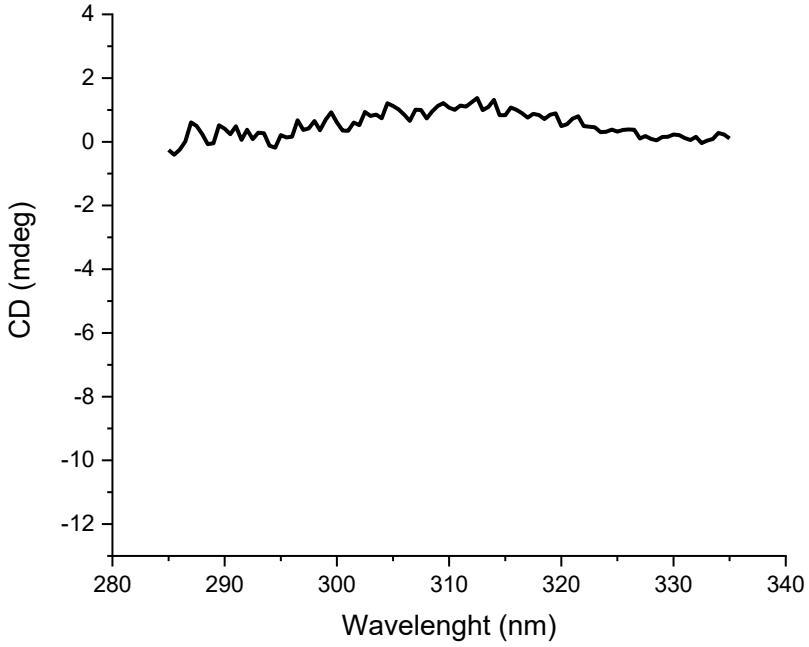

Figure A39. CD spectrum of cage **R@1** formed using Blueberry juice as complex mixture.

A2.10.8. Apple juice-1@1

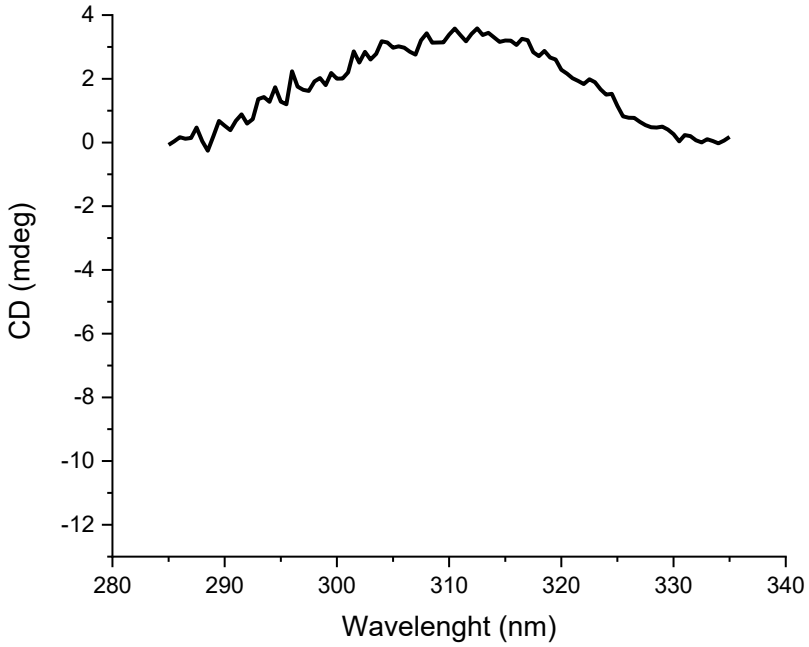

Figure A40. CD spectrum of cage **R@1** formed using Apple juice as complex mixture.

A2.10.9. Apple juice-2@1

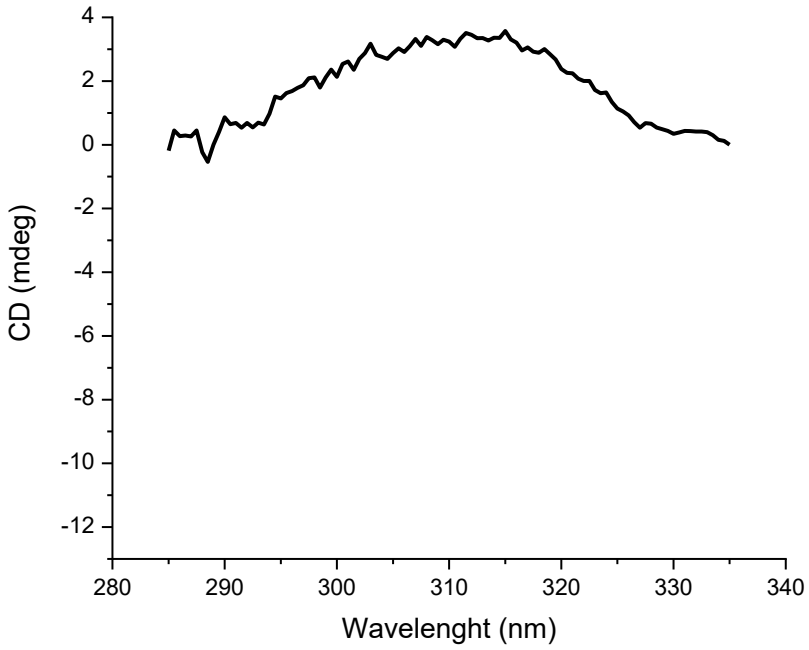

Figure A41. CD spectrum of cage **R@1** formed using Apple juice as complex mixture.

A2.10.10. Apple juice-3@1

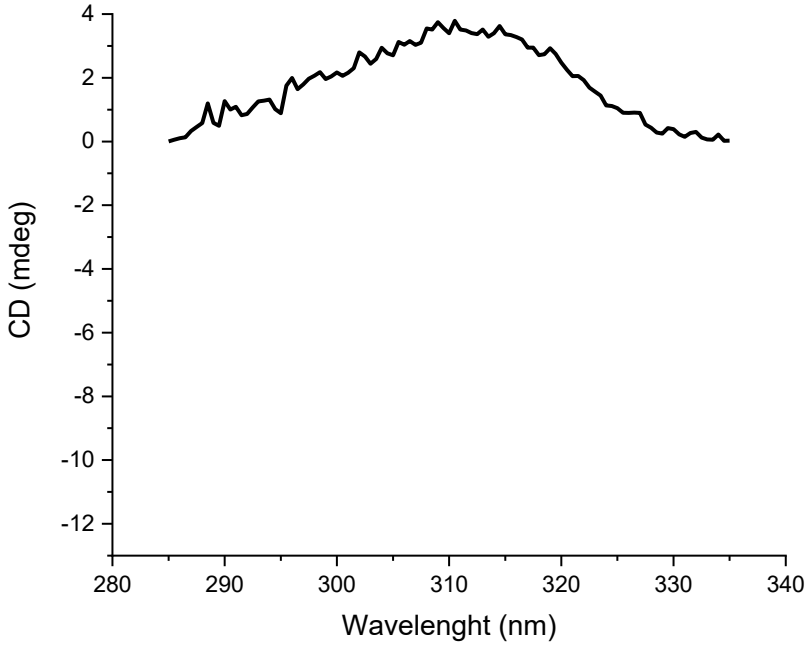

Figure A42. CD spectrum of cage **R@1** formed using Apple juice as complex mixture.

A2.10.11. Pear juice-1@1

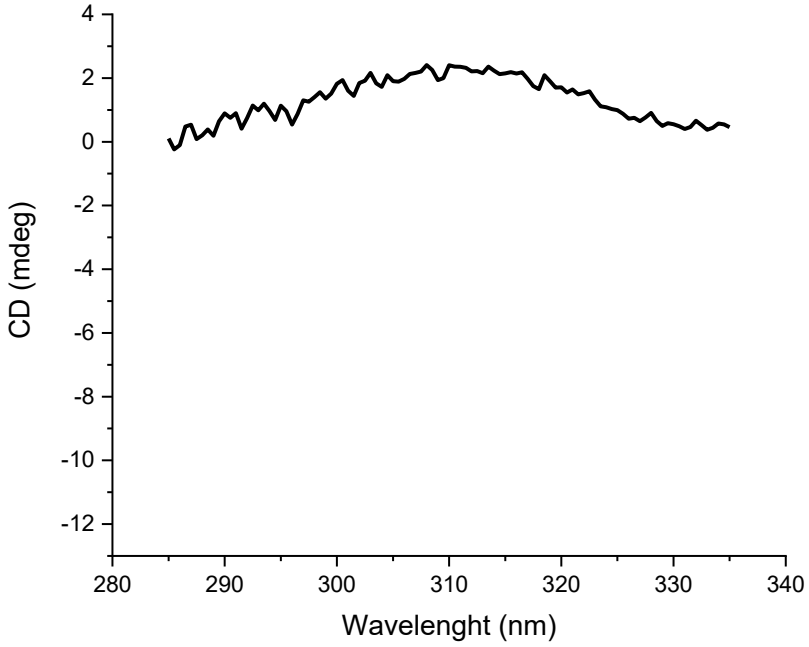

Figure A43. CD spectrum of cage **R@1** formed using Pear juice as complex mixture.

A2.10.12. Pear juice-2@1

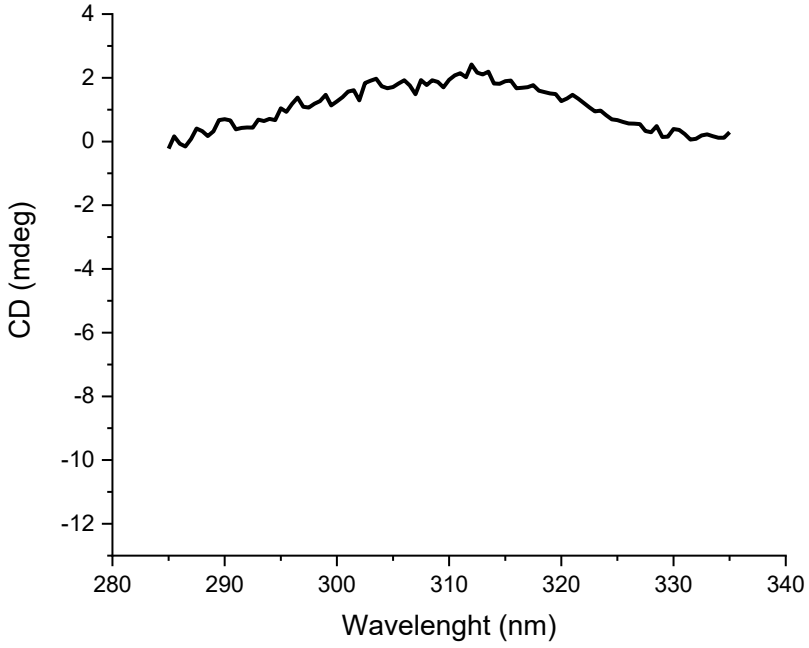

Figure A44. CD spectrum of cage **R@1** formed using Pear juice as complex mixture.

A2.10.13. Pear juice-3@1

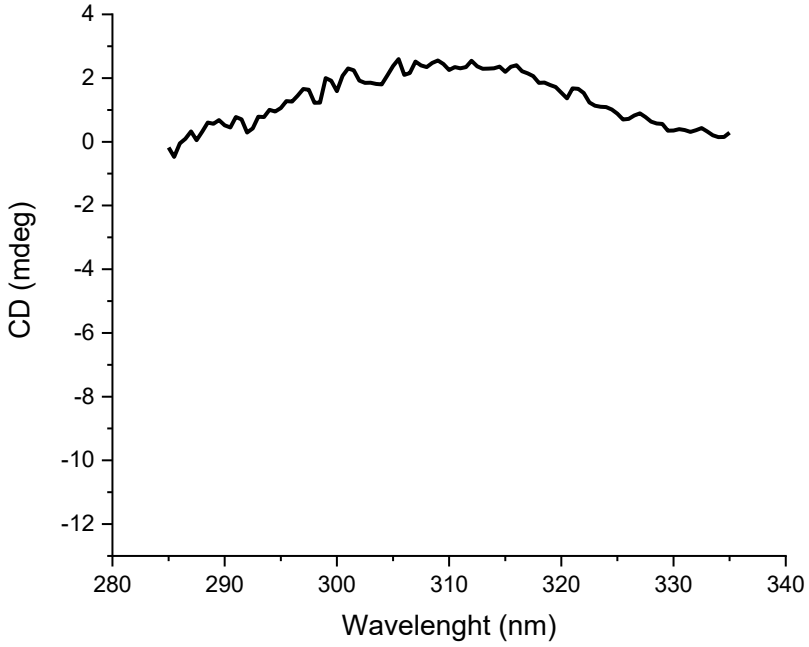

Figure A45. CD spectrum of cage **R@1** formed using Pear juice as complex mixture.

A2.10.14. Orange Juice@1

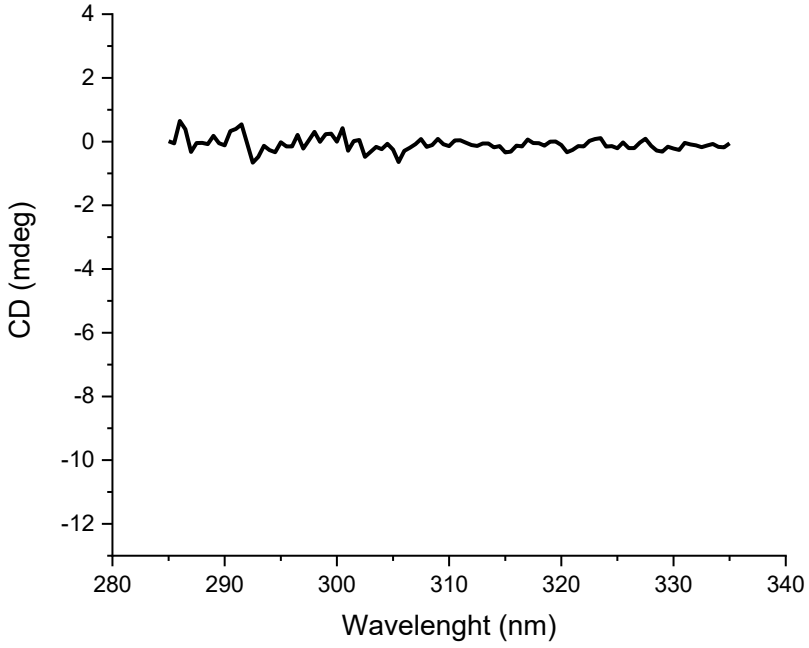

Figure A46. CD spectrum of cage **R@1** formed using Orange squeezed juice as complex mixture.

A2.10.15. Lemon Juice@1

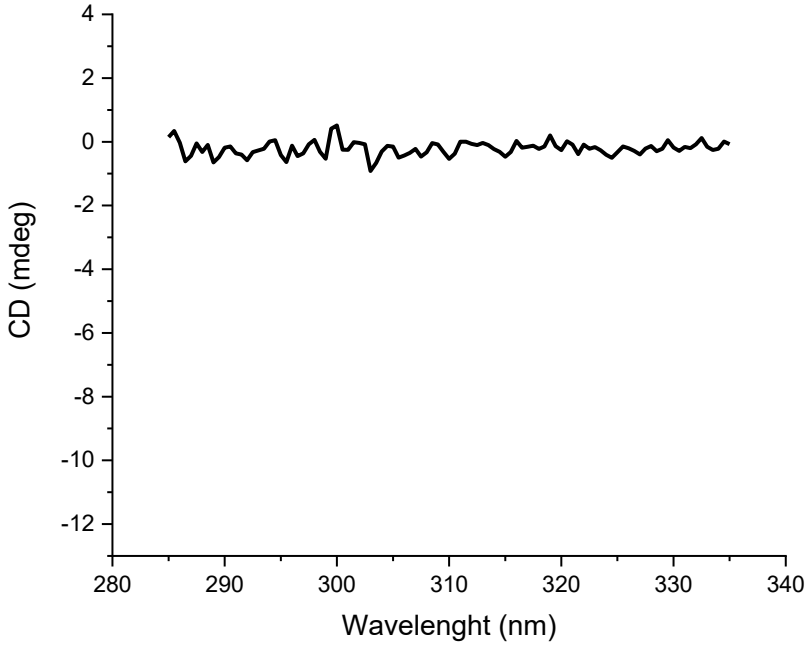

Figure A47. CD spectrum of cage **R@1** formed using Lemon squeezed juice as complex mixture.

A2.11. Quantification of Dicarboxylic acids Content in the Complex Mixtures for the PCA Analysis

In order to determine the concertation of Tartaric and Malic in the complex mixtures, the concentration of cages **L-Tar@1** and **L-Mal@1** has been determined using *p*-xylene as internal standard.

Table A7. Quantification of **L -Tartaric** and **L-Malic** acids content in the complex mixtures.

Complex Mixture	L-Tartaric Acid (g/L)	L-Malic Acid (g/L)
Prosecco	1.3	1.6
Chianti	2.4	n.d
Chardonnay	1.5	1.6
Valpolicella	2.0	0.3
Müller-Thurgau	1.5	1.7
Barbera	2.5	n.d
Blueberry Juice-1	n.d	1.4
Blueberry Juice-2	n.d	2.5
Blueberry Juice-3	n.d	2.1
Apple Juice-1	n.d	4.7
Apple Juice-2	n.d	3.9
Apple Juice-3	n.d	4.0
Pear Juice-1	n.d	2.1
Pear Juice-2	n.d	2.7
Pear Juice-3	n.d	2.1
Lemon Juice	n.d	n.d
Orange Juice	n.d	n.d

A2.11.1. Prosecco@1

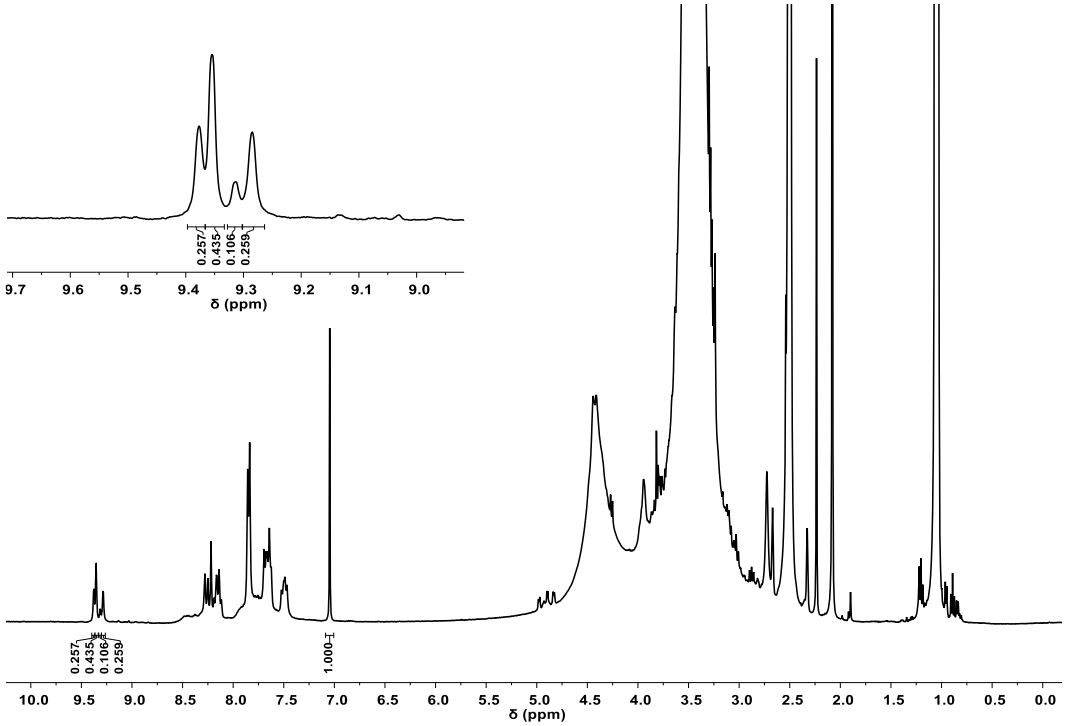

Figure A48. ^{1}H-NMR spectrum (400 MHz, 301 K, DMSO-d_6) of the system formed adding Prosecco wine without pre-treatment to the DMSO-d_6 solution containing complex **2** and ethylenediamine.

A2.11.2. Chianti@1

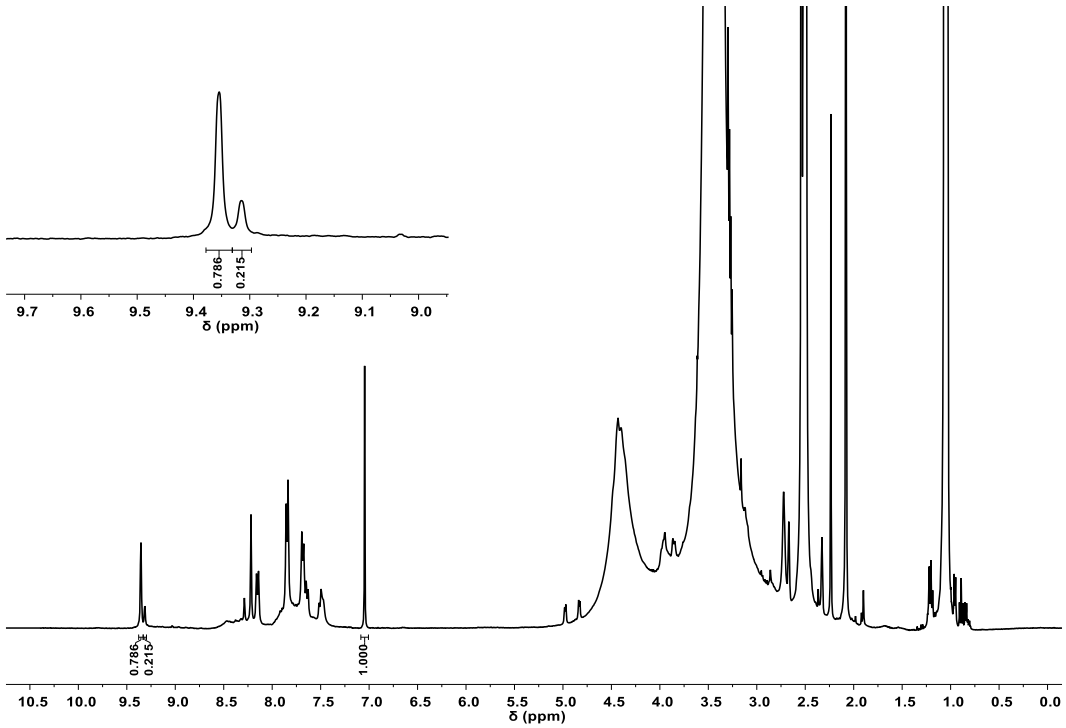

Figure A49. ^{1}H-NMR spectrum (400 MHz, 301 K, DMSO-d_6) of the system formed adding Chianti wine without pre-treatment to the DMSO-d_6 solution containing complex **2** and ethylenediamine.

A2.11.3. Chardonnay@1

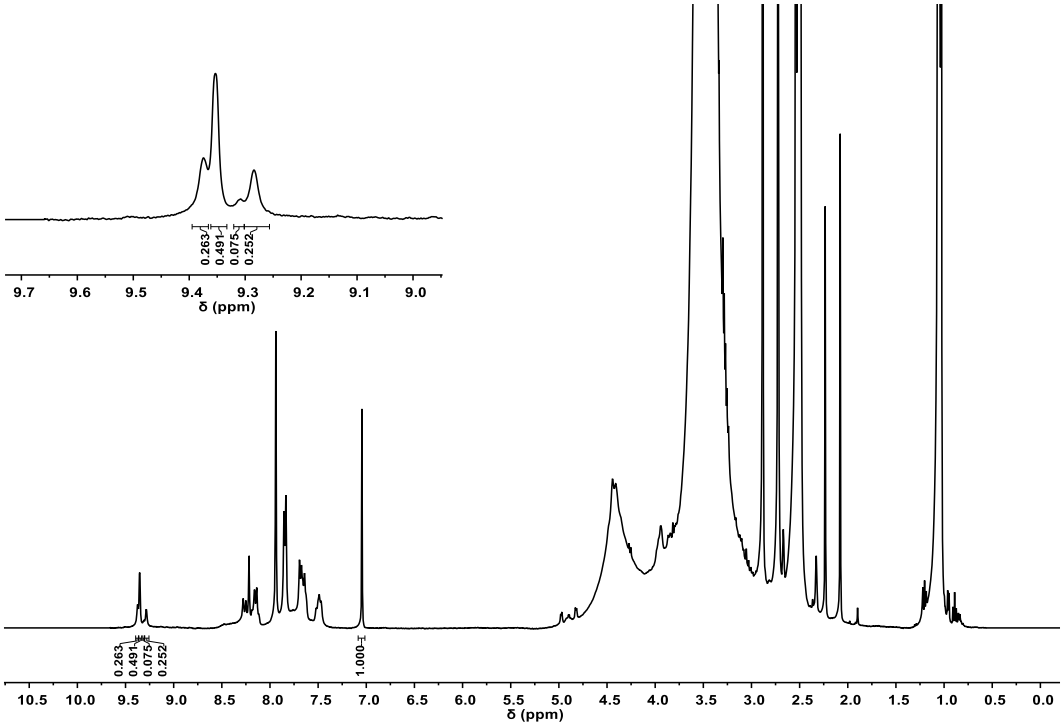

Figure A50 ^{1}H-NMR spectrum (400 MHz, 301 K, DMSO-d_6) of the system formed adding Chardonnay wine without pre-treatment to the DMSO-d_6 solution containing complex **2** and ethylenediamine.

A2.11.4. Valpolicella@1

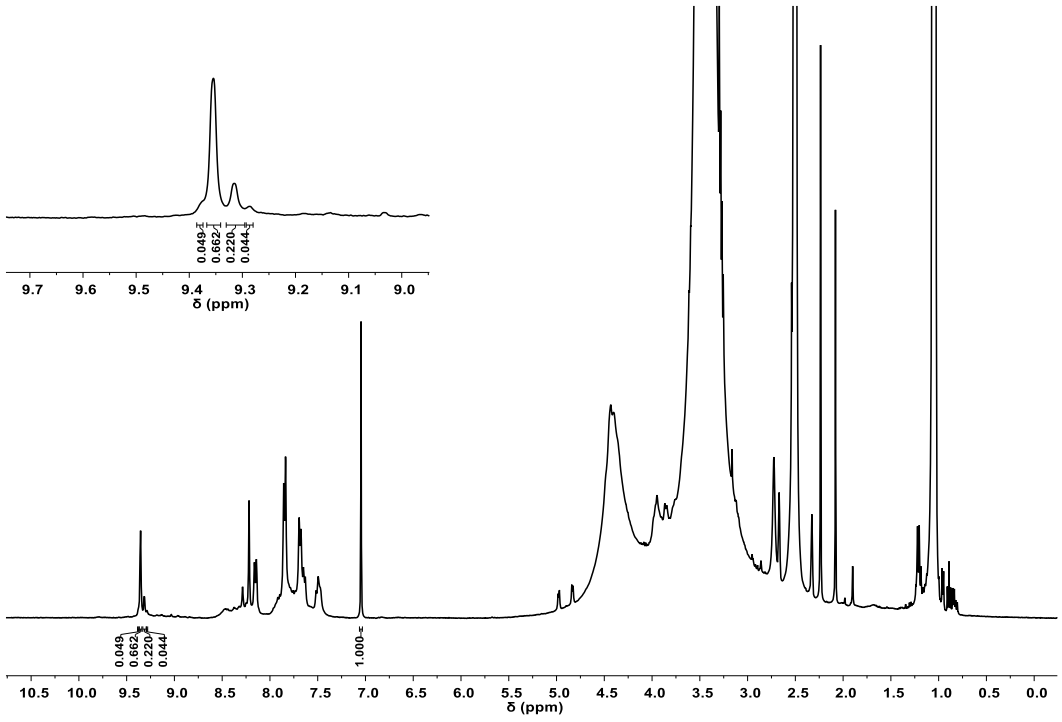

Figure A51. ^{1}H-NMR spectrum (400 MHz, 301 K, DMSO-d_6) of the system formed adding Valpolicella wine without pre-treatment to the DMSO-d_6 solution containing complex **2** and ethylenediamine.

A2.11.5. Müller-Thurgau@1

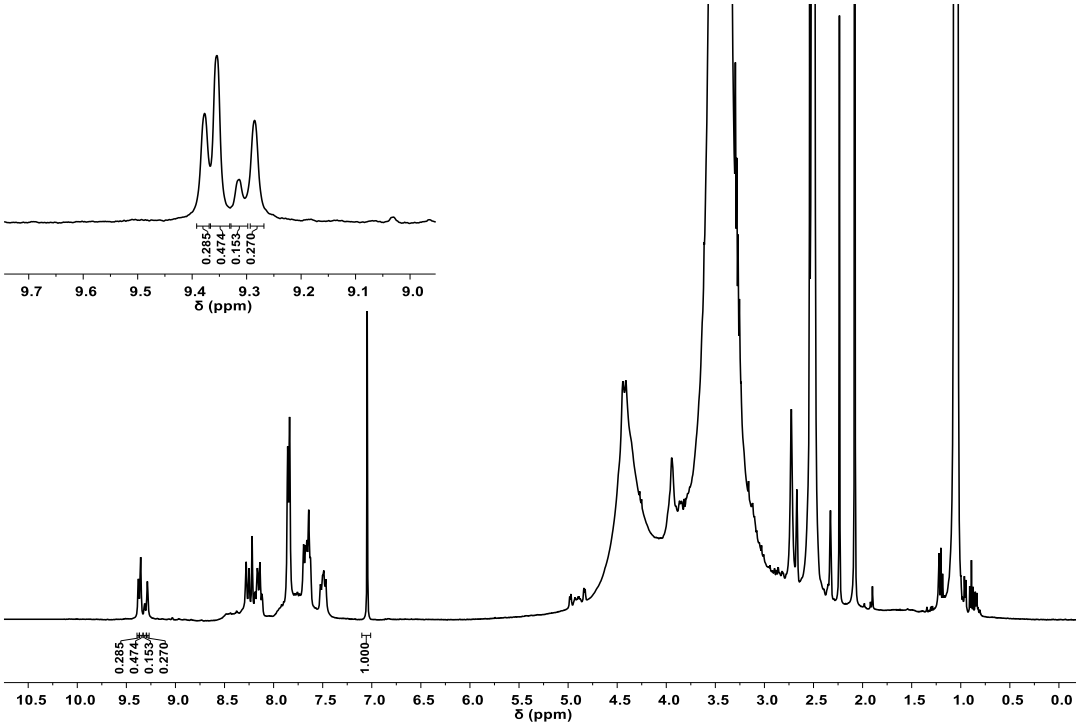

Figure A52. ^{1}H-NMR spectrum (400 MHz, 301 K, DMSO-d_6) of the system formed adding Müller-Thurgau wine without pre-treatment to the DMSO-d_6 solution containing complex **2** and ethylenediamine.

A2.11.6. Barbera@1

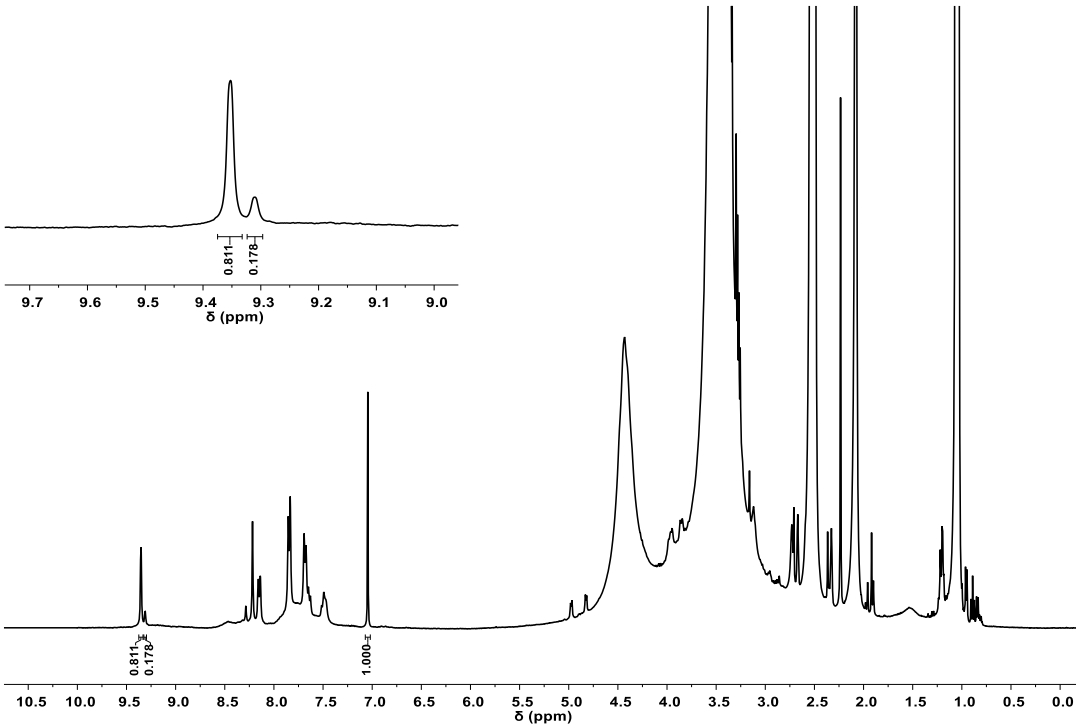

Figure A53. ^{1}H-NMR spectrum (400 MHz, 301 K, DMSO-d_6) of the system formed adding Barbera wine without pre-treatment to the DMSO-d_6 solution containing complex **2** and ethylenediamine.

A2.11.7. Blueberry juice-1@1

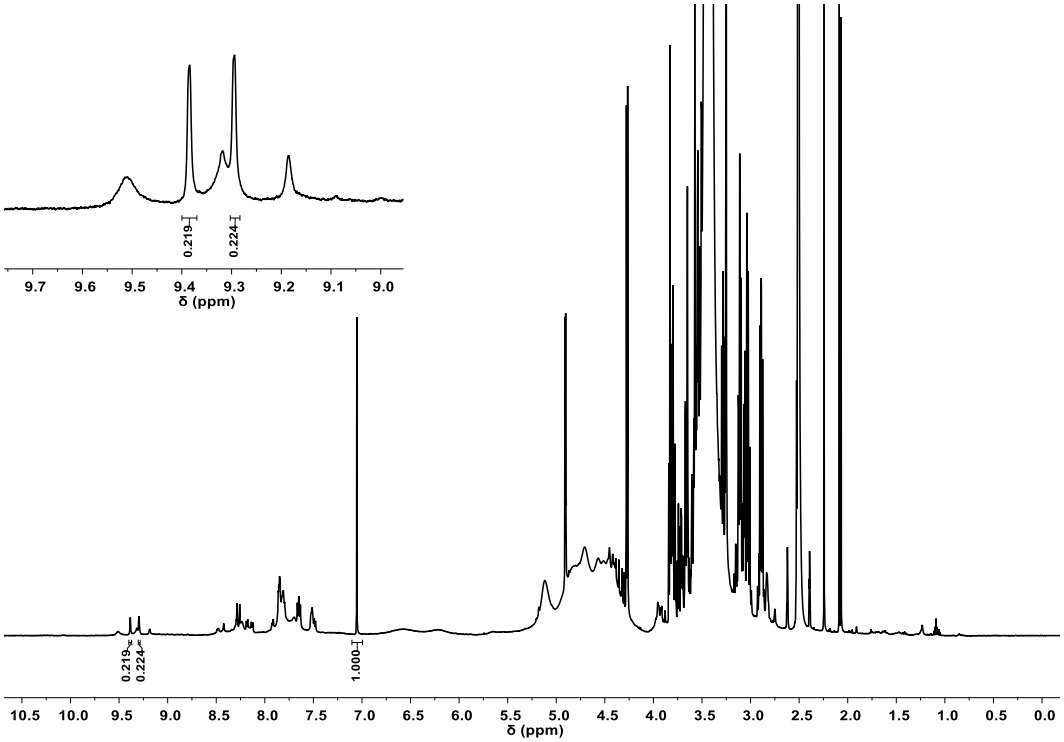

Figure A54. ^{1}H-NMR spectrum (600 MHz, 301 K, DMSO-d_6) of the system formed adding Blueberry juice without pre-treatment to the DMSO-d_6 solution containing complex **2** and ethylenediamine.

A2.11.8. Blueberry juice-2@1

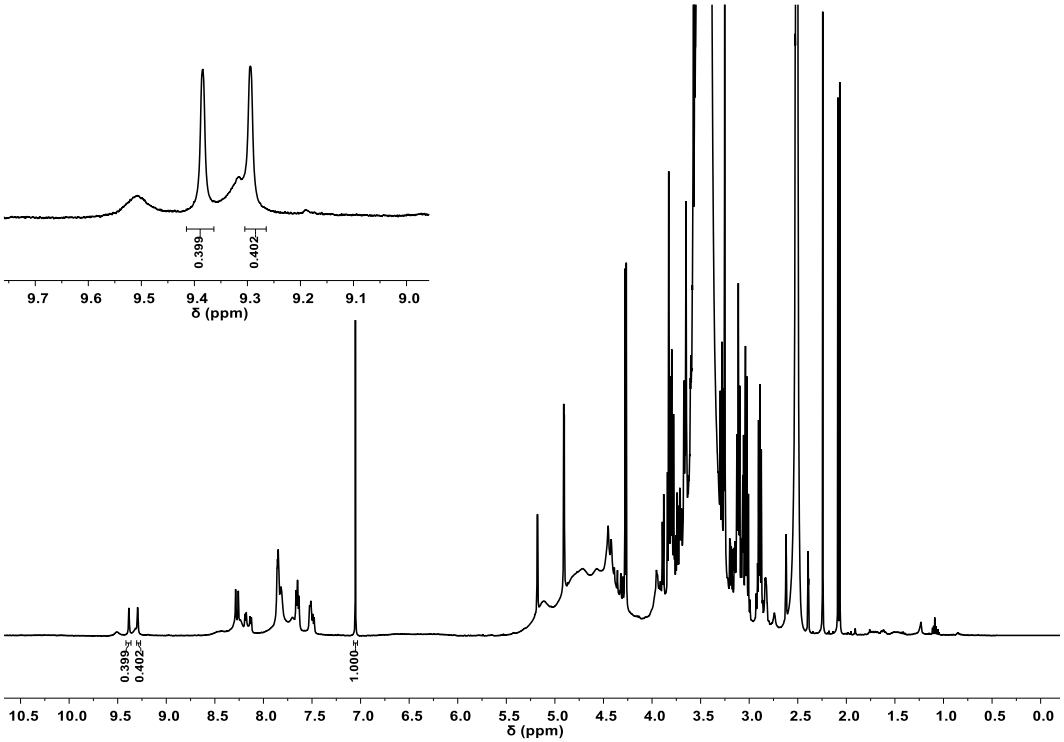

Figure A55. ^{1}H-NMR spectrum (400 MHz, 301 K, DMSO-d_6) of the system formed adding Blueberry juice without pre-treatment to the DMSO-d_6 solution containing complex **2** and ethylenediamine.

A2.11.9. Blueberry juice-3@1

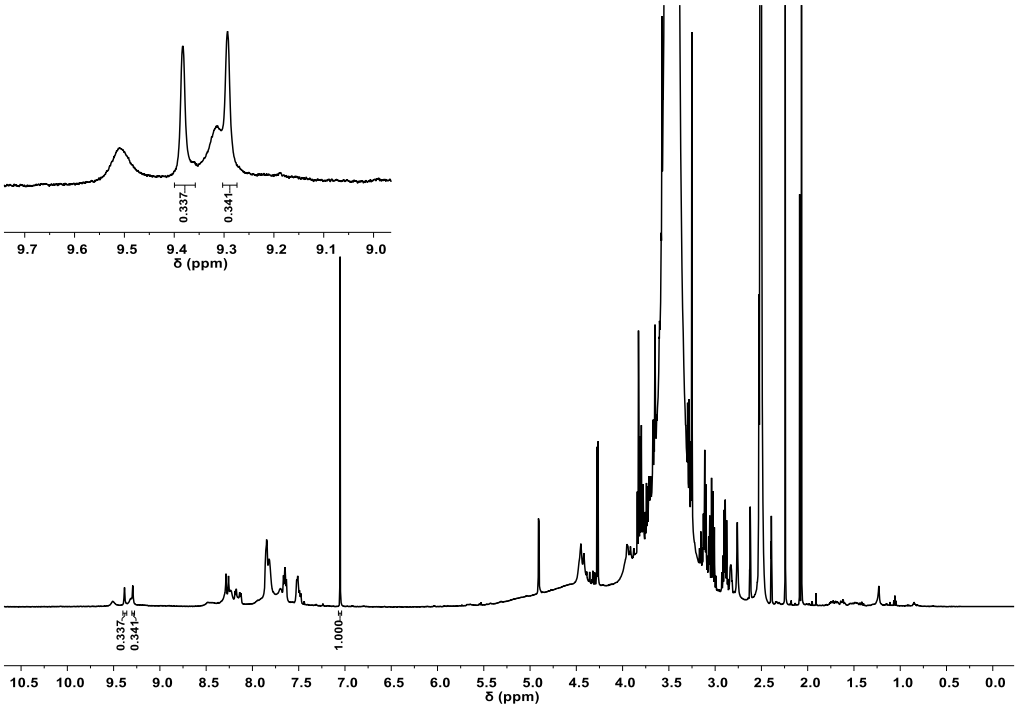

Figure A56. ^{1}H-NMR spectrum (600 MHz, 301 K, DMSO-d_6) of the system formed adding Blueberry juice without pre-treatment to the DMSO-d_6 solution containing complex **2** and ethylenediamine.

A2.11.10. Apple Juice-1@1

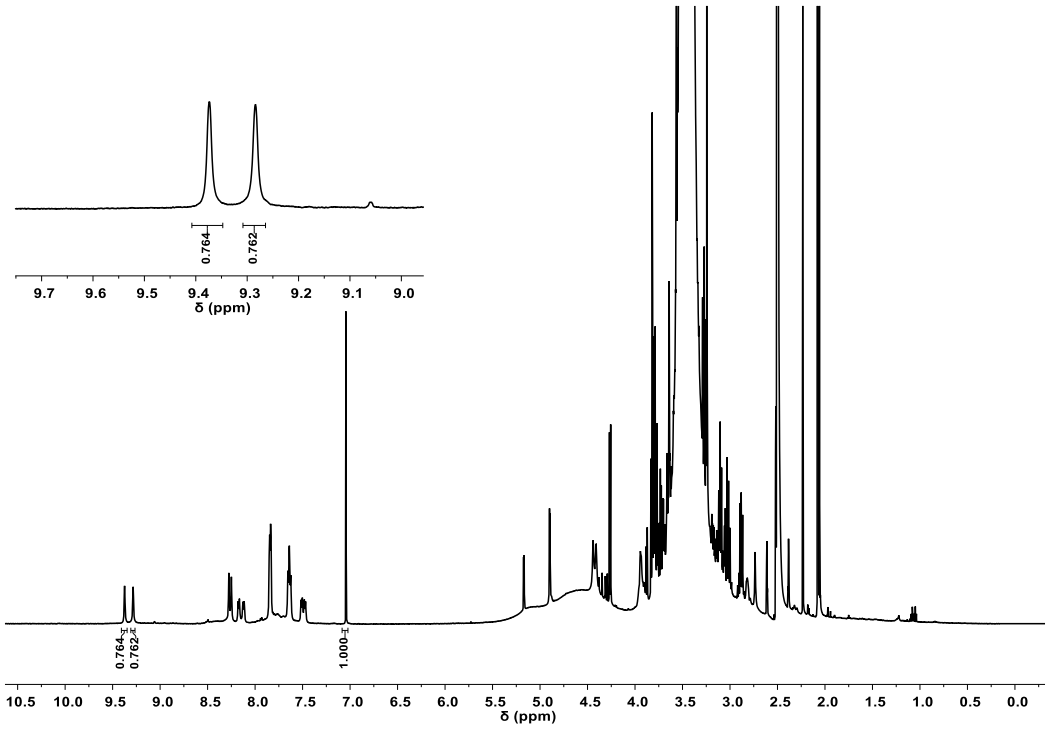

Figure A57. ^{1}H-NMR spectrum (400 MHz, 301 K, DMSO-d_6) of the system formed adding Apple juice without pre-treatment to the DMSO-d_6 solution containing complex **2** and ethylenediamine.

A2.11.11. Apple Juice-2@1

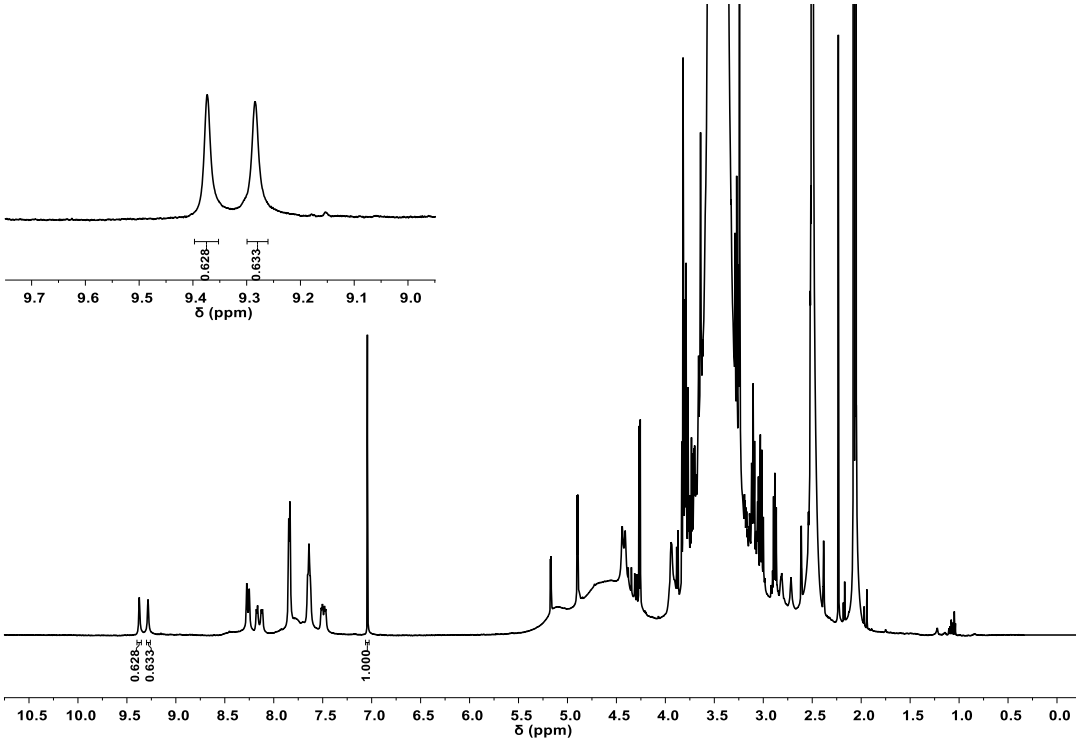

Figure A58. ^{1}H-NMR spectrum (600 MHz, 301 K, DMSO-d_6) of the system formed adding Apple juice without pre-treatment to the DMSO-d_6 solution containing complex **2** and ethylenediamine.

A2.11.12. Apple Juice-3@1

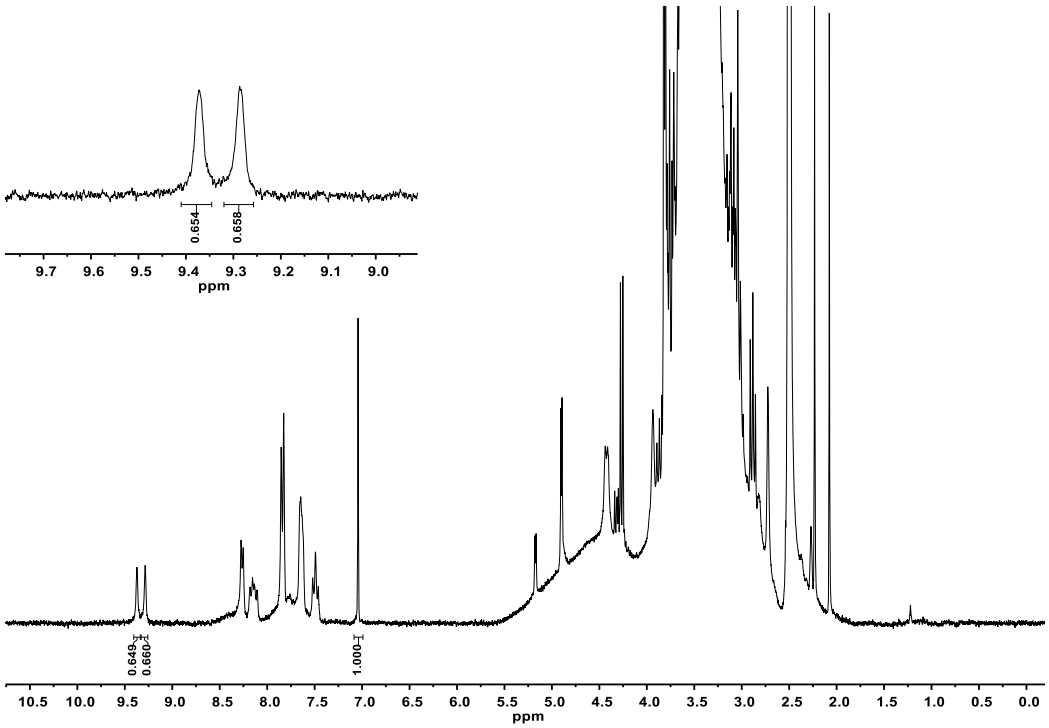

Figure A59. ^{1}H-NMR spectrum (300 MHz, 301 K, DMSO-d_6) of the system formed adding Apple juice without pre-treatment to the DMSO-d_6 solution containing complex **2** and ethylenediamine.

A2.11.13. Pear Juice-1@1

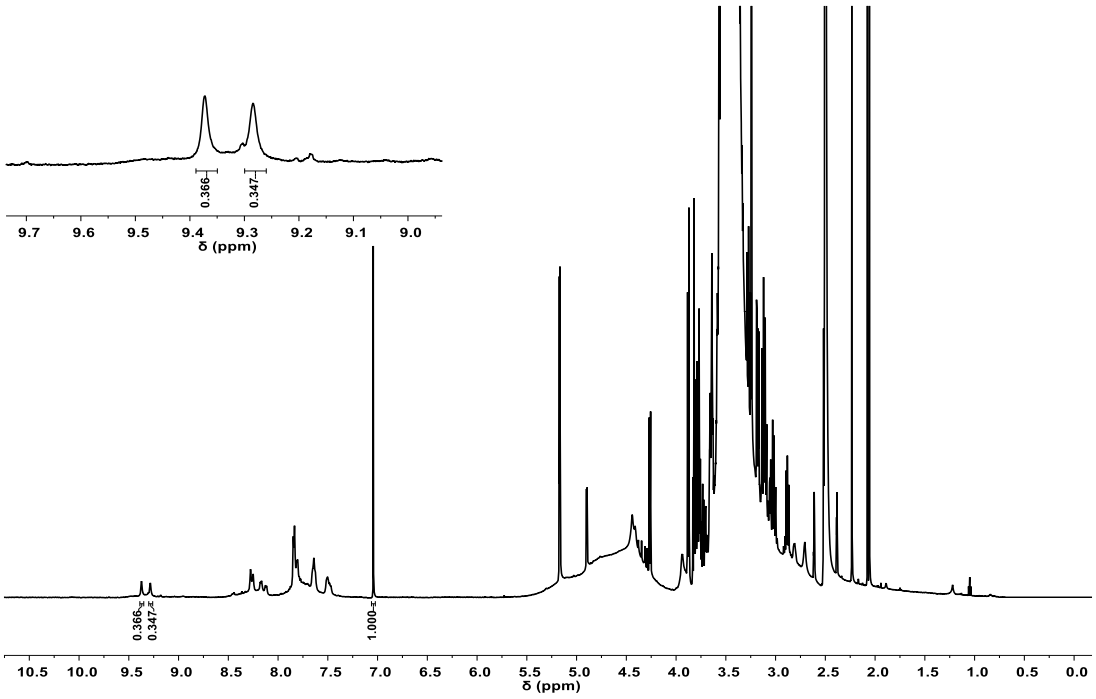

Figure A60. ^{1}H-NMR spectrum (400 MHz, 301 K, DMSO-d_6) of the system formed adding Pear juice without pre-treatment to the DMSO-d_6 solution containing complex **2** and ethylenediamine.

A2.11.14. Pear Juice-2@1

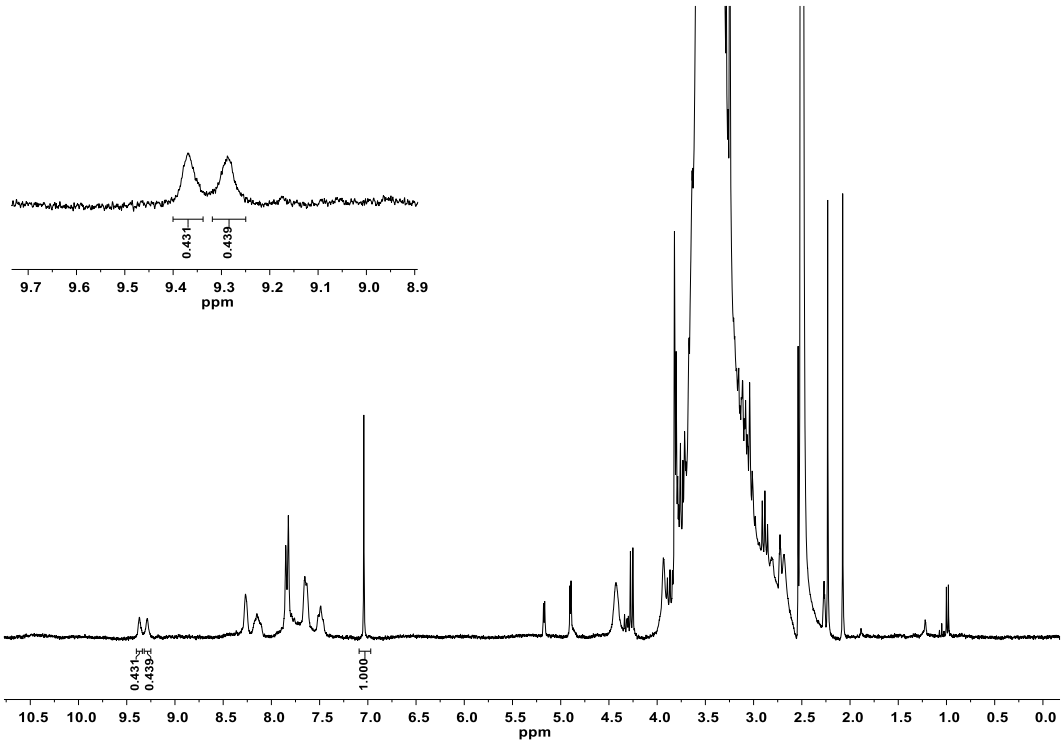

Figure A61. ^{1}H-NMR spectrum (300 MHz, 301 K, DMSO-d_6) of the system formed adding Pear juice without pre-treatment to the DMSO-d_6 solution containing complex **2** and ethylenediamine.

A2.11.15. Pear Juice-3@1

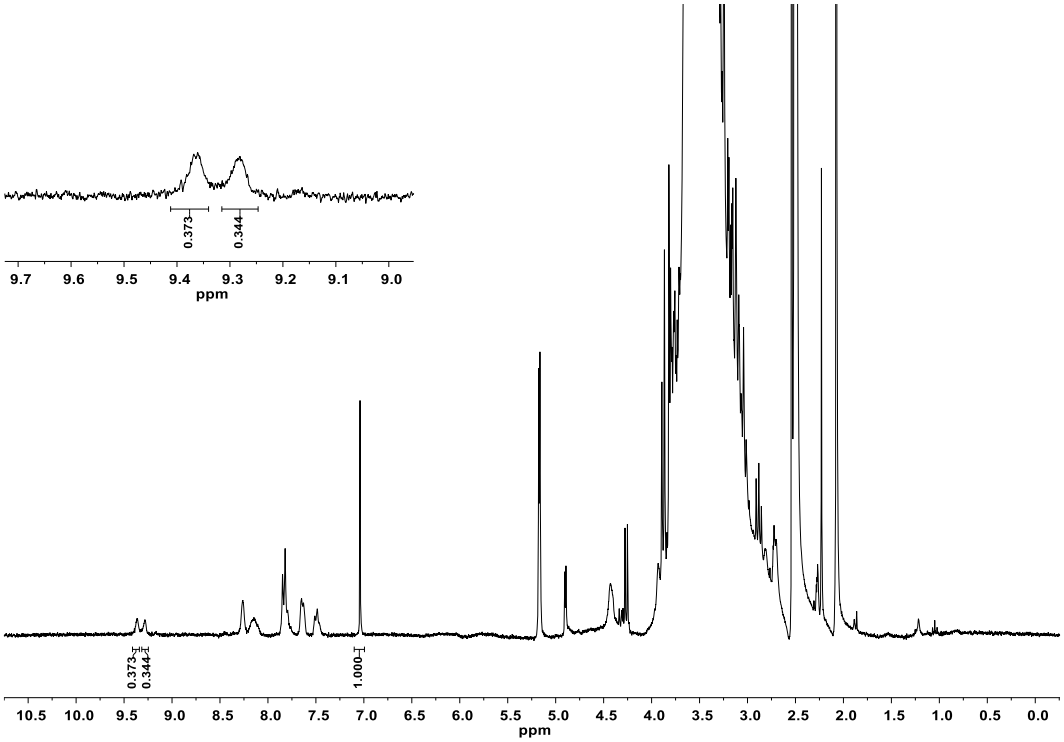

Figure A62. ^{1}H-NMR spectrum (300 MHz, 301 K, DMSO-d_6) of the system formed adding Pear juice without pre-treatment to the DMSO-d_6 solution containing complex **2** and ethylenediamine.

A2.11.16. Lemon Juice@1

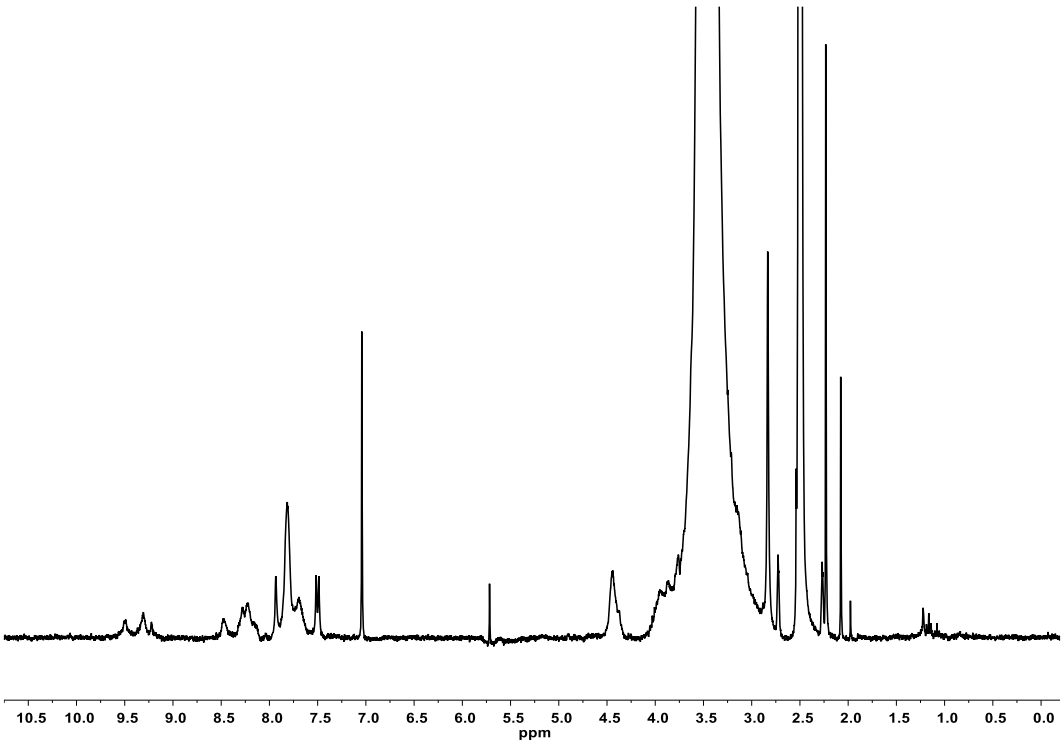

Figure A63. ^{1}H-NMR spectrum (300 MHz, 301 K, DMSO-d_6) of the system formed adding Lemon juice without pre-treatment to the DMSO-d_6 solution containing complex **2** and ethylenediamine.

A2.11.17. Orange Juice@1

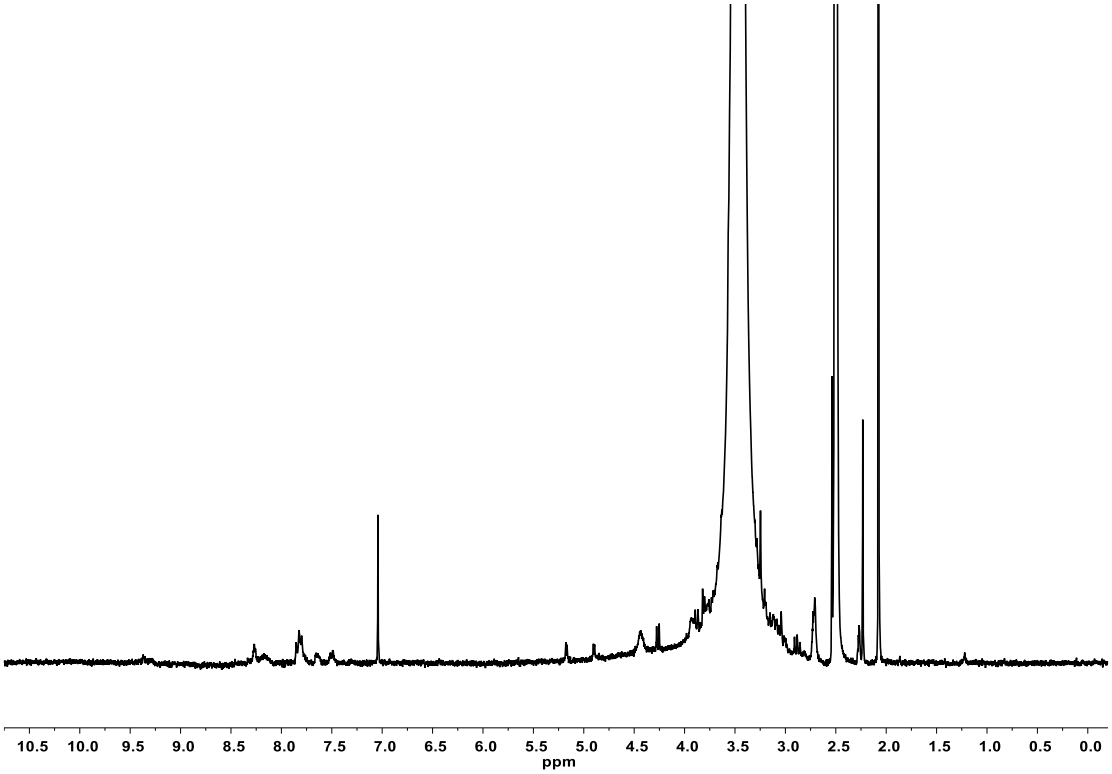

Figure A64. ^{1}H-NMR spectrum (300 MHz, 301 K, DMSO-d_6) of the system formed adding Orange juice without pre-treatment to the DMSO-d_6 solution containing complex **2** and ethylenediamine.

A2.12. References

[1] Gaussian 16, Revision C.01, M. J. Frisch, G. W. Trucks, H. B. Schlegel, G. E. Scuseria, M. A. Robb, J. R. Cheeseman, G. Scalmani, V. Barone, G. A. Petersson, H. Nakatsuji, X. Li, M. Caricato, A. V. Marenich, J. Bloino, B. G. Janesko, R. Gomperts, B. Mennucci, H. P. Hratchian, J. V. Ortiz, A. F. Izmaylov, J. L. Sonnenberg, D. Williams-Young, F. Ding, F. Lipparini, F. Egidi, J. Goings, B. Peng, A.Petrone, T. Henderson, D. Ranasinghe, V. G. Zakrzewski, J. Gao, N. Rega, G. Zheng, W. Liang, M. Hada, M. Ehara, K. Toyota, R. Fukuda, J. Hasegawa, M. Ishida, T. Nakajima, Y. Honda, O. Kitao, H. Nakai, T. Vreven, K. Throssell, J. A. Montgomery Jr., J. E. Peralta, F. Ogliaro, M. J. Bearpark, J. J. Heyd, E. N. Brothers, K. N. Kudin, V. N. Staroverov, T. A. Keith, R. Kobayashi, J. Normand, K. Raghavachari, A. P. Rendell, J. C. Burant, S. S. Iyengar, J. Tomasi, M. Cossi, J. M. Millam, M. Klene, C. Adamo, R. Cammi, J. W. Ochterski, R. L. Martin, K. Morokuma, O. Farkas, J. B. Foresman, D. J. Fox, Gaussian, Inc., Wallingford CT, 2016.

[2] 2016. GaussView, Version 6, Dennington, R., Keith, T. A., Millam, J. M., Semichem Inc., Shawnee Mission, KS.

[3] T. Bruhn, A. Schaumlöffel, Y. Hemberger and G. Bringmann, *Chirality*, 2013, **25**, 243–249.

[4] Gaussian 16, Revision C.01, Frisch, M. J., Trucks,.

[5] E. Debie, E. De Gussem, R. K. Dukor, W. Herrebout, L. A. Nafie and P. Bultinck, *ChemPhysChem*, 2011, **12**, 1542–1549.

[6] R. Evans, Z. Deng, A. K. Rogerson, A. S. McLachlan, J. J. Richards, M. Nilsson and G. A. Morris, *Angew. Chem. Int. Ed.*, 2013, **52**, 3199–3202.

[7] A. Macchioni, G. Ciancaleoni, C. Zuccaccia and D. Zuccaccia, *Chem. Soc. Rev.*, 2008, **37**, 479–489.

A3. Appendix to Chapter 3

A3.1. Disassembly and Assembly cycle of cage C_6@2 using PHQ

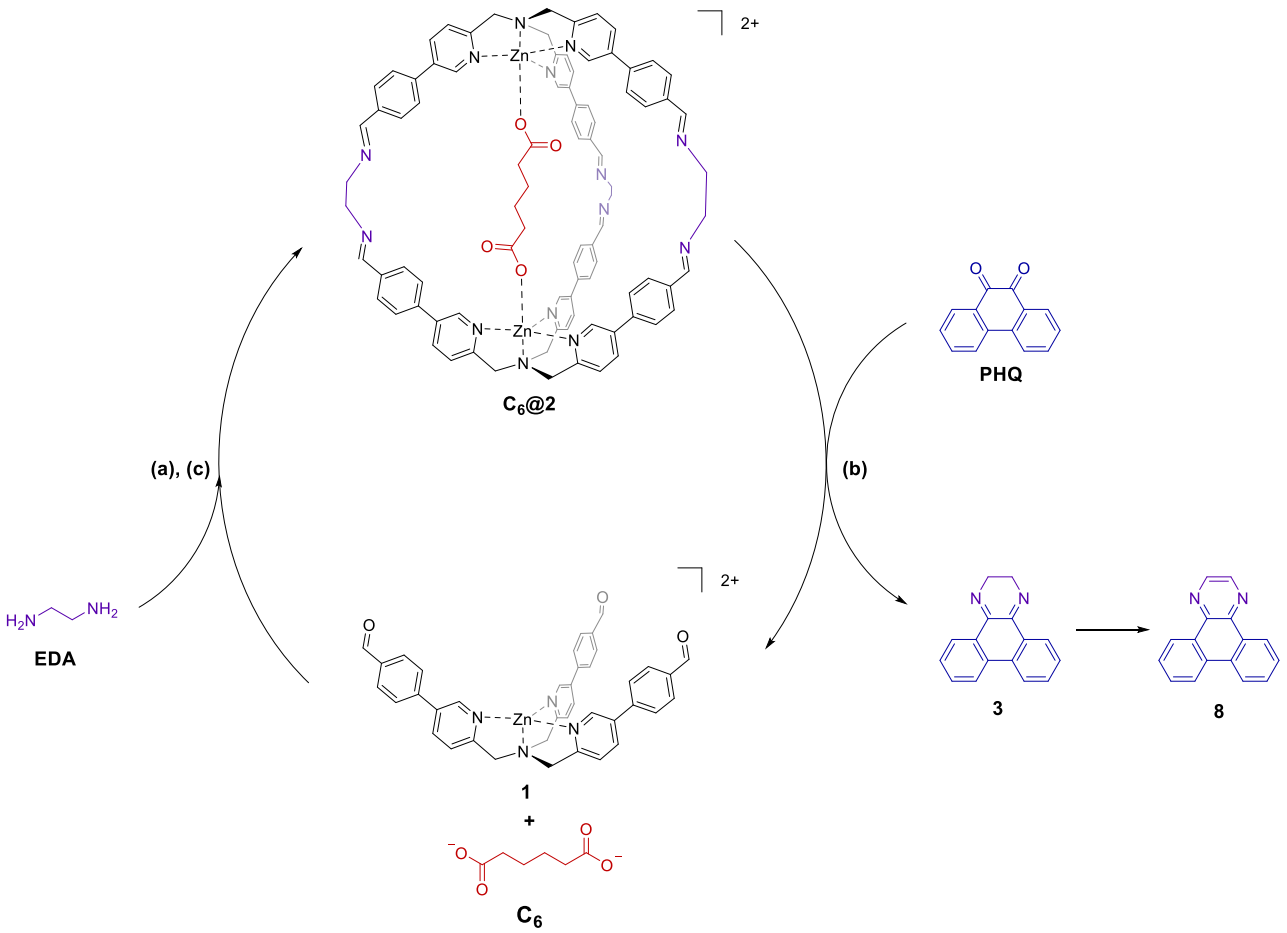

Procedure for the assembly/disassembly cycle. Perchlorate counterions are removed for clarity.

a) Formation of cage C_6@2:

To 350 µL (0.70 µmol) of a solution 0.002 M of complex **1** in DMSO-d_6, 18 µL (0.35 µmol) of a solution 0.02 M in DMSO-d_6 of a dicarboxylic acid **C_6,** 87 µL (1.75 µmol) of a solution 0.02 M in DMSO-d_6 of ethylenediamine, and 30 µL (0.60 µmol) of a solution 0.02 M in DMSO-d_6 of 1,3,5-trimetoxybenzene were added in a NMR tube and left at room temperature for 12 h. After 12 h, ^{1}H-NMR confirmed the complete formation of cage **C_6@2** (yield 95% determined *via* ^{1}H-NMR on internal standard 1,3,5-trimetoxybenzene).

b) Disassembly of cage C_6@2with PHQ:

After the complete formation of cage **C_6@2**, 44 µL (1.75 µmol) of a solution 0.04 M in DMSO-d_6 of 1,3-phenantrenequinone **PHQ** were added to the NMR tube and the mixture was left for 10 days at room temperature. ^{1}H-NMR confirmed the complete disassembly of the cage as confirmed by the disappearance of the imine peak at 8.4 ppm and the formation of the aldehyde peak of complex **1** at 10 ppm.

c) Assembly of cage C_6@2 with ethylenediamine:

After 10 days 87 µL (1.75 µmol) of a solution 0.02 M in DMSO-d_6 of ethylenediamine were added to the NMR tube and the mixture was left for 12 h at room temperature. ^{1}H-NMR confirmed the formation of cage **C_6@2** (yield 85 % determined *via* ^{1}H-NMR on internal standard 1,3,5-trimetoxybenzene).

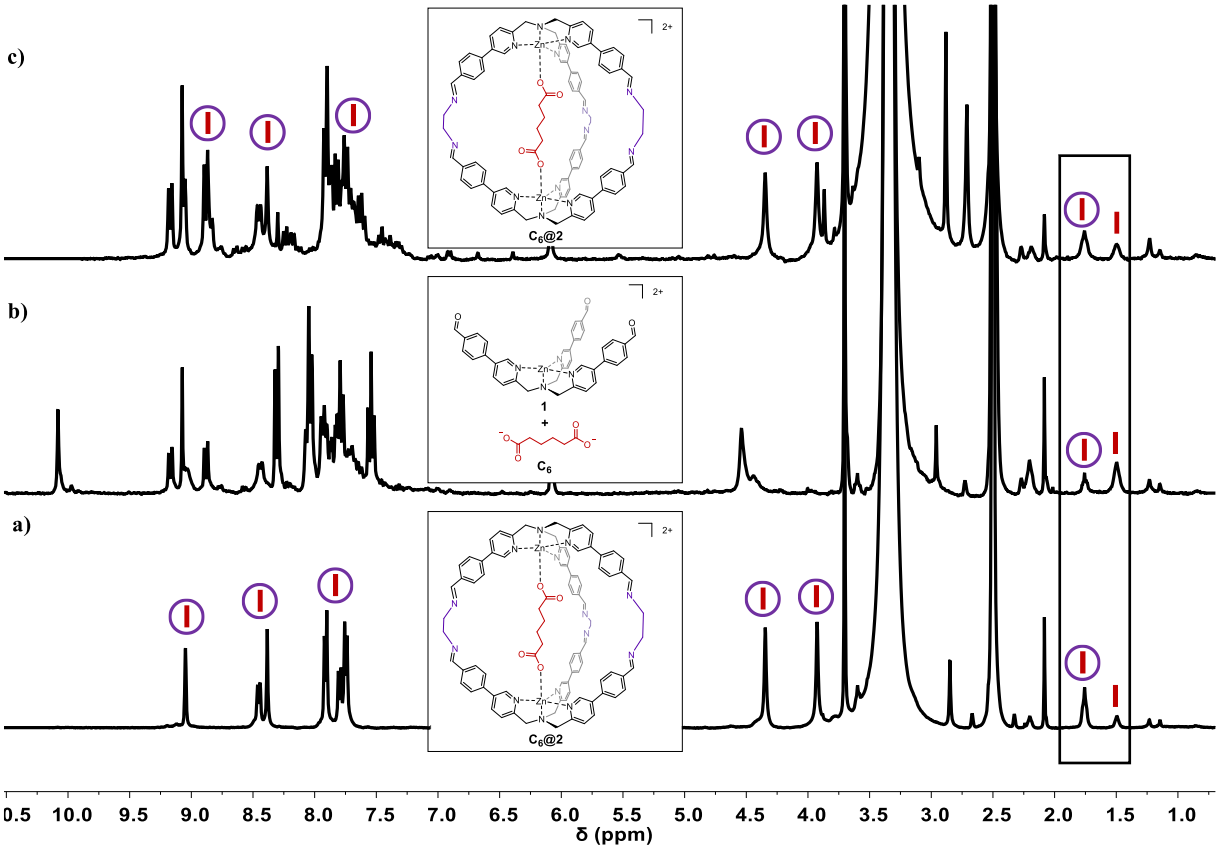

Figure A1. ^{1}H-NMR (DMSO-d_6, 400 MHz) of a) cage **C_6@2**, b) 15 days after the addition of **PHQ**, and c) 12 h after the addition of ethylenediamine. The purple circle indicates cage **2**, red stick indicates **C_6**.

A3.2. Cage to Cage conversion with *p*-XDA

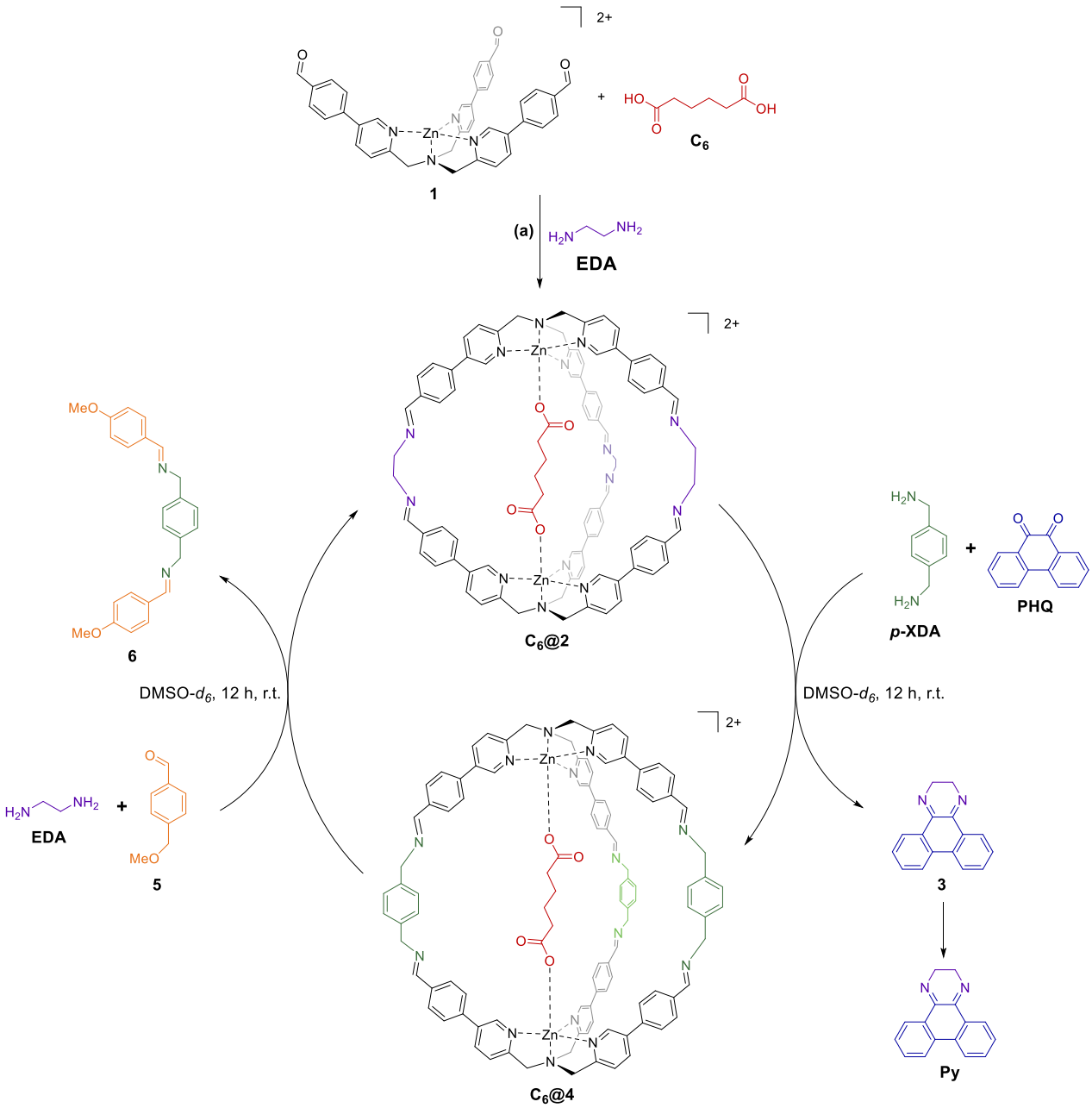

Procedure for the cage to cage transformation. Perchlorate counterions are removed for clarity.

a) Formation of cage C6@2:

To 350 µL (0.70 µmol) of a solution 0.002 M of complex **1** in DMSO-*d*6, 18 µL (0.35 µmol) of a solution 0.02 M in DMSO-*d*6 of a dicarboxylic acid **C6**, 87 µL (1.75 µmol) of a solution 0.02 M in DMSO-*d*6 of ethylenediamine, and 30 µL (0.60 µmol) of a solution 0.012 M in DMSO-*d*6 of *p*-xylene were added in a NMR tube and left at room temperature for 12 h. After 12 h, ^{1}H-NMR confirmed the complete formation of cage **C6@2** (yield 95% determined *via* ^{1}H-NMR on internal standard *p*-xylene).

b) Cage to cage conversion from C_6@2 to C_6@4 with PHQ:

After the complete formation of cage **C_6@2**, 87 µL (1.75 µmol) of a solution 0.02 M in DMSO-d_6 of *p*-xylylenediamine and 44 µL (1.75 µmol) of a solution 0.04 M in DMSO-d_6 of 1,3-phenantrenequinone **PHQ** were added to the NMR tube and the mixture was left for 12 h at room temperature. After 12 h, ^{1}H-NMR confirmed the formation of cage **C_6@4** (ESI analysis showed the presence of a minor species in which one arm was substituted with ethylenediamine instead of *p*-xylylenediamine).

c) Cage to cage conversion from C_6@4 to C_6@2:

After the formation of cage **C_6@4**, 87 µL (1.75 µmol) of a solution 0.02 M in DMSO-d_6 of ethylenediamine and 44 µL (1.75 µmol) of a solution 0.04 M in DMSO-d_6 of *p*-methoxybenzaldehyde were added to the NMR tube and the mixture was left for 12 h at room temperature. After this time, ^{1}H-NMR confirmed the re-formation of cage **C_6@2** (yield 72 % determined *via* ^{1}H-NMR on internal standard *p*-xylene).

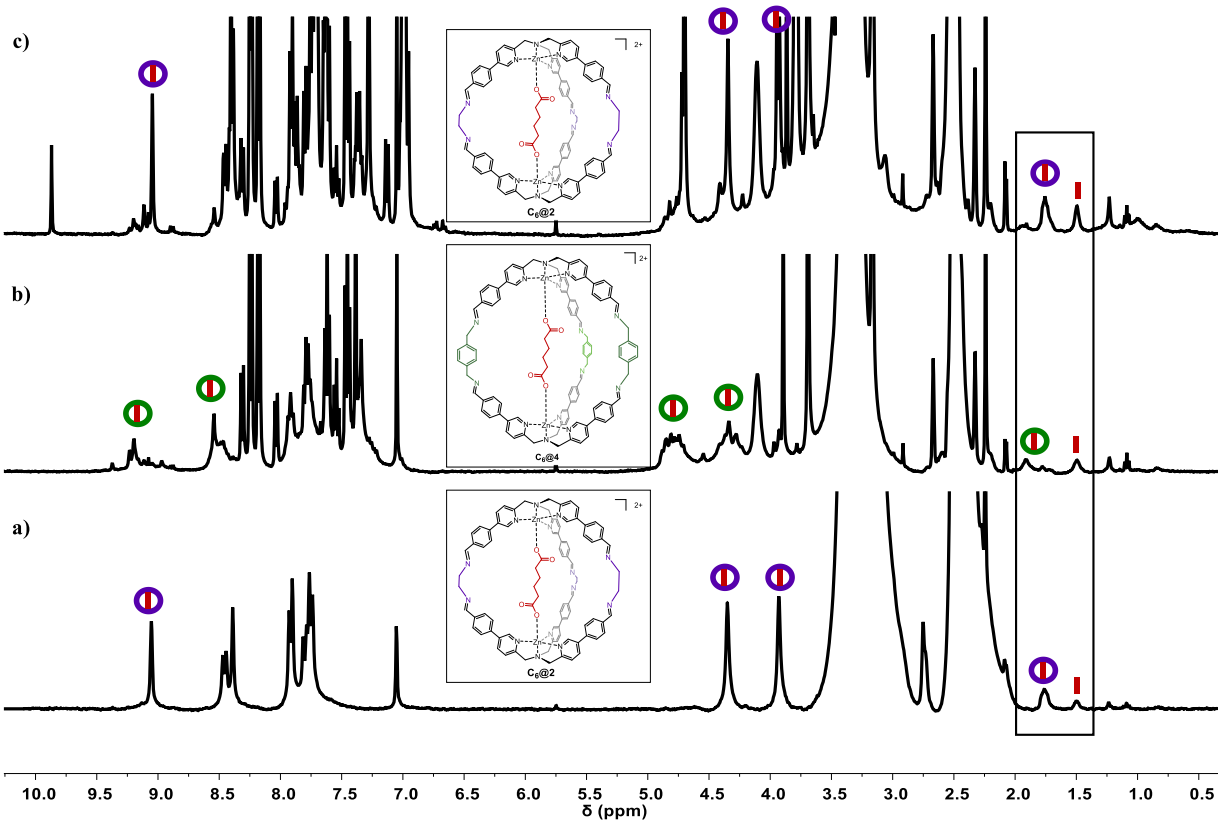

Figure A2. ^{1}H-NMR (DMSO-d_6, 400 MHz) of a) cage **C_6@2**, b) 12 h after the addition of *p*-xylylenediamine and **PHQ** that led to the formation of cage **C_6@4**, and c) 12 h after the addition of ethylenediamine and *p*-methoxybenzaldehyde that allow the re-formation of cage **C_6@2**. The purple circle indicates cage **2**, the green circle indicates cage **4**, red stick indicates **C_6**.

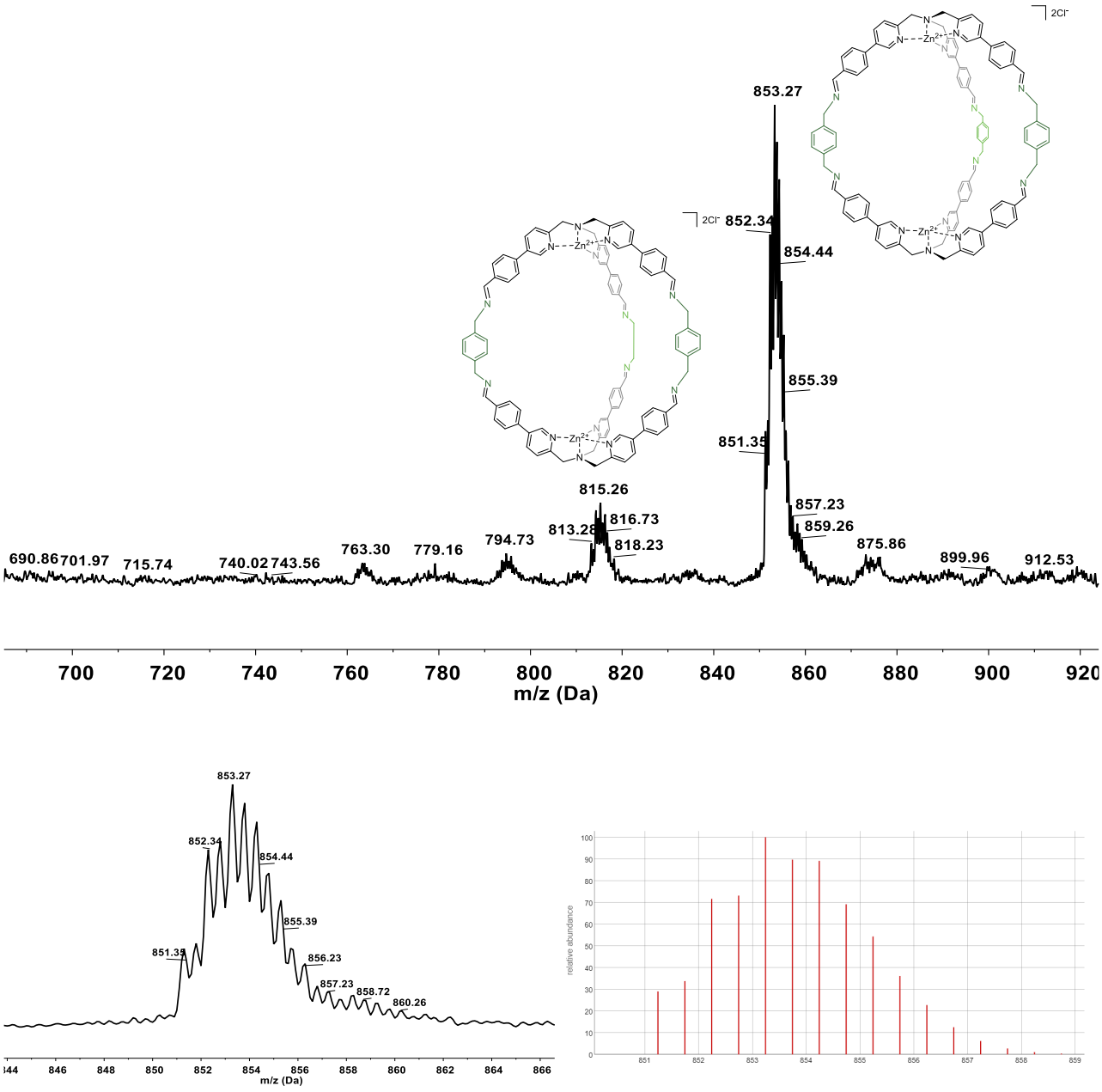

Figure A3. Experimental, and calculated ESI-MS pattern (in CH_3CN/0.1% HCOOH) of the reaction mixture. Due to the low affinity of the guest, only the empty cage is observed.

A3.3. Cage-to-Cage Competing Guests

A3.3.1. Guest substitution

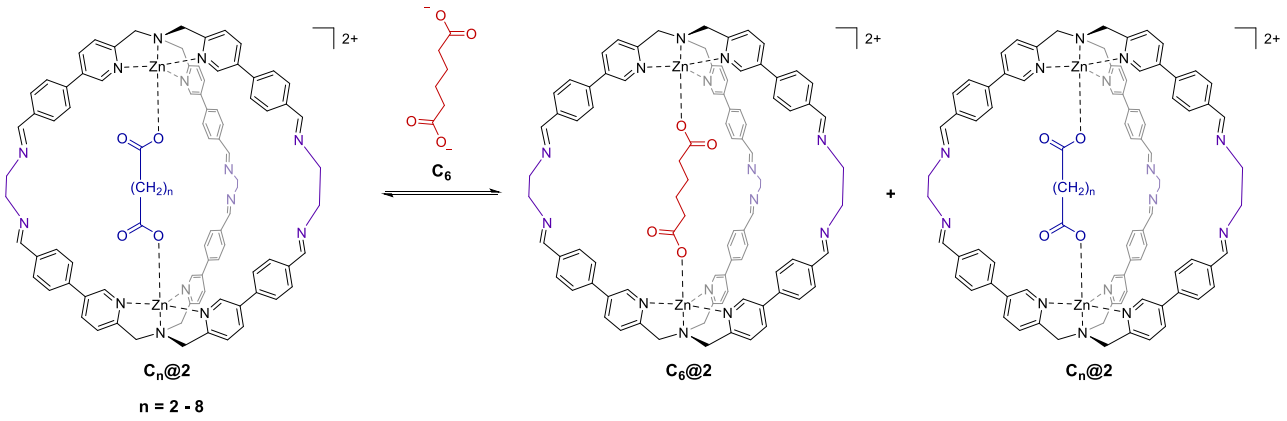

General procedure for the guest substitution inside molecular cages **C_n@2**. Perchlorate counterions are removed for clarity.

To 350 µL (0.70 µmol) of a solution 0.002 M of complex **1** in DMSO-d_6, 18 µL (0.35 µmol) of a solution 0.02 M in DMSO-d_6 of a dicarboxylic acid **C_n** (ranging from Succinic **C_4** to decandioic **C_{10}**), 87 µL (1.75 µmol) of a solution 0.02 M in DMSO-d_6 of ethylenediamine, and 30 µL (0.60 µmol) of a solution 0.012 M in DMSO-d_6 of *p*-xylene were added in a NMR tube and left at room temperature for 12 h (yield >95% Determined *via* ^{1}H-NMR on internal standard *p*-xylene). After 12 h 18 µL (0.35 µmol) of a solution 0.02 M in DMSO-d_6 of adipic acid **C_6** were added to the NMR tube and the ratio between the two different cages was determined by integration of the α-pyridine protons peak around 9 ppm.

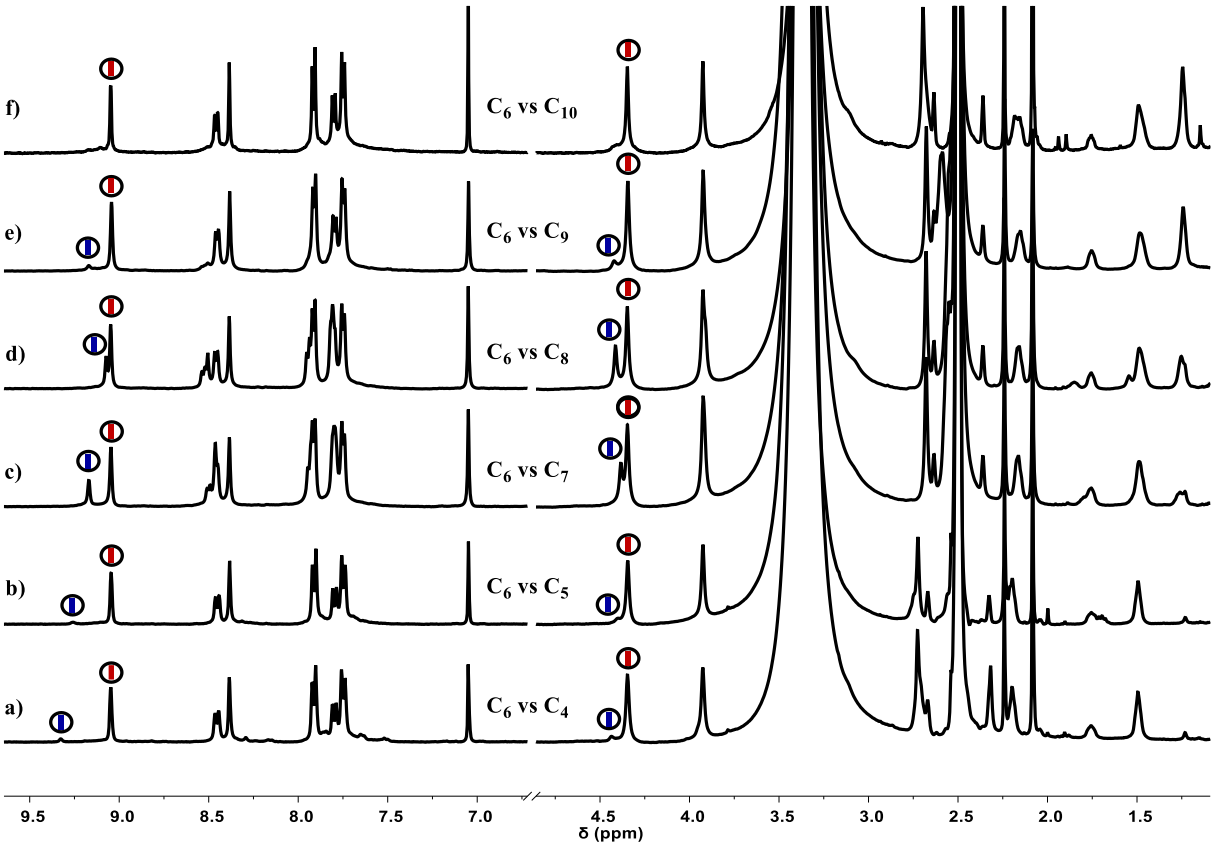

Figure A4. ^{1}H-NMR (DMSO-d_6, 500 MHz) of each mixture of cage **C_n@2** after the addition of the competitor. The black circle indicates cage **2**, red stick indicates acid **C_6**, blue stick indicates acid **C_n**: (a) **C_4**, (b) **C_5**, (c) **C_7**, (d) **C_8**, (e) **C_9**, (f) **C_{10}**.

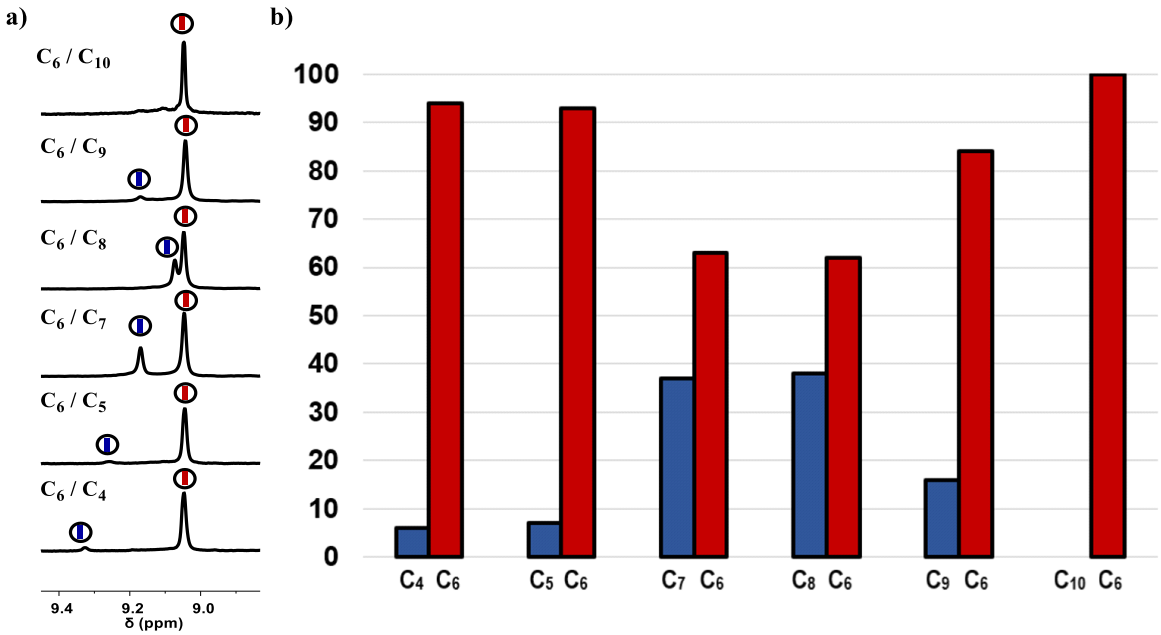

Figure A5. a)Partial ^{1}H-NMR (DMSO-d_6, 500 MHz) that highlights the α-pyridine protons peak of the cages The black circle indicates cage **2**, red stick indicates acid **C_6**, blue stick indicates acid **C_n**. b) Percentage of bound guest obtained by integration of the α -pyridine protons peak.

A3.3.2. Guest substitution from C_{10} to C_6

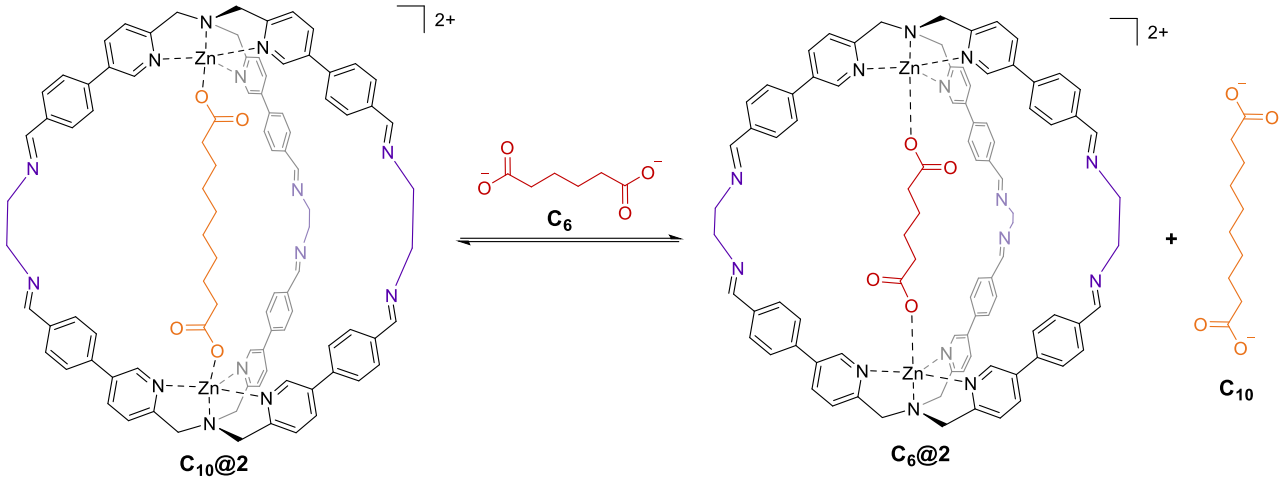

Procedure for the guest displacement. Perchlorate counterions are removed for clarity.

To 350 µL (0.70 µmol) of a solution 0.002 M of complex **1** in DMSO-d_6, 18 µL (0.35 µmol) of a solution 0.02 M in DMSO-d_6 of a dicarboxylic acid **C_{10}**, 87 µL (1.75 µmol) of a solution 0.02 M in DMSO-d_6 of ethylenediamine **EDA**, and 30 µL (0.60 µmol) of a solution 0.012 M in DMSO-d_6 of *p*-xylene were added in a NMR tube and left at room temperature for 12 h (yield >95% Determined *via* ^{1}H-NMR on internal standard *p*-xylene). After 12 h 36 µL (0.35 µmol) of a solution 0.01 M in DMSO-d_6 of dicarboxylic acid **C_6** were added to the NMR tube in 4 aliquots. At the end, the complete exchange of the guest from **C_{10}** to **C_6** occurred, obtaining the selective uptake and release of the guests.

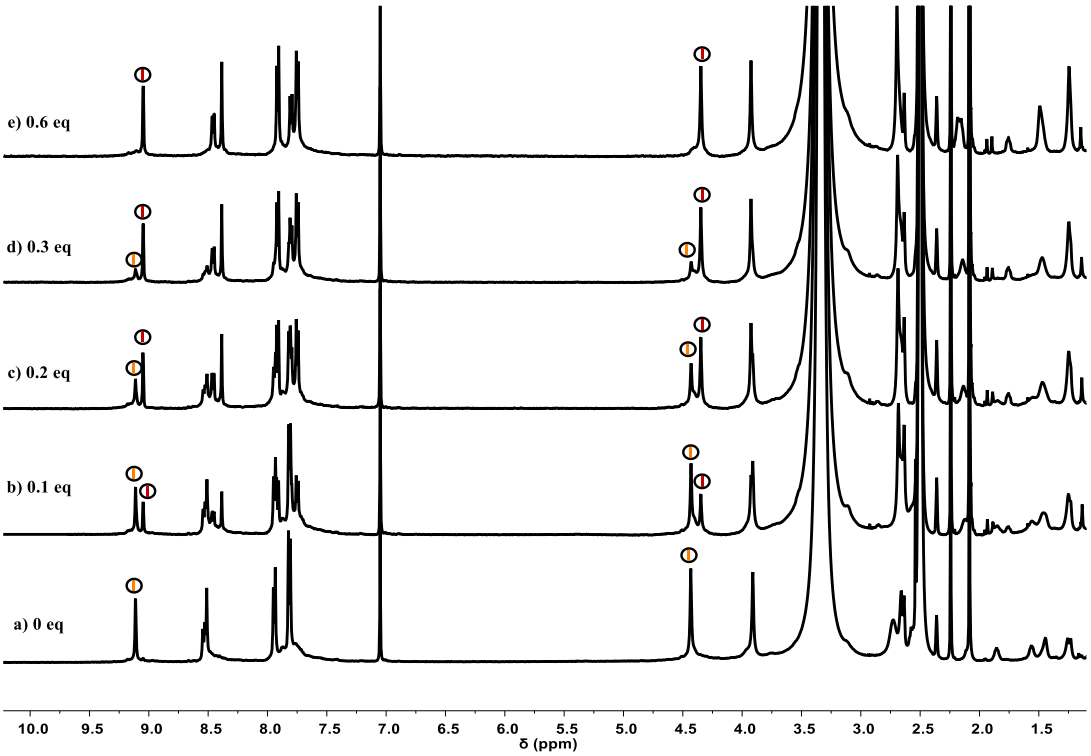

Figure A6. ^{1}H-NMR (DMSO-d_6, 500 MHz) titration experiment of the preformed cage **C_{10}@2** using adipic acid **C_6** as competitor. The black circle indicates the cage, orange stick indicates **C_{10}** while the red stick indicates **C_6**.

A3.4. Cage to Cage conversion with selective release and uptake of the guests

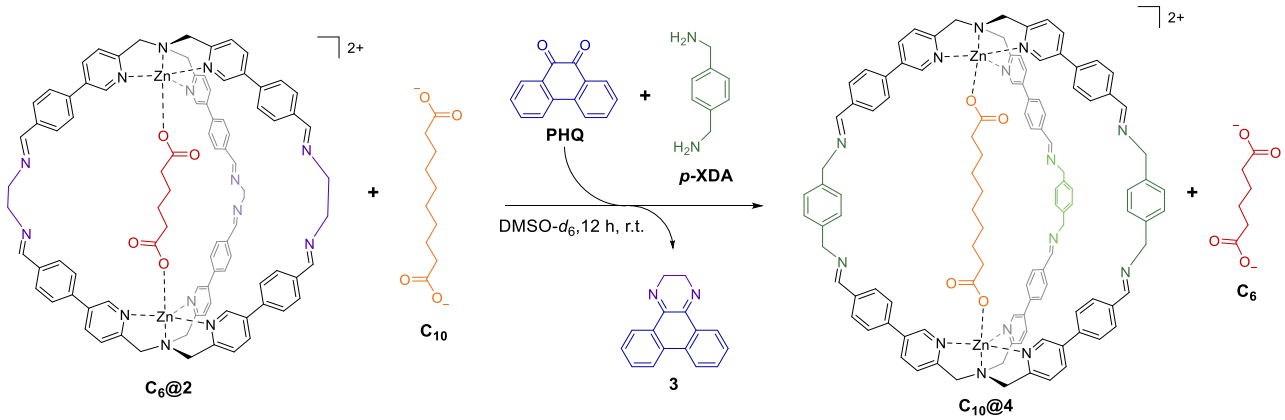

Procedure for the cage to cage transformation. Perchlorate counterions are removed for clarity.

To the prepared mixture in which **C_{10}** was substituted with **C_6** as guest in cage **2**, 87 µL (1.75 µmol) of a solution 0.02 M in DMSO-d_6 of *p*-xylylenediamine ***p*-XDA** and 44 µL (1.75 µmol) of a solution 0.04 M in DMSO-d_6 of 1,3-phenantrenequinone **PHQ** were added to the NMR tube and the mixture was followed by NMR for 12 h at room (yield >95% Determined *via* ^{1}H-NMR on internal standard *p*-xylene). At the end of the reaction, the complete cage conversion from **C_6@2** to **C_{10}@4** occurred with the selective uptake and exchange of the guest from **C_6** to **C_{10}**.

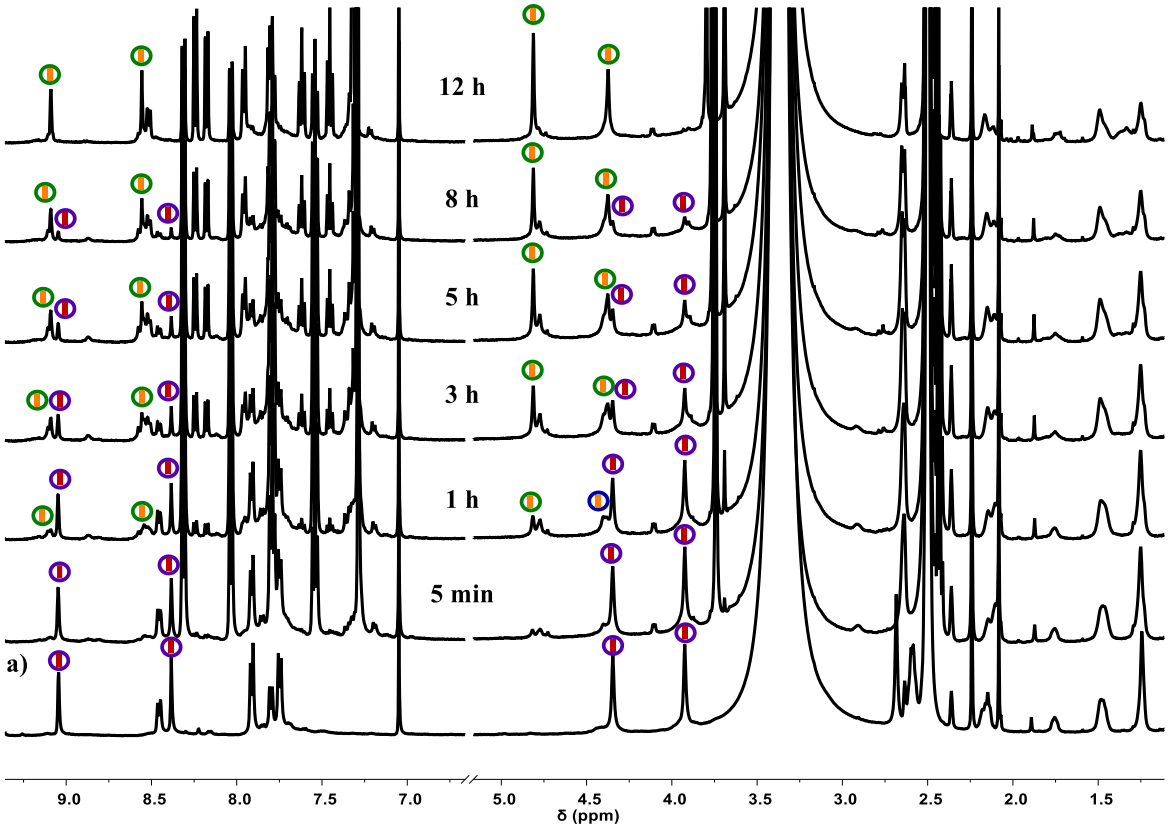

Figure A7. ^{1}H-NMR (DMSO-d_6, 500 MHz) spectra in time progression of the cage **C_6@2** after the addition of 2.5 equiv. of ***p*-XDA** and 2.5 equiv. of **3**. Times are related to the addition of **3** and ***p*-XDA**. a)Spectrum of **C_6@2** before the addition of the subcomponents. The green circle with the orange stick indicates **C_{10}@4** while the purple circle with the red stick indicates **C_6@2**.

A3.5. Chiral cage Assembly-Disassembly-Assembly with enantiomers

A3.5.1. Selective encapsulation using a racemic mixture

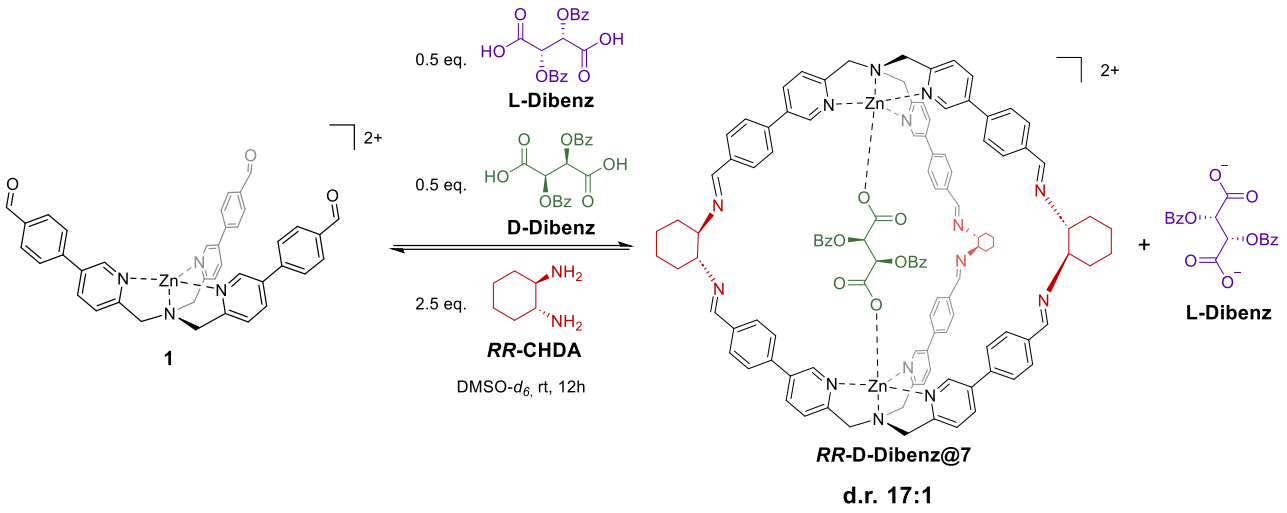

Procedure for the selective encapsulation. Perchlorate counterions are removed for clarity.

To 350 µL (0.70 µmol) of a solution 0.002 M of complex **1** in DMSO-d_6, 18 µL (0.35 µmol) of a solution 0.02 M in DMSO-d_6 of a dicarboxylic acid **D-Dibenz**, 18 µL (0.35 µmol) of a solution 0.02 M in DMSO-d_6 of a dicarboxylic acid **L-Dibenz**, 87 µL (1.75 µmol) of a solution 0.02 M in DMSO-d_6 of (1*R*,2*R*)-(-)-1,2-diaminocyclohexane ***RR*-CHDA**, and 30 µL (0.60 µmol) of a solution 0.012 M in DMSO-d_6 of 1,3,5-trimetoxybenzene were added in a NMR tube and left at room temperature for 12 h (yield >95% Determined *via* ^{1}H-NMR on internal standard 1,3,5-trimetoxybenzene). From the NMR, a preference for the encapsulation of **D-Dibenz** was observed, with a diastereomeric ratio 17:1.

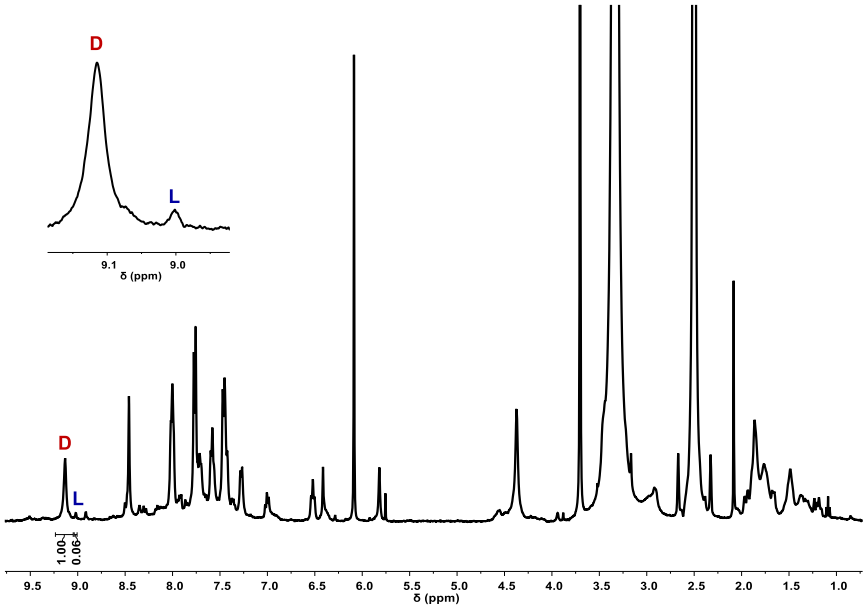

Figure A8. ^{1}H-NMR (DMSO-d_6, 400 MHz) of cage 5 in the presence of a racemic mixture of Benzoyl-tartaric acid **Dibenz**. From integration of the α -pyridine protons peak, a preference for the encapsulation of **D-Dibenz** was observed, with a diastereomeric ratio 17:1.

A3.5.2. Cage-to-Cage Enantiomeric Competing Guests

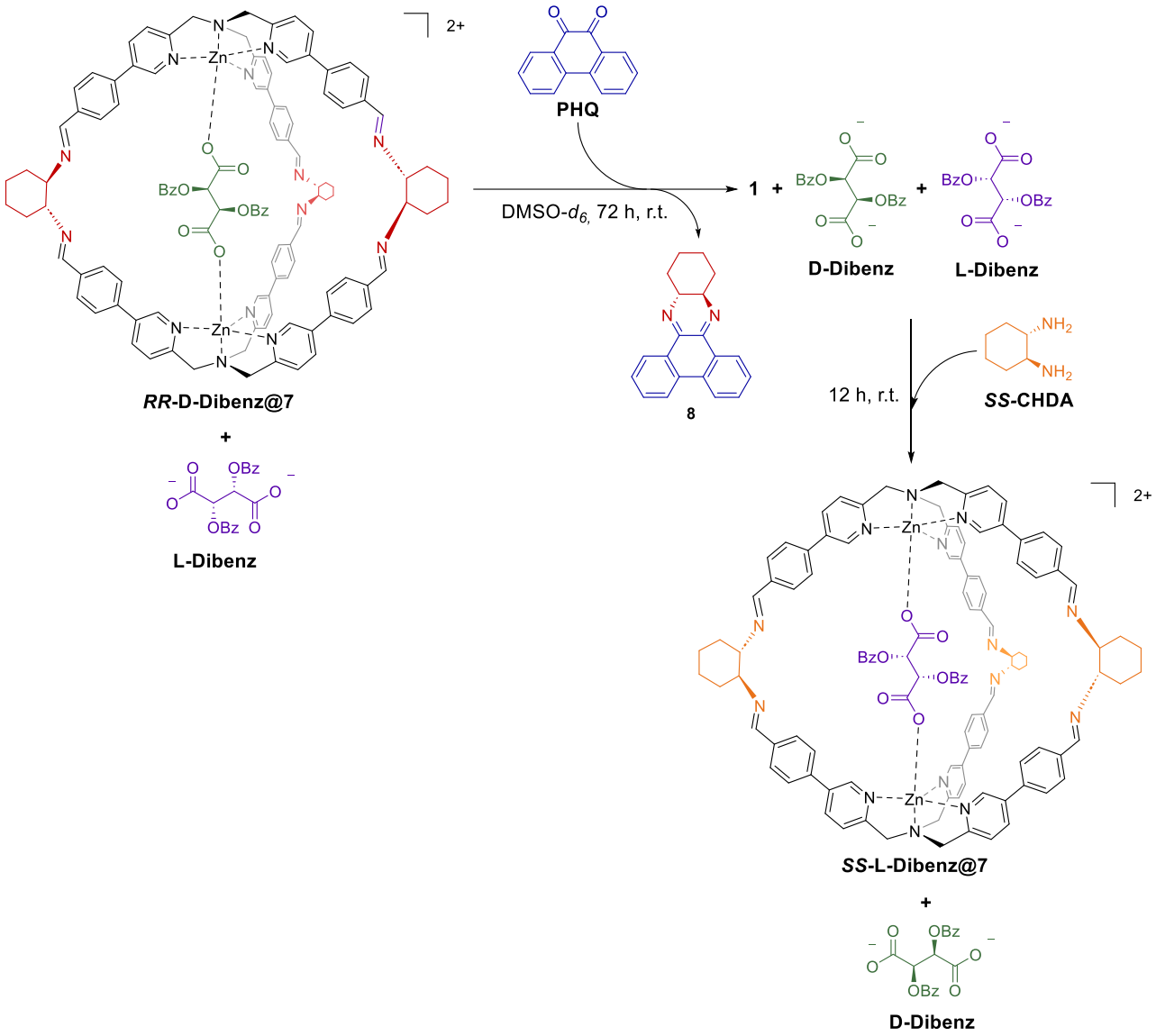

Procedure for the cage to cage transformation. Perchlorate counterions are removed for clarity.

a) Disassembly of cage ***RR*-D-Dibenz@7** with **PHQ**:

After 12 h, 44 µL (1.75 µmol) of a solution 0.04 M in DMSO-d_6 of 1,3-phenantrenequinone **PHQ** were added to the previously prepared mixture in the NMR tube, and the solution was left for 72 h at room temperature. ^{1}H-NMR showed the complete disassembly of the cage as confirmed by the disappearance of the imine peak at 8.5 ppm and the formation of the aldehyde peak of complex **1** at 10 ppm.

b) Assembly of cage ***SS*-L-Dibenz@7** with ***SS*-CHDA**:

After 72 h, 87 µL (1.75 µmol) of a solution 0.02 M in DMSO-d_6 of (1*S*,2*S*)-(+)-1,2-diaminocyclohexane ***SS*-CHDA** were added to the NMR tube and the mixture was left for 12 h at room temperature. ^{1}H-NMR confirmed the formation of cage ***SS*-L-Dibenz@7** (yield 55 % determined *via* ^{1}H-NMR on internal standard 1,3,5-trimetoxybenzene).

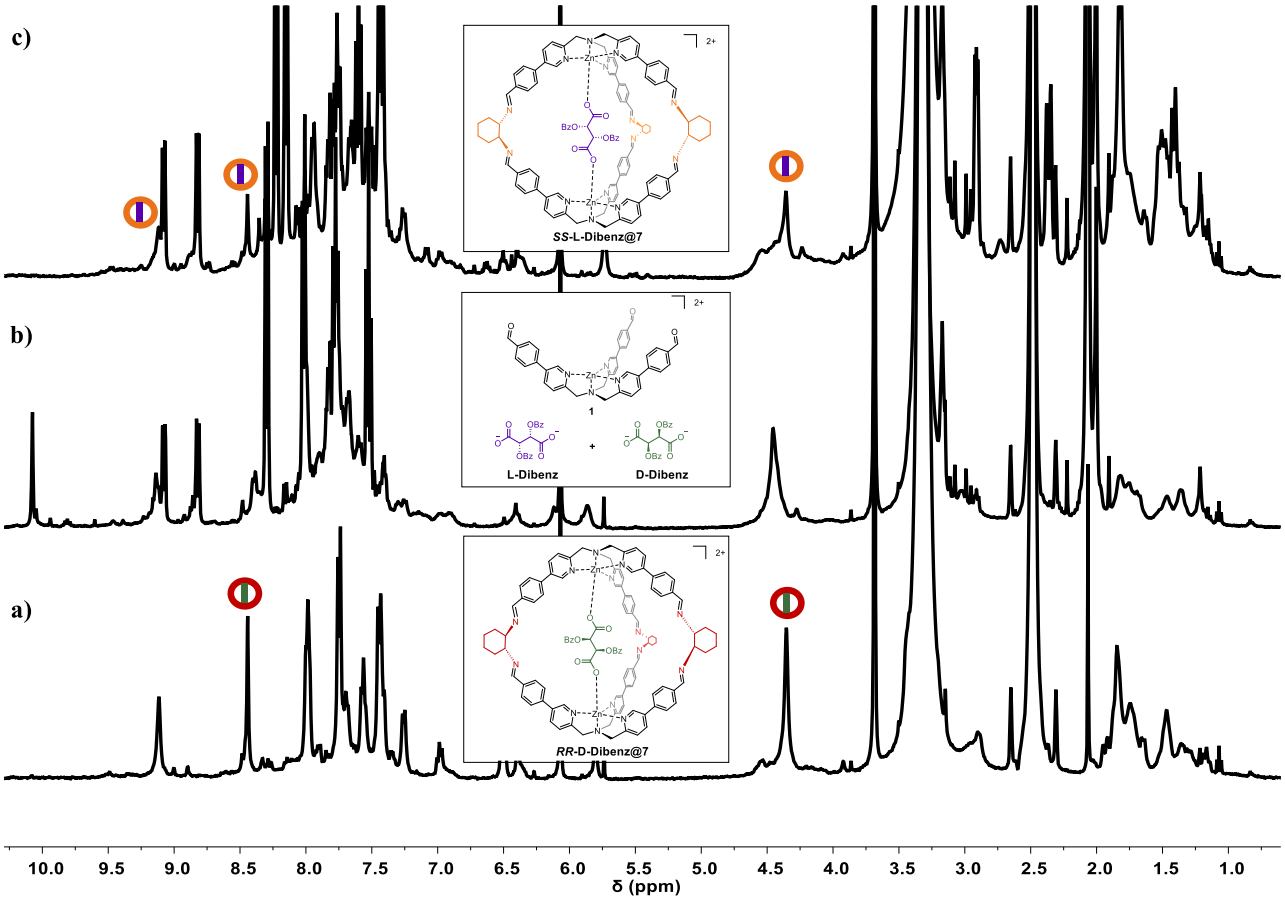

Figure A9. ^{1}H-NMR (DMSO-d_6, 400 MHz) of a) cage ***RR*-D-Dibenz@7**, b) 72 h after the addition of **PHQ**, and c) 12 h after the addition of *S*,*S*- diaminocyclohexane ***SS*-CHDA** that led to the formation of cage ***SS*-L-Dibenz@7**. The red circle indicates cage ***RR*-7**, orange circle indicates cage ***SS*-7**, green stick indicates **D-Dibenz**, and purple stick indicates **L-Dibenz**.

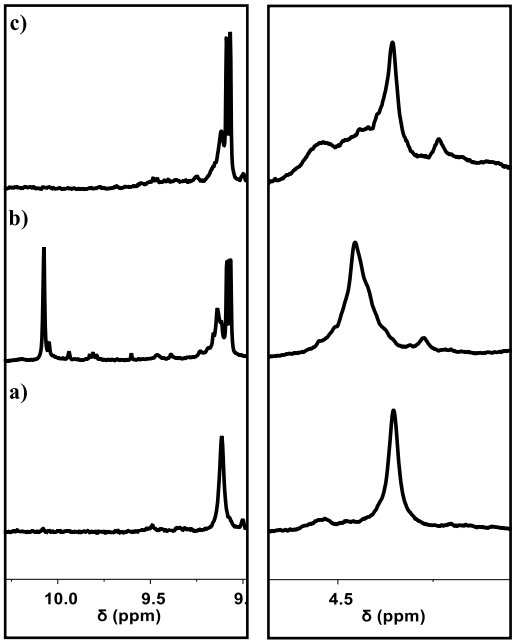

Figure A10. Partial ^{1}H-NMR (DMSO-d_6, 400 MHz) of the α -pyridine protons peak. (left) and the CH_2 benzylic protons of the TPMA scaffold (right). a) cage ***RR*-D-Dibenz@7**, b) 72 h after the addition of **PHQ**, and c) 12 h after the addition of *S*,*S*- diaminocyclohexane ***SS*-CHDA** that led to the formation of cage ***SS*-L-Dibenz@7**.

A3.5.3. Cage-to-Cage Pseudo-Enantiomeric Competing Guests

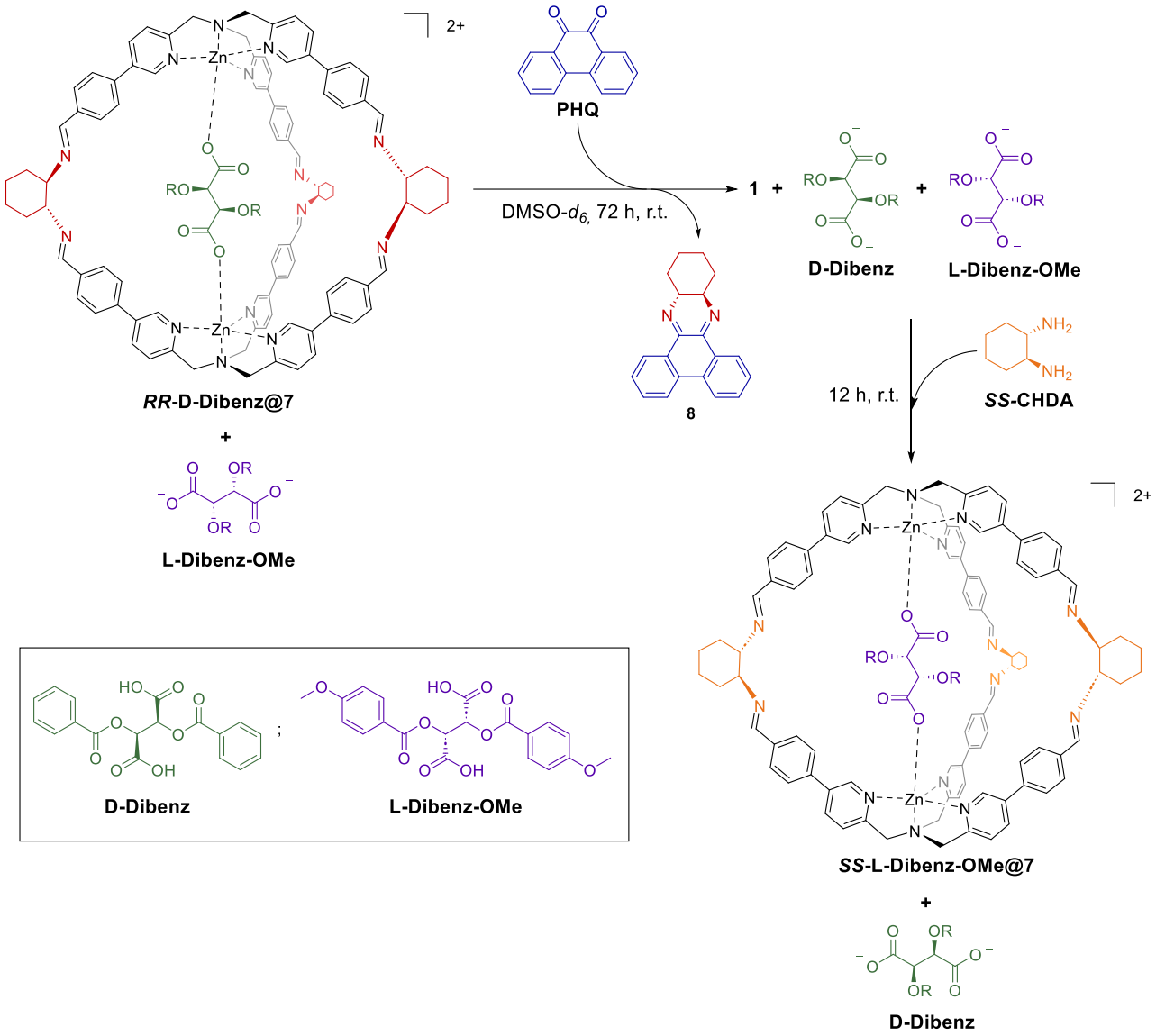

Procedure for the cage to cage transformation. Perchlorate counterions are removed for clarity.

To 350 µL (0.70 µmol) of a solution 0.002 M of complex **1** in DMSO-d_6, 18 µL (0.35 µmol) of a solution 0.02 M in DMSO-d_6 of a dicarboxylic acid **D-Dibenz**, 18 µL (0.35 µmol) of a solution 0.02 M in DMSO-d_6 of a dicarboxylic acid **L-Dibenz-OMe**, 87 µL (1.75 µmol) of a solution 0.02 M in DMSO-d_6 of (1*R*,2*R*)-(-)-1,2-diaminocyclohexane, and 30 µL (0.60 µmol) of a solution 0.012 M in DMSO-d_6 of 1,3,5-trimetoxybenzene were added in a NMR tube and left at room temperature for 12 h (yield >95% Determined *via* ^{1}H-NMR on internal standard 1,3,5-trimetoxybenzene). From the NMR, a preference for the encapsulation of **D-Dibenz** was observed.

a) Disassembly of cage ***RR*-D-Dibenz@7** with **PHQ**:

After 12 h, 44 µL (1.75 µmol) of a solution 0.04 M in DMSO-d_6 of 1,3-phenantrenequinone **PHQ** were added to the previously prepared mixture in the NMR tube, and the solution was left for 72 h at room temperature. ^{1}H-NMR showed the complete disassembly of the cage as confirmed by the disappearance of the imine peak at 8.5 ppm and the formation of the aldehyde peak of complex **1** at 10 ppm.

b) Assembly of cage ***SS*-L-Dibenz-OMe@7** with ***SS*-CHDA**:

After 72 h, 87 µL (1.75 µmol) of a solution 0.02 M in DMSO-d_6 of (1*S*,2*S*)-(+)-1,2-diaminocyclohexane ***SS*-CHDA** were added to the NMR tube and the mixture was left for 12 h at room temperature. ^{1}H-NMR confirmed the formation of cage ***SS*-L-Dibenz-OMe@7** (yield 50 % determined *via* ^{1}H-NMR on internal standard 1,3,5-trimetoxybenzene).

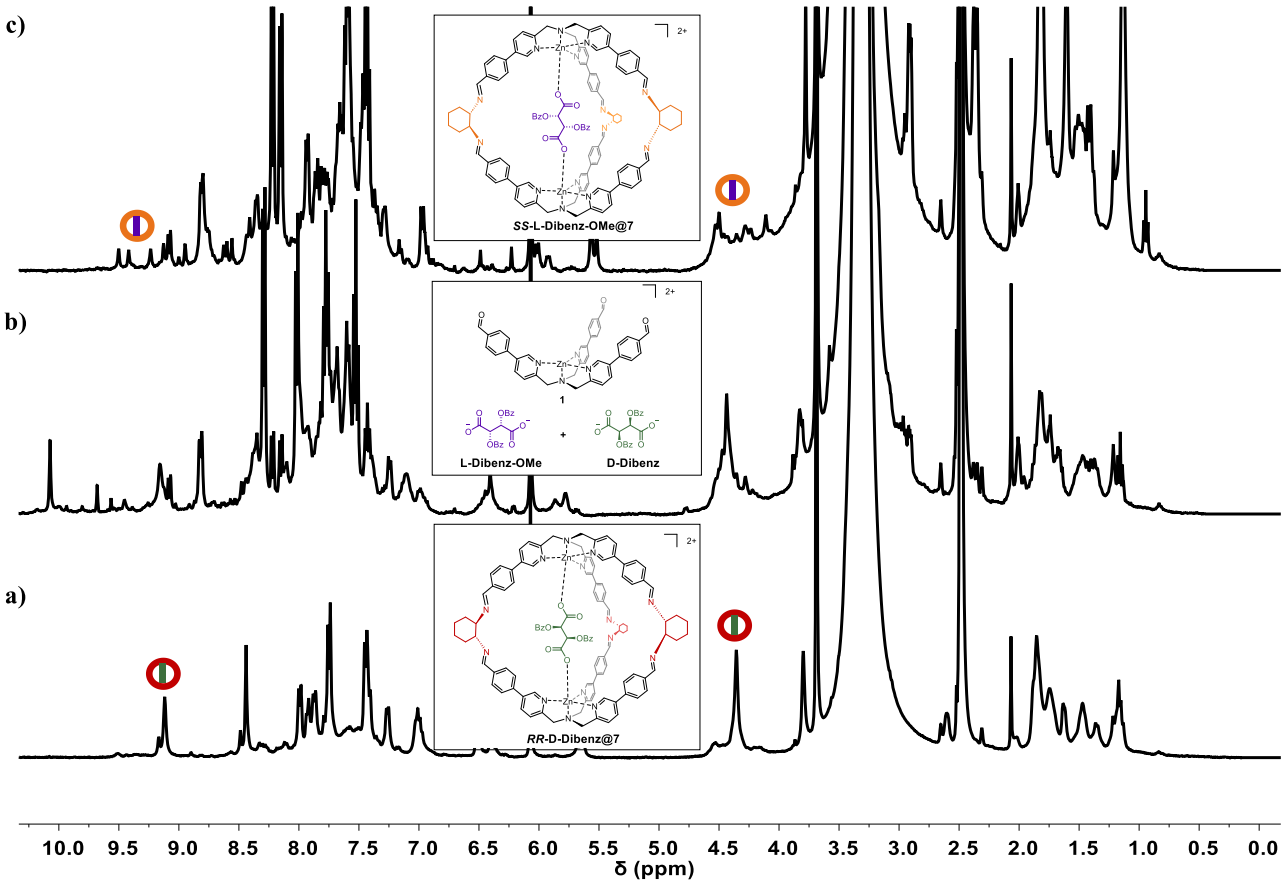

Figure A11. ^{1}H-NMR (DMSO-d_6, 400 MHz) of a) cage ***RR*-D-Dibenz@7**, b) 72 h after the addition of **PHQ**, and c) 12 h after the addition of *S*,*S*- diaminocyclohexane ***SS*-CHDA** that led to the formation of cage ***SS*-L-Dibenz@7**. The red circle indicates cage ***RR*-7**, orange circle indicates cage ***SS*-7**, green stick indicates **D-Dibenz**, and purple stick indicates **L-Dibenz-OMe**.

A3.6. NMR and ESI characterizations

A3.6.1. C_6@2

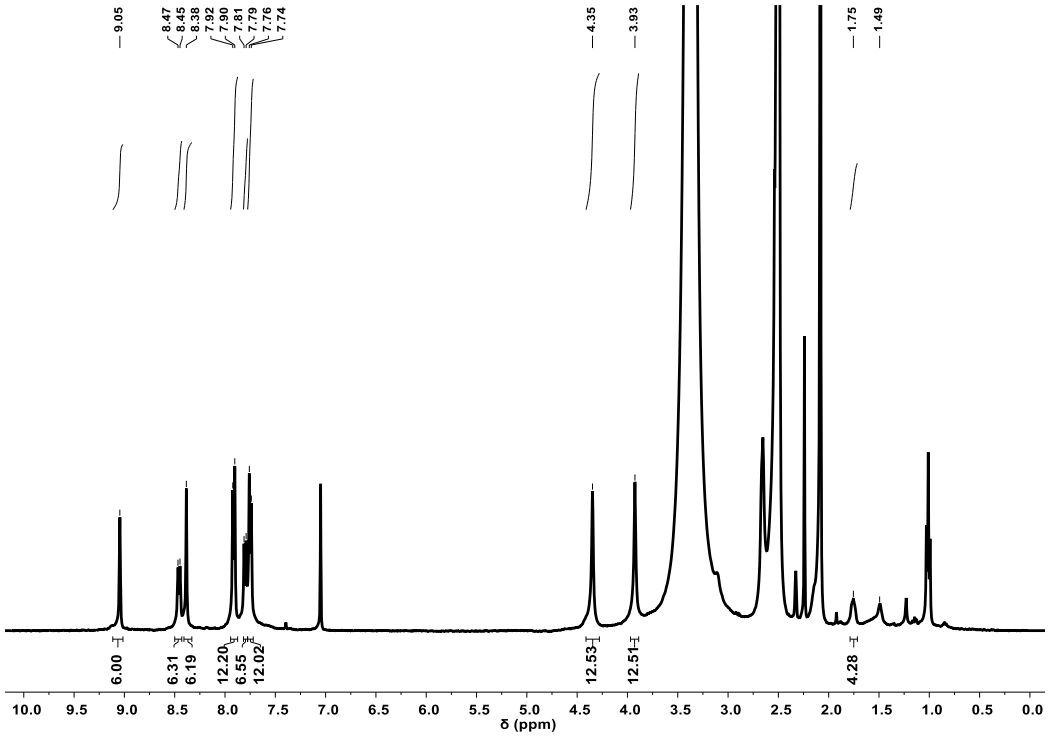

Figure A12. ^{1}H-NMR spectrum (400 MHz, 301 K, DMSO-d_6) of cage **C_6@2**.

A3.6.2. C_{10}@2

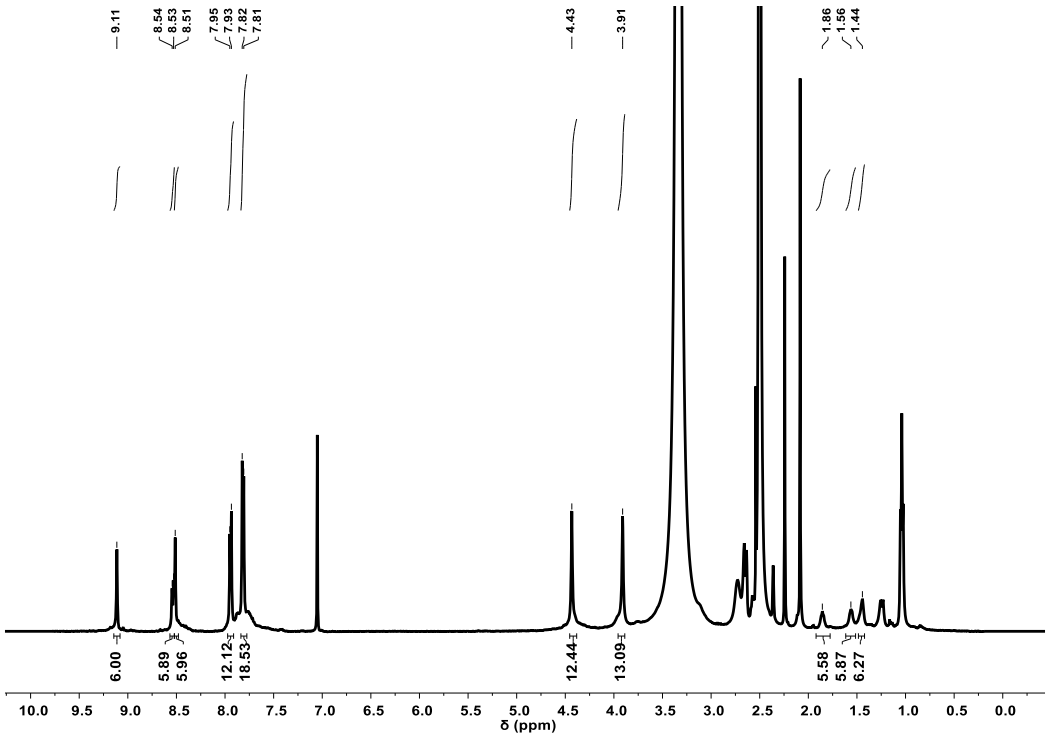

Figure A13. ^{1}H-NMR spectrum (500 MHz, 301 K, DMSO-d_6) of cage **C_{10}@2**.

A3.6.3. C_6@4

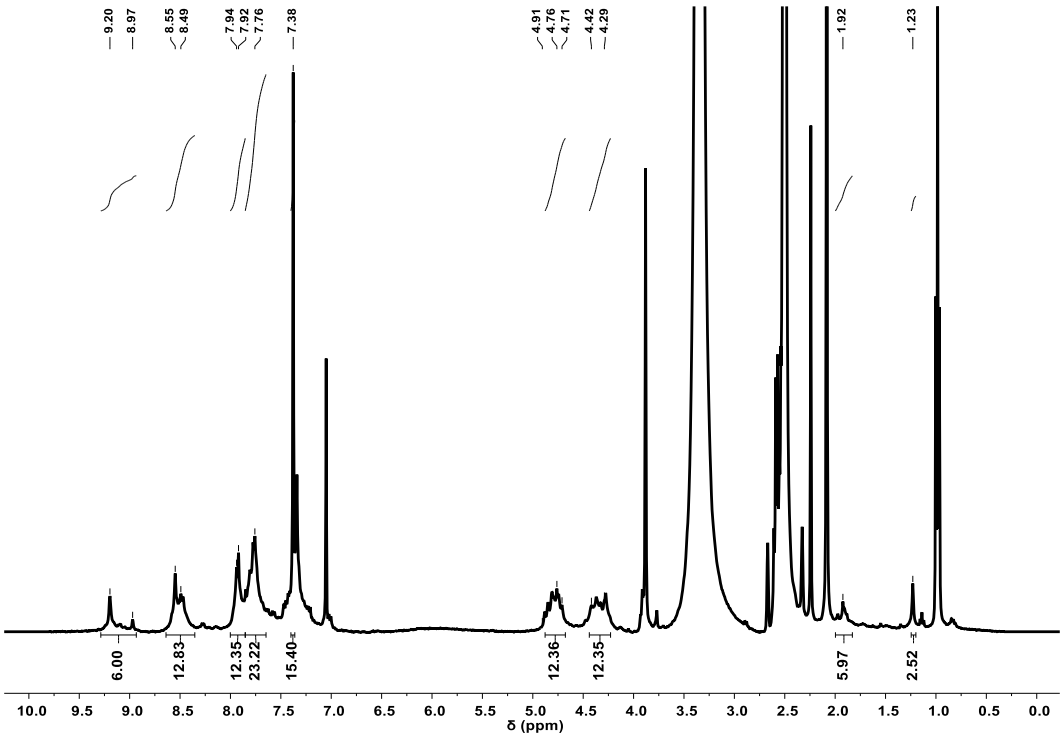

Figure A14. [1]H-NMR spectrum (400 MHz, 301 K, DMSO-d_6) of cage **C_6@4**.

A3.6.4. C_{10}@4

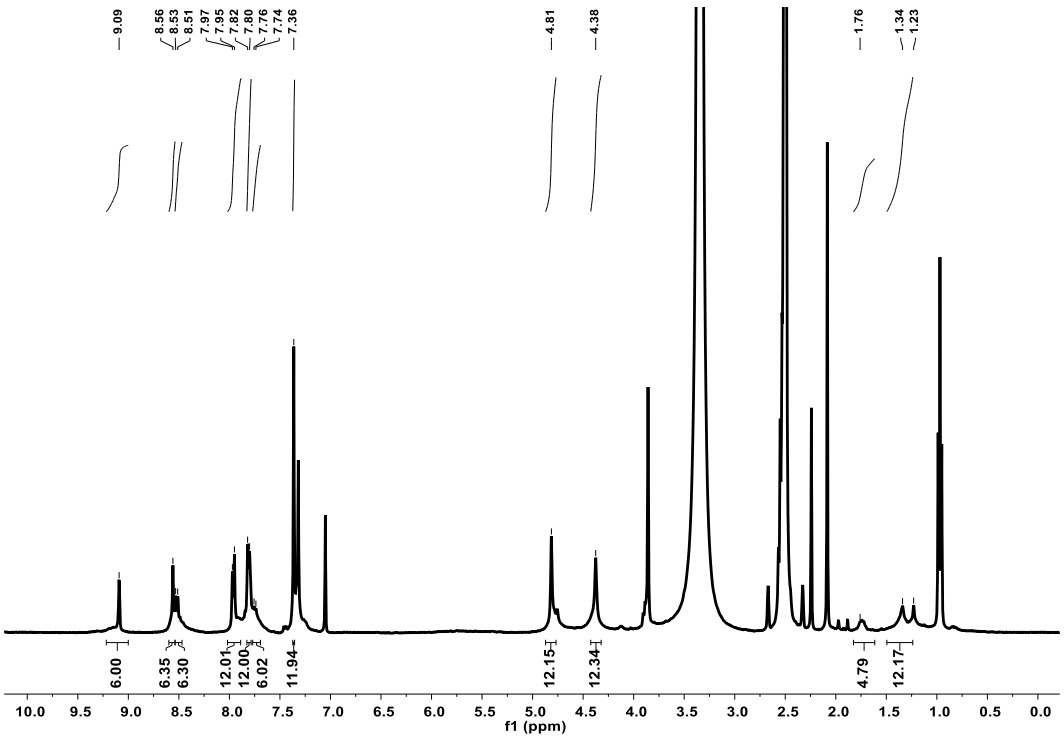

Figure A15. [1]H-NMR spectrum (400 MHz, 301 K, DMSO-d_6) of cage **C_{10}@4**.

A3.6.5. *RR*-L-Dibenz@7

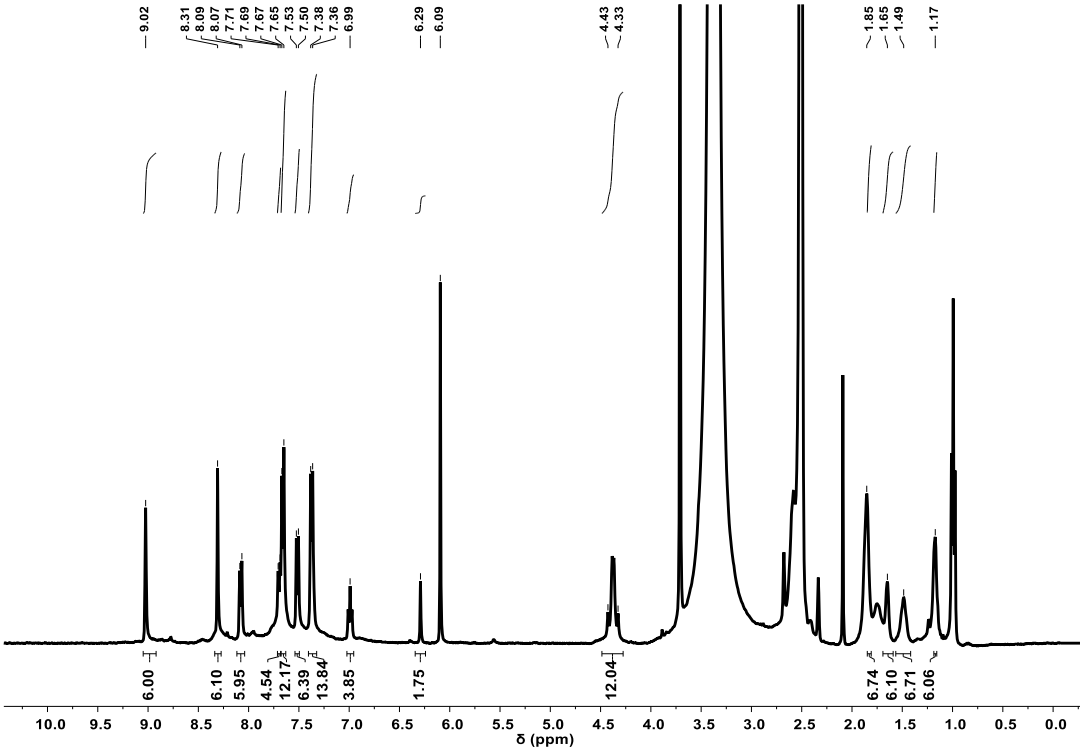

Figure A16. ^{1}H-NMR spectrum (400 MHz, 301 K, DMSO-d_6) of cage ***RR*-L-Dibenzoil@7**.

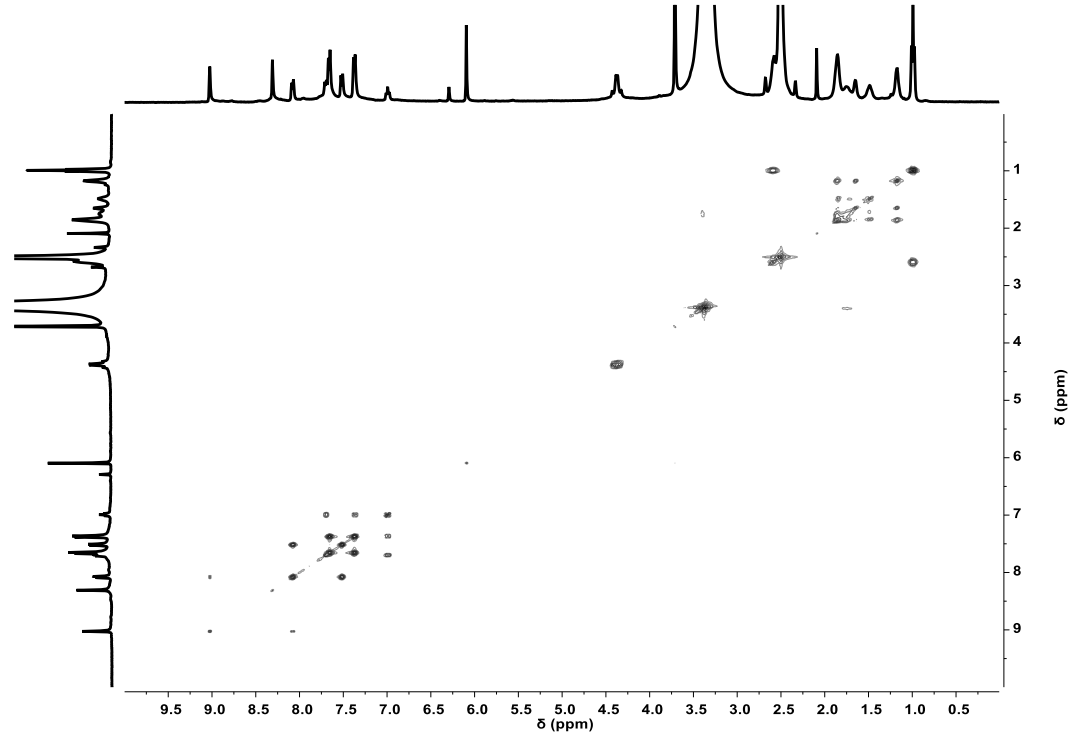

Figure A17. ^{1}H-^{1}H COSY spectrum (500 MHz, 301 K, DMSO-d_6) of cage ***RR*-L-Dibenzoil@7**.

A3.6.6. *RR*-D-Dibenz@7

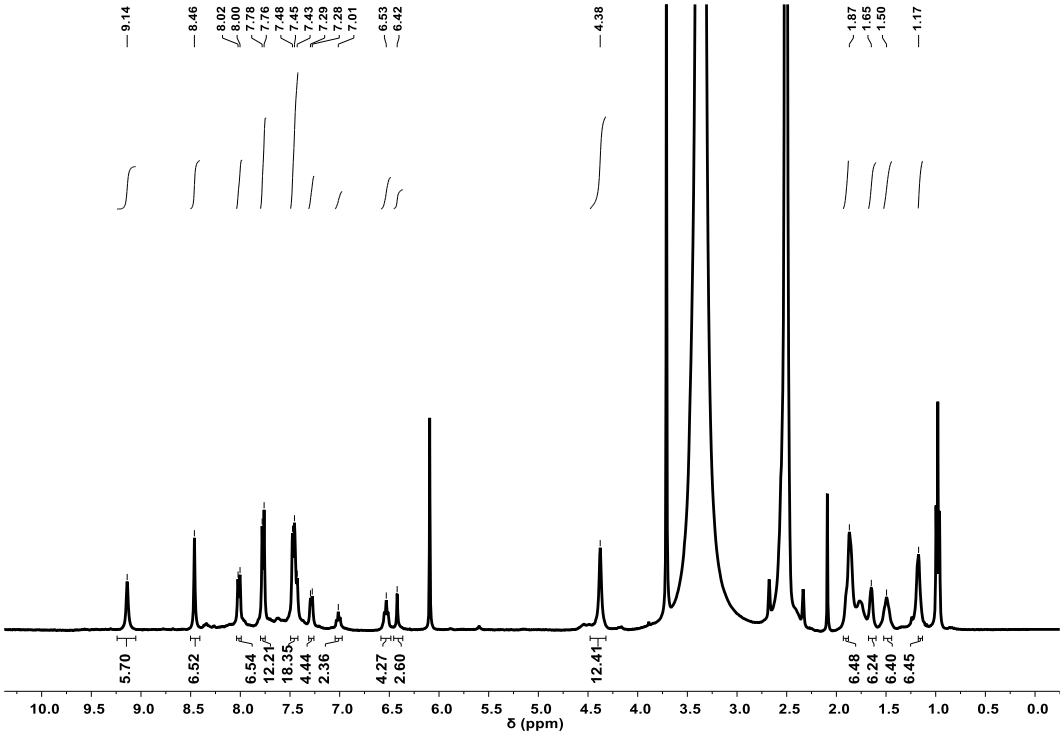

Figure A18. ^{1}H-NMR spectrum (400 MHz, 301 K, DMSO-d_6) of cage ***RR*-D-Dibenzoil@7**.

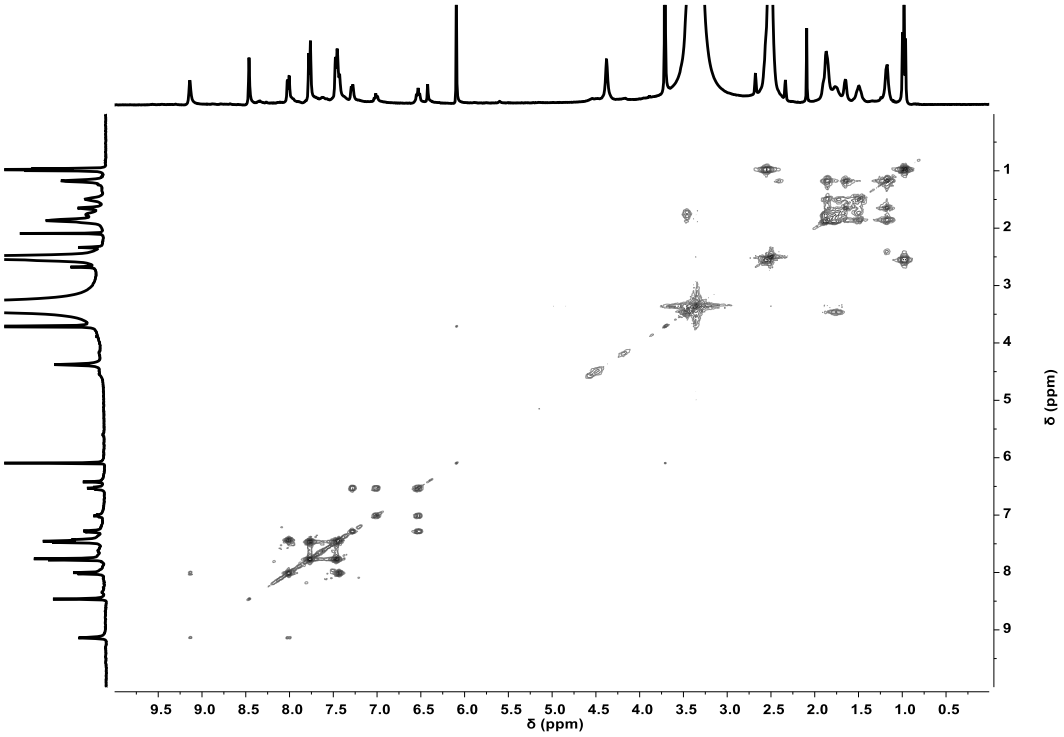

Figure A19. ^{1}H-^{1}H COSY spectrum (500 MHz, 301 K, DMSO-d_6) of cage ***RR*-D-Dibenzoil@7**.

A3.6.7. *RR*-L-Dibenz-OMe@7

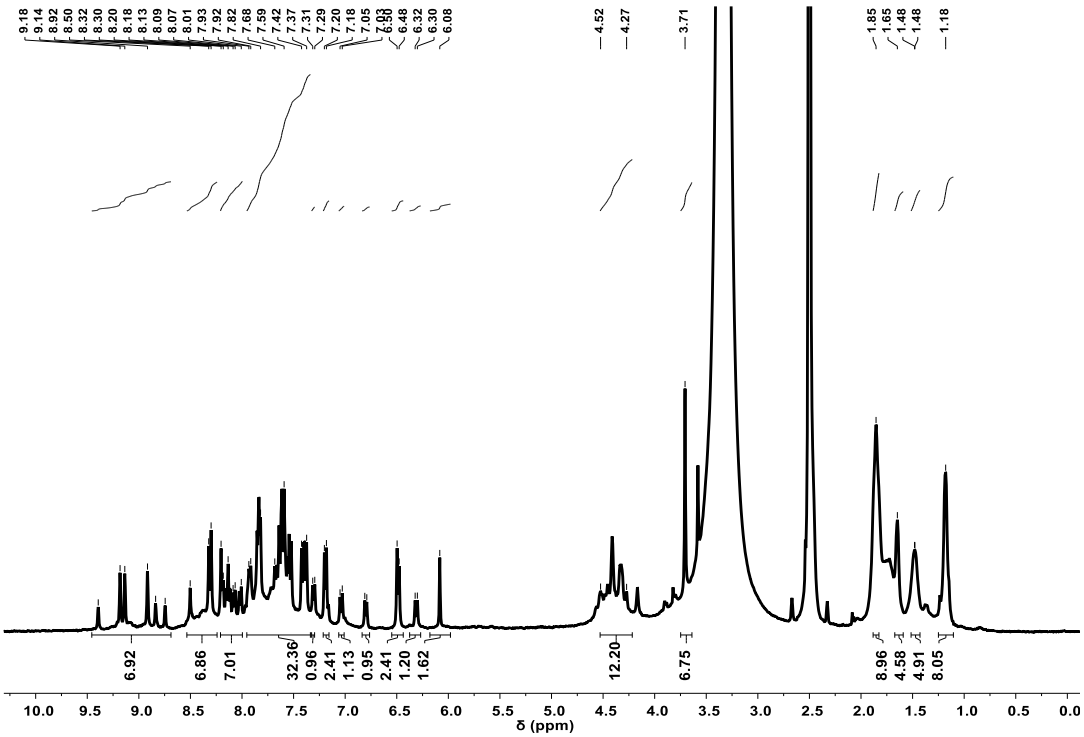

Figure A20. ^{1}H-NMR spectrum (400 MHz, 301 K, DMSO-d_6) of cage ***RR*-L-Dibenzoil-OMe@7**.

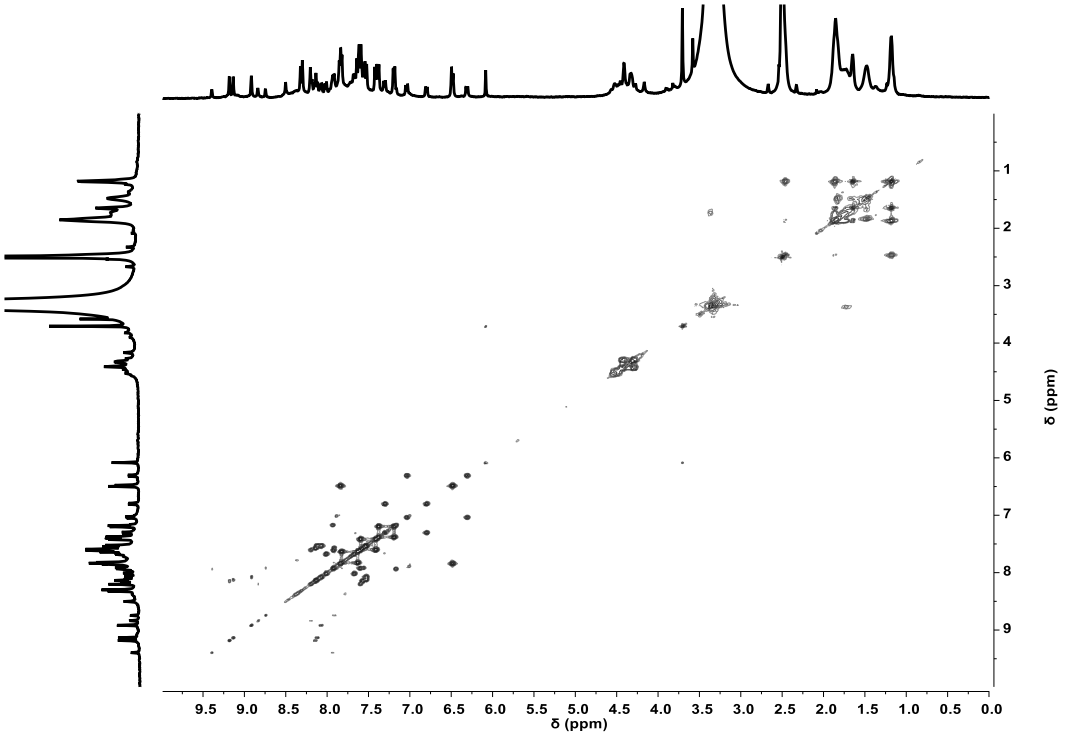

Figure A21. ^{1}H-^{1}H COSY spectrum (500 MHz, 301 K, DMSO-d_6) of cage ***RR*-L-Dibenzoil-OMe@7**.

A3.6.8. *RR*-D-Dibenz-OMe@7

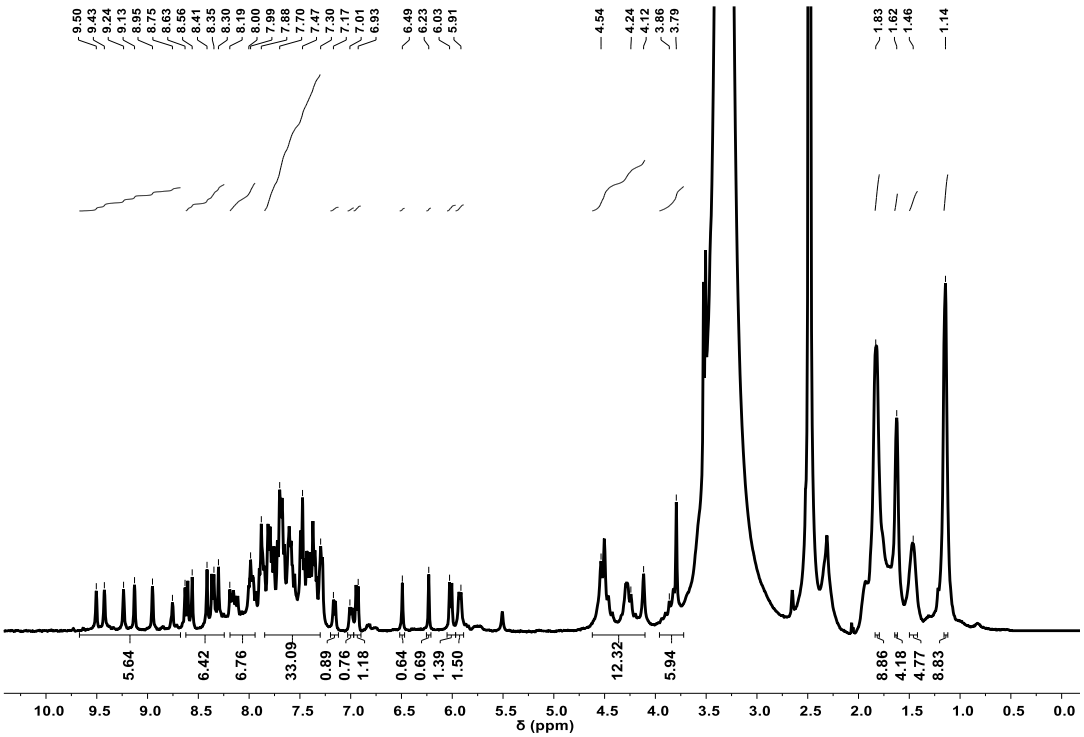

Figure A22. ^{1}H-NMR spectrum (400 MHz, 301 K, DMSO-d_6) of cage ***RR*-D-Dibenzoil-OMe@7**.

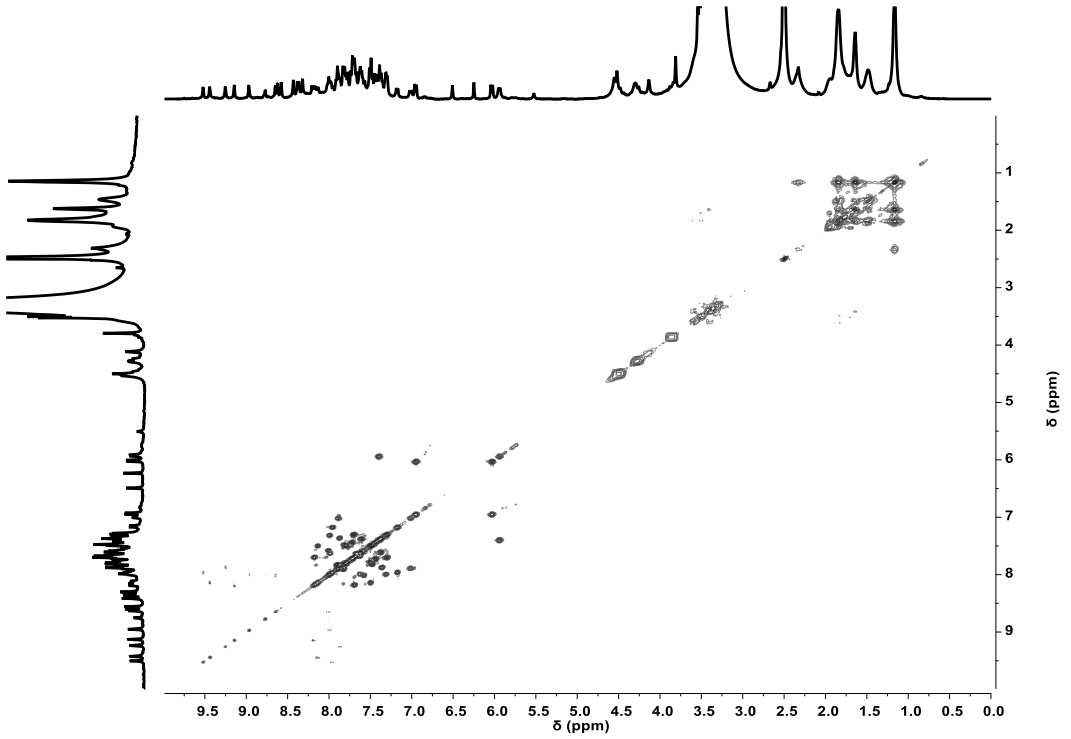

Figure A23. ^{1}H-^{1}H COSY spectrum (500 MHz, 301 K, DMSO-d_6) of cage ***RR*-D-Dibenzoil-OMe@7**.

A3.6.9. ESI-MS spectrum of cage *RR*-D-Dibenzoil@7

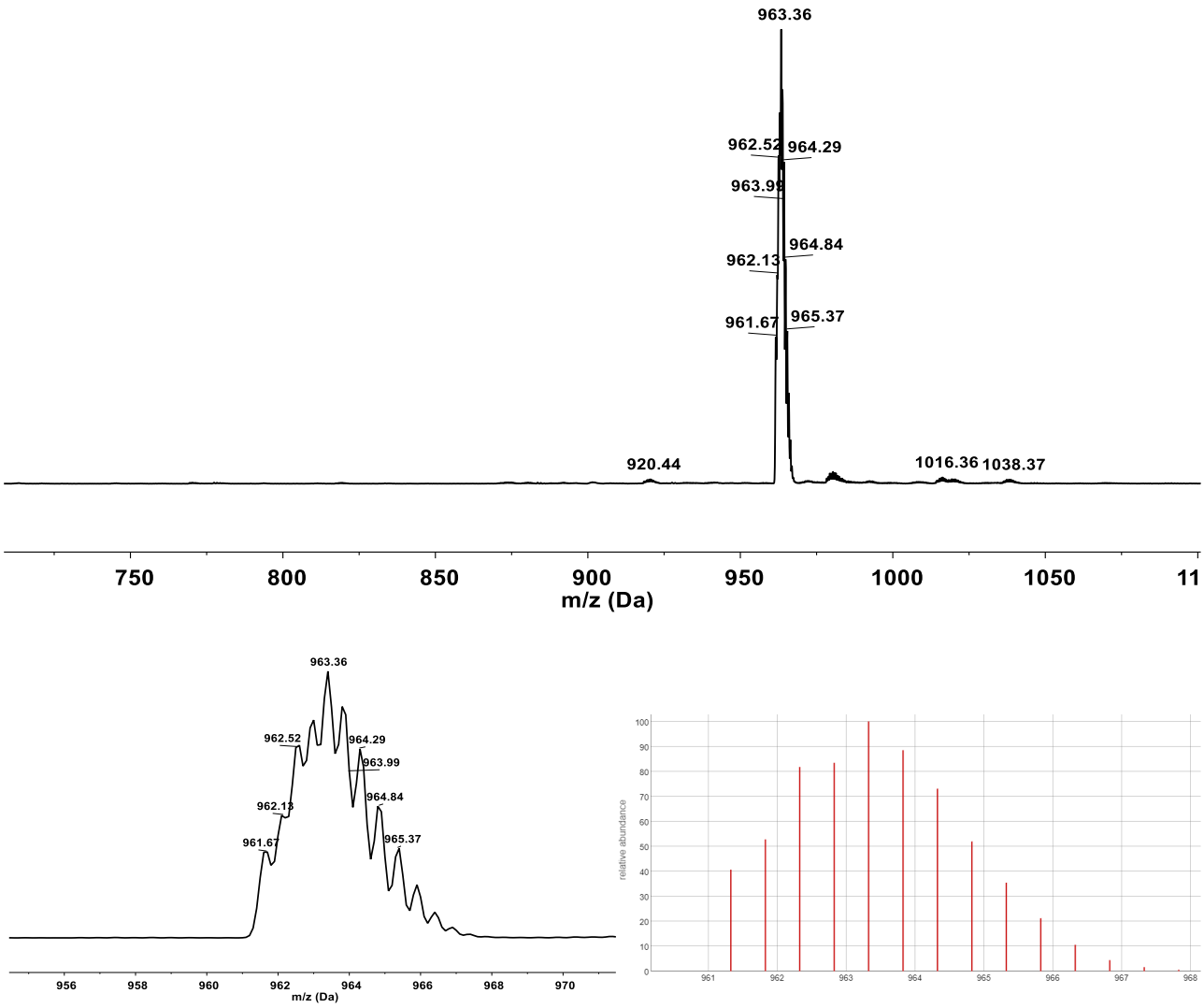

Figure A24. Experimental, and calculated ESI-MS pattern (in CH_3CN/0.1% HCOOH) of cage ***RR*-D-Dibenzoil@7.**

A3.6.10. ESI-MS spectrum of cage *RR*-D-Dibenzoil-OMe@7

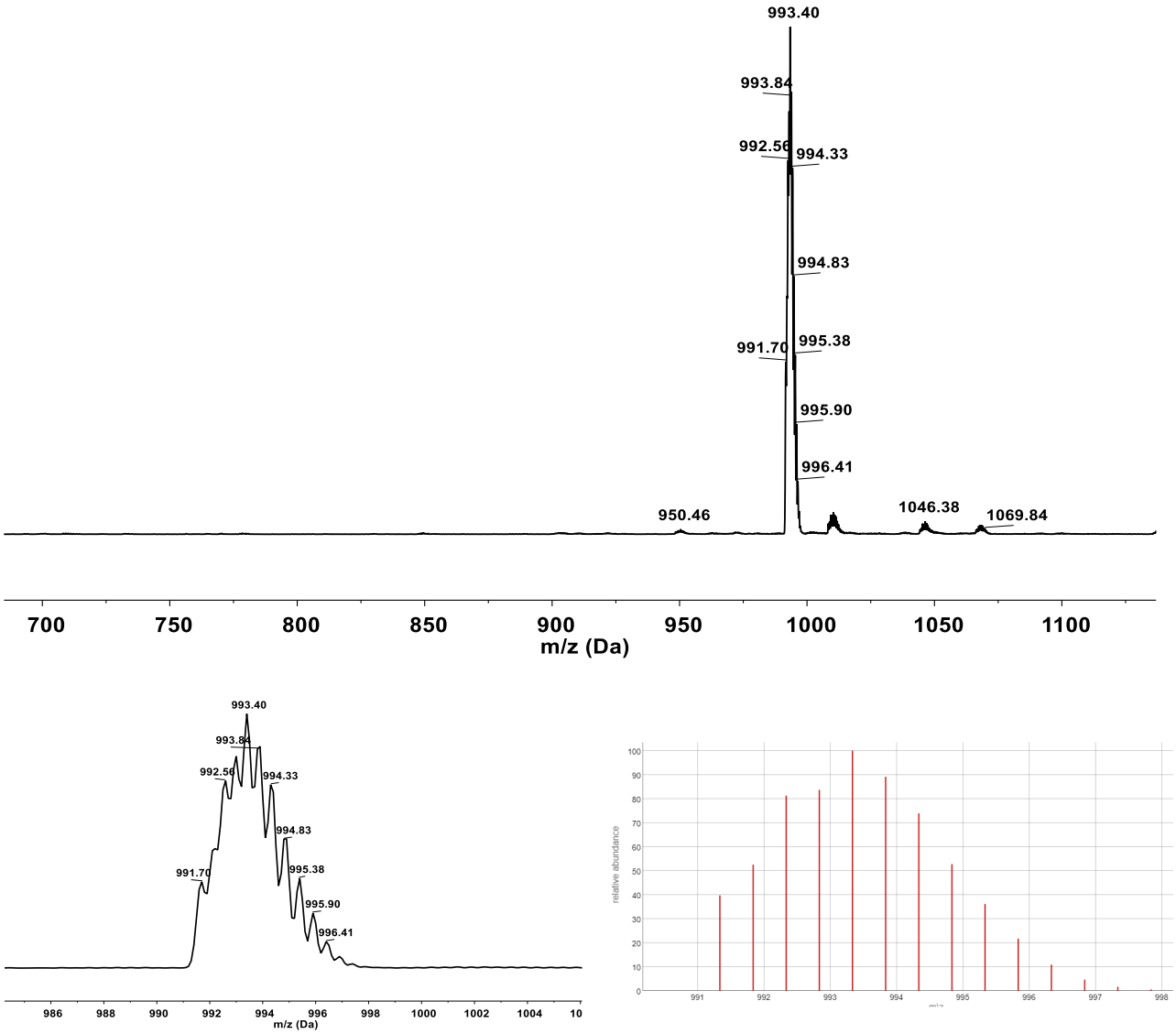

Figure A25. Experimental, and calculated ESI-MS pattern (in CH_3CN/0.1% HCOOH) of cage ***RR*-D-Dibenzoil-OMe@7.**

A4. Appendix Chapter 4

A4.1. CD measurements

CD measurements for compounds ***S*-4**, ***R*-4**, ***S*-5**, and ***S*-6** were performed in Milli-Q water with a concentration equal to $1.0 \cdot 10^{-4}$ M (0.1 cm cuvette).

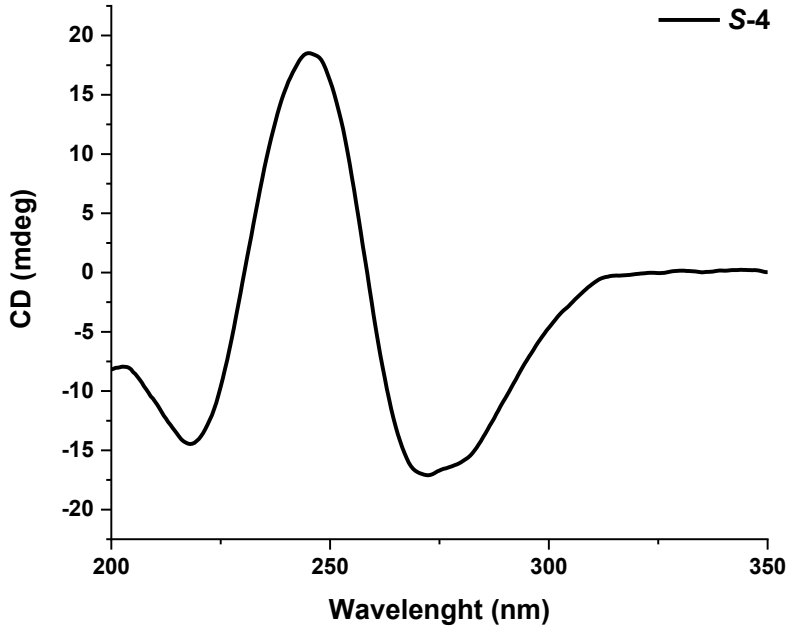

Figure A1. Circular Dichroism spectrum of compound ***S*-4**.

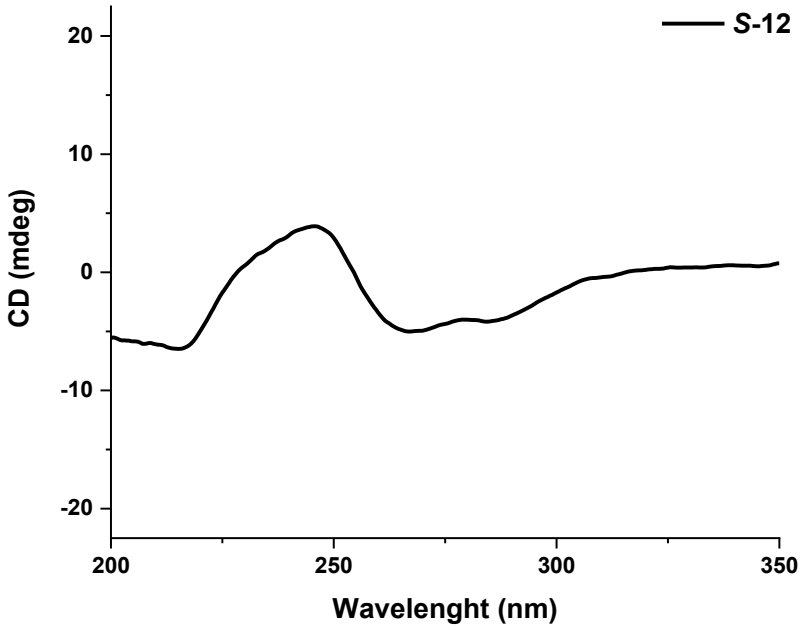

Figure A2. Circular Dichroism spectrum of compound ***S*-12**.

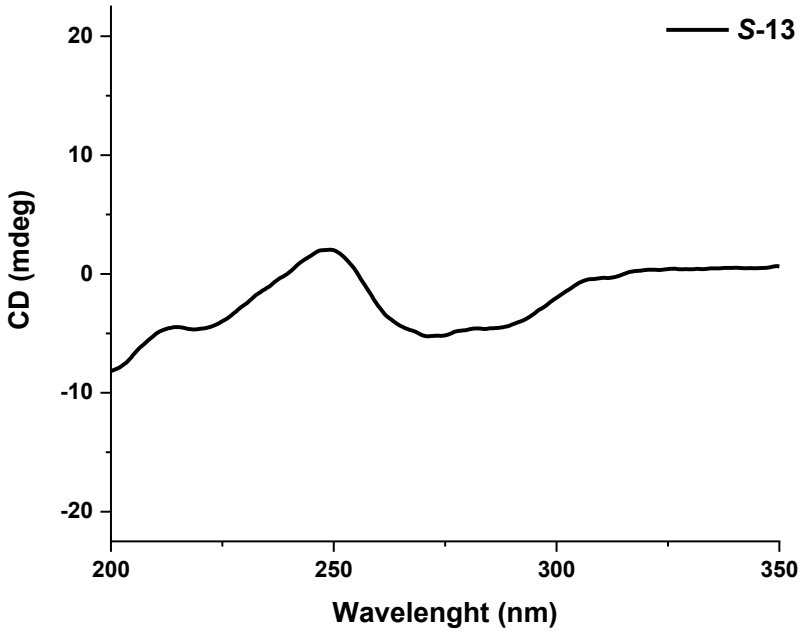

Figure A3. Circular Dichroism spectrum of compound ***S*-13**.

A4.2. Kinetic Experiment for the formation of cage C_3@3

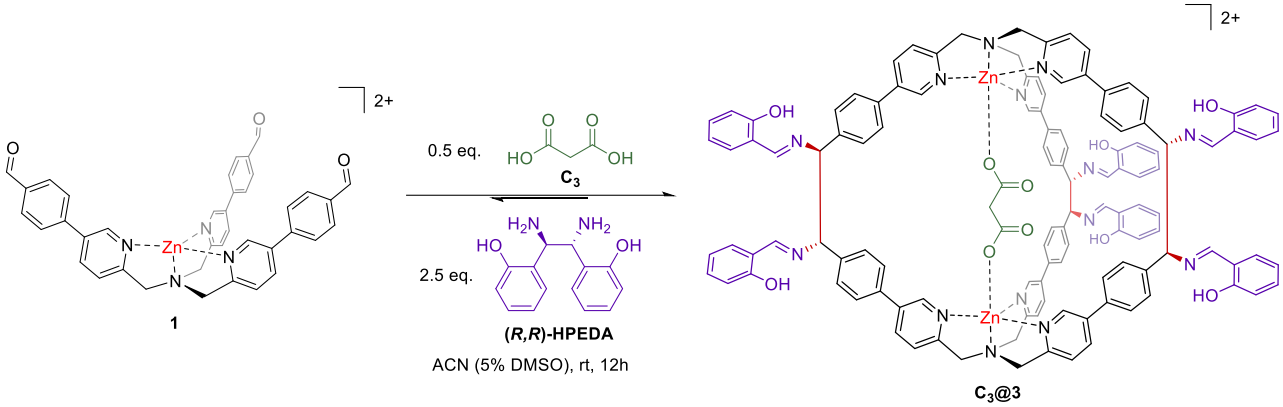

To 500 µL (1.0 µmol) of a solution 0.002 M of complex **1** CD_3CN, 50 µL (0.5 µmol) of a solution 0.01 M in CD_3CN of malonic acid (**C_3**) and 125 µL (2.5 µmol) of a solution 0.02 M in CD_3CN/DMSO-*d_6* (1:1) of **(*R*,*R*)-HPEDA** were added in a NMR tube. The formation of cage **C_3@3** was followed for 24 h at *via* ^{1}H-NMR. (yield > 97% determined *via* ^{1}H-NMR based on internal standard *p*-xylene).

^{1}H NMR (400 MHz, 301 K, CD_3CN/5% DMSO-*d_6*) δ 13.03 (s, 6H), 9.19 (s, 6H), 8.60 (s, 6H), 8.23 (d, *J* = 8.1, 6H), 7.65 (d, *J* = 8.1 Hz, 6H), 7.56 (d, *J* = 7.9 Hz, 12H), 7.38 (d, *J* = 7.9 Hz, 12H), 7.31 – 7.27 (m, 12H), 6.86 – 6.83 (m, 12H), 4.98 (s, 6H), 4.39 – 4.02 (m, 12H).

HRMS (m/z): $[M]^{2+}$ calcd. for $[C_{123}H_{98}N_{14}O_{10}Zn_2]^{2+}$, 1031.4979; found 1031.3010.

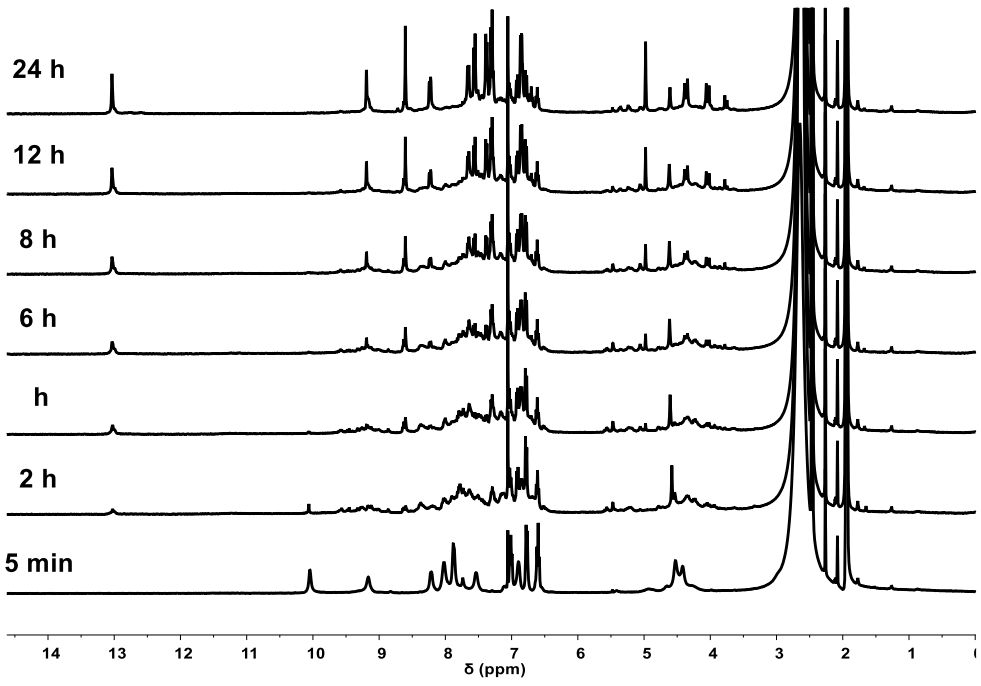

Figure A2. ^{1}H-NMR spectra (300 MHz, 301 K, CD_3CN/5% DMSO-d_6) during time after after the addition of Malonic Acid (**C_3**) (0.5 eq.) and **(R,R)-HPEDA** (2.5 eq) to the solution of complex **1** (1 eq.).

A4.3. Effect of the length of the diacid on the Diaza-Cope rearrangement

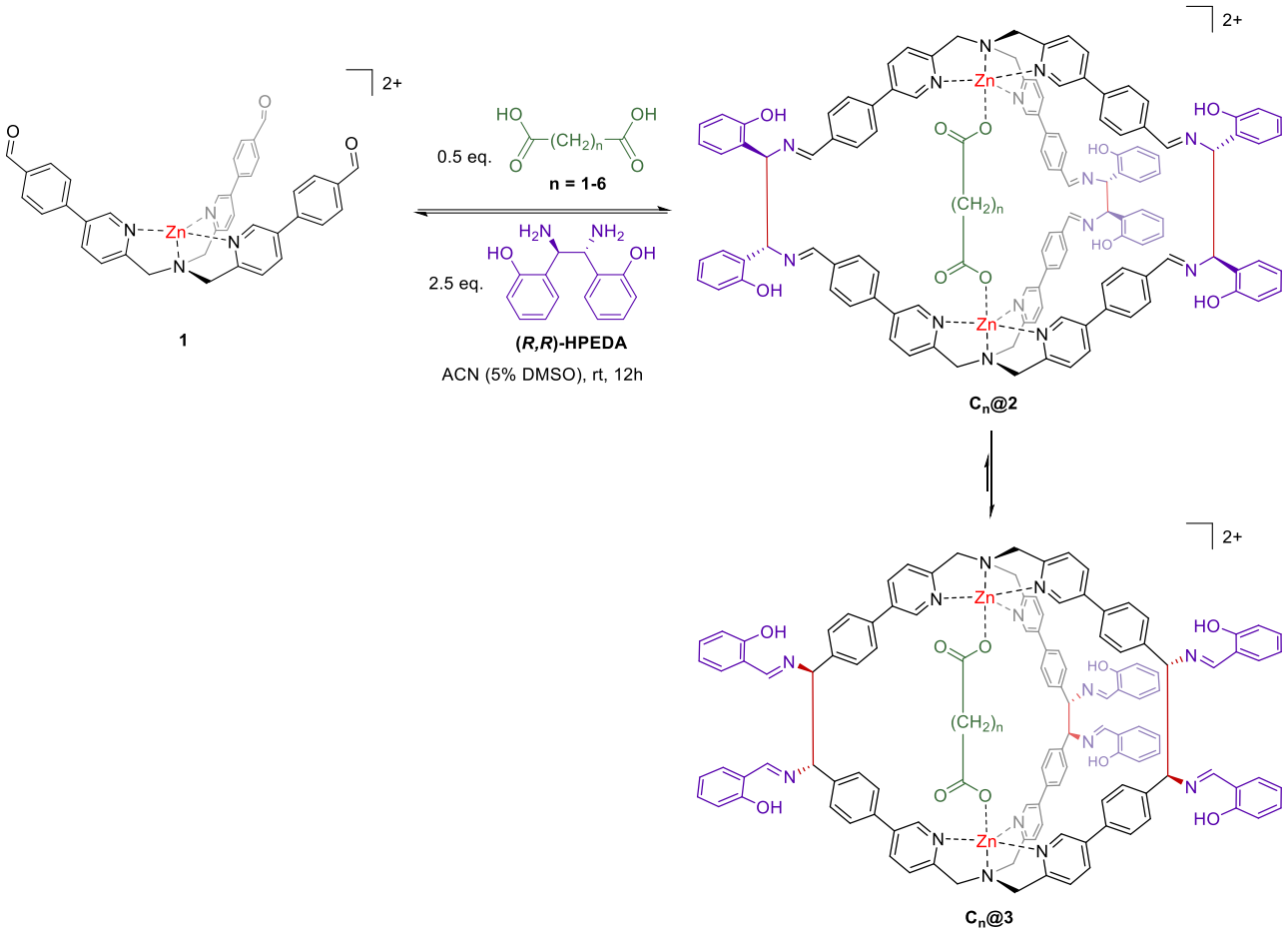

General procedure for the kinetic experiment. Perchlorate counterions are removed for clarity.

To 350 µL (0.70 µmol) of a solution 0.002 M of complex **1** in CD_3CN, 18 µL (0.35 µmol) of a solution 0.02 M in CD_3CN of a dicarboxylic acid **X,** 87 µL (1.75 µmol) of a solution 0.02 M in DMSO-d_6 of **(*R*,*R*)-HPEDA**, and 30 µL (0.60 µmol) of a solution 0.02 M in DMSO-d_6 of 1,3,5-trimetoxybenzene were added in a NMR tube. The reaction was followed for 24 h *via* ^{1}H-NMR.

The concentration of **1**, **C_n@2**, **C_n@3** were determined via ^{1}H-NMR by integration of the relative peaks using 1,3,5-trimetoxybenzene as internal standard.

Concentration of the intermediate species was determined using the equation:

$$[\mathbf{Intermediates}] = \frac{[\mathbf{1}]_0}{2} - \frac{[\mathbf{1}]_t}{2} - [\mathbf{C_n@2}]_t - [\mathbf{C_n@3}]_t$$

With $[\mathbf{1}]_0 = 1.44 \cdot 10^{-3}$ M

A4.3.1. Malonic Acid (C_3)

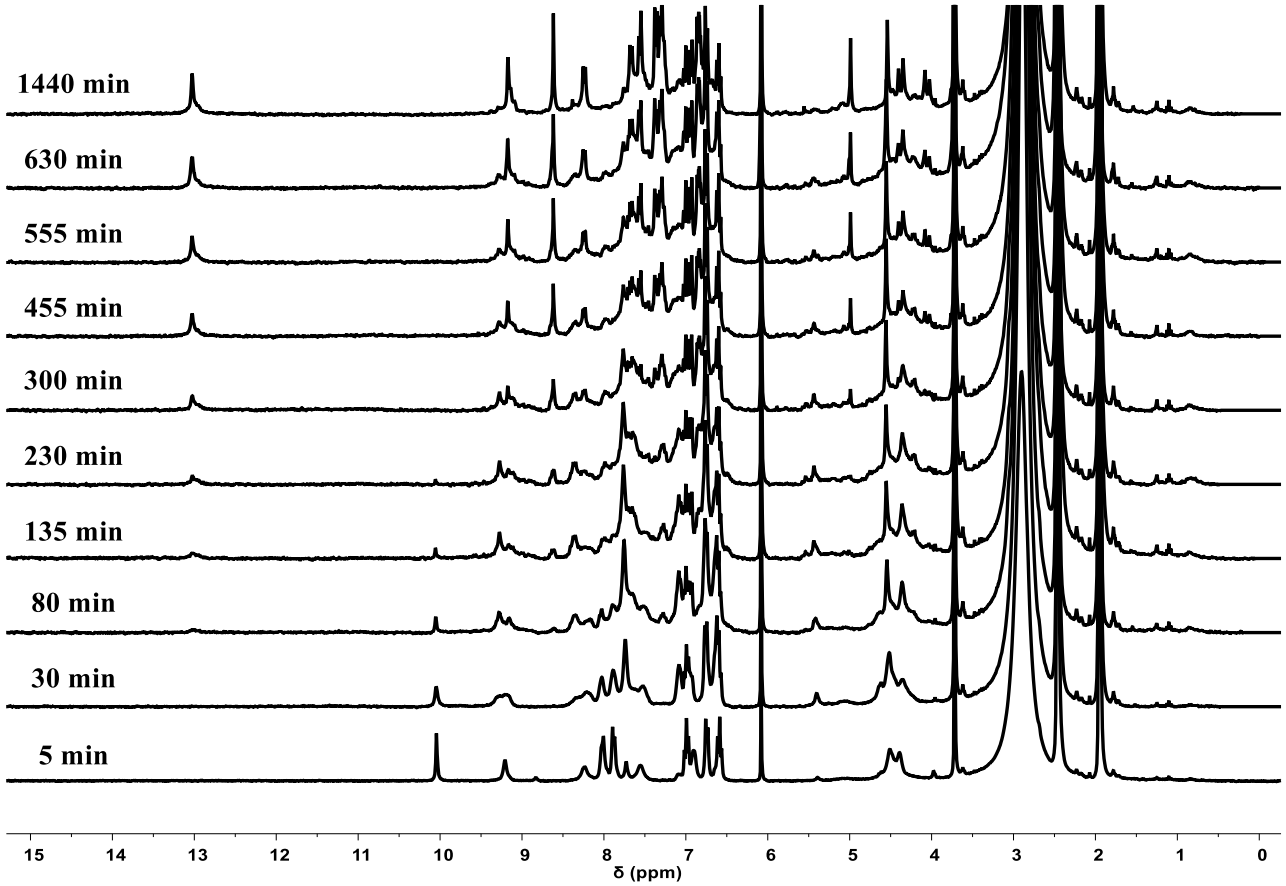

Figure A3. ^{1}H-NMR spectra (300 MHz, 301 K, CD_3CN/DMSO-d_6) during time after after the addition of Malonic Acid (**C_3**) (0.5 eq.) and **(R,R)-HPEDA** (2.5 eq) to the solution of complex **1** (1 eq.). The peak at 6.1 ppm corresponds to the internal standard 1,3,5-trimetoxybenzene.

Table A1. [**1**] determined by integration of the 3 protons at 10.03 ppm, [**C_3@2**] determined by integration of the 6 protons at 5.40 ppm, [**C_3@3**] determined by integration of the 6 protons at 5.00 ppm using 1,3,5-trimetoxybenzene as internal standard.

Time (min)		[1]/2 M	[C_3@2] (M)	[C_3@3] (M)	[Intermediates] (M)
5		6,75E-04	5,52E-05	0	0,00E+00
30		3,19E-04	2,76E-04	0	1,25E-04
80		1,04E-04	2,52E-04	0	3,64E-04
135		5,52E-05	2,33E-04	0	4,32E-04
230		1,23E-05	1,96E-04	5,52E-05	4,56E-04
300		0	1,84E-04	1,23E-04	4,13E-04
455		0	1,72E-04	1,90E-04	3,58E-04
555		0	1,47E-04	2,70E-04	3,03E-04
630		0	1,29E-04	3,56E-04	2,35E-04
1440		0	0	6,38E-04	8,20E-05

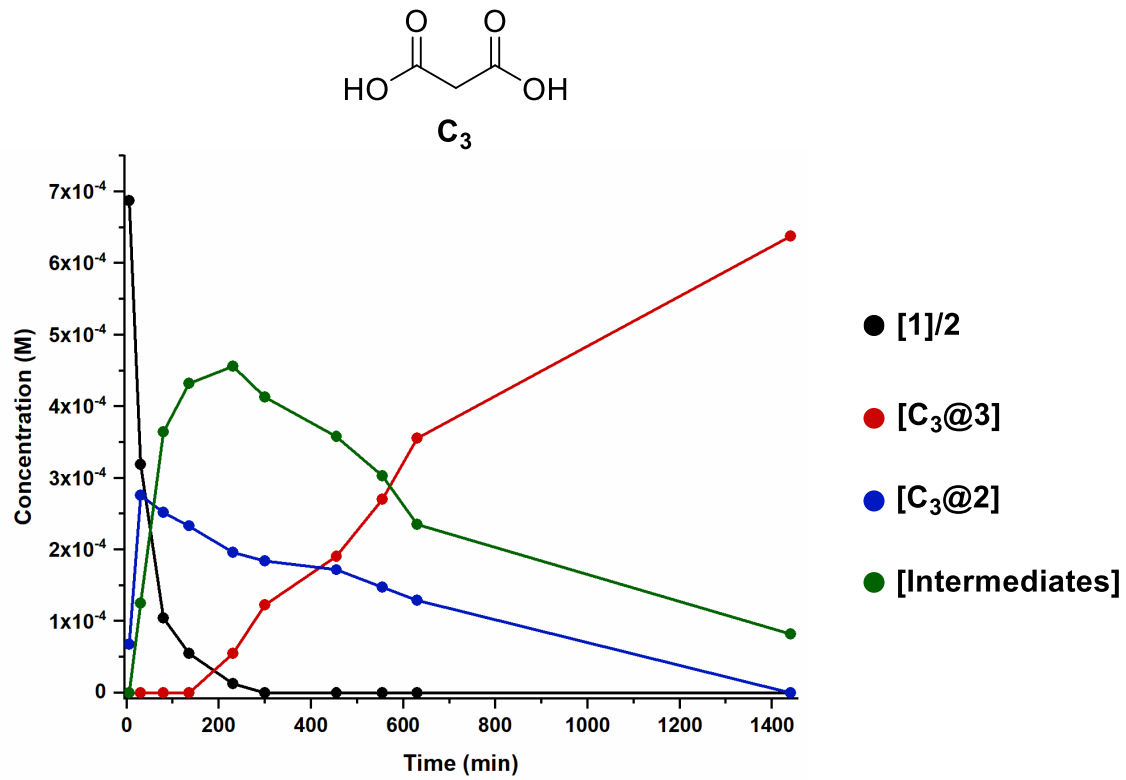

Figure A4. Kinetic profiles obtained for the differents species.

A4.3.2. Succinic Acid (C_4)

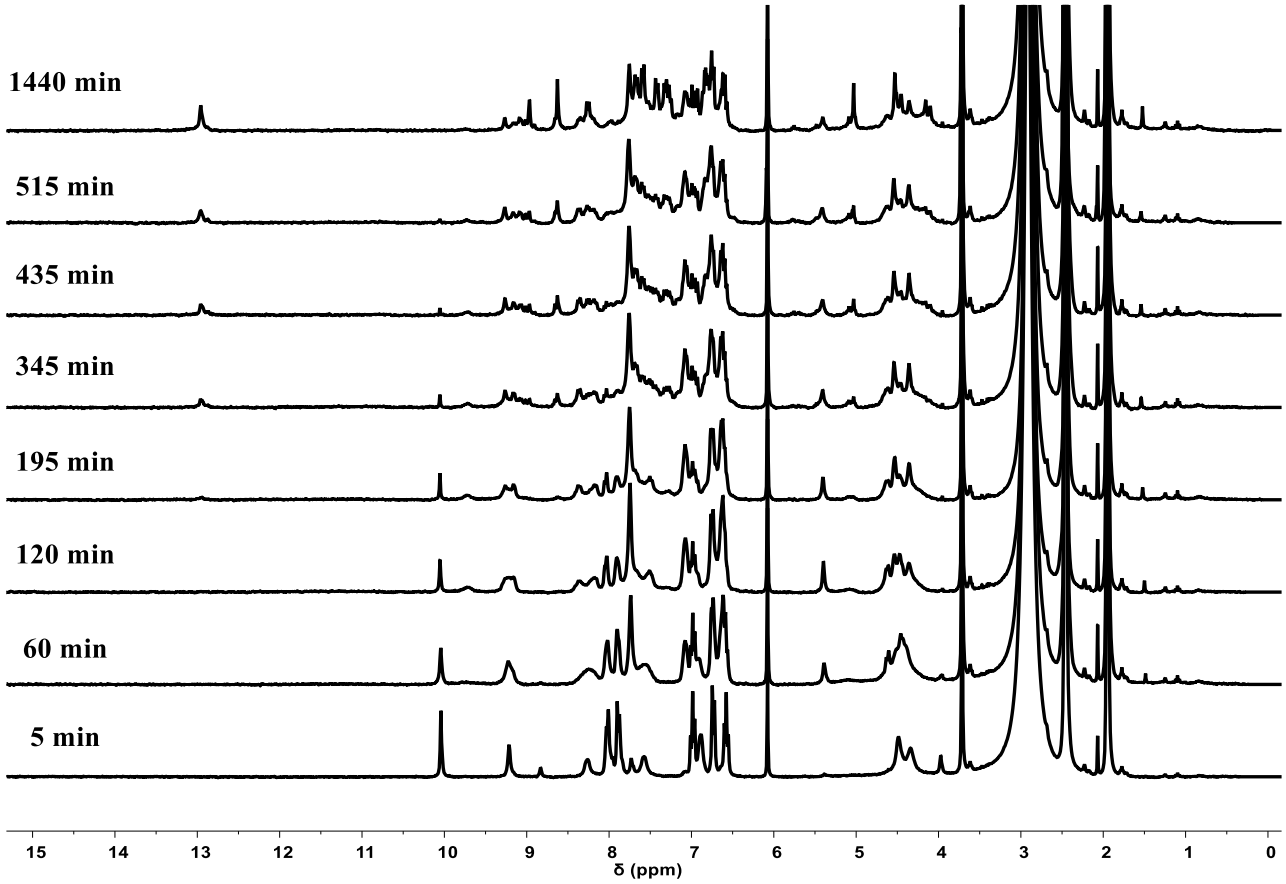

Figure A5. ^{1}H-NMR spectra (300 MHz, 301 K, CD_3CN/DMSO-d_6) during time after after the addition of Succinic Acid (**C_4**) (0.5 eq.) and **(R,R)-HPEDA** (2.5 eq) to the solution of complex **1** (1 eq.). The peak at 6.1 ppm corresponds to the internal standard 1,3,5-trimetoxybenzene.

Table A2. [**1**] determined by integration of the 3 protons at 10.03 ppm, [**C_4@2**] determined by integration of the 6 protons at 5.40 ppm, [**C_4@3**] determined by integration of the 6 protons at 5.00 ppm using 1,3,5-trimetoxybenzene as internal standard.

Time (min)	[1]/2 M	[C_4@2] (M)	[C_4@3] (M)	[Intermediates] (M)
5	6,75E-04	4,91E-05	0	0
60	4,42E-04	3,01E-04	0	0
120	2,82E-04	3,31E-04	0	1,07E-04
195	1,66E-04	2,70E-04	0	2,84E-04
345	5,52E-05	2,33E-04	8,59E-05	3,46E-04
435	3,07E-05	2,15E-04	9,82E-05	3,76E-04
515	2,45E-05	2,09E-04	1,23E-04	3,64E-04
1440	0	1,72E-04	3,01E-04	2,48E-04

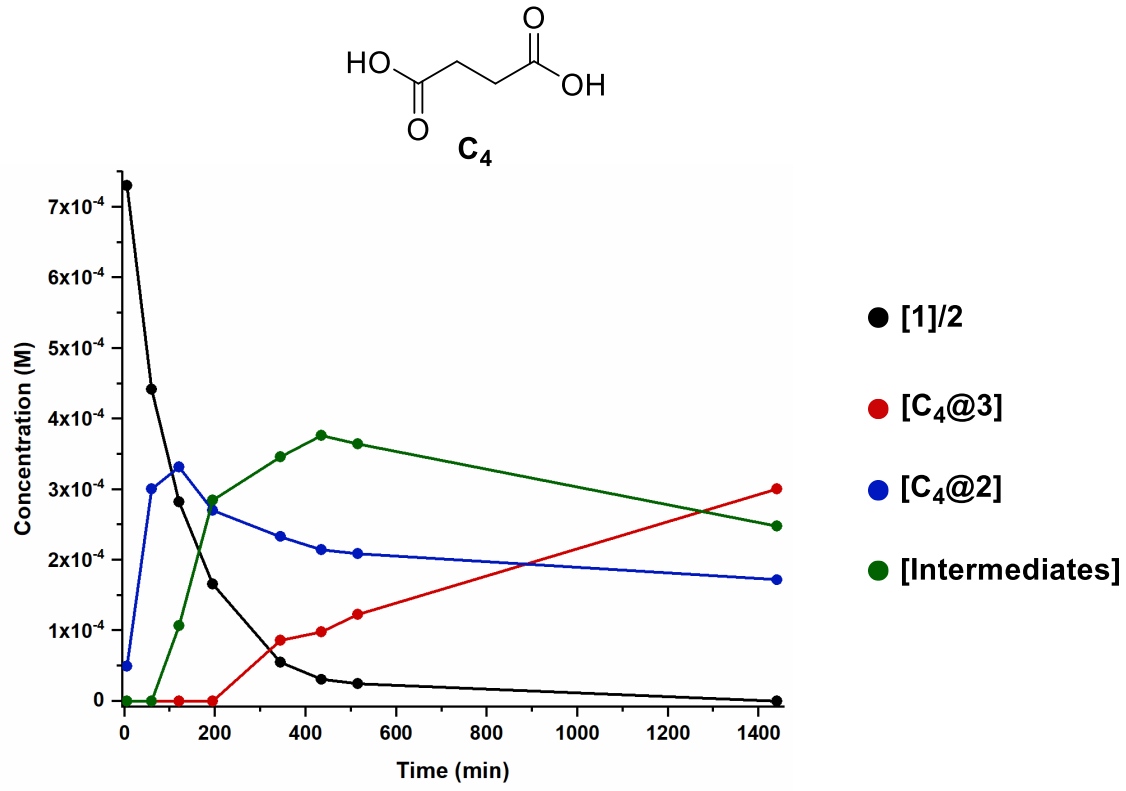

Figure A6. Kinetic profiles obtained for the differents species.

A4.3.3. Glutaric Acid (C_5)

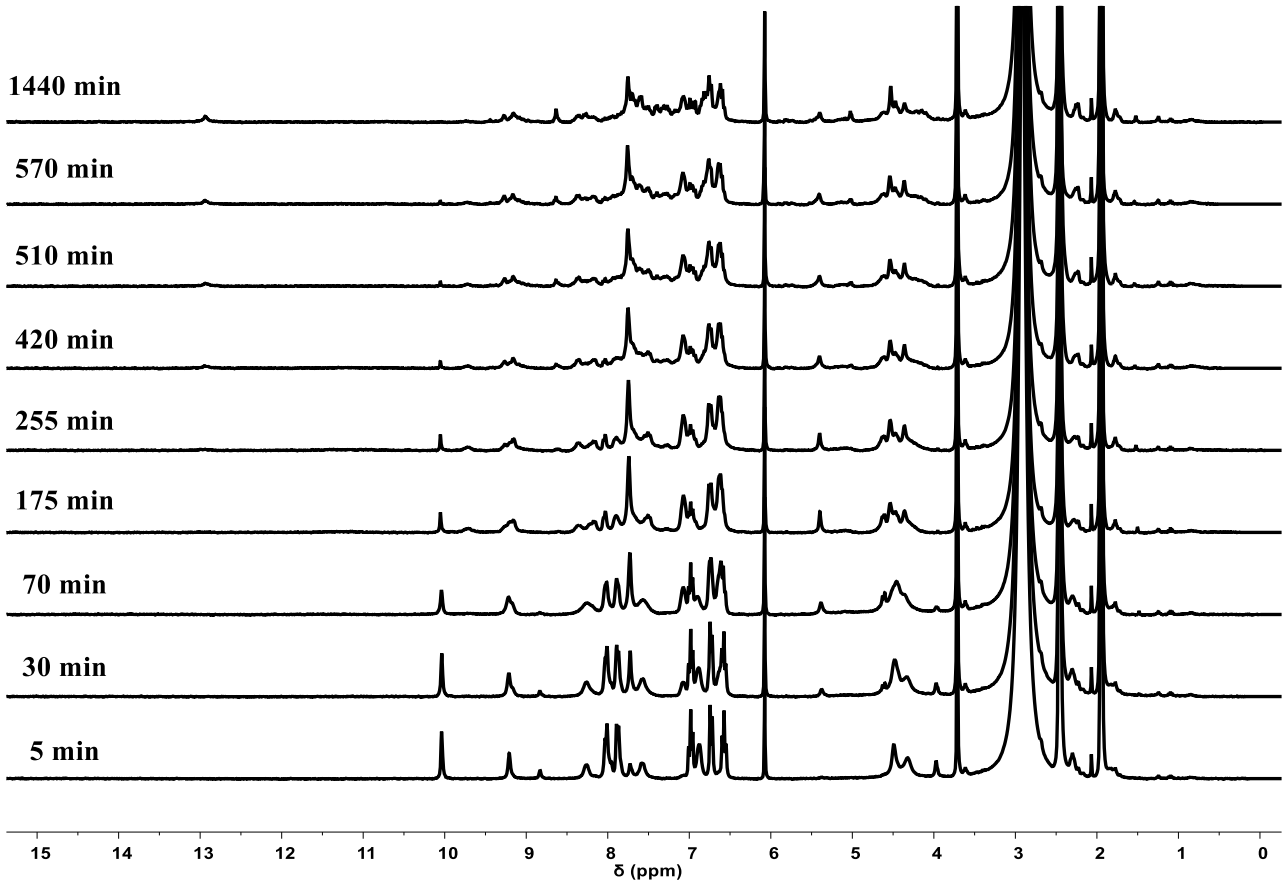

Figure A7. ^{1}H-NMR spectra (300 MHz, 301 K, CD_3CN/DMSO-d_6) during time after after the addition of Glutaric Acid (**C_5**) (0.5 eq.) and **(R,R)-HPEDA** (2.5 eq) to the solution of complex **1** (1 eq.). The peak at 6.1 ppm corresponds to the internal standard 1,3,5-trimetoxybenzene.

Table A3. [**1**] determined by integration of the 3 protons at 10.03 ppm, [**C_5@2**] determined by integration of the 6 protons at 5.40 ppm, [**C_5@3**] determined by integration of the 6 protons at 5.00 ppm using 1,3,5-trimetoxybenzene as internal standard.

Time (min)	[1]/2 M	[C_5@2] (M)	[C_5@3] (M)	[Intermediates] (M)
5	6,99E-04	3,07E-05	0	0
30	5,83E-04	1,84E-04	0	0
70	4,48E-04	3,01E-04	0	0
175	2,27E-04	3,31E-04	0	1,62E-04
255	1,41E-04	3,25E-04	0	2,54E-04
420	6,75E-05	3,01E-04	6,75E-05	2,84E-04
510	4,29E-05	2,64E-04	7,36E-05	3,40E-04
570	2,45E-05	2,39E-04	1,04E-04	3,52E-04
1440	0	1,72E-04	2,15E-04	3,33E-04

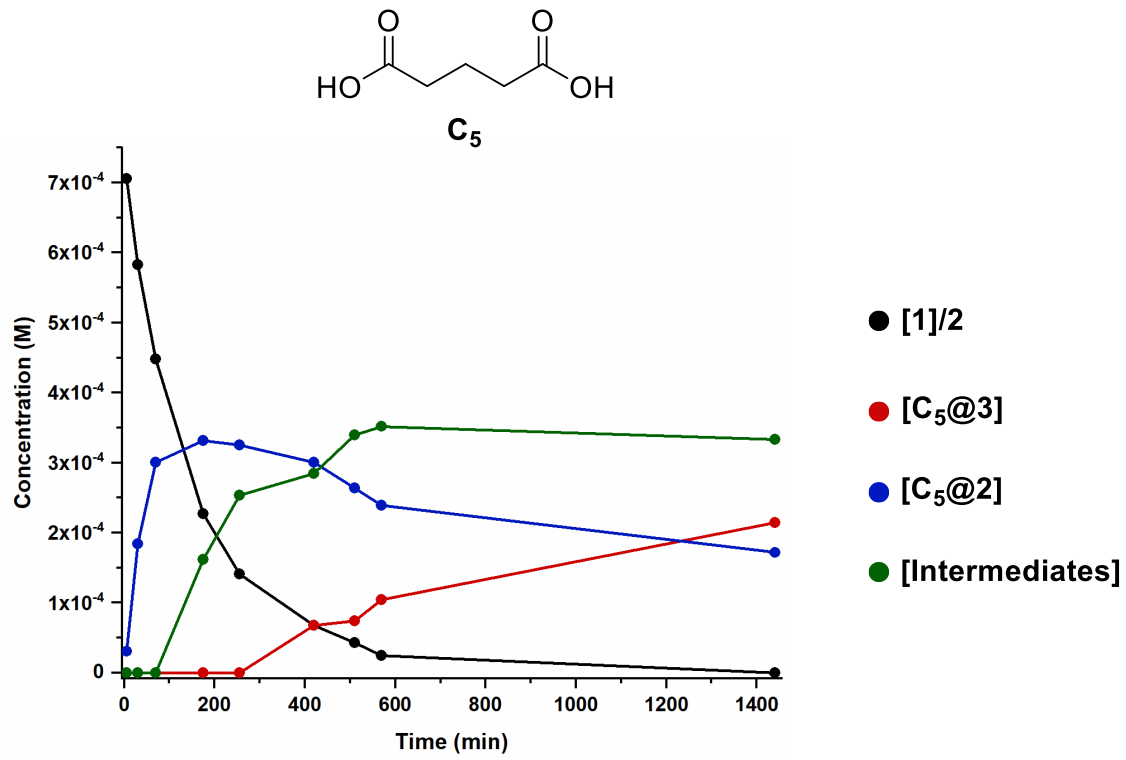

Figure A8. Kinetic profiles obtained for the differents species.

A4.3.4. Adipic Acid (C_6)

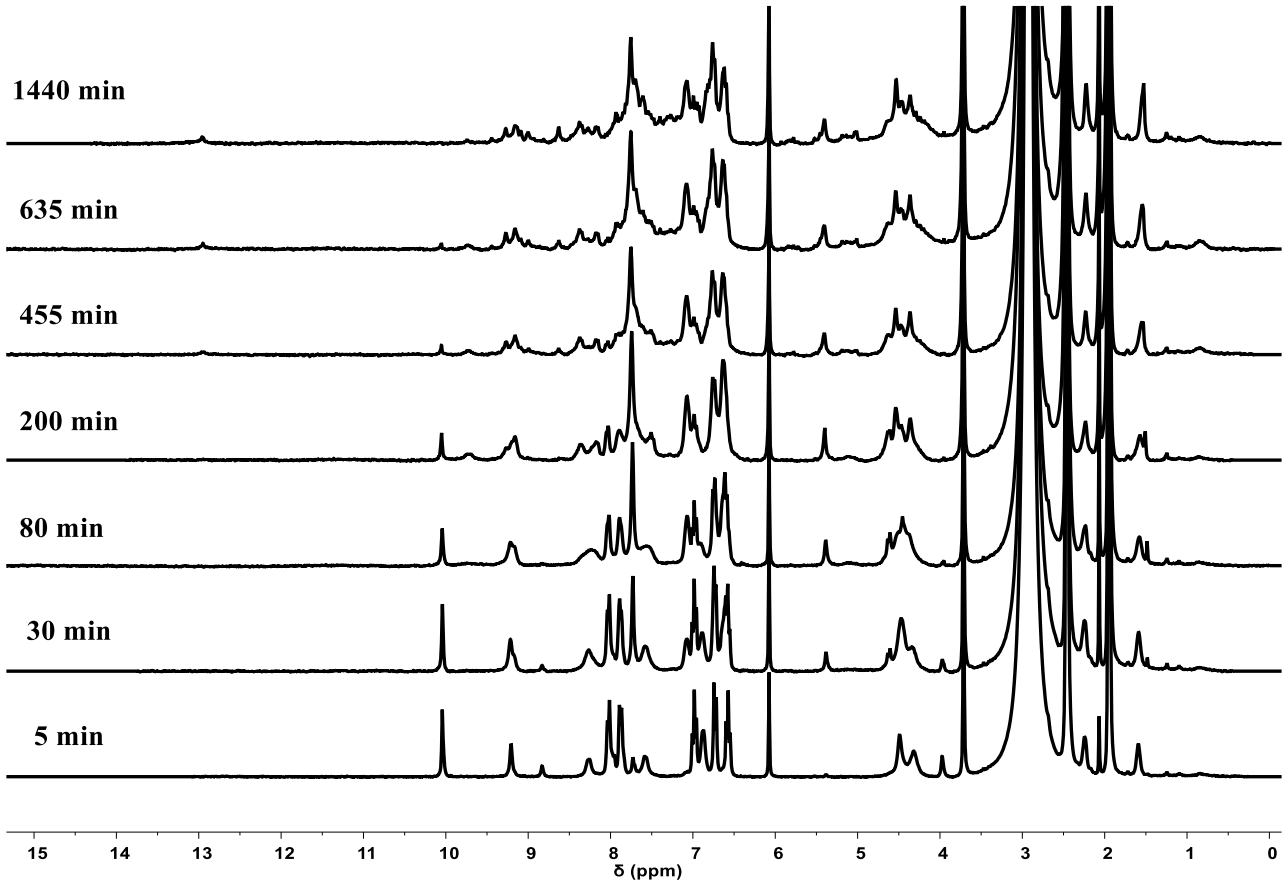

Figure A9. ^{1}H-NMR spectra (300 MHz, 301 K, CD_3CN/DMSO-d_6) during time after after the addition of Adipic Acid (**C_6**) (0.5 eq.) and **(R,R)-HPEDA** (2.5 eq) to the solution of complex **1** (1 eq.). The peak at 6.1 ppm corresponds to the internal standard 1,3,5-trimetoxybenzene.

Table A4. [**1**] determined by integration of the 3 protons at 10.03 ppm, [**C_6@2**] determined by integration of the 6 protons at 5.40 ppm, [**C_6@3**] determined by integration of the 6 protons at 5.00 ppm using 1,3,5-trimetoxybenzene as internal standard.

Time (min)	[1]/2 M	[C_6@2] (M)	[C_6@3] (M)	[Intermediates] (M)
5	6,99E-04	1,84E-05	0	0
30	4,97E-04	2,21E-04	0	0
80	3,68E-04	3,13E-04	0	3,90E-05
200	2,09E-04	3,50E-04	0	1,62E-04
455	7,36E-05	2,82E-04	1,84E-05	3,46E-04
635	2,45E-05	2,64E-04	5,52E-05	3,76E-04
1440	0	2,52E-04	7,36E-05	3,95E-04

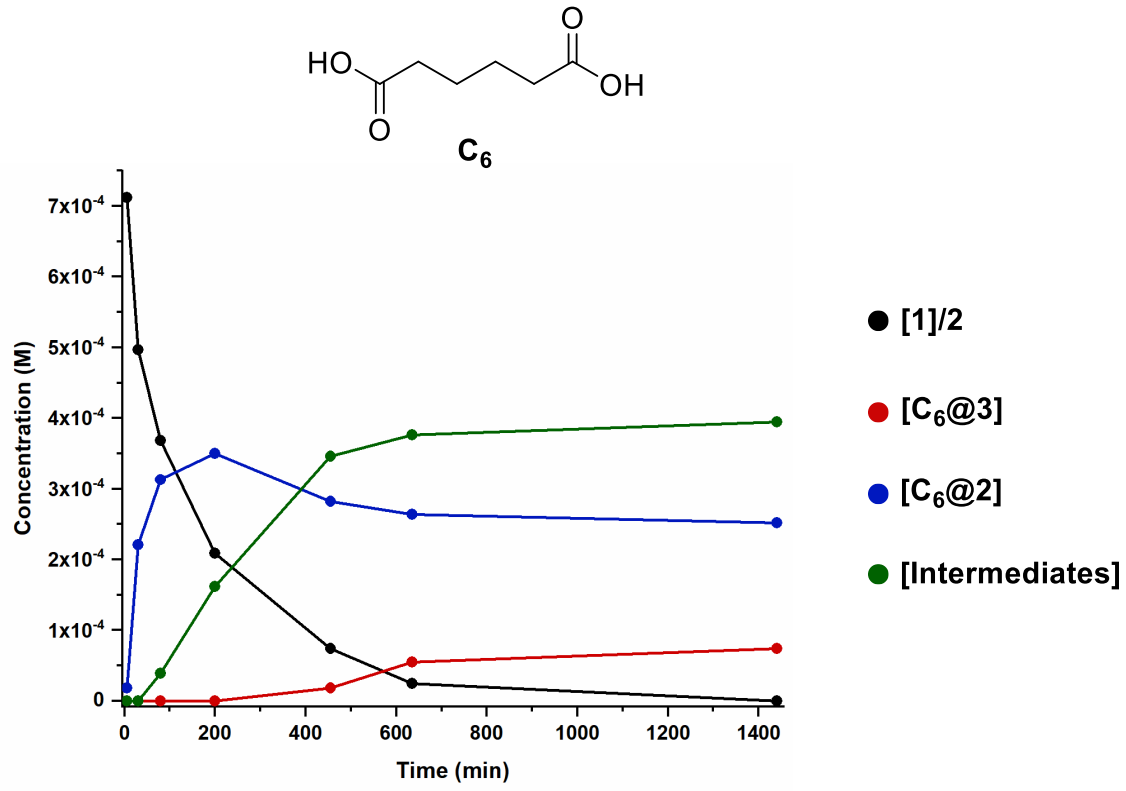

Figure A10. Kinetic profiles obtained for the differents species.

A4.3.5. Pimelic Acid (C_7)

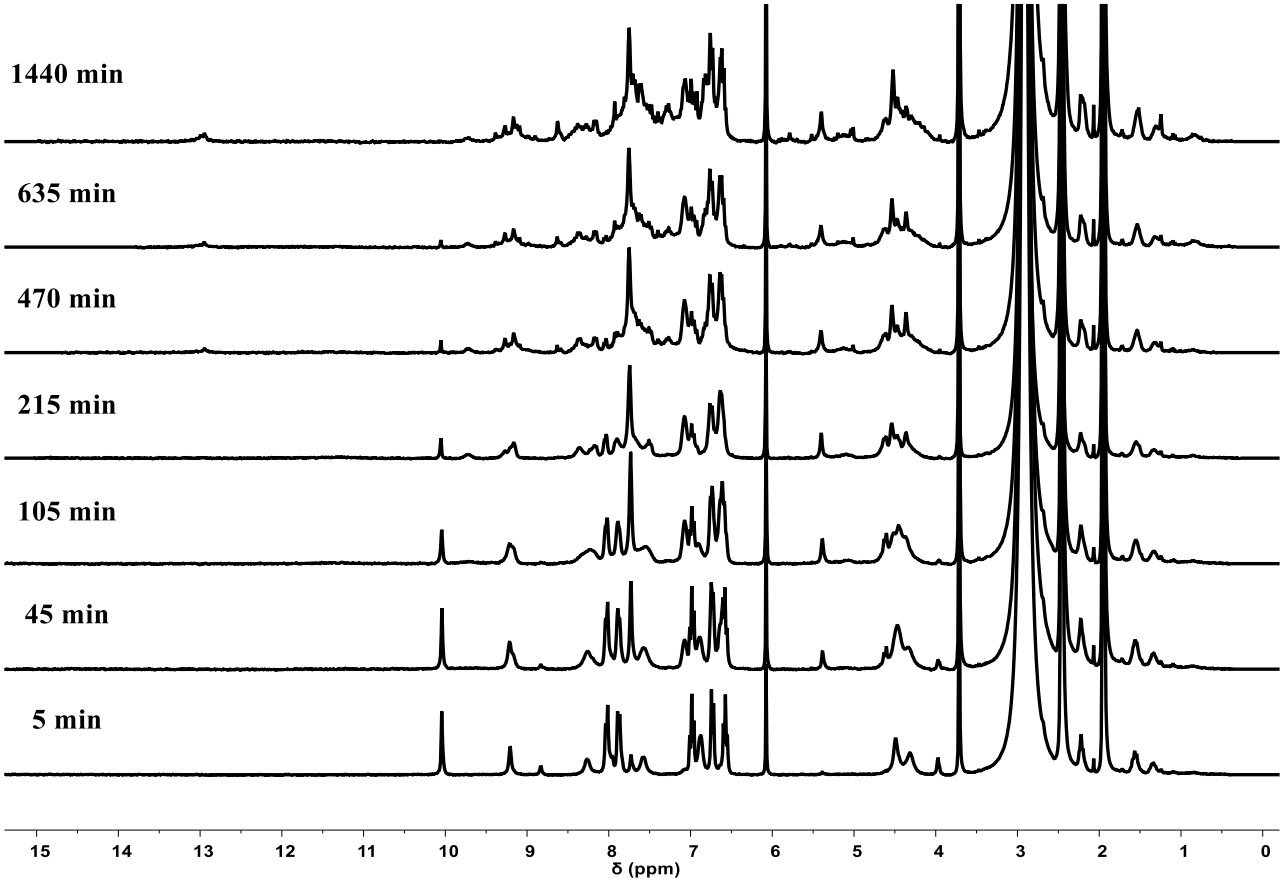

Figure A11. ^{1}H-NMR spectra (300 MHz, 301 K, CD_3CN/DMSO-d_6) during time after after the addition of Pimelic Acid (**C_7**) (0.5 eq.) and **(R,R)-HPEDA** (2.5 eq) to the solution of complex **1** (1 eq.). The peak at 6.1 ppm corresponds to the internal standard 1,3,5-trimetoxybenzene.

Table A5 [**1**] determined by integration of the 3 protons at 10.03 ppm, [**C_7@2**] determined by integration of the 6 protons at 5.40 ppm, [**C_7@3**] determined by integration of the 6 protons at 5.00 ppm using 1,3,5-trimetoxybenzene as internal standard.

Time (min)	[1]/2 M	[C_6@2] (M)	[C_6@3] (M)	[Intermediates] (M)
5	7,12E-04	2,45E-05	0	0
45	5,52E-04	2,15E-04	0	0
105	3,62E-04	3,37E-04	0	2,06E-05
215	2,09E-04	3,74E-04	0	1,37E-04
470	7,98E-05	3,01E-04	3,07E-05	3,09E-04
635	1,84E-05	3,07E-04	4,91E-05	3,46E-04
1440	0	2,52E-04	6,75E-05	4,01E-04

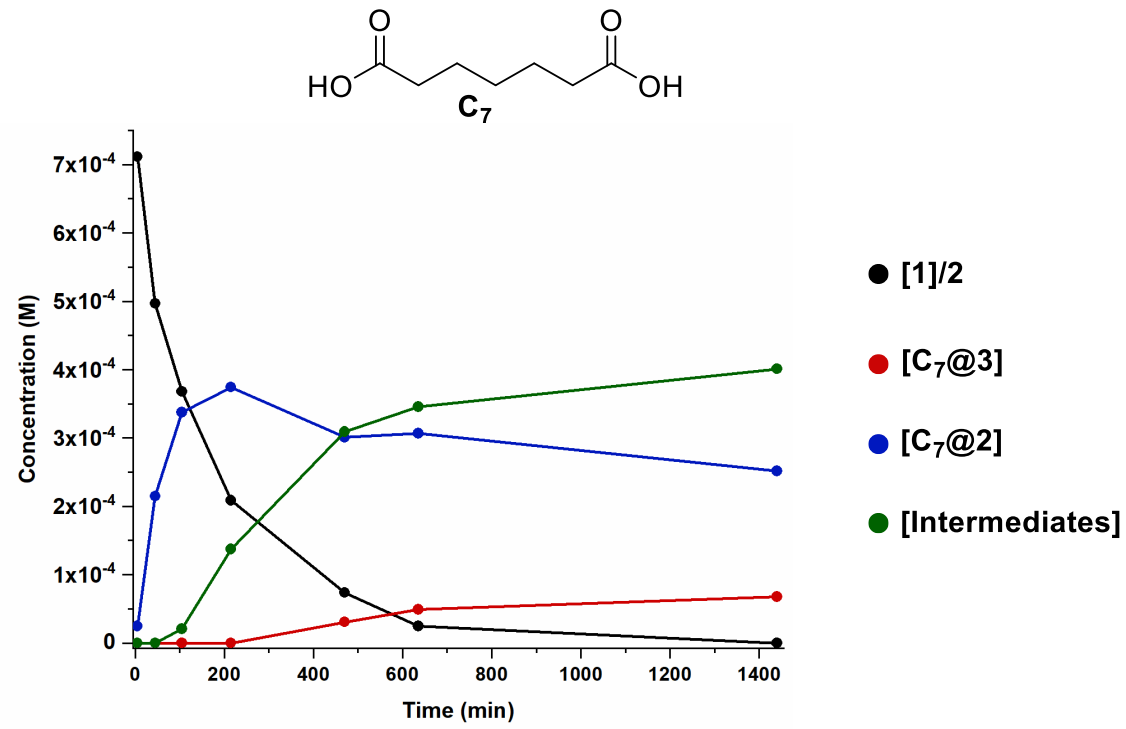

Figure A12. Kinetic profiles obtained for the differents species.

A4.3.6. Triggering Experiment

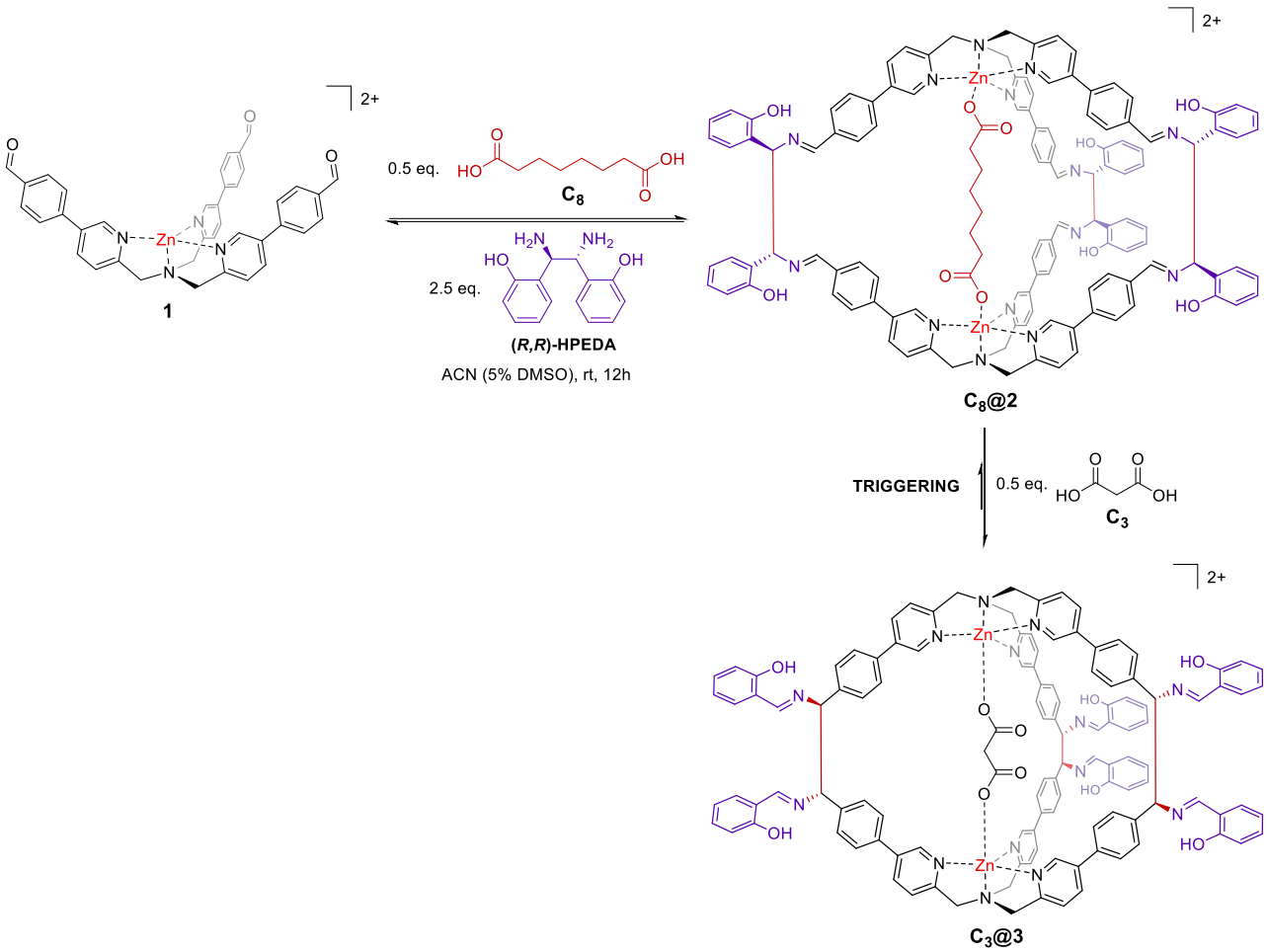

To 350 µL (0.70 µmol) of a solution 0.002 M of complex **1** in CD_3CN, 18 µL (0.35 µmol) of a solution 0.02 M in CD_3CN of a suberic acid **C_8,** 87 µL (1.75 µmol) of a solution 0.02 M in DMSO-*d_6* of **(*R*,*R*)-HPEDA**, and 30 µL (0.60 µmol) of a solution 0.02 M in DMSO-*d_6* of 1,3,5-trimetoxybenzene were added in a NMR tube. The reaction was followed for 24 h *via* ^{1}H-NMR.

After 24 h, 18 µL (0.35 µmol) of a solution 0.02 M in CD_3CN of a malic acid **C_3** were added in the NMR tube. The reaction was followed for 24 h *via* ^{1}H-NMR.

The concentration of **1**, **C_n@2**, **C_n@3** were determined via ^{1}H-NMR by integration of the relative peaks using 1,3,5-trimetoxybenzene as internal standard.

Concentration of the intermediate species was determined using the equation:

$$[\mathbf{Intermediates}] = \frac{[\mathbf{1}]_0}{2} - \frac{[\mathbf{1}]_t}{2} - [\mathbf{C_n@2}]_t - [\mathbf{C_n@3}]_t$$

With $[\mathbf{1}]_0 = 1.44 \cdot 10^{-3}$ M

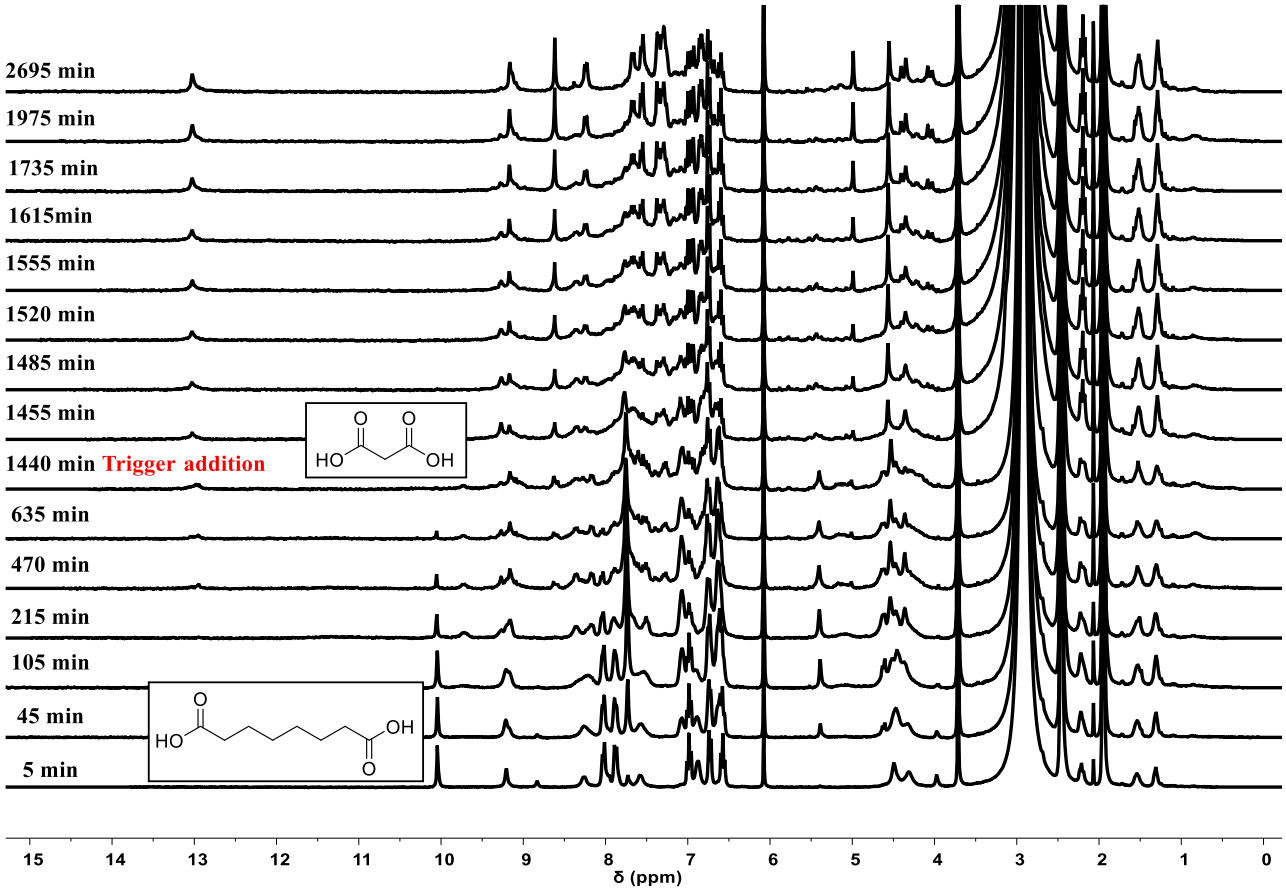

Figure A13. ^{1}H-NMR spectra (300 MHz, 301 K, CD_3CN/DMSO-d_6) during time after after the addition of Suberic Acid (**C_8**) (0.5 eq.) and **(R,R)-HPEDA** (2.5 eq) to the solution of complex **1** (1 eq.). After 1440 min Malonic Acid (**C3**) (0.5 eq.) was added to the NMR tube.The peak at 6.1 ppm corresponds to the internal standard 1,3,5-trimetoxybenzene.

Table A6. [**1**] determined by integration of the 3 protons at 10.03 ppm, [**C_8@2**] and [**C_3@2**] determined by integration of the 6 protons at 5.40 ppm, [**C_8@3**] and [**C_3@3**] determined by integration of the 6 protons at 5.00 ppm using 1,3,5-trimetoxybenzene as internal standard.

	Time (min)	[**1**]/2 **M**	**[C_8@2] (M)**	**[C_8@3] (M)**	**[Intermediates] (M)**
	5	7,06E-04	1,23E-05	0	0,00E+00
	45	5,28E-04	2,33E-04	0	0,00E+00
	105	3,68E-04	3,50E-04	0	1,86E-04
	215	2,27E-04	3,93E-04	0	2,14E-04
	470	7,98E-05	3,44E-04	1,84E-05	3,18E-04
	635	4,91E-05	3,13E-04	4,29E-05	3,40E-04
	1440	0	2,70E-04	5,52E-05	3,95E-04
Addition of Malonic Acid (C_3)	**Time (min)**	[**1**]/2 **M**	**[C_3@2] (M)**	**[C_3@3] (M)**	**[Intermediates] (M)**
	1455	0	1,47E-04	8,59E-05	4,87E-04

1485	0	1,23E-04	1,09E-04	4,88E-04
1520	0	1,10E-04	1,41E-04	4,69E-04
1555	0	9,82E-05	1,48E-04	4,73E-04
1615	0	8,59E-05	1,80E-04	4,54E-04
1735	0	4,29E-05	2,66E-04	4,11E-04
1975	0	0	4,06E-04	3,14E-04
2695	0	0	6,41E-04	7,94E-05

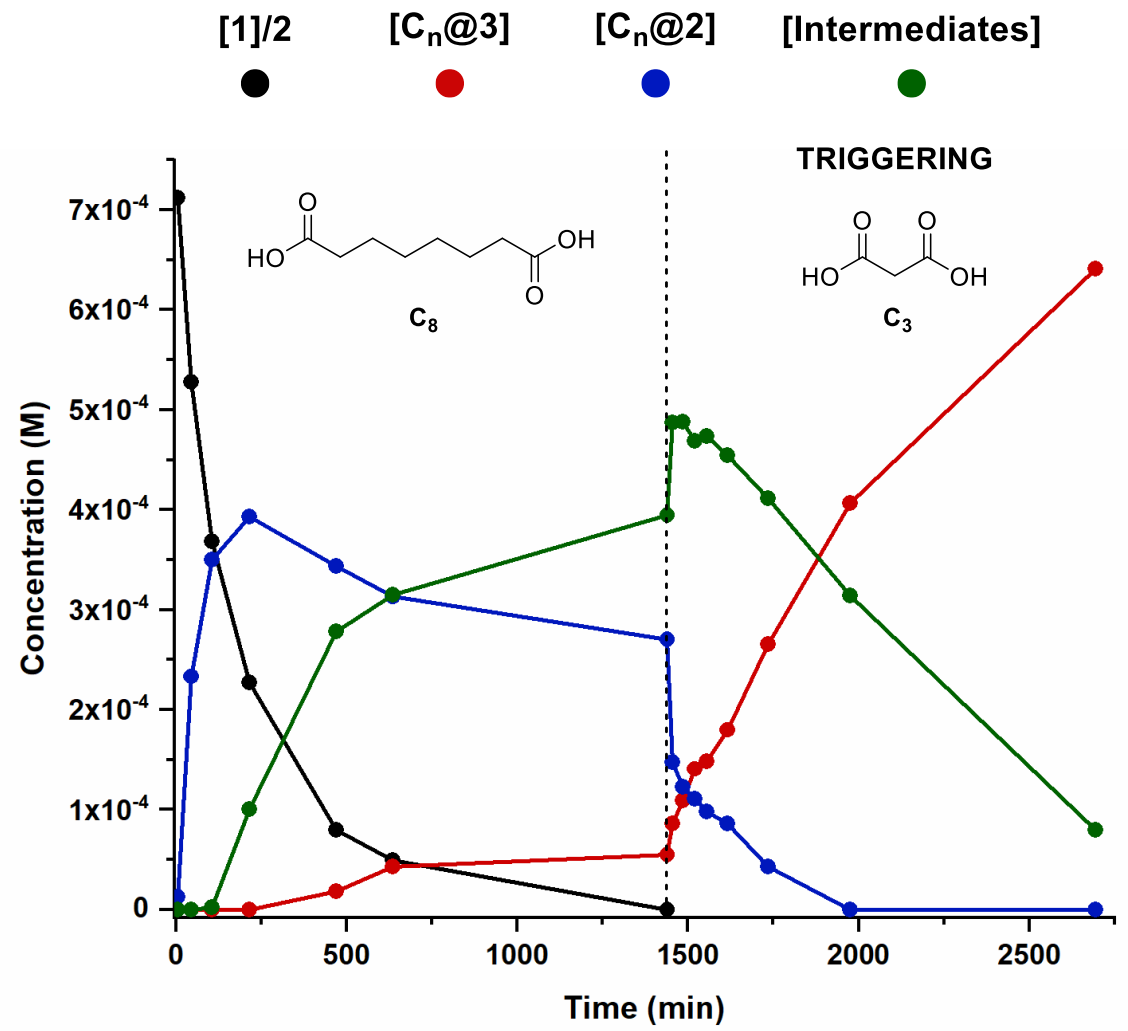

Figure A14. Kinetic profiles obtained for the differents species.

A4.4. Computational Studies

The geometry optimization of cage **C_3@3** was run with Gaussian 16 package[1,2] (DFT B3LYP/6-31G(d)). The initial structure before geometry optimization was taken from an optimized structure reported in another study.[28] From computational studies we have confirmed that short diacids tend to pre-organize the system in this conformation and thus allow for the reaction to proceed faster. While in the case of longer guests, the diamine linkers assume an antiperiplanar conformation, thus leading to an increasing distance between the two carbons and a loss of pre-organization.

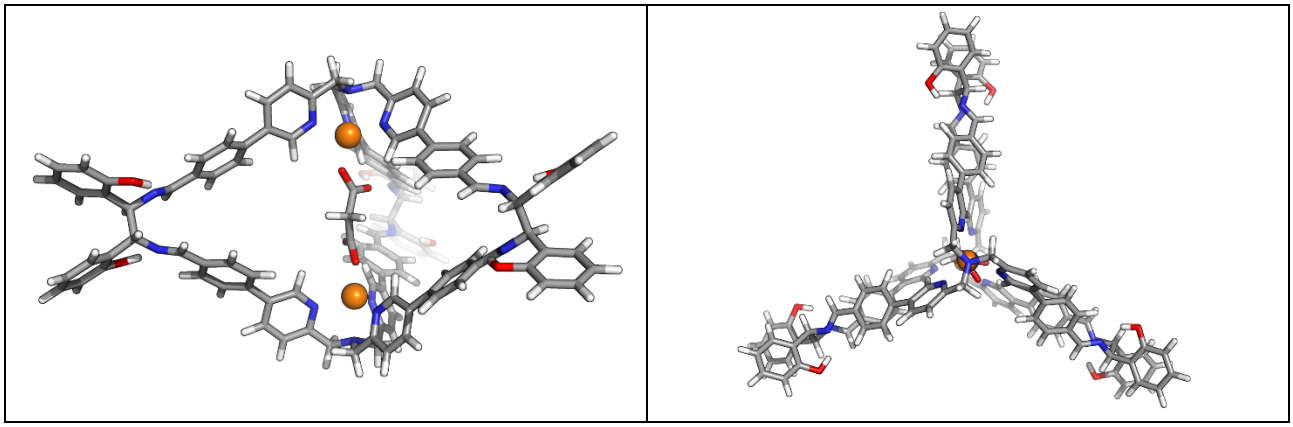

Figure A15. B3LYP/6-31G(d) minimized structure for the cage **C_3@3**.

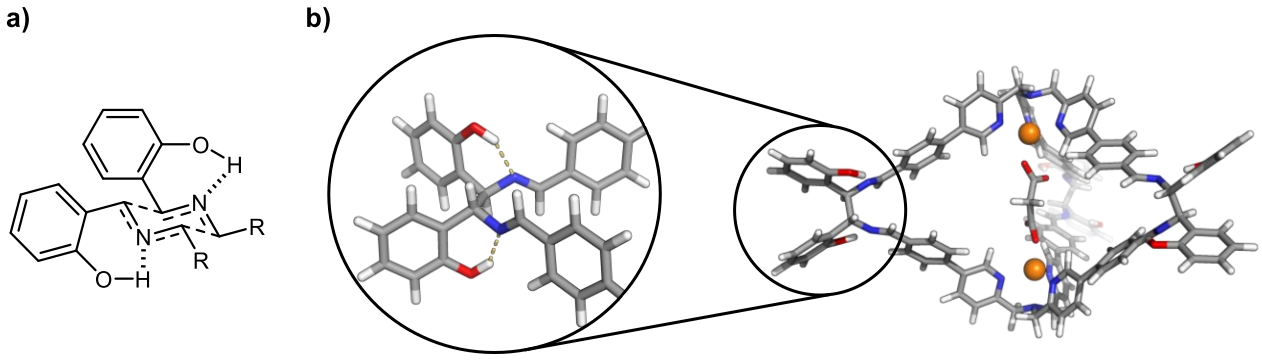

Figure A16. a) Diaza-Cope transition state[32] and, b) highlight of the imine conformation in cage **C_3@3**.

A4.5. X-Ray Analysis

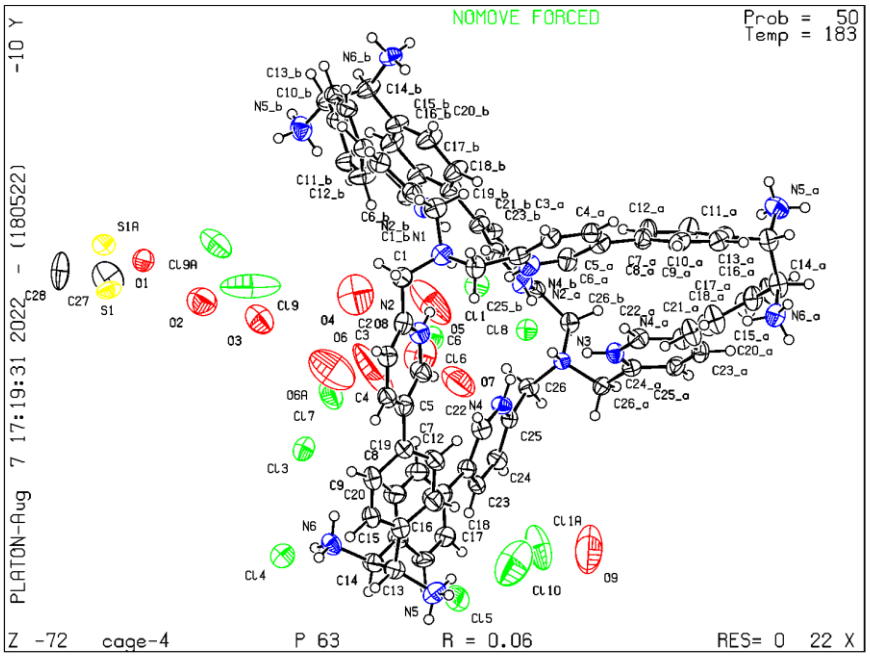

Figure A17. Crystal structure of cage ***S*-4**.

Table A8. Crystal data and structure refinement for kon. For kon. U(eq) is defined as one third of the trace of the orthogonalized U^{ij} tensor.

Identification code	cage-4	
Empirical formula	C78 H86 Cl14 N14 x 1.5 DMSO x 18 H2O x 7HCl	
Formula weight	2412.59	
Temperature	183.00 K	
Wavelength	0.71073 Å	
Crystal system	Hexagonal	
Space group	$P6_3$ (no. 173)	
Unit cell dimensions	a = 18.0982(8) Å	□= 90°.
	b = 18.0982(8) Å	□= 90°.
	c = 23.6018(10) Å	□ = 120°.
Volume	6694.9(7) $Å^3$	
Z	2	
Density (calculated)	1.197 Mg/m^3	
Absorption coefficient	0.507 mm^{-1}	
F(000)	2518	
Crystal size	0.21 x 0.15 x 0.11 mm^3	
Theta range for data collection	2.410 to 24.999°.	
Index ranges	-21<=h<=21, -21<=k<=21, -26<=l<=28	

Reflections collected	93713
Independent reflections	7599 [R(int) = 0.0649]
Completeness to theta = 24.999°	99.8 %
Absorption correction	Semi-empirical from equivalents
Max. and min. transmission	0.9191 and 0.8681
Refinement method	Full-matrix least-squares on F^2
Data / restraints / parameters	7599 / 1 / 496
Goodness-of-fit on F^2	1.118
Final R indices [I>2sigma(I)]	R1 = 0.0566, wR2 = 0.1447
R indices (all data)	R1 = 0.0638, wR2 = 0.1505
Absolute structure parameter	0.040(18)
Extinction coefficient	n/a
Largest diff. peak and hole	0.550 and -0.305 e.$Å^{-3}$

Table A10. Atomic coordinates (x 10^4) and equivalent isotropic displacement parameters ($Å^2$x 10^3).

	x	y	z	U(eq)
Cl(1)	6667	3333	6085(1)	51(1)
Cl(3)	4552(1)	6016(1)	5757(1)	47(1)
Cl(4)	3333	6667	4227(1)	50(1)
Cl(5)	2674(2)	4180(2)	1914(1)	74(1)
Cl(6)	7580(1)	5802(1)	2945(1)	58(1)
Cl(7)	6463(2)	6864(2)	4012(1)	86(1)
Cl(8)	6667	3333	3886(1)	39(1)
O(1)	8383(7)	9469(6)	7583(6)	61(3)
C(27)	8677(19)	10566(19)	6769(10)	90(7)
C(28)	8541(19)	10972(11)	7816(10)	86(7)
S(1)	8098(3)	10111(3)	7372(2)	49(1)
S(1A)	9015(11)	10466(12)	7456(13)	65(7)
O(2)	7211(6)	8022(6)	7532(4)	88(2)
O(3)	7003(6)	7270(6)	6616(4)	84(2)
O(4)	7441(17)	6020(16)	5673(6)	118(7)
O(6)	5790(30)	5160(20)	5670(20)	250(20)
O(6A)	6250(20)	6230(30)	5307(11)	168(12)
O(8)	6680(8)	5316(7)	4091(4)	48(2)
N(1)	6667	3333	7622(4)	39(2)
N(2)	5583(4)	3700(4)	6922(3)	41(1)

N(3)	6667	3333	2331(3)	25(2)
N(4)	5751(3)	3870(3)	3023(2)	36(1)
N(5)	1290(4)	2897(4)	4881(3)	54(2)
N(6)	2792(4)	5211(4)	5101(2)	42(1)
C(1)	6341(5)	3894(5)	7811(3)	41(2)
C(2)	5569(5)	3752(4)	7495(3)	40(2)
C(3)	4853(5)	3720(5)	7732(3)	40(2)
C(4)	4205(5)	3662(4)	7386(3)	40(2)
C(5)	4256(5)	3612(4)	6802(3)	42(2)
C(6)	4967(5)	3621(5)	6584(3)	43(2)
C(7)	3589(5)	3561(4)	6405(3)	39(1)
C(8)	3099(5)	3933(4)	6550(3)	42(2)
C(9)	2524(5)	3929(5)	6170(3)	39(2)
C(10)	2418(5)	3580(5)	5629(3)	42(2)
C(11)	2876(6)	3178(6)	5485(4)	55(2)
C(12)	3462(6)	3176(5)	5881(4)	52(2)
C(13)	1840(5)	3685(5)	5208(3)	45(2)
C(14)	2339(5)	4422(5)	4777(3)	44(2)
C(15)	2923(5)	4324(5)	4366(3)	44(2)
C(16)	2622(5)	3979(5)	3838(3)	44(2)
C(17)	3168(5)	3913(5)	3443(3)	45(2)
C(18)	3985(5)	4159(5)	3580(3)	39(2)
C(19)	4296(5)	4512(6)	4119(3)	50(2)
C(20)	3761(5)	4595(6)	4497(3)	51(2)
C(21)	4573(4)	4071(4)	3179(3)	36(1)
C(22)	5194(5)	3914(5)	3380(3)	40(2)
C(23)	4516(4)	4123(4)	2586(3)	37(1)
C(24)	5094(4)	4075(4)	2236(3)	38(1)
C(25)	5742(4)	3963(4)	2460(3)	31(1)
C(26)	6445(4)	3970(4)	2122(3)	34(1)
Cl(9)	8238(3)	8223(6)	5704(3)	170(4)
Cl(10)	1730(11)	1808(8)	4309(7)	179(6)
O(5)	7230(20)	4860(20)	4947(8)	178(16)
O(7)	5410(16)	3737(16)	4994(11)	117(7)
O(9)	1670(30)	470(18)	4113(15)	183(15)
Cl(1A)	2087(7)	1600(5)	3978(3)	114(3)
Cl(9A)	9168(10)	9046(11)	5982(5)	91(4)
O(5A)	6221(15)	4737(13)	4919(8)	104(6)

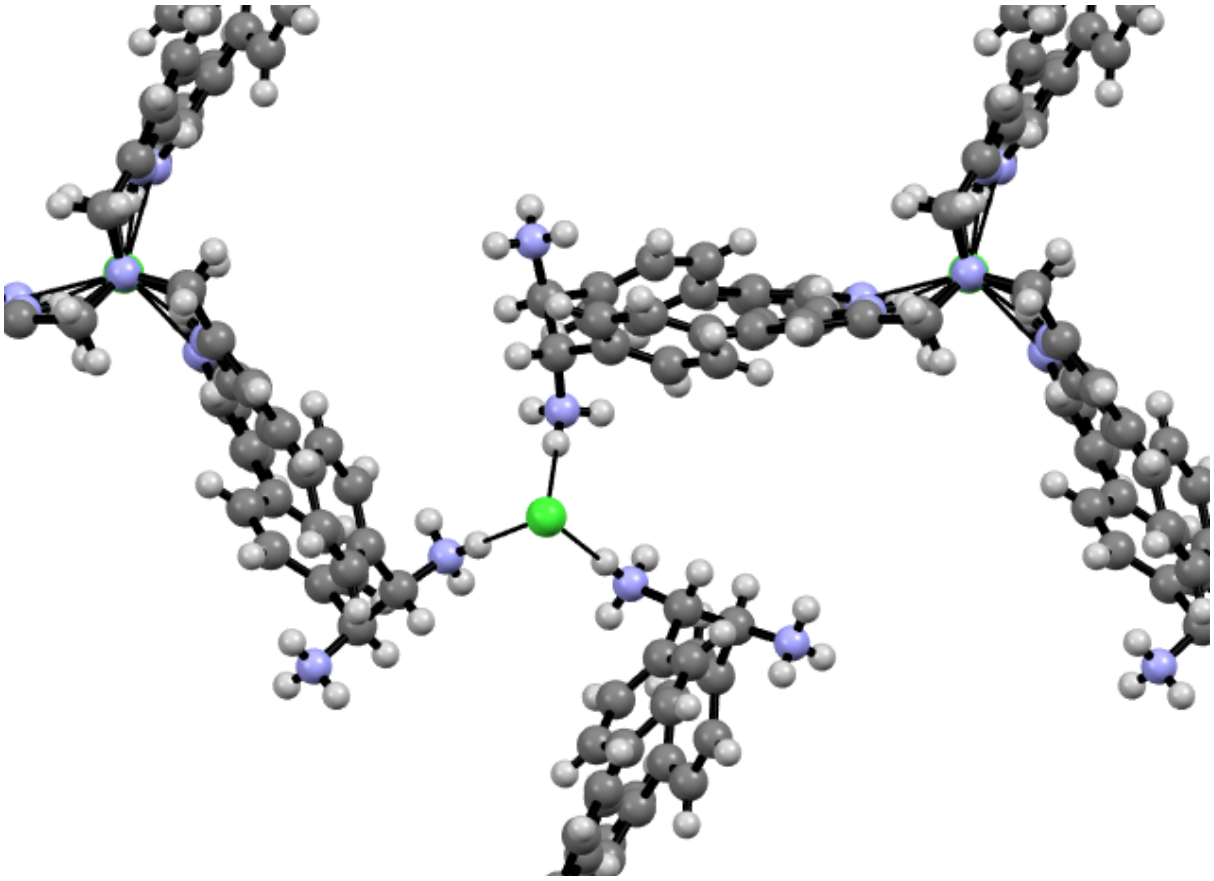

Figure A18. Highlight of the bridged chloride anions among ammonium groups of the cages.

A4.6. NMR and HRMS Characterization

A4.6.1. 4-(6-((bis(pyridin-2-ylmethyl)amino)methyl)pyridin-3-yl)benzaldehyde (7)

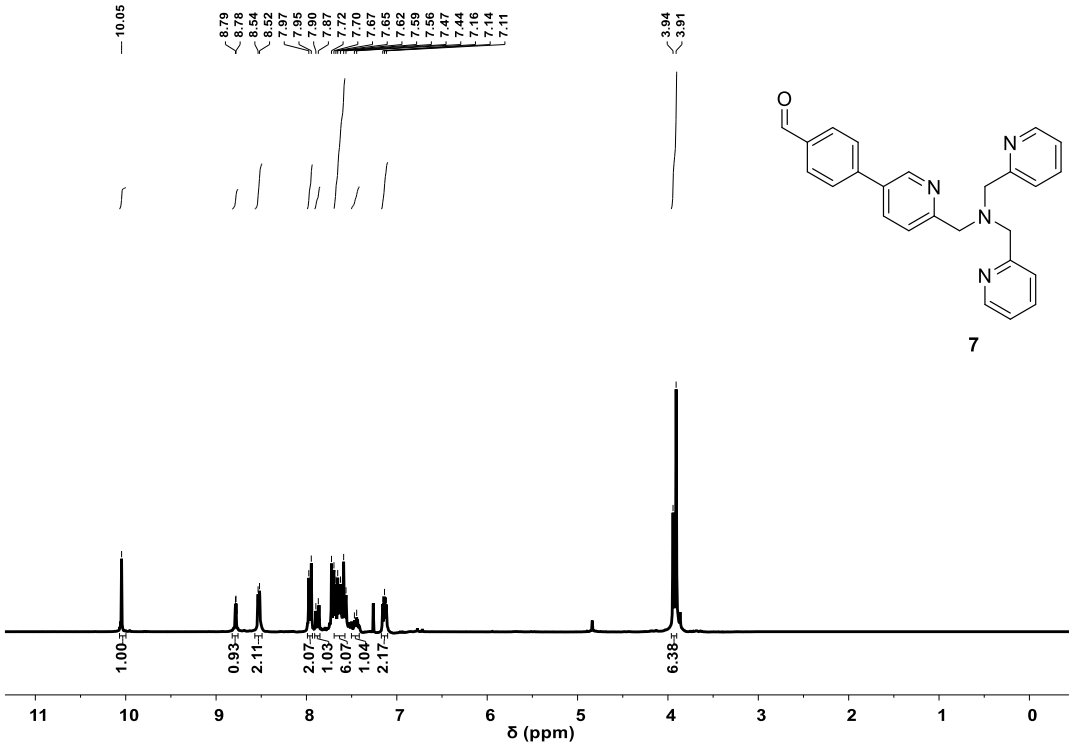

Figure A19. ^{1}H-NMR spectrum (300 MHz, 301 K, $CDCl_3$) of compound **7**.

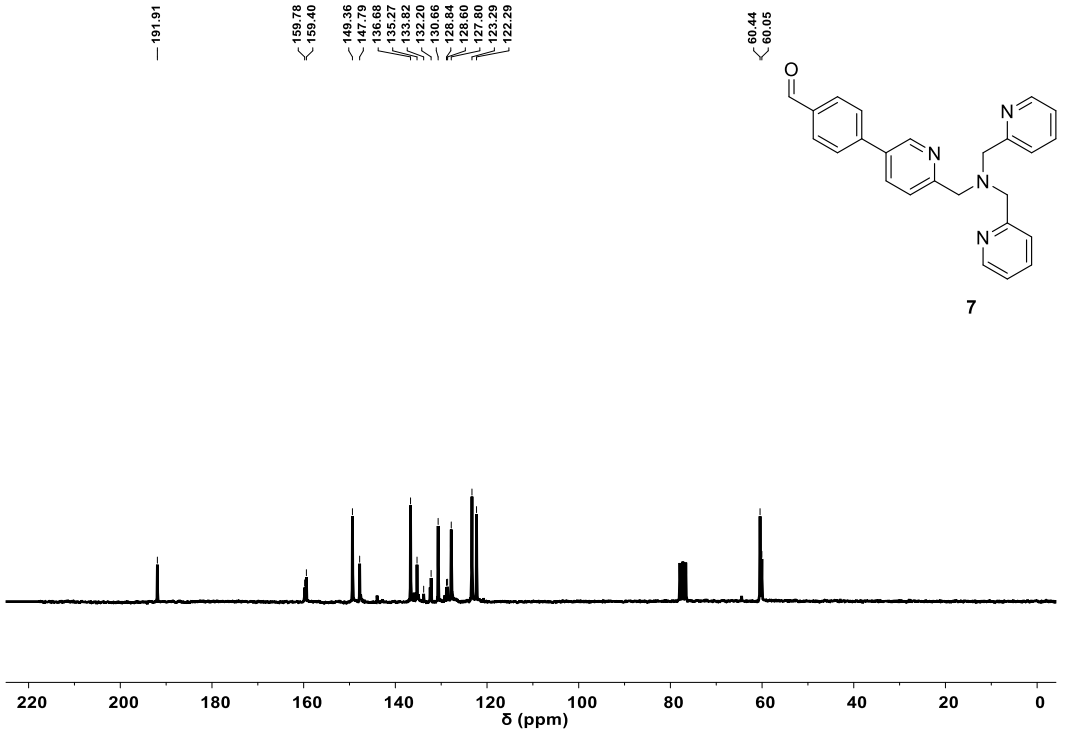

Figure A20. ^{13}C-NMR spectrum (50 MHz, 301 K, $CDCl_3$) of compound **7**.

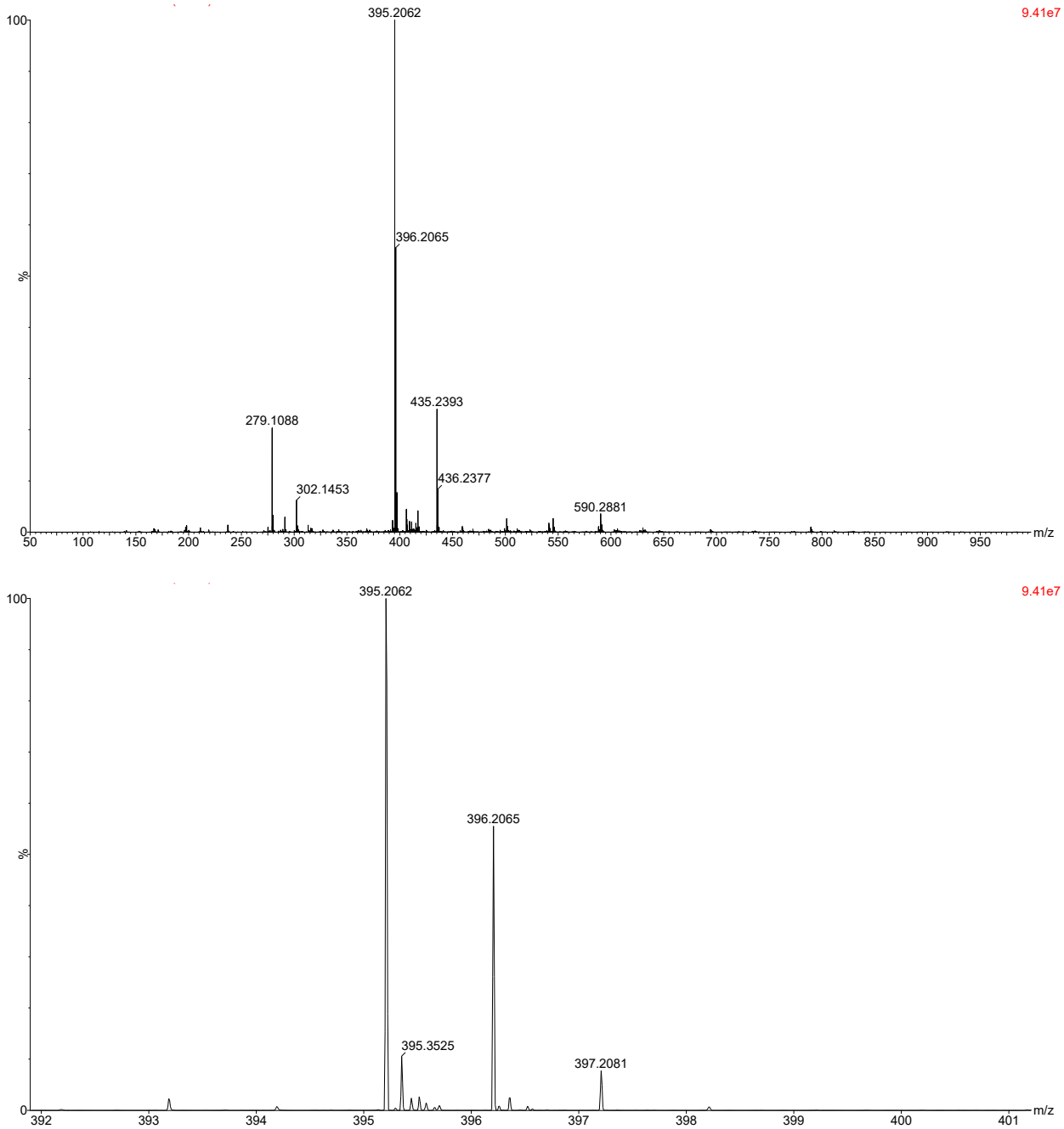

Figure A21. Experimental HRMS pattern of **7** for $[M+H]^+$ adduct in CH_3CN/H_2O (50:50)/0.1% HCOOH.

A4.6.2. Complex 8

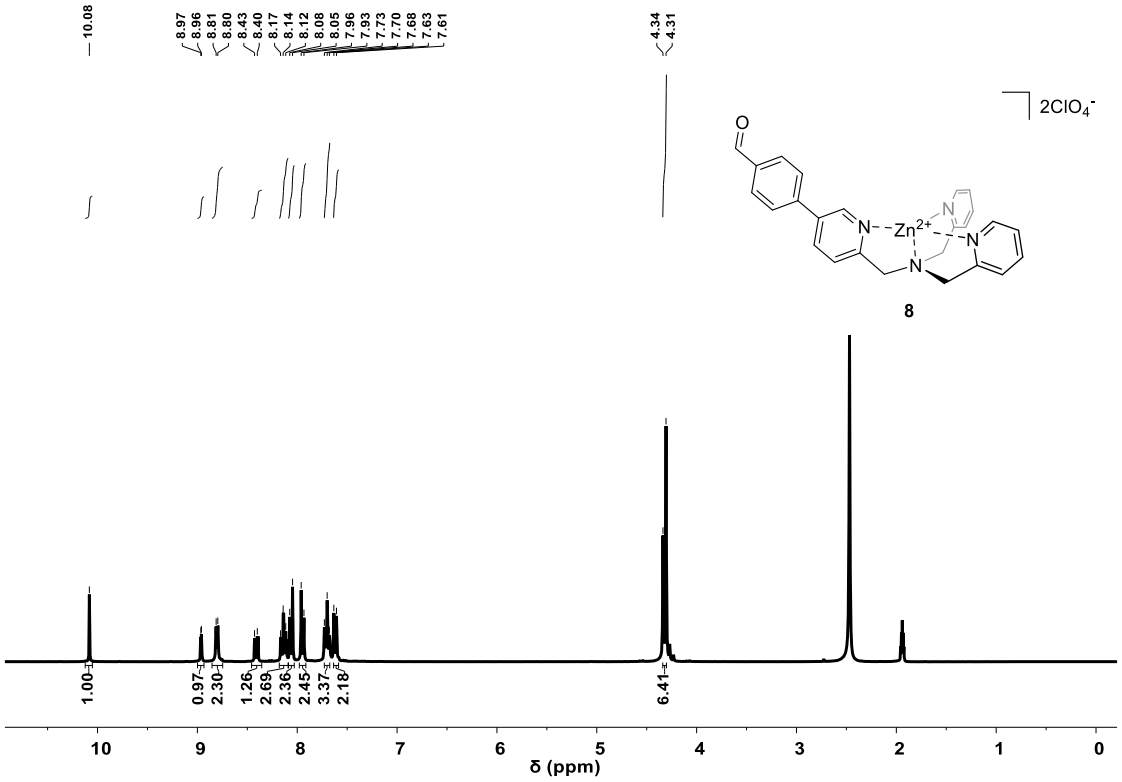

Figure A22. ^{1}H-NMR spectrum (300 MHz, 301 K, CD_3CN) of complex **8**.

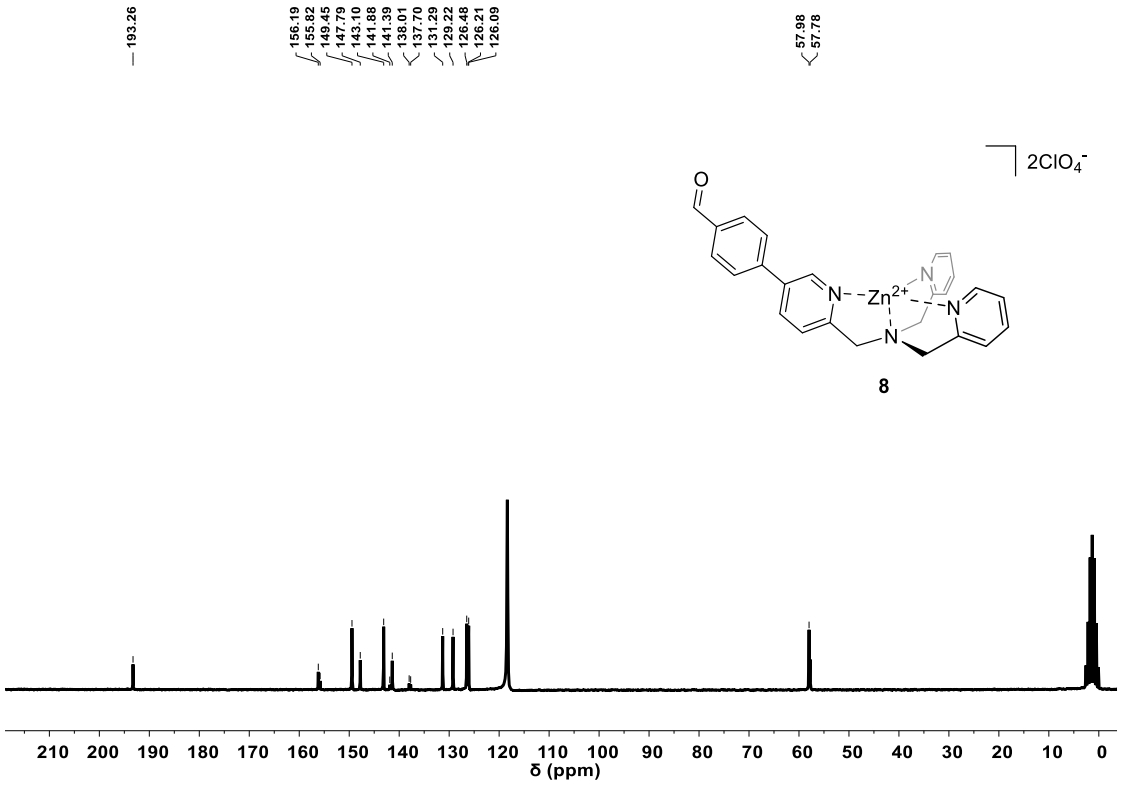

Figure A23. ^{13}C-NMR spectrum (50 MHz, 301 K, CD_3CN) of complex **8**.

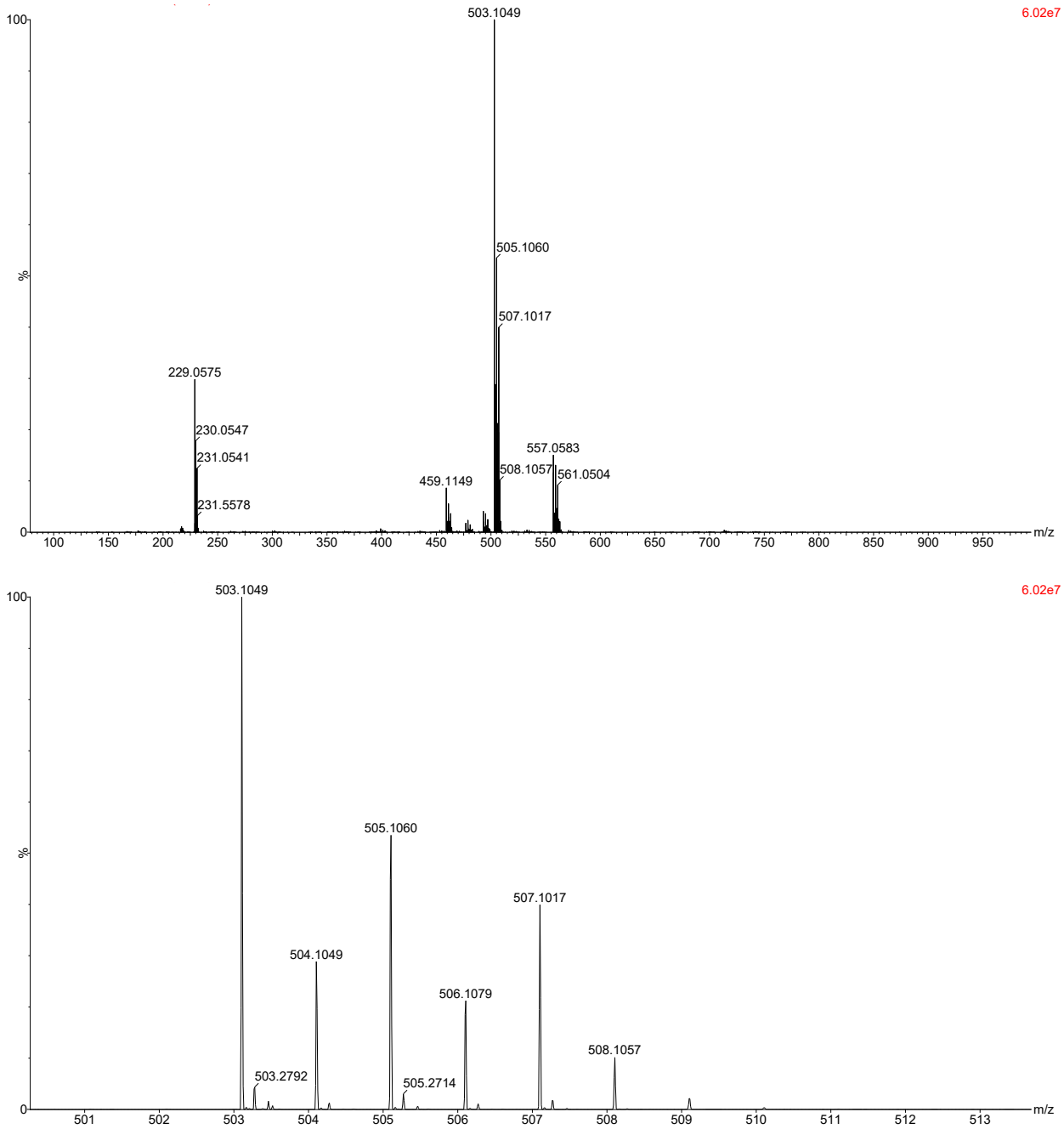

Figure A24. Experimental HRMS pattern of **8** for $[M+CHCOO]^+$ adduct in CH_3CN/H_2O (50:50)/0.1% HCOOH.

A4.6.3. 1-(5-bromopyridin-2-yl)-N-((5-bromopyridin-2-yl)methyl)-N-(pyridin-2-ylmethyl)methanamine (9)

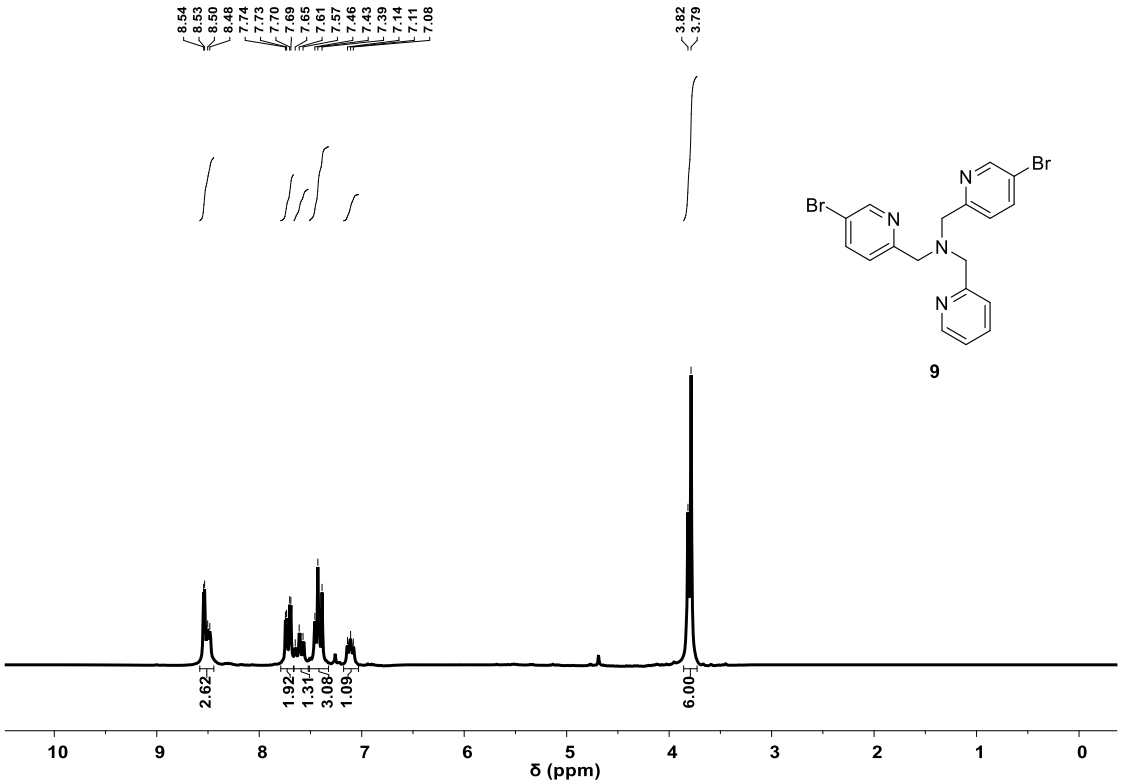

Figure A25. ^{1}H-NMR spectrum (300 MHz, 301 K, $CDCl_3$) of compound **9**.

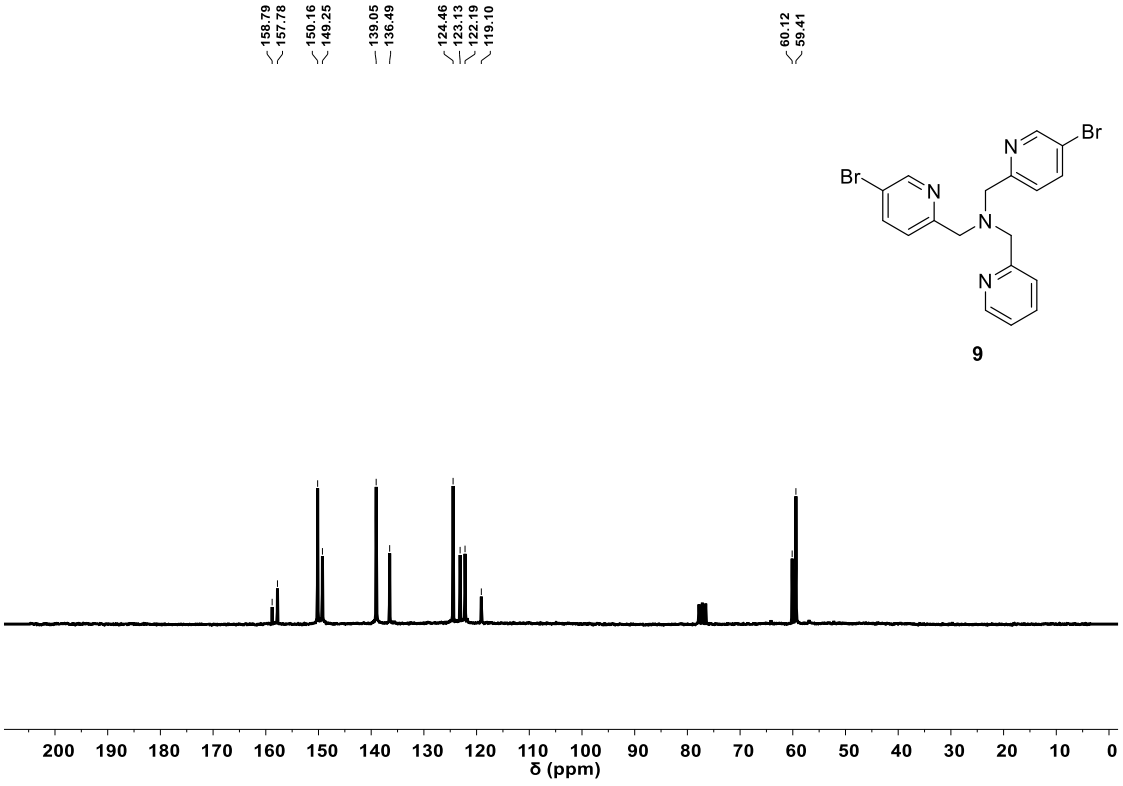

Figure A26. ^{13}C-NMR spectrum (50 MHz, 301 K, $CDCl_3$) of compound **9**.

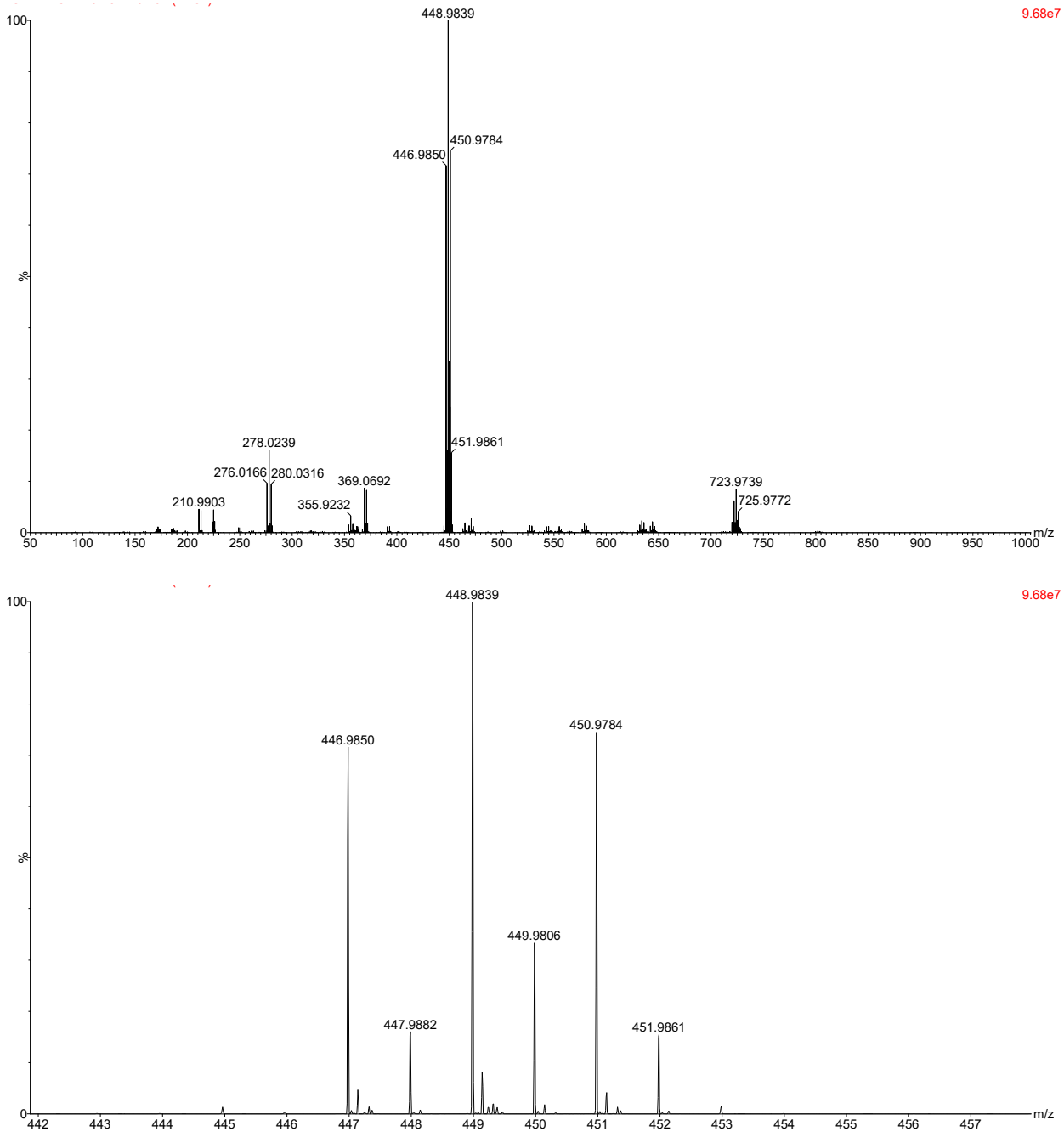

Figure A27. Experimental HRMS pattern of **9** for $[M+H]^+$ adduct in CH_3CN/H_2O (50:50)/0.1% HCOOH.

A4.6.4. 4,4'-((((pyridin-2-ylmethyl)azanediyl)bis(methylene))bis (pyridine-6,3-diyl))dibenzaldehyde (10)

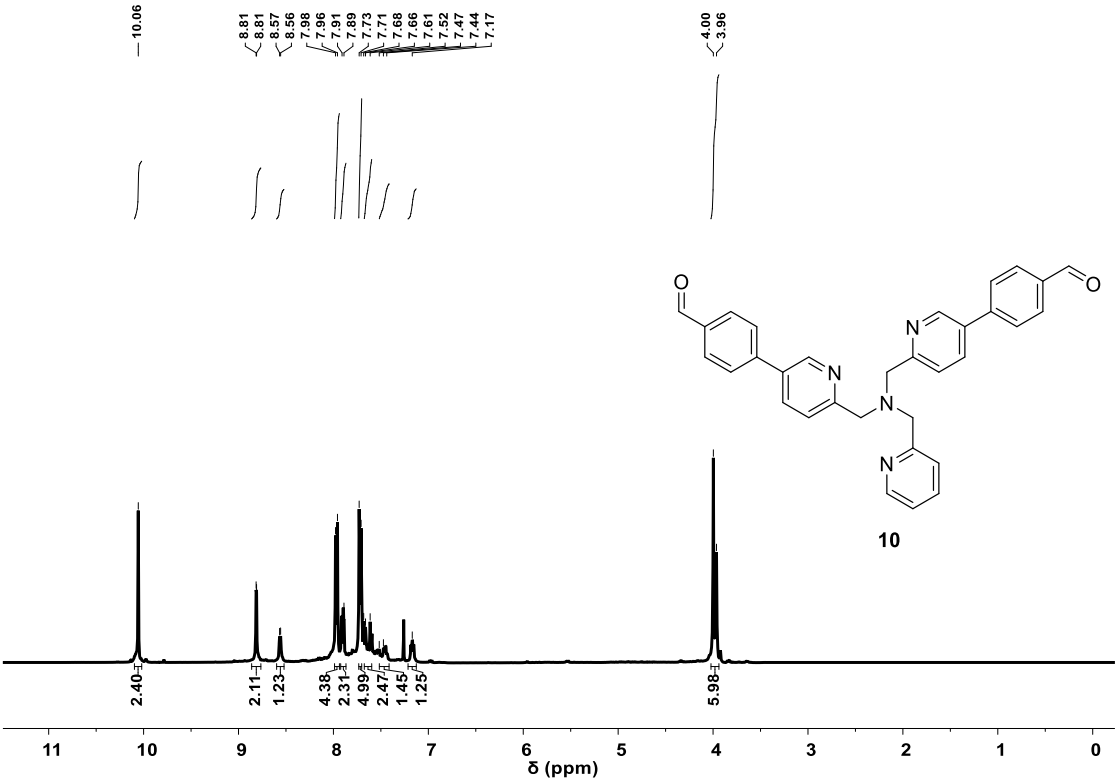

Figure A28. ^{1}H-NMR spectrum (400 MHz, 301 K, $CDCl_3$) of compound **10**.

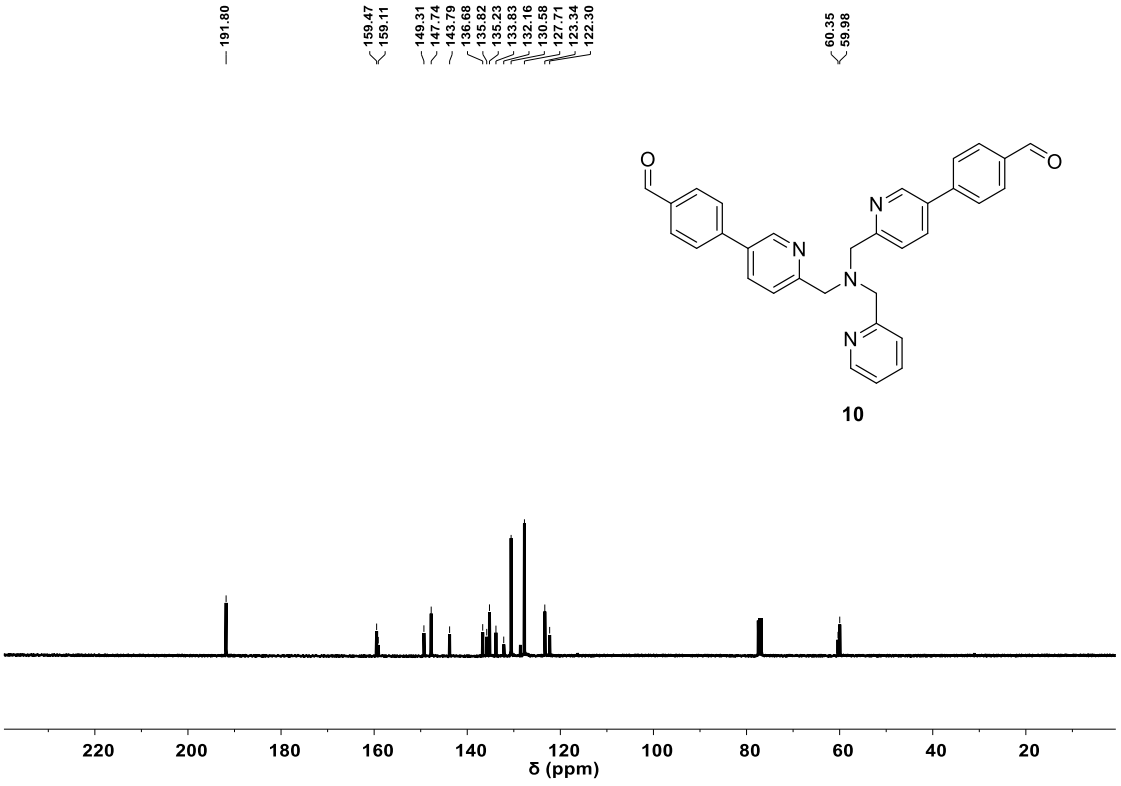

Figure A29. ^{13}C-NMR spectrum (101 MHz, 301 K, $CDCl_3$) of compound **10**.

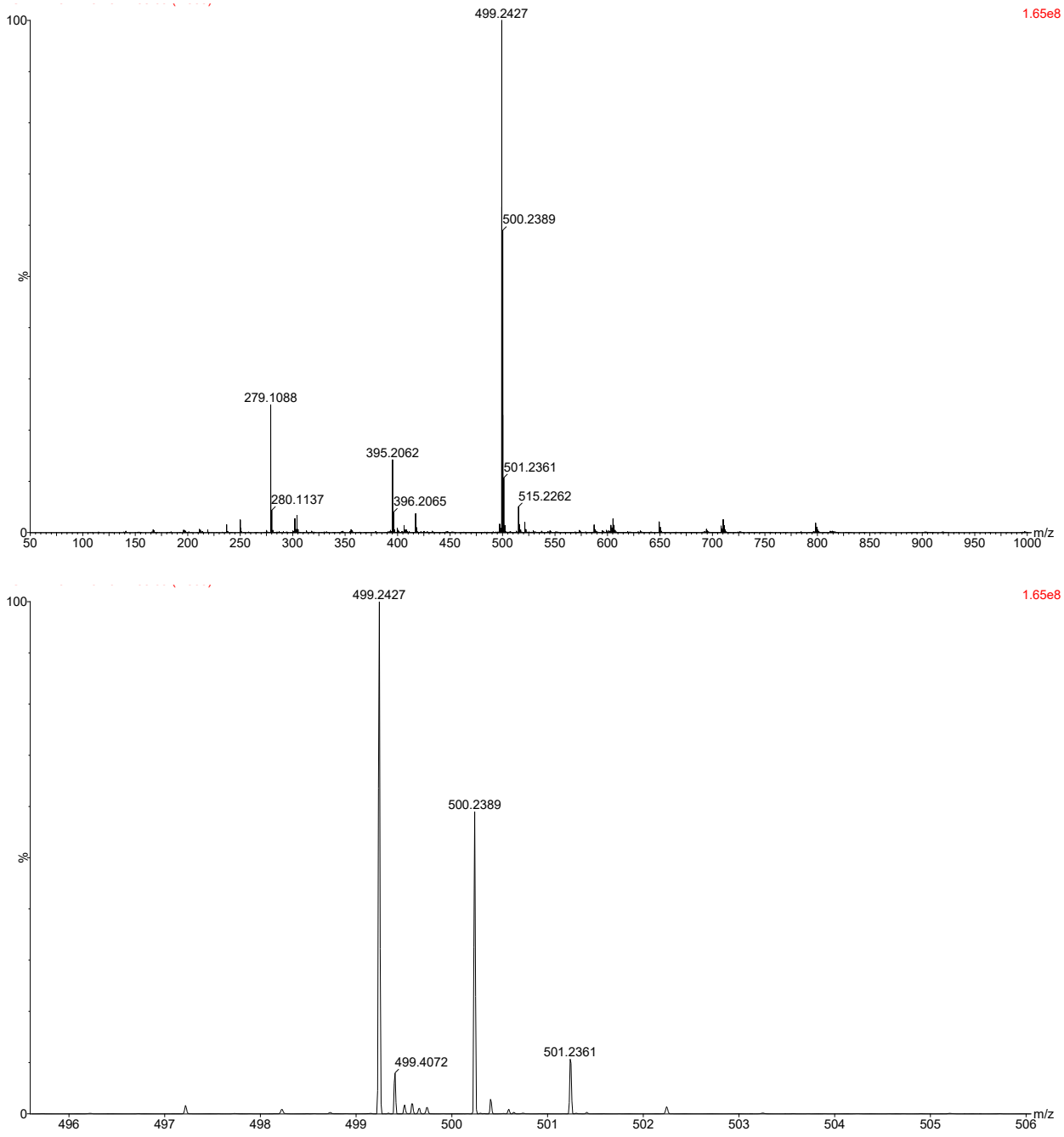

Figure A30. Experimental HRMS pattern of **10** for $[M+H]^+$ adduct in CH_3CN/H_2O (50:50)/0.1% HCOOH.

A4.6.5. Complex 11

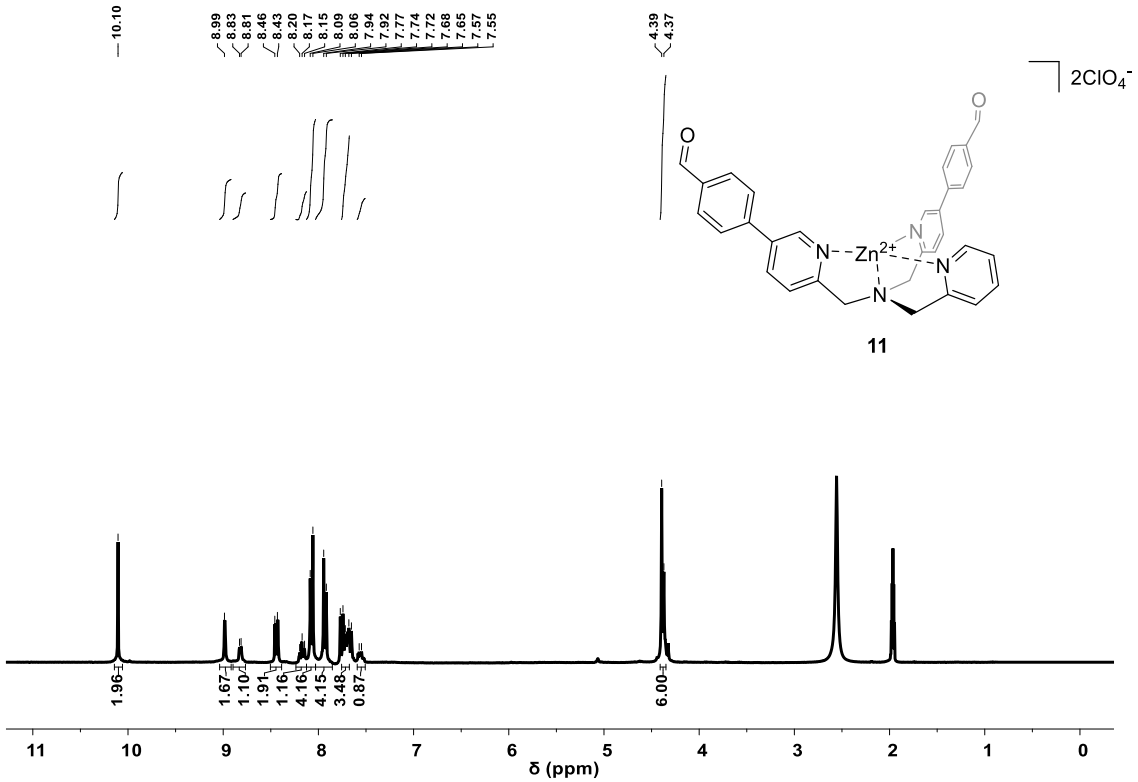

Figure A31. ^{1}H-NMR spectrum (300 MHz, 301 K, CD_3CN) of complex **11**.

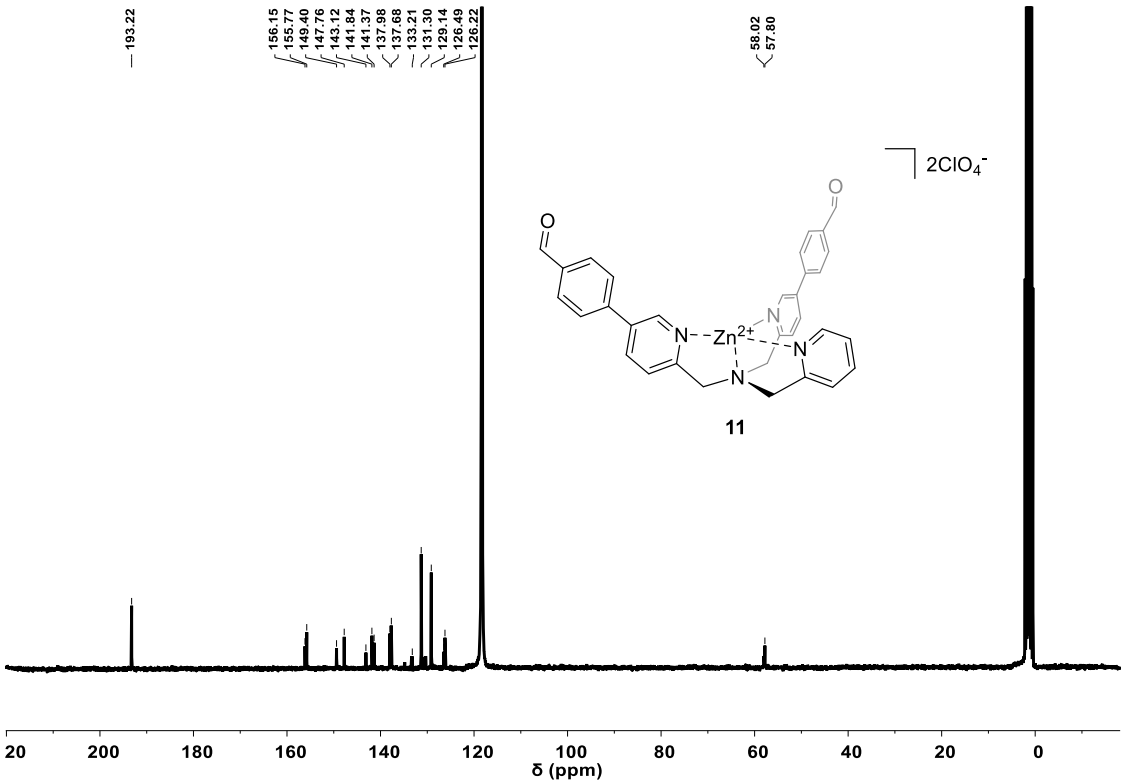

Figure A32. ^{13}C-NMR spectrum (75 MHz, 301 K, CD_3CN) of complex **17**.

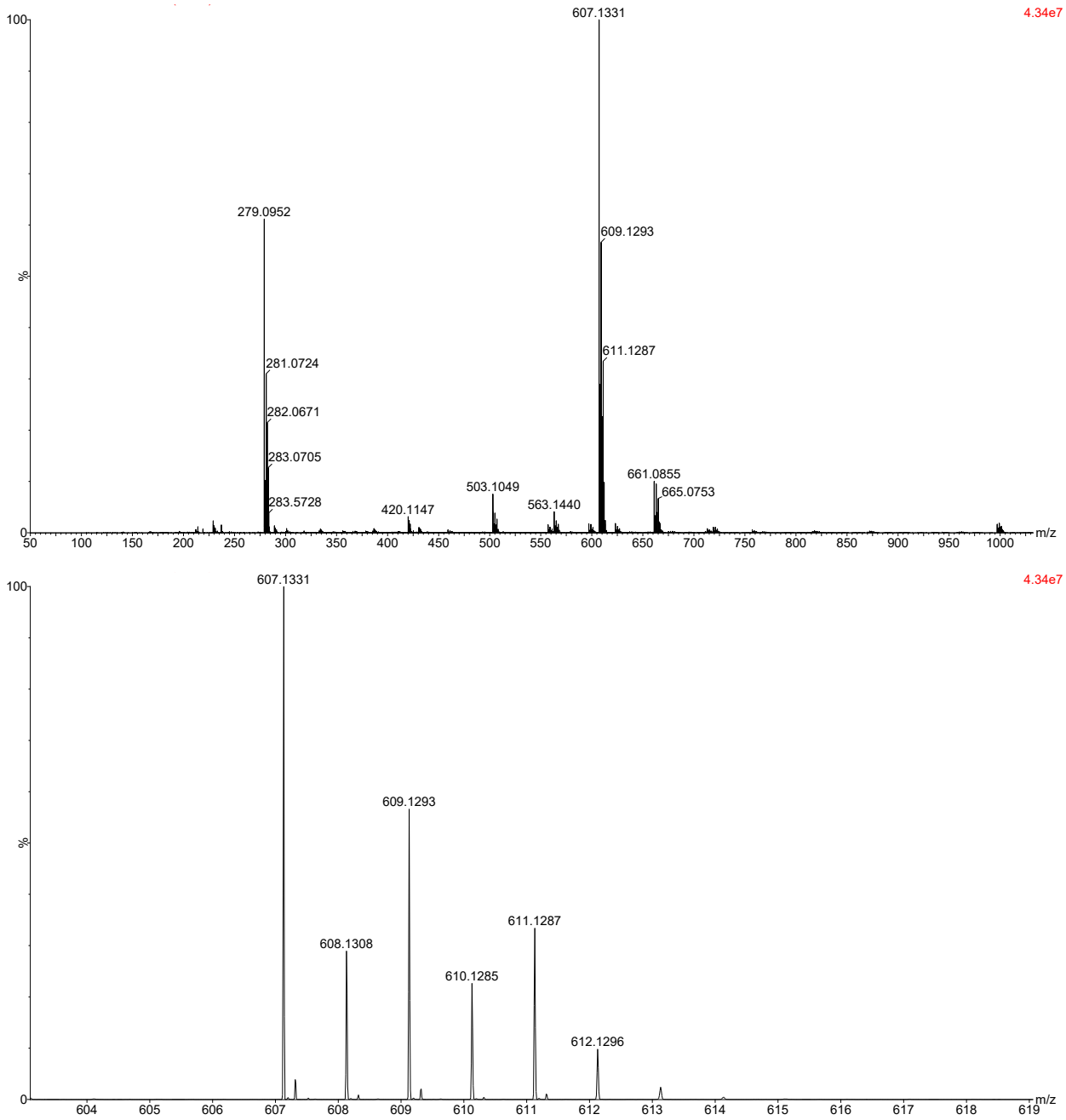

Figure A33. Experimental HRMS pattern of **11** for $[M+CHOO]^+$ adduct in CH_3CN/H_2O (50:50)/0.1% HCOOH.

A4.6.6. Cage C_3@3

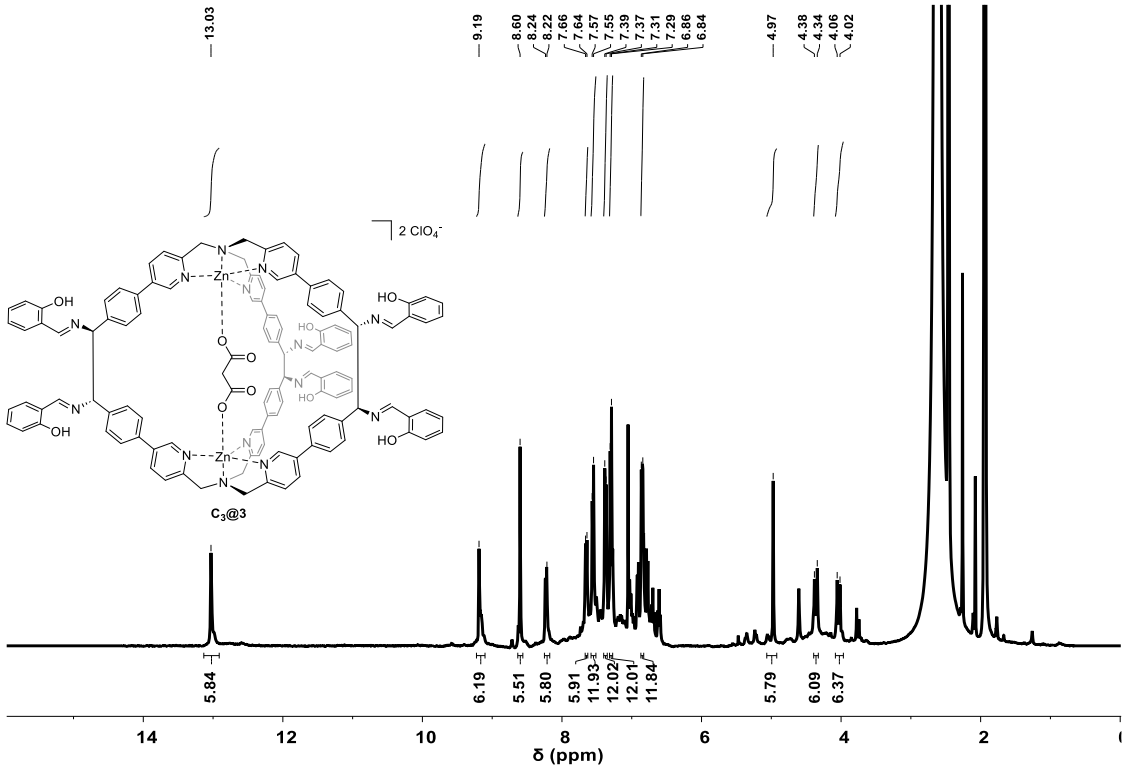

Figure A34. ^{1}H-NMR spectrum (400 MHz, 301 K, CD_3CN/5% DMSO-d_6) of cage **C_3@3**.

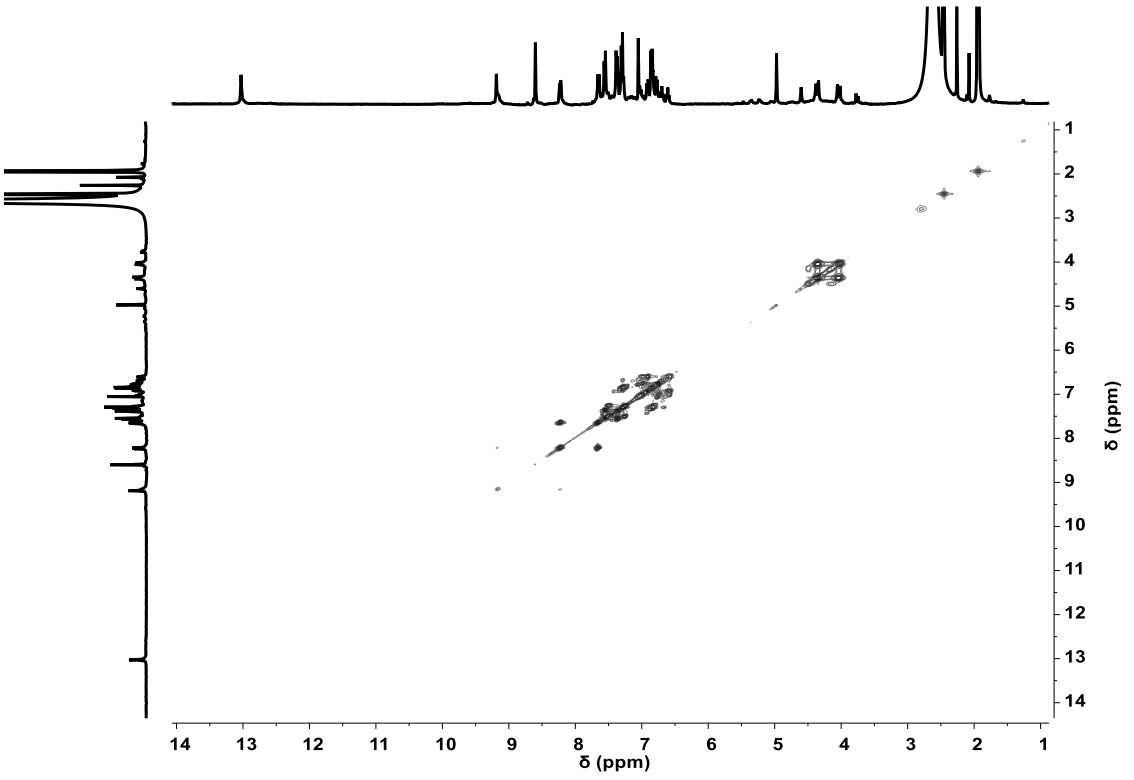

Figure AS35. ^{1}H-^{1}H COSY spectrum (400 MHz, 301 K, CD_3CN/5% DMSO-d_6) of cage **C_3@3**.

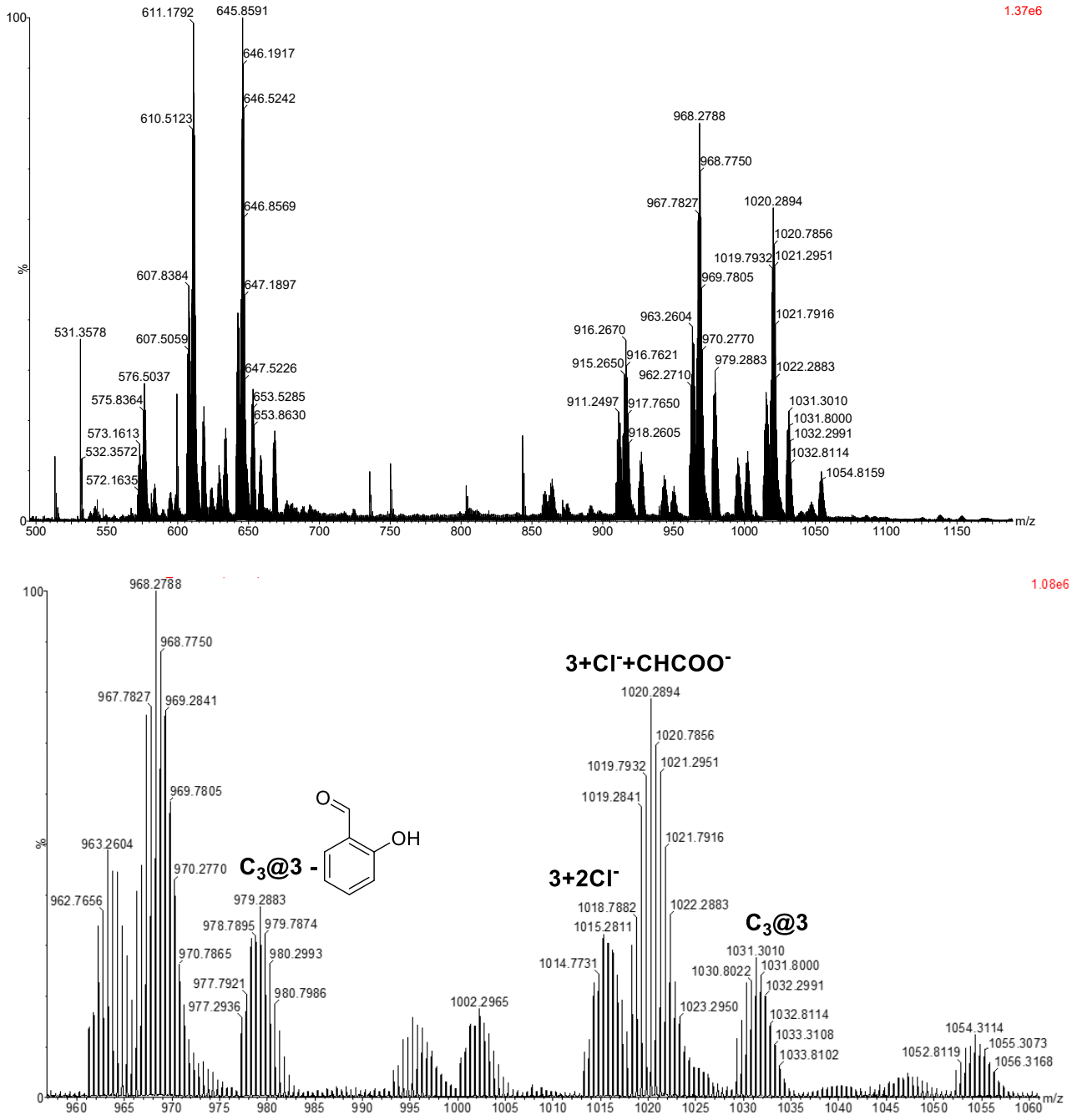

Figure A36. Experimental HRMS pattern of **C_3@3** for $[M]^{2+}$ adduct in CH_3CN 0.1% HCOOH. **3** corresponds to the cage without **C_3**.

A4.6.7. Compound *S*-4

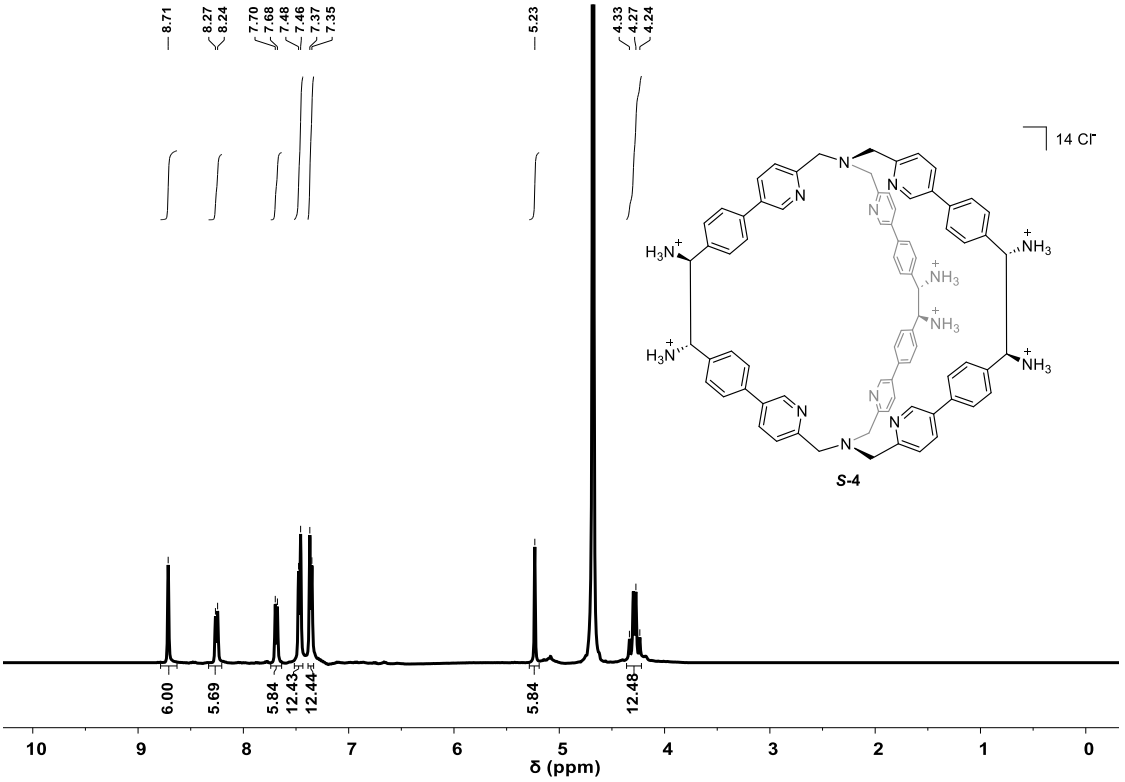

Figure A37. ^{1}H-NMR spectrum (400 MHz, 301 K, D_2O) of compound ***S*-4**.

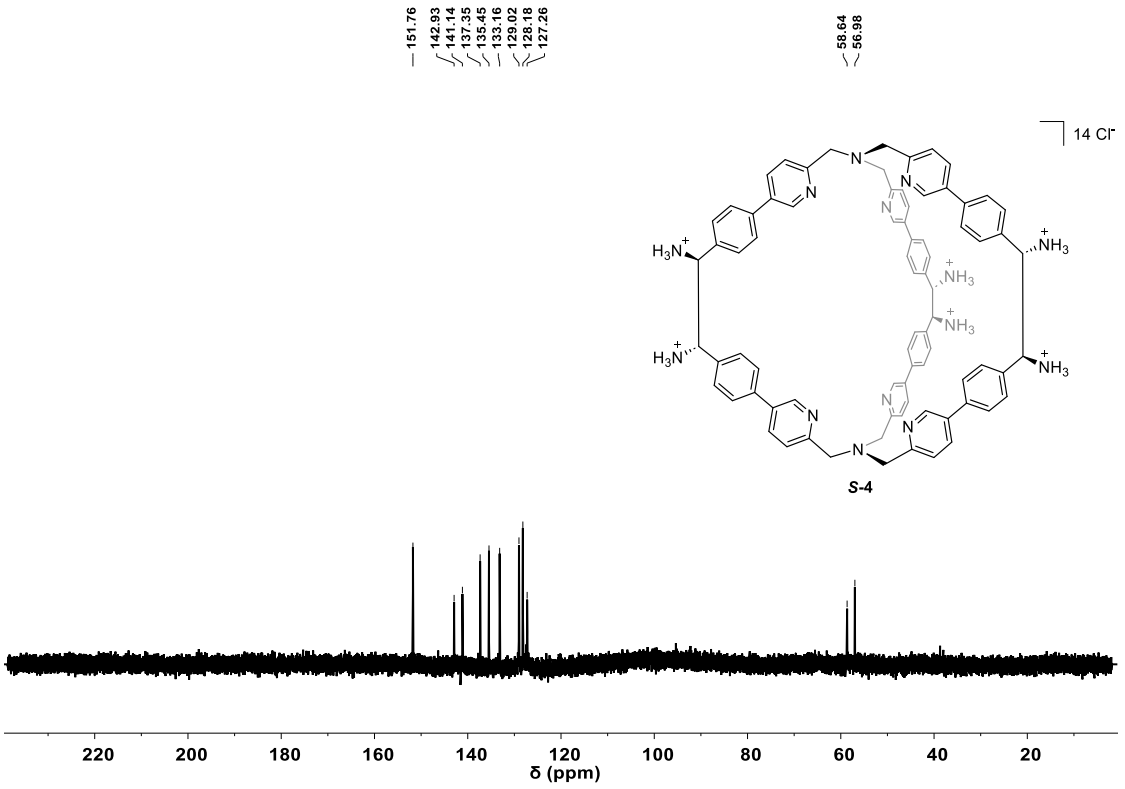

Figure A38. ^{13}C-NMR spectrum (101 MHz, 301 K, D_2O) of compound ***S*-4**.

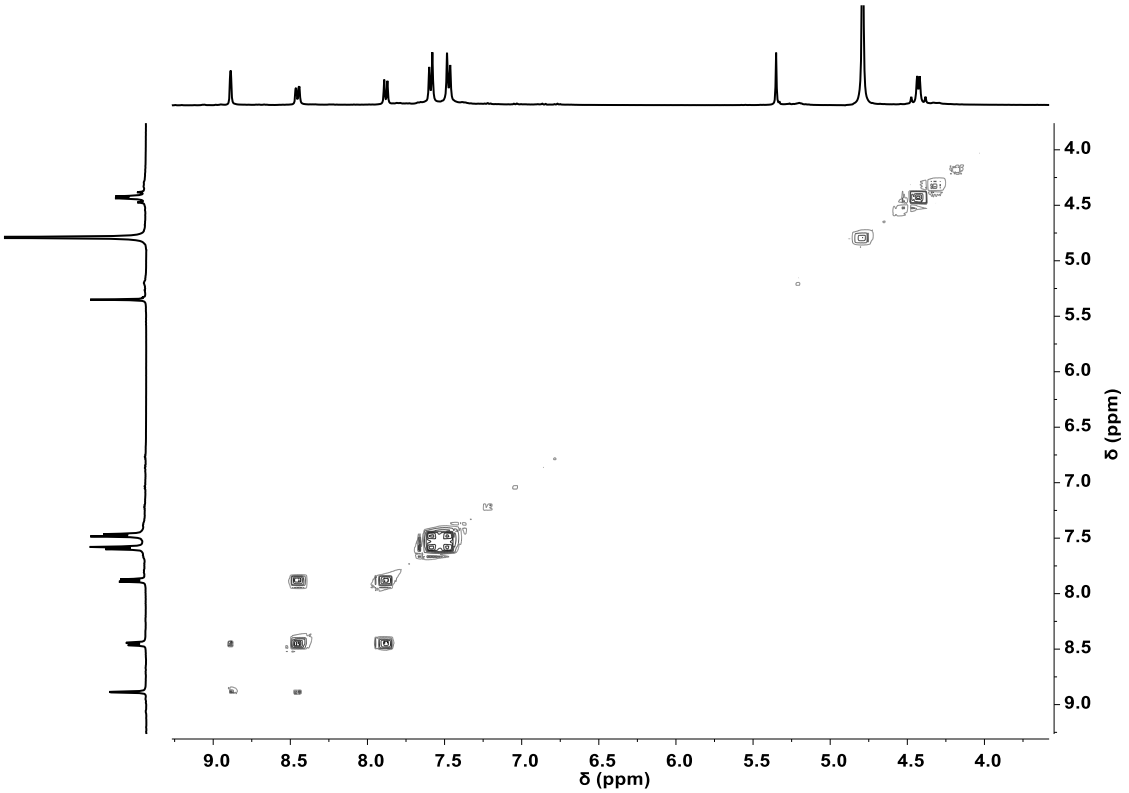

Figure A39. ^{1}H-^{1}H COSY spectrum (400 MHz, 301 K, D_2O) of compound ***S*-4**.

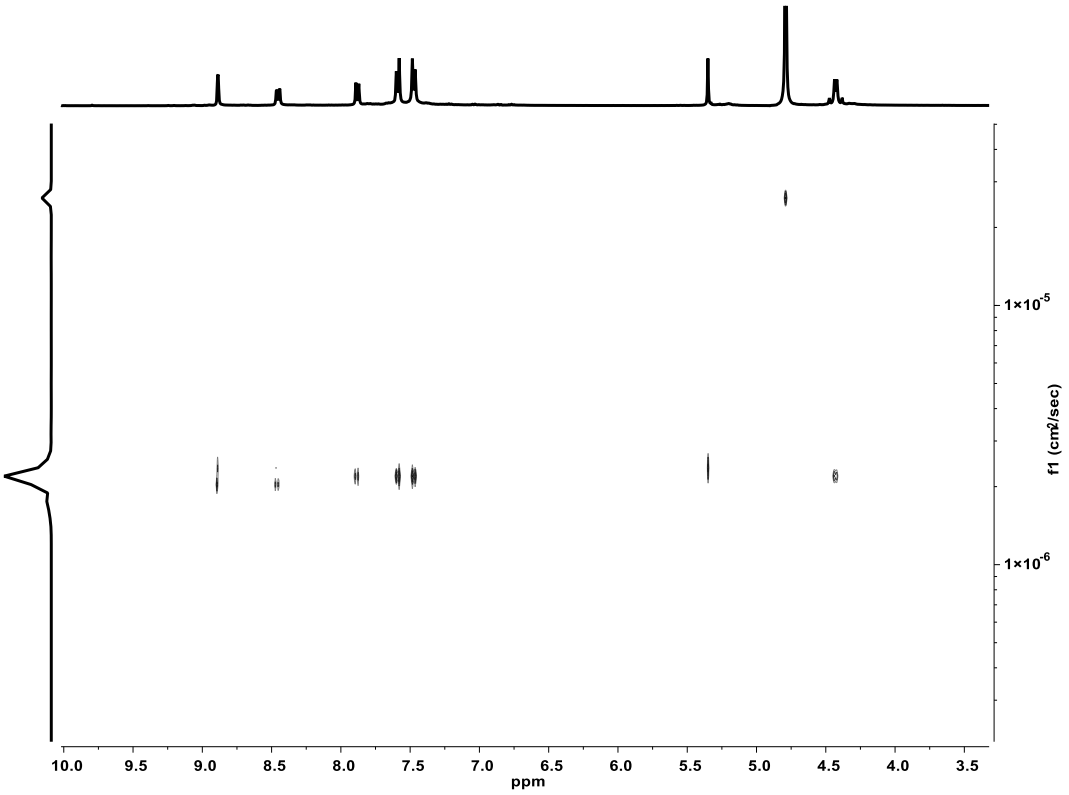

Figure A40. DOSY spectrum (400 MHz, 301 K, D_2O) of compound ***S*-4**.

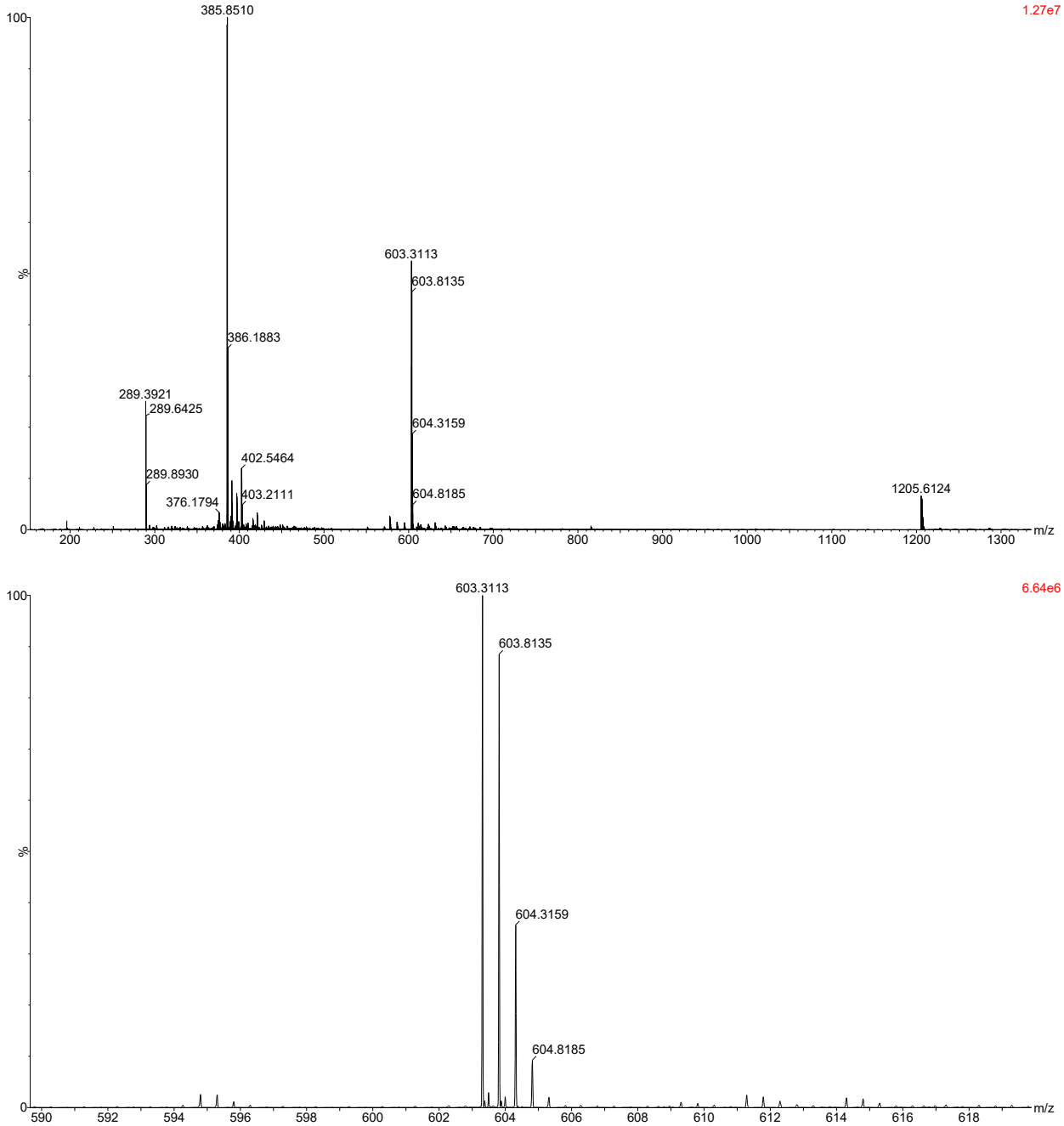

Figure A41. Experimental HRMS pattern of ***S*-4** for $[M+2H]^{2+}$ adduct in CH_3CN/H_2O (50:50)/0.1% HCOOH.

A4.6.8. Compound *S*-Zn-4

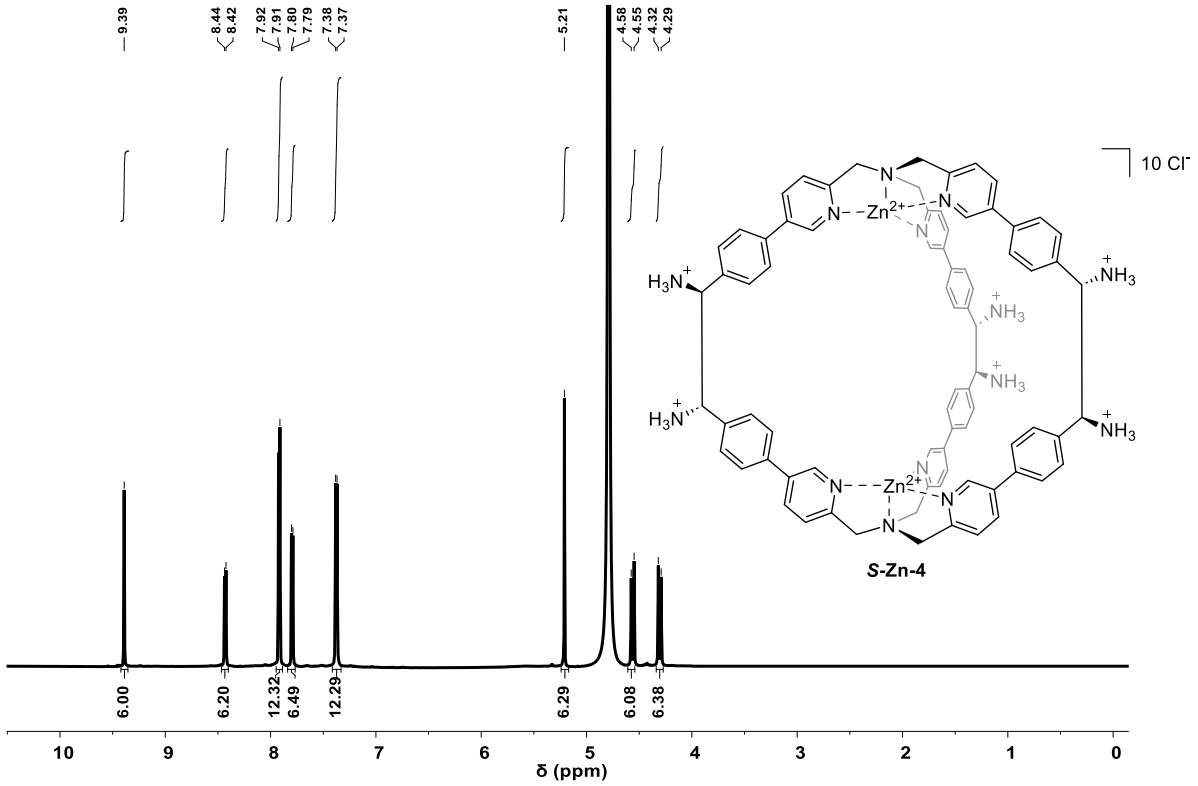

Figure A42. ^{1}H-NMR spectrum (400 MHz, 301 K, D_2O) of compound ***S*-Zn-4**.

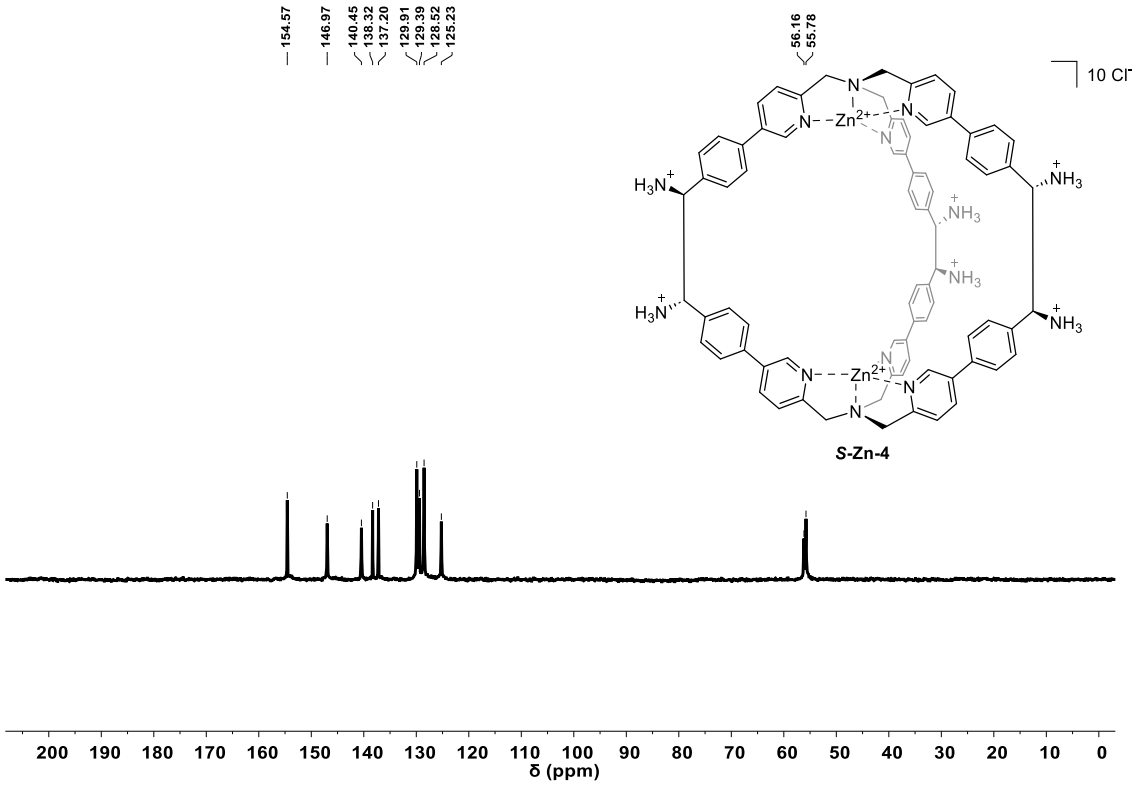

Figure A43. ^{13}C-NMR spectrum (101 MHz, 301 K, D_2O) of compound ***S*-Zn-4**.

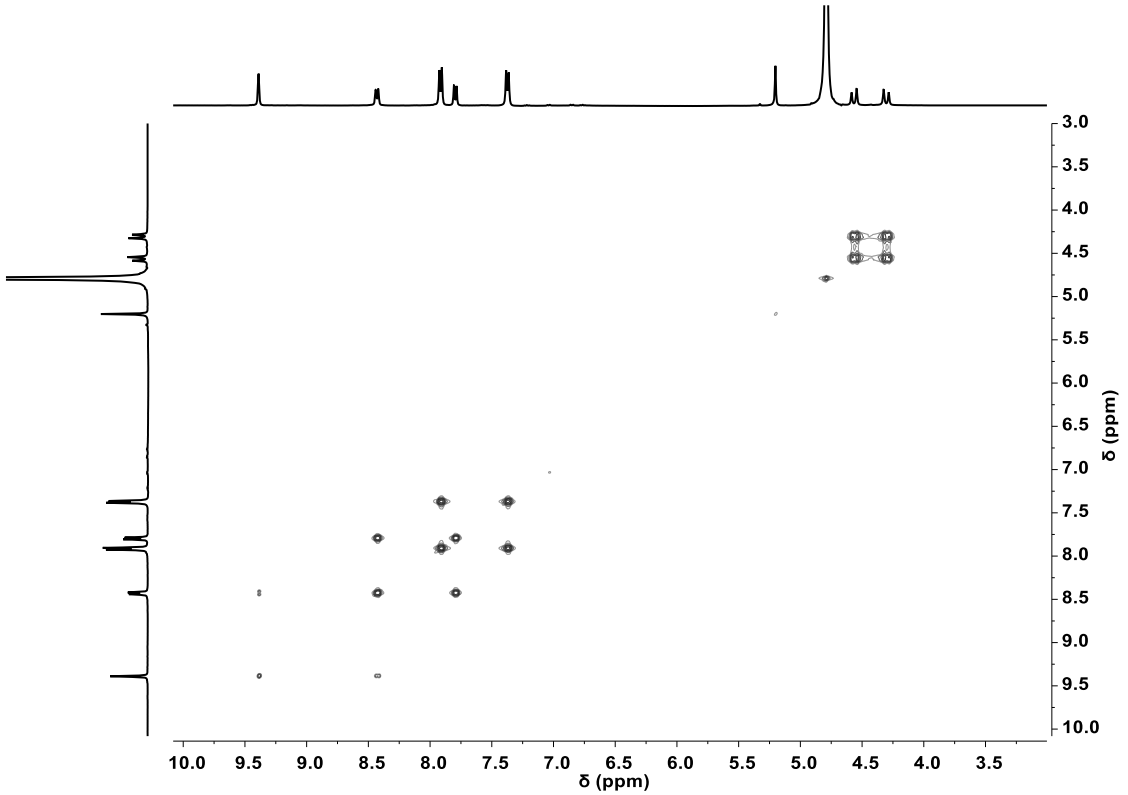

Figure A44. ^{1}H-^{1}H COSY spectrum (400 MHz, 301 K, D_2O) of compound ***S*-Zn-4**.

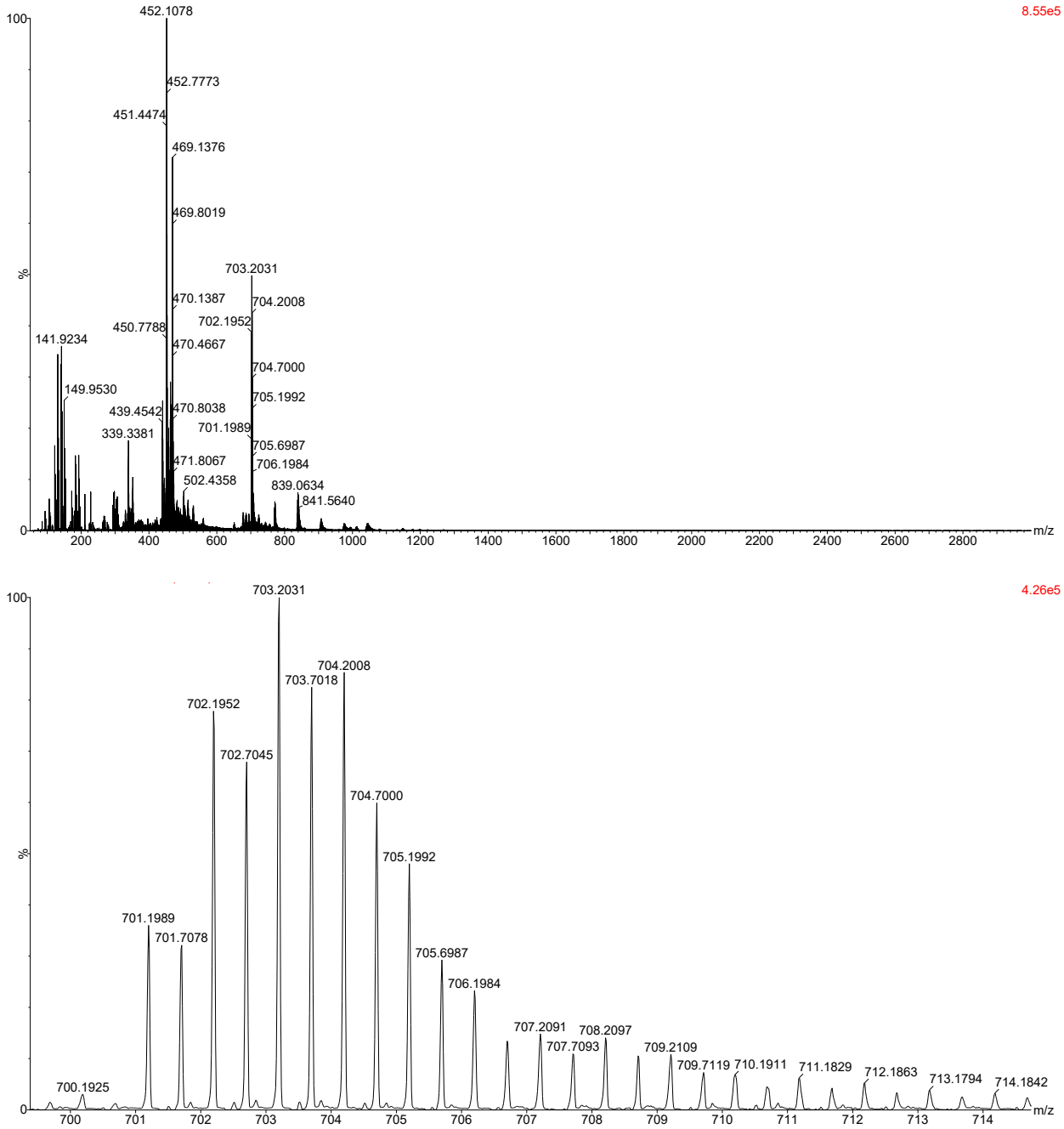

Figure A45. Experimental HRMS pattern of ***S*-Zn-4** for $[M+2Cl]^{2+}$ adduct in CH_3CN/H_2O (50:50)/0.1% HCOOH.

A4.6.9. Compound *S*-12

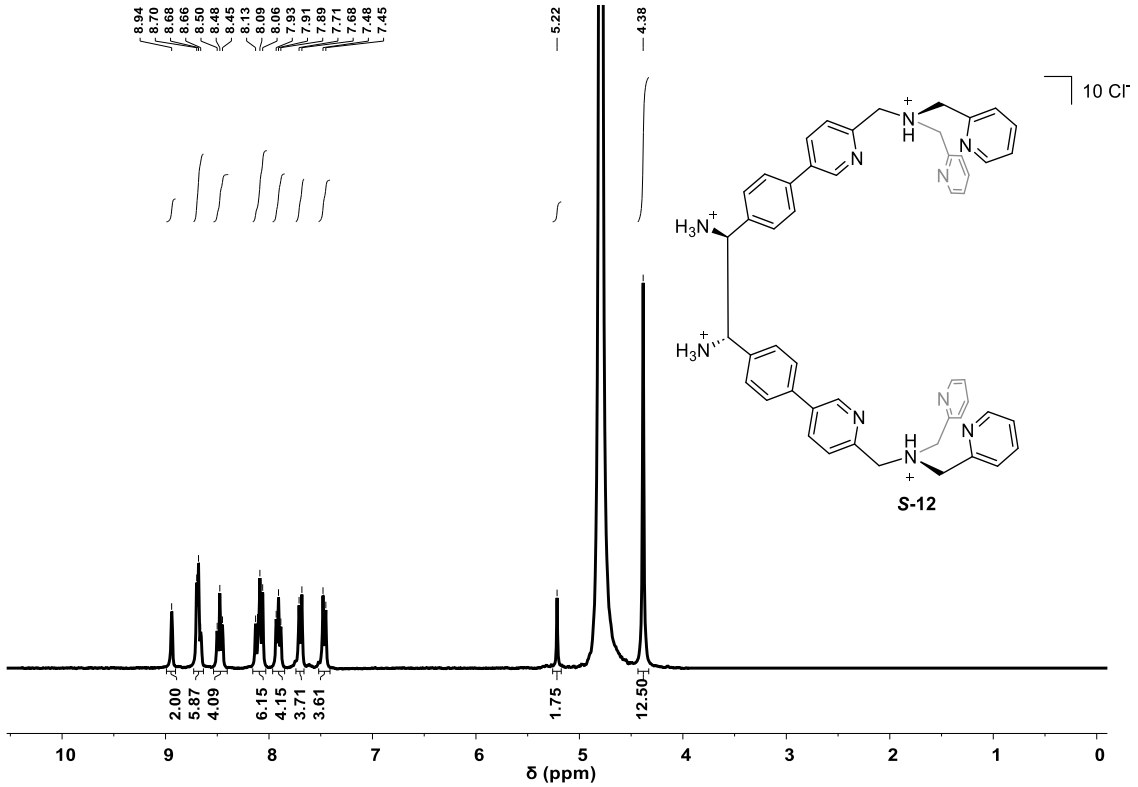

Figure A46. ^{1}H-NMR spectrum (400 MHz, 301 K, D_2O) of compound ***S*-12**.

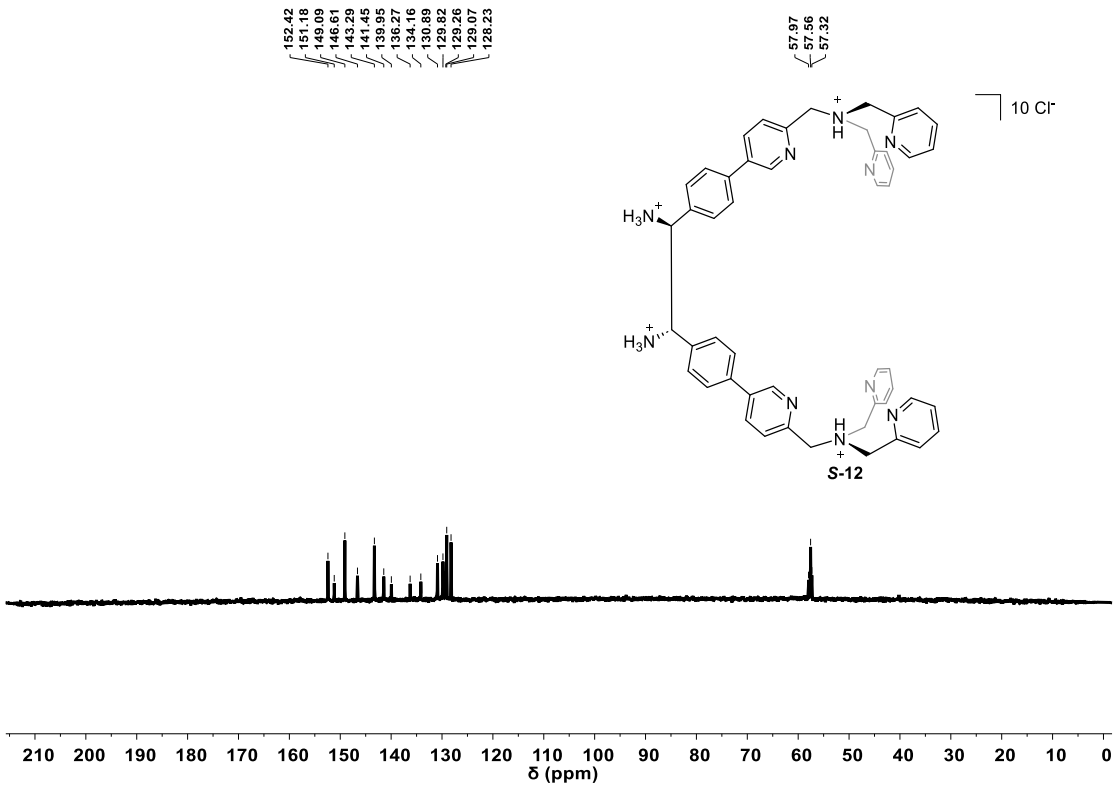

Figure A47. ^{13}C-NMR spectrum (101 MHz, 301 K, D_2O) of compound ***S*-12**.

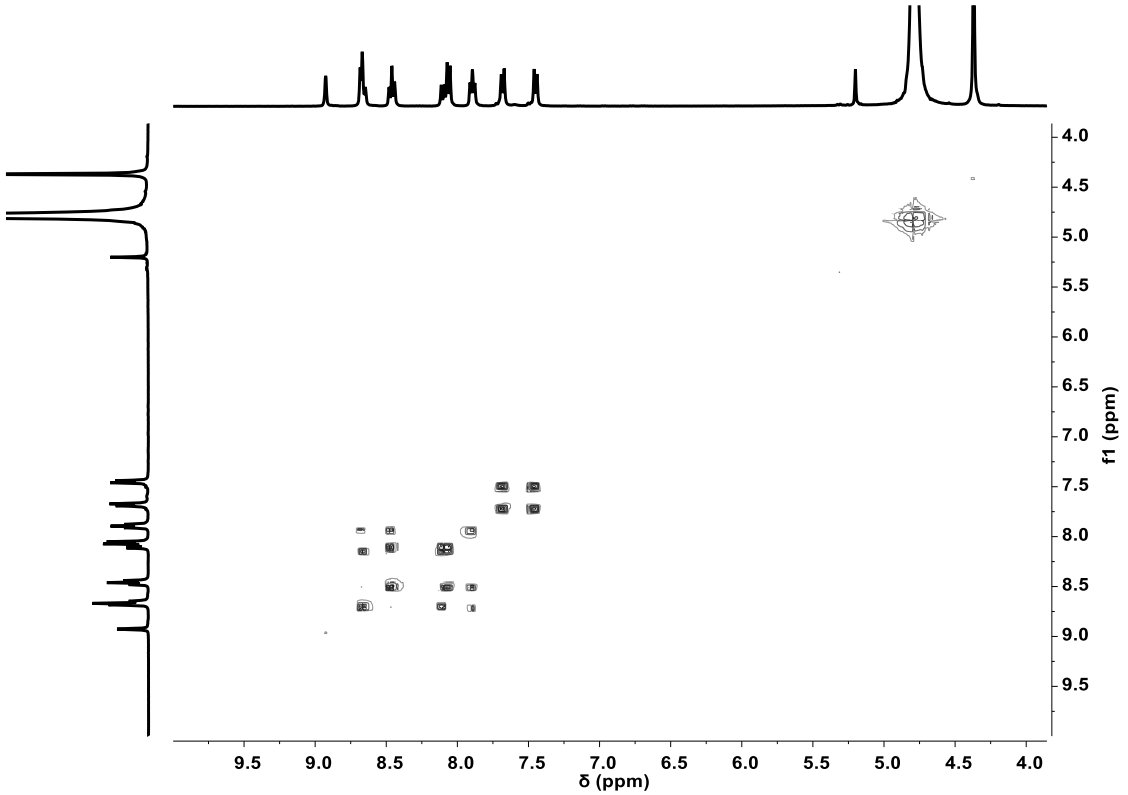

Figure A48. ^{1}H-^{1}H COSY spectrum (400 MHz, 301 K, D_2O) of compound ***S*-12**.

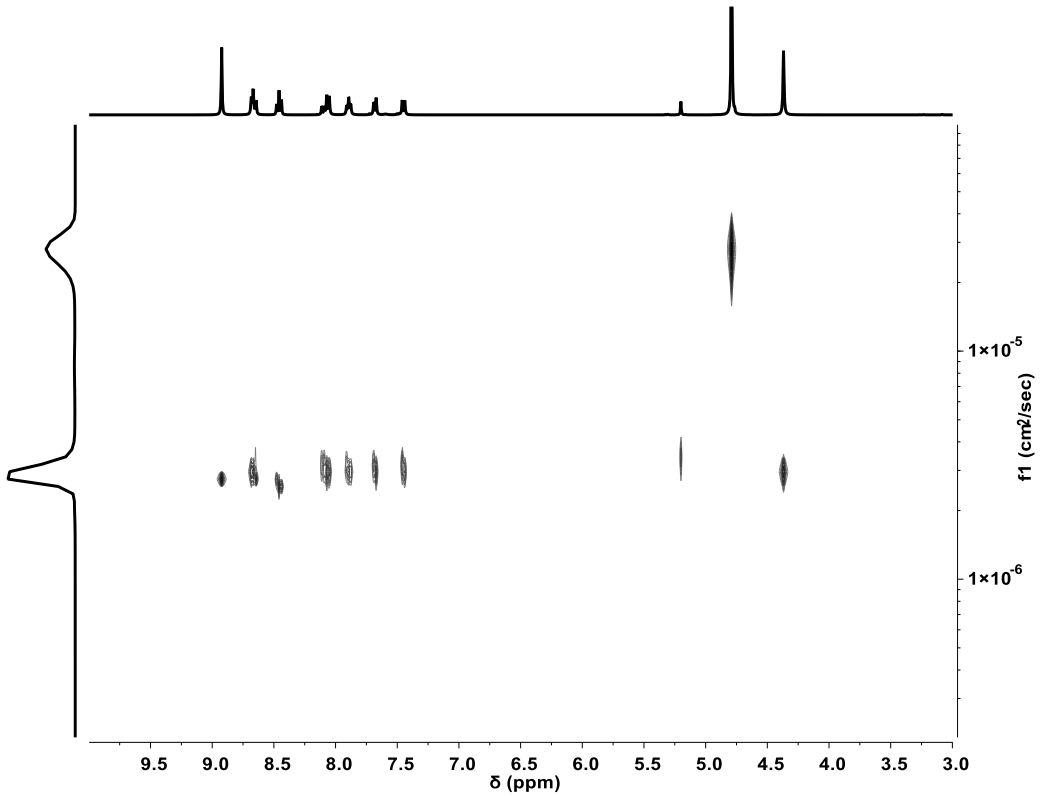

Figure A49. DOSY spectrum (400 MHz, 301 K, D_2O) of compound ***S*-12**.

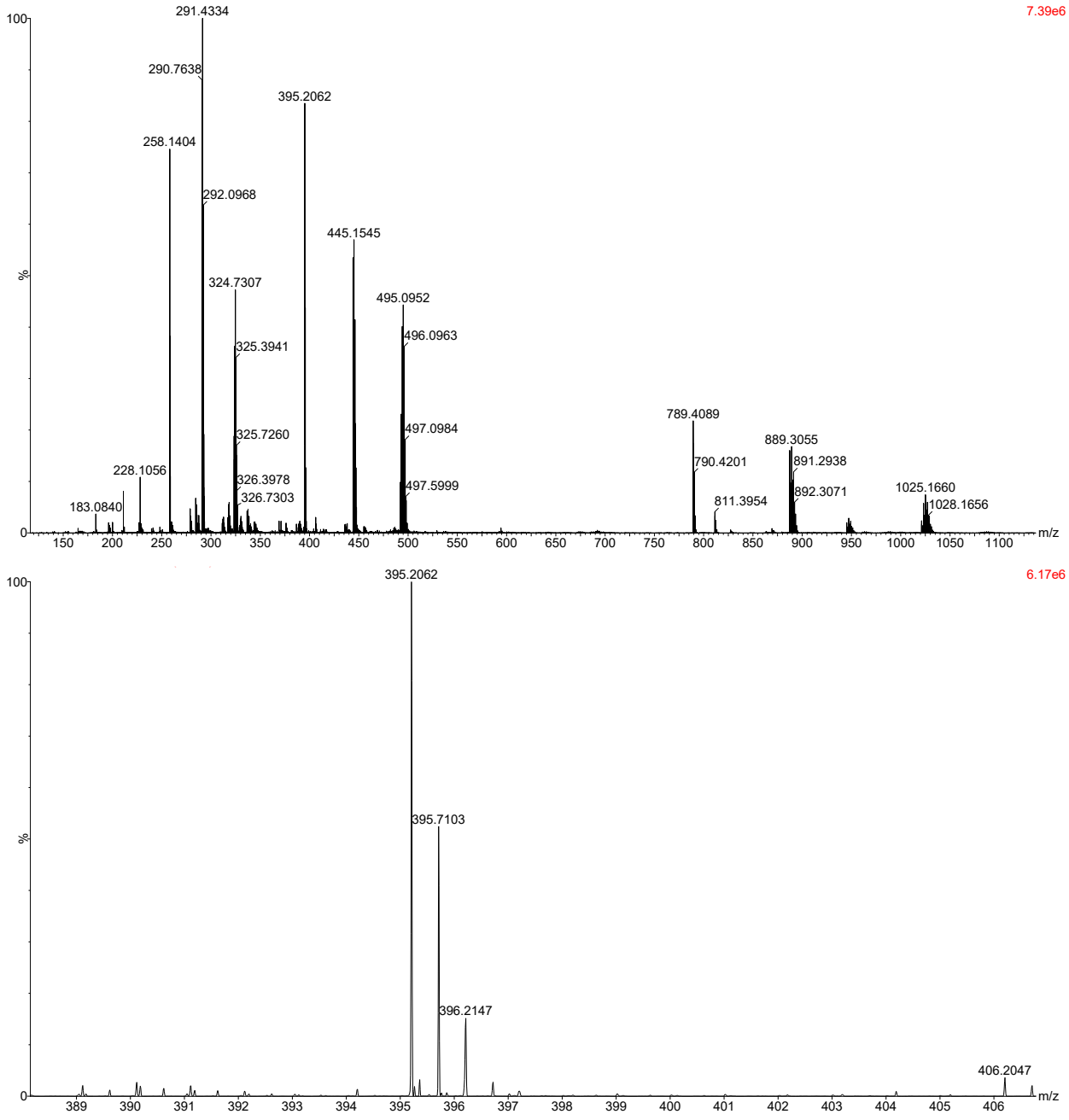

Figure A50. Experimental HRMS pattern of ***S*-12** for $[M+2H]^{2+}$ adduct in CH_3CN/H_2O (50:50)/0.1% HCOOH.

A4.6.10. Compound *S*-13

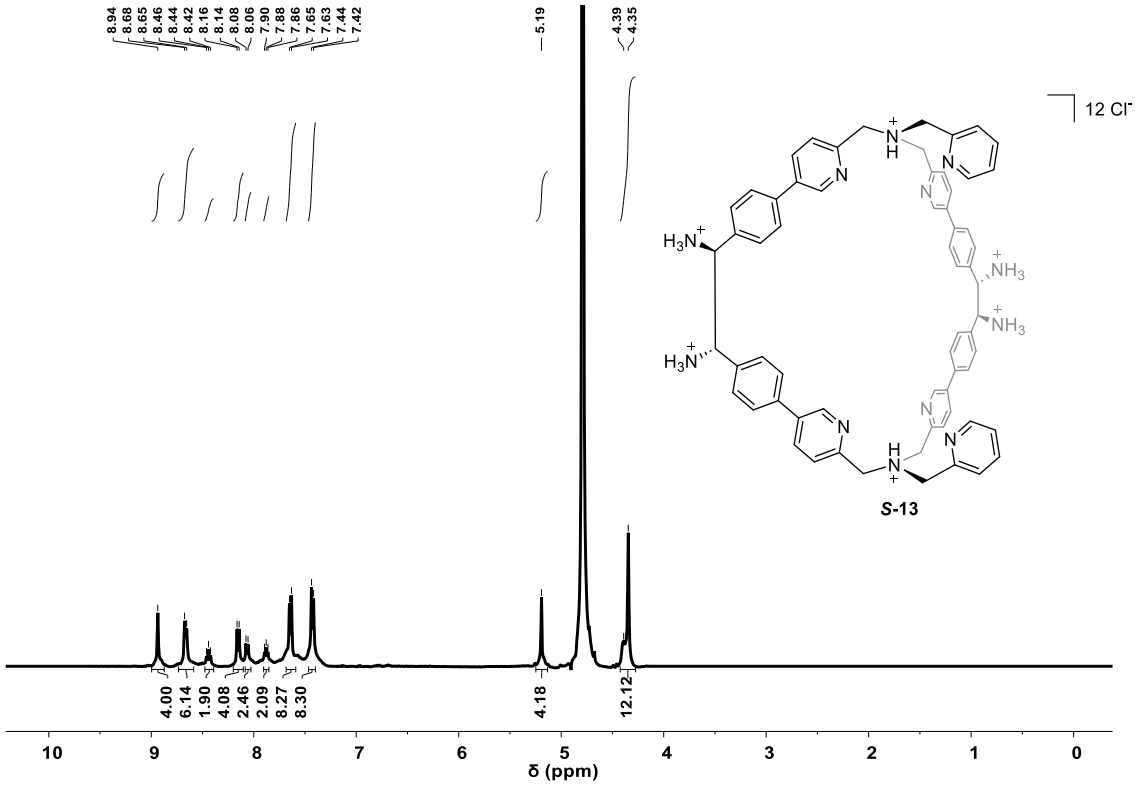

Figure A51. ^{1}H-NMR spectrum (400 MHz, 301 K, D_2O) of compound ***S*-13**.

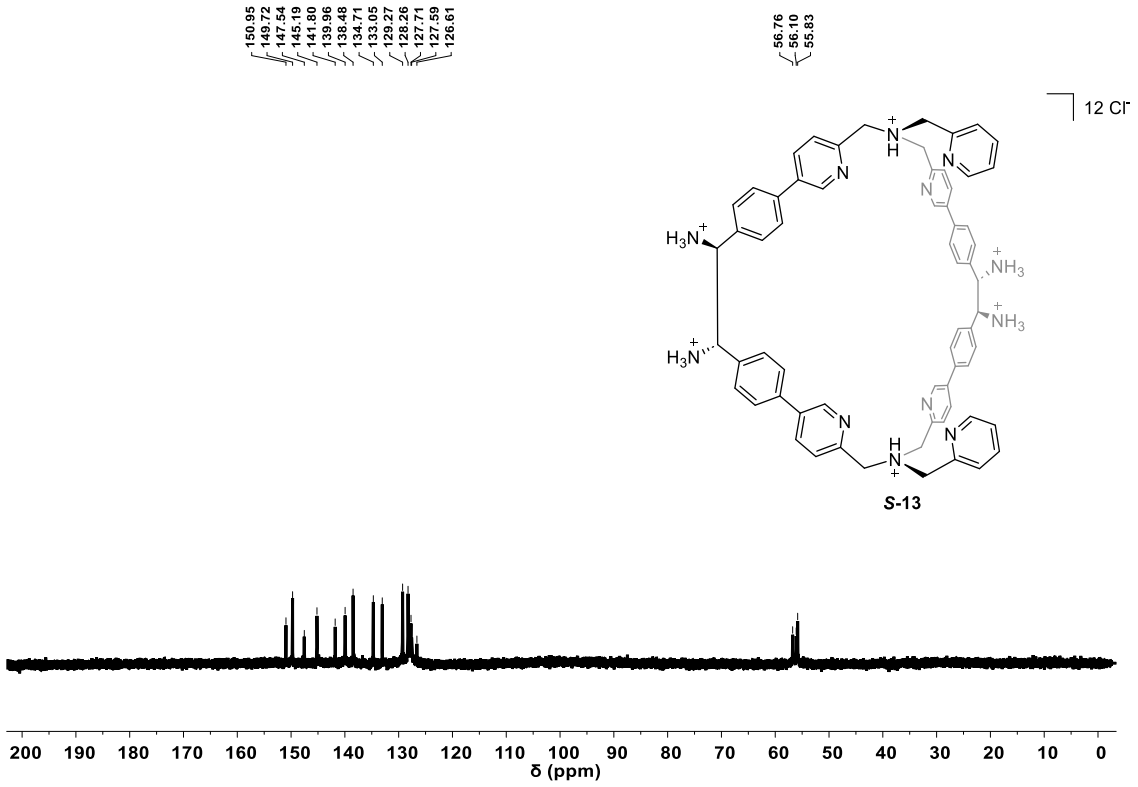

Figure A52. ^{13}C-NMR spectrum (101 MHz, 301 K, D_2O) of compound ***S*-13**.

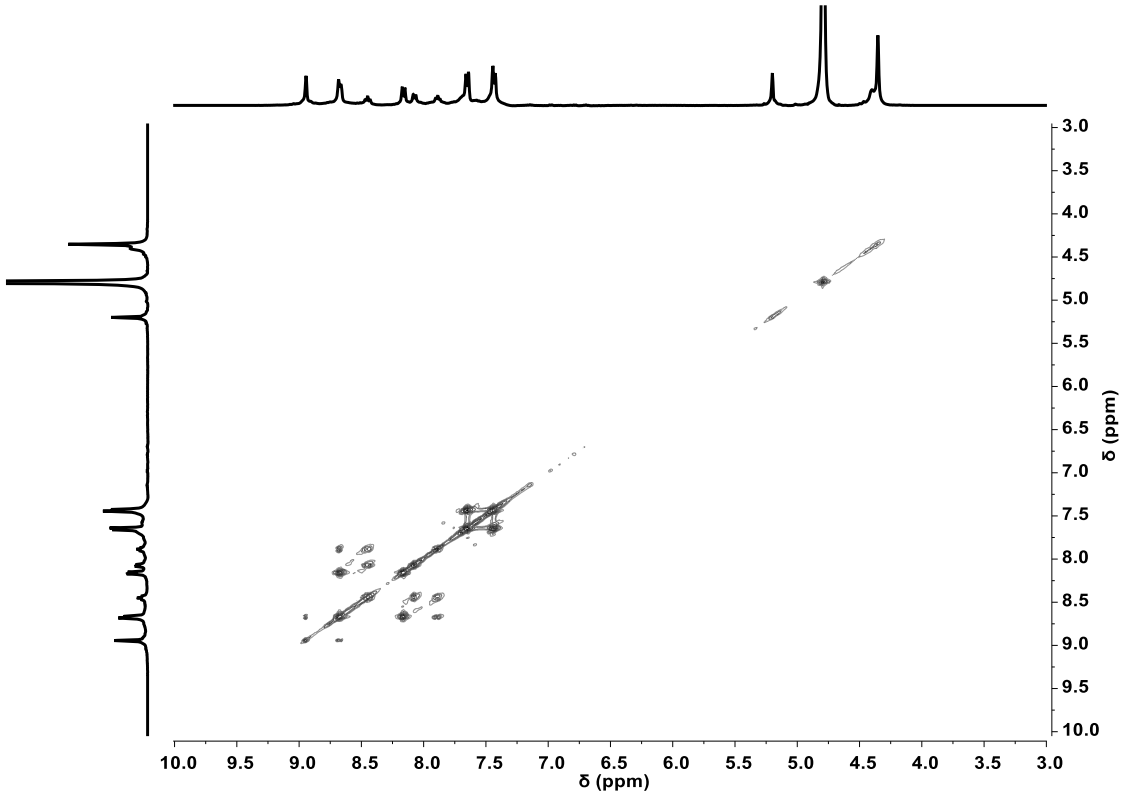

Figure A53. ^{1}H-^{1}H COSY spectrum (400 MHz, 301 K, D_2O) of compound ***S*-13**.

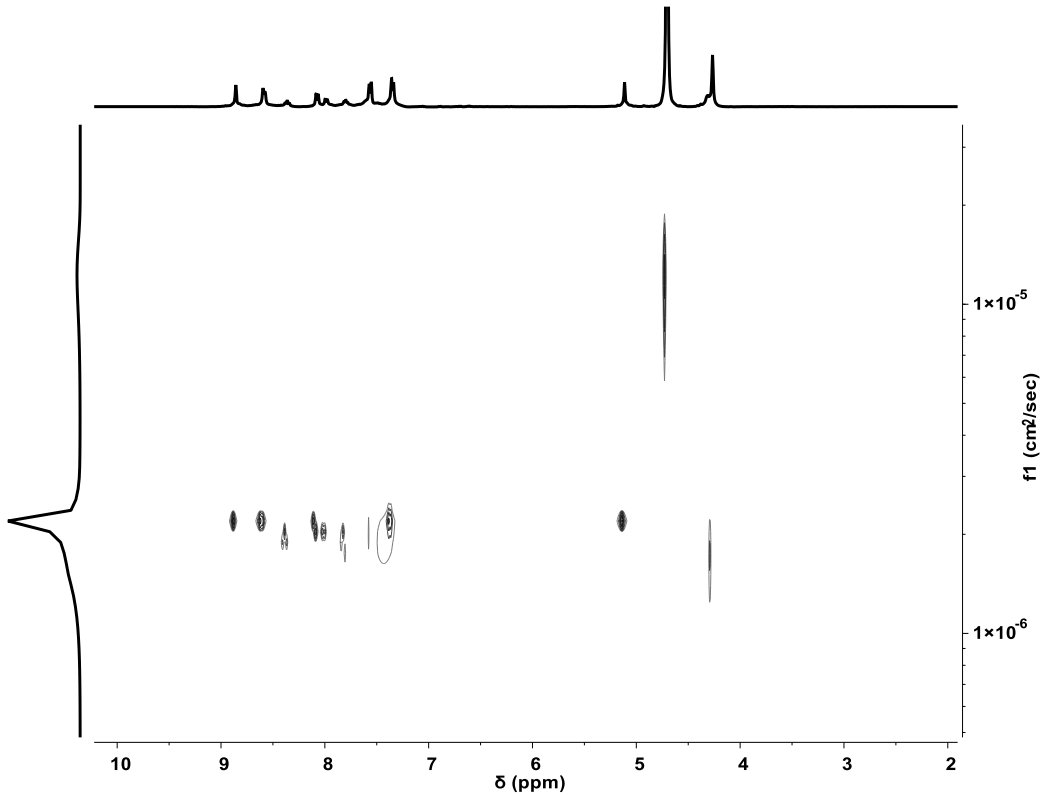

Figure A54. DOSY spectrum (400 MHz, 301 K, D_2O) of compound ***S*-13**.

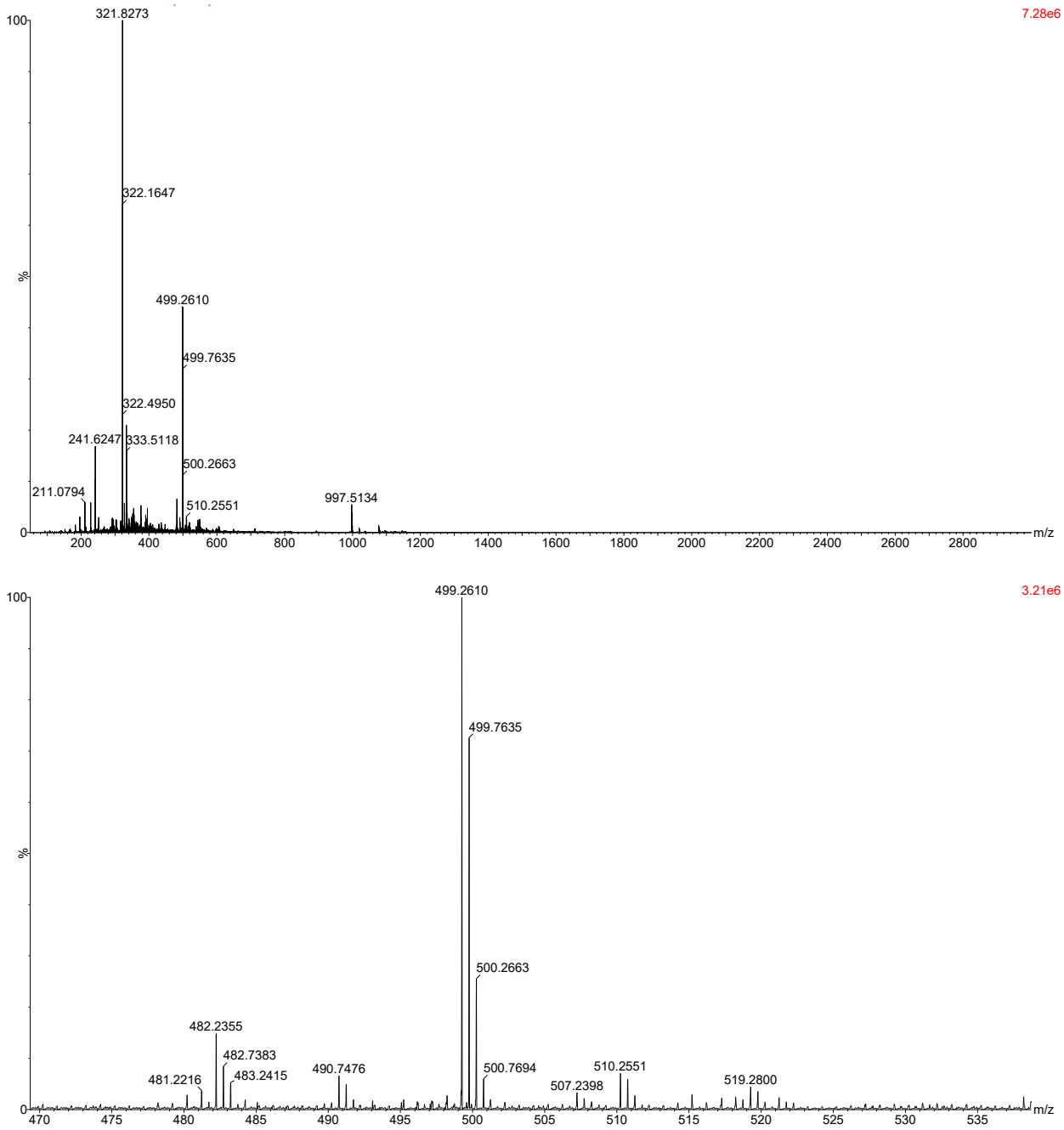

Figure A55. Experimental HRMS pattern of ***S*-13** for $[M+2H]^{2+}$ adduct in CH_3CN/H_2O (50:50)/0.1% HCOOH.

A4.6.11. Compound *S*-4 at pD = 1

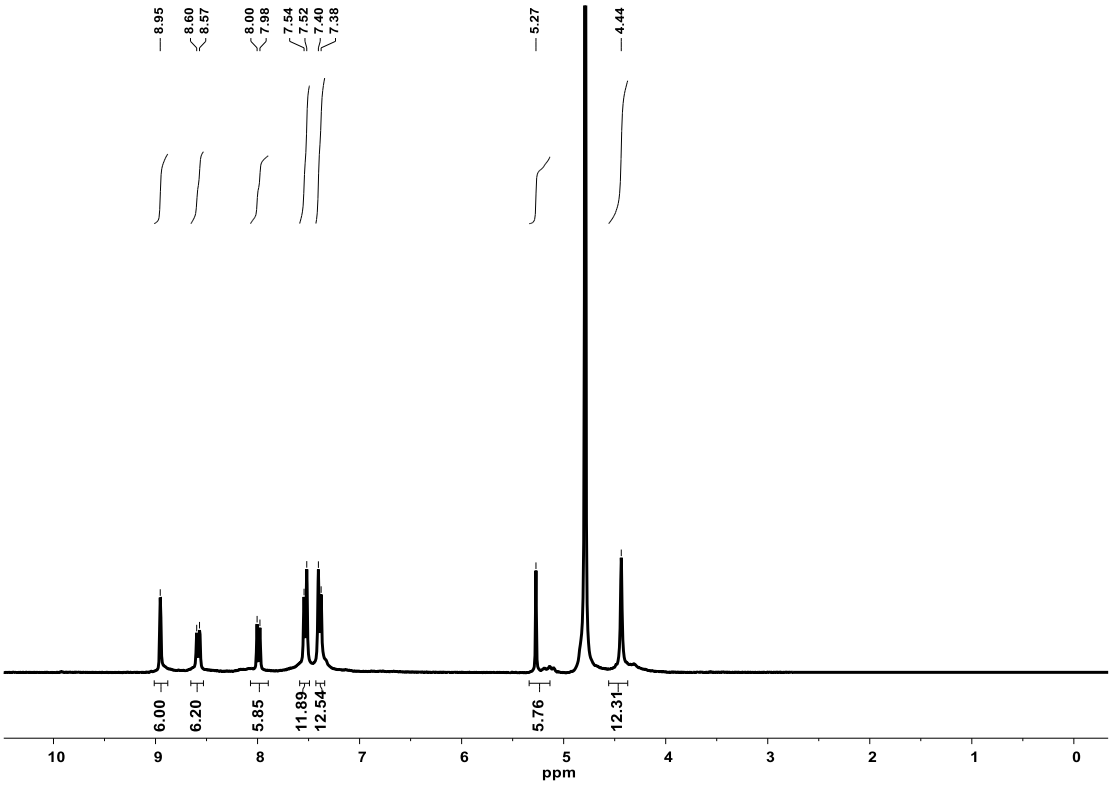

Figure A63.56 ^{1}H-NMR spectrum (300 MHz, 301 K, D_2O) of compound ***S*-4** at pD = 1 after two weeks.

A4.7. Coordinates of optimized structure C_3@3

Symbol	X	Y	Z
C	-9,98521	-5,4244	-0,59406
C	-0,39317	10,8271	-0,68552
C	10,19067	-4655	-0,77299
N	-9,07982	-4,62806	-1,41827
N	-0,01394	9,62275	-1,42122
N	8,8901	-4,55267	-1,43167
C	-7,8794	-5,0043	-1,61502
C	8,30727	-3,42603	-1,54902
C	-0,8536	8,68204	-1,59953
C	-6,9521	-4,23187	-2,46101
C	-5,57615	-4,49634	-2,41988
C	-7,42644	-3,23183	-3,32648
C	-4,68966	-3776	-3,21662
H	-5,1985	-5,27716	-1,76445
C	-6,54632	-2,52726	-4,13382
H	-8,49161	-3,03071	-3,36885
C	-5,16423	-2,78901	-4,09405
H	-3,62949	-4,01224	-3,18948

H	-6,93065	-1,75489	-4,79427
C	-0,52269	7,47617	-2,38012
C	-1,39048	6,37504	-2,37584
C	0,64351	7,41707	-3,16172
C	-1,10991	5,24372	-3,13874
H	-2,30175	6,41163	-1,78414
C	0,91747	6,29666	-3,9307
H	1,3144	8,26921	-3,1764
C	0,04087	5,19528	-3,94056
H	-1,81505	4,41709	-3,14982
H	1,82541	6,26973	-4,52669
C	7,03022	-3,2757	-2,27011
C	6,50865	-4,32555	-3,04503
C	6,33553	-2,05831	-2,22867
C	5,34999	-4,1443	-3,78374
H	7,04131	-5,26953	-3,08505
C	5,16508	-1,87788	-2,96272
H	6,72787	-1,23632	-1,63506
C	4,66939	-2,91158	-3,77321
H	4,96705	-4,96878	-4,37856
H	4,66438	-0,91403	-2,9438
C	0,30012	4,05435	-4,84676
C	0,77495	4,26973	-6,15074
C	0,05966	2,72388	-4,47654
C	0,96219	3,19673	-7,01287
H	0,95906	5,28173	-6,49742
H	-0,28046	2,47006	-3,47788
C	0,6758	1,9102	-6,56621
H	1,30685	3,35538	-8,03013
C	3,52502	-2,69025	-4,68636
C	2,42655	-1,88508	-4,34499
C	3,53305	-3,24042	-5,97743
H	2,32693	-1,42814	-3,36425
C	2507	-2,94793	-6,86693
H	4,36822	-3,85362	-6,30043
C	1,47505	-2,11021	-6,45921
H	2,5224	-3,33785	-7,88007
C	-4,24789	-2,07342	-5,00948
C	-2,99028	-1,61154	-4,59528
C	-4,59893	-1,84294	-6,34896
H	-2,65758	-1,70451	-3,56696
C	-3,70771	-1,20358	-7,20244
H	-5,55451	-2,19469	-6,72556
C	-2,4718	-0,79797	-6,70719
H	-3,95966	-1,03573	-8,24521
H	8,74523	-2,50626	-1,13544
H	-1,87191	8,73378	-1,18835
N	1,43026	-1,60383	-5,20745
N	0,23796	1,68544	-5,3106

N	-2,12553	-0,99834	-5,4213
C	-1,4586	-0,08159	-7,57478
C	0,86261	0,69764	-7,45576
C	0,36295	-1,71035	-7,40421
H	0,69755	-1,81613	-8,44704
H	-0,49028	-2,38708	-7,2759
H	1,87177	0,29652	-7,30496
H	0,79332	0,98867	-8,51432
H	-1,59457	-0,35748	-8,63136
H	-1,62841	0,99997	-7,50673
N	-0,09824	-0,35145	-7,10108
Zn	-0,18462	-0,30867	-4,7705
H	-7,4817	-5,92426	-1,16334
C	-10,1895	-4,65712	0,7726
C	9,98626	-5,42211	0,59375
C	0,39069	10,82725	0,68563
N	-8,88881	-4,55455	1,43117
N	9,08055	-4,6258	1,41766
N	0,01179	9,62285	1,4214
C	-8,30628	-3,42776	1,54856
C	0,85164	8,68228	1,59957
C	7,88051	-5,00287	1,61512
C	-7,02926	-3,27713	2,26965
C	-6,50742	-4,32688	3,04451
C	-6,3349	-2,05954	2,2283
C	-5,34884	-4,14535	3,78328
H	-7,03981	-5,27101	3,08443
C	-5,16453	-1,87882	2,9624
H	-6,72746	-1,23762	1,63473
C	-4,6686	-2,91243	3,77286
H	-4,96569	-4,96976	4,37807
H	-4,6641	-0,91484	2,94355
C	6,95299	-4,23063	2,46106
C	7,42712	-3,23038	3,3264
C	5,57712	-4,49549	2,42004
C	6,54685	-2,52598	4,13373
H	8,49224	-3,02899	3,36867
C	4,69047	-3,7753	3,21675
H	5,19963	-5,27649	1,76471
C	5,16483	-2,78811	4,09406
H	6,93101	-1,75347	4,79412
H	3,63036	-4,01182	3,18968
C	0,52104	7,47633	2,38017
C	-0,64507	7,41695	3,16186
C	1,38907	6,37538	2,37579
C	-0,91872	6,29647	3,93085
H	-1,31615	8,26895	3,17661
C	1,10881	5,24399	3,1387
H	2,30028	6,41217	1784

C	-0,04188	5,19528	3,94062
H	-1,82661	6,26934	4,52691
H	1,81413	4,41751	3,1497
C	4,24836	-2,0727	5,00951
C	4,59938	-1,84217	6,34899
C	2,99065	-1,61109	4,59533
C	3,70803	-1,20301	7,20249
H	5,55503	-2,19373	6,72557
H	2,65794	-1,70414	3,56702
C	2,47204	-0,79764	6,70725
H	3,95994	-1,03514	8,24526
C	-0,30082	4,05429	4,84683
C	-0,06011	2,72387	4,47658
C	-0,77559	4,26957	6,15085
H	0,27998	2,47014	3,47789
C	-0,96258	3,19651	7,01297
H	-0,95987	5,28152	6,49757
C	-0,67599	1,91004	6,56627
H	-1,30721	3,35508	8,03026
C	-3,52435	-2,69085	4,6861
C	-2426	-1,88548	4,34481
C	-3,53241	-3,24098	5,97719
H	-2,32641	-1,42848	3,36411
C	-2,50648	-2,94831	6,86677
H	-4,36752	-3,8543	6,30013
C	-1,47462	-2,11046	6,45911
H	-2,52191	-3,3382	7,87992
H	1,86989	8,73421	1,18826
H	7,48336	-5,9234	1,16414
N	-0,23814	1,68538	5,31064
N	2,12578	-0,99805	5,42136
N	-1,42982	-1,60407	5,20735
C	-0,36261	-1,71048	7,40416
C	1,4587	-0,08148	7,57487
C	-0,86261	0,69744	7,4558
H	-0,79337	0,98847	8,51437
H	-1,87171	0,29617	7,30499
H	1,62837	1,00011	7,50694
H	1,5947	-0,35744	8,63143
H	-0,69723	-1,81638	8,44697
H	0,49072	-2,38708	7,27583
N	0,0984	-0,3515	7,10113
Zn	0,18484	-0,3086	4,77052
H	-8,74449	-2,50808	1,13504
H	1,46339	10,82911	0,44669
H	-1,46587	10,82867	-0,44657
H	10,59629	-3,66289	-0,52989
H	9,55193	-6,40231	0,35218
H	-9,5507	-6,40452	-0,35251

H	-10,5952	-3,66508	0,52936
C	-11,297	-5,61589	-1,33762
C	-11,9333	-6,86258	-1,32318
C	-11,9193	-4,5465	-2,01787
C	-13,1678	-7,05415	-1,9399
H	-11,4556	-7,68948	-0,80326
C	-13,1601	-4,73596	-2,6345
C	-13,7819	-5,98102	-2,59009
H	-13,6457	-8,02842	-1,91054
H	-13,6127	-3,89359	-3,14838
H	-14,7453	-6,11551	-3,07411
C	-11,1522	-5,3904	1,69322
C	-12,4672	-4,93334	1,83717
C	-10,7622	-6,55854	2,38355
C	-13,3919	-5,62032	2,62101
H	-12,7707	-4,03279	1,30884
C	-11,6897	-7,25149	3,16778
C	-12,9976	-6,78706	3,28033
H	-14,4087	-5,25127	2,71264
H	-11,3591	-8,14731	3,68427
H	-13,7087	-7,33408	3,89329
C	-0,05421	12,04829	-1,52539
C	-0,95595	13,11593	-1,60428
C	1,17981	12,15303	-2,20327
C	-0,64608	14,2758	-2,31132
H	-1,90848	13,03797	-1,08582
C	1,4942	13,31777	-2,91032
C	0,58802	14,37394	-2,95852
H	-1,35805	15,0942	-2,35349
H	2,45172	13,36785	-3,41939
H	0,84357	15,27327	-3,51211
C	0,05137	12,04841	1,5254
C	0,95282	13,11631	1,60425
C	-1,1827	12,15286	2,20323
C	0,6426	14,27614	2,3112
H	1,90538	13,03857	1,08584
C	-1,49744	13,31756	2,91018
C	-0,59156	14,37399	2,95834
H	1,35433	15,09474	2,35334
H	-2455	13,36741	3,41922
H	-0,84738	15,27328	3,51186
C	11,15354	-5,38845	-1,69328
C	12,46868	-4,93151	-1,83701
C	10,76367	-6,55668	-2,3835
C	13,39347	-5,61869	-2,6205
H	12,77207	-4,03087	-1,30879
C	11,69133	-7,24985	-3,16737
C	12,99928	-6,78554	-3,27969
H	14,41033	-5,24974	-2,71196

H	11,3608	-8,14574	-3,68379
H	13,7105	-7,33271	-3,89237
C	11,29788	-5,6134	1,33767
C	11,93425	-6,86004	1,32339
C	11,91983	-4,54398	2,01816
C	13,16861	-7,05152	1,94048
H	11,45682	-7,68695	0,80327
C	13,16044	-4,73335	2,63517
C	13,78238	-5,97835	2,59092
H	13,64663	-8,02575	1,91123
H	13,61287	-3,89097	3,14922
H	14,74568	-6,11277	3,07525
C	-0,5182	-0,21603	-0,56178
H	-1,1365	0,64352	-0,40755
H	-1,10678	-1,10294	-0,45287
C	0,07804	-0,16933	-1,97009
O	1,28505	0,02103	-2,16585
O	-0,7967	-0,32897	-2,92724
O	-11,3575	-3,30018	-2,08975
H	-10,3991	-3,41598	-1,90597
O	-9,49216	-7,06353	2,3049
H	-8,91786	-6,32551	2,00399
O	9,49358	-7,06152	-2,30509
H	8,91928	-6,32335	-2,00447
O	11,35789	-3,29771	2,09001
H	10,39973	-3,41334	1,90535
O	2,11041	11,14884	-2,18555
H	1,62955	10,32782	-1,94164
O	-2,11302	11,14841	2,18552
H	-1,63189	10,32747	1,94187
C	0,61867	-0,22364	477
O	0,31202	-0,3494	1,86806
O	1,8166	-0,11956	0,1059

A4.8. References

[1] Gaussian 16, Revision C.01, M. J. Frisch, G. W. Trucks, H. B. Schlegel, G. E. Scuseria, M. A. Robb, J. R. Cheeseman, G. Scalmani, V. Barone, G. A. Petersson, H. Nakatsuji, X. Li, M. Caricato, A. V. Marenich, J. Bloino, B. G. Janesko, R. Gomperts, B. Mennucci, H. P. Hratchian, J. V. Ortiz, A. F. Izmaylov, J. L. Sonnenberg, D. Williams-Young, F. Ding, F. Lipparini, F. Egidi, J. Goings, B. Peng, A.Petrone, T. Henderson, D. Ranasinghe, V. G. Zakrzewski, J. Gao, N. Rega, G. Zheng, W. Liang, M. Hada, M. Ehara, K. Toyota, R. Fukuda, J. Hasegawa, M. Ishida, T. Nakajima, Y. Honda, O. Kitao, H. Nakai, T. Vreven, K. Throssell, J. A. Montgomery Jr., J. E. Peralta, F. Ogliaro, M. J. Bearpark, J. J. Heyd, E. N. Brothers, K. N. Kudin, V. N. Staroverov, T. A. Keith, R. Kobayashi, J. Normand, K. Raghavachari, A. P. Rendell, J. C. Burant, S. S. Iyengar, J. Tomasi, M. Cossi, J. M. Millam, M. Klene, C. Adamo, R. Cammi, J. W. Ochterski, R. L. Martin, K. Morokuma, O. Farkas, J. B. Foresman, D. J. Fox, Gaussian, Inc., Wallingford CT, 2016.

[2] 2016. GaussView, Version 6, Dennington, R., Keith, T. A., Millam, J. M., Semichem Inc., Shawnee Mission, KS.